THE MAGNETIC SUSPENSION OF WIND TUNNEL MODELS FOR DYNAMIC TESTING

by

M.J. Goodyer, D.C.Ae., C.Eng., A.M.I.Mech.E., A.F.R.Ae.S.,

of the Department of Aeronautics and Astronautics,

University of Southampton.

A thesis submitted for the degree of

Doctor of Philosophy.

December, 1967.

CONTENTS

ABSTRACT

FACULTY OF ENGINEERING AND APPLIED SCIENCE.

AERONAUTICS AND ASTRONAUTICS.

Doctor of Philosophy.

THE MAGNETIC SUSPENSION OF WIND TUNNEL MODELS FOR DYNAMIC TESTING.

by Michael John Goodyer.

To aid the prediction of aircraft stability, wind tunnel measurements are made on models performing unsteady motions. Normally the model is mechanically supported. The resultant flow interference is particularly severe with the type of sting support used in tests at the high forcing frequencies sometimes required for dynamic similarity of oscillatory motions.

Wind tunnel models had previously been suspended in steady flow using controlled electro-magnetic fields, with the elimination of flow interference. The purpose of the work described in the thesis was to investigate practically the feasibility of magnetic suspension for dynamic tests and to develop suitable measuring techniques.

Existing magnetic suspension systems incorporated control of model position in five rigid body degrees of freedom, leaving roll motions free. For measurements on non-axisymmetric models, it is necessary to control all six degrees of freedom. A satisfactory low speed roll control system was developed for models having wings and fins.

The suspension system may be used directly as a force and moment balance. The drag forces produced by bodies of revolution were measured at subsonic Mach numbers. Dynamic tests included roll damping and pitch stability derivative measurements on delta planform models. Difficulties involved in the separation of unsteady aerodynamic loads from relatively large inertia forces led to the concept of a tuned model in which, at the resonant frequency, inertia forces are balanced by internal spring forces. Aerodynamic damping forces then dominate and can be measured accurately. The tuned model was difficult to suspend with adequate stability margin until special feedback control characteristics were incorporated.

It has been demonstrated that steady load measurements can be made to an accuracy of 2% and dynamic loads to 10%. The system has been proved for subsonic operation; it is anticipated that problems associated with supersonic speeds can be overcome.

ACKNOWLEDGEMENTS

Research and Development on this scale must be a team effort, and I would like to express my thanks to:

Mr. Peter Tanner, for long hours (often night hours) spent developing the large power amplifiers to a state where they have performed faultlessly for a period of about four years. This reliability contributed in a major way to the subsequent developments in magnetic suspension techniques;

Mr. Tom Kelley, our technician, who has been responsible for the manufacture of the majority of the mechanical parts of the system. His insistence on good workmanship, in the long run has saved us a good deal of time. Temporary jobs have a habit of becoming permanent; and finally my Supervisor, Dr. M. Judd, who has helped me in so many ways. I would like to mention specifically our many discussions on the subject, which have helped to clarify half-conceived ideas, and have undoubtedly been a source of inspiration.

I am grateful to those members of the staff of the Aerodynamics Division of N.P.L. for agreeing to monitor the work; to D.S.I.R., later S.R.C., for placing the research contracts, and to my wife for typing the Thesis.

1. Introduction.

Contents:

1.1 The Basic Principles and Advantages of Magnetic Suspension.

Objects which are sufficiently strongly magnetised may be suspended in magnetic fields, with no other means of support. A simple form of suspension system might consist of a bar magnet suspended with its axis vertical and one of its poles positioned closely beneath a solenoid-like electro-magnet, also with its axis vertical. In this case, a force of attraction between the magnets would be arranged to just oppose the gravitational force. For stability, a fundamental requirement is that either the strength of magnetisation of the suspended object, or the strength of the suspending field, should be controlled automatically as a function of the position of the object. In this case the vertical position would be monitored, and the signal used to control a field strength. This suspension system would have control in one degree of freedom - vertical translation. Other modes of motion have pendulum-like stability.

Such a system would allow a model containing a magnet to be suspended in a wind tunnel free from flow interferences which would otherwise be caused by mechanical supports.

This is one of the advantages of magnetic suspension applied

to wind tunnel models. In the case of low speed wind tunnels, interference to boundary layer flow by support wires or struts is avoided. In high speed flow where a sting is the usual form of support, disturbance of the base flow over the model is eliminated. A second advantage to be gained by eliminating sting support is that the design of the tail region of the model is not compromised in any way by sting thickness.

The suspension system with control in one degree of freedom which has been described, in some circumstances could be employed in a vertical wind tunnel where the additional force applied to the model, which would be an aerodynamic drag force, would be directed vertically and opposed by a change of field strength. However, one would rely on any other aerodynamic forces or moments not producing instabilities in the five uncontrolled degrees of freedom. Furthermore, it would only be possible to control movement of the model, by changes of field strength, in one degree of freedom. For wind tunnel work a more versatile suspension system would normally be required allowing control to be exercised over more than one degree of freedom. For example, as well as providing control over the magnetic force opposing the drag force, it is desirable to be able to control incidence. However, at any but zero incidence there would generally be an aerodynamic lift force and pitching moment which would tend to move the model in a direction which could not be corrected by changes of field strength. If wind tunnel measurements are required on a model at incidence to the flow, as well as providing means for opposing drag force a magnetic suspension system must oppose lift force and pitching moment. A still more general case would be a requirement to yaw the model, in which case control of the model in more degrees of freedom would be required.

Once a requirement exists for opposing two or more mutually perpendicular aerodynamic force components, these forces having magnitudes comparable with or greater than the model weight, there is more freedom of choice of wind tunnel arrangement. One is no longer confined to a vertical working section as the simplest configuration.

Control over model position in several degrees of freedom can be achieved by constructing the suspension system out of several separate magnets, the strength of each magnet being controllable and influencing model motion desirably in just one degree of freedom. The suspension magnets are exclusively electro-magnets todate, although there is no fundamental reason why moveable permanent magnets could not be used. Electro-magnets are chosen because they offer the simplest method of controlling the field strength generated at the model. The electro-magnet array is positioned around the model but clear of the gas stream.

Most wind tunnel models have a relatively high length : diameter ratio, and have a length comparable with the working section width. The characteristic shape suggests that the model should contain a bar magnet running length-wise through the fuselage, and the size of the model, compared with the tunnel dimensions, suggests that a horizontal working section should be used with two suspension electro-magnets arranged over the ends of the model. Each electro-magnet would attract the near end of the model, supporting half of the weight. The system would be unstable with fixed-strength suspension magnets as has been mentioned, and in this case the current supply to the electro-magnets would be governed by the position of the near end of the model.

It is common to monitor model position optically; the position signal is then used in a servo loop to control current. This pair of electromagnets would be capable of controlling model motion in two degrees of freedom, vertical translation and pitch (or yaw, depending on the roll attitude of the model), and can oppose a vertical aerodynamic force and moment as well as the gravitational force. Similar electromagnets alongside the working section can provide control in two more degrees of freedom. The main aerodynamic force that remains to be opposed is the drag force, and for this purpose a solenoid coil is normally wound around the wind tunnel and controlled by the axial position of the model.

These particular suspension system principles, which were pioneered by O.N.E.R.A.[2]*, provide model control in five degrees of freedom, and have formed the basis of several suspension systems now in use and the basis of all systemswhich control more than three degrees of freedom.

1.2 The Object of the Work at Southampton University on Magnetic Suspension Systems.

This suspension system has its origins in discussions between Professor J.P. Jones and Dr. M. Judd of this Department on techniques that might be suitable for making dynamic measurements with wind tunnel models. It was suggested that a wind tunnel magnetic suspension system of a type which had been developed at O.N.E.R.A. in France, details of which had just been published, might prove a useful research tool for dynamic measurements provided that suitable techniques

* References are collected in Section 15.

could be developed.

A contract was negotiated between the University and the Directorate of Scientific and Industrial Research (D.S.I.R.) for a feasibility study on the application of magnetic suspension to dynamic measurements. The study began in 1959 and was carried out by Dr. Judd. The conclusions were that there were good prospects of making such measurements, with the important advantages over mechanical systems used for dynamic measurements that different modes of model motion would be available without changing the basic arrangement of the system, and that the support sting would be eliminated. Dynamic measurements usually involve model oscillation at frequencies and amplitudes where inertia forces are high, and for this reason the support sting tends to be robust and sting interference effects are aggravated.

D.S.I.R., and later the Science Research Council, then supported the University with a contract for the construction of a magnetic suspension system. The contract was monitored through the National Physical Laboratory, and construction began in 1962.

The object was to construct a magnetic suspension system which would be capable of making dynamic measurements with winged models, using an existing high speed (Mach 1.8) wind tunnel.

1.3 The Research and Development Programme.

The original intention was to construct a suspension and balance system which would be capable of controlling model position in five degrees of freedom, leaving roll uncontrolled, and capable of making five corresponding force or moment measurements. The principal modes of oscillatory model motion for which the system was designed were pitching and lateral heaving. Suspension magnet principles based

on those described in section 1.1 were chosen, but the moments and forces that would be required to induce the model motions dictated a particular magnet arrangement that is unique. The lateral electro-magnets, which were to be used to induce model oscillation, were duplicated with one pair each side of the wind tunnel, forming a symmetrical arrangement of magnets.

A feature of magnetic suspension systems is that the wind tunnel working section is largely enclosed by the electro-magnets and model position monitoring equipment, and is therefore rather inaccessible. In the case of this system the working section is virtually completely surrounded by this equipment, and optical flow studies are not possible, nor would the system be easily adapted to a transonic working section. A second feature is that as there is no connection with the model, point data such as pressures and temperatures are not easily obtained, and telemetry techniques are normally employed.

A considerable engineering effort is required to produce a suspension system, and during the time that this suspension system was being developed some new principles were evolved. Hitherto, only axi-symmetric bodies had been suspended, but for a magnetic suspension system to be really useful it is necessary to have the capability of suspending aeroplane-like models. When a model carries wings it is necessary to have control in roll in order to trim the roll attitude. Several principles for controlling roll were proposed and evaluated, theoretically and experimentally, some of the principles making use of the unique arrangement of electro-magnets, and one roll control system was adopted making this the first six component magnetic suspension system and balance.

When the balance had been developed to a satisfactory state for suspension with six degree of freedom control in still air, the balance was adapted to a low speed wind tunnel to gain operational experience, and to prove some of the equipment.

With a six component balance, models can be forced in almost any mode by oscillating appropriate magnetic fields. The control systems were adapted to provide a variety of modes. The forces or moments generated by a model, whether aerodynamic or due to its inertia, are opposed by the suspension magnets and are therefore dependent on the current flowing in the electro-magnet coils. Current calibrations may be used to give overall force and moment data.

The high speed wind tunnel required some modification for the magnetic suspension system : the existing working section was magnetic and therefore unsuitable. A new non-magnetic non-conducting working section was manufactured, and fitted with plain convergent liners to allow the air speed range to be extended gradually. The model control systems were developed to a state giving an acceptably steady model at speeds close to Mach 1.

The equipment that had been commissioned at this stage included six power amplifiers, six independent automatic control systems including model position monitoring equipment, the electro-magnet coil array and cooling system (the power dissipation in the coils was rather high), a suitable working section for the high speed wind tunnel, and various pieces of calibration equipment.

During the development of the system it had become apparent that some difficulties of measurement could arise in the case of dynamic measurements with a magnetic suspension system. It was

anticipated that it would be difficult to separate relatively small aerodynamic force components from the large inertia forces involved with an oscillating model. There was particular interest in the measurement of an aerodynamic damping force with a model oscillating sinusoidally. This force results in a phase difference between the force applied to the model and its motion. When the dominant force is the inertia force, the phase difference is small and difficult to measure. For an accurate measurement pure wave-forms are required.

The results of some work which were published at this time[17] confirmed these suspicions. The work was carried out at M.I.T. on a five component magnetic balance, suspending a model in a hypersonic wind tunnel, and was concerned with the measurement of the aerodynamic damping of a body of revolution oscillating in pitch. Acceptable measurements were not possible because the poor quality of both the motion and applied moment signal wave-forms did not allow the accurate measurement of relative phase angles.

It was also recognised that the frequency or amplitude of model oscillation were rather restricted, and also the wave-forms of the current and model oscillations would be distorted due to non-linearities in the power amplifiers. For these reasons there was a requirement for some alternatibe means of measuring damping forces. The solution was a "tuned" model, which, as a result of its construction, had one resonant mode of motion. The model was easily excited in this mode at the resonant frequency, and the excitation force applied to the model by the suspension magnets in this case was only required to overcome damping forces.

The tuned model overcame most of the problems of measurement, and greatly extended the useful frequency range of oscillations. However, the model was difficult to suspend and required a considerable effort on control system design to obtain stability, whereas the conventional solid models were relatively easy to stabilise. A control system was evolved which allowed suspension over a restricted range of wind tunnel Mach number. The remaining work in the programme was the development of measurement equipment suitable for tuned models, and the measurement of the aerodynamic damping of pitching oscillations of one particular model.

Concurrently with the development of the Southampton University magnetic suspension system, there were systems under development in several other organisations. The main object with some of these systems was to suspend bodies of revolution for studies of base flows, rather than to produce wind tunnel balances.

This covers the work reported in this Thesis, which begins with a basic description of the magnetic suspension systems suitable for wind tunnel work which were in use in France and the U.S.A. in the late 1950's. In subsequent chapters a good deal of emphasis is placed on the development of equipment and suspension techniques in order to achieve satisfactory dynamic measurements.

2. A Review of Two Existing Suspension Systems.

When the suspension system described in this Thesis was projected there existed only two magnetic suspension systems providing control of the position of the suspended object in more than one degree of freedom. One of these, controlling in three degrees of freedom, had been developed as a free gyro. support but was suitable for application to the suspension of wind tunnel models, where it could be used as a three component balance. The other was a wind tunnel model magnetic suspension system controlling in five degrees of freedom, in use as a five component balance. These two systems are fundamentally different in their approach to suspension, and have formed the basis for several later wind tunnel systems. In this Chapter the main features of each are described. A discussion of the relative merits then leads to the logical choice of one as a basis for the design of a suspension system suitable for dynamic measurements.

Section

Contents:

2.1 A Suspension System Controlling in Three Degrees of Freedom.

This suspension system was developed at the University of Virginia, and the work was reported by Jenkins and Parker[5]. The electro-magnets were capable of subjecting the suspended object to three force components, which were arranged to be mutually at right angles for convenience, but no moments could be applied. The suspended object was a soft iron sphere, magnetised by a pair of

Helmholtz-like coils, the sphere being situated at the centre of the coils in the region of uniform field. When applied to a wind tunnel, these coils would be wound around the tunnel working section. A magnet in such a uniform field experiences no net force, for which a non-uniform field is required.

A non-uniform field is generated by a single coil, but in the general case a magnet in such a field would experience a force through its centre and a pure couple. Variation of the current in the coil changes the magnitudes of both. In order to exert a pure force, the suspended magnet can be subjected to fields from a pair of similar coils, one each side of the magnet in the manner of Helmholtz coils but with the current flowing in opposite sense in the two coils. The mechanism of the production of the force can be explained qualitatively with the aid of the sketch below, where the magnetising Helmholtz coils have been omitted, and the force-producing coils are represented by bar magnets. The field produced by a coil is similar to that produced by a bar magnet, provided that the bar magnet is co-axial with the coil.

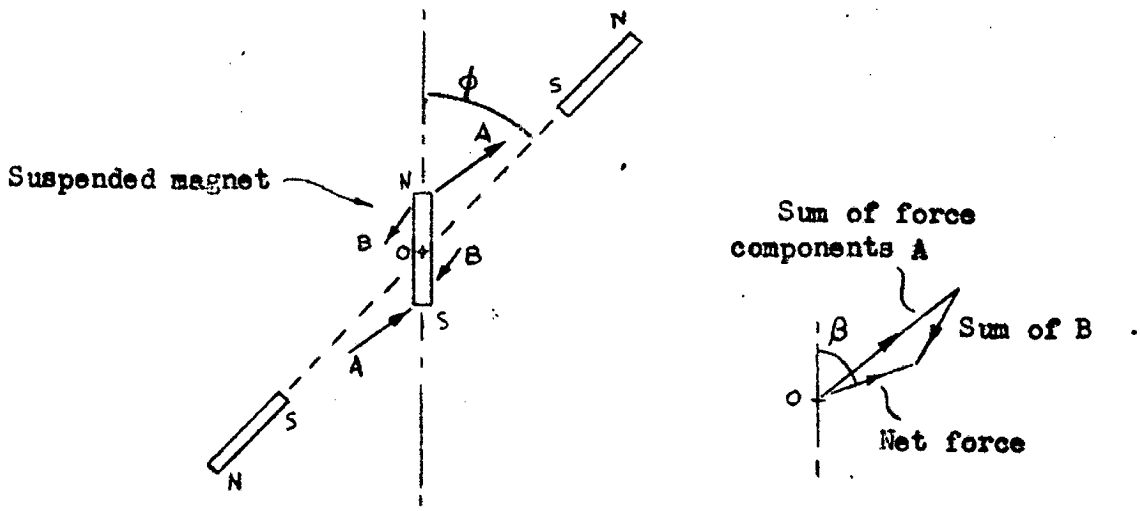

This sketch represents a general case where the force coil axis makes an angle ϕ with the direction of magnetisation of the suspended magnet (this direction, which is vertical in the sketch, would be the axis of the Helmholtz coils). The force coils produce a net force through O at angle β to the vertical in this sketch $(\beta \neq \phi)$, but no moment. . By a suitable choice of ϕ, the angle β can be made 90°. This pair of force coils would then produce a horizontal force and be able to control position in the horizontal direction.

A similar pair of coils rotated 90° about the vertical axis would allow similar control along a second axis perpendicular to the first. Neither of these pairs of coils would be capable of supporting the weight of the model, and for this purpose a third pair is required, positioned with their axes on the vertical axis. The array of coils would provide position control along three mutually perpendicular axes.

This system was later developed into a successful three component wind tunnel balance, with some modification to the coil arrangement to suit the application. A similar system was built at Princeton University[6] simply as a model support for wake studies in hypersonic flow.

For the purpose of measuring the aerodynamic damping of a particular mode of motion it is a requirement that the mode should be produced, normally as a continuously forced or a decaying sinusoidal oscillation, and the resultant damping forces measured. In the case of a suspension system of this type, capable of producing translational

modes of motion and also capable of measuring the forces producing and resisting the motion, information on damping would be available provided that no significant unwanted mode of motion was produced. Continuous pitching oscillations cannot be forced with this system, but the decaying oscillation technique could be applied, the initial disturbance of the model possibly being induced mechanically.

For a model to resonate in pitch, a pitching stiffness must exist. This could be produced by offsetting the centre of gravity of the model, by using a non-spherical magnetic core in the model, and there could be a contribution from the airflow over the model. For a stable pitching oscillation the aerodynamic damping must be positive, which could be a restriction on the range of shapes that could be suspended, wind-on.

The problems which could arise with this balance, when applied to dynamic measurements can be summarised as:

(i) Excitation in heave may be accompanied by rotary modes of motion.

(ii) Aerodynamic pitching moment, or rolling moment, cannot be opposed by the suspension magnets.

(iii) The aerodynamic damping of pitching oscillations must always be positive.

Evidently a suspension system was required which could provide model control and forcing in more degrees of freedom.

2.2 The Five Component Magnetic Balance.

Magnetic suspension systems of this type were developed at O.N.E.R.A. and first reported[2] in 1957. The basic principles have been described in Chapter 1. In that case the electro-magnet layout is described as the L-arrangement, because of the arrangement of magnets

above and alongside the wind tunnel, controlling vertical and horizontal motions. These magnets control four degrees of freedom including two rotary modes of motion. The fifth degree of freedom, axial motion, is controlled by a coil around the wind tunnel as has already been explained. Later suspension systems at R.A.E. Farnborough[3] and at M.I.T.[4] were based on this electro- magnet arrangement.

A variation on this arrangement which also provides control in five degrees of freedom was available. The variation consisted of a movement of the four electro-magnets controlling vertical and lateral motions to symmetrical positions roughly at 45° to the horizontal above and either side of the tunnel. In these positions the coils can exercise proper control over the model, and all four coils help to support the model. The main advantage was that a clear horizontal Schlieren path was available. This is known as the V-arrangement as used now by O.N.E.R.A. and projected for a system at A.E.D.C.

The advantages of five component balances of the L or V types over the three component balance were that model oscillations could be forced by the electro-magnets, giving more control over the frequency of oscillation, and that negative aerodynamic stiffness and damping could be countered by stiffness and appropriate artificial damping introduced by the automatic position control systems. This allows a much wider range of models to be suspended, and the advantages together result in the five component balance being the more suitable type for dynamic measurements.

It is desirable that the available frequency of model

oscillation should give a frequency parameter similar to that obtained in full scale. This generally results in a requirement for relatively high frequencies of model oscillation. In order to extend the frequency range, a variation of the L-arrangement was adopted for the magnetic suspension system built at Southampton University, the variation being the addition of an extra pair of electro-magnets alongside the wind tunnel opposite to the normal lateral position control magnets. This is referred to as the $\perp$ - arrangement. The immediate advantage was that the maximum lateral force or moment capacity was increased. However, the arrangement of the lateral magnets, which is unique to this suspension system, had other important advantages resulting from the symmetry of the arrangement. One of these advantages was that roll control could be incorporated, an important requirement for the suspension of winged models.

Both of the existing suspension systems described above used optical systems to monitor model position, and it was decided to adopt the same method for this suspension system, in view of the proven suitability.

3. The Principles of Force and Moment Generation.

There are several quite different ways in which magnetic fields might be used for controlling the position of a model in a wind tunnel. The disturbing forces acting on the model are gravitational and aerodynamic, and in this Chapter the principles are given of the various methods by which the forces may be counteracted using magnetic fields.

Contents:

3.1 Introduction.

There are two broad classes into which the techniques available for control of model position by magnetic fields may be divided,

(i) the sum of the disturbances could be directly countered by magnetic forces and moments applied to magnetic material or electro-magnets within the model, or

(ii) the attitude relative to the airstream of parts of the model, or the whole model, could be controlled by magnetic fields in order to produce an aerodynamic force to counteract the gravitational force, or to eliminate some aerodynamic forces or moments, giving an indirect control over model position.

The general principles in either category could be selected in different combinations to provide the most convenient solution to the problems of suspending different models.

The suspension system which has been built at Southampton University was designed for operation under category (i) conditions, but experience has shown that some models are not adaptable to adequate control in all degrees of freedom at the higher air speeds that are available with the particular wind tunnel in use. Serious consideration is now being given to the possibility of utilising category (ii) control in circumstances where no serious restrictions would be imposed on the range of available aerodynamic data.

The control principles which are available are described qualitatively in the following sections. In Chapters 5 and 6 quantitative magnetic force and moment data coming under category (i) is given for some models in the suspension system.

3.2 Direct Control by Magnetic Forces and Moments.

3.2.1 The magnetic suspension system was designed for a supersonic wind tunnel having a horizontal working section, and for models which would typically be missile-like, or a body carrying slender delta wings. With these types of model a relatively long magnetic core lying in the general direction of the tunnel axis can be contained within the model, and magnetic forces and moments were generated in the following manner to give control over the model in six degrees of freedom.

The forces and moments which the suspension system are required to produce on the model are referred to a system of orthogonal axes centred on the model, with one axis along the tunnel centre-line, a vertical axis, and a second horizontal axis transverse to the tunnel, say x, y and z axes respectively.

A pair of similar electro-magnets were arranged over the

wind tunnel in the manner shown schematically on Fig. 3.1 (a), each magnet being separately energised. If the electro-magnets have equal energisation producing equal pole-strengths, the net force on a model positioned symmetrically below the electro-magnets would act vertically through the centre O of the model. In this way the gravitational force and a vertical aerodynamic force could be counteracted. In the special case where the strengths of the four poles depicted on Fig. 3.1 (a) are independant, the net vertical force would be proportional to the sum of the currents in the coils of the two electro-magnets. It is assumed for simplicity that the complimentary poles to S_1 and N_1 are far enough away from the model to exert negligible force.

If the electro-magnets are energised to different levels, the effect on a model in the same position would be to produce a force on the model in the plane of the figure which can be resolved into vertical and horizontal components through the centre O, together with a moment about the axis normal to the figure through O, i.e. a moment about the z-axis, see Fig. 3.1 (b). For the simplified system described in the previous paragraph this moment and the force in the x direction would be proportional to the difference between the strengths of the electro-magnets (i.e. to the ampere-turns on each magnet) and the force component in the y direction would be proportional to the sum of the strengths. Hence this type of electro-magnet will in general allow control of two quantities with one interaction, and it is convenient to regard the y force component and moment about the z-axis as the controlled quantities and the x-force component as an interaction.

Movement of the model from its position of symmetry changes the distribution of the forces shown on Fig. 3.1 (a) and several other interactions can arise. As one particular example of this, movement in the x-direction can have a relatively large effect on the x force component, but initially only a small effect on the y force component and the moment about the z-axis. The x force component from such a pair of electro-magnets has been used for resisting drag forces on a model[12], and some details of force calibration and measurement techniques are given in Chapters 5 and 10 respectively, and a simple theory assessing some of the potentialities is given in Section 3.2.2 below.

This form of control over a degree of freedom may be regarded as "passive" control, in that no special provision is made to change the current supply to the electro-magnets as a result of changes of model position. This form of control may be compared with "active" control, where the field from a magnet controlling a particular mode of motion is varied depending on movement in that mode. The field could be varied either by current changes to the electro-magnet, or by movement of the magnet. The former method has been chosen, and has the advantage that force or moment can vary linearly with current, whereas for the latter method force would not vary linearly with displacement of the electro-magnets. Another advantage of control by current change is that forces of repulsion or attraction are available from the same electro-magnet, a feature which is used in the control of two degrees of freedom with this suspension system.

Passive control in category (i) can be used to simultaneously control several degrees of freedom (however, all six degrees of freedom cannot be simultaneously controlled in this way[13]). The

characteristics of this form of control are that relatively low stiffness is provided, and near zero damping. Methods for providing this form of stiffness in the rolling mode are discussed in Chapter 6, which make use of the magnetic field generated by the electro-magnets supporting the weight of the model, numbered 4 and 5 on Fig. 3.2. It is a simple procedure to suspend a model under active control in two degrees of freedom and passive control in the remainder.

The two force components and the moment into which the forces originating from the pair of electro-magnets shown on Fig. 3.1(a) can be resolved, are affected by any motion of the model. The motions themselves can be resolved into translations along and rotations about the three axes which have been defined, but the relative importance of the effects varies from one degree of freedom to another. Some of the more important effects of model movement can be largely eliminated by introducing more symmetry into the layout of the electro-magnets, as shown on Fig. 3.1 (c). This particular arrangement has been chosen for the electro-magnets controlling movement of the model across the wind-tunnel, and hence the diagram represents a horizontal section through the wind-tunnel axis, and the electro-magnets would be required in general to exert a force component along the z-axis and a moment about the y-axis. It would be arranged for the force component to be generated by the electro-magnet poles A attracting the model with the same forces as poles B repel the model. Initial movement of the model in the z-direction has only a small effect on the magnitude of the force, whereas the arrangement shown on Fig. 3.1 (a) shows a strong dependence of force on model movement towards or away from the electro-magnets. A moment about the y-axis together with a force

in the z-direction would be produced by energising the upstream poles more strongly than the downstream poles, and again the force and moment would be relatively insensitive to small displacements in the z-direction.

A schematic diagram of the complete suspension magnet array is given on Fig. 3.2. One additional electro-magnet is shown: the drag coil. This has been arranged to produce a force in the upstream direction to oppose the drag force, and was positioned upstream of the model so that the field from the coil tended to magnetise the model.

The electro-magnets arranged alongside the model can produce a moment about the x-axis on a suitable model, thus allowing control of roll. A rolling moment can be produced by varying the force from the lateral magnets attracting the model. In the case where only a rolling moment is required, the four windings of the lateral magnets are arranged to attract the model core equally, and by varying the force of attraction a varying rolling moment can be produced either on a suitably shaped magnetic core in the model or on electro-magnets carried in the model. The principles are described in Chapter 6 and Appendix IV. The three functions performed by the lateral electro-magnets required three independantly controllable power supplies and two alternative wiring arrangements for these are shown on Figs. 3.3 and 3.4.

The windings are shown on horseshoe shaped soft iron yokes; the considerable air gaps in the magnetic circuits have the effect of making the strength of any one pole largely dependant on the net ampere-turns in the windings on the leg of the iron horseshoe forming

that pole.

The production of the forces and moments by the electro-magnets giving direct control of the model position is summarized in Table 3.1:

Forces along axes			Depend primarily on
x	...	...	NI_1
y	...	...	$NI_4 + NI_5$
z	...	...	$NI_2 + NI_3 - NI_6 - NI_7$
Moments about axes			
x	...	...	$NI_2 + NI_3 + NI_6 + NI_7$
y	...	...	$-NI_2 + NI_3 + NI_6 - NI_7$
z	...	...	$NI_4 - NI_5$

Notes: (i) The axis system is defined on Fig. 3.2.

(ii) NI is the net ampere-turn product for the windings in an electro-magnet.

(iii) The suffix attached to NI corresponds with a coil number marked on Fig. 3.2.

(iv) Moments are positive in the clockwise sense.

(v) Positive values of NI correspond with a coil tending to attract the near end of the model.

TABLE 3.1 The Method of Producing Forces and Moments Allowing Six Degrees of Freedom Control.

Note that many interactions can occur in the form of secondary forces or moments from the electro-magnets, or result from movement of the

model away from what could be regarded as the "normal" position on the tunnel axis. Some of the interactions are discussed in Appendices III and IV, and where they effect model stability, in Chapter 7.

3.2.2 In the special case where the drag force (the component along the x-axis) is relatively low it is possible to make use of the force component in this direction produced by the lift coils numbered 4 and 5 on Fig. 3.2. which arises when the model is displaced in the x-direction. This force component has the nature of a positive-stiffness spring, and produces stability in this degree of freedom without use of the drag coil. However, the damping of the model is low, and the stiffness produces a resonant system in this particular degree of freedom.

A simple theory can be developed for a hypothetical arrangement of model and suspension magnet, shown on Fig. 3.5. The model has a pole length s equal to the distance between the poles of the suspension electro-magnets, and it constrained to move axially at a constant distance g from the suspension magnets. Three of the four forces acting on the model have components resisting the applied drag force.

In the undisturbed state, with the model in equilibrium under the suspension magnet, the current levels in the two legs of this electro-magnet are equal. However, as the model moves away from equilibrium under the action of the drag force the current levels rise, but by different amounts in the two legs.

It is assumed that the pole strength of a particular leg of the suspension magnet is proportional to the current flow in the coil on that leg. Hence the forces between poles are given by

$$f_1 = \frac{k I_1 p}{m_1^2} \qquad \text{where} \quad m_1^2 = m_2^2 = d^2 + g^2$$

$$f_2 = \frac{k I_2 p}{m_2^2} \qquad \text{and } k \text{ is a constant}$$

$$f_3 = \frac{k I_2 p}{m_3^2} \qquad \text{where} \quad m_3^2 = (s+d)^2 + g^2$$

$$f_4 = \frac{k I_1 p}{m_4^2} \qquad \text{where} \quad m_4^2 = (s-d)^2 + g^2$$

By taking vertical components of f_1 and f_3, the net vertical force on p_1 can be obtained:

$$k p g \left(\frac{I_1}{m_1^3} - \frac{I_2}{m_3^3} \right)$$

and similarly the net vertical force on p_2 is

$$k p g \left(\frac{I_2}{m_2^3} - \frac{I_1}{m_4^3} \right)$$

If the centre of gravity of the model is assumed to lie mid-way between p_1 and p_2, each of the above equations can be equated to $\frac{1}{2}$ W and the resulting pair of simultaneous equations solved to give I_1 and I_2 :

$$I_2 = \frac{\frac{s^2 W}{2kp}\left(\frac{M_1^3 + M_4^3}{G} \right)}{\left[\left(\frac{M_4}{M_1} \right)^3 - \left(\frac{M_1}{M_3} \right)^3 \right]}$$

where M is a non-dimensionalised form of m given by $M = m/s$, similarly $G = g/s$.

and $$I_1 = \frac{s^2 W}{2kp} \left[\frac{M_1^3}{G} + \left(\frac{M_1}{M_3} \right)^3 I_2' \right]$$

where $$I_2' = \frac{2kp}{s^2 W} I_2$$

similarly one can define $I_1' = \frac{2kp}{s^2 W} I_1$

Both I_1' and I_2' , the non-dimensional currents in the legs of the suspension electro-magnet, are functions only of the geometry of the system.

By resolving the force components f_1 to f_4 in a horizontal direction, a non-dimensional axial force due to model displacement can be obtained in terms of non-dimensional distances and currents:

$$\frac{2f}{W} = \frac{DI_1'}{M_1^3} + \frac{DI_2'}{M_1^3} + \frac{(1-D)I_1'}{M_4^3} - \frac{(1+D)I_2'}{M_3^3}, \text{ where } D = d/s,$$

hence the axial force depends on geometry and model weight, but is independent of the state of magnetisation of the magnetic core of the model.

The changes of current that would occur in the coils of the suspension magnet as the model is moved away from equilibrium by aerodynamic drag are shown on Fig. 3.6 for one particular geometrical arrangement. It can be seen that the upstream coil would demand the greatest current change; movement of the model downstream by one-third of its pole-length would double the current required by the upstream suspension electro-magnet coil, and increase by 50% the current required by the downstream coil.

At first sight it might be thought that this drag-resisting technique would lose effectiveness with the model displaced a long way from equilibrium, because of a rapidly weakening magnetic field. This would certainly occur with fixed currents in the suspension magnets. The dashed curve on Fig. 3.7 shows the variation of axial force with displacement, for constant current. A condition of neutral stability would be reached when the model had been displaced about half its pole-length. However, in this position the suspension magnets would not support the model weight. In fact, the system progressively increases its stiffness with increasing displacement, due to the rapid rise of current in the

coils. This is shown with a full line on Fig. 3.7.

The drag force that this system can resist depends upon the continuous current overload that can be tolerated. Typically this might be 50%, in which case a drag force equal to about 60% of the model weight could be accepted.

As the displacement of the model in the x-direction depends on the force component in this direction, force can be calibrated against displacement, allowing the measurement of drag. Further details are given in Chapters 5 and 10.

3.3 Indirect Control by Magnetic Fields.

Indirect control of the model position could take several forms, but it is unlikely that this approach could be applied to the complete control of the model. It is the object of this section to propose several ways in which indirect control could be provided for motions in some degrees of freedom, but it must be emphasized that no practical work has been carried out to test the feasibility of the proposals.

The basic principle of indirect control is the use of magnetic fields generated by electro-magnets disposed around the wind tunnel to make adjustments to the model so that a net force or moment on the model can be reduced to zero. The particular model motions, and the forces or moments controlling these motions, which are amenable to this form of control will be treated separately.

In the case of a winged model positioned in the tunnel with its wings horizontal, in principle it would be possible to adjust the incidence to the flow such that the lift force balances the weight, thus relieving the lift magnets of part of their load.

In effect the model would be "flown" in the tunnel. A similar form of control could be exercised over lateral motions. A limited range of variation of incidence would be available by varying tunnel speed or model weight. However, the drag force would require balancing by a force from the drag coil in the case of a horizontal wind tunnel.

An alternative approach to controlling vertical, lateral or rolling motions of a model in a horizontal wind tunnel might be achieved by employing a more complex model carrying internally moveable magnets. Fields applied to the model could in principle be arranged to move the magnets which in turn could be arranged to operate flying controls, and in this way the applied fields would become transmission links to the model. Alternative forms of link may be more economical, for example a radio or an optical link, but one advantage of a magnetic link would be a reduction of model complexity, an important consideration with small models. In the case of lateral or roll control, this method would merely allow the model to be trimmed for flight in the tunnel.

On a more modest scale, a fairly simple indirect method of controlling the rolling motions of certain types of model will now be described. If the model carries a fin, when yawed to the flow the model experiences an aerodynamic rolling moment which could be used for controlling roll. The roll attitude would then be dependant on and controlled by variations of yaw attitude, but the mean yaw attitude would be zero and the mean roll attitude would be "normal". In practice many aerodynamic experiments do not require any steady-state variation of these attitudes.

This completes the description of the known available methods of magnetic control, and the direct techniques are

described more fully in later chapters. The six degrees of freedom were arranged to be automatically controlled using feedback of model attitude signals, to control the current supplies to the electro-magnets.

3.4 LIST OF SYMBOLS USED IN CHAPTER 3

Symbol	Meaning
d	Model displacement downstream from equilibrium position.
D	d/s
f	Axial force component.
$f_1 - f_4$	Forces between poles.
g	Perpendicular distance between model axis and suspension magnet poles.
G	g/s
I	Current in electro-magnet.
k	A constant.
m_1 to m_4	Defined on Fig. 3.5
NI	Ampere-turn product.
p	Pole strength.
s	Distance between the poles of the suspension magnets.
W	Model weight.
x, y, z	A set of axes.

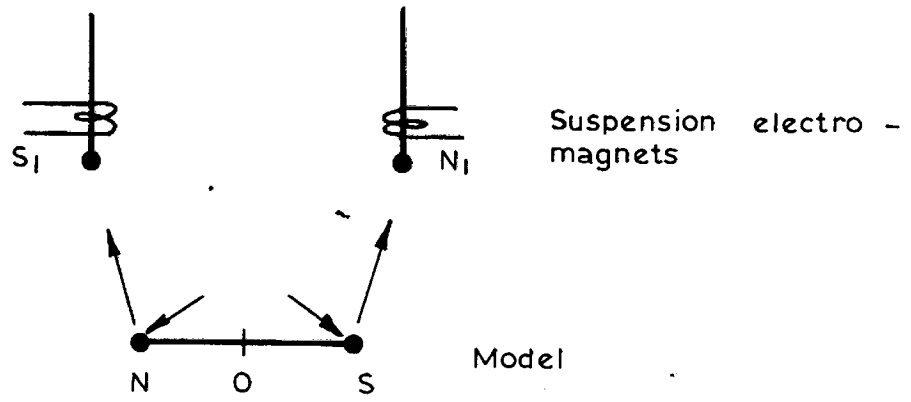

(a) FOUR FORCE COMPONENTS ACTING ON A MODEL.

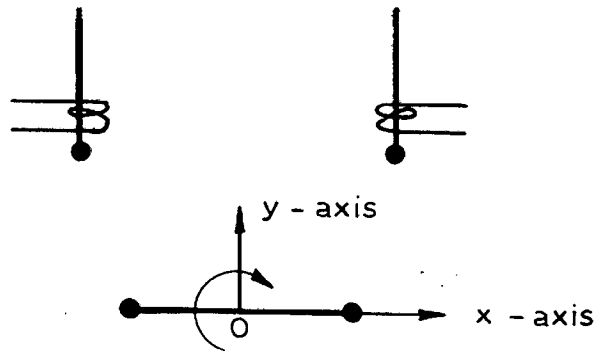

(b) RESOLUTION OF FORCES INTO TWO COMPONENTS AND A MOMENT.

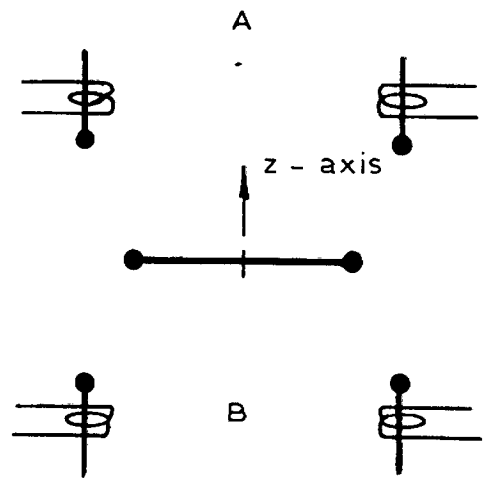

(c) A SYMMETRICAL PAIR OF ELECTRO - MAGNETS, AS USED FOR LATERAL CONTROL.

Fig. 3.1

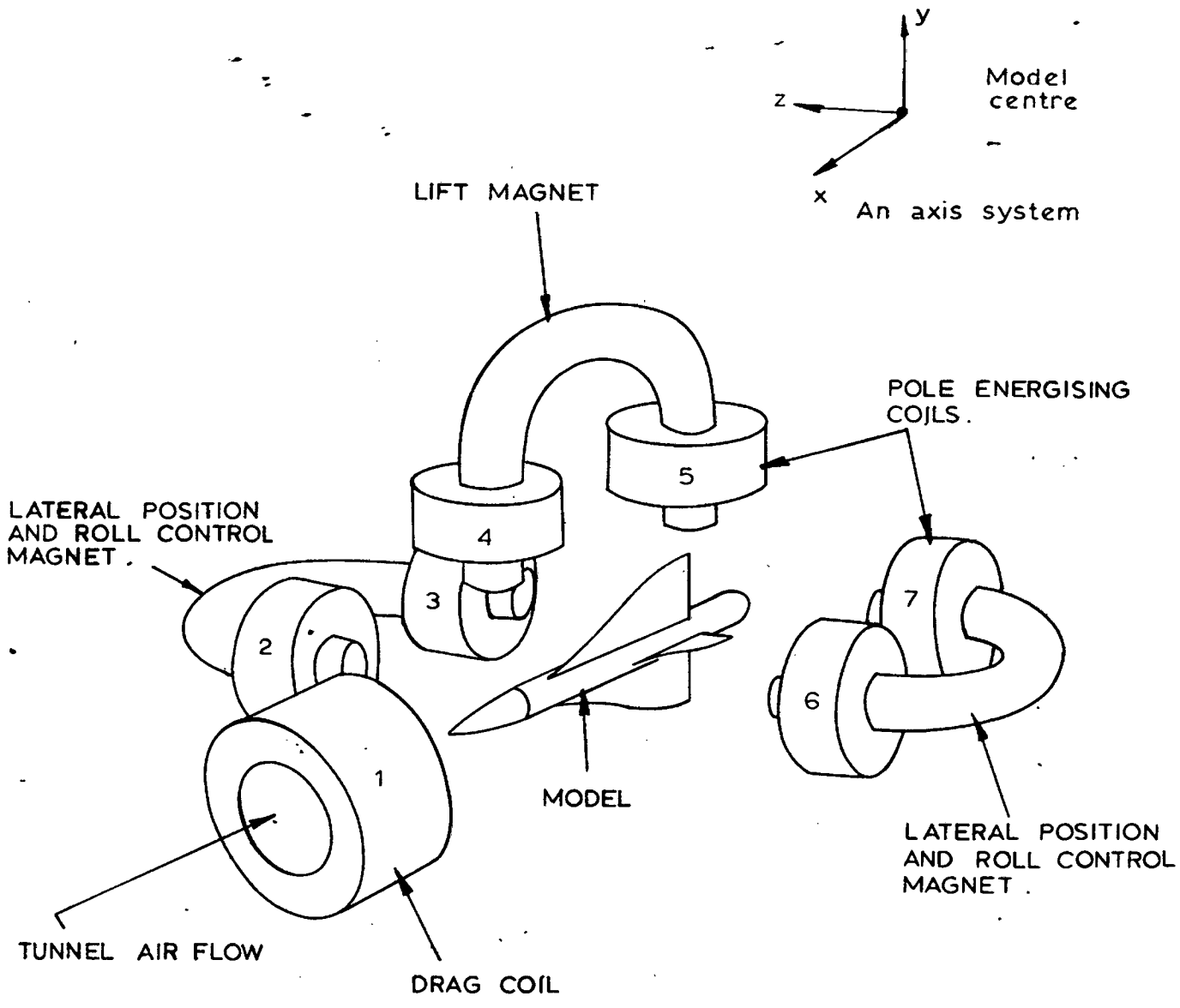

Fig. 3.2. A schematic diagram of the suspension magnet array of a six component magnetic wind tunnel balance and suspension system.

WIRING ARRANGEMENT; ZERO COUPLING IN THE CASE OF SYMMETRICAL FORCING IN LATERAL PITCH.

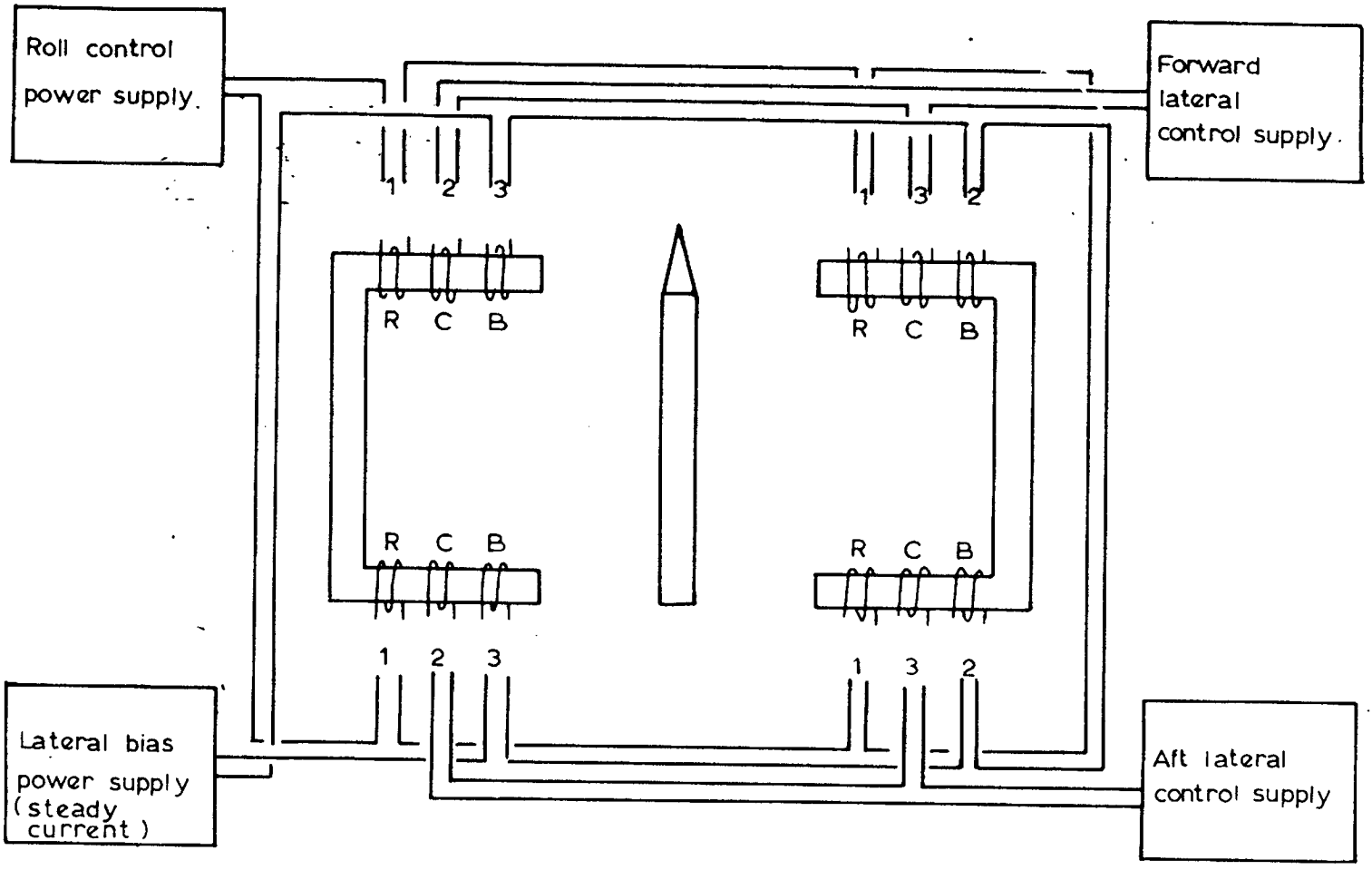

R WINDING SECTION RESERVED FOR ROLL CONTROL
C: " " " LATERAL
B: " " " BIAS
SECTIONS NUMBERED 1 AND 2 ATTRACT THE NEAR END OF THE MODEL.
" " 3 REPEL " " "

Fig.3.3 A plan view of the lateral electro-magnets showing a wiring arrangement for lateral and roll control. (Shaped-core model)

WIRING ARRANGEMENT, ZERO COUPLING IN THE CASE OF SYMMETRICAL FORCING IN LATERAL HEAVE.

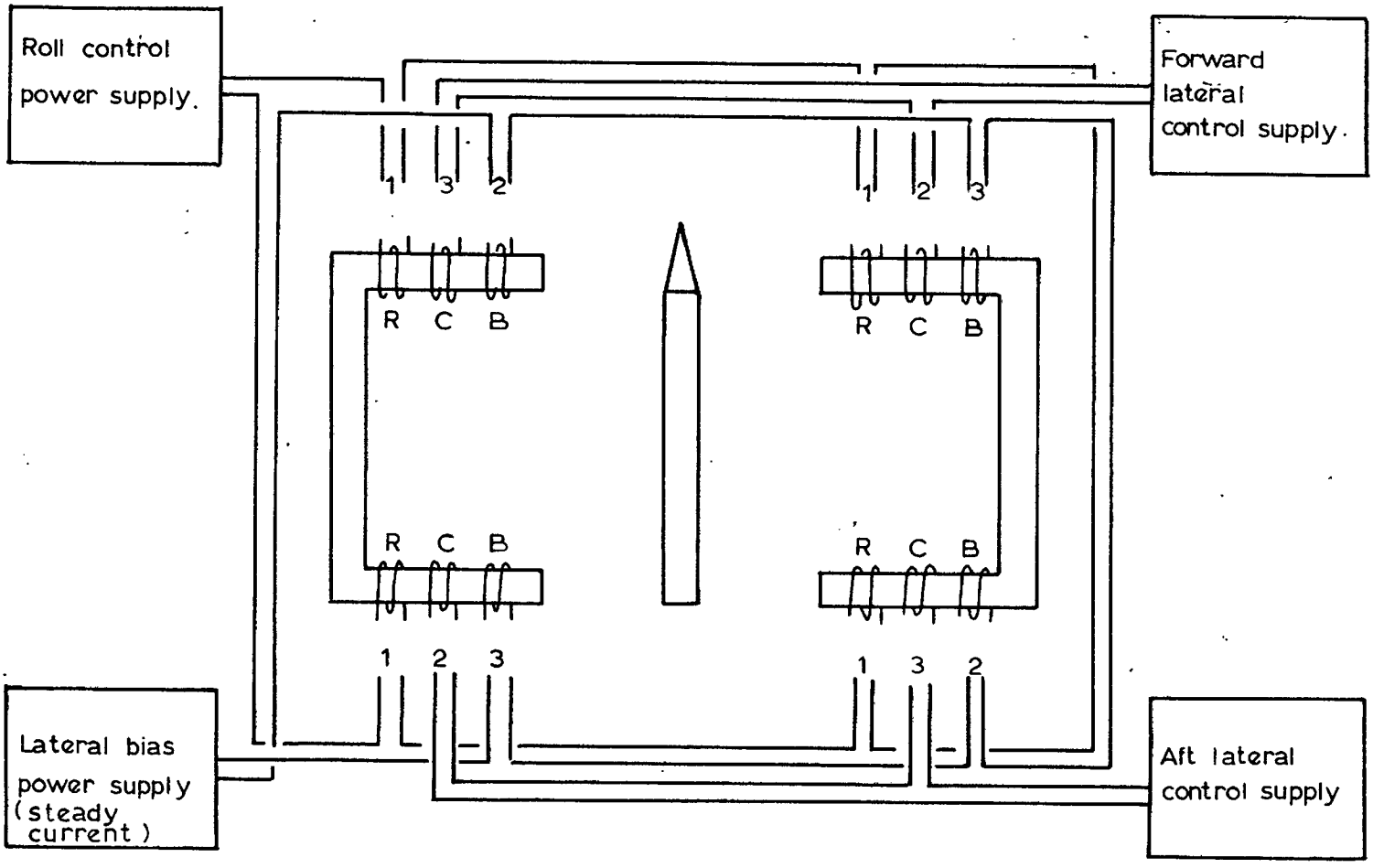

R : WINDING SECTION RESERVED FOR ROLL CONTROL
C : " " " LATERAL "
B : " " " BIAS
SECTIONS NUMBERED 1 AND 2 ATTRACT THE NEAR END OF THE MODEL.
" " 3 REPEL " " "

Fig. 3.4 A plan view of the lateral electro-magnets showing a wiring arrangement for lateral and roll control. (Shaped-core model)

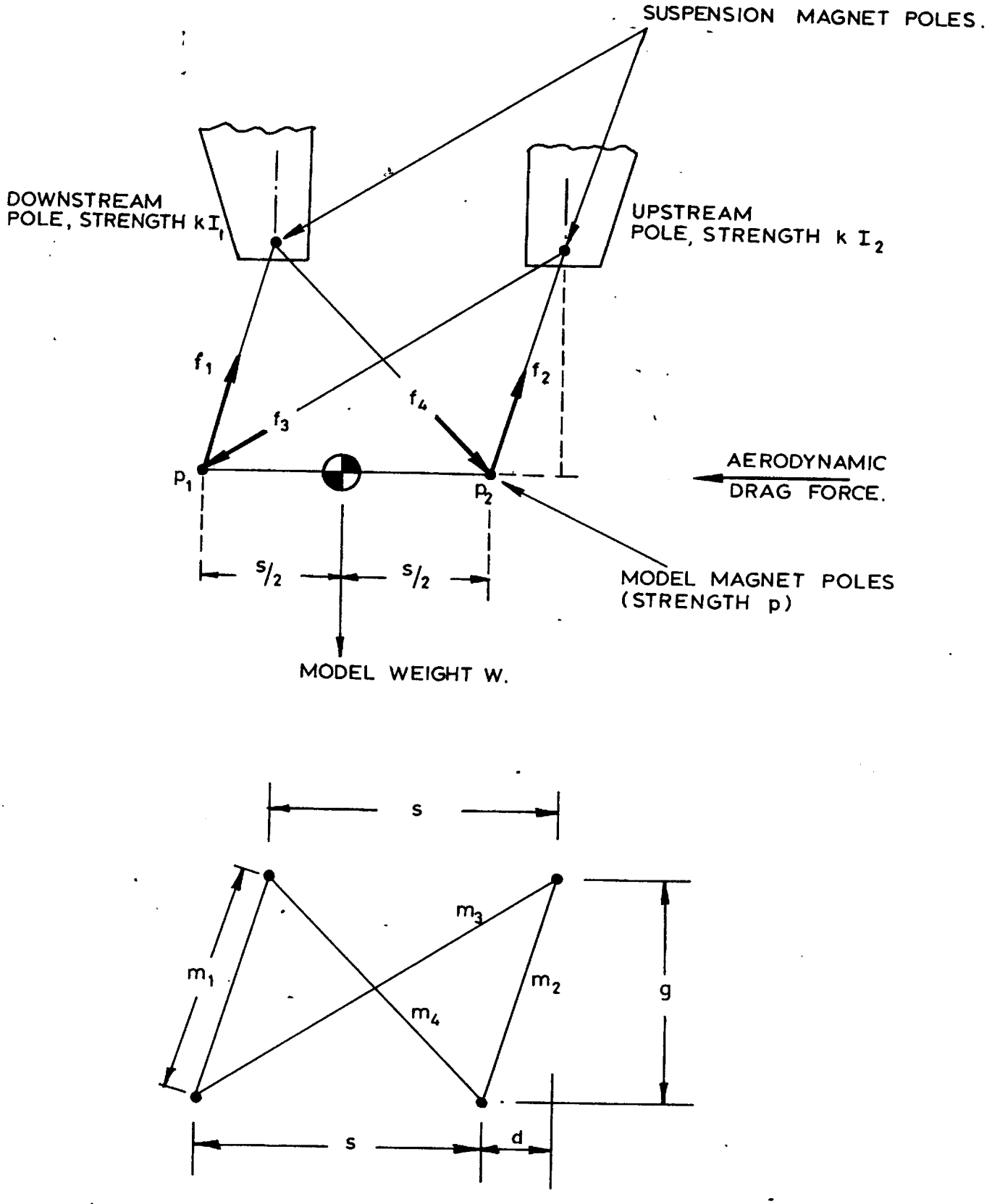

Fig. 3.5 The geometrical arrangement of a magnetically suspended model resisting a drag force by means of horizontal force components from the suspension magnet.

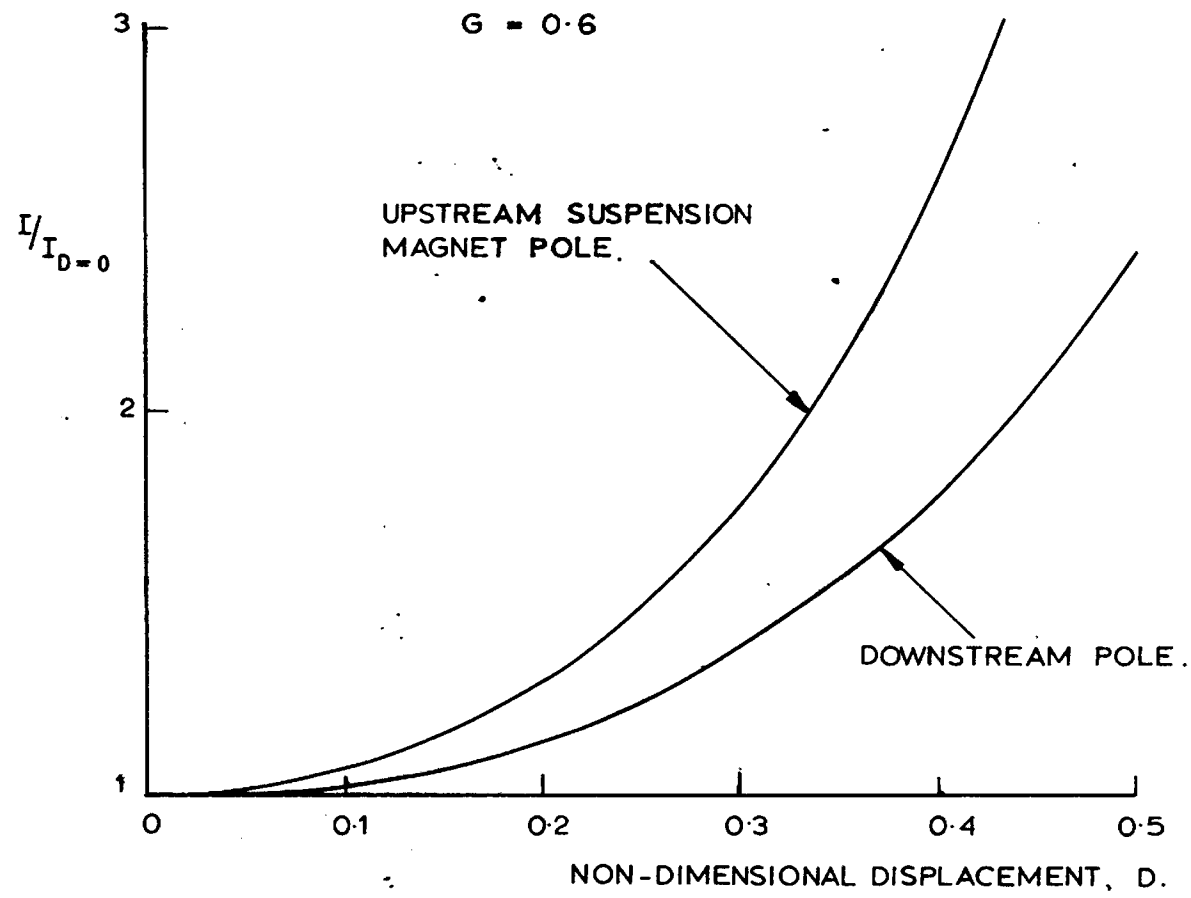

Fig. 3.6 The variation of current requirements with the axial displacement of the model.

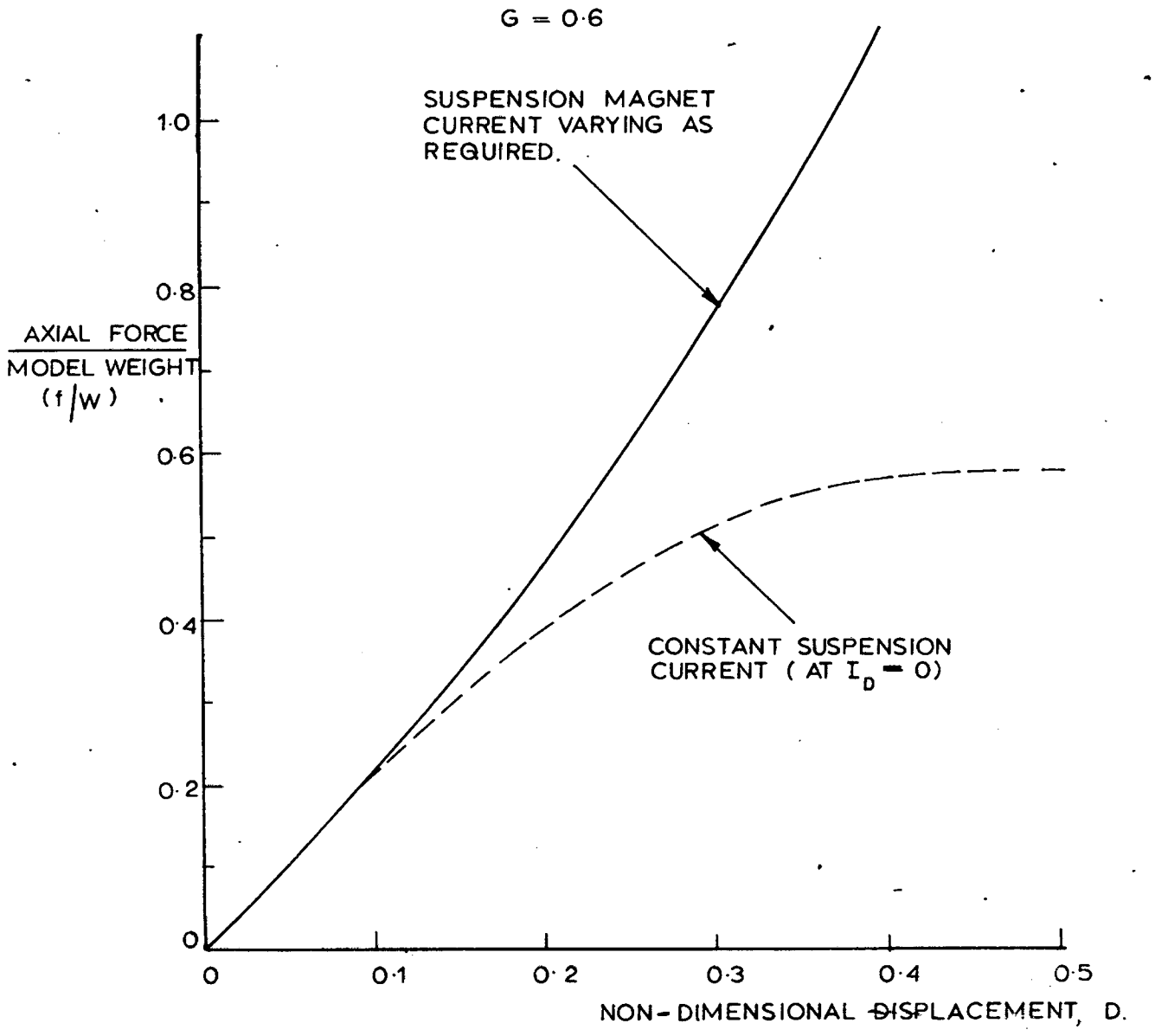

Fig 3.7 The axial force characteristic of a model suspended horizontally in a four component magnetic balance.

4. A Description of the Suspension System Electro-Magnets.

The design of the electro-magnet array for the suspension and control of models in six degrees of freedom in a high speed wind tunnel is given in this chapter, and attention is drawn to the influence that these magnets have on the design of the other equipment and services that comprise a complete suspension system.

Contents:

4.1 Introduction.

The disposition of the electro-magnets around a model has been given on Fig. 3.2. The factors influencing the design of the magnets include the model size, the proportion of magnetic to non-magnetic material in the model, the electrical power requirements, the inductances of the coils, the separation of the model from the magnets, and the aerodynamic forces.

Provided that increases of model weight are accompanied by a proportional increase of magnetic material, then the absolute weight of the model is not important. However, the ratio of the model length to the distance between a pair of electro-magnets (say the pair 4 and 5 on Fig. 3.2) can have a large influence on the required sizes of the electro-magnets. It can be shown that the ratio should ideally lie near unity, the requirements for electro-magnet strength rising sharply for values outside the range 0.5 to 1.5. Some theoretical data on this point is given in Appendix IV, and experimental data in Chapters 5 and 6.

The maximum size of a model is determined by the cross sectional dimensions of the wind tunnel working section, and in the case of a supersonic wind tunnel by the flow Mach number. For the high speed wind tunnel for which the suspension system was designed, at a representative Mach number the maximum length of magnetic core in the model would be about 5". This dimension, together with the separation distances dictated by the tunnel working section, formed a starting point for the coil design.

The suspension system has been used in conjunction with a low speed wind tunnel as well as the high speed tunnel. The main design and development effort has centred around the high speed tunnel, some features of which are described below where they effect the design of the electro-magnets. The low speed wind tunnel is described in Chapter 10.

4.2 The High Speed Wind Tunnel.

This is an existing tunnel, based on a basic design of the National Physical Laboratory, and is a return circuit induced flow tunnel covering a speed range from subsonic up to about Mach 1.8, the inducing air supply being dried and supplied at 200-300 lb./in.^{2} A detailed description is available in reference 15.

The main feature affecting the design of the magnetic suspension system was the working section. The original section had inside cross sectional dimensions of about 9" deep by 6" wide, and the construction was mainly of cast iron and steel. This part of the tunnel circuit required replacing by a non-magnetic working section, with access for model launching and position monitoring equipment. It was decided to reduce the vertical dimension to 8" in order to reduce

the separation between the model and the support magnets and hence reduce the electrical power requirements. The minimum top wall thickness that could be conveniently provided was about $\frac{3}{4}$", giving a model to lift magnet pole face separation of about $4\frac{3}{4}$". In the case of the lateral magnets the separation was about $3\frac{5}{8}$". The working section is described in detail in Chapter 11.

In order to minimise the inductance of the coils, and hence the voltage amplitudes, it was decided to confine dynamic measurements to motions in the horizontal plane and to divide the forces between electro-magnets on both sides of the wind tunnel. Some of the additional advantages to be gained from this arrangement are

(i) some force interactions were eliminated,

(ii) the demagnetisation of the model which might be possible with just one electro-magnet during the repulsion part of a cycle would be eliminated by magnetising forces from the opposite magnet

(iii) it was possible to incorporate roll control.

During the course of the development of this suspension system, large force and moment requirements associated with dynamic measurements were eliminated by the tuned model, leaving the requirements dominated by steady forces. At the maximum speed of the tunnel and with a representative model suspended with its wings in the vertical plane these were:

Vertical force: $\frac{1}{2}$ lb.; Drag force: 1 lb.;

Lateral force: 4 lb.; Pitching moment: 4 lb.in.

Drag forces were to be opposed by a solenoid-like coil wound around the wind tunnel upstream of the model. The field from

this coil would be magnetising. It was decided to use an air-cored coil mainly because the amount of iron which could be incorporated was limited. The steady force requirement for this coil is tabulated above, but with a supersonic wind tunnel the starting loads can be several times the steady load, and it was not feasible to design a drag coil to cope with the starting load. Hence a mechanical launcher would be required for operation at high speeds. In order to minimise the resistance and inductance of the drag coil it was wound directly onto the wind tunnel walls which were locally thinned down. The wall thickness was determined by stresses raised by the static pressure differential that exists across an atmospheric wind tunnel, the pressure difference depending on Mach number but being typically 12 p.s.i.

The layout of electro-magnets that had been chosen made access to the model rather restricted. The underside of the tunnel was accessible, together with the upper corners, and it was decided to utilise these regions for the model position monitoring equipment which required windows to be let into the tunnel. The whole of the underside in the region of the model was made transparent, together with smaller windows in the top corners. Model viewing was through a mirror looking upwards into the working section. Access to the model, for launching purposes, was through a door in the side of the wind tunnel in an extension of the working section between the suspension system and the tunnel compressed air injector.

4.3 Electro-magnet Design.

The coil and iron core design was carried out by Judd[14], based on a set of force and moment requirements dictated by model design, anticipated aerodynamic loads, and the forces and moments

required to induce oscillatory motions of the model for derivative measurements. At the time these requirements were assessed, the concept of the tuned model had not been evolved, and the dynamic requirements were based on those for forcing a solid model. Large inertia forces exist with a solid model, when oscillating at the required frequency and amplitude (in the pitching mode these were 50 cycles per second 2 degrees respectively).

The lift and lateral electro-magnets consisted of six coils wound on three horse-shoe shaped iron cores, forming the three separate assemblies shown on Fig. 3.2. All coils and cores were identical, for convenience.

The shape of a horse-shoe electro-magnet is shown on Fig. 4.1. The cores consisted of about 190 laminations of Stalloy grade 74 magnetic steel each 0.014" thick bolted together between outside laminations $\frac{1}{8}$" thick to give a total thickness of 3". The laminations were each insulated on one side. The coils were wound from 12 S.W.G. copper wire coated with Pirelli Pigenestor enamel, onto brass formers. The formers were split electrically in order to avoid a "shorted turn" effect. The insides of the formers were insulated and the coils wound by hand in three separate sections of three layers per section. In this way different sections of each coil could be supplied from different power supplies or connected in series as required. The total number of turns per leg was approximately 400. The windings were enclosed by a brass cover with an araldite re-inforced split.

It had been decided to oil cool the coils to increase the steady-state current capacity, and the cover was made liquid-tight

to enable oil to be pumped around the coil. There were several advantages to be gained from using forced cooling. These were:

(i) For a given ampere-turn product, the coils could be more compact, allowing the legs to be placed closer together thus reducing the minimum length of model which could be suspended.

(ii) The leakage flux could be minimised as a result of a shorter coil.

(iii) The coil circuit inductance would be reduced, easing the problem of model stabilisation, and reducing the voltage amplitude required to induce oscillatory motion of the model.

The drag coil, enclosed in a split former bolted and sealed to the wind tunnel, was wound from the same gauge of wire. The coil was kept as close as practically possible to the lift and lateral electro - magnets in order to make the coil as effective as possible, and the coil was kept short in the axial direction to limit the area of thinner wind tunnel wall.

It was anticipated that the drag coil would be required to withstand the highest steady current levels on this suspension system, and particular attention was paid to the provision of gaps between the windings and the former, and between windings, to allow free passage for the cooling oil. In order to limit the amount of relative movement of the wires over a period of time in this loosely wound coil, occasional patches of Araldite resin adhesive were pressed into the windings, which on hardening gave a rigid but open winding to allow the passage of cooling oil. The coil was designed to be wound in two sections, the first (inner) section of 500 turns and the outer section of 400 turns. The length of

wire in the two sections would be roughly equal, giving equal resistances, and they were to be supplied in parallel from the single power supply.

The magnet array was mounted on a Dural channel framework, which in turn was supported on a welded steel base. The framework is shown on Figs. 10.1 and 11.2. There were many possible electrical loops in the frame, and any of these could have acted as a shorted turn and hence could have added to the effective inductances of the coils. For this reason all loops in the Dural part of the frame were broken electrically, including the frames supporting the position monitoring equipment.

The coils were cooled by transformer oil pumped from a reservoir. Two pumps were used, one for the drag coil, the other for the remaining coils. The pipe-work between coils and between the reservoir and coils was 1" diameter copper, and here again any possible electrical circuits were broken by short lengths of plastic tube. Oil returning from the coils was arranged to pass through a shell-tube heat exchanger which in turn was cooled by mains water. Pressure relief valves were incorporated in the system to limit the pressures to which the flat-sided covers surrounding the coils could be subjected. The maximum steady-state currents that the coils will tolerate in the cooled and un-cooled condition are given in the following chapter.

The forces and moments that the coils can develop depend on the magnetic core in the model. Data for several different cores is also included in the following chapter.

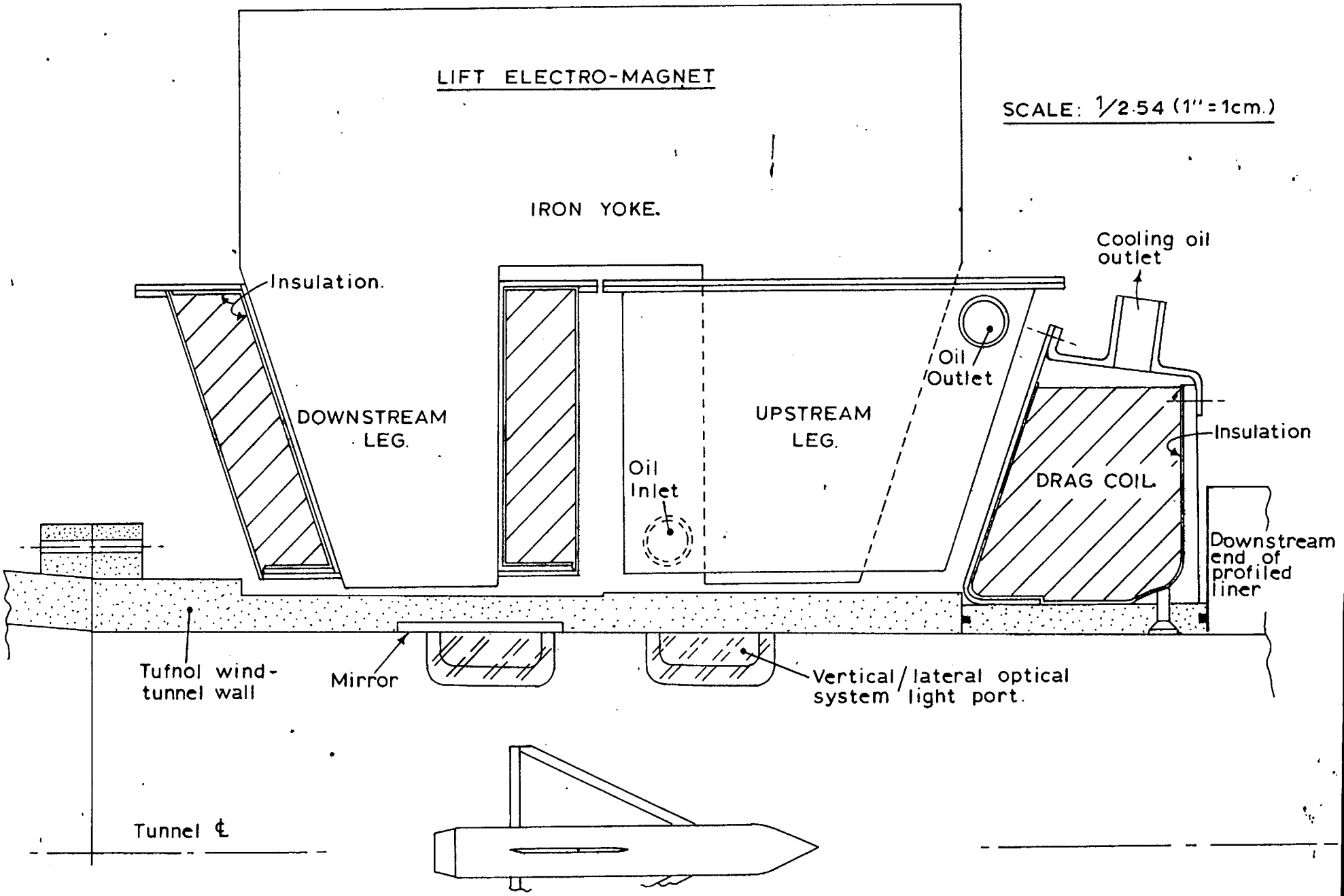

Fig. 4.1.' A vertical cross section along the high speed wind tunnel axis.

5. Electro-Magnet Force, Moment and Heating Data.

The aerodynamic and inertial forces and moments acting on a model are opposed by magnetic fields generated by the electro-magnets surrounding the wind tunnel, and either the current flowing in the coils, or the displacement of the model in the fields, may be used as a measure of the forces or moments. In this Chapter some calibration techniques are described and calibration constants given for a selection of models, together with data on current limitations set by coil heating.

Contents:

5.1 Introduction.

In general a force or moment exerted on a model by the suspension magnet array is a function of coil current, the model magnetic core design, material and state or magnetisation, and model position. Another longer term effect could be changes in the characteristics of the coils; it might be possible for a loosely wound coil to move as a result of magnetic forces between turns, or for coils to move relative to one another for similar reasons.

The state of magnetisation of a soft-iron model core varies strongly with the applied field. With this suspension system, the field is always magnetising, and has magnetising field

contributions from the lift magnet, the roll control sections of the lateral magnets, and from the drag coil. Consequently a single calibration such as drag force against drag coil current is not possible for "soft" magnetic model cores; the drag force acting on a particular core in one position would be a function of the current flowing in several different coils. For reasons such as this, a "hard" magnetic core material has been used in most instances on this suspension system.

The chosen core material was Alcomax III because of its relatively high coercive force. The cores were magnetised when received from the manufacturers, but to make sure that they were magnetised as strongly as possible, they were re-magnetised in a nominal 10^4 oersted field. After re-magnetisation, no long-term change in the state of magnetisation was detected. This may have been a result of the magnetising effect of the suspension system fields.

Some initial force and moment calibrations were carried out by Judd , on a range of Alcomax III cores held in a jig and subjected to a field from the first suspension electro-magnet to be built for this suspension system. During these measurements it was established that force of attraction was proportional to the sum of the current in the windings on the two legs of the electro-magnet yoke. Similarly the force of repulsion was proportional to the current sum, flowing in the opposite sense of course, provided that the force did not exceed about 1 lb. With greater repulsive forces the core began to de-magnetise. It was also established that the moment acting on a model was dependant on the difference between the

current in the two coils.

This chapter deals with the calibrations made with specific models while magnetically suspended, excluding the rolling moment calibrations which are separately covered in Chapter 6, and only those calibrations which were of direct interest in particular experiments have been made, with a small range of models. The calibrations were:

(i) low drag force (data used in Chapter 10),

(ii) Drag force - drag coil current (data used in Chapters 7, 12),

(iii) force and moment from the lift magnet (data used in Chapter 7) ,

(iv) force and lateral moment from the lateral magnets (data used in Chapters 7, 13)

The calibration constants and the measurement techniques are given in the following sections, together with data on the performance of the coil cooling system.

5.2 Low Drag Forces.

The measurement of low drag forces was confined to one basic model design. The principle of the measurement of low drag forces using field stiffness from the lift magnet has been described in Chapter 3. The basic model, a 10.2 oz. body of revolution, consisted of a parallel sided brass tube with a faired Dural nose, and Dural tail plug, containing a 6" long $\frac{1}{2}$" dia. Alcomax III core. An outline drawing of the model is shown on Fig. 10.3 and the experimental work was carried out with a low speed wind tunnel, described in Chapter 10.

The drag measurement technique required the axial position of the model to be monitored. For convenience an existing optical system was used, consisting of a light beam shining across the blunt

tail of the model, the part of the beam passing the model being focussed onto a silicon solar cell (see Chapter 8 for details of the optical system). The output from the cell was amplified using an operational amplifier, and fed to a valve voltmeter for position indication.

An accurate method was required for applying small drag forces to the model. The technique adopted was to tape a loop of thread to the model (at two points on a diameter to avoid applying pitching or yawing moments) and to attach this to a second thread anchored downstream of the model as shown on Fig. 5.1. The downstream section of the wind tunnel was removed during calibration. This force application method is virtually frictionless, and the drag force can be calculated simply from the applied calibration weight and the measured angles of the threads.

An example of a calibration is given on Fig. 5.2. For consistent results it was necessary to prevent the model from pitching out of alignment with the tunnel axis when displaced by the drag force. Optical position sensors were used to monitor the vertical position of the nose and tail of the model, and these enabled the two positions to be held constant to $\pm$ 0.001 inch. during any one test, which effectively suppressed the pitch interaction.

Zero incidence was ensured by machining a jig, which located on a tunnel side-wall and bottom, to hold the model in the correct attitude allowing the optical system outputs corresponding with zero incidence to be noted. These light beams, about $4\frac{1}{2}$" apart, shone past a parallel part of the fuselage.

The calibration did not exhibit short-term changes (say within one day), but in the longer term changes did occur. It is

possible that the changes were a result of changes in the sensitivity of the axial position monitoring optical system.

From the scatter obtained in the calibration points it is probable that a calibration constant obtained from the line through the points would be accurate to better than $\pm$1%, and that any single calibration point in the region of 0.01 lb. drag force would be accurate to about $\pm$1%.

The upper limit to the drag force that might be resisted by this type of suspension system appears to be fairly clearly limited by the current overload permissible in the upstream weight-supporting electro-magnet. The current overload is limited by coil heating. If a heat production rate 100% above normal could be tolerated, the theoretical model considered in Chapter 3 could accept a drag force equal to 55% of the model weight. However, this would require a model displacement downstream equal to 22% of the pole-length of the model. A limit to the acceptable displacement, set by the fuselage or the optical system, could be a second factor limiting the maximum drag force.

A third but less easily defined limit to the maximum drag force that could be resisted in practice might be set by turbulence-induced oscillations of the model in the direction of the tunnel axis. The oscillations result from the fact that this mode of motion is resonant and lightly damped. The exitation forces may increase with increased air speed and hence drag force. The axial position of the model was measured with a valve-voltmeter having a relatively heavily damped needle which effectively damped the position oscillations at the drag force levels reached. With the low speed wind tunnel, the maximum drag force was about 5% of the model weight. The maximum drag force applied during calibration was 10% of the

model weight.

5.3 High Drag Forces.

The upper drag force requirement for the suspension system was set at 1 lb., and the drag force was opposed by a force from the drag coil. The current supply to the drag coil was automatically controlled by feedback of the model axial position to the drag coil power supply. Calibrations of drag force were obtained simply by suspending the model with automatic position control, and applying known drag forces to the model. Precautions were taken to ensure that the applied force was truly axial, and that the model did not change its position during calibration. Examples of calibrations are given on Figs. 5.3 and 5.4 respectively for a tuned model and a solid body of revolution. Drag measurements with these models are reported in Chapter 12, and the calibration data has been used in Chapter 7 for an assessment of the stability of the position control loop. Both models had Alcomax III permanent magnet cores. At the present time only half of the drag coil has been wound, but in the case of both models the calibrations show that a drag force of $\frac{1}{2}$ lb. would require about 50 amperes to this section. The drag power supply is capable of supplying more than 100 amps. which can be fed to two winding sections connected in parallel. The safe operating time at this current level is discussed in section 5.6. In the case of the solid model, zero drag force corresponds with a drag coil current of $1\frac{1}{2}$ amperes; during this calibration the model was positioned a small distance upstream of its equilibrium position under the lift magnets, requiring a small force from the drag coil to oppose the restoring force from the lift magnets. Over a period of about 6 months the drag calibration for the tuned model changed about 6%.

5.4 Lift Magnet Forces and Moments.

The lift electro-magnets have only been used as a means of model suspension, rather than as a balance, and the force and moment calibrations were only required to assist in the development of the position stabilisation system associated with these magnets. High accuracy was not required, and it was decided to invoke the conclusions mentioned in 5.1 that the vertical force and moment on the model would be directly proportional to the sum and difference respectively of the currents in the two coils, for a fixed model position, giving

$$\text{force} \quad f = b_1 (i_f + i_a)$$

$$\text{moment} \quad m = a_1 (i_f - i_a)$$

where a_1, b_1 are force and moment calibration constants, and i_f, i_a are the currents in the forward and aft coils.

The constant b_1 was simply determined from the current in the two coils required to support the weight of the model. The procedure for determining the constant a_1 was to add various weights to a suspended model near the nose and tail, and determine the constant from the changes of applied moment and suspension magnet currents. The values are tabulated below:

Model	Tuned	Solid
b_1 lb./amp.	0.023	0.0208
a_1 lb.ft./amp.	0.00433	0.00365

These constants apply to models suspended on the wind-tunnel axis.

5.5 Lateral Magnet Force and Moment.

Model lift force and pitching moment were measured with these magnets, and accurate calibration constants were required. The calibrations are dependant (among other factors) on the position of

the model along the tunnel axis. This position, determined by the centering forces from the lift magnets and the roll control sections of the lateral magnets, with zero drag coil current, was taken as normal for the tuned model, for which force and moment calibration constants have been determined. The wiring arrangement for the lateral magnets was as shown on Fig. 3.3; one wiring section per lateral leg was used for the production of the lateral force and the moment about the vertical axis (through the centre of the magnets over the wind tunnel).

It was found that force and moment were not given by current sum and difference as had been determined for a magnet symmetrically positioned relative to the electro-magnet poles. This may have been due to the normal position of the model core being displaced from this position of symmetry. Several factors can cause axial displacement of the model, for example the effect of a c.g. position displaced axially from the centre, the effect of inclination of the tunnel axis to the horizontal, or variation of the cross-section of the model core along its length.

The lateral magnet system could be calibrated for a range of lateral forces and moments on a "carpet" basis, but in order to simplify the use of the system as a balance it was decided to postulate simple relationships between force, moment and the two current supplies involved, and to test the validity of the assumptions by experiment.

The currents controlling lateral position, i_f and i_a for the upstream and downstream legs respectively are functions of the externally applied lateral force f and moment m :

$$i_{f,a} = \phi_{1,2}(f, m).$$

By linearising these equations for small changes in the variables, the currents can be written

$$\Delta i_f = \left(\frac{\partial i_f}{\partial f}\right)_m \cdot \Delta f + \left(\frac{\partial i_f}{\partial m}\right)_f \cdot \Delta m \qquad \text{——5.1}$$

$$\Delta i_a = \left(\frac{\partial i_a}{\partial f}\right)_m \cdot \Delta f + \left(\frac{\partial i_a}{\partial m}\right)_f \Delta m \qquad \text{——5.2}$$

Put

$$a = \left(\frac{\partial i_f}{\partial f}\right)_m , \quad b = \left(\frac{\partial i_f}{\partial m}\right)_f$$

$$c = \left(\frac{\partial i_a}{\partial f}\right)_m , \quad d = \left(\frac{\partial i_a}{\partial m}\right)_f$$

then from equations 5.1 and 5.2,

$$\left.\begin{aligned} \Delta m &= \frac{\frac{a}{c}\Delta i_a - \Delta i_f}{\left(\frac{a}{c}d - b\right)} \\ \Delta f &= \frac{\frac{b}{d}\Delta i_a - \Delta i_f}{\left(\frac{b}{d}c - a\right)} \end{aligned}\right\} \qquad \text{——5.3}$$

The constants $\left(\frac{\partial i_f}{\partial f}\right)_{m=0}$ and $\left(\frac{\partial i_a}{\partial f}\right)_{m=0}$ may be determined from the current changes resulting from the application of a pure force to the model, and similarly the constants $\left(\frac{\partial i_f}{\partial m}\right)_{f=0}$ and $\left(\frac{\partial i_a}{\partial m}\right)_{f=0}$ by applying a pure couple. However, it was convenient to apply forces to the model via threads from one side only, hence it was possible to apply a pure force but not a pure couple. Moments could only be applied in conjunction with a force. However, having determined

a and c from a force calibration, the constants b and d could be determined in the following way:

equations 5.3 may be transposed to give

$$\left.\begin{aligned} b.\Delta m &= \Delta i_f - a.\Delta f \\ d.\Delta m &= \Delta i_a - c.\Delta f \end{aligned}\right\} \qquad \text{——— 5.4}$$

and by applying a range of force/moment combinations to the model, values of $b\Delta m$, $d\Delta m$ could be plotted against Δm, and the constants b and d determined from the slopes of the lines. Fixed values of Δm at different values of Δf giving the same values of $b\Delta m$, $d\Delta m$, would be a test of the invariance of b, d with Δf.

The forces were applied to the tuned model (this model is described in Chapter 13; it has a resiliently mounted magnetic core, but for the purposes of this calibration the core was locked to the outer shell to avoid the effects of core movement on calibrations) at two points via threads passing over a pulley system held in a jig temporarily attached to the inside of the wind tunnel, clear of the magnetically suspended model and position monitoring beams.

The curves from which the constants a and c were determined are given on Fig. 5.5, and the constants were

c = 0.0382 amp./gm.

a = 0.0330 amp./gm.

Plots of $b\Delta m$ and $d\Delta m$ against Δm, derived from equations 5.4 are given on Fig. 5.6. Each point is marked with the simultaneously applied force, in gm. The slopes of the lines gave b = -0.0071 amps./gm.cm. and d = 0.0077 amps./gm.cm.; there did not appear to be any variation of slope with applied force.

The force and moment equations 5.3 with the constants substituted become:

$$\Delta m = 0.00525\ (0.864\ \Delta i_a - \Delta i_f) \quad \text{lb.ft.} \qquad \text{\_\_\_\_\_} 5.5$$

$$\Delta f = 0.0315\ (0.972\ \Delta i_a + \Delta i_f) \quad \text{lb.} \qquad \text{\_\_\_\_\_} 5.6$$

where Δi_a, Δi_f are the changes of current in amperes from those values required to oppose the current in the bias sections while producing zero lateral force and moment. It is estimated that these equations would give force and moment accurate to about $\pm$5%. A more refined calibration technique would be required to improve on the accuracy.

5.6 Coil Heating and Cooling.

The features of the temperature variations of the coils and coolant (oil) that are of main interest may be identified as

(i) The initial heating rate. This is of interest if oil cooling is not used, particularly when high currents are in use and operation is likely to be terminated at a time set by the windings reaching some limiting temperature.

(ii) The relationship between equilibrium winding temperature and current with natural cooling. This is of interest when protracted periods of suspension are required, say for calibration, and when the currents might be low enough not to require forced cooling. The time constant associated with the heating, defined as the time required for the coil to reach $1 - 1/e$ of the equilibrium temperature rise, is also of interest.

(iii) The variation with current of the equilibrium temperature rise of the coils when oil cooled, relative to the temperature of the oil supply, and the time constant of this temperature change.

(iv) The variation of the temperature of the supply of cooling oil to the coils with heat dissipation by the heat exchanger.

(v) The rates of coil cooling expressed as time constants, for natural cooling and forced cooling, with no current flowing.

5.6.1 Initial heating rates. A theoretical rate of temperature rise may be calculated by equating the wattage dissipation with heat absorbtion by the copper. The gauge of wire used in the electromagnets had a resistance of 0.0291 ohms/lb. at 20°C, and using a specific heat of 0.1 C.H.U./lb.°C. the rate of temperature rise would be given by

$$\frac{dT}{dt} = 0.0092\ i^2 \quad ^\circ C/min., \text{ at } 20^\circ C.$$

where T is the temperature of the wire and i is the current flow, amps.

The various measured rates of temperature rise lay in the range equal to and $\frac{2}{3}$ of the theoretical rate given above, when uncooled or oil cooled. In the case of the drag coil, a typical current at the drag force of 1 lb. for which the system was designed would be 50 amps, hence $\frac{dT}{dt} \doteq 23^\circ C./min.$ The high speed wind tunnel has a running time of less than one minute, and this rate of temperature rise would be quite acceptable. However, calibration of drag force against current can require much longer times of operation.

5.6.2. The equilibrium temperatures of uncooled coils. In the case of the lift and lateral magnets it has been found that operation without oil cooling - with no oil in the tanks - is possible with some models for long periods, somewhat simplifying this part of the suspension system. The time to reach equilibrium is very long, and

the measurements of heating rates have been terminated after about 70 minutes heating. However, if the temperature-time curve is assumed to have an exponential form then the time constant and equilibrium temperature can be calculated from the slope of the measured temperature-time curve at two points. For the lift and lateral magnets the time constant determined in this way was approximately 80 minutes, and the equilibrium temperature rise was given by

$$\Delta T = 0{\cdot}6\, i^2 \quad ^\circ C$$

where i is the current in amperes.

For example, at 12 amps. the temperature rise would be about 86°C above room temperature, giving an equilibrium coil temperature of around 100°C. This may be acceptable.

The temperatures of the coils were estimated from variations of resistance, and hence are mean values. It is possible that local hot spots could exist in the coils, or that inner regions would stabilise at a higher temperature than regions on the outside. The coils were wound in three separate sections, connected in series during the measurement of heating rates, and the average temperature of each section was estimated from individual resistance changes; within the limits of measurement the three sections heated at the same rate and tended towards the same equilibrium temperature. This shows that there is no significant temperature gradient through the coil, but does not rule out the possibility of hot-spots. A local hot-spot could occur if cooling oil access was locally restricted.

The example given above, where the steady state temperature rise was 86°C, would correspond with a coil resistance change of

about 34% above the room temperature value. In the case of the coils on the lift and lateral magnets there were relatively larger resistors connected in series, having zero change of resistance with temperature. Hence the effect of changes of coil temperature on the demands from the power supplies, and on the problem of model stabilisation where circuit resistance is important, were small.

5.6.3 Coil temperature changes with oil cooling. The data on the steady-state values of the difference between the average winding temperature and the temperature of the supply of cooling oil can be correlated approximately by

$$\Delta T \doteqdot 0.028\, i^2 \ ^{\circ}C.,$$

the constant here being only 5% of that obtained without oil cooling. This is a very useful reduction of temperature rise; provided that the temperature of the oil supply is reasonably low, continuous operation at current levels in the range 45-50 amperes is possible. This can be most usefully exploited with the drag coil.

There was a significant reduction of heating time constant with oil cooling. The time constant was approximately three minutes, with equilibrium well established in under 20 minutes.

5.6.4 The performance of the oil cooler. The cooling oil leaving the coils was cooled in a heat exchanger by mains water. The water flow rate was 2½ gallons per minute, and the oil flow rate about 5 gallons per minute from each pump.

At 7kW heat generation rate in the coils under equilibrium conditions the oil cooler maintained an oil delivery temperature to the coil of 20°C above the cooling water supply temperature. This heat dissipation rate is near the maximum that would be required,

hence cooling oil should always be available at temperatures not exceeding about 35°C. The oil temperature excess over the water temperature did not vary in direct proportion to the heat generation rate; the tendency was for the temperature excess / - heat generation rate curve to increase in slope with increasing heat generation rate.

5.6.5 Coil cooling rates. The rate at which the coils cooled after switching-off the current sometimes determines the rate at which experiments may be carried out.

Natural cooling, with no oil in the tanks, was rather slow. Measured time constants of cooling were of the same order as the heating time constants - about 80 minutes. However with oil flowing the constants were much more satisfactory, again being comparable with the heating time constants of 3 minutes. This particular feature of oil cooling - the rapid reduction of coil temperature following current shutdown - is probably the most useful, in practice.

5.7 LIST OF SYMBOLS USED IN CHAPTER 5.

Symbol	Meaning
a_1	Lift magnet moment calibration constant.
b_1	" " force " "
a	$\left(\frac{\partial i_f}{\partial f}\right)_m$
b	$\left(\frac{\partial i_f}{\partial m}\right)_f$
c	$\left(\frac{\partial i_a}{\partial f}\right)_m$
d	$\left(\frac{\partial i_a}{\partial m}\right)_f$
f	Force
i	Current
m	Moment
T	Temperature
t	Time

Suffixes

f	Forward (upstream) coil.
a	Aft coil.

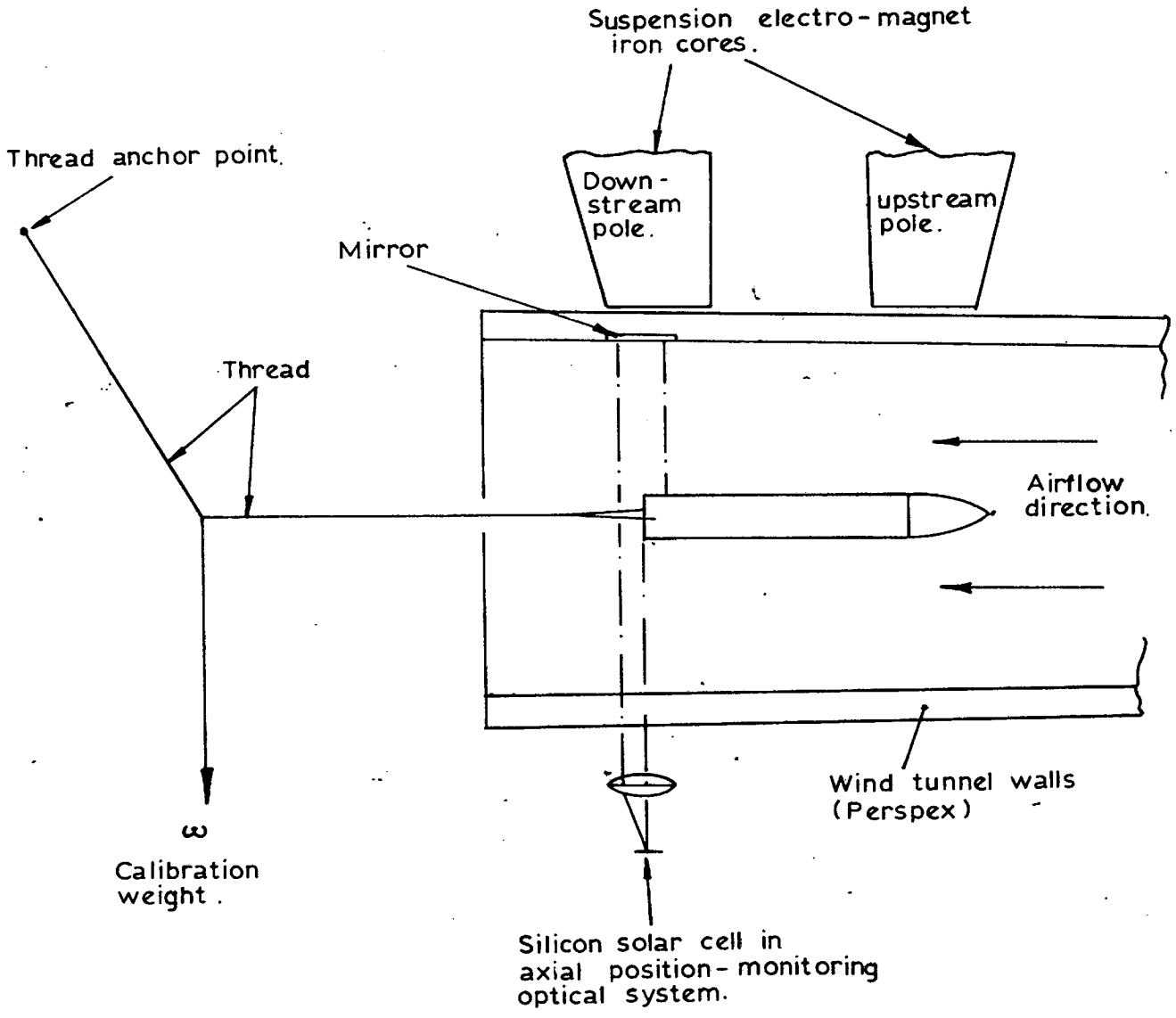

Fig. 5.1. Schematic diagram of the drag force - axial position calibration arrangement.

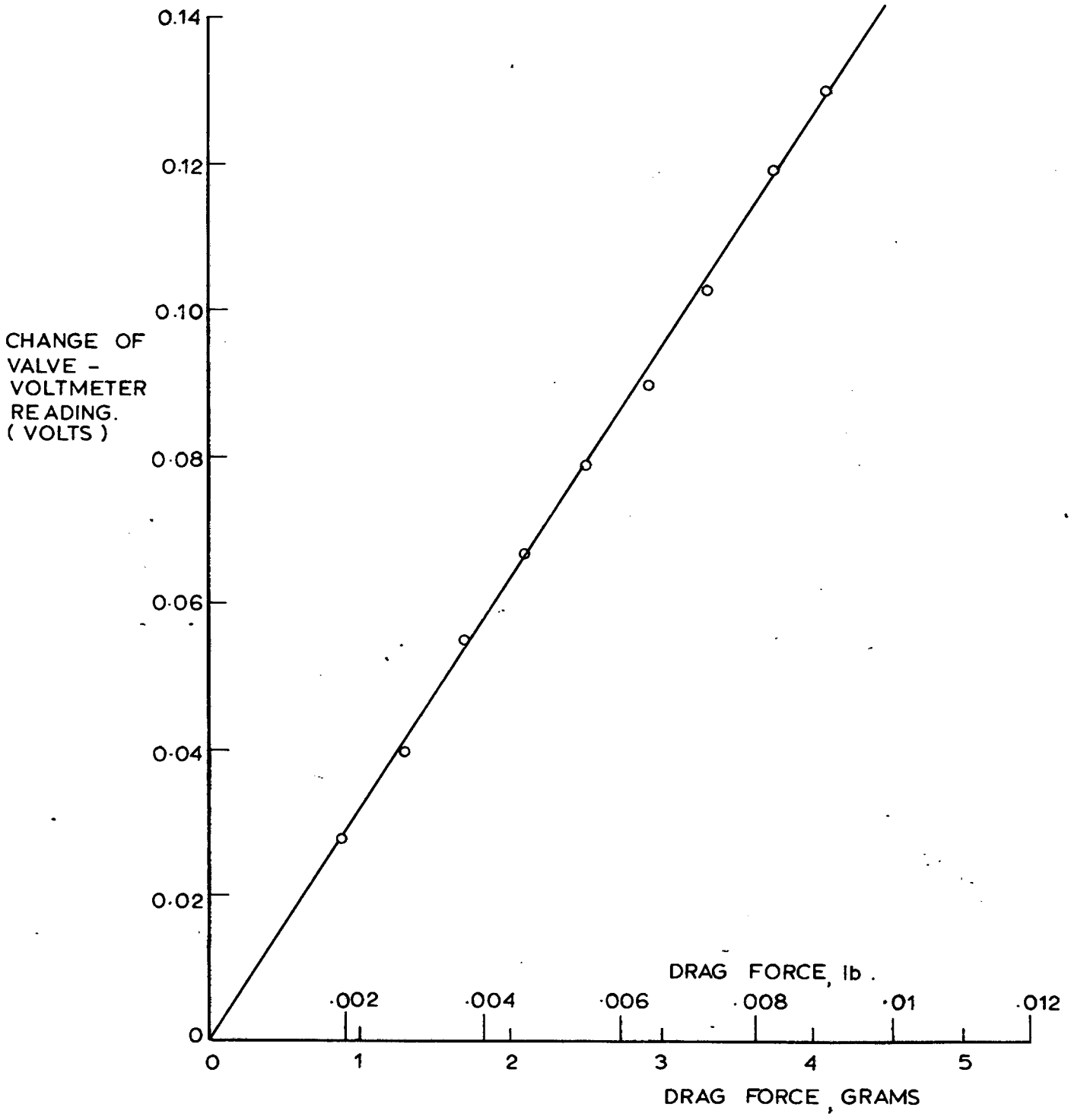

Fig. 5.2. A drag-force calibration of the optical system.

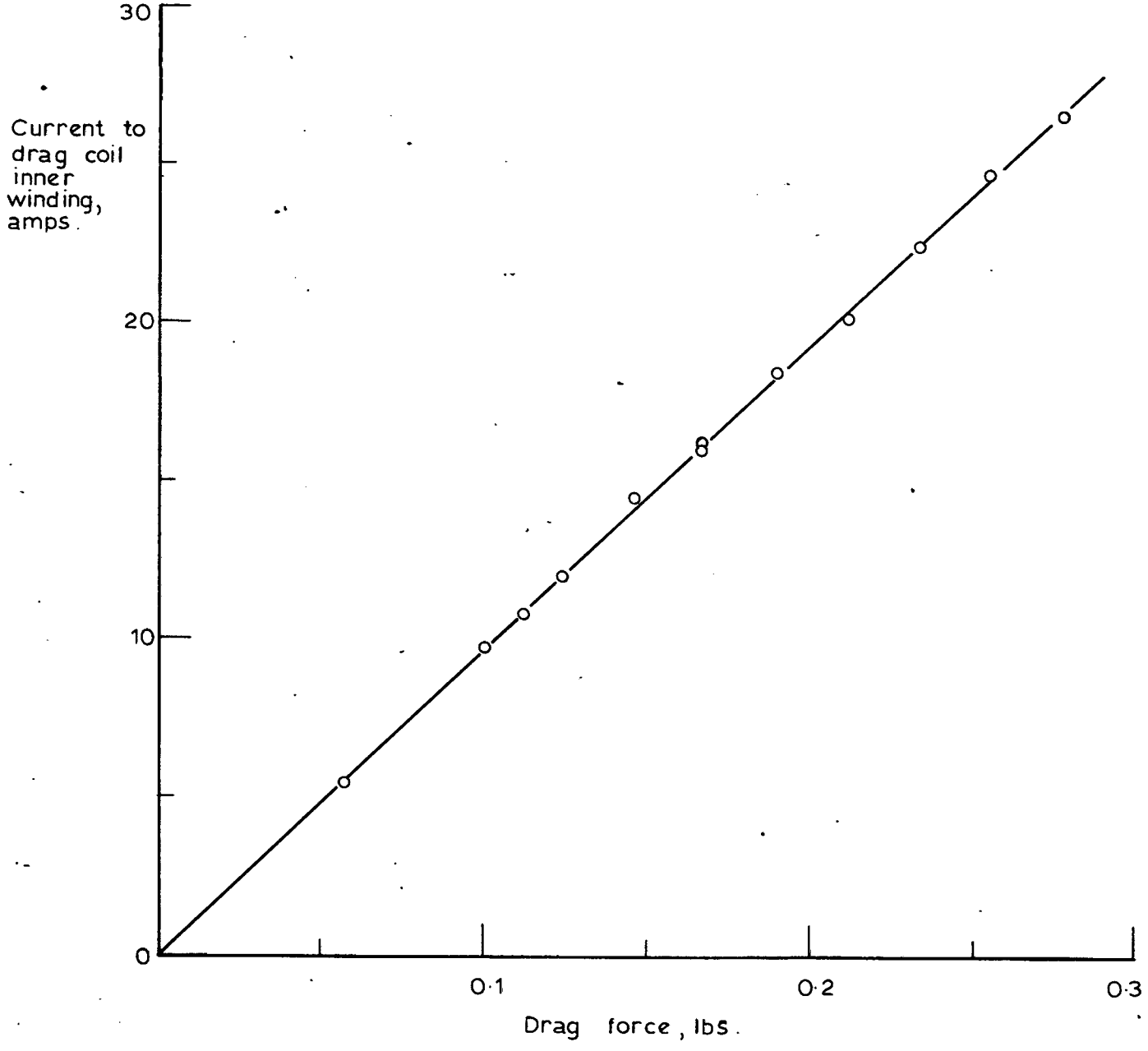

Fig. 5.3 A calibration of drag force against drag coil current for the tuned model.

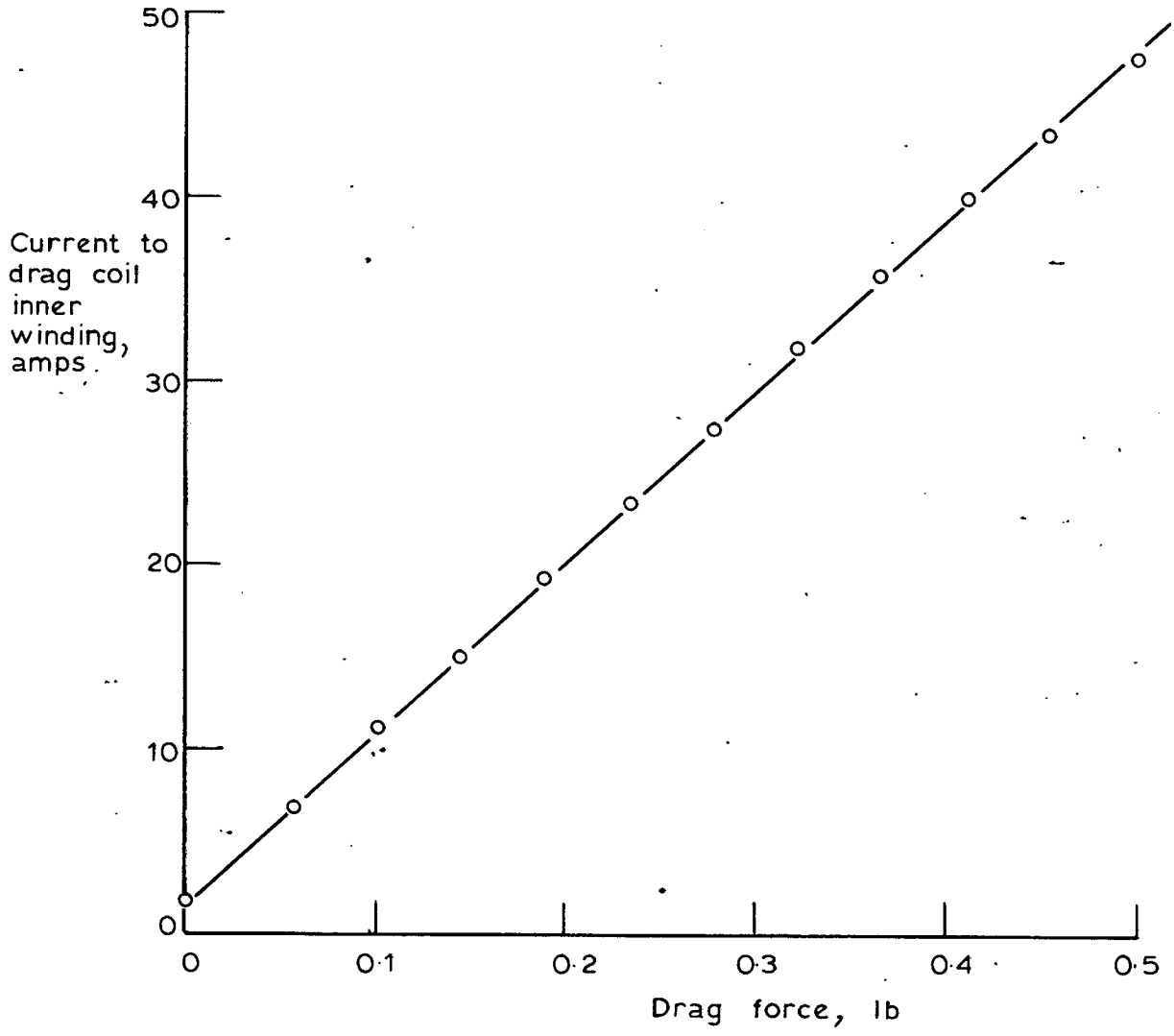

Fig. 5.4 A calibration of drag force against drag coil current for the solid body of revolution.

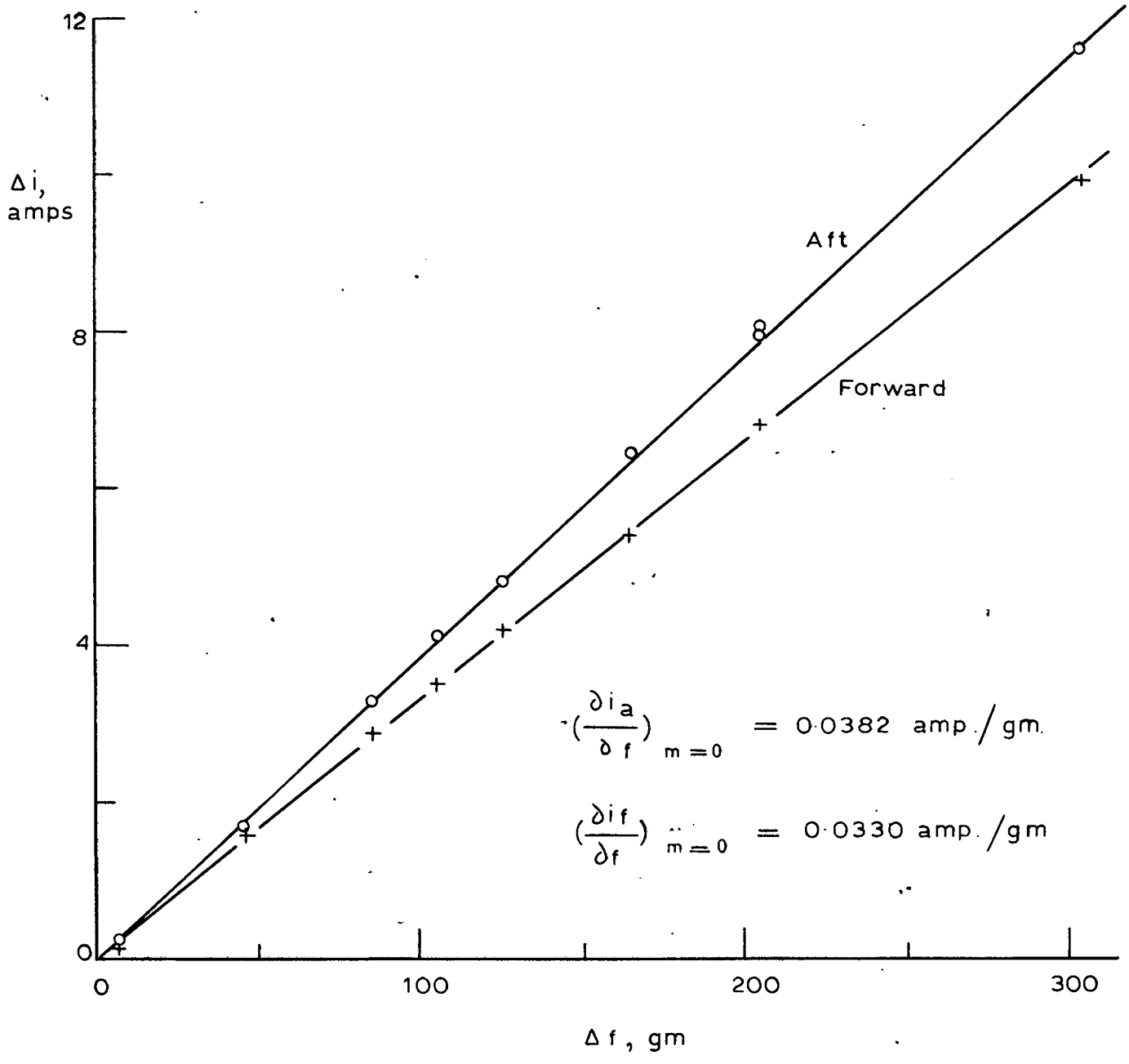

Fig. 5.5. A force calibration of the lateral electro-magnets acting on the tuned model.

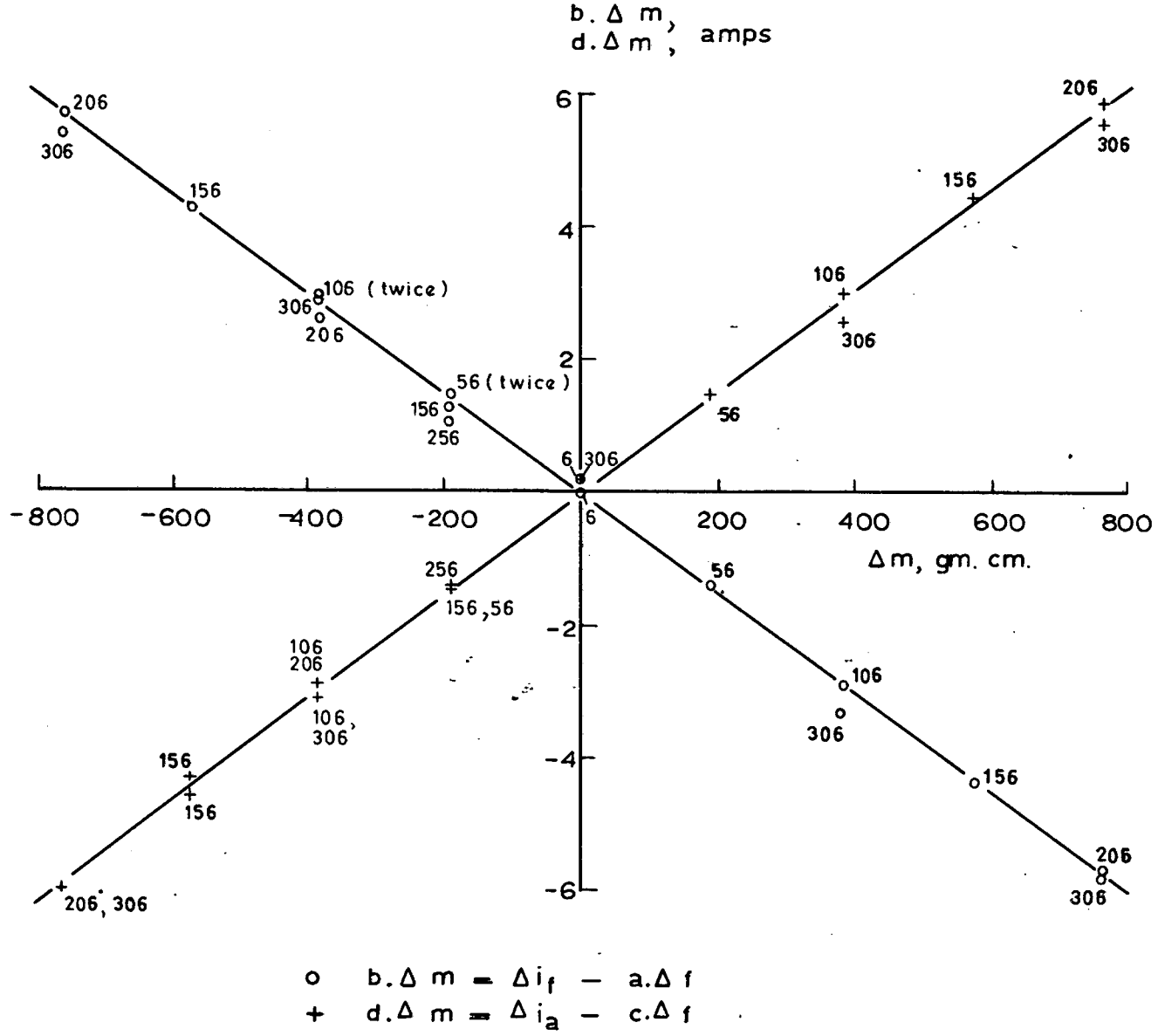

Fig. 5.6 Moment calibration curves for the lateral electro-magnets acting on the tuned model.

6. The Control of Rolling Motion.

The versatility of magnetic suspension systems can be increased to the extent that it becomes feasible to suspend and make measurements on aeroplane-like models instead of the more missile-like models or bodies of revolution to which magnetic balances had hitherto been confined, if roll is controlled.

In this Chapter the various techniques which are available for controlling roll are described and assessed.

Contents:

6.1 Introduction.

The magnetic suspension systems which had been developed elsewhere for wind tunnel applications were designed to control the models in three[5,6] or five[2,3,4] degrees of freedom. In no case was a roll control system in use, although concurrently with the developments at Southampton University there was a proposal from M.I.T.[7] for an A.C. coil system described below, but the scheme was

not applied to a magnetic suspension system.

In the context of this work, in order to consider a particular mode of motion controlled, there must be positive stiffness, damping near critical, and it must be possible to adjust the attitude of the model, within limits, by controls external to the model. This has become the normal practice for up to five degrees of freedom, the exception being rolling motions. However, a considerable amount of wind-tunnel testing has been possible in the past without the installation of proper control in roll, because in some circumstances the precise maintenance of roll attitude is not necessary; for example, the testing of bodies of revolution does not require roll attitude control. Similarly, the measurement of the zero incidence drag of a finned missile, or base pressure measurements, are practicable without the knowledge of or control over the roll attitude, provided that the model can be prevented from spinning under the action of the air stream.

Before considering methods of controlling roll, two methods of providing some stiffness in roll to prevent rotation about the model axis should be explained. Firstly, stiffness is produced by offsetting the centre of gravity so that it swings about the axis of rotation of the model defined by the outside contour rotating in the optical system. Some stiffness from this source is difficult to avoid in practice. The second method consists of providing the model with a magnetic core which is not axisymmetric, typically by providing a magnetic fin at the end of the model, the fin being attracted by the nearest lift magnet pole. The fin adopts a vertical attitude in the absence of disturbing rolling moments. Disturbances

can arise from at least two sources, one example being aerodynamic out-of-trim in the model which can result in varying attitudes in roll depending on air speed, the second occurring when a lateral force is applied to the model by the lateral magnets, either to resist an aerodynamic force or moment or to deliberately oscillate the model for the purpose of making aerodynamic derivative measurements. In the second case the disturbance is periodic and can result in large roll amplitudes of motion at low frequencies and at frequencies near to the natural frequency in roll. An improvement on this scheme is to use a pair of identical fins on opposite sides of the model, near an end, manufactured from a permanent magnet material. The lift magnet attracts the upper fin more strongly than the lower, providing the necessary stiffness, but forces from the lateral magnets do not disturb the model in roll provided that the fins remain vertical and that the intensity of magnetisation of the fins is equal and remains constant. The variation of rolling moment with angular displacement in roll is fundamentally different for 1 or 2 fins. In the case of a single fin, the moment reaches a maximum at a displacement of about 90° from equilibrium, whereas for two fins the maximum moment occurs near 45° displacement and is zero at 0°, 90° etc. It sometimes occurs that asymmetry in the state of magnetisation of a geometrically symmetrical core can produce a roll stiffness in the manner of a magnetic fin.

Neither of these schemes, the offset centre of gravity or magnetic asymmetry, provides any significant damping in roll, nor does it allow the correction of roll attitude during a tunnel test, which might require correction because of wing defects, or as a result of a

rolling moment generated due to yaw, for example. Some possible techniques for providing proper control in roll will now be considered.

There are at least six different methods under the following headings that might be used for controlling the roll attitude of a model.

Aileron control

D.C. - coil

A.C. - coil

E - coils

Shaped Cores

L_v control

6.2 Aileron Control.

In some circumstances it may be practical to control roll by fitting the model with working ailerons, operated by a mechanism mounted on the model. Many detail arrangements can be proposed; the operating mechanism could be electrical, pneumatic using ram air exhausting downstream of the tail, or magnetic operated by varying fields applied to the model. An electrical system could be rather heavy, because a power supply, amplifier, motor and some attitude monitoring system would need to be carried within the model; however, it must be classed as a possible technique. The ram-air system might consist of a bellows-operated aileron (or pair of ailerons) but some control of the air supply to the bellows would be required. In a high speed wind tunnel the total to static pressure ratio and the total pressure in the working section can be very high, providing a useful source of energy. Alternatively the controlled supply of ram-air could be exhausted through suitably directed jets, in the wings

to provide rolling moment by reaction.

Developments along one of these lines may be desirable, because the aileron roll control system promises the useful characteristic of increasing moment capacity with dynamic head.

6.3 The D.C. - Coil Roll Control System.

6.3.1 Active Coil.

This system consists of one or more coils wound in a fin or wing mounted on the model and energised by a battery also carried on the model. With the fins arranged vertically or horizontally, suitably chosen coils would experience forces tending to roll the model. A diagram showing the field distribution in the vertical plane through the legs of a typical horseshoe shaped lift electro-magnet is shown in Fig. 6.1, together with a suitable location of a coil. Depending to some extent on the shape and position of this coil, with the current flowing the top edge would experience a lateral force which would produce the required moment about the axis of the model, together with a force component through the axis which would require balancing by the lateral magnets. By varying the current level in the coil the rolling moment can be varied. One possible method of automatically controlling this current would be to install a feedback system and amplifier similar to that suggested for the aileron control system. This system is shown schematically in Fig. 6.2. This roll control system would be suitable for the L or V magnet layouts described in reference 1.

6.3.2 Passive Coil.

A lateral control system consisting of two similar electromagnets, one each side of the tunnel, can be used to generate varying

field strengths in the model region, and this gives one the opportunity to generage varying rolling moments on a model mounted coil carrying a steady current, with the consequent simplification of the model design. The moment generating equipment carried on the model would then consist of the coil and energising cell.

The model can be arranged to carry one or more coils, supplied with a steady current from a battery carried on the fuselage, and the interacting coil and lateral magnet fields can generate controllable rolling moments, as well as other forces and moments. A map of the local field strengths and directions is shown on Fig. 6.3 for the suspension system in use at Southampton University, taken in one quadrant of a horizontal plane through the four equally energised poles of the two horseshoe comprising the lateral magnet system. There are regions in this field were a coil, lying in a horizontal plane, would generate insignificant moments in the rolling sense. However, some regions are of particular interest, namely those where strong cross-field components exist, as marked on the diagram. Coils of suitable size situated in these regions can produce moments, and one particular design of coil is shown superimposed on Fig. 6.3. The coil has been chosen with a view to adaptation to the fins of a missile type model, where only the downstream region of strong cross field would be used. Fig. 6.4 is a photograph of a model carrying such coils; each coil consisted of 58 turns of 26 s.w.g. wire, the coil thickness was 1/16 ins, and the overall span 4⅛ ins. The model also carries a fin and roll optical grid.

6.3.3 <u>The Moment Capability of Fin Coils</u>.

The coils have been used for the measurement of moment-

current relationships under the two different operating conditions discussed, namely constant lift magnet energisation with zero field from the lateral magnets, varying the fin coil current in order to hold the roll attitude of the model constant when subjected to varying rolling moments (the "active coil" system), and constant fin coil current with constant lift magnet field strength, varying the lateral electro-magnet field strength in order to hold the model roll attitude constant (the "passive coil" system).

Rolling moments were applied to the model by attaching arms to the fuselage, mid-way along, and hanging moment weights at the ends of the arms.

The model was magnetically suspended for these measurements and, to avoid changes of the intensity of magnetisation of the lift magnets, which would itself have resulted in moment changes on the model, it was necessary to adopt the technique of transferring weights from one arm to the other when a moment change was required.

Some results of measurements taken with the "active coil" moment system with the fins in both the vertical plane and the horizontal plane are given on Fig. 6.5. The inverse slope of these curves has been used as a measure of the moment generating ability of the active fin coil system and, for the two cases just mentioned, the slopes are 16.7 and 14.5 gm.cm. per ampere in the fin coils. Some data on the variation of the slope with roll attitude is given on Fig. 6.6.

The "passive coil" system was investigated at steady coil current levels up to one amp. The resistance of the pair of coils in series was 1¼ ohms; hence the maximum power consumption was 1¼ watts. For these measurements, the current required to be supplied to the

roll sections of the lateral electro-magnets to hold the attitude of the model constant after a moment change had been applied has been plotted on Fig. 6.7 for various fin coil current levels. The fin coils were in the horizontal plane. The inverse slope of these curves, λ , varies linearly with fin coil current, reaching a value of 0.007 gm.cm/NI. (ampere-turn) in each lateral leg, at a fin current level of 1 amp. Measurements were also made in the passive mode of operation with the coils mounted vertically, and at 1 amp fin current level λ was 0.0051. The variation between these limits of attitude roughly follows a $\cos 2\theta$ curve. During all of these tests on the fin coils the D.C. power to the coils was not carried on the model, but, for convenience, was supplied externally through thin flexible leads. However, suitable batteries are available.

6.4 The A.C. Coil System.

A variation on the model mounted coil type of roll control system has been proposed[7] in the United States. The coil in this case consisted of a loop of heavy gauge wire passed around the perimeter of the model. In line with the axis of the coil there would be an A.C. electro-magnet used to generate alternating currents in the coil on the model. A second A.C. electro-magnet, operating at the same frequency as the first, would be arranged with its axis in the plane of the model coil, alongside the wind tunnel working section. By varying the phase relationship between the two A.C. electro-magnets, clockwise or anticlockwise periodic rolling moments can be produced.

6.5 The E-coil System.

This roll control system was a proposal reported by Stephens.[8] The rolling moment would be produced by a magnetic field acting on a

model containing a reverse-curved magnetic core. In order to assist with the explanation of the method by which a controllable rolling moment could be generated, a schematic diagram of the core, and the electro-magnets which would be used for the production of the rolling moment, is given on Fig. 6.8.

The model core is shown lying in the horizontal plane, and the electro-magnets which would be E-shaped are shown lying in the vertical plane. The model core would consist of three separate parts, identified as a, b and c on Fig. 6.8, section b being larger than a and c. The action of electro-magnet poles N_1, S_1 on core a would produce a rolling moment and pitching moment in the same sense as those produced by N_3, S_3 acting on core c, whereas N_2, S_2 acting on core b would produce a rolling moment in the same sense but a pitching moment of opposite sense. By suitable choice of core and electro-magnet proportions, the pitching moments could be arranged to cancel, leaving a net rolling moment. This argument, which is much simplified, ignores forces or moments generated by, for example, electro-magnet poles N_3, S_3 acting on a and b.

6.6 Roll Control using "Shaped Cores".

If a model containing a magnetic core having a non-circular cross section is suspended under the lift magnets, it will adopt one of several preferred roll attitudes. For example, if the cross section of the core is rectangular, or elliptical, the major axis of the cross section will adopt a vertical attitude, and there can be two stable positions in roll for the model. With a square cross section there are four stable equilibrium attitudes.

This property of such cores can be used to control roll, with a suitable lift and lateral electro-magnet system. As just

described, the roll attitude is stable for disturbances inside an arc approaching 90° either side of the mean in the case of a rectangular core, but the damping is almost non-existent and the stiffness rather low. Also, changes of roll attitude of a given model cannot be selected. However, if two identical lateral electromagnets are arranged one either side of the wind tunnel, attracting the model equally strongly, it is possible to induce the model to adopt one of two attitudes by varying the current supplied to the lateral magnets. The suspension system at Southampton University has been constructed in this way. At low lateral magnet current levels, the model will adopt an attitude with its major axis vertical, but with the lateral magnets pulling on the model there is a critical current level to these magnets above which the model adopts an attitude with its major axis horizontal, and the attitude remains constant at higher current levels. This system is now a two position control; the major axis can be either vertical or horizontal.

The stiffness in roll depends upon the current level in the lateral magnets. At all times it is relatively low, but at a critical current level in the lateral magnets the stiffness, and hence natural frequency in roll, tends to zero. The model becomes neutrally stable in roll.

With very little alteration this system can be adapted to one giving an infinitely variable selection of roll attitude, within limits. The alteration simply consists of adding a bob-weight to the model to offset the centre of gravity in such a way that, with zero current to the lateral magnets, the model adopts an attitude with the major axis a few degrees out of vertical. As the current supply to the lateral magnets is increased, the model gradually rolls over to a

nearly horizontal attitude. Thus, within an arc of somewhat less than 90°, any roll attitude can be selected.

There remained two major steps to turn this roll attitude selection system into one giving proper control in roll.

Firstly, the effective stiffness required increasing, from a level giving the rather low naturaly frequency in roll of 1-2 c/s, and secondly some damping was required.

The "applied moment" - "roll attitude" characteristic of a shaped core suspended with zero net lateral field quite closely follows a $\sin 2\theta$ law, where θ is the displacement of the major axis of the cross section from the vertical. Hence the maximum moment capabilities are realised with the core set at 45° to the vertical. This attitude of the major axis was chosen as normal. When positioned in this way the core experiences a moment from the lift magnets tending to restore it to the vertical; this must be opposed by an equal and opposite moment from the lateral magnets. For a given position of the model, the restoring moment is dependent on the current in the two legs of the lift electro-magnet and is therefore constant in the absence of aerodynamic forces. By optically monitoring the roll attitude of the model and feeding the signal, via a compensation network to the power amplifier supplying the roll sections of the lateral magnets, a stable roll control system can be obtained giving the required increase of stiffness and good damping.

On Fig. 6.9 an end view of a rectangular cross-sectioned core is shown, together with points corresponding with the poles in each adjacent end of the three horseshoe electro-magnets. As will be shown later, in addition to force components acting through the core

axis, the weight-supporting-pole B generates an anti-clockwise moment about the model axis, which is very nearly a maximum for a given pole strength with the core in the position shown. Similarly each lateral pole generates its own force components and moment, but in the case of these poles the force components cancel one another for equal lateral (horseshoe) pole strengths whereas the moments generated are additive and in opposite sense to that generated by B. Consequently, such a core suspended magnetically would experience a fixed anti-clockwise moment from the support magnet, which can be opposed by an equal and opposite moment as a result of the two lateral magnets attracting the core equally with an appropriate field strength. Because of the cancellation of force components from the lateral magnets, they have no influence upon the lateral position of the model. By varying the strength of the lateral poles away from that value which just has the effect of opposing the fixed anti-clockwise moment resulting from the support magnet field, the magnetic core of the model can be made to oppose a disturbing rolling moment that might be applied to the model.

This roll control principle can allow the exertion of a lateral force and moment about the vertical axis upon the model by the lateral magnets without at the same time changing the magnitude of the rolling moment. The mechanism for the simultaneous control of lateral bodily motions and rolling motions of the model with the lateral electro-magnets will now be discussed.

It would be possible to exert a lateral force on the magnetic core of the model by increasing the strength of the pole of one of the lateral magnets, say pole C in Fig. 6.9, but if this was done without changing the strength of pole D there would be a change

of rolling moment generated by the shaped core because the net moment generated by the two lateral magnets is additive. To avoid this rolling moment change the technique can be adopted of reducing the strength of one of the lateral electro-magnet poles by the same amount that the other has its strength increased. In this way the net rolling moment would remain constant while the required lateral force would be generated. If corresponding changes equal in magnitude but of opposite sign (because of the opposite polarity) were made at the other ends of the two lateral horseshoe magnets, a lateral force would be generated on the core, the line of action of the force passing through the centre of the model. Similarly, if changes of the same sign were made at the other ends of the lateral magnets, a pure moment about the vertical axis would be generated on the model.

Schematic wiring diagrams for the lateral electro-magnets are given on Figs. 3.3 and 3.4. A constant current power supply is used for lateral bias, the remaining three supplies being controllable and operated by signals from appropriate optical systems. All power supplies have uni-directional outputs.

6.6.2 The theoretical behaviour of a particular type of shaped core has been investigated, the assumed cross section having a slender rectangular form. The analysis and some theoretical results are given in Appendix IV. For part of the analysis the magnetic poles in the core were assumed to consist of uniform line distributions near the ends of the core, rather than to be the point sources of magnetism assumed in classical theory. In practice a slender core would not be used, but the theory was useful in illustrating trends. The mathematical model is shown in Fig. 6.10,

where the force δf generated by an element of the model under the action of the nearest suspension magnet pole $+p$ is shown resolved into three components. With a symmetrically disposed model the axial component δf_a will be cancelled by an opposite force at the other end of the core. Components δf_v and δf_h contribute to the rolling moment (measured about the axis of the model). The net forces and rolling moment generated on the line distribution of poles by both poles of the suspension magnet have been calculated, and presented in non-dimensional form.

The main conclusions are listed in Table 6.1.

$\oint \delta f_v$	insensitive to θ proportional to b (valid only for low values of b) proportional to x_o dependent on a. Peak values occur at low positive values of a.
$\oint \delta f_h$	Small, generally less than 1% of $\oint \delta f_v$ for cores of practical sizes.
Rolling moment	proportional to sin 2θ proportional to b proportional to x_o^3 dependent on a. Peak values occur at low positive values of a

TABLE 6.1 The Effects of Geometry on Forces and Rolling Moment Produced by a Shaped Core.

On this suspension system the main aerodynamic measurements were to be made with model motions in the plane containing the lateral horseshoe electro-magnets. The sensitivity of a rolling moment

calibration to changes of model position in this plane required investigation. The results of the analysis showed that the lateral force and rolling moments produced on the model by the lateral magnets were relatively insensitive to small changes of model position in the horizontal plane, as a result of the symmetry of the system.

The selection of the cross-sectional shape of the magnetic core is clearly an important factor in determining the moment that can be generated by a model, and the problem arises of selecting the optimum core shape. This has been answered in two different ways. For the type of suspension system on which this work has been done, having a lateral control magnet on each side of the wind tunnel, the optimum shape contained within a circular envelope is that shown in the end view sketch below:

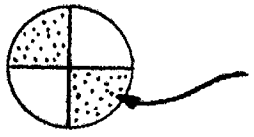

However, the shape is not particularly easy to produce except by casting, in the brittle "hard" magnetic materials, and the most suitable shape of cores having a rectangular cross section has also been calculated using a magnetic pole theory. The details are given in Appendix IV. The conclusion was that over a wide range of core sizes the maximum rolling moment would be given by a width to thickness ratio of 0.58. In fact, the choice of aspect ratio of the cross section is compromised to some extent by considerations other than that of moment generation. For ease of suspension of heavy models, or in order to excite an oscillation in yaw more easily, a higher value than that quoted might be chosen. Alternatively, if the main interest was that of oscillating the model to measure roll derivatives the choice might

be for a thinner core with lower inertia.

Having determined a suitable cross-sectional shape, it remained to find out how rolling moment capacity was affected by the scale of the cross section. The simple theory of Appendix IV indicated that rolling moment capacity varied very nearly as the fourth power of the model scale, and this was borne out experimentally where indices between 3 and 4 were obtained for different sized cores of the same length and material.

6.6.3 Some measurements have been made of the magnitudes of the rolling moments that can be generated by several different cores. The technique used was to suspend a model with the core in the 45° attitude, and to hang weights on a pair of horizontal moment arms fixed to the model. In order to generate a change of moment, while at the same time keeping the restoring moment from the lift magnets constant, it was necessary to hang a selection of weights on the arms, and to transfer a suitable weight from one side to the other as previously described. After a moment change had been selected, the resultant change of roll attitude was corrected by changing the strength of the lateral magnets.

On Fig. 6.11 the model used for moment measurements is shown standing next to a selection of mild steel cores. When magnetically suspended, this model was positioned with the Perspex pointer vertical and with the cylindrical Dural endpieces in the vertical/lateral optical system beams. The variation of lateral electro-magnet roll section current with applied moment (to hold the roll attitude constant) for the core fitted with end-pieces in Fig. 6.11 is shown on Fig. 6.12. On this calibration one winding

section per lateral leg was used for applying rolling moment, and the ordinate scale shows the current in amperes in each of these windings. The non-linearity of the curves was probably due to a changing state of magnetisation of the soft iron core. The field from the roll control sections is magnetising, and the cores are more effective from the point of view of moment generation at the higher roll current levels.

Fig. 6.13 shows a curve of applied rolling moment plotted against N.I. (ampere-turns) per lateral horseshoe leg, for a mild steel core of overall diameter 3/4". A moment range close to $\pm$ 1 oz. inch. about a mean level was achieved. The non-linearity near one end of the line was again probably due to the reduction of intensity of magnetisation of the core under conditions of low current in the roll sections. Permanent magnet cores do not exhibit this non-linearity.

The inverse slope of such a curve (or that of the linear part of the curve for a 'soft' magnetic core) given the symbol λ, is used as a measure of the moment generating ability of a core in this suspension system.

Table 6.2 gives a selection of core shapes and materials, and the measured value of λ for each. Further information is given in reference 10.

All of the cores listed in table 6.2. had an overall length of 5 inches. Core 1 had a rectangular cross-section 3/4" x 3/8", and cores 2 were manufactured from round bar by machining diametrically opposite flats to give a width to diameter ratio of about 0.7. Cores 3 were the 5/8" diameter cores numbered

		MAGNETIC MATERIAL	SPAN OF MAJOR AXIS.	λ oz-INCH / NI IN EACH LATERAL LEG. $\times 10^4$
1.	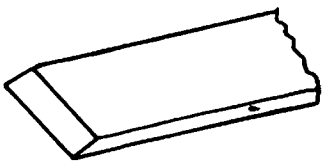	MILD STEEL	$\frac{3}{4}$"	2·63
2.	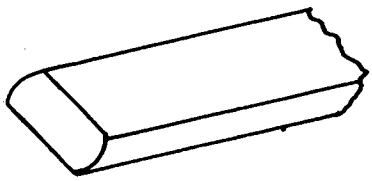	MILD STEEL AND ALCOMAX III	$\frac{1}{2}$" AND $\frac{5}{8}$"	<table><tr><th></th><th>$\frac{1}{2}$"</th><th>$\frac{5}{8}$"</th></tr><tr><td>M.S.</td><td>0·447</td><td>0·965</td></tr><tr><td>ALCIII</td><td>0·264</td><td>0·527</td></tr></table>
3.	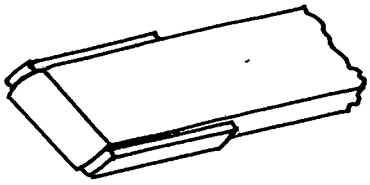	MILD STEEL AND ALCOMAX III	$\frac{3}{4}$"	M.S. 1·95 ALC III 0·917
4.	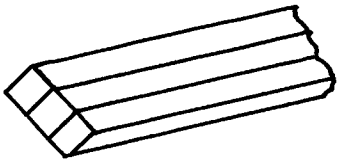	MILD STEEL	$\frac{3}{4}$"	1·792
5.	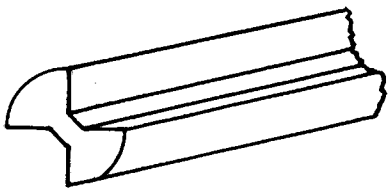	"	$\frac{5}{8}$"	1·09
6.	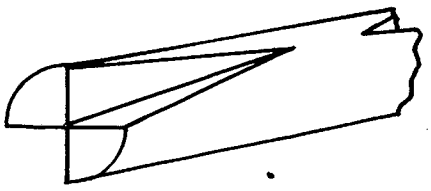	"	$\frac{5}{8}$"	1·205
7	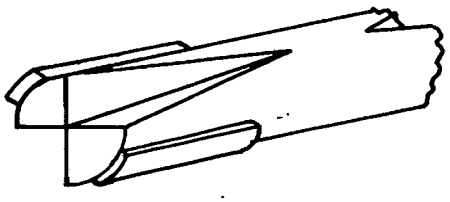	"	$\frac{3}{4}$"	2·115
8.	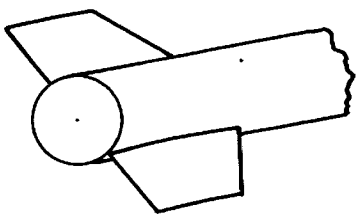	"	$2\frac{3}{4}$"	4·5

Table 6.2 A selection of Shaped Cores and their rolling moment performance.

2 with the addition of four mild steel pole pieces each 1" long by 0.3" wide by one-sixteenth inch thick.

Core No. 4 was a sandwich consisting of 1/4" square mild steel strips each side of a 1/4" square Dural strip. The cores numbered 1 - 3 were not the best that could be devised. Improved rolling moment capacity could be obtained for a given overall size of core with most of its material in diametrically opposite quadrants, as No. 5. In this case an improvement of 13% was recorded over the 5/8" diameter mild steel core No. 2. The theory behind this shape of core is given in Appendix IV.

Consideration of the flux distribution through a bar magnet suggested that the ends of the magnet, which contribute the major part of the rolling moment, were not fully magnetised because of saturation in the mid region of the core. With the object of increasing the total flux passing through the mid region and thereby increasing the flux density near the poles, a modification of No. 5 was tested, shown as No. 6 in table 6.2. An improved value of λ was recorded of about 25% over the corresponding core No. 2.

The addition of the mild steel pole-pieces showed only an 8% improvement of the corresponding core No. 3. Finally table 6.2 shows a model design, numbered 8, which is not strictly a shaped core, which consisted of a pair of steel fins attached to an otherwise conventional model, the fins being positioned in the 45° attitude and having the dimensions of root chord 1", tip cord 3/4" and thickness 0.087". In practice these fins might be two out of a cruciform set of fins, the other pair being non-magnetic. The high value of λ obtained is an illustration of the powerful effect that span has on moment, mentioned in section 6.6.2.

The effect of model core length on its force and moment capabilities was investigated using permanent magnet Shaped Cores ranging in length from somewhat shorter to much longer than would be used in practice with this suspension system. Fig. 6.14 shows the variation with core length of the suspended weight per ampere in the suspension magnet coils. The curve peaks with a value of the core overall length somewhat greater than the geometric centre to centre distance between the suspension magnet poles (about 7 inches), which was predicted in theory. A comparable curve showing the dependence of rolling moment capacity on core length is shown in Fig. 6.15.

The measured variation of λ with roll attitude followed a $\sin 2\theta$ law very closely. This property is useful for purposes of control because it results in negligible change of system calibration for small deviations of the roll attitude of the model core away from the normal 45° attitude. The measured sensitivity of λ to roll attitude is shown on Fig. 6.16.

In order to check on the sensitivity of λ to changes of model position in the horizontal plane, calibrations of a permanent magnet core in the 45° attitude (core No. 3 of table 6.2) were made with the model pitched about its centre 2.8° each way. The changes of calibration resulting from displacement away from zero pitch were inside 2%.

6.6.4 The advantage to be gained by fitting a shaped core with pole-pieces has been exploited in the construction of a model for the suspension system. The pole-pieces were let into slots in the model fuselage, as shown on Fig. 6.17; an optical grid is mounted inside

the fin and is covered with acetate film. The same model is shown on Fig. 6.18, subjected to a forced oscillation in roll while suspended in the six component balance.

The magnetising effect on the model core of the field generated by the lateral magnets precludes the use of soft magnetic cores in the model. Experience has shown that with this type of roll control system a model containing a soft iron core tends to heave vertically with variations of the current in the roll sections of the lateral magnets; the changing suspension current requirements with roll-sections current is shown on Fig. 6.19 for a selection of 5 inch long mild steel cores.

The particular wiring arrangement adopted for the lateral magnets has about 132 turns (one third of the total) on each leg allocated to roll control, and the power supplies are each capable of producing a maximum of 33 amps. Hence the moment range that can be generated on the permanent magnet core numbered 3 in table 2 is $\pm$ 0.2 oz. inch, whereas the fin arrangement of number 8 will generate a range close to $\pm$ 1 oz. inch with this wiring arrangement.

Stabilisation of the model in roll is achieved by using "proportional plus first derivative" feedback, a simple lead-lag circuit providing the necessary phase lead at low frequencies. Details of the compensation circuit are given in Chapter 7.

6.7 Motoring.

A model containing a Shaped Core can be induced to run as a synchronous motor by feeding cyclically varying currents to the lateral magnets of a $\perp$ type suspension system, and then mechanically spinning the model up to synchronous speed to allow the lock-on.

Speeds greater than 1000 r.p.m. have been produced on a 3/4" diameter body of revolution.

The maximum average moment that can be produced during one cycle is given by

$$\bar{M} = 1/2\ k\ .\ i_o$$

where i_o is the amplitude of the A.C. component of current fed to the roll sections

and k is the change of moment generated on the shaped core when in the 45° attitude per ampere change of current in the roll sections

but when generating this mean moment the model would be on the point of slipping out of synchronisation with the field.

The moment is not steady during the cycle, and the rotary motion of the model has sinusoidal perturbations. However, the technique could be useful for use in measuring roll derivatives, because it avoids the problem of opposing the inertia forces which exist when oscillatory techniques are used with a solid model.

The models were worked slowly up the speed range. The mean roll current level was set to a value giving the model neutral stability in roll and a current ripple was superimposed by a forcing signal fed into the compensation circuits (see Chapter 7) at about 10 cycles per second, corresponding with a model rotational speed of 300 r.p.m. The model was then spun by hand to a speed above synchronous speed. On slowing down, on some occasions the model would lock onto the oscillating field and hold the necessary mean rotational speed. The forcing frequency was then slowly increased, raising the model rotational speed. Normally synchronisation was

lost at around 1000 r.p.m.; the technique was more successful when a light braking moment was applied to the model.

From plots of the variation of angular velocity with time it would appear that the model tended to oscillate in a phase sense relative to the forcing field. This was not surprising as there was no feedback between model speed and field frequency. It is possible that an improved performance would be obtained with some feedback to dampen the phase oscillation.

6.8 L_v Roll Control.

It has been explained that one of the reasons for requiring a roll control system was to counteract out-of-trim of the wings. Circumstances could arise where this was the only requirement. For example in the measurement of lift, drag, pitching moment and pitching derivatives of an aeroplane model one would only be concerned that the model maintained its proper roll orientation relative to the suspension magnet array, and during the measurements the aerodynamically induced rolling moments could be relatively small.

Within these terms of reference, it might be possible to arrange a roll control system making use of the rolling moment due to side-slip, L_v. Aeroplane models would probably have an appreciable moment capacity from this source, mainly as a result of the fin.

At the present time this is only a proposal, and the method for putting the scheme into practice can only be suggested. There are two conditions of suspension to be considered, (a) wind off, and (b) wind on. It would be necessary to monitor roll attitude.

(a) Wind Off. For this phase, it would probably be necessary to prevent large errors in roll attitude from occurring, because of the difficulties that arise with winged models from the wings interrupting the optical system beams when the model is too far from its "normal" attitude, and in the case of a tuned model the model cannot be allowed to roll far from the normal attitude because of interactions caused by the tuned mode.of motion becoming influenced by control systems not adapted to the tuned mode.

For this case, either the "shaped core" roll control system could be retained, or some passive stiffness in roll could be introduced, for example by letting small permanent magnets into the wings (this stiffness could be relatively high because of the span which would be available).

(b) Under wind-on conditions, in order to generate an aerodynamic rolling moment it would be necessary to yaw the model. It should be emphasized here that the moment would mainly be required to trim out defects in the construction of the model, and hence the required yaw angle should be small. It may be possible to utilise the roll attitude signal to control either one of the electro-magnets controlling yaw, or both in opposition, (in the case of this suspension system, this would mean control of the lift magnets) and to arrange yaw to be introduced dependent on the roll signal. The error could be effectively reduced to zero by incorporating integral control in the feed-back loop.

6.9 A summary of the discussion on Roll Control.

The choice of technique for controlling roll depends on the design of the suspension system magnet array and on the model

design. At Southampton University the ⊥ type of suspension system is in use, and for this apparatus a Shaped Core roll control system has been developed for use with winged models.

The moment capacity of shaped cores is strongly dependent on the span of the major axis of the core. Some models cannot accomodate a core with a large-span major axis set at 45° to the vertical. In these cases, it is suggested that either the aileron control or L_v control should be developed, because a minimum re-design of the basic suspension system would be required, and the moment capacity would vary in proportion to the likely aerodynamic disturbances.

6.10 LIST OF SYMBOLS USED IN CHAPTER 6

a	defined on Fig. 6.10
b	thickness of core cross-section
i_o	amplitude of an oscillatory current
k	moment calibration
L	aerodynamic rolling moment
$\bar{M}$	maximum mean moment
v	side-slip velocity component
x_o	semi-width of the major axis of the cross-section
θ	roll attitude
λ	moment capacity of shaped cores, or fin coils

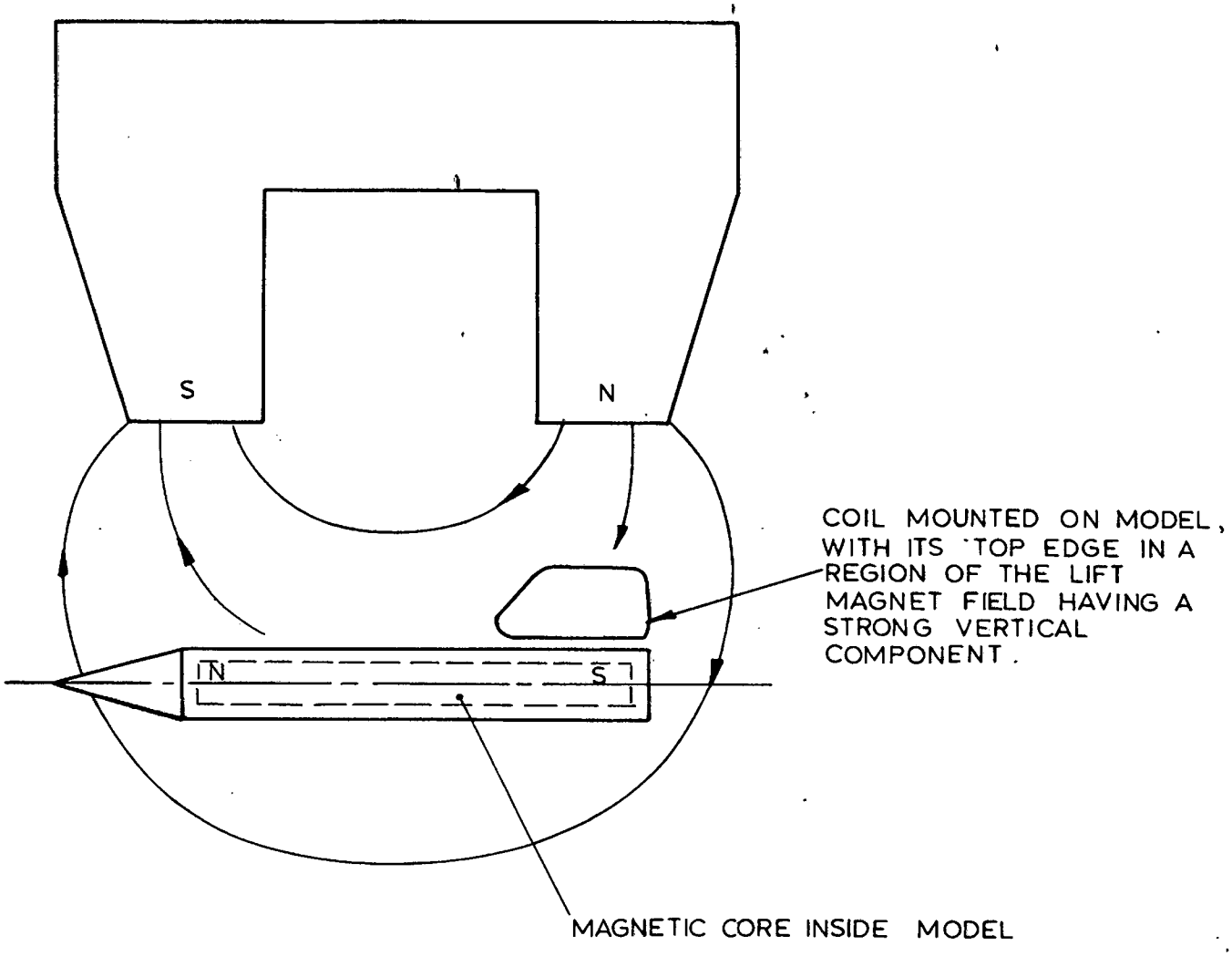

Figure 6.1 A schematic diagram of a model and rolling moment - generating coil in the lift magnet field.

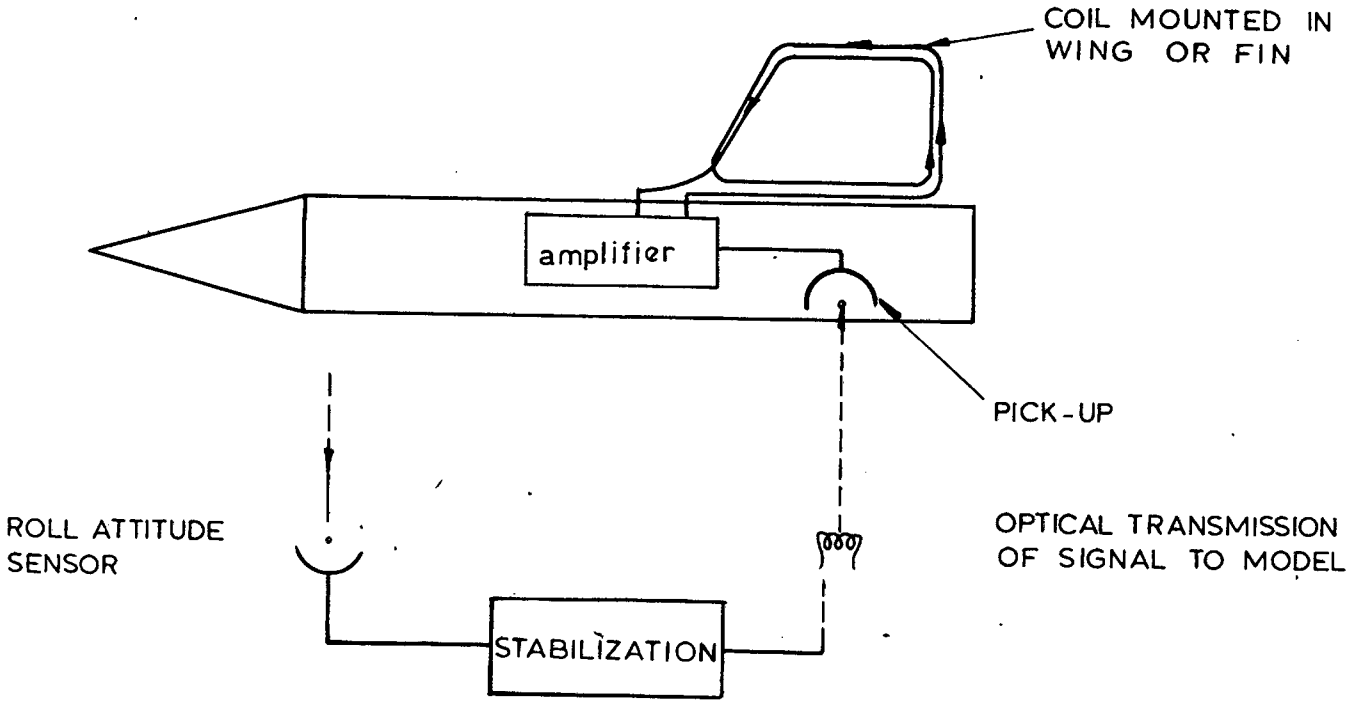

Figure 6.2 An "active coil" control and feedback system.

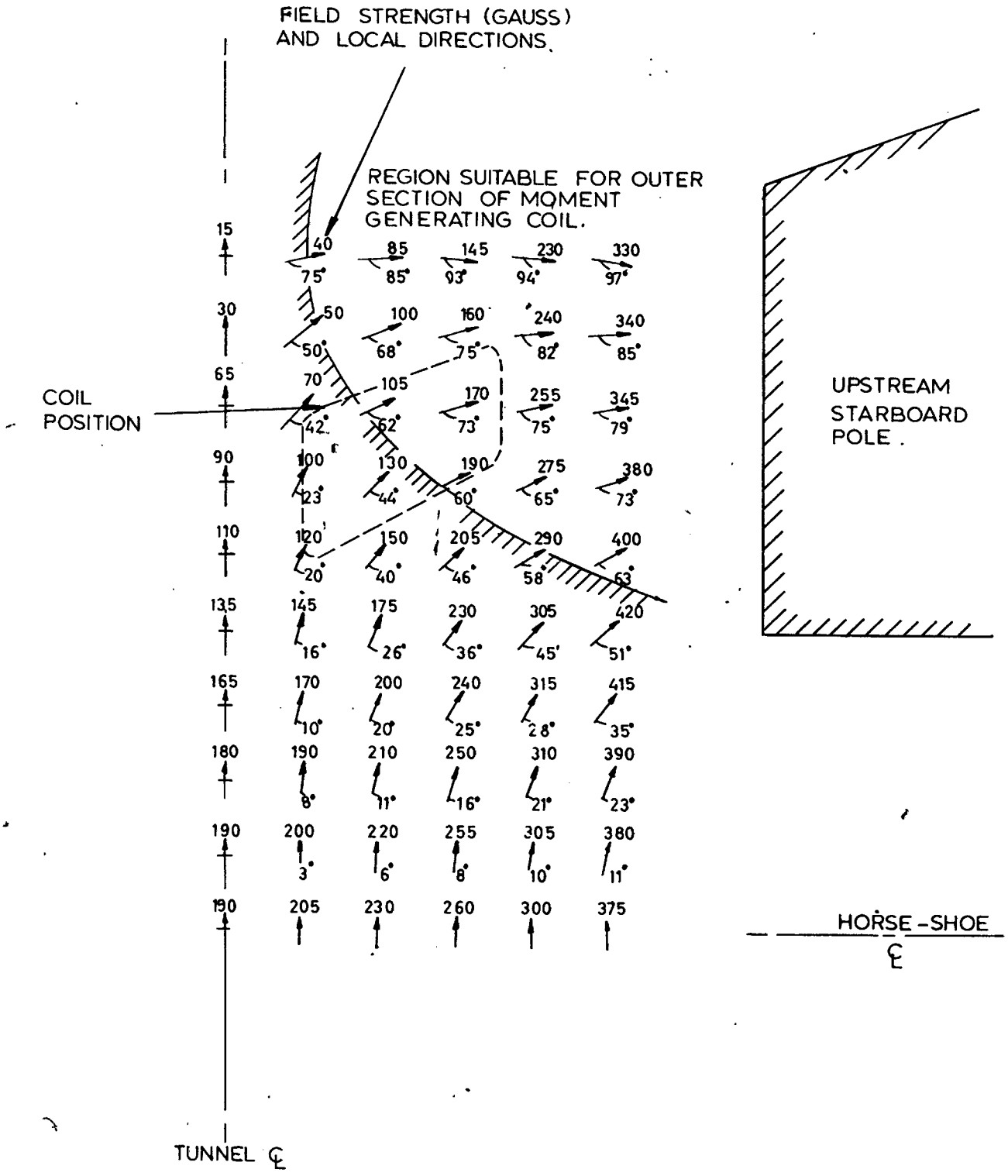

Fig. 6.3 Field strength and directions in a horizontal plane through the tunnel axis. All lateral legs energised at 2640 NI attracting the model.

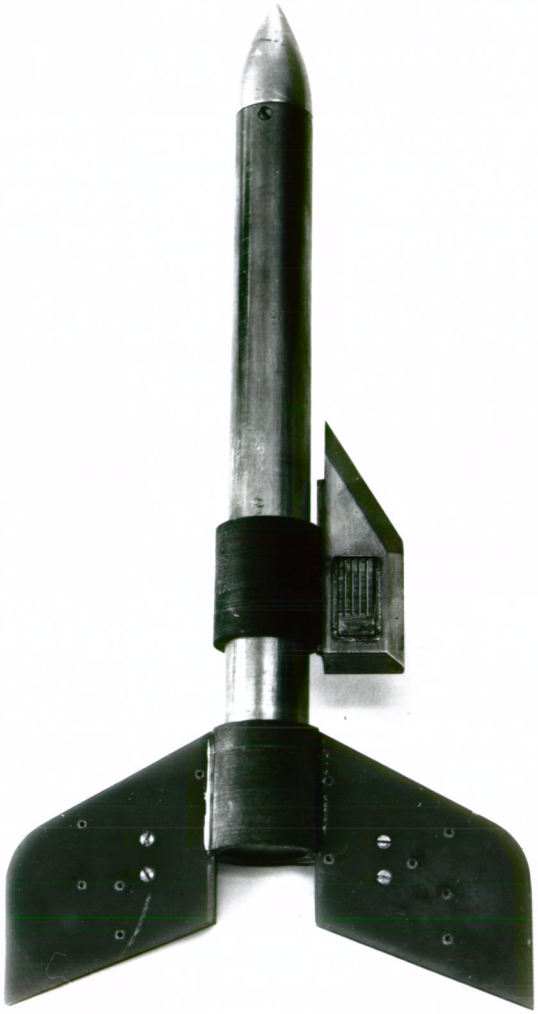

Fig. 6.4. A model carrying a pair of fin coils and an optical grid. These components were added to an existing model, for demonstration purposes.

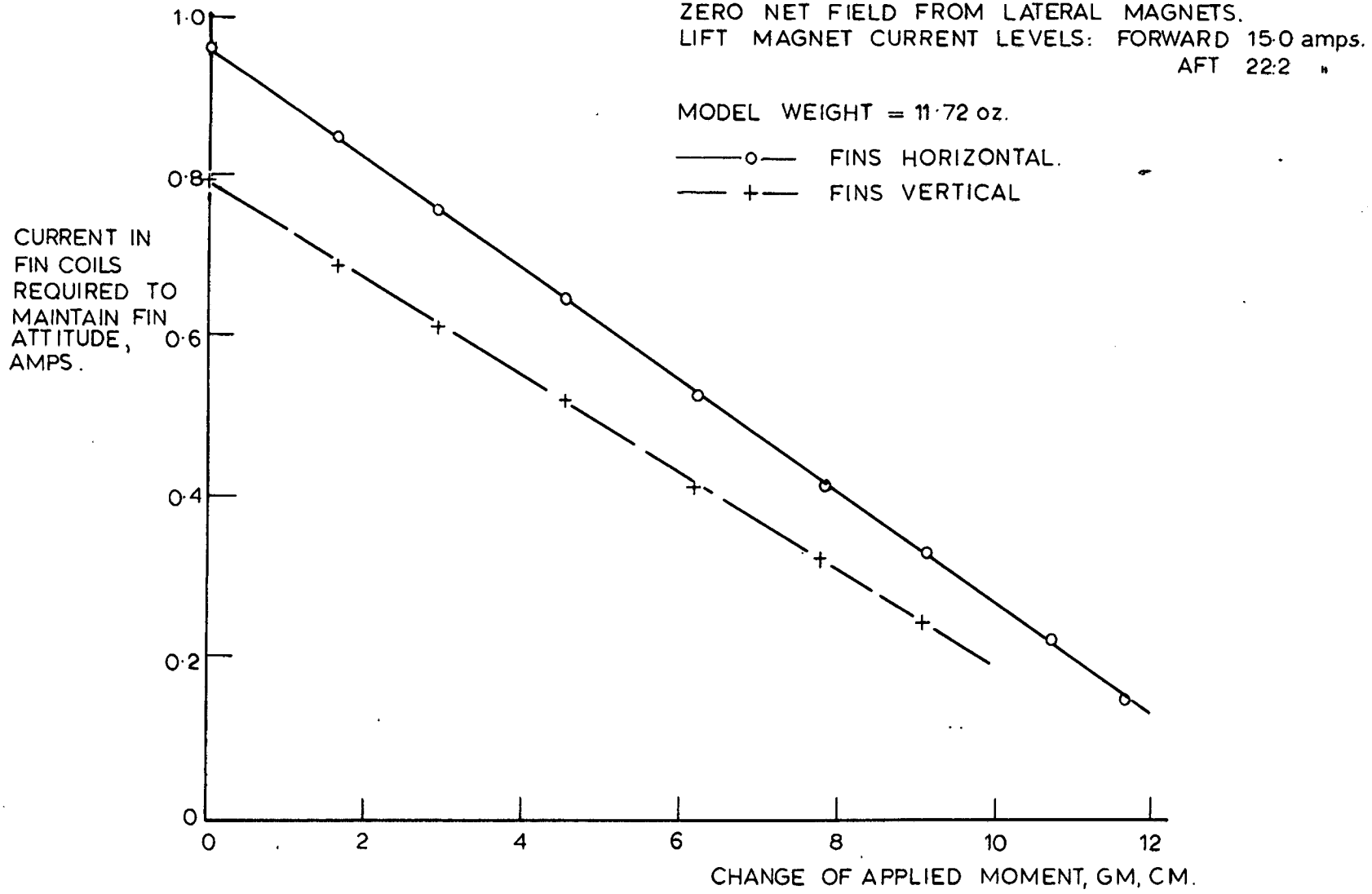

Fig. 6.5 Moment generated by fin coils in lift magnet field.

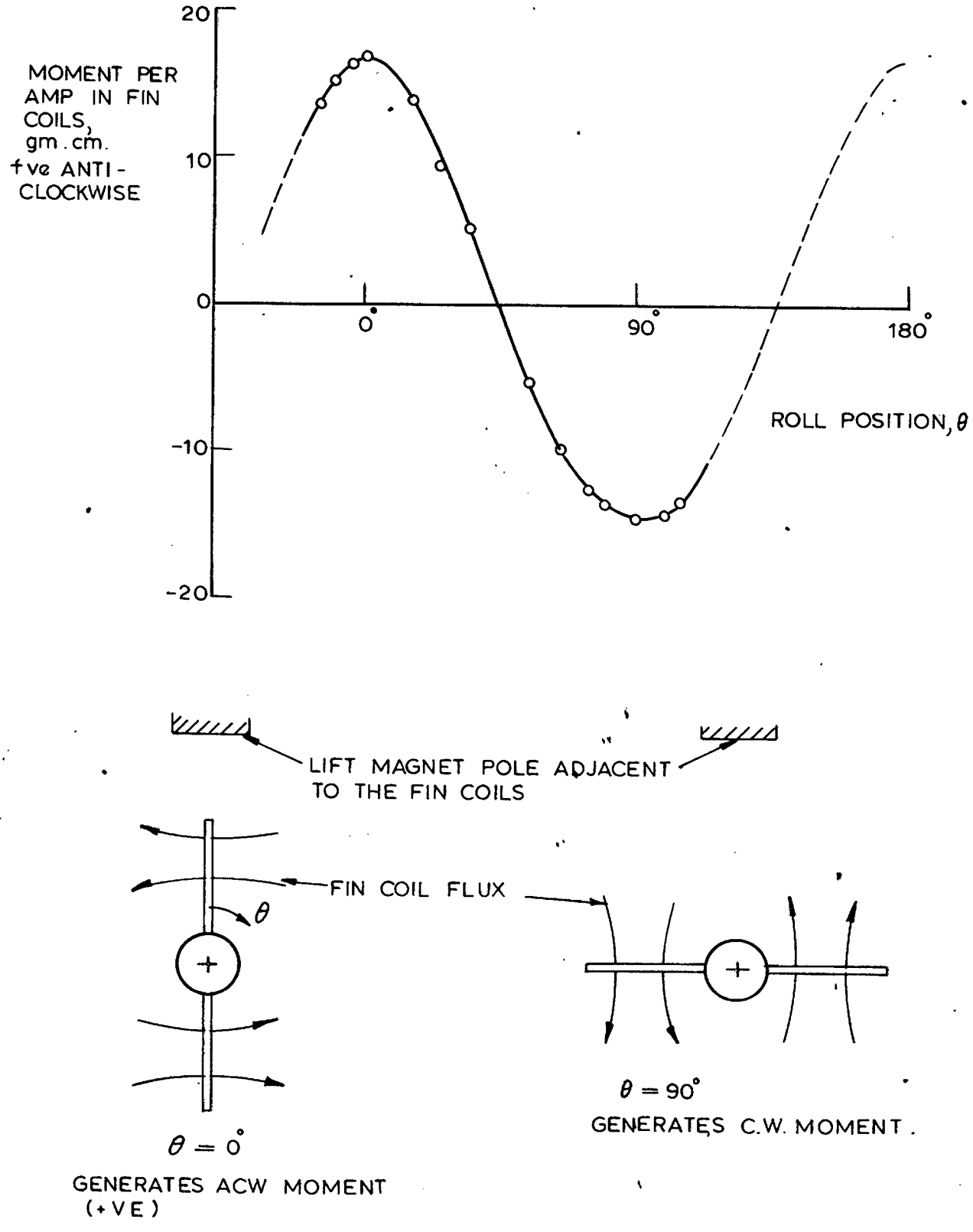

Fig 6.6 Moment generating ability of fin coils under the action of the lift electro-magnets. The lateral magnets are producing zero net field.

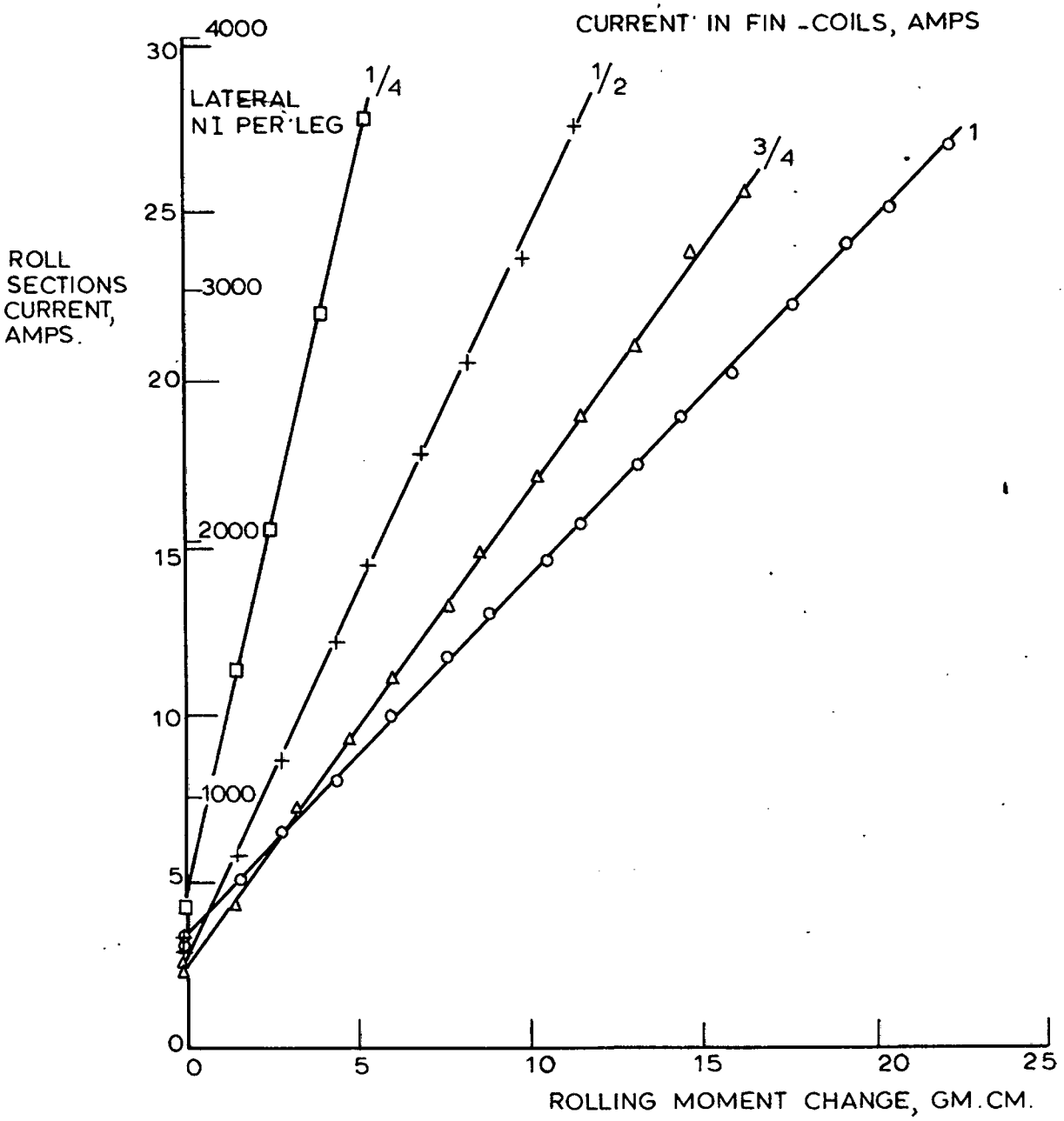

Fig. 6.7
Moment - roll sections current curves for coil-in-fin rolling moment generator .

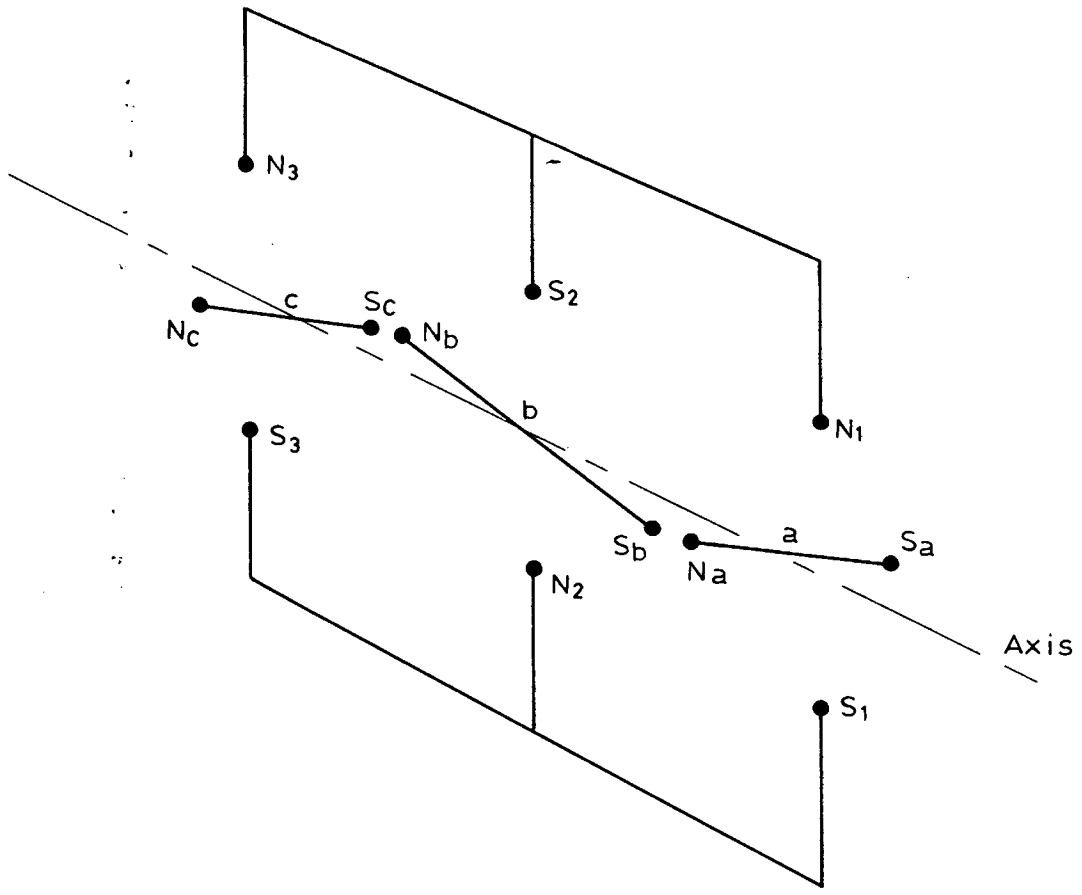

Fig. 6.8. A proposed roll control system using E-coils.

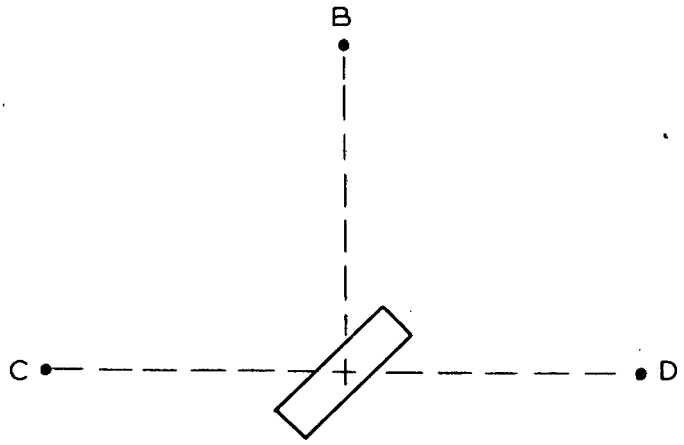

Fig. 6.9. A view along the axis of the model, taken in a plane through the upstream poles of the support and lateral horse-shoe electro-magnets.

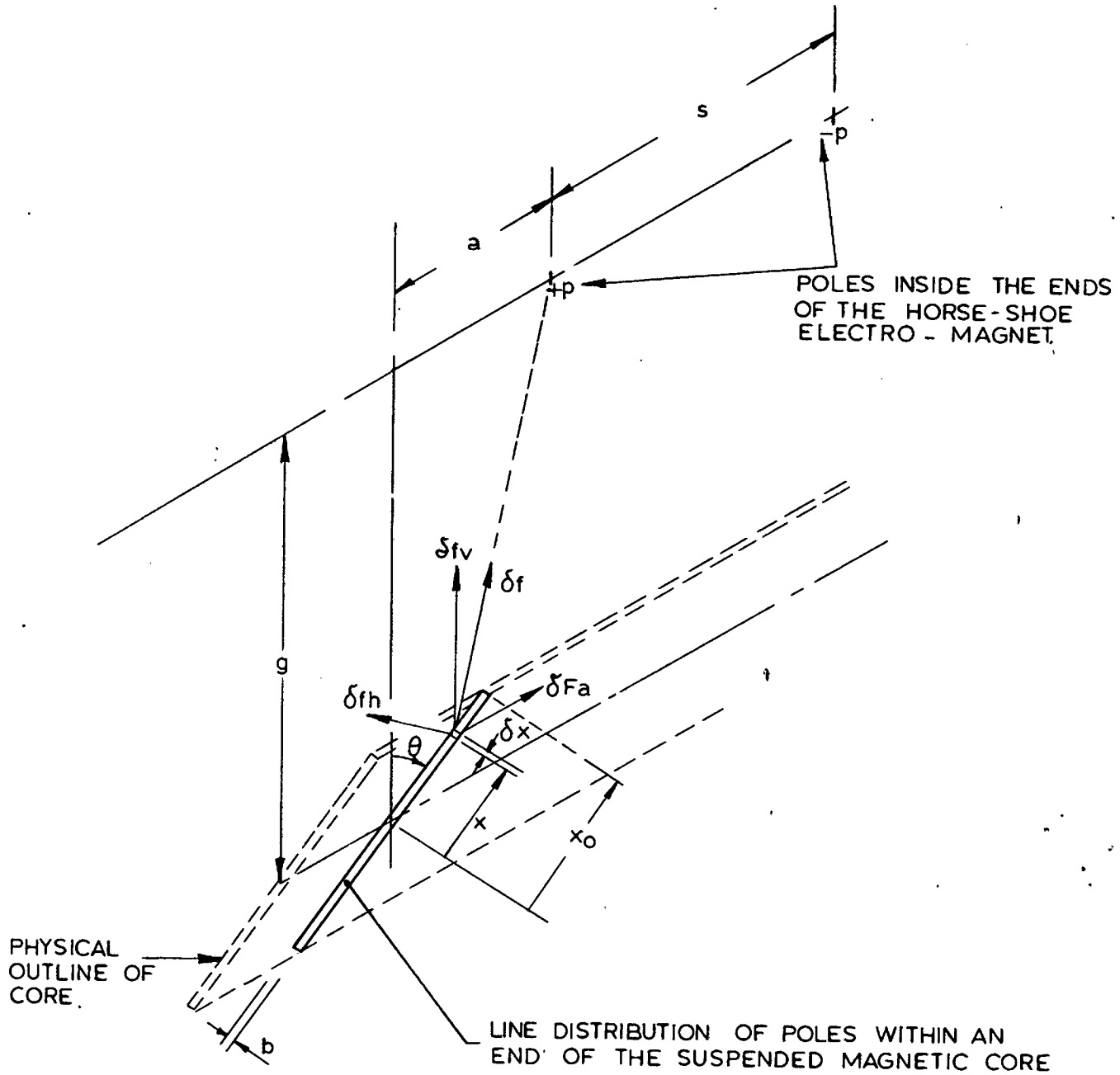

Fig 6.10 The "slender core" mathematical model.

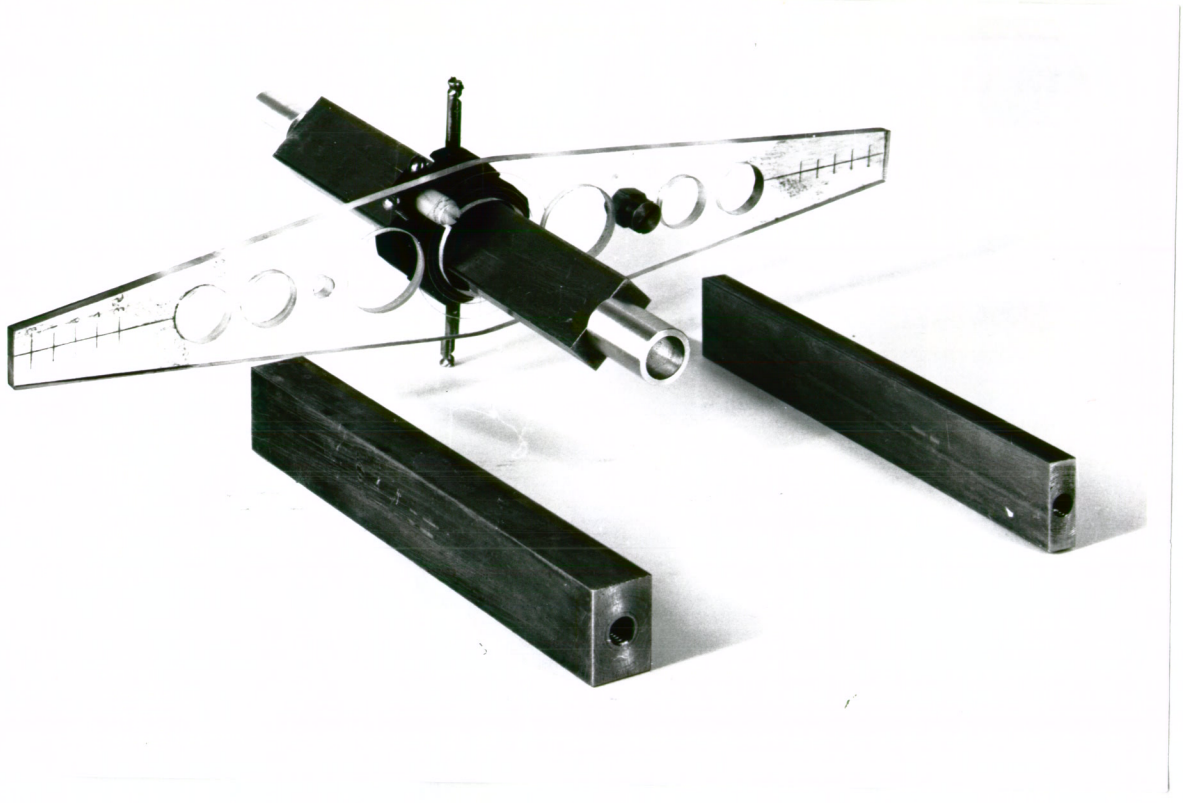

Fig. 6.11. A model which has been used for the measurement of the rolling moment capacity of Shaped Cores. A selection of cores stand alongside.

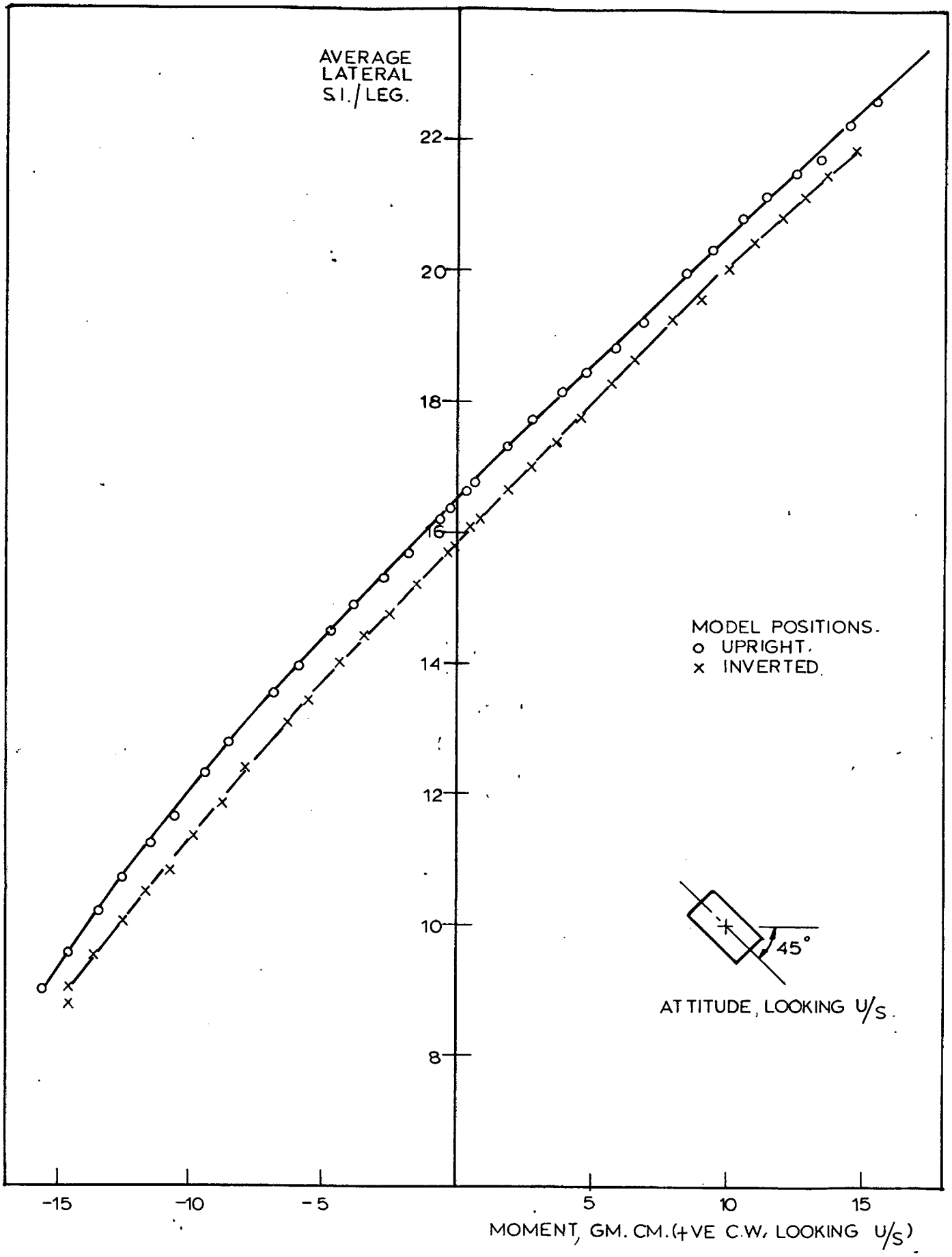

Fig. 6.12. Shaped - core moment curves.
Mild. steel core 5" long, cross-section $\frac{3}{4}" \times \frac{3}{8}"$

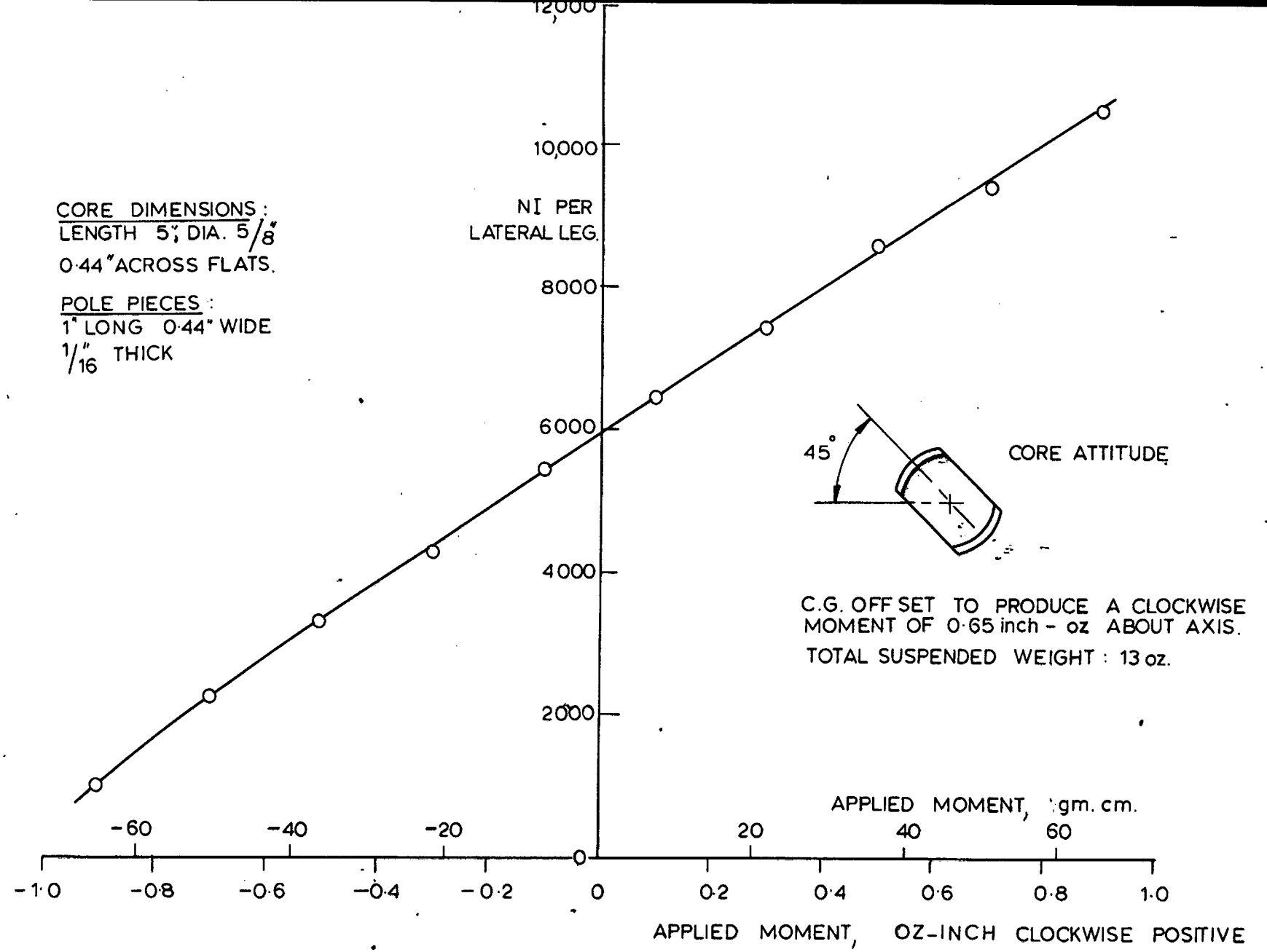

3.13 Applied moment - ampere turn curve for a mild steel "shaped core."

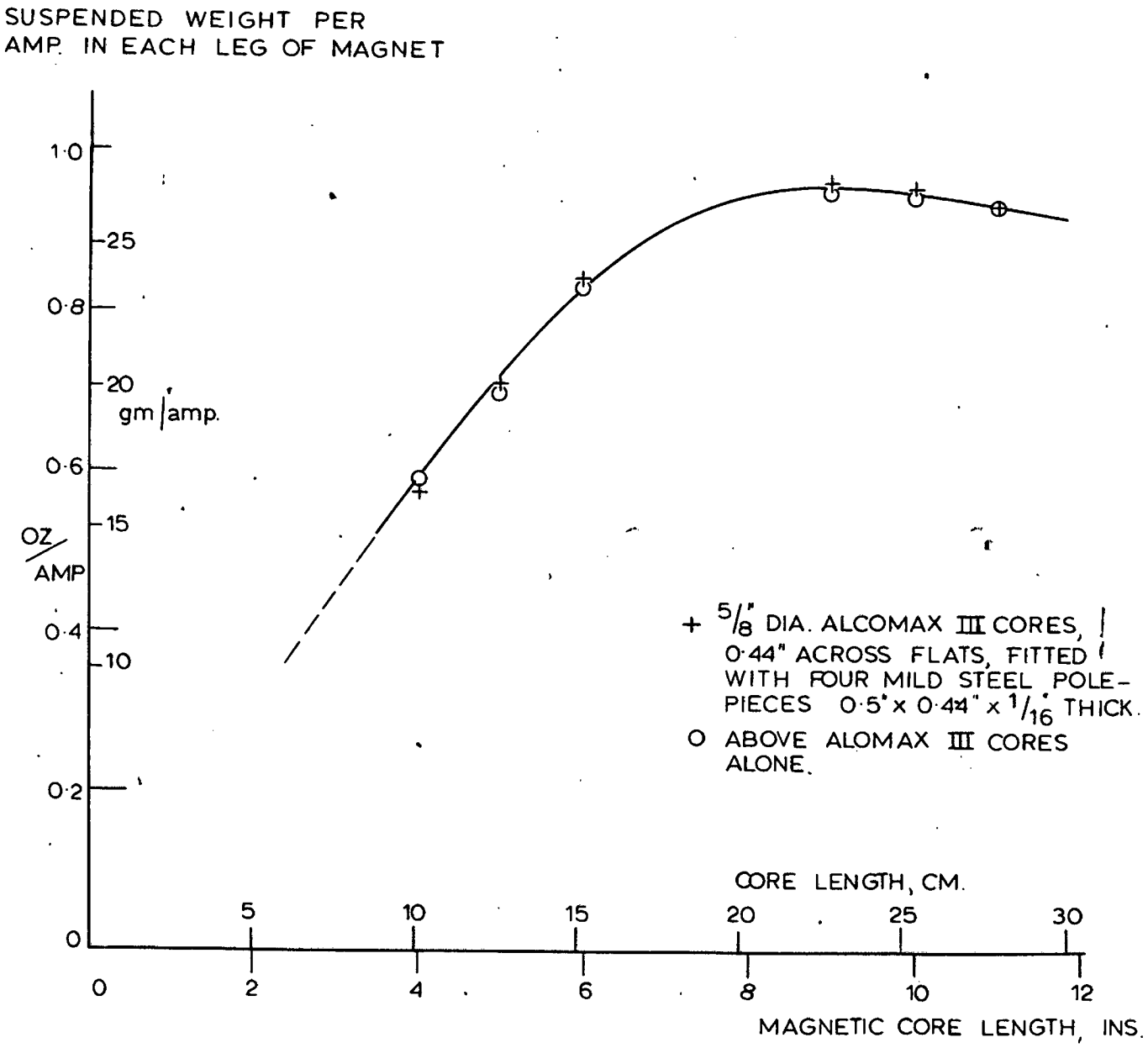

Fig. 6.14.
The variation of suspension current requirements with the length of the shaped magnetic core.

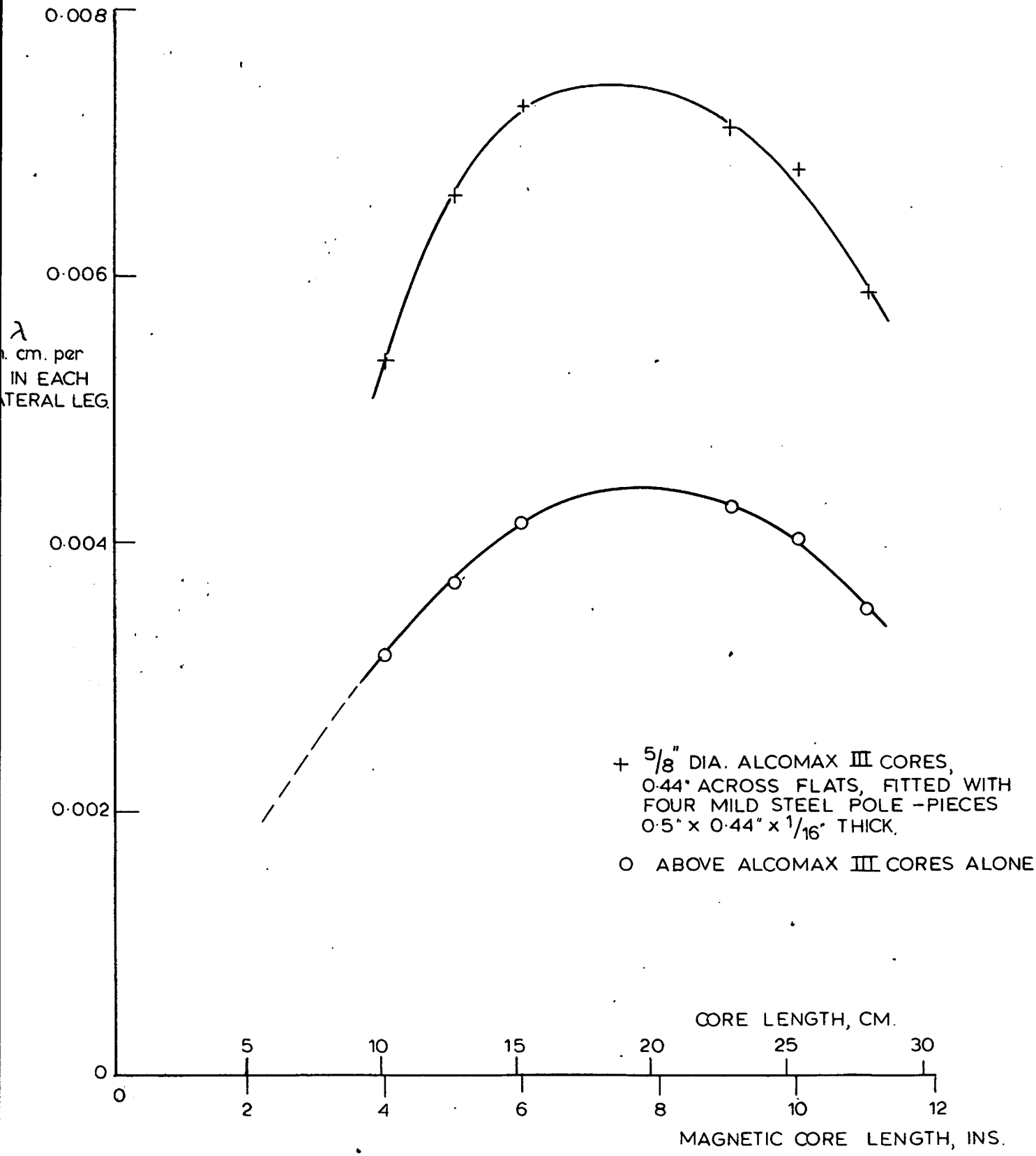

Fig. 6 15. The variation of λ with core length.

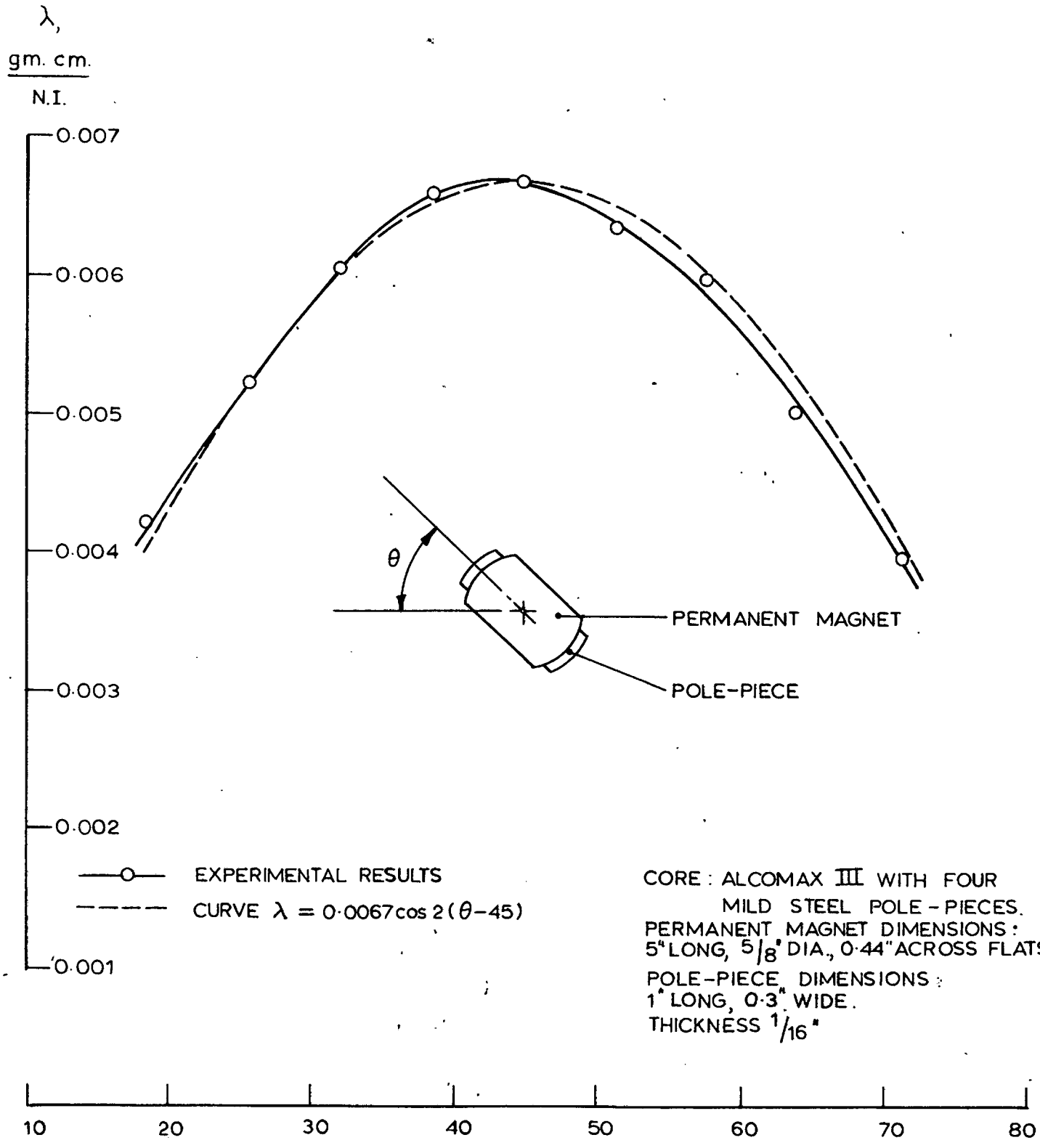

Fig. 6.16

The variation of λ with roll attitude θ for a "shaped core" roll control model.

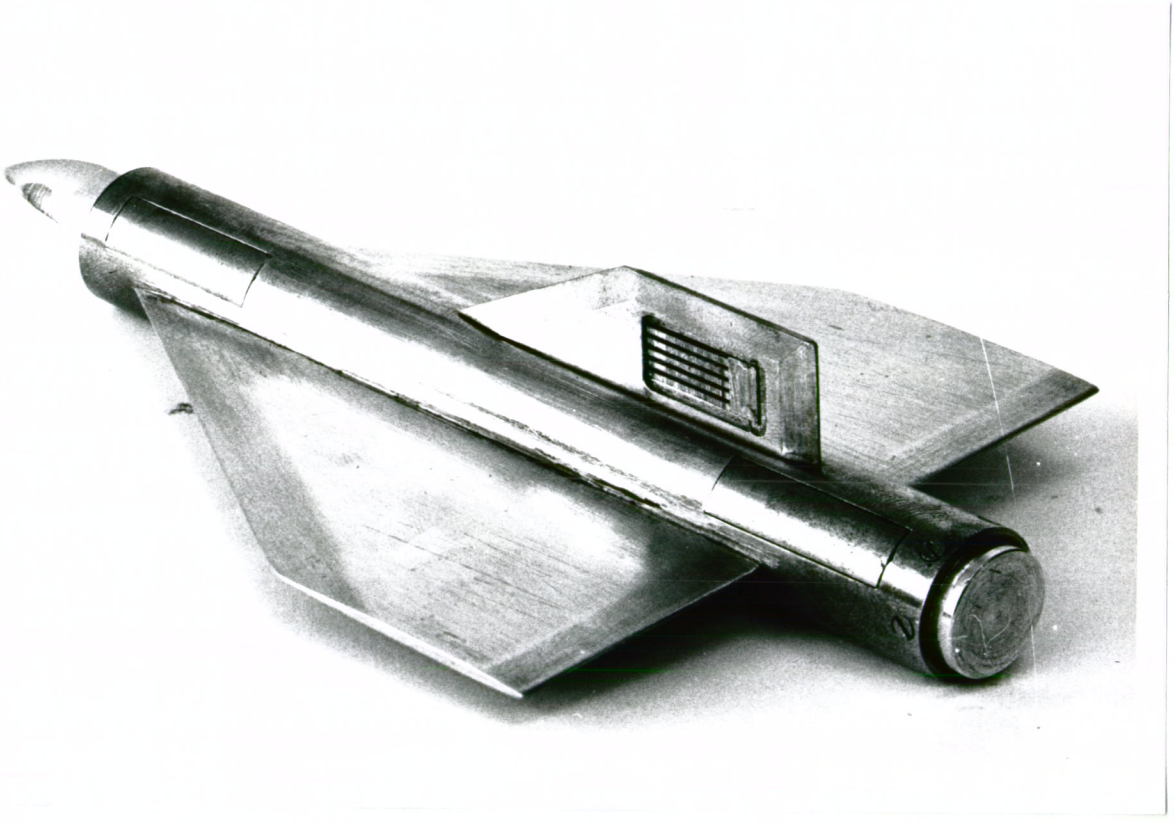

Fig. 6.17. A model adapted for suspension and control in six degrees of freedom.

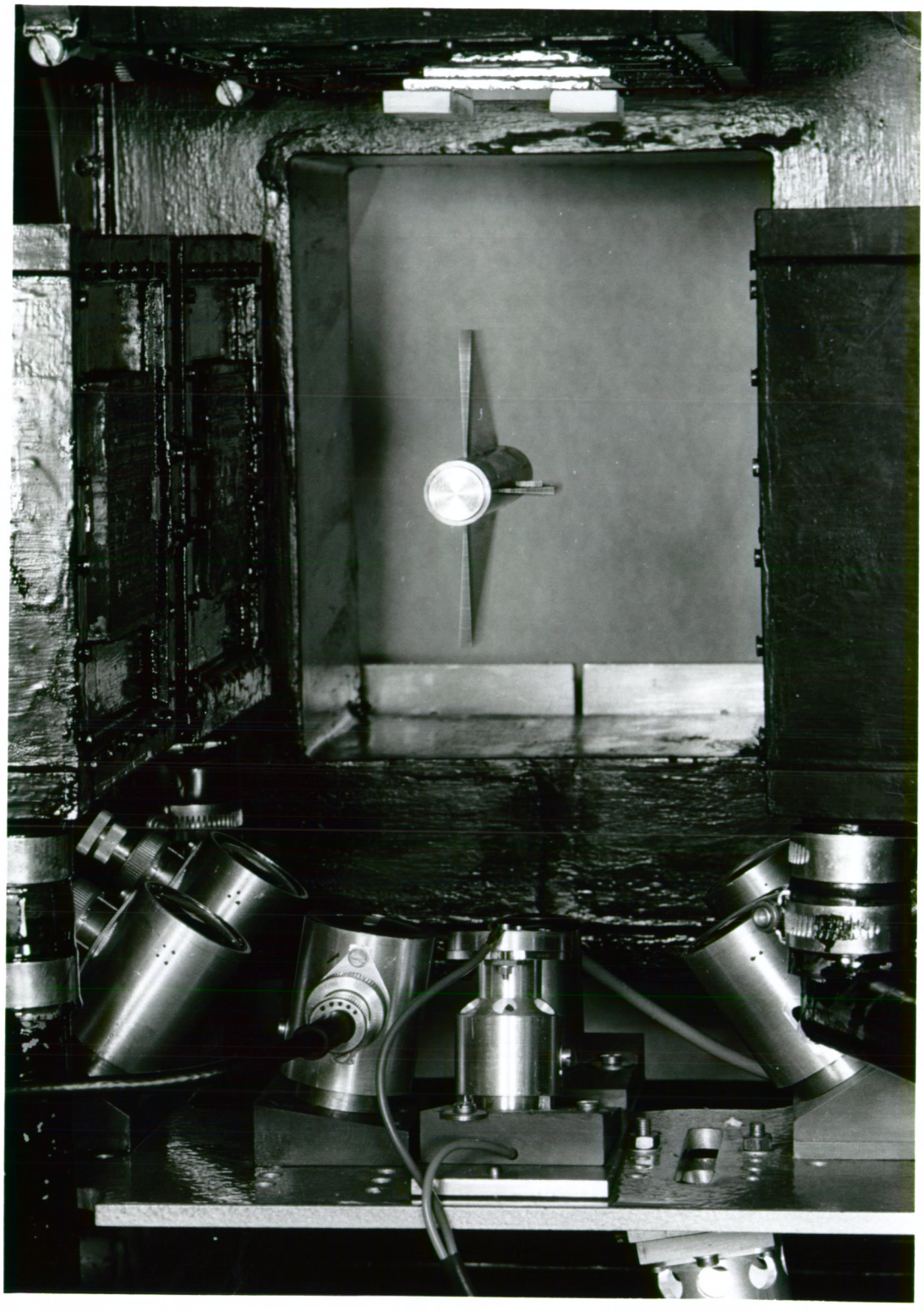

Fig. 6.18. A model subjected to a forced oscillation in roll while suspended in the six component balance.

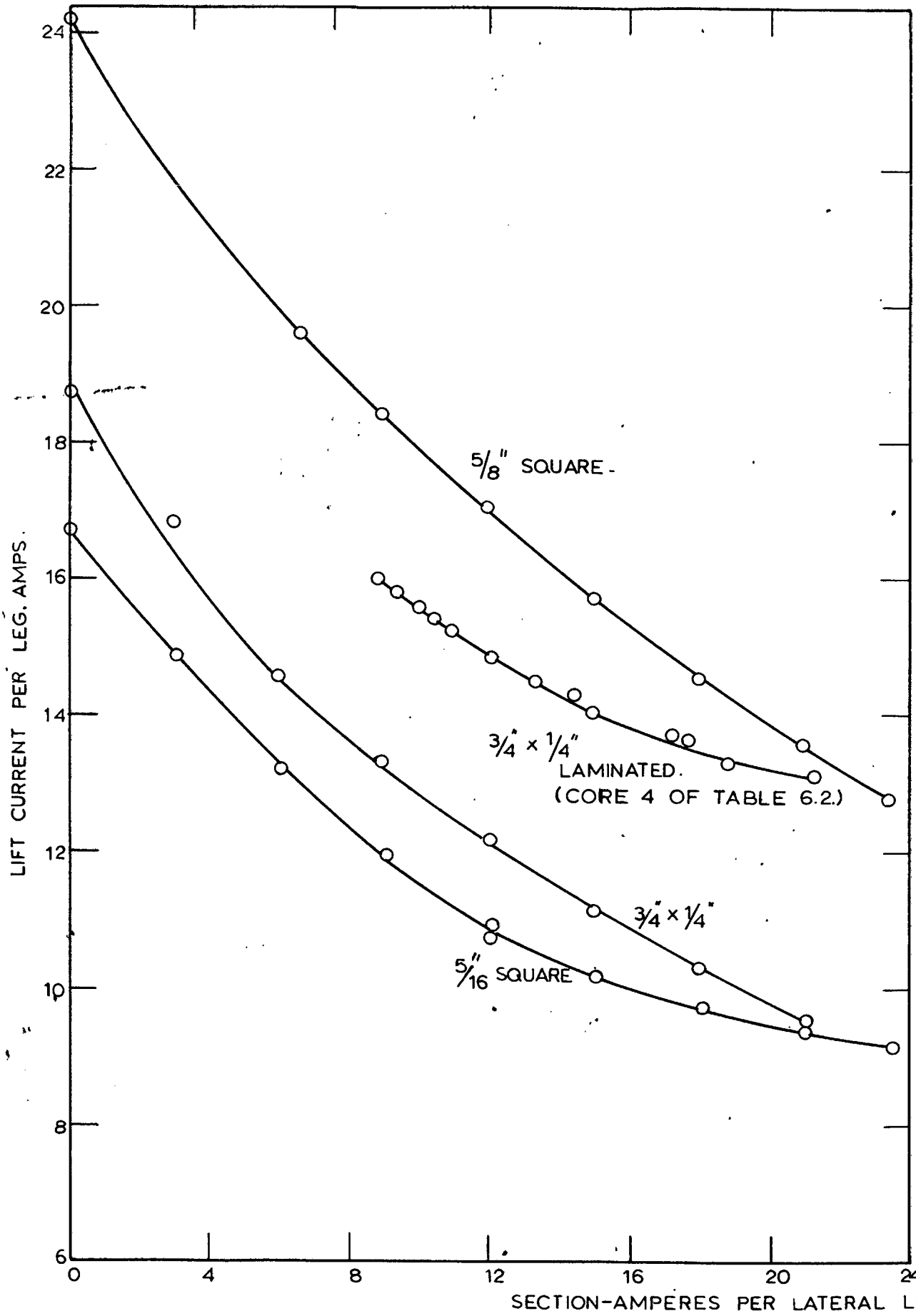

Fig. 6.19 Suspension currents for mild steel cores.

7. Control System Stabilisation.

A discussion of the techniques employed for stabilising models under magnetic suspension, and the characteristics of the six position control loops.

Contents:

7.1 Introduction.

The motions of the model must be automatically controlled in six degrees of freedom; for each of these a separate closed feedback loop is required. In addition to the model each loop consists of a model position sensor, position signal compensator, power supply and electro-magnet. Without signal compensation the closed feedback loops are inherently unstable when the natural damping of the model itself is low. This damping can be appreciable when the model is in an air stream. However, in still air the damping forces, which might arise from the generation of eddy-currents and from the air around the model, are low. The main de-stabilising feature of the feedback loop is the inductance of the electro-magnet which causes current changes to lag changes in applied voltage. If the lag could be made sufficiently small, then it might be possible to magnetically suspend a model without compensation, but in these circumstances the wind-off damping would be low: the motion of the model following a disturbance would

be a poorly damped oscillation. However, this is an over-simplification of the problem of model position stabilisation. In practice the motions of the model must be artificially damped by forces generated by the electro-magnet system, and the reasons for this will be shown in the following sections.

Many workers[1,2] in this field have reported on techniques for model stabilisation and control in up to 5 degrees of freedom. However, there are several reasons for discussing the subject further:

(a) the model was to be fully controlled in six degrees of freedom,

(b) the electro-magnet system produced unusual field gradients in the region of the model,

(c) solid-model resonances had previously been ignored,

(d) the tuned model required special consideration.

In the following sections, the stability problem is analysed and details of the stabilisation circuits are given.

7.2 The Component Transfer Functions.

For a theoretical assessment of model stability we require the various component transfer functions. The component parts of any one loop may be broken down into: the position sensor; the model; the magnetic fields; the coil; the power amplifier; the compensation circuits. In this section the general form of the transfer functions of all of these components except the compensation circuits are presented.

7.2.1 Model position sensors: For the detection of the motion of the model, optical systems are used, and these produce voltage signals which are proportional to model position. The sensors are designed to give an output corresponding with the normal position of the model, which selects the steady-state current level, and in writing down the

transfer function (T.F.) it is usual to use the change of signal output e_1 corresponding with a movement x of the model away from equilibrium

$$\text{i.e. the optical system T.F.} = \frac{e_1}{x}$$

and this is a constant over the frequency range of interest, namely D.C. to about 100 cycles/sec.

7.2.2 The model: The nature of the transfer function depends on the mode of motion being controlled and on the operating conditions of the model. We will begin by considering a simple case, that illustrated schematically on Fig. 7.1 (a). In this case, for this mode of motion, the model is not subject to any stiffness to ground, but there is some damping present represented by the dashpot producing a force $-c\dot{x}$ on the model, with the sign convention that upward directed force and motion are positive. Examples of the occurance of this mode are

(i) roll control

(ii) vertical motions in circumstances where roll is not being controlled, and the drag force is zero. In this case the damping coefficient is positive but small.

The T.F. is defined as $\frac{X}{F}$ (in the case of roll, on Fig. 7.1, x corresponds with an angle of roll, and the mass m with the rolling moment of inertia).

The equation of motion of this model is

$f = m\ddot{x} + c\dot{x}$ where f is the magnetic force applied to the model.

Using the notation $D = \frac{d}{dt}$, $f = (mD^2 + cD)x$

from which the T.F. is given by $\frac{x}{f} = \frac{1}{mD^2 + cD}$

If we consider sinusoidal variations in f, say $f = Fe^{j\omega t}$ giving a response $x = Xe^{j\omega t}$, then we may write $j\omega$ for D giving

$$\frac{X}{F} = \frac{-1}{m\omega^2 - cj\omega} = \frac{m\omega^2 + cj\omega}{m^2\omega^4 + c^2\omega^2} \qquad \text{7.1}$$

For any value of c, $\frac{X}{F} \to 0$ as $\omega \to \infty$.

For $c = 0$, $\frac{X}{F} \to -\infty$ as $\omega \to 0$, but in general c will not be zero, in which case the real (in-phase) part of the response will tend to the finite value $\frac{X}{F} = -\frac{m}{c^2}$ as $\omega \to 0$, and the quadrature component of the response tends to $-\infty$. The locus of each of the cases $c = 0$ and positive c are shown schematically on Fig. 7.1 (a) for the frequency range from near zero to infinity.

The second case, shown on Fig. 7.1 (b), is more common in a magnetic suspension system, and is different from the first in having some stiffness to ground, represented schematically by the spring of stiffness k. The stiffness has two sources:

(i) aerodynamic stiffness, which could be positive or negative

(ii) magnetic stiffness, positive with this suspension system.

This latter stiffness is complicated, in that it can vary between modes of motion, and can also vary wind-on to wind-off, and it arises as a result of a tendency for the model to align itself with the electro-magnets. For example, a model which is just suspended beneath the lift magnet, with none of the other magnets operating, will align itself along the wind-tunnel axis. If moved bodily to one side and released, the model oscillates with a lateral heaving motion typically at 1½ cycles per second. When released from a

position rotated away from equilibrium in a horizontal plane, the model oscillated about a vertical axis through its centre at a frequency which was typically 3 cycles per second. The stiffnesses are explained in the sketches below.

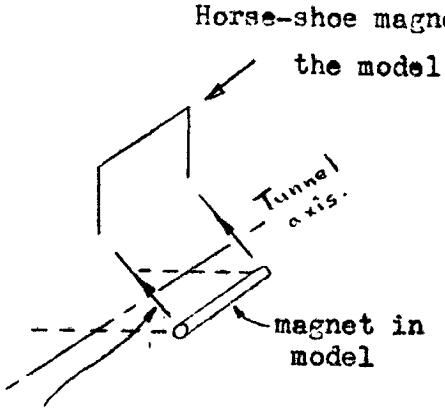

Horizontal components of these forces produce a heaving motion.

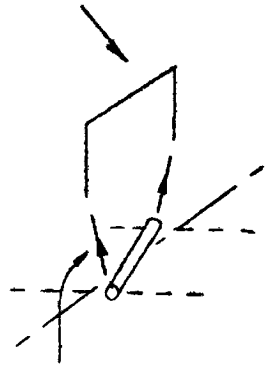

Horizontal components of these forces produce a pitching motion.

Displacement in combined pitch and heave result in lightly damped combined oscillations at the same frequencies, and it would appear that the two motions can exist separately.

There is a similar tendency for alignment in the rotary sense with the field from the drag coil, and at the higher drag forces that are available the natural frequency of rotation of the model can rise to around 7 cycles per second.

The origin of the stiffness in a rotary sense from the drag coil can be explained by considering the drag coil to be a bar-magnet on the tunnel axis, attracting the model. The forces which appear

when the model is displaced are explained in this sketch:

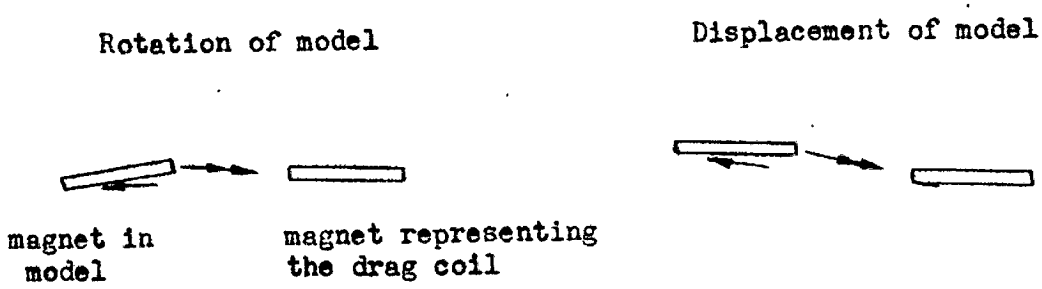

The displacement of the force vectors, coupled with their opposite directions produces an appreciable moment on the model, but only a small vertical force.

These various stiffnesses must be taken into account when considering the stability of motions in the horizontal plane.

Consider now motions in the vertical plane, and the sources of magnetic stiffness affecting these motions. Under wind-off conditions, the drag coil force is zero, and similarly the force from the lateral magnets (in both cases this assumes that the model is resting in its equilibrium position, on the tunnel axis). With wind-on, there will be a rotary stiffness from the drag coil field, and there could be a significant lateral aerodynamic force on the model. In the case of an L-type of suspension system, the production of a lateral force would result in stiffnesses in rotation and heave in the vertical plane through the model axis: the mechanism is identical to that already described for horizontal motions under the action of the

lift magnet. However, with a symmetrical pair of lateral magnets operating on the push-pull system, the positive stiffness produced by the magnet attracting the model is cancelled by a negative stiffness produced by the magnet repelling the model. Consequently, a force or moment in the horizontal plane produced by a symmetrical pair of lateral horseshoe electro-magnets has no effect on the stiffnesses in the vertical plane. A rolling moment generated by the lateral magnets does produce positive stiffness in the vertical plane, because for the purpose of producing the rolling moment both lateral horseshoe magnets are arranged to attract the model .

The remaining motion which is affected by magnetic stiffnesses is that of motion along the tunnel axis, controlled by the drag coil. The tendency of the model to centralise itself under the lift magnet is one source of stiffness in this direction. Additionally, forces from the lateral pair of magnets used for the purposes of roll control increase the stiffness (with an L-type of suspension system, the production of a lateral force would result in additional fore-and-aft stiffness, but this is not the case with an $\perp$ - type of magnet arrangement).

The equation of motion for a mode having stiffness to ground is

$$m D^2 x + c D x + k x = F$$

where k is defined on Fig. 7.1 (b)

from which $$\frac{X}{F} = -\left\{\frac{m\omega^2 - k + cj\omega}{(m\omega^2 - k)^2 + (c\omega)^2}\right\} \qquad \text{7.2}$$

With $c = 0$, $\frac{X}{F} \rightarrow \pm \infty$ at the natural frequency ω_0 defined by $m\omega_0^2 = k$; $\frac{X}{F} = \frac{1}{k}$ at zero frequency, and

$\frac{X}{F} \rightarrow 0$ as $\omega \rightarrow \infty$. The locus is shown as a broken line on Fig. 7.1 (b).

With positive damping, the response at ω_o is no longer infinite: the real (in-phase) component is zero, but the complex (in quadrature) component is $-1/c\omega_o$, giving the response locus shown on Fig. 7.1 (b) as a continuous line.

The magnitude of the response at the resonant frequency is sensitive to changes of damping, in lightly damped systems, and responses at the various resonant modes caused by the magnetic stiffnesses could be used in order to measure aerodynamic damping. However, the frequencies available are rather low in practice, particularly in the heaving modes, and the tuned model has been devised in order to provide a resonance at a higher frequency. A tuned model is shown schematically on Fig. 7.2 in one form, consisting of two separate masses connected by a spring of constant k, and with damping between the masses. A magnetic force f is shown applied to mass m_2 which therefore must be magnetic, and we assume mass m_1 to be non-magnetic.

The equations of motion of the system are given in Appendix I, and the solutions for this system with periodic exitation are

$$\left.\begin{aligned} \frac{X_1}{F} &= \frac{k + c\omega j}{m_1 m_2 \omega^4 - k\omega^2(m_1+m_2) - jc\omega^3(m_1+m_2)} \\ \frac{X_2}{F} &= \frac{k - m_1\omega^2 + j\omega c}{m_1 m_2 \omega^4 - k\omega^2(m_1+m_2) - jc\omega^3(m_1+m_2)} \end{aligned}\right\} \quad \text{——— 7.3}$$

The undamped ($c=0$) resonant frequency is given by

$$m_1 m_2 \omega^4 = k\omega_o^2 (m_1 + m_2)$$

from which $$\omega_o^2 = \frac{k(m_1+m_2)}{m_1 m_2}$$

Consider first the motion of mass 1, with $c = 0$.

As $\omega \to 0$, $\frac{X_1}{F} \to -\infty$. In the whole frequency range below resonance, $k(m_1 + m_2) > m_1 m_2 \omega^2$ and $\frac{X_1}{F}$ is negative, and similarly above resonance $\frac{X_1}{F}$ is positive.

The minimum response in the frequency range below resonance is given when $|m_1 m_2 \omega^4 - k\omega^2(m_1 + m_2)|$ is a maximum, and this occurs when

$$\omega^2 = \frac{k(m_1 + m_2)}{2 m_1 m_2} = \omega_0^2/2$$

and at this frequency

$$\frac{X_1}{F} = \frac{-4 m_1 m_2}{k(m_1 + m_2)^2}$$

Above resonance, the response locus is a line from $+\infty$ at ω_0 tending to zero as $\omega \to \infty$. The undamped response locus is shown as a broken line on Fig. 7.2 (a).

With finite damping, the response $\frac{X_1}{F}$ tends to $-\infty$ as $\omega \to 0$ and to zero as $\omega \to \infty$. The usual case is positive damping, and in these circumstances the imaginary part of the response is positive in the whole range $0 < \omega < \infty$. The locus of the response with positive damping is also shown on Fig. 7.2 (a) as a continuous line. The response is characterised by a phase which changes rapidly with frequency near resonance, with light damping.

Now consider the response of the mass m_2 to the applied periodic force f, initially with $c = 0$. $\frac{X_2}{F} = \pm\infty$ at ω_0, and as $\omega \to 0$, $\frac{X_2}{F} \to -\infty$. In the range $0 < \omega < \omega_0$ there is a frequency given by $k = m_1 \omega_a^2$ where the response is zero (the anti-resonance). In the frequency range $0 < \omega < \omega_a$ the response

is negative; in the range $\omega_a < \omega < \omega_o$ the response is positive, and in the range $\omega_o < \omega < \infty$ the response is negative again, giving the locus shown as a broken line on Fig. 7.2 (b).

With positive damping, it can be shown that the imaginary part of the response $\frac{X_2}{F}$ is always negative, and is zero at $\omega = 0$ and $\omega = \infty$, and similarly the real part of the response is $-\infty$ at $\omega = 0$ and zero at $\omega = \infty$. At the undamped natural frequency ω_o the real part of the response is negative, and the locus of the response $\frac{X_2}{F}$ of a damped tuned model is shown as a continuous line on Fig. 7.2 (b).

The example of a tuned model which has been considered above is a relatively simple case, which could occur in practice, for example it would closely represent a model tuned in the rolling mode when suspended wind-off. However, the most general case is that shown schematically on Fig. 7.3. The force is shown applied to mass 2 (magnetic), and mass 1 is non-magnetic. The response of mass 1 to the periodic force f is given by

$$\frac{X_1}{F} = \frac{A + Bj}{C + Dj} \qquad \text{7.4}$$

where $A = k_1$; $B = c_1\omega$

$$C = m_1 m_2 \omega^4 - \omega^2\left[m_1(k_1+k_2) + m_2(k_1+k_3) + c_1c_2 + c_2c_3 + c_3c_1\right] + k_1k_2 + k_2k_3 + k_3k_1$$

$$D = \omega\left[c_3(k_1+k_2) + c_2(k_1+k_3) + c_1(k_2+k_3)\right] - \omega^3\left[m_2(c_1+c_3) + m_1(c_1+c_2)\right]$$

Undamped resonance occurs when $C = 0$, giving a quadratic in ω^2 and two resonant frequencies. In practice the closest that can be approached to undamped conditions is suspension with the wind off, and if the model is constructed with the magnet (mass 2) spring-mounted inside a shell (mass 1) forming the aerodynamic shape of the

model, then k_3 is an aerodynamic stiffness which will be zero wind-off. In this case the undamped natural frequencies are given by

$$m_1 m_2 \omega^4 - \omega^2 (m_1 k_1 + m_1 k_2 + m_2 k_1) + k_1 k_2 = 0$$

where k_1 is the stiffness of the spring connecting the masses and k_2 is a magnetic stiffness.

Between resonances, the minimum undamped response of mass 1 occurs at a frequency given by $\omega^2 = \dfrac{k_1 (m_1 + m_2) + k_2 m_1}{2 m_1 m_2}$

At zero frequency $\dfrac{X_1}{F} = \dfrac{1}{k_2}$, and at infinite frequency $\dfrac{X_1}{F} = 0$

However, with this type of model the situation where all sources of damping can be assumed zero does not arise. In particular, the internal spring k_1 itself appears to introduce some damping which is present at all times. Wind-off, the damping c_3 is usually very low (measured values are given in Appendix III) and can be ignored, and similarly c_2 wind-off or wind-on with the model arrangement described above. Under wind-off conditions this leaves a model system consisting of the two masses, springs k_1 and k_2 and damping c_1. The responses $\dfrac{X_1}{F}$ and $\dfrac{X_2}{F}$ are given on Fig. 7.3. Consider first the response $\dfrac{X_1}{F}$. At zero frequency, the movement of m_1 is in-phase with the force (and $\dfrac{X_1}{F} = \dfrac{1}{k_2}$), and remains nearly so for low frequencies. As ω passes through ω_{oa}, the lower resonant frequency, there is a rapid change of phase from nearly in-phase through 90° lag to near anti-phase, and as ω passes through the upper resonant frequency ω_{ob} the phase changes rapidly from anti-phase to nearly in-phase. The frequency ω_ℓ marked on the response loci is the frequency at which the same model would resonate with the core locked to the outer shell.

The changes that occur with wind-on are due to the addition of the aerodynamic stiffness k_3 and the aerodynamic damping term c_3. The effects of these will be treated separately.

The addition of a positive stiffness k_3 has the effect of raising both resonant frequencies, and in addition to this the response at zero frequency is reduced to $\frac{1}{\left[k_2\left(1+\frac{k_3}{k_1}\right)+k_3\right]}$.

The main effects of the addition of a small value of positive aerodynamic damping $(+ve.\ c_3)$ are to reduce the amplitudes of the responses at frequencies near the two resonances.

The response of mass 2 to force f can also be written in the form (see Appendix I)

$$\frac{X_2}{F} = \frac{A + Bj}{C + Dj} \qquad \text{——————7.5}$$

where $A = k_1 - m_1\omega^2$; $B = \omega(c_1 + c_3)$

and C and D are as defined for equation 7.4.

The response locus will be described as applicable to the model arrangement described above, namely one comprising a non-magnetic shell m_1 containing a spring-mounted magnet m_2, with c_2 assumed zero. The characteristics of the wind-off response locus, where we assume $k_3 = c_3 = 0$ are similar to the locus of $\frac{X_1}{F}$ at frequencies up to anti-resonance at frequency ω_a. However, above this frequency the locus lies entirely in the lower half of the diagram and with light damping the two parts of the model move nearly in anti-phase.

The principal changes wind-on are as follows. With the addition of positive k_3, the resonant frequencies increase; with the addition of positive c_3 the response is generally reduced, particularly near the resonances ω_{oa} and ω_{ob}.

7.2.3 The power supplies. The characteristics of the power supplies expressed in transfer function form are simply a constant gain, for relatively small changes of output voltage about a mean level, and for frequencies which are well below the firing frequency of the rectifiers, at present 150 cycles per second. The upper limit to the forcing frequency for an acceptable output current waveform is about 25 cycles per second: over the frequency range from D.C. to 25 cycles per second, we assume that the power supplies give an output voltage e_3 which varies in direct proportion to and in phase with an input voltage signal e_2.

7.2.4 The coils. These have an inductance which can provide a significant lag in the frequency range of interest, and the transfer function can be expressed as

$$\frac{I}{e_3} = \frac{1/R}{1 + \tau j\omega} \qquad \text{——— 7.6}$$

where I = current

e_3 = e.m.f. applied to coil

R = coil circuit resistance

τ = coil circuit time constant

= L/R

L = coil inductance

and the phase lag is $\tan^{-1} \tau$. This lag can be reduced by increasing the circuit resistance by adding series resistance, but the steady-state power and voltage requirements increase in direct proportion to R and a compromise has to be adopted which does in fact result in the circuit having an appreciable time constant.

7.2.5 The electro-magnet force-current relationships. The force f between any given electro-magnet and model is a function of the current i supplied to the coil and a measure of the separation of coil and model y ,

$$\text{i.e.} \quad f = \phi(i, y)$$

Linearising for small changes we have

$$\delta f = \left(\frac{\partial f}{\partial i}\right)_y \delta i + \left(\frac{\partial f}{\partial y}\right)_i \delta y \qquad \text{——— 7.7}$$

For a permanent magnet model and an air-cored solenoid, or a solenoid having an unsaturated iron core and an appreciable air gap in its magnetic circuit, $\left(\frac{\partial f}{\partial i}\right)_y$ is a constant for all values of i , whereas for small changes in y

$$f \propto \frac{1}{y^n} \text{ at constant current,}$$

where $n > 2$ and can be assumed constant.

Then $\left(\frac{\partial f}{\partial y}\right)_i \propto \frac{-1}{y^{n+1}}$ a constant for small changes in y. However, $\left(\frac{\partial f}{\partial y}\right)_i$ is also directly proportional to current for the magnet system which is considered here, and equation 7.7 may be rewritten

$$\delta f = b_1 \delta i + b_2 \delta y \qquad \text{——— 7.8}$$

where $b_1 = \left(\frac{\partial f}{\partial i}\right)_{\bar{y}}$, $b_2 = \left(\frac{\partial f}{\partial y}\right)_{\bar{i}}$

and $\bar{y}, \bar{i}$ are the datum values of y and i .

The surface relating f to i and y is, in schematic form:

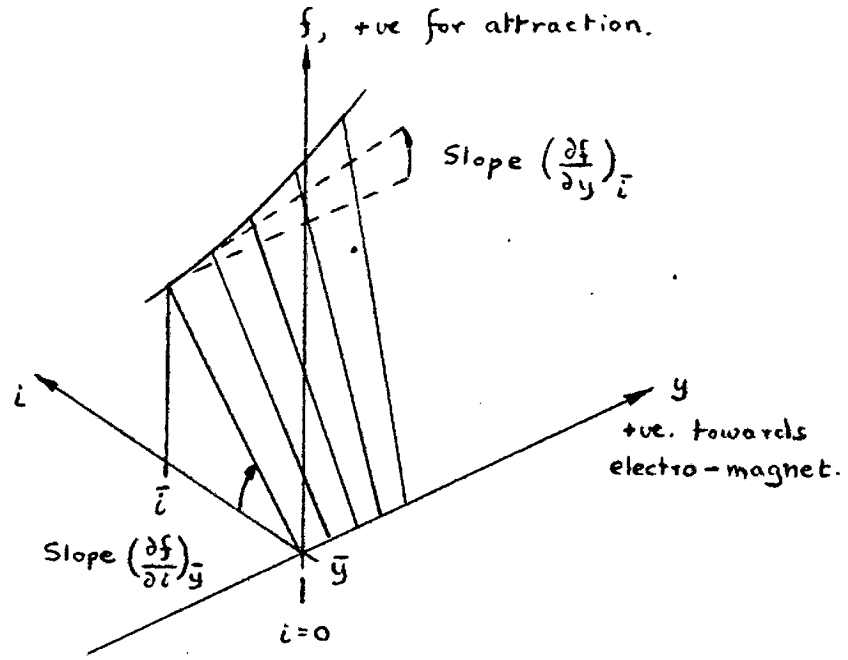

. The positive value of $\left(\frac{\partial f}{\partial y}\right)_{\bar{i}}$ has the effect of a negative spring stiffness in the system, a negative stiffness caused by the field gradient. This can be shown by combining a model transfer function as derived in Section 7.2.2 which will be written now as

$$\frac{X}{F} = \phi(j\omega) \qquad \text{_____7.9}$$

with the electro-magnet force-current relationship given by equation 7.8.

In combining these two relationships, equation 7.8 is now re-written in the form

$$f = b_1 i + b_2 \bar{i} x \qquad \text{_____7.10}$$

where f = increase of force from a datum value, taken as positive when the electro-magnet is attracting the model

i = increase of current from the datum value

x = change of model position from the datum position $\bar{y}$, motion towards the electro-magnet taken as positive,

and b_1, b_2, $\bar{i}$ are as previously defined, and are positive.

Substituting for F from equation 7.10 into 7.9 and re-arranging we have

$$\frac{X}{I} = \frac{b_1}{\frac{1}{\phi(j\omega)} - \bar{i}\, b_2} \qquad \text{7.11}$$

Taking now the simple case of a solid model with a positive field stiffness and with zero damping (equation 7.2 with $c=0$)

$$\phi(j\omega) = \frac{-1}{m\omega^2 - k}$$

then

$$\frac{X}{I} = \frac{-b_1}{m\omega^2 - k + \bar{i}\, b_2}$$

where $\bar{i}\, b_2$ appears as a constant term of opposite sign to the positive spring stiffness k. Consequently, with the electro-magnet attracting the model, the field gradient effectively applies a spring of negative stiffness to the model. Conversely a magnet repelling the model would produce a spring of positive stiffness, and in the case of a model placed mid-way between a pair of similar electro-magnets, one attracting the model and one repelling, the effects of the field gradients cancel.

7.3 <u>The Compensation Circuits and Loop Nyquist Plots</u>.

The transfer function of the compensation circuit must be chosen to stabilise an otherwise unstable closed control loop. Of the various transfer function forms so far considered, only the T.F. of the model varies fundamentally from one controlled degree of freedom to another. However, because of these variations coupled with the different component constants (for example: inductance, optical system gain), the required characteristics of the compensation circuits also vary and each degree of freedom must be considered separately.

In the calculation of the various transfer functions, it is necessary to draw on a great deal of data, and it is not convenient to describe the method of derivation of this data in this section. For the detailed information refer to the following sections:

The constant b_1 for some models, Chapter 5.

Optical system performance, Chapter 8.

Coil resistances, inductances, the constant b_2 for some coil : model combinations, and the field stiffnesses, Appendix III.

In the following sections of this Chapter, details are given of the six independent control systems which have been developed, and the open loop responses are estimated.

7.3.1 The lift magnet system. Models which are not tuned in this mode of motion will be considered, suspended in conditions where field stiffnesses are negligible. The situation is appropriate to a model suspended wind-off, without roll control.

The lift electro-magnet is horseshoe shaped, with a separate winding on each leg. The theoretical approach is to assume that each leg can be treated separately as a one degree of freedom system and supports half of the model weight.

Each lift magnet control loop consists of:

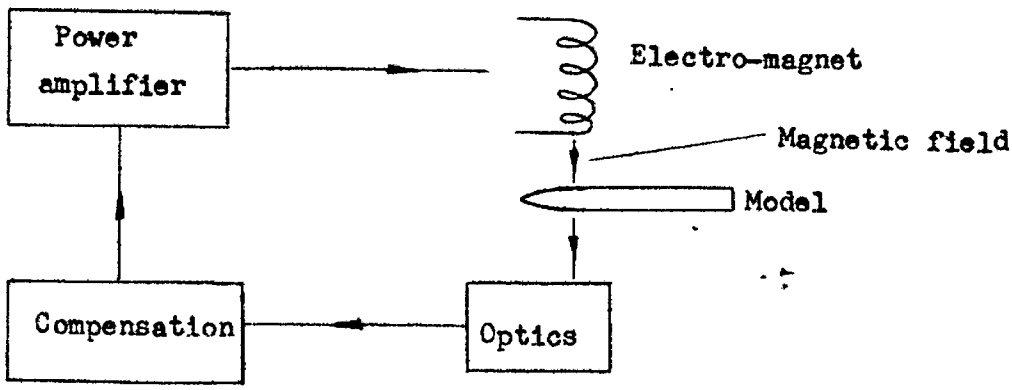

A schematic diagram showing the transfer function $\frac{X}{F}$ for a lightly damped model combined with the field gradient effect is shown on Fig. 7.4 (a). The response of the current in the electromagnet to the e.m.f. generated by the power amplifier is shown on Fig. 7.4 (b) and these two T.F.'s are combined on Fig. 7.4 (c). The optical system and power amplifier merely change the gain of the system. It can be seen that the locus of the open loop response of Fig. 7.4 (c) results in an unstable system when the natural damping of the model is low as occurs in all degrees of freedom, wind-off. It is necessary to move the part of the locus near the -1 point anticlockwise on the diagram until it passes the other side of the -1 point. This operation is effected electrically by the compensation circuits, and the requirement is for some phase lead over part of the frequency range. The simple lead-lag circuit shown below has the required characteristics:

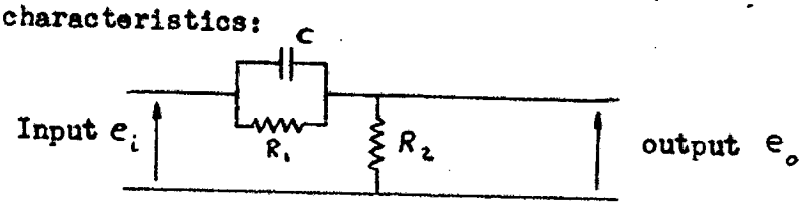

and the transfer function of this circuit is

$$\frac{e_o}{e_i} = a\left\{\frac{1 + \tau_1 j\omega}{1 + a\tau_1 j\omega}\right\} \quad \text{where} \quad a = \frac{R_2}{R_1+R_2} < 1$$

$$= \text{D.C. gain},$$

$$\text{and} \quad \tau_1 = R_1C.$$

The gain at $\omega = \infty$ is unity, and the phase lead at frequency ω is given by $\tan^{-1} \frac{\omega\tau_1(1-a)}{1 + a\tau_1^2\omega^2}$.

The locus of the response e_o/e_i is a semicircle as shown on Fig. 7.4 (d) and the maximum phase lead of $\sin^{-1}\frac{1-a}{1+a}$ occurs at

frequency $\omega = \frac{1}{\tau_1\sqrt{a}}$ where the gain is $\sqrt{a}$. In practice this lead-lag circuit has been combined with a feedback gain-stabilised operational amplifier to maintain sufficient loop gain.

With suitable choice of constants a and τ_1 in the lead-lag circuit, a suitable range of frequencies can be rotated in the Nyquist plot to give a stable model with the Nyquist plot shown on Fig. 7.4 (e), provided that the loop gain is set correctly.

Adjustment for loop gain is conveniently provided in the compensation circuits. The minimum value of gain is dictated by the zero frequency point on the locus passing the -1 point (at this condition there is insufficient gain to compensate for the field gradient); the maximum gain is dictated by the approach of the cross over point on the negative real axis to the -1 point. With a locus running very close to the -1 point the system damping is low.

The transfer functions of the components are as follows:-

(i) The model.

For the purpose of the analysis of the stability of the two degrees of freedom controlled by the lift magnets, the motion of the model is separated into a vertical heaving mode and a pitching mode about the horizontal axis through the model centre. As examples two models will be considered:

(i) A tuned model (see Fig. 13.5)

(ii) A body of revolution (see Fig. 10.3)

These models weigh respectively 9.14 oz. and 10.2 oz., and with c = o the transfer functions $\frac{X}{F} = \phi(j\omega)$ are respectively

$\frac{-1}{0.0056\,\omega^2}$ and $\frac{-1}{0.0098\,\omega^2}$ ft/lb. from equation 7.1, for the case of bodily heaving motions.

The field gradient effect is included by substituting these T.F.'s into equation 7.11 where the constants b_1 are respectively 0.023 and 0.0208 lb/amp. (see Chapter 5) at the normal model position (i.e. on the tunnel centre-line) and the constants $i b_2$ are respectively 1.86 lb/ft. and 2.05 lb/ft. The T.F.'s $\frac{X}{I}$ including field gradient effects, for heaving motion become respectively

$$\frac{-0.023}{0.0086\omega^2 + 1.86} \quad \text{and} \quad \frac{-0.0208}{0.0098\omega^2 + 2.05} \text{ ft/amp.}$$

The case of pitching motions of the model, pitching about the horizontal axis through the model centre, can be separately considered by assuming that each leg of the lift magnet provides half of the moment required to produce the angular accelerations. If we write the moment of inertia of the model about this axis as $2z$ and the angular displacement from the horizontal as ψ, then the moment about this axis per leg of the electro-magnet is $m = z\ddot{\psi}$ and ψ is related to the displacement of the model in the optical system by $\psi = x/\ell$ for small angles of displacement. For sinusoidal motions,

$$\frac{x}{m} = \frac{-\ell}{z\omega^2}$$

where ℓ is the distance from the pitching axis to the monitoring plane.

Referring to one end of the model and one leg of the lift magnet, the moment applied to the model by the electro-magnet is given by $m = a i$

where a is the calibration constant

and i is the coil current

The model transfer function for this mode of motion becomes

$$\frac{x}{i} = -\frac{\ell a}{z\omega^2}$$

The normal value for l for the two models considered in this section was approximately 0.2 ft., for the tuned model $Z = 1.391/10^4$ slug ft^2., and for the tuned model and lift magnets $a = 0.00433$ lb.ft/amp, hence the model transfer function becomes $\frac{x}{i} = \frac{-3.11}{\omega^2}$ for the pitching mode.

Note that the field gradient effects are of opposite sense for the two ends of the model in the case of pitching motion and can be ignored.

For the solid model the transfer function for pitching motion becomes $$\frac{x}{i} = \frac{-1.52}{\omega^2}$$

(ii) The electro-magnet current T.F. I/e_3.

The T.F. is given by equation 7.6 where the constants are $R = 2.61$ ohms and $\tau = 0.03$ sec.:

$$\frac{I}{e_3} = \frac{0.383}{1 + 0.03\,j\omega} \quad \text{amps/volt.}$$

(iii) The optical system.

The optical system in the lift-magnet control system has an output of 156 volts/ft. with the working section of the wind-tunnel in position, measured at the output of the summing amplifier shown on Fig. 8.1 (b), and the transfer function is $\frac{e_1}{X} = 156$ volts/ft.

(iv) The power amplifier.

Over the full range of the output from the power amplifier there is an appreciable variation of gain, as shown in Chapter 9, but in the normal working current region the variation of output voltage with input voltage is fairly linear with a slope of 54.6 hence the g ain of the power amplifier is taken as

$$\frac{e_3}{e_2} = 54.6$$

(v) The compensation circuit.

This circuit, providing gain adjustment for the loop in addition to the required phase-lead, has been developed to a point where it is suitable for suspending a wide range of models with permanent magnet or soft-iron cores. Normally the only adjustment that is necessary to maintain stability when changing models is the loop gain.

One of the requirements of a magnetic suspension system is a model which is held fairly rigidly in position, and this implies a requirement for a relatively high loop gain which in turn requires the phase lead of the compensation circuit to be high in the range of frequencies which give near unity open loop gain. The basic lead-lag circuit which has been described provides a fairly constant lead over a range of frequencies, but if this lead is high (approaching 90°) given by $\alpha \ll 1$, the ratio of the zero frequency gain to the infinite frequency gain $= \frac{1}{\alpha}$ is high. The low D.C. gain can be recovered by incorporating an amplifier in series with the loop as already mentioned, but the practical problem arises that any electrical noise in the loop ahead of the compensation circuit becomes strongly amplified. An alternative approach to obtaining a large lead-angle is to stage some lead-lag circuits in series (the theory is presented in Appendix II). In this way it is possible to reduce the ratio of infinite frequency gain to D.C. gain with any given overall maximum lead below 90°, or to increase the maximum lead beyond the 90° limit of a single stage. For the lift compensation circuits, two lead-lag stages are used in series, and in addition to these there is a simple low-pass filter included to reduce the high frequency gain. The filter introduces a phase lag into the circuit, but the time constant was chosen such that

the lag only became significant at high frequencies. To compensate for the low frequency attenuation of the lead-lag circuits, each has been followed by an operational amplifier having a gain with feedback of about 10.

The circuit for lift magnet loop stabilisation is shown on Fig. 7.5 (a) and the component values are given in Appendix III. The input is from the summing amplifier giving the vertical position signal of the model (the signal on Fig. 8.1 (b) shown as - (A+B)) and the first lead-lag stage and amplifier is C_1 with R_1 - R_3. This is followed by the low-pass filter R_4 with C_2 and then by the second lead-lag stage C_3 with R_5 - R_7. Loop gain variation is by adjustment of potentiometer R_9. Also shown on this circuit diagram is a voltage divider R_{11} which is arranged to feed a D.C. bias voltage into the compensation circuit output amplifier in order to bias the output voltage level. This allows for the selection of the required mean output current from the power amplifier.

The overall T.F. of this compensation circuit gives the locus shown below:

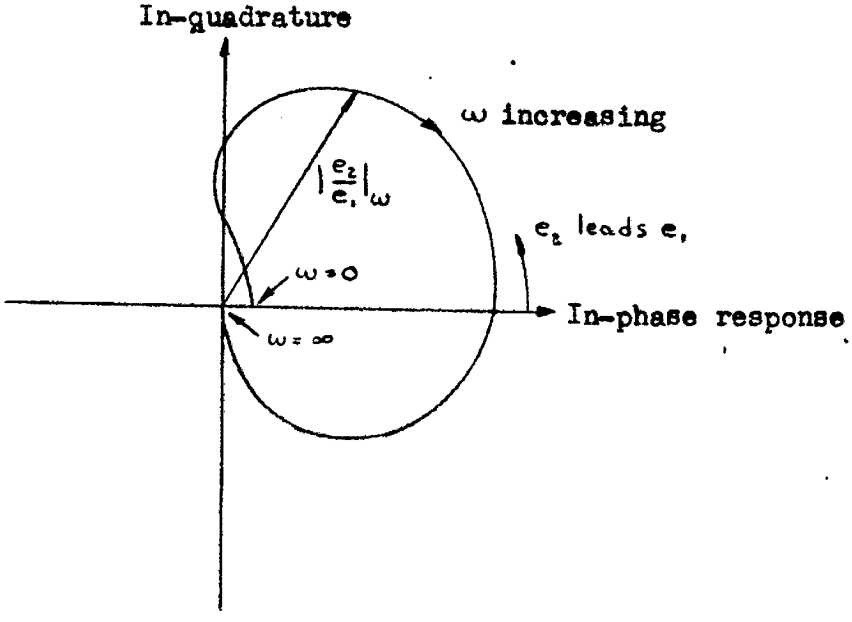

The measured gain and phase characteristics are plotted on Figs. 7.6 and 7.7 respectively at a gain setting suitable for the 10.2 oz. body of revolution. The phase lead provided by the circuit is greater than 90° over the frequency range 12 - 35 c.p.s., but above this range of frequency the lead falls rapidly towards zero if no filter is used and towards a 90° lag with the filter in circuit. The high frequency attenuation of the filter is also shown on Fig. 7.6, and is responsible for the loop in the lower right quadrant of the above sketch.

This completes the description of the component transfer functions involved in the lift magnet control system. In constructing the open loop Nyquist plot it is necessary to consider the complete frequency range from D.C. to infinity in order to be confident that the locus has the desired characteristics. However, in the case of the two lift control loops, at low frequencies involving phase angles where the approximation "sin lead = lead" is valid, and where the low pass filter is producing negligible lag, the net lead in the open control loop is given by

$$\omega \left(2\tau_1 - \tau \right) .$$

where $\tau_1 = 0.024$ sec.

and $\tau = 0.03$ sec.

Hence at low frequencies, there is always a phase lead and the Nyquist plot lies entirely in the lower left quadrant. At D.C. conditions the loop gain is

$$\frac{-b_1}{i b_2} \cdot \frac{1}{R} \cdot \frac{e_3}{e_2} \cdot \frac{e_2}{e_1} \cdot \frac{e_1}{X} = -85.5$$

Nyquist plots for the frequency range from 15 c.p.s. to 50 c.p.s. are shown on Fig. 7.8 for the two models pitching and

heaving, for a gain setting that in practice was suitable for the solid model but too high for the tuned model. The gain and phase margins are tabulated below:

	Heaving Mode		Pitching Mode	
	Gain Margin	Phase Margin	Gain Margin	Phase Margin
Solid Model	0.44	15°	0.57	20½°
Tuned Model	0.16	10½°	0.30	5½°

The gain and phase margins for the tuned models were too low, resulting in a poorly damped model, but a reduction of the loop gain has the effect of increasing the gain and phase margins, but also steady state errors. Note that the accuracy of the calculated margins quoted above depends on the accuracy with which the various transfer functions are known. The inductances of the coils in particular are doubtful, because the effects of mutual inductance between the two legs of the lift magnet have not been determined with any certainty.

With the loop closed, that is with a model suspended, the potentiometer R_{11} on Fig. 7.5 (a) becomes a model position adjuster. For example, suppose R_{11} was moved from the normal position giving the correct current output to suspend a model in the correct position in the wind tunnel, to a setting which resulted in a reduced current supply to the coil with the same position signal input to the compensation circuits. There would now be insufficient magnetic force to support the whole of the weight of the model, and it would move downwards until the input signal to the compensation circuits and hence power amplifier was restored to a level feeding sufficient current to the coil to support the model in its new position. The same procedure is used in order to oscillate the

model, by feeding an oscillating signal via a suitable resistor to the input of amplifier No. 3 on this diagram.

There are two useful measures of the quality of the performance of the closed loop. One is the steady-state stiffness of the suspension defined as applied force per unit displacement of the model away from equilibrium, and this can be measured by applying weights to the model and measuring the displacement, or it can be calculated from the measured characteristics of the components in the loop. However, the stiffness varies with model design and position, and both must be specified. The stiffness may be calculated as follows for bodily displacement:

$$\delta f = \left(\frac{\partial f}{\partial i}\right)_{\bar{x}} \delta i + \left(\frac{\partial f}{\partial x}\right)_{\bar{i}} \delta x \quad \text{(from equation 7.7)}$$

and $$\left(\frac{\delta i}{\delta x}\right)_{\omega=0} = -\frac{e_1}{x} \cdot \left(\frac{e_2}{e_1}\right)_{\omega=0} \cdot \frac{e_3}{e_2} \cdot \left(\frac{i}{e_3}\right)_{\omega=0}$$

and the stiffness is given by

$$-\frac{\delta f}{\delta x} = \left(\frac{\partial f}{\partial i}\right)_{\bar{x}} \frac{e_1}{x} \left(\frac{e_2}{e_1}\right)_{\omega=0} \cdot \frac{e_3}{e_2} \cdot \left(\frac{i}{e_3}\right)_{\omega=0} - \left(\frac{\partial f}{\partial x}\right)_{\bar{i}}$$

For the lift control system and solid body of revolution $\left(\frac{e_2}{e_1}\right)_{\omega=0} = 2.12$ using the gain setting of Fig. 7.6, $\left(\frac{i}{e_3}\right)_{\omega=0} = \frac{1}{R} = 0.383$ amp/volt,

$\frac{e_1}{x} \cdot \frac{e_3}{e_2}$ = 8500 volts/ft., $\left(\frac{\partial f}{\partial x}\right)_{\bar{i}} = \bar{i} b_2 = 2.05$ lb./ft.

and $\left(\frac{\partial f}{\partial i}\right)_{\bar{x}}$ = 0.0208 lb/amp.

from which the steady-state stiffness

= 141.7 lb/ft.

Another measure of the quality of the suspension of the model is the transient motion of the model following release from a position away from equilibrium. For the model to be acceptably steady when suspended in the wind tunnel and subjected to excitation

forces from turbulence in the air stream, the suspension system damping cannot be too low. To put a scale on damping, a damping ratio of 0.1 would in this context be regarded as low, the desirable range would be 0.3 to 0.6, and critical damping would be rather high. The Nyquist plot on Fig. 7.8 for the solid model would indicate a damping ratio of about 0.15, too low on the above scale. However, transient tests indicated somewhat higher damping, and the performance of the two suspension circuits has been adequate for the model test conditions encountered so far.

The changes that occur in the Nyquist plot when field stiffnesses are introduced are mainly evident at the low frequency end of the locus. As positive field stiffness is increased from zero, the zero frequency point moves further to the left of the diagram until a condition is reached where positive field stiffness (which can arise from the field generated by the drag coil and from the roll control sections on the lateral electro-magnets) balances the negative stiffness due to the gradient of the lift magnet field. At this condition the zero frequency point extends to $\pm \infty$, and further increase of field stiffness brings the point from $+\infty$ towards zero on the real (in-phase) axis. However, the line joining the steady-state point to the high frequency end of the locus is a large loop in the lower two quadrants. The shape of the locus at frequencies above about 20 c.p.s. is hardly affected by the level of field stiffnesses reached on this suspension system.

The different phase and gain margins which are calculated for a given model in each mode of oscillation suggest that there could be an optimum spacing in a fore-and-aft sense for the optical

monitoring system, giving superimposed Nyquist plots for the two modes of motion. Variation of the spacing (distance 2ℓ) will not affect the locus of the Nyquist plot for the heaving mode, or the stiffness of the suspension in this mode, but there would be the possibility of moving the plot for the pitching mode by means of a variation in ℓ. For example, in the case where the pitching mode plot had the lower gain and phase margins, the maximum loop gain would probably be dictated by the damping of this mode, whereas the heaving mode could stand a higher loop gain. A change of ℓ to achieve superposition would permit the loop gain to be increased resulting in the same Nyquist plot for the pitching mode as originally, but with increased stiffness in the heaving mode. Such a value of the spacing of the optical beams might be referred to as an optimum, and be identified by the symbol ℓ_o.

Ignoring field gradient and stiffness effects we have for the heaving mode $\frac{x}{I} = \frac{-b_1}{m\omega^2}$ and for the pitching mode $\frac{x}{I} = \frac{-\ell a}{z\omega^2}$. The remaining terms in the loop are common to the two modes, and hence for identical Nyquist plots the above T.F.'s must be identical, giving $\ell_o = \frac{b_1 z}{ma}$

For the tuned model, ℓ_o = 0.086 ft. giving a total distance between the planes of the monitoring systems of 2.06", and for the solid model the optimum distance would be 3.35". By adopting these values, and adjusting the loop gains, the stiffness in heave for the tuned model and the stiffness in pitch for the solid model could be increased.

It should be noted that these values of the spacings are only optimum for the lift magnet system; the optimum for lateral position control would in general be different, and the optimisation

of the spacing would be affected by any differences in the inductances of the coils under pitching and heaving modes.

7.3.2 Drag coil control system. The axial position sensor and power amplifier have constant gains (see section 3 of Chapter 8 and section 2 of Chapter 9 respectively) together giving a gain product of 968 volts/ft., and the coil circuit time constant and resistance give a transfer function

$$\frac{I}{e_3} = \frac{0{\cdot}69}{1 + 0{\cdot}05j\omega} \quad \text{amps/volt.}$$

leaving the compensation circuit and the field and model transfer functions to be considered. In this section the latter will be presented in combination for the tuned model, with account taken of the field stiffnesses in the fore-and-aft sense generated by the lift electro-magnets and the roll control sections of the lateral electro-magnets, at the normal steady-state current levels.

In determining the field gradient constant $\left(\frac{\partial f}{\partial x}\right)$ for the lift magnet it was possible to use a representative mean lift current which in practice was more-or-less constant, in the main being dictated by the model weight and magnetic core properties. However, in the case of the drag coil current there was no similar typical mean level, consequently two mean current levels have been chosen representative of the range of conditions so far encountered with the tuned model. The current levels correspond with drag forces of zero and $\frac{1}{4}$ lb., and are 0 and 25.4 amps respectively. The model transfer function is given by equation 7.2, but the measured natural damping coefficient c was very low (see Appendix III) in this degree of freedom wind-off as was the calculated value wind-on, and each have been taken as zero (i.e. $C = 0$ in equation 7.2). The locus of

the T.F. is shown schematically on Fig. 7.1 (b). Including the field gradient effect of the drag coil and the force-current relationship, both for the model in its normal position (centred between the lift and lateral magnet poles), the transfer function $\frac{X}{I}$ becomes

$$\frac{b_1}{m\omega^2 - k + \bar{\iota} b_2}$$ from equations 7.2 and 7.11.

and for the zero drag case, $\bar{\iota} = 0$.

With appropriate numerical constants included, the T.F.'s become

Drag zero

$$\frac{X}{I} = \frac{-0.01}{0.0177\omega^2 - 4.68}$$

Drag $\frac{1}{4}$ lb.

$$\frac{X}{I} = \frac{-0.01}{0.0177\omega^2 - 2.71} \quad \text{ft./amp.}$$

where the field stiffness k, which is appropriate to normal lift and roll control current levels, is derived in Appendix III.

During the process of development of the magnetic suspension system, the first serious efforts at obtaining a good performance from the drag coil control loop were made with the solid body of revolution, where drag forces close to $\frac{3}{4}$ lb. were encountered during tests at wind speeds up to the region of Mach 1. The characteristics of the compensation circuits developed at that time for that particular model are shown on Figs. 7.9 and 7.10. An integral control system was also developed, the characteristics of which will be described later. It was found that the same compensation circuit would control the tuned model quite well at low drag force levels, without modification, and the calculated Nyquist plot is given here for the tuned model. The main differences between this locus and that already given for the lift control loops are caused by the field stiffness which in the absence of drag control produce a lightly damped (see Appendix III)

fore-and-aft oscillation of the model at around 2½ cycles per second wind-off, and by the effect of the integral control.

The compensation circuit for the drag control loop is shown on Fig. 7.11, and the component values are given in Appendix III. A selection of calculated low frequency Nyquist plots is shown on Fig. 7.12. Consider first the no-integrator curves. For both drag force levels the loci extend to $\pm\infty$ as a result of the assumption of zero natural damping, at the resonant frequencies generated by the net effect of field stiffnesses and drag coil field gradient. At zero drag force, the resonant frequency is 2.59 c.p.s., and at this frequency there is introduced into the loop a phase lag caused by the inductance of the drag coil amounting to 39° and a phase lead in the compensation circuits of 58°, resulting in a net lead of 19°. Above about 2 c.p.s. the locus extends in very nearly a straight line at close to this lead angle, to ∞ at 2.59 c.p.s., and returns from $-\infty$ again in nearly a straight line at low frequencies in the lower left quadrant of the plot. This curve is shown on Fig. 7.12. The locus corresponding with a drag force of ¼ lb. is similar except that the resonant frequency is somewhat lower at 1.98 c.p.s., because of the negative stiffness generated by the drag coil field, and the net lead at resonance is also lower at 17°.

At frequencies above about 10 c.p.s., the difference between the Nyquist plots for the two drag force levels is very small, and the locus for the upper end of the frequency range is presented as a single curve on Fig. 7.13. For this model, the phase margin is rather low at 11½°, and the compensation circuit is probably not the best that could be devised for this particular model. With an upward extension of the wind speed range and a corresponding increase

of drag force beyond $\frac{1}{4}$ lb. it would probably be necessary to modify the compensation circuit for the tuned model.

During the programme of tests on the body of revolution at relatively high tunnel speeds, it was useful to be able to increase and decrease the wind speed fairly rapidly to conserve the stored compressed air supply for the tunnel. With a drag coil control loop compensation circuit as described above, there was a model position change accompanying a wind speed change, with corresponding changes to the value of $\left(\frac{\partial \xi}{\partial t}\right)_x$ which is used for drag force measurement. In addition to this, there was a danger of the model moving out of the range of control provided by the optical system. Consequently as wind speed and drag force changed, it was necessary to adjust the model position setting potentiometer (R_{11} on Fig. 7.11) to return the model to its correct axial position, and the rate at which speed changes could be effected was rather low.

It is possible to automatically maintain zero model position error, under steady-state conditions, by integrating the position error with respect to time, andusing the resulting integrated signal in such a way that the current supply to the drag coil is biased to move the model mean position in a direction reducing the rate at which the value of the time integrated position error is increasing. The integrating circuit which was used is shown on Fig.7.11, and comprises component R_{12} - R_{18} and C_4 and operational amplifiers 4 and 5. The action of the integrator is de-stabilising in that it produces another phase lag in the loop. However, if the response rate of the integrator is kept to a low value, the effects on the compensation

circuit phase and gain characteristics can be restricted to low frequencies, where the Nyquist plot is well clear of the -1 point. The action of the integrator is explained by the following sketches in a qualitative sense:

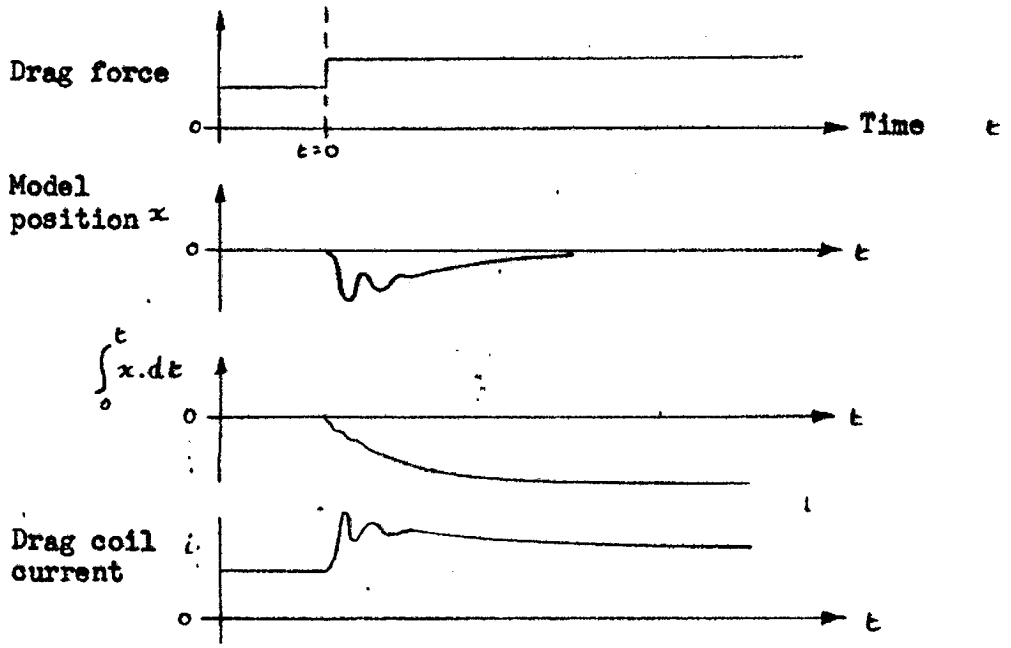

A step increase of drag force is shown applied at t = o, followed by a model movement away from the initial equilibrium position to a new equilibrium position further away from the drag coil, following a short period transient oscillation. The integrating circuit begins to develop an e.m.f. proportional to $\int x.dt$ which is used in a sense which tends to increase the drag coil current i. However, the forces on the model are in a state of equilibrium, and the effect of the signal from the integrator is to draw the model forward so that the position signal reaching the input of the compensation circuit maintains a quasi constant

magnetic force equal to the drag force following the step. The requirement for a constant force is obtained by a coil current which automatically falls from its value following the transient oscillation to a slightly lower level as a result of the field gradient, as the model moves forward to its correct position.

With the integrator in operation, the model position adjuster R_{11} does not function - the integrator backs off any e.m.f. change from this potentiometer. In order to change the model equilibrium position it is necessary to change the setting of another potentiometer, R_{13}, which is used to feed a signal into the integrator amplifier 4 backing-off the position signal. Any change in the setting of R_{13} will result in a change of integrator output and hence a change of model position.

The measured effects on the compensation network response are shown on Figs. 7.9 and 7.10. At frequencies above about 3 c.p.s. the integrator has negligible effect, but with reducing frequency the gain increases above that obtained with no integrator, theoretically tending towards infinite gain at zero frequency, while the phase tends towards a 90° lag.

This position error integrator proved to be very useful in practice: it became a standard procedure to suspend the model wind-off with its position set with the integrator turned on, controlling the fore-and-aft position of the model with a very low current passing through the drag coil (a current of less than 2 amperes) and therefore with the model drawn a little forward of its normal position against the field stiffness generated by the lift magnets. For example, at a current of 1 amp. the force on the model

would be about 0.01 lb. from the drag coil ($b_1 \doteq 0.01$ lb/amp) and from the normal lift-magnet field stiffness of about 1½ lb/ft. with the solid body of revolution, the forward movement of the model would be about 0.08". The operation of the tunnel was then much simplified by the integrator taking care of the model position during rapid changes of tunnel air speed, facilitating single-handed management of the complete system.

As an example of the effect that the addition of an integrator of this type in parallel with the lead-lag circuits would have, the Nyquist plot has been calculated using the measured characteristics of the compensation network with the integrator operating, for the tuned model. The changes are illustrated qualitatively by the diagram below:

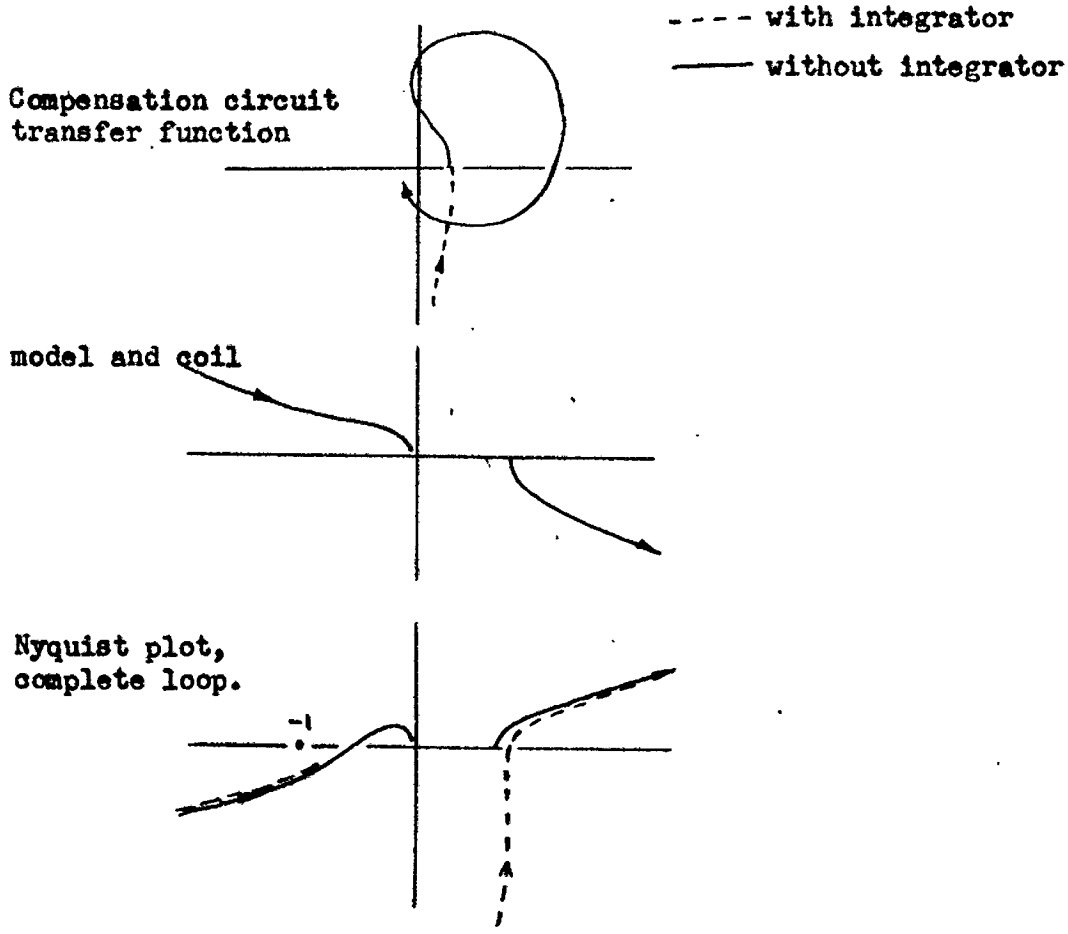

The combination of the upper two T.F.'s results in the Nyquist plot which, with the integrator operating, extends to $-j\infty$ at zero frequency, instead of beginning on the positive real axis. The calculated locus for low frequencies is shown on Fig. 7.12, for two values of drag force.

7.3.3 The roll control system. The gains of the roll optical system and power amplifier are 3.4 volts/radian and 32.9 volts/volt, giving $\frac{e_1}{\phi} \cdot \frac{e_3}{e_i}$ = 111.7 volts/radian, assumed independant of frequency.

The windings on the lateral horseshoe electro-magnets which are used for controlling roll, combined with an external load resistor, have a total resistance of 2.09 Ω and inductance of 0.04H giving a transfer function.

$$\frac{I}{e_3} = \frac{0.478}{1 + 0.0191 j\omega}$$

For the roll control system there is no field stiffness, and for small displacements in roll about the mean position there is no field gradient, consequently the roll control current is related to rolling moment by

$$\frac{M}{i} = \frac{0.63}{10^4} \quad \text{lb.ft/amp.}$$

for the tuned model, which will be considered throughout this section.

The compensation circuit developed for models of this type is shown on Fig. 7.14 (the component values are given in Appendix III) and consists of a single lead-lag stage followed by a low-pass filter, with provision for attitude and gain adjustment. The characteristics of the circuit, measured from the output of position signal amplifier

No. 1 to the filter output, are shown on Fig. 7.16 for the normal gain setting. The amount of phase-lead generated in the compensation circuit is modest, and would peak at about 56° at 5¼ c.p.s. were it not for the phase-lag introduced by the filter just becoming noticeable at this frequency.

The formation of the roll loop Nyquist plot is explained on Fig. 7.17, by means of an assembly of transfer functions of the various parts of the loop formed into groups. The model transfer function, Φ/M, which for the rolling mode is given by equation 7.1 with Φ in place of X (this is a good approximation, but the model can be subject to a stiffness producing a low frequency resonance - see a later note in this section) is shown schematically with positive damping. The second group consists of the coils of the electro-magnets controlling roll, and the magnetic moment generated on the model by these coils, and relates rolling moment to e.m.f. applied to the coils. The general shape of this T.F., M/e_3, is a first order lag. The final group consists of two fixed gains, the position signal amplifier and power amplifier $\frac{e_1}{\phi} \cdot \frac{e_3}{e_2}$ in combination with the compensation circuit transfer function e_2/e_1 giving e_3/ϕ These are presented in the sense which results in the magnetic moment from the coil tending to reduce the model position-error, producing the moment through the feedback circuit. The value of the wind-off model damping coefficient is very low (see Appendix III) and has been taken as zero in calculating the loop Nyquist plot for this case. Hence the model transfer function is dependant only on the inertia in roll (given in Appendix III):

$$\frac{\Phi}{M} = -\frac{10^4}{0.195\omega^2}$$

The aerodynamic damping in roll is relatively important, and as the damping effect varies with air speed the damping coefficient corresponding with the ¼ lb. drag air speed has been estimated at $^{12.7}/_{10^4}$ lb.ft/radian per sec. The model T.F. becomes, for this wind-on condition:

$$\frac{\Phi}{M} = \frac{-10^4}{0.195\omega^2 - 12.7j\omega}$$

The roll control loop Nyquist plots corresponding with the above two conditions are plotted on Fig. 7.18. There is a pronounced difference between the two curves; under wind-on conditions the damping is relatively high, but the margins, wind-off, indicate low damping.

In order to check on the validity of this method of calculating the response locus, for the roll control system the closed loop response has been measured. The technique which was used was to feed an oscillatory signal into the input of No. 1 operational amplifier (see Fig. 7.14) and to measure the model response. The definition of the loop transfer function is illustrated by the sketch below:

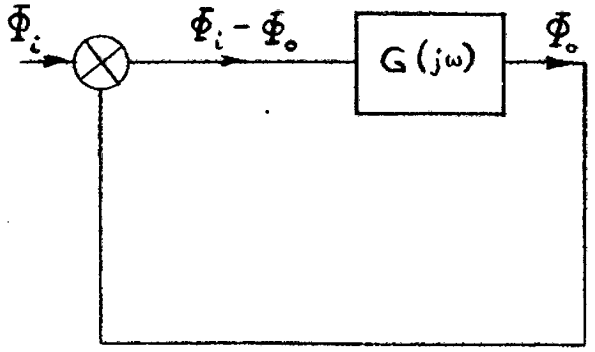

We can regard Φ_o as the model position signal and Φ_i as the voltage disturbance fed into No. 1 amplifier, then $\Phi_i - \Phi_o$ is the signal fed into the compensation circuit. The differencing device in the sketch is assumed to have unity gain, consequently the e.m.f. selected by the wiper of R_3 had to be divided by the gain of the amplifier in order to refer the signal to the amplifier output. By measuring this output, an e.m.f. proportional to $\Phi_i - \Phi_o$ was obtained, similarly by measuring the disturbance signal, and correcting for gain, a signal proportional to Φ_i . From the phase difference and amplitudes of these signals, Φ_o could be obtained, hence the loop transfer function $\frac{\Phi_o}{\Phi_i - \Phi_o} = G(j\omega)$. The locus of this function over the frequency range ω is the Nyquist plot. This is also shown on Fig. 7.18 for the frequency range $5\frac{1}{2}$ to $12\frac{1}{2}$ cycles/second, measured under wind-off conditions. The general agreement between the two wind-off curves is fair, but these latter measurements indicated larger gain and phase margins. The measured values are compared in the following table:

	Phase margin	Gain margin
Calculated from the individual T.F.'s for the wind-off condition:	7.0°	0.22
Closed loop measurements, wind-off:	10.7°	0.29
Calculated from the individual T.F.'s for specific wind-on condition:	> 90°	0.82

The last feature of the closed control loop to be checked was the transient response of the model following a disturbance in roll; the check was simply by displacing the model by hand a few degrees from its equilibrium attitude and watching the motion

subsequent to release. A typical oscilloscope trace has been re-plotted on Fig. 7.15. The motion appears to consist of a small amplitude oscillation of about 7 c.p.s. superimposed on a simple decay having a time constant of about one-tenth of a second.

The tuned model exhibited a low-frequency resonance in roll, with the roll control system inoperative, possibly resulting either from an offset c.g. or some magnetic asymmetry in the model core material. This stiffness will vary from model to model and could be positive or negative. In the case of the tuned model, the measured stiffness was + $2.1/10^4$ lb.ft./radian, (see Appendix III) Such a stiffness would produce a resonance in roll at about 0.5 c.p.s., but the effect on the Nyquist plot in the frequency range shown on Fig. 7.18 is negligible.

The compensation circuit described above has not been optimised for any particular model. However, the performance obtained with the complete system in this state has proved adequate for several models todate. It is quite possible that improvements would have to be made before a model could be satisfactorily suspended at increased air speeds. The maximum air speed at which any model has been suspended with control in six degrees of freedom was with the tuned model (with wings as shown on Fig. 13.5) at a Mach number of 0.35 at atmospheric total pressure.

7.3.4. Lateral position control - solid models. It is in this plane that models have been built with resonant motions, and two separate types of position control system have been developed to accomodate the different characteristics of solid and tuned models. In this section details are given of the identical pair of solid model

lateral control systems, which, compared with the tuned model systems, have a high loop gain.

The optical system and power amplifier gain product give

$$\frac{e_3}{e_2} \cdot \frac{e_1}{x} = 8500 \text{ volts/ft.}$$

and the coil transfer function, from equation 7.6. using the circuit resistance of 2.4 ohms and coil inductance of approximately 0.02 H is

$$\frac{I_1}{e_3} = \frac{0.417}{1 + 0.00833\omega j}.$$

Note that the relatively low value of the inductance was a result of the arrangement of the coil wiring: for each end of the model, one winding section from the left hand and right hand electro-magnets were connected in series. One section alone has the relatively low inductance of a little under 0.01 H, and as the two horseshoe magnets were separated by a considerable air gap, the total inductance of the control circuit was simply the sum of the separate coil inductances.

The field gradient at the tunnel centre-line is zero for the symmetrical pair of lateral magnets, hence $b_2 = 0$ for this control system. The force-current constant $\left(\frac{\partial F}{\partial i}\right)_x = b_1$ has not been measured for the solid model and for this reason an accurate Nyquist plot cannot be drawn. However, values of the constant for other electro-magnet/model combinations suggest that for this model and the lateral electro-magnets (using one winding section per leg for lateral control) b_1 would be of the order of 0.02 lb/amp. For this reason, and for the reasons that aerodynamic forces and moments can be important factors in the control loop wind-on, a Nyquist plot has only been calculated for the wind-off condition and is confined to lateral heaving modes of motion.

Solid models are subject to magnetic stiffness in the horizontal plane from the lift magnets, wind-off, and from the lift and drag coil under wind-on conditions. The magnetic stiffnesses from the drag coil have not been measured.

The natural frequency of heaving oscillation in the horizontal plane, induced by the lift magnets, for the solid body of revolution is 1.68 cycles per second giving a magnetic stiffness per $\frac{1}{2}$ model of 1.095 lb/ft. The model transfer function, from equation 7.2 with c assumed zero (the wind-off damping factor is given in Appendix III at 7.47×10^{-4} lb. per ft./sec.) becomes

$$\frac{X}{F} = \frac{-1}{0.0098\omega^2 - 1.095} \quad \text{ft/lb.}$$

The compensation circuits which have been used for lateral position control were very similar to those used in the lift control circuits. For the forward lateral control system the circuit was as shown on Fig. 7.5. (a) and for aft lateral control the circuit was as Fig. 7.5 (b). The component values are given in Appendix III, and the circuit characteristics are shown on Fig. 7.19. The maximum phase lead was 96° at 24 c.p.s.

The loop Nyquist plot has been calculated using the above data and is shown on Fig. 7.20 for the frequency range from 5 to 70 cycles per second. In addition to the normal locus, in order to show the effect of phase lead in the compensation circuit a second curve is shown which is the Nyquist plot which would be obtained with a compensation circuit having a constant gain equal to the D.C. gain shown on Fig. 7.19, and no phase change with frequency. Judging from the shape and frequency distribution of the latter curve, and bearing

in mind that the gain of a compensation circuit corresponding with maximum phase lead can be several times the D.C. gain of the circuit, one would expect that a compensation circuit with this value of D.C. gain should provide its maximum phase lead at a frequency above 20 cycles per second. As already mentioned, the lead provided by the lateral compensation circuits provided a peak at about 24 c.p.s. The lead of this circuit exceeded the phase lag of the coil over the whole frequency range from D.C. up to about 55 c.p.s. The main problem with extending this frequency range even higher was that of noise amplification: increasing the lead angle at higher frequencies inevitably increases the loop gain at high frequencies and generally results in unwanted electrical noise being circulated around the loop, possibly causing amplifier saturation.

In order to examine the net lead through the open loop at low frequencies the following approximate approach can be useful. The main contributors to phase changes are the coil and the compensation circuit. The phase lag of the coil is given by $\tan^{-1} \tau_c \omega$, where $\tau_c = L/R$ and at low phase angles the lag can be written as $\tau_c \omega$. In the compensation circuit there are two lead-lag elements and a low-pass filter in series. At low frequencies the lead in one of the elements is approximately $\tau_1 \omega$ where τ_1 is a time constant of the lead lag circuit (see section 7.3.1). If we write the low frequency lead in the second lead-lag circuit as $\tau_2 \omega$ and the low frequency phase lag in the low pass filter as $\tau_f \omega$, then the net phase lead at low frequencies is $\omega(\tau_1 + \tau_2 - \tau_c - \tau_f)$. Provided that $\tau_1 + \tau_2 > \tau_c + \tau_f$ there will be a phase lead through the loop. For the lateral position control systems, $\tau_1 + \tau_2 = 0.0352$ sec. $\tau_c = 0.00833$ sec. and $\tau_f = 0.001$ sec., and hence the net phase lead is positive and is given by

0.0259ω for low values of the individual phase lead and lag angles.

The steady-state stiffness of the complete model with this lateral control circuit, with respect to bodily displacements, given by the product of each of the transfer functions (excluding the model transfer function X/F) under steady state conditions, was approximately 20 lb/inch.

7.3.5 Lateral position control - tuned model. A wind tunnel model has been specially devised in order to facilitate the measurement of oscillatory derivatives. The main feature of the model is the spring-connected two-mass construction, the transfer functions for which are given in section 2.2 of this chapter. Practical considerations dictate that one of the masses should be the outer shell of the model, forming the aerodynamic shape and including wing surfaces, and the other mass should be the magnetic core. The model has been designed for one mode of oscillation, namely rotary motion about the vertical axis through the centre of the model. This mode of motion resonates under the action of field stiffnesses and the stiffness of the spring connecting the masses, and must be controlled by the lateral electro-magnets. The model was suspended with its wings in the vertical plane, hence the model resonated in pitch.

The model position must be monitored in order to complete the feedback loop, and as there are two parts to the model, either or both could be monitored. If both were to be monitored, optical systems extra to those already installed for solid models would be required; in view of the complication which this would produce (there was very little space around the wind tunnel for the additional light

sources and pick-ups, and the model design would be complicated by the necessity to provide light beam modulation by both main parts of the model) it was decided to monitor just one of the masses and to attempt to stabilise both the pitching mode having two resonances and the heaving mode having one resonant frequency, with the same compensation circuit.

The early demonstration tuned models consisted of a bar magnet suspended in the normal set of light beams, and a second mass suspended by leaf springs in the manner of a pendulum below the bar magnet and clear of the light beams. A range of resonant frequencies from 20 to 60 c.p.s. was produced by varying the spring torsional stiffness and the moment of inertia of the non-magnetic mass.

A magnet rotated away from the axial direction in the horizontal plane is subject to a restoring moment from the lift magnet system, and from the drag coil with the wind on, and the transfer function for pitching motions with the magnetic core being monitored by the optical system is given by response $\frac{X_2}{F}$ on Fig. 7.3 (b) and by equation 7.5. The open loop response would be similar in general shape to Fig. 7.3. (b) except that the lag introduced by the coil inductance would take the part of the response in the frequency range from about ω_ℓ to ω_a and from $\omega_{o\ell}$ to $\omega = \infty$ across the negative real axis into the upper left quadrant (the first may not occur with heavy damping of the model motion from c_1, c_2, c_3). With zero damping the response locus would twice pass the wrong side of the -1 point and result in an unstable model, but by introducing some phase-lead into the compensation circuit the excursion into the upper left quadrant can be confined to frequencies above the upper

resonant frequency and the model may be stabilised in pitch for a range of values of loop gain. The tuned model behaves as a solid model as far as bodily heaving motions are concerned, and the same simple phase-lead compensation circuit can also be arranged to stabilise this mode motion, completing the control of the two degrees of freedom which are under discussion.

The second possibility was to monitor the non-magnetic mass, mass m_1 on Fig. 7.3, and in practice this was the most convenient way to monitor a wind tunnel model as a result of the preferred construction where the core was hidden inside the non-magnetic shell. The response locus $\frac{X_1}{F}$ is given on Fig. 7.3 (a) and by equation 7.4. As this model has been the subject of a good deal of experimental effort, the problem of stabilisation with shell-monitoring will be dealt with in some detail for the particular case of the model used for pitching derivative measurement.

The theoretical undamped response $\frac{\Theta_1}{M}$ for this model is given on Fig. 7.21, where the moments of inertia are

non-magnetic shell $I_1 = 1.088/10^4$ slug ft^2

magnetic core $I_2 = 1.695/10^4$ slug ft^2

and the stiffnesses are

torsion spring $k_1 = 0.893$ lb.ft. per radian

field stiffness $k_2 = 0.1147$ " " "

for the two cases of the model behaving as a two-mass system, and with the core locked behaving as a solid model.

In practice, for the still-air case the damping coefficients c_2 and c_3 are very low, and can be assumed zero. The value of the coefficient c_1 has been determined from measurements made with the model

suspended and forced near the upper resonant frequency by the lateral magnets and has been taken as 0.000411 lb.ft./radian per second for the purposes of computing the model transfer function.

The phase differences between the shell motion and the moment applied to the core for the undamped case are:-
over the frequency range from 0 to the lower resonance : in phase
between resonances : phase difference of 180^{o}
above upper resonance : in phase.

In the loop Nyquist plot drawn for the damped model (c_1 as above, $c_2 = c_3 = o$) the lower reasonance appears as a large loop well clear of the -1 point, but the response at frequencies above the lower resonance requires special consideration because of the unusual characteristics of the model. The calculated response of this model over the frequency range from 5 c.p.s. to infinity is given on Fig. 7.22. When suspended using the same compensation circuit that had been developed for lateral control of the solid model, the tuned model was violently unstable, and the reason for this can be seen by drawing the theoretical loop Nyquist plot. This is given on Fig. 7.23, where the large upper resonance loop results in a complete encirclement of the -1 point. With this particular compensation circuit a stable model could only be achieved by reducing the loop gain to 1-2% of that used for the solid model resulting in very low stiffness of model suspension, or by locking the core. With negative aerodynamic damping the gain would have to be reduced still further.

One possible way of increasing the loop gain would be to adjust the maximum phase lead of the compensation circuit to just match the coil phase lag at a frequency corresponding with the inter-

resonance depression, around 13 c.p.s. for this model, and then to adjust the loop gain to obtain stability. The construction of the Nyquist plot would be as given below in qualitative form:

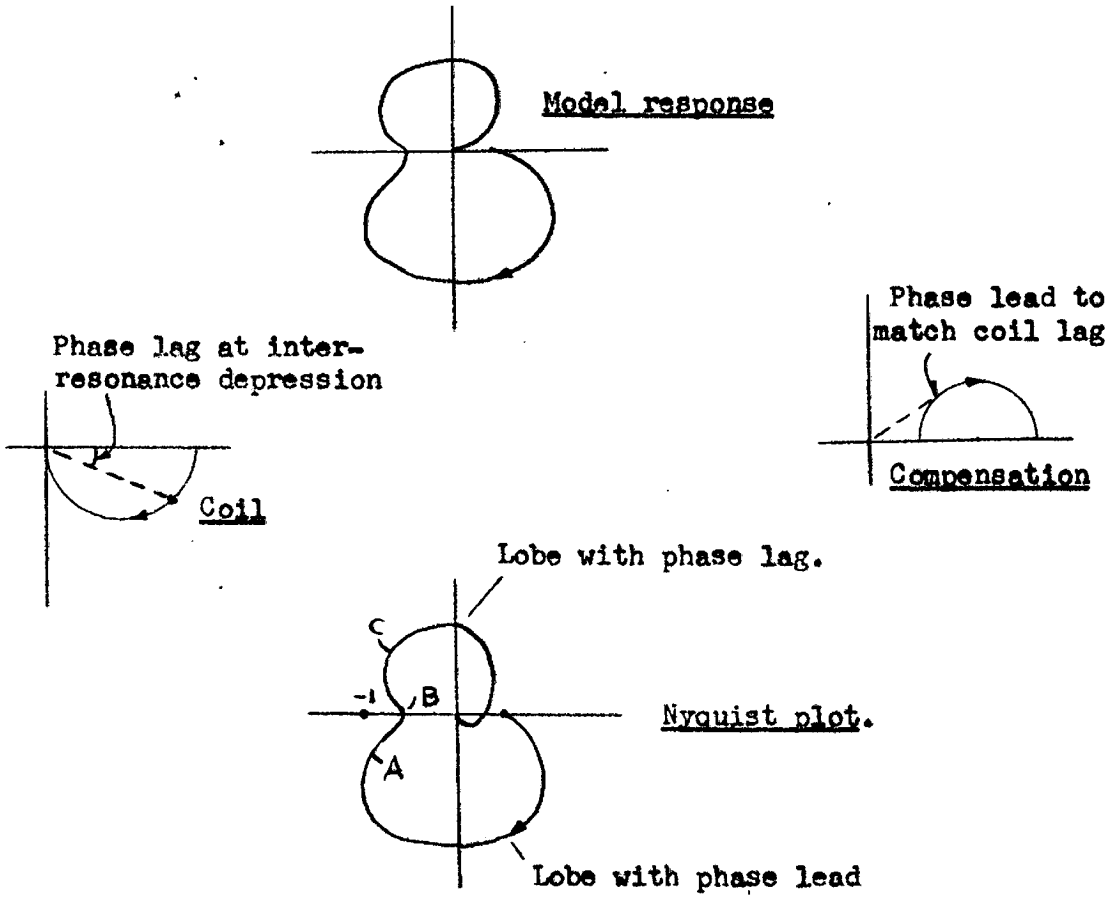

The lower resonance lobe is given phase lead in order to move the region marked A away from the -1 point. The inter-resonance depression has no net phase change and this minimum in the model response locus is arranged to coincide with the negative real axis between the origin and the -1 point by adjustment to loop gain, point B on the diagram above. In order to remove the region just below upper resonance from the -1 point, region C, frequencies above the depression are shown with phase lag.

The maximum D.C. gain of such a compensation circuit for the above model and for the normal lateral control power amplifiers, optical systems etc., would be 0.081 for a gain margin of 0.5. This is about 5% of the gain which had been used for the solid model. Aerodynamic damping would probably have little effect on the permissible gain.

A second possible approach to raising the loop gain would be to utilise a compensation circuit having a normal lead-lag stage or stages in conjunction with a sharp cut-off low pass filter, or a notch filter, arranged to reduce or eliminate the open loop response at frequencies near the upper resonance, thus in principle suppressing the lobe shown on Fig. 7.23. Apart from the filter introducing unwanted phase lags at lower frequencies which would require compensation, the main disadvantage of this type of control system would be the low damping that would be available at the upper resonant frequency of the model: the resonance would not be damped by the control system because of the zero response of the loop to model motion at the resonant frequency. There would also be the possibility of model divergence with negative aerodynamic damping, model exitation at resonance resulting from aerodynamic turbulence or from ripple in the current supply to the electro-magnets, and the problem of adjusting the filter characteristics to suit changes of natural frequency of oscillation that would accompany changes of aerodynamic stiffness or of magnetic stiffness.

A third solution to the problem of suspending with adequate loop gain, and the solution which was adopted, was to introduce a phase inverting compensation network. The principle of this control

system was to introduce a phase change of 180° into the control loop (additional to any phase lead required to compensate for coil lag) at a frequency below upper resonance such that the upper resonance lobe was moved from the upper half of the Nyquist plot to the lower half; in this way the position control system could produce some damping for the potentially troublesome upper resonance without having the maximum loop gain limited by the relatively large values of the response ω/M obtained between or near the resonances. At the same time this control circuit would need to provide conventional compensation for the lower part of the frequency range from D.C. to near the inter-resonance depression frequency (this would be the anti resonant frequency for an undamped model). The network which was developed to provide these characteristics consisted of a phase inversion section, set to produce a 180° phase lead at the required frequency, in series with a section providing phase lead to compensate for coil lag, and is shown on Fig. 7.24. The resistor values are in Ohms, and the capacitor values in Farads. A block diagram of the phase inversion section is shown below:

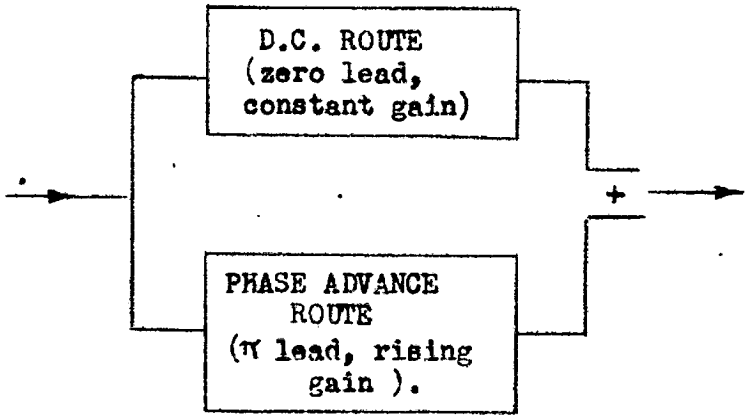

The circuit has been arranged to provide low d.c. gain through the phase advance route, allowing the d.c. route to dominate the output at low frequencies, and to provide rising gain with frequency in the phase advance route so that at higher frequencies the output is dominated by the phase advance route. At some intermediate frequency, referred to as the centre frequency, the gains of the two routes are matched and as the signals are equal in amplitude but in antiphase the net output is zero. Hence this part of the compensation circuit acted as a notch filter, with the notch at the centre frequency, and the components were chosen so that the centre frequency could be set below the upper resonant frequency of the model. Below the centre frequency, the output signal from the phase advance section was nearly in phase with the input, and above the centre frequency the output signal was nearly in antiphase.

Staged lead-lag circuits were chosen to provide the total of 180° phase lead required, and the control network currently in use comprises four lead-lag elements in series, each producing a maximum of 45° lead. The lead was only maintained over a relatively narrow band of frequencies, and the components were chosen to provide this value of phase lead at frequencies near the centre frequency and the model upper resonant frequency. Above and below this frequency range the phase lead was less than 180°; however over the high frequency range the loop gain was inherently low because of low model and coil response and hence reduced lead did not result in instability, and over the lower frequency range the dominating d.c. route provided the required in-phase signal for the correct positioning of the low frequency response of the open loop in the Nyquist plot. The phase inversion section was arranged in series with a normal phase lead

section, consisting in this case of three lead-lag stages in series followed by a low pass filter, with provision for loop gain and model position adjustment. A large number of lead-lag stages were used in order to minimise the loop gain at high frequencies (see Appendix II), but even so it was necessary to filter the compensation circuit output rather heavily in order to prevent power amplifier saturation from spikes.

The mechanism of the production of damping forces by this control system can be explained by considering the closed loop performance when a part of the model is forced (by some external means) say at the upper resonant frequency. Suppose a periodic force was applied to the magnetic core. For low values of c_1, at the undamped resonant frequency the motion of the core and shell would be very nearly in antiphase, and a position signal would be fed into the compensation circuit in phase with the shell, in antiphase with the core. At this frequency the phase inversion section of the compensation network would be arranged to produce a signal in phase with the core motion and in antiphase with the shell. The signal would then proceed to the phase-lead section, the power amplifier and electro-magnet and appear partly as a force having a component in antiphase with the core motion, a force which opposes the motion of the core with the nature of a spring stiffness, and as a result of the phase lead generated in the lead section of the compensation circuit being greater than the phase lag of the coil at this frequency, a component in quadrature leading antiphase relative to the core motion. This force component has the characteristics of a damper, being a force which opposes motion and is a maximum when the core velocity is a maximum.

Hence there would be a net inflow of energy to the closed loop from the externally applied force, and hence the closed loop could not be unstable at this particular frequency.

The gain and phase variations with frequency for the phase inversion section of Fig. 7.24 are shown on Figs. 7.25 and 7.26(a) respectively, for two selected values of centre frequency. The main features of the gain curves are (i) the rapidly increasing gain with frequency above the centre frequency, this being the main reason for the requirement for a low pass filter in the loop, and (ii) varying d.c. gain with selected centre frequency resulting from a d.c. route gain which changes with the selected frequency. The phase-changes shown on Fig. 7.26 (a) occur over a narrow band of frequencies, but because of the output signal attenuation near the centre frequency it was not possible to measure the output phase with any certainty. However, from the measurements that were possible it can be claimed that the nominal 180° phase change occurred within a range $\pm$ 1 c.p.s. about the centre frequency. Below the centre frequency the output signal was in-phase with the input within $\pm 2^{\circ}$, and with increasing frequency above the centre frequency the phase lead falls (eventually reaching zero theoretically at infinite frequency) as a result of reducing phase lead in each of the four lead-lag elements.

The characteristics of the phase-lead section of the compensation network are given on Fig. 7.27, measured at one gain setting. The rather heavy filtering of the output signal which was necessary is apparent on this figure; a considerable amount of the lead which would otherwise be generated in this section was lost in the filter. The overall phase and gain characteristics of the compensation network are given separately on Figs. 7.26 (b) and

7.28, measured at a gain setting suitable for the tuned model, and the same information is shown plotted in the phase plane on Fig. 7.29.

From the preceeding discussion on closed loop damping, it is evident that a centre frequency set at or very near to the upper resonant frequency of the model would result in poor damping of model oscillations at this frequency. A Nyquist plot has been drawn for the tuned model (upper undamped resonant frequency 18.66 c.p.s.) using the measured compensation circuit characteristics when centred at 18.5 c.p.s. and is given on Fig. 7.30. The near-zero loop response in this frequency range has virtually completely suppressed the upper resonance lobe; the model is known to be stable in this condition but the control system is not capable of generating significant forces (or more strictly moments as we are considering rotary motions) at 18-19 cycles per second.

A second Nyquist plot is given on Fig. 7.31 for a centre frequency of 17.5 c.p.s. This was the normal setting of the centre frequency for this model, and the upper resonance lobe can now be seen expanded mainly in the lower half of the diagram but still leaving a gain margin of 0.38 at this particular gain setting. Uncertainty about the inversion circuit characteristics near the centre frequency leave the response locus shape in doubt from $16\frac{1}{2}$ - $18\frac{1}{2}$ c.p.s.

An interesting demonstration of the generation of damping forces by the control system at a frequency near the upper resonance is given by suspending the tuned model, and forcing the upper resonant frequency by feeding signals into both of the lateral compensation network phase inversion sections, and monitoring model

lateral position and the current difference $i_f - i_a$ on the oscilloscope while the forcing signal is switched off. The current and position traces, which are reproduced on Fig. 7.32, can be divided into four regions, labelled A-D on the upper trace on Fig. 7.32 which was for the case just described, the case of switching off the forcing signal.

The section of trace A shows the model resonating under the action of a relatively small moment amplitude indicated by the current trace. The position signal trace was in phase with the motion of the model, but the current signal was filtered and hence subject to a phase lag. At point B the forcing signal was switched off, indicated by the abrupt change of phase of the current signal. During section C there is a sharp increase of current and hence moment amplitude, phased approximately 180° differently relative to the position trace compared with section A, and a decay of the amplitude of motion. The remaining part D of the trace merely shows the steady-state current and position signals.

The lower trace shows the reverse procedure : switching on a fixed amplitude of forcing signal. Following switch-on there is a period during which the current amplitude is relatively high, but the current signal diminishes as the amplitude of oscillation increases until the steady-state oscillation is obtained as labelled A in the upper trace.

The compensation network in this form allowed the model to be suspended with a d.c. gain over the network of 0.217, about 13% of the d.c. gain used for the solid model. This was still rather low, and would probably need improvement before the tunnel speed range

could be extended much above the maximum of 380 ft./sec. so far reached with this model. Increase of loop gain might be achieved by increasing the compensation network phase lead, particularly in the frequency range 20–25 c.p.s., possibly by adding an additional passive lead-lag stage at the beginning of the phase lead section.

Any compensation network which was chosen to stabilise the tuned mode of motion must also be capable of stabilising the remaining mode of motion in the two degrees of freedom controlled by the lateral magnets, in this case heaving motions.

Under wind-off conditions we can assume that the transfer function $\frac{X}{F}$ is given by equation 7.2 with $c = 0$. The field stiffness k for the tuned model was approximately 1.2 lb./ft. per half-model, and the T.F. becomes

$$\frac{X}{F} = \frac{-1}{0{\cdot}0086\,\omega^2 - 1{\cdot}2} \qquad \text{ft./lb.}$$

The force-current calibration $\frac{F}{I} = b_1$ was taken as 0.031 lb./amp. (there was no field gradient to take into account for this magnet system).

The remainder of the loop component transfer functions are as given for the pitching mode discussed above, and the resulting Nyquist plot has the form:

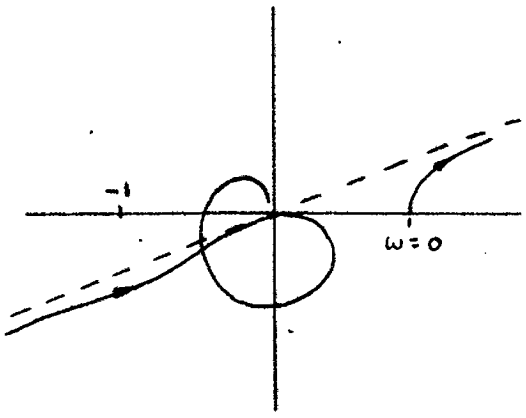

The broken line corresponds with the net phase lead through the loop at the resonant frequency in heave. With increasing frequency above the resonance the locus tends to the origin at the compensation network centre frequency, and at higher frequencies reappears as a lobe which crosses the negative real axis well clear of the -1 point. The calculated Nyquist plot for part of the frequency range is given on Fig. 7.33, using the compensation network characteristics with the centre frequency set at 17.5 c.p.s.

It can be seen that the high values of compensation network gain above the centre frequency result in quite a large open loop response, the locus is positioned such that the loop would require a large increase of gain before this particular mode of motion became unstable. This suggests that closer spacing of the lateral monitoring beams (a lower value of l) might be advantageous in allowing the loop gain to be increased in the case of a pitch-tuned model to result in an increased stiffness of suspension with respect to heaving motion, the increase possibly being of the order of 100% with adequate damping.

However, there is an altogether different approach which should be investigated and which might offer greater stiffness in heave with a pitch-tuned model. The proposed technique would offer separate control of the pitch and heave modes, each with the most suitable compensation circuit and hence highest gain. Signals proportional to lateral displacement and pitch displacement would be required and could be obtained by summing and differencing the lateral position signals , or to provide for unequal spacing of the monitoring planes fore and aft of the pitching axis, in the latter case the differencing could be through circuits having unequal gain. The phase

compensated signals would in turn be summed and differenced to provide the two power amplifier input drives. In this manner it may be possible to increase the stiffness of lateral bodily displacement to a value equal to that attainable with a solid model, about seven times the stiffness obtained with the control system in use at present.

A clear requirement for the steady-state stiffness of the lateral position control system is that it should be capable of preventing a lateral divergence of the model under the action of aerodynamic forces or moments. For a model suspended with its wings in the vertical plane, any rotation of the model about a vertical axis would produce a lift force and could in general produce a pitching moment which must be resisted by the lateral control system. Considering just the lift force, for static stability the control system must be capable of producing a restoring force to balance the lift force due to incidence. The system will automatically provide this force as a result of bodily movement of the model across the tunnel such that the position-error signals generate via the control circuits the necessary currents in the electro-magnets. For static stability it is necessary for the rate of increase of restoring pitching moment with incidence from the lateral magnets to exceed the rate of increase of aerodynamic pitching moment. Referring pitching moments to the vertical axis through the tunnel centre-line, then the magnetic restoring moment due to model incidence can be written

$$M_m = a\,(i_f - i_a)$$
$$= ag\,(x_f - x_a)$$

where $g = \frac{e_1}{x} \cdot \frac{e_2}{e_1} \cdot \frac{e_3}{e_2} \cdot \frac{f}{e_3}$ (d.c. values for this quasi-steady analysis)

and suffix f refers to the forward end

a " " " aft "

The incidence of the model to the airflow is given by

$$(x_f - x_a)\frac{1}{2l} = \theta$$

hence $$M_m = 2gal\theta \qquad \text{——— 7.9}$$

The aerodynamic moment M_a due to incidence, taken as positive when tending to increase incidence, is given by

$$M_a = q S \bar{c} \frac{dC_m}{d\theta} \cdot \theta \qquad \text{——— 7.10}$$

where C_m is a pitching moment coefficient. The derivative $\frac{dC_m}{d\theta}$ can vary from one model design to another, but is assumed constant for small incidence changes for any particular model.

For the particular case of control by a symmetrical pair of electro-magnets, as in the case of lateral control, field gradient effects on force-current or moment-current calibrations are zero for small movements of the model about the tunnel axis, and hence from equation 7.9 we may write

$$\frac{\partial M_m}{\partial \theta} = 2agl$$

and from 7.10 $$\frac{\partial M_a}{\partial \theta} = q S \bar{c} \frac{dC_m}{d\theta}$$

For static stability it is necessary to satisfy the relationship $$\frac{\partial M_m}{\partial \theta} > \frac{\partial M_a}{\partial \theta}$$

and hence $$2agl > q S \bar{c} \frac{dC_m}{d\theta} \qquad \text{——— 7.11}$$

In the stability criterion 7.11, the terms on the left hand side are positive, and similarly q and $S\bar{c}$. Hence with negative $dC_m/d\theta$ the criterion is satisfied, but for a model with positive $dC_m/d\theta$ there would be an upper limit to the variable q (the atmospheric wind tunnel for which the magnetic suspension system has been designed generates a maximum q of about 910 lb.ft.^{2} at Mach 1.45)

for which the model positioning system would be statically stable. The value of g is directly proportional to the d.c. gain of the compensation network, and hence it could be desirable to have high compensation network gain in order to satisfy static stability with some models at high values of q.

To illustrate this point one can estimate the value of q at which the tuned model (which has a positive value of $\frac{dC_m}{d\theta}$, see Chapter 13) would become neutrally stable at the gain which is attainable with the present compensation circuits.

At d.c. conditions $g = 770$ amps./ft.

$a = 0.00489$ lb.ft./amp.

$2l \doteqdot 0.43$ ft.

and $2ag\ell = 1.62$ lb.ft.

From the steady pitching moment measurements made with this model at $q = 42$ lb./ft.^{2} the product $S\bar{c}\frac{dC_m}{d\theta} = 0.00269$ and the value of q giving $2ag\ell = qS\bar{c}\frac{dC_m}{d\theta}$ would be 600 lb./ft.^{2}, corresponding with Mach 0.75, hence for operation with this model at Mach 1.45 the loop gain would require increasing by 50% to maintain neutral stability, and possibly by 100% for there to be an adequate safety margin.

While discussing the subject of model control at high air speeds, it would be appropriate to mention some additional aspects of lateral position control which might involve some system modification in the future.

Firstly, there would be an upper limit to the steady pitching moment that can be applied to a model by the electro-magnets in the case of a pitch-tuned model, set by the moment required to rotate the magnetic core of the model to a position where it just

touched the outer shell. The moment is given by the product of the spring torsional stiffness and the permissible relative rotation of the core. In the case of the tuned model under discussion in this section, the angular displacement limit was $\pm$ 1.95°, the spring torsional stiffness 0.893 lb.ft/radian and hence the maximum moment was $\pm$ 0.034 lb.ft. In the case of a model stabilised by a phase-inversion network the limit to the rotation of the core relative to the shell is less than this because of an instability which occurs when the core touches the shell: when touching occurs the model transfer function is no longer given by the equations in this chapter, and hence the compensation networks no longer have the correct characteristics. Raising the upper natural frequency of the model by increasing the spring stiffness would raise the moment limit.

This raises a second problem which could become severe with high speed operation of the tunnel. When launching the tuned model into the suspension system by hand, the model had a tendency to oscillate in pitch until released into full control by the magnetic suspension system. It is possible that the action of holding the model changed the dynamic characteristics of the model to the extent that the lateral compensation networks were not matched to the model. A mechanical launcher will be necessary for supersonic operation of the tunnel, and the restraint offered by the launcher might result in a similar instability unless the shell of the model is held rigidly to prevent position error signals causing core movement within the model. Rapid release of the model might then avoid a build-up of oscillation amplitude before the suspension control system takes over. However, rapid release may not be a desirable feature for other reasons: the present opinion is that it would be

useful to "loosely restrain" the model mechanically until a check can be made that the model is satisfactory under magnetic control. Also, rapid release could be followed by a bodily divergence of a winged model in a direction normal to the wing surfaces, irrespective of whether the model is solid or tuned, if the model produces a large zero incidence aerodynamic pitching moment.

It has been mentioned earlier in this section that the development effort to date has concentrated on stabilising the tuned model using position sensors monitoring the outer shell of the model. However, there are prospects of higher attainable loop gain with a sensing system either monitoring the magnetic core only, or monitoring the outer shell at each end of the model in the conventional way but adding to the system a device giving a signal dependent on the position of the core relative to the shell. Compensation networks designed for such monitoring systems might also eliminate the launching instability.

7.4 A Summary of the Discussion on Control.

(i) Solid models: adequate position control can probably be provided for suspension up to the limit of the high speed wind tunnel (Mach 1.8) in five degrees of freedom. Experience has shown that extension of the speed range above 400 ft./sec. would probably require increased moment capacity in roll.

(ii) Tuned models: adequate position control for operation at high speed can be provided in three degrees of freedom, but the lateral stiffness at present provided in pitch and heave would not be adequate, and increased moment capacity in roll would probably be required. The provision of model restraint during launch may introduce control problems.

(iii) Nyquist plots: these may be calculated from the transfer functions of the components, or can be estimated from the measured open loop response. Unless all transfer functions are known with good accuracy, the latter method is to be preferred.

7.5 LIST OF SYMBOLS USED IN CHAPTER 7.

Symbol	Meaning
a	Magnetic restoring moment per unit current difference between the lift magnet coils or the lateral position control coils.
b_1	The force-current calibration constant with the model in its normal position.
b_2	The variation of the magnetic force on the model with distance moved towards an electromagnet, per ampere in the windings.
c	A damping coefficient.
$\bar{\bar{c}}$	Mean aerodynamic chord.
D	The operator d/dt.
e_1	The output of an optical pick-up amplifier.
e_2	The output of a compensation circuit.
e_3	The voltage output of a power amplifier.
f	Force.
$\|F\|$	The amplitude of a periodic force.
g	Current change per unit model displacement under steady-state conditions.
i	Current.
$\bar{i}$	Mean current level.
$\|I\|$	The amplitude of a periodic current.
j	$\sqrt{-1}$
k	A spring constant.
l	Half of the separation, measured in the windward direction, of the vertical or lateral position monitoring beams.
L	Coil inductance.
m	Mass.
M	Moment.

Symbol	Meaning
M_a	Aerodynamic moment.
M_m	Magnetic moment.
q	$\frac{1}{2}\rho v^2$
R	Circuit resistance.
S	Wing area.
t	Time.
v	Air velocity in the wind tunnel working section.
$\|X\|$	Amplitude of model motion in the x - direction.
x	The change of model position from a datum position as monitored by an optical system.
y	The separation of a model from an electro-magnet.
$\bar{y}$	The datum separation distance between a model and an electro-magnet.
z	Half of the moment of inertia of a model in yaw.
θ	Angular displacement of the model centre-line in pitch (note that this symbol refers to a model suspended with its wings vertical).
ρ	Air density in tunnel working section.
$\|\Theta\|$	The amplitude of a periodic pitching motion.
τ	A time constant.
τ_1	A time constant of a lead-lag network.
τ_c	A coil time constant, $= L/R$.
ϕ	Angular displacement of the model in roll.
$\|\Phi\|$	The amplitude of a periodic displacement in roll.

Symbol	Meaning
ψ	Angular displacement of the model in yaw.
ω	Angular frequency.
ω_o	Resonant frequency.
ω_{oa}	The lower resonant frequency of a tuned model.
ω_{ob}	The upper resonant " " " "
ω_a	The antiresonant frequency
ω_l	The resonant frequency of a tuned model with the core locked to the outer casing.

MODEL SYSTEM

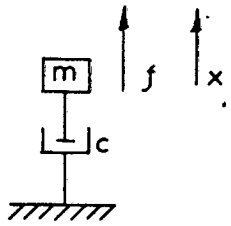

(a)

FREQUENCY RESPONSE $\frac{X}{F}$

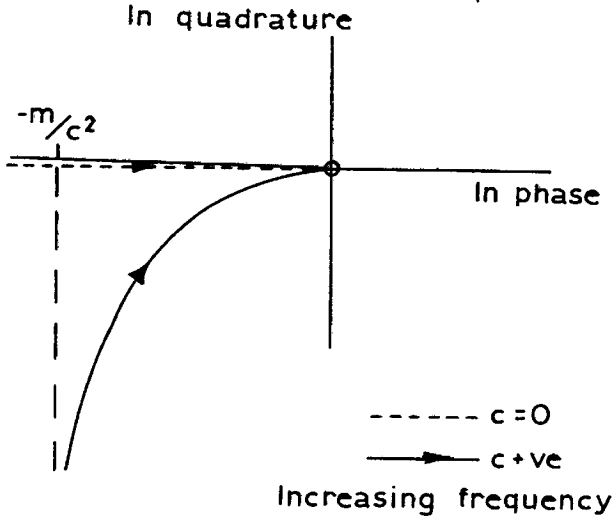

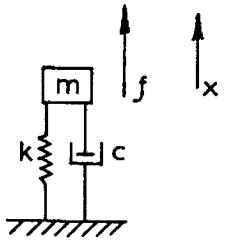

(b)

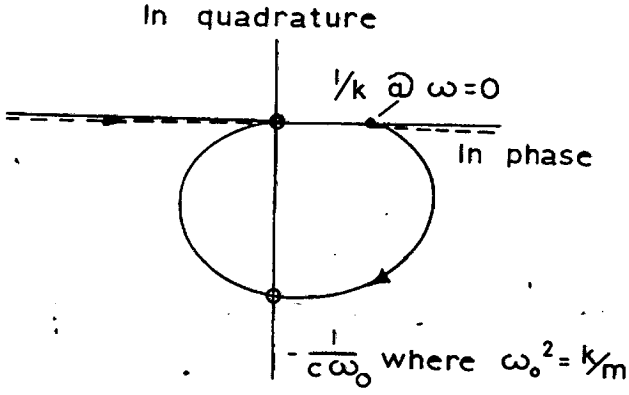

Fig. 7.1. The responses of models consisting of a single mass.

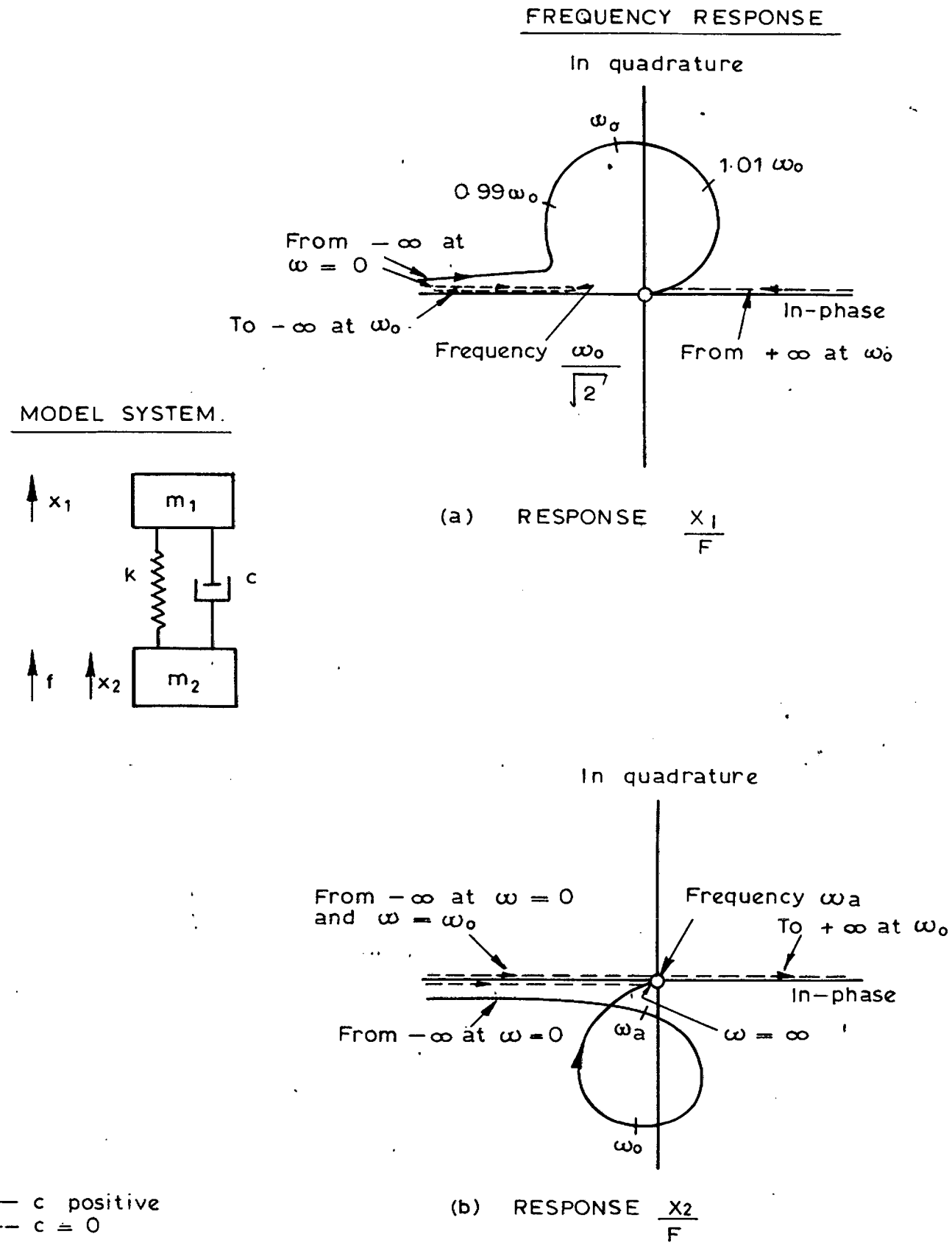

Fig. 7.2. The frequency response of a tuned model.

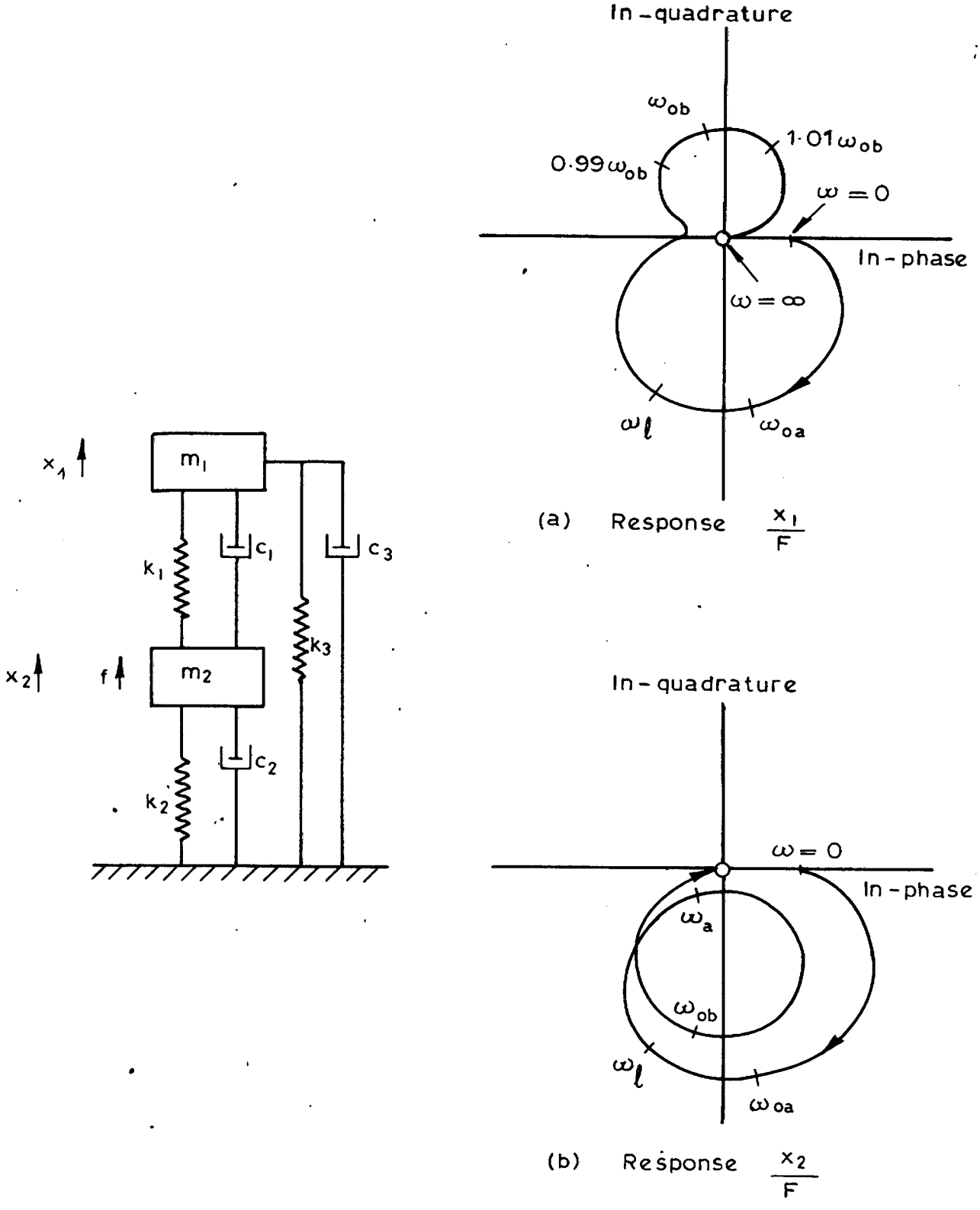

Fig. 7·3 The tuned model — general case.

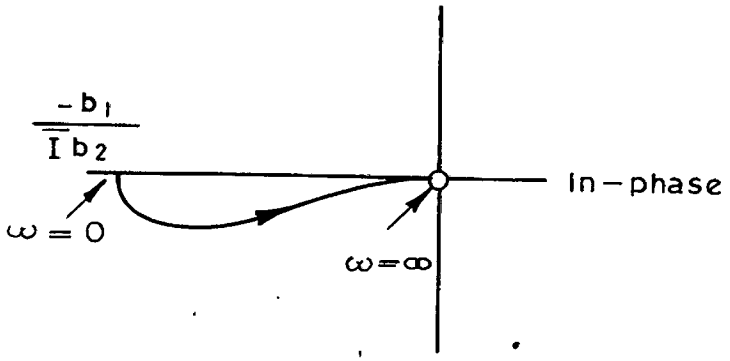

(a) Model and coil magnetic field transfer function $\frac{X}{I}$

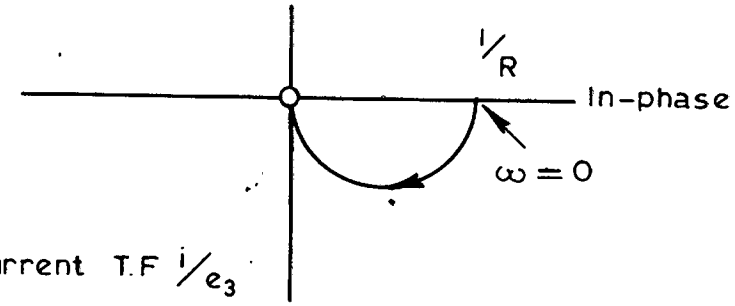

(b) Electro magnet current T.F i/e_3

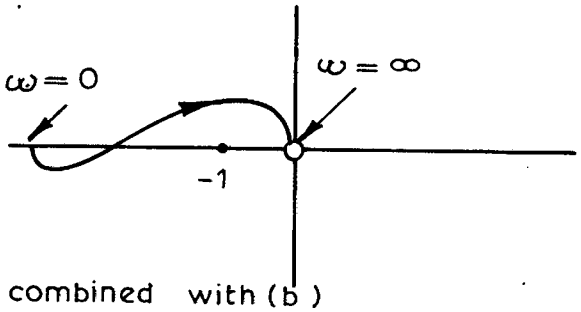

(c) Nyquist plot of (a) combined with (b)

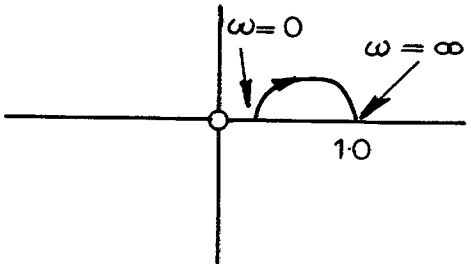

(d) Lead-lag circuit T.F.

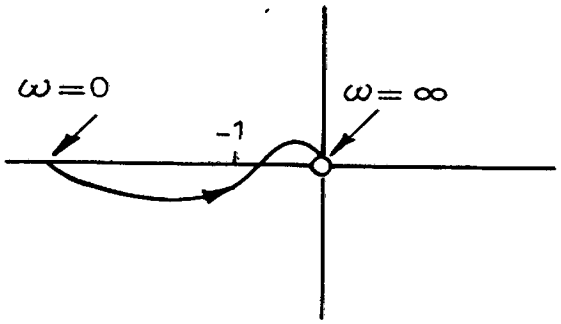

(e) Combination of (d) with (c)

Fig. 7·4 The formation of the lift magnet control loop Nyquist plot.

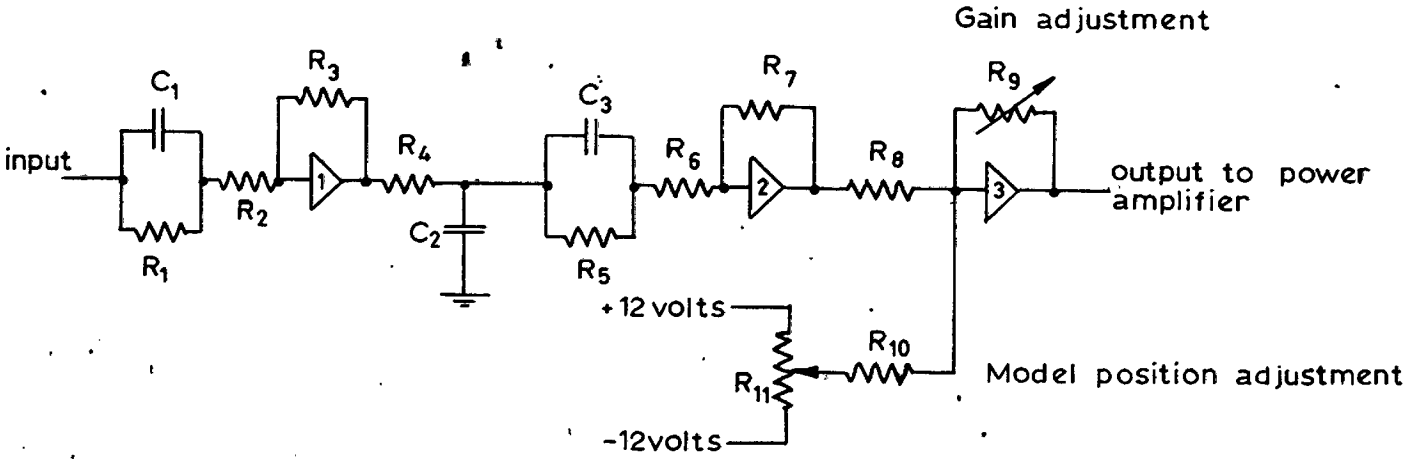

Fig. 7.5(a)

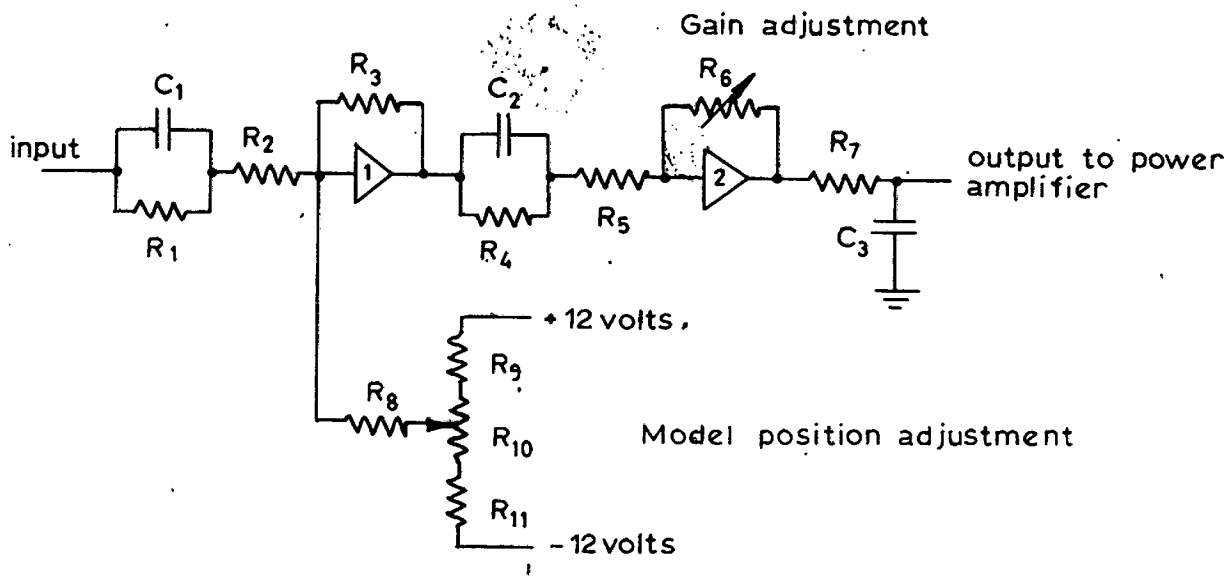

Fig. 7.5(b) Two and three operational-amplifier stabilisation networks, providing two lead-lag stages in series, together with loop gain and model position adjustment.

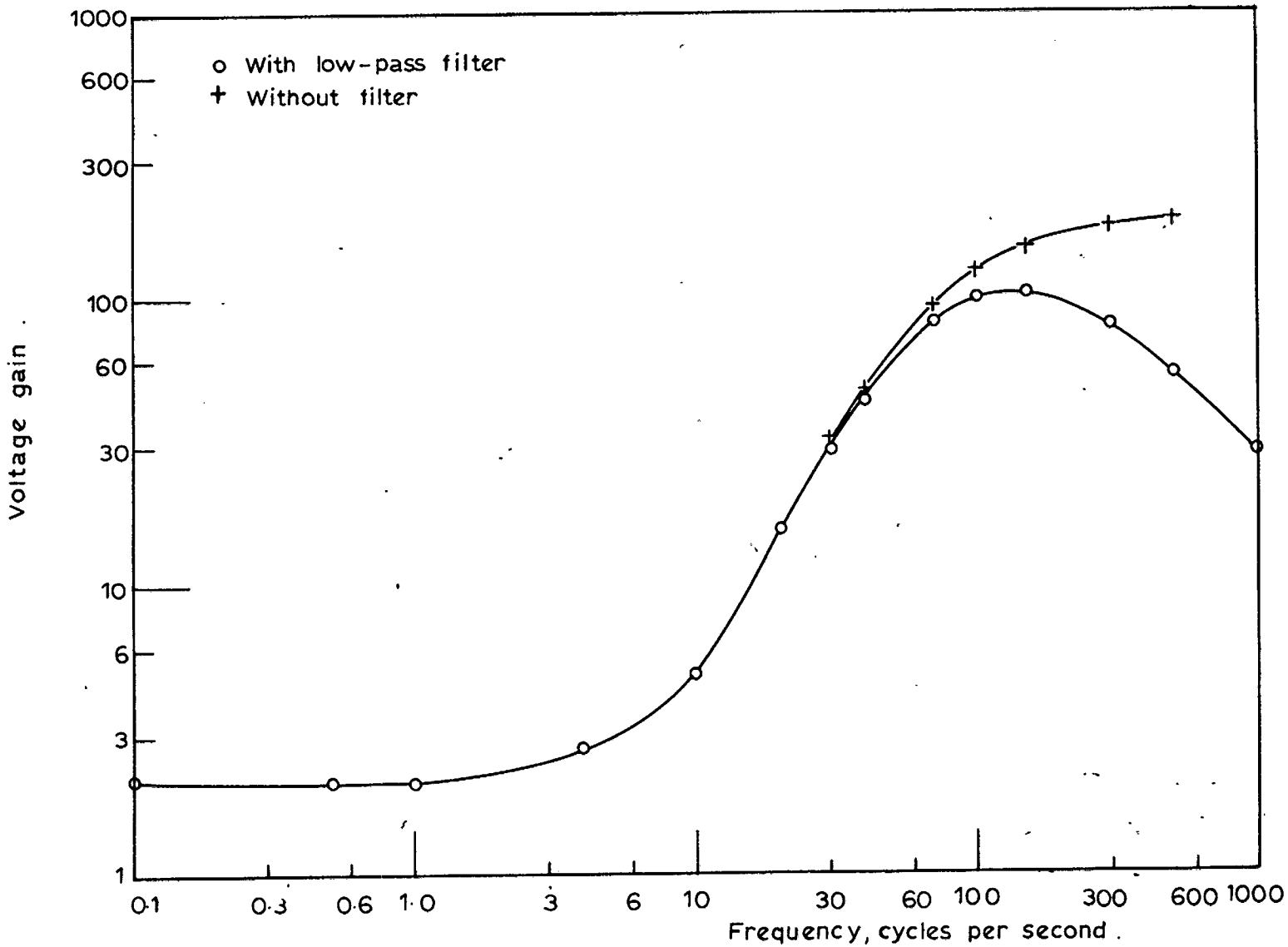

Fig. 7.6 Forward vertical compensation circuit gain characteristics.

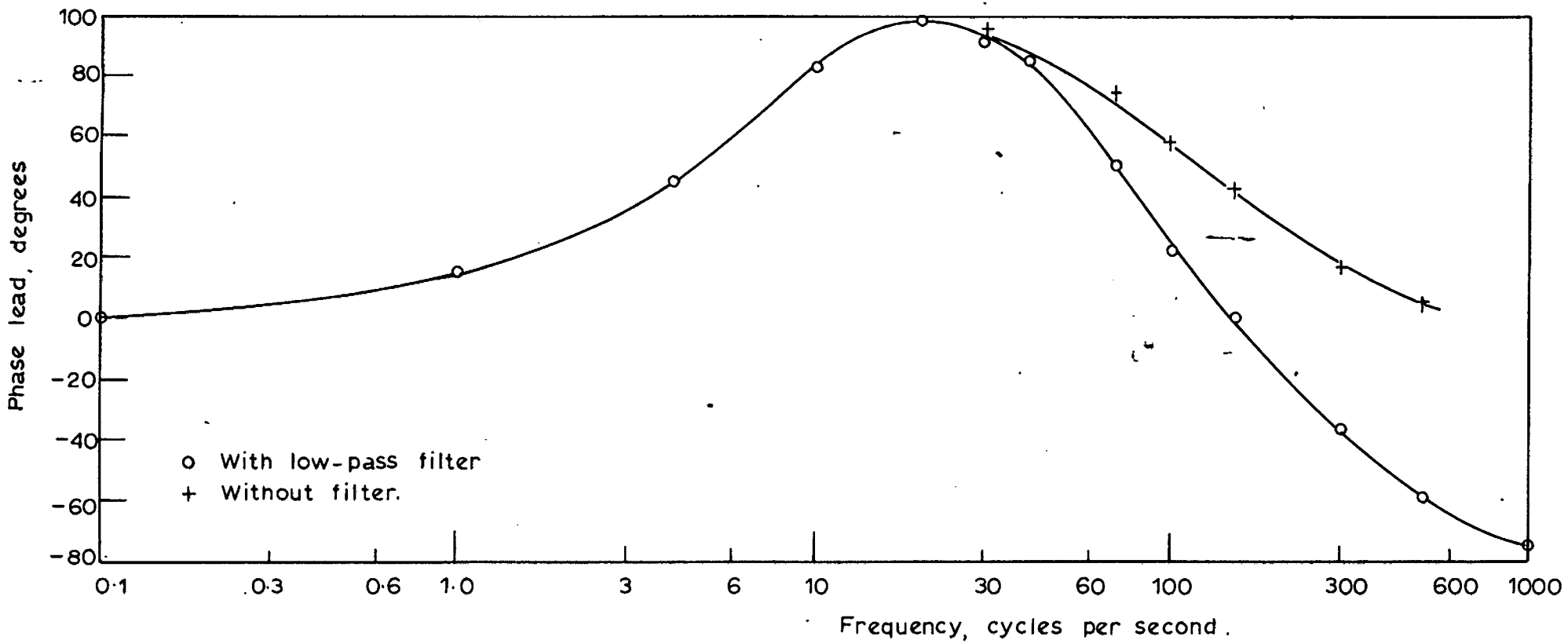

Fig.7.7 Forward vertical compensation circuit phase characteristics.

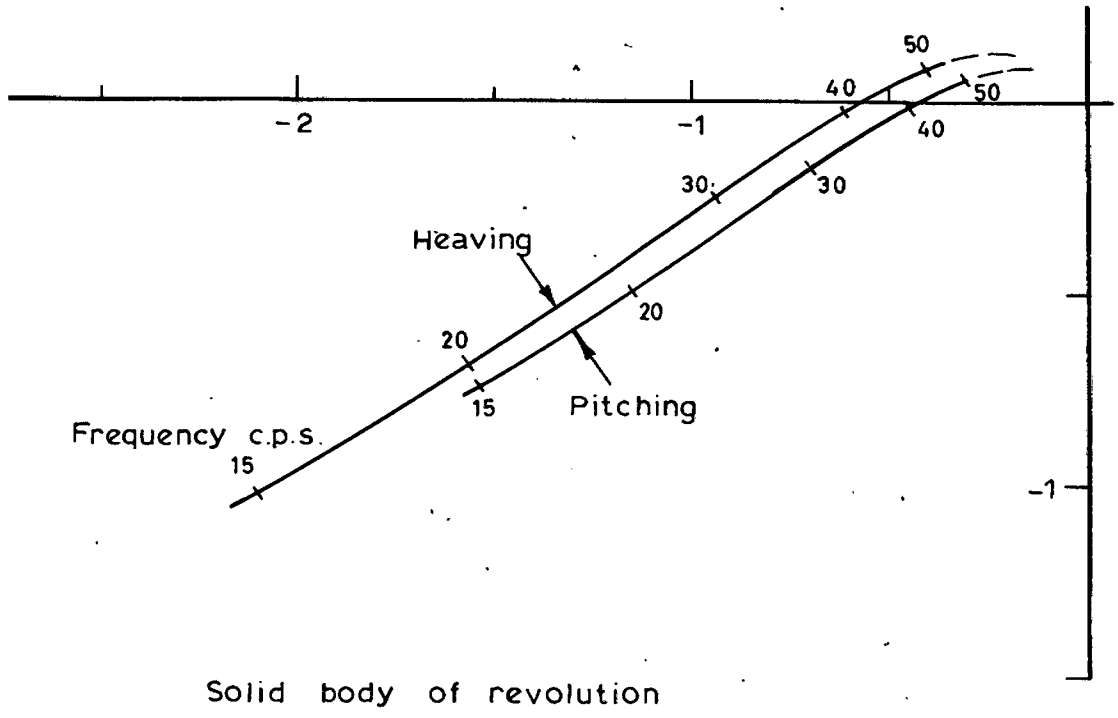

Solid body of revolution

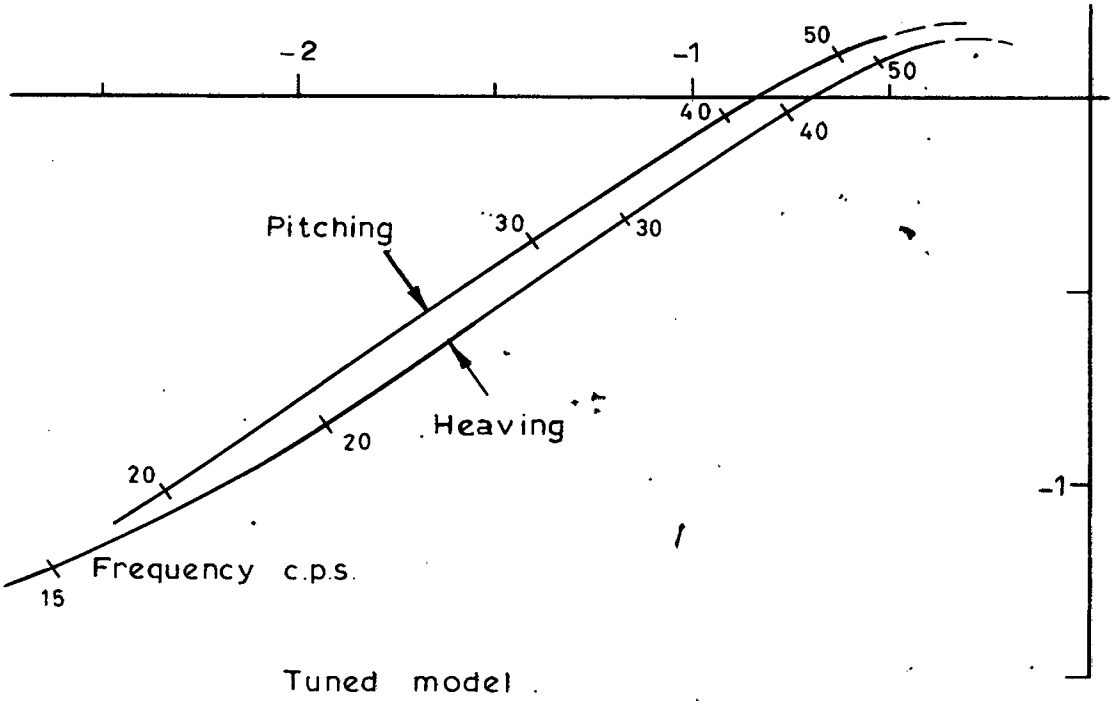

Tuned model

Fig. 7.8 Nyquist plots for two models, main suspension magnet system.

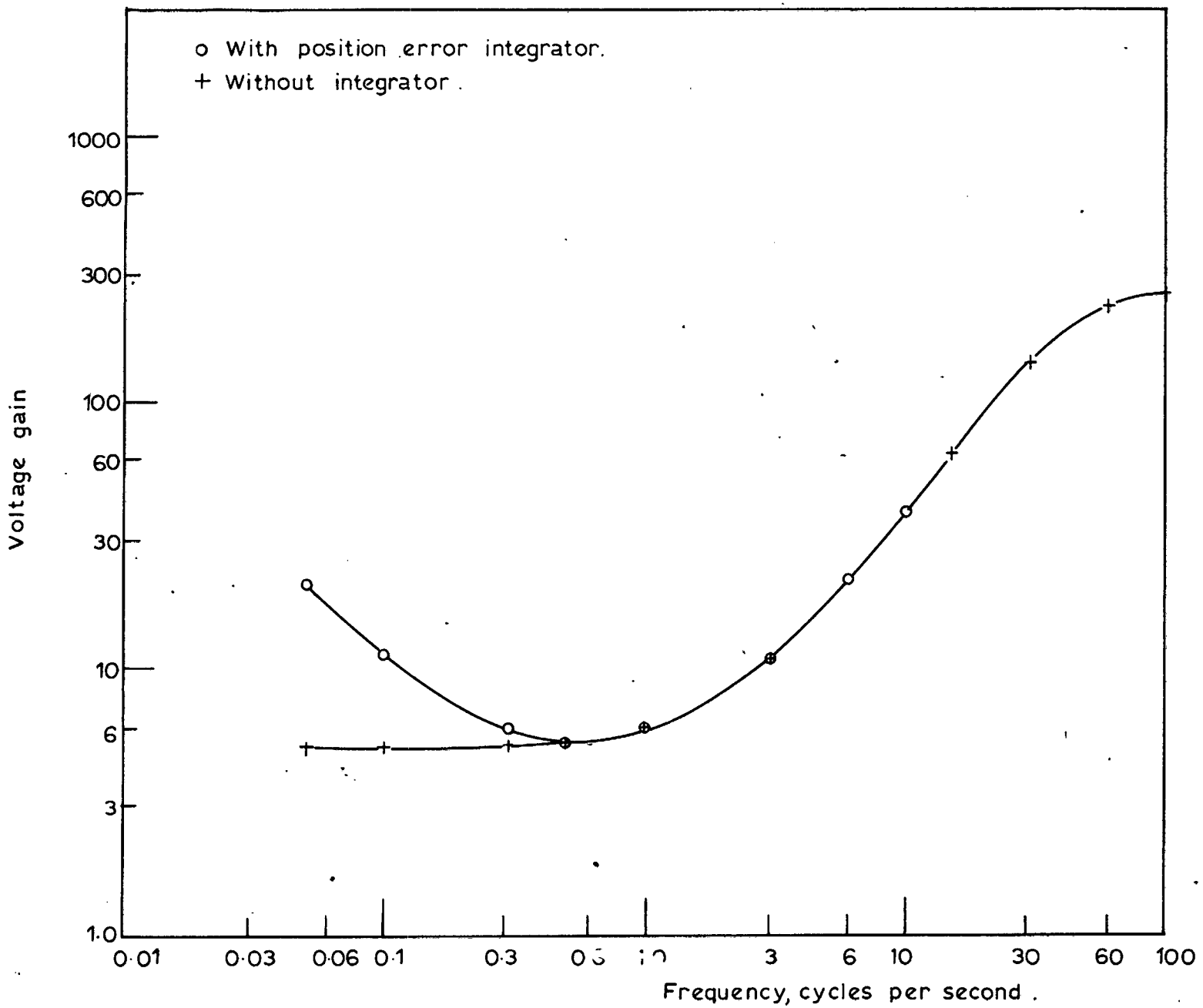

Fig. 7.9 Drag-control compensation circuit gain characteristics.

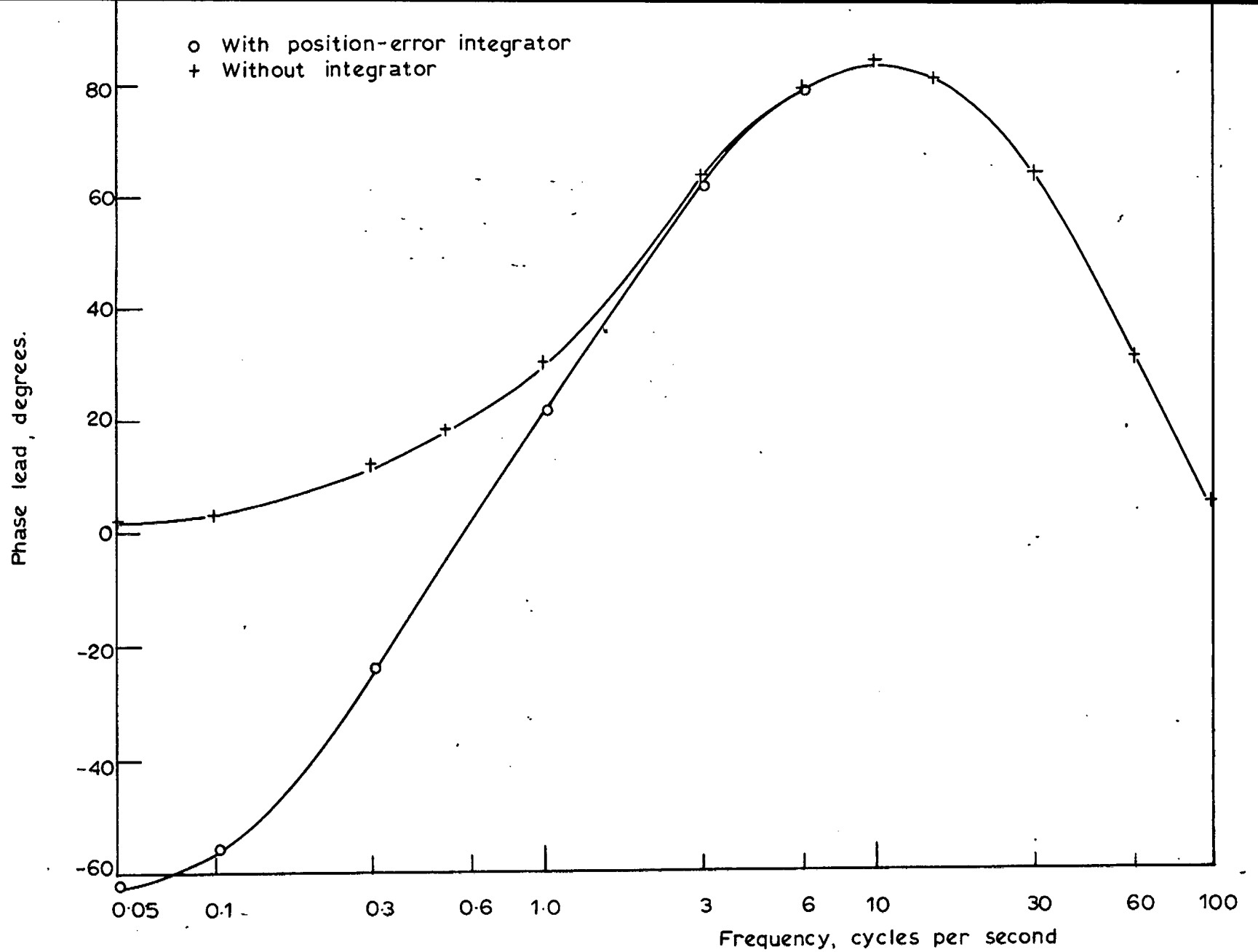

Fig. 7.10 Drag control compensation circuit phase characteristics.

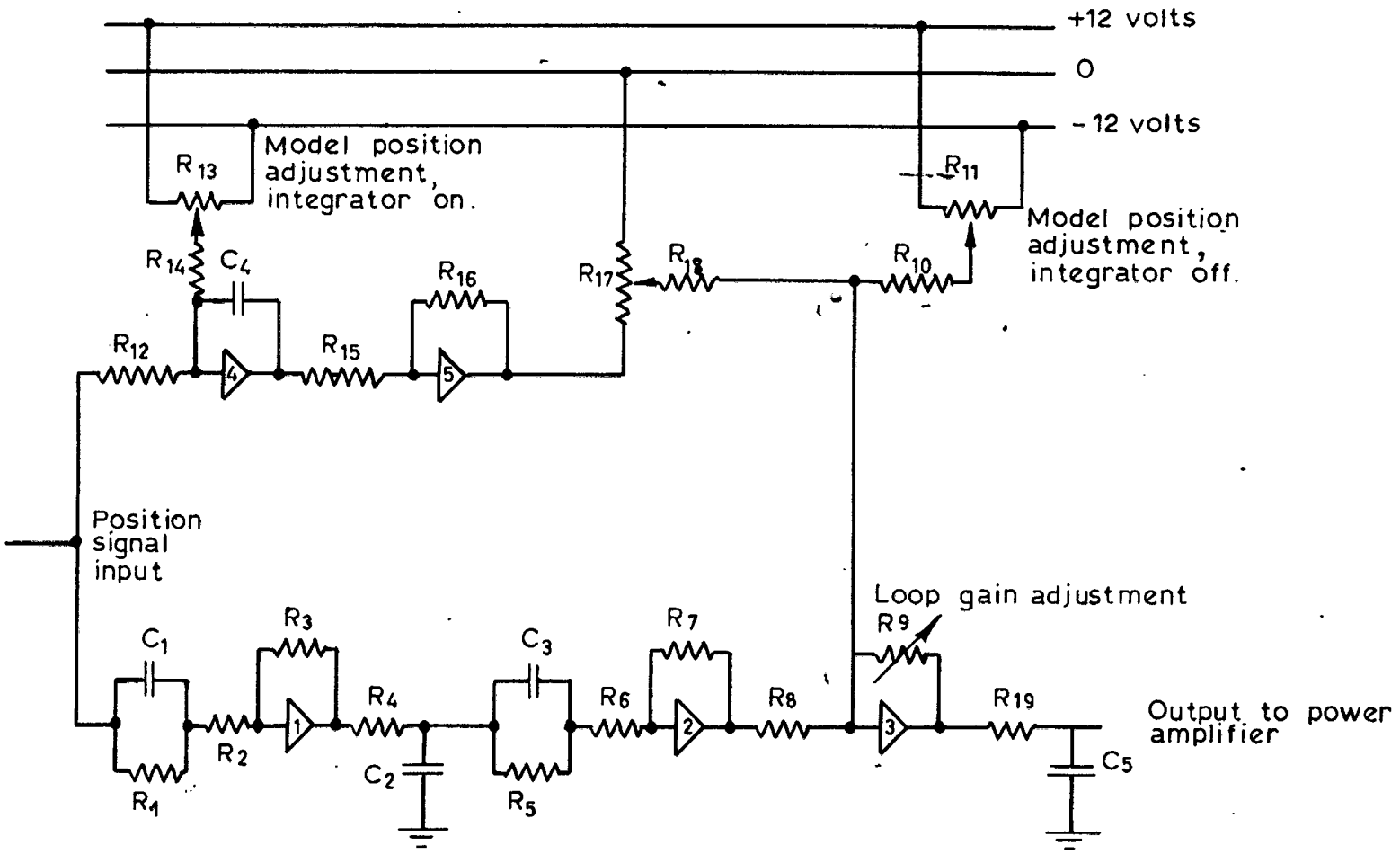

Fig. 7.11. The drag coil control loop compensation circuit, including a positioning-error integrator.

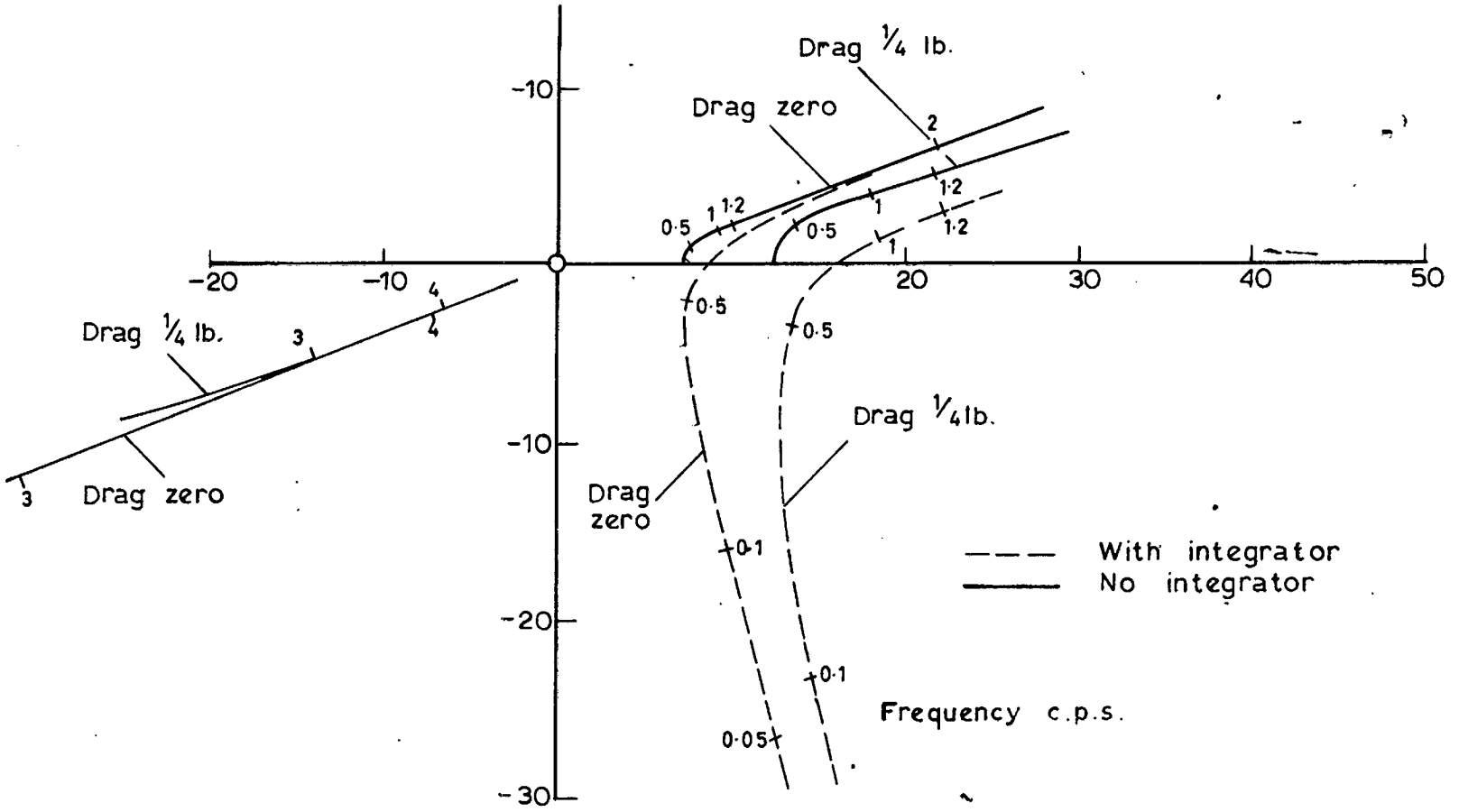

Fig. 7.12 The calculated low frequency Nyquist plot for drag control system, with tuned model .

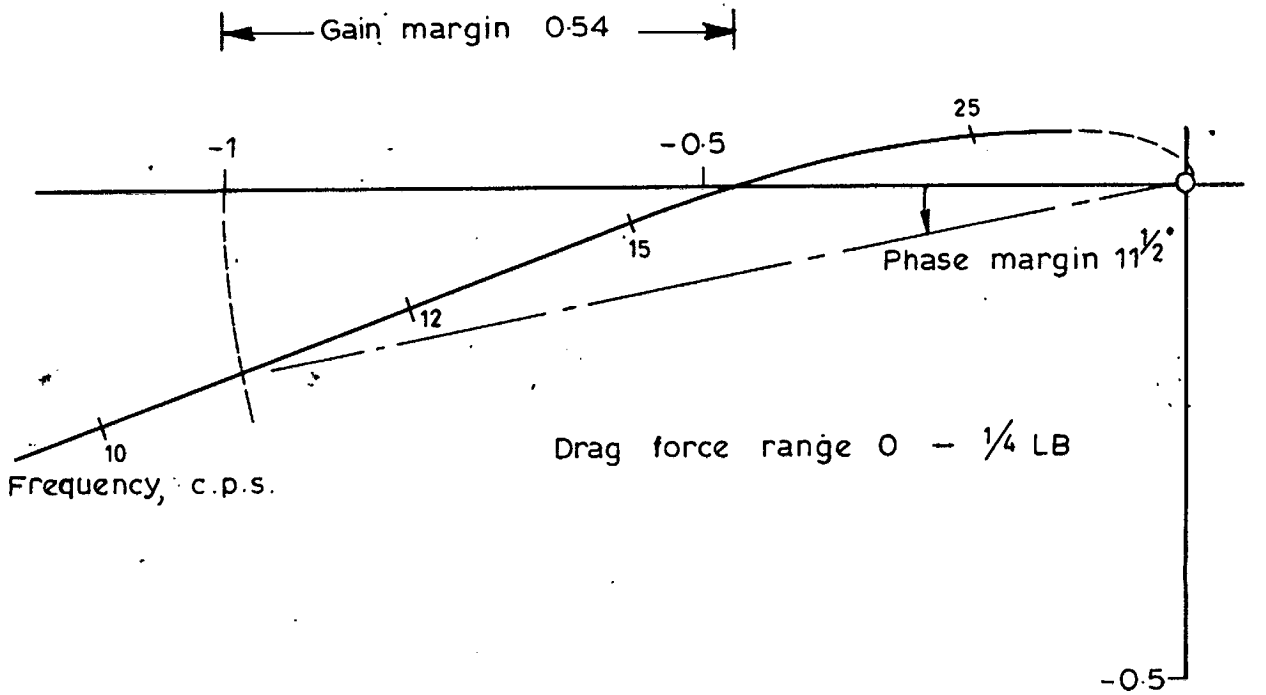

Fig. 7.13 The calculated high frequency Nyquist plot for drag control system, with tuned model.

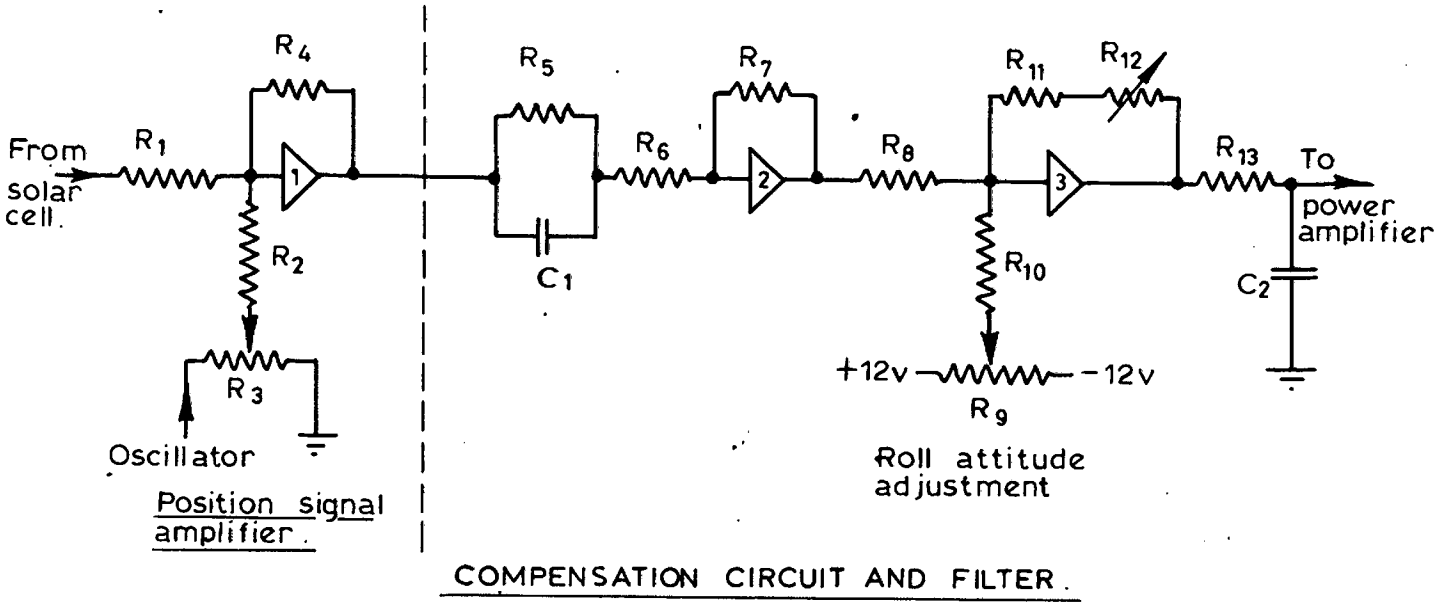

Fig. 7.14 The roll control system position signal amplifier and compensation circuit.

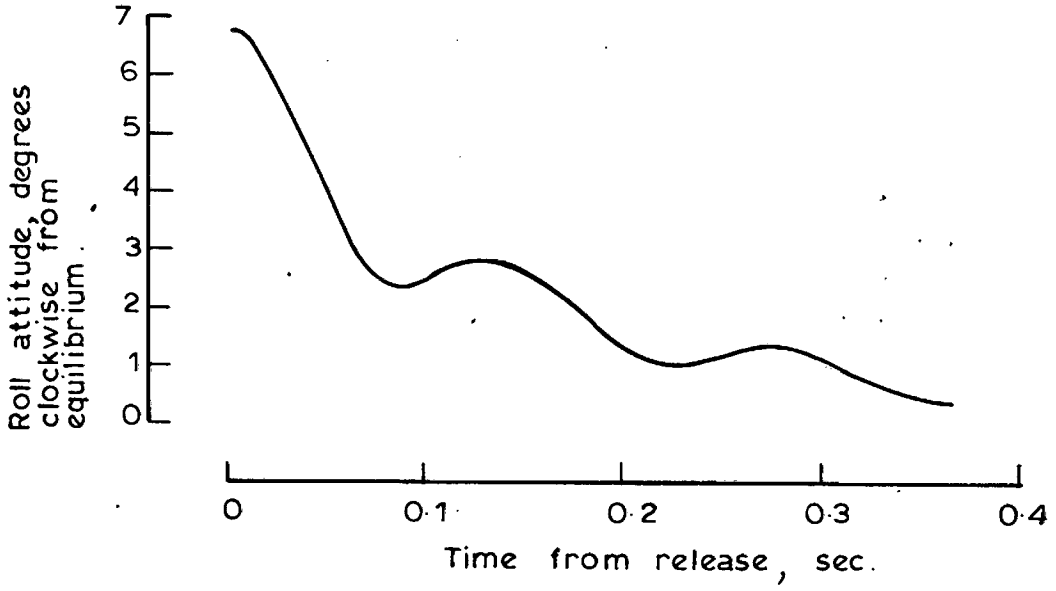

Fig. 7.15 The motion of a model following release from a displacement-in-roll away from equilibrium.

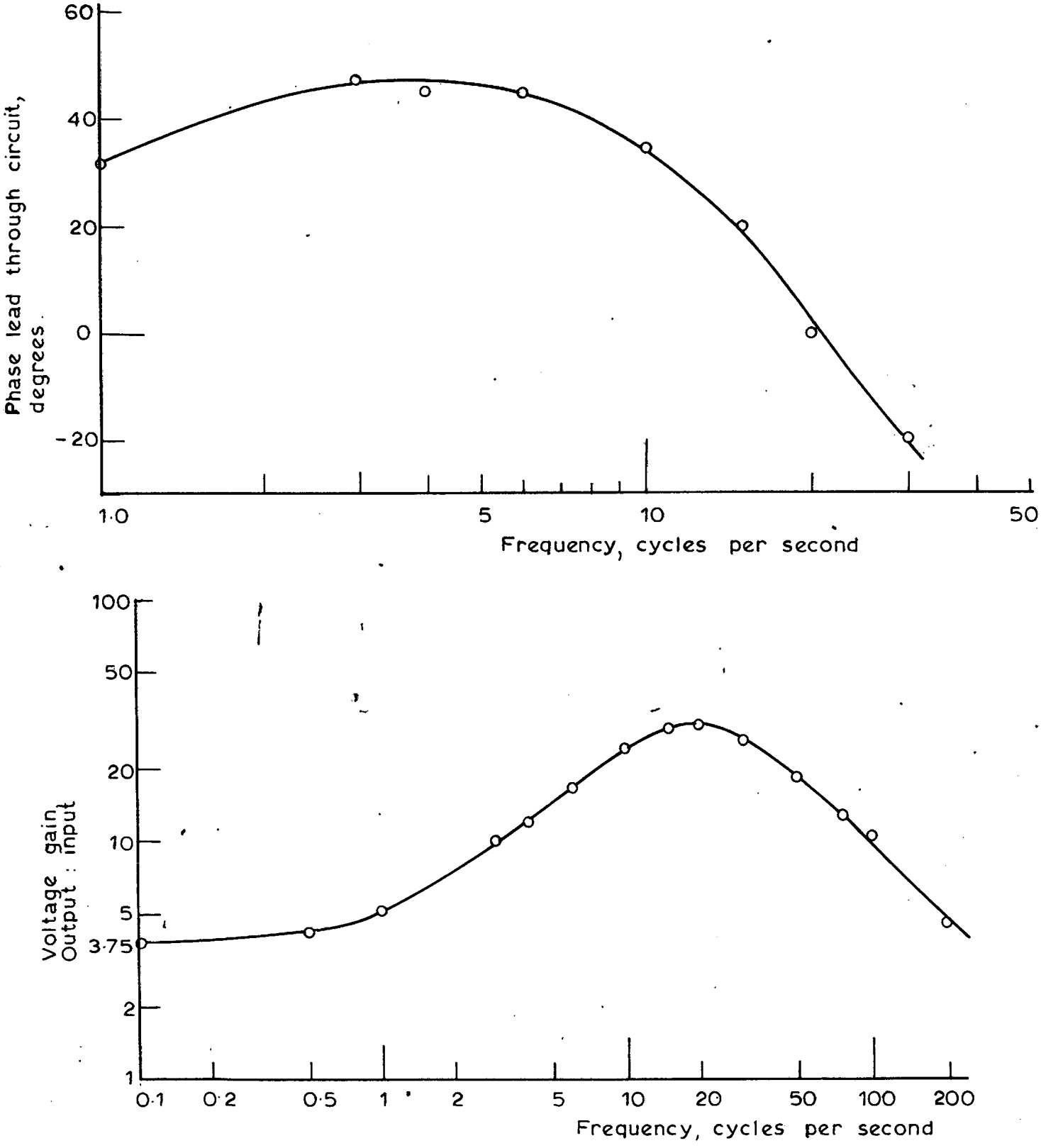

Fig. 7·16 The measured gain and phase characteristics of the roll control system compensation circuit.

COMPONENT GROUPS

1. THE MODEL:

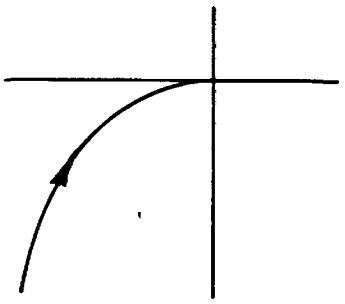

Motion in-phase with applied moment.

Positive moment and displacement

2. COILS AND MAGNETIC FIELDS:

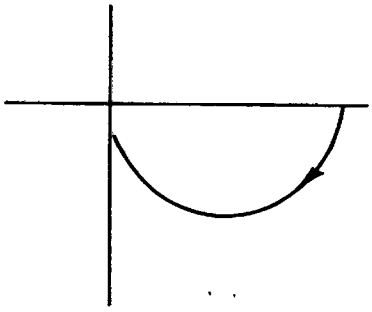

Moment in-phase with applied e.m.f

3. POSITION SIGNAL AMPLIFIER, COMPENSATION CIRCUIT AND POWER SUPPLY:

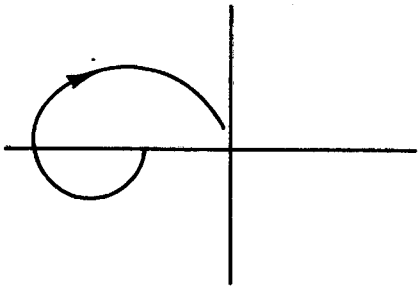

E.m.f. to coil in-phase with model motion.

COMBINATION OF 2 & 3

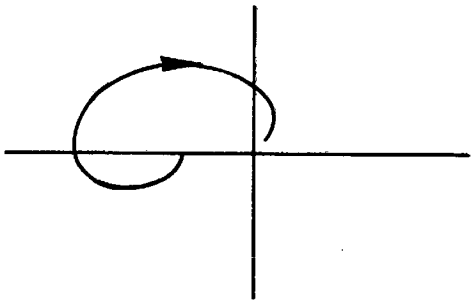

Moment in phase with model motion.

NYQUIST PLOT OF LOOP.

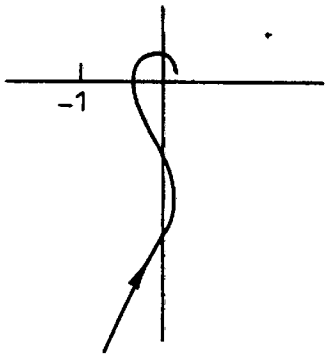

Fig. 7.17 The formation of the roll control loop Nyquist plot from the individual transfer functions of the component parts presented in three groups.

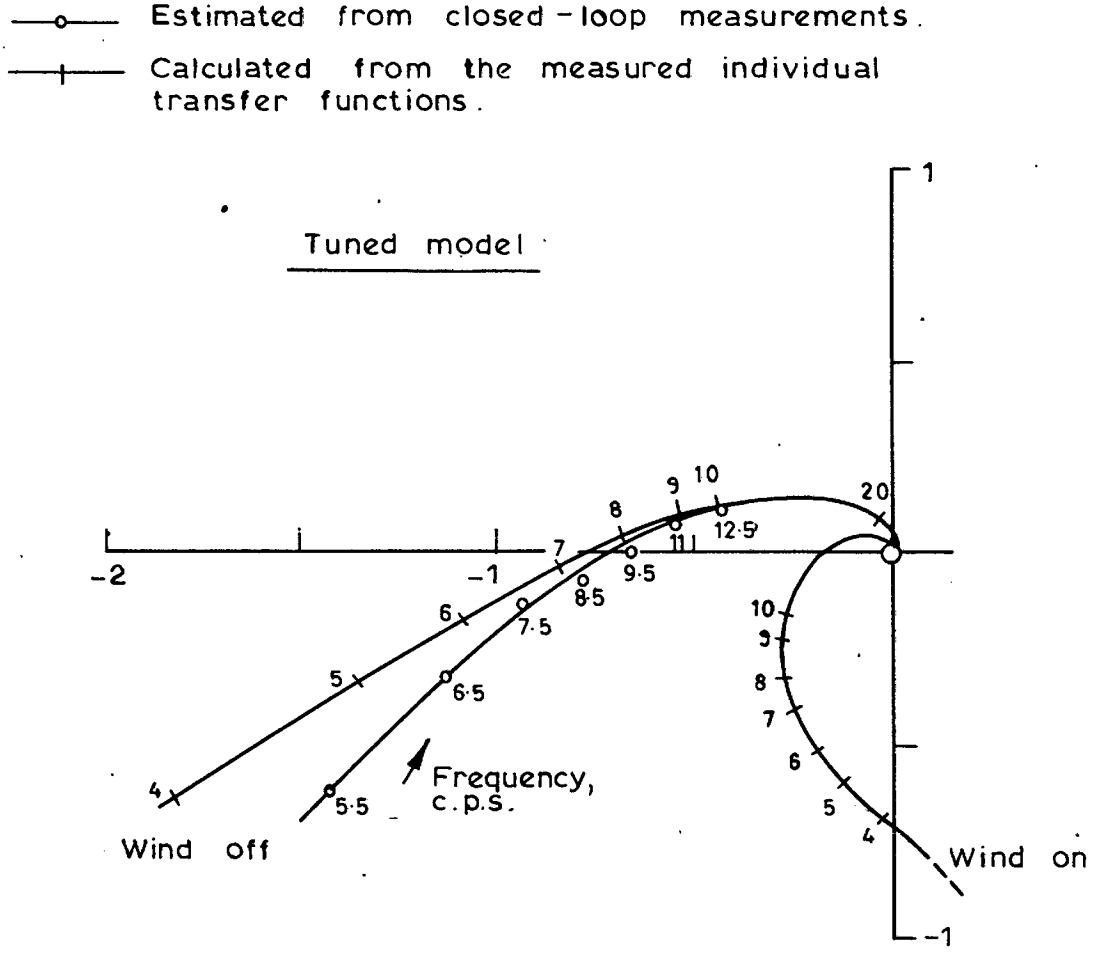

Fig. 7.18 Nyquist plot, roll control system.

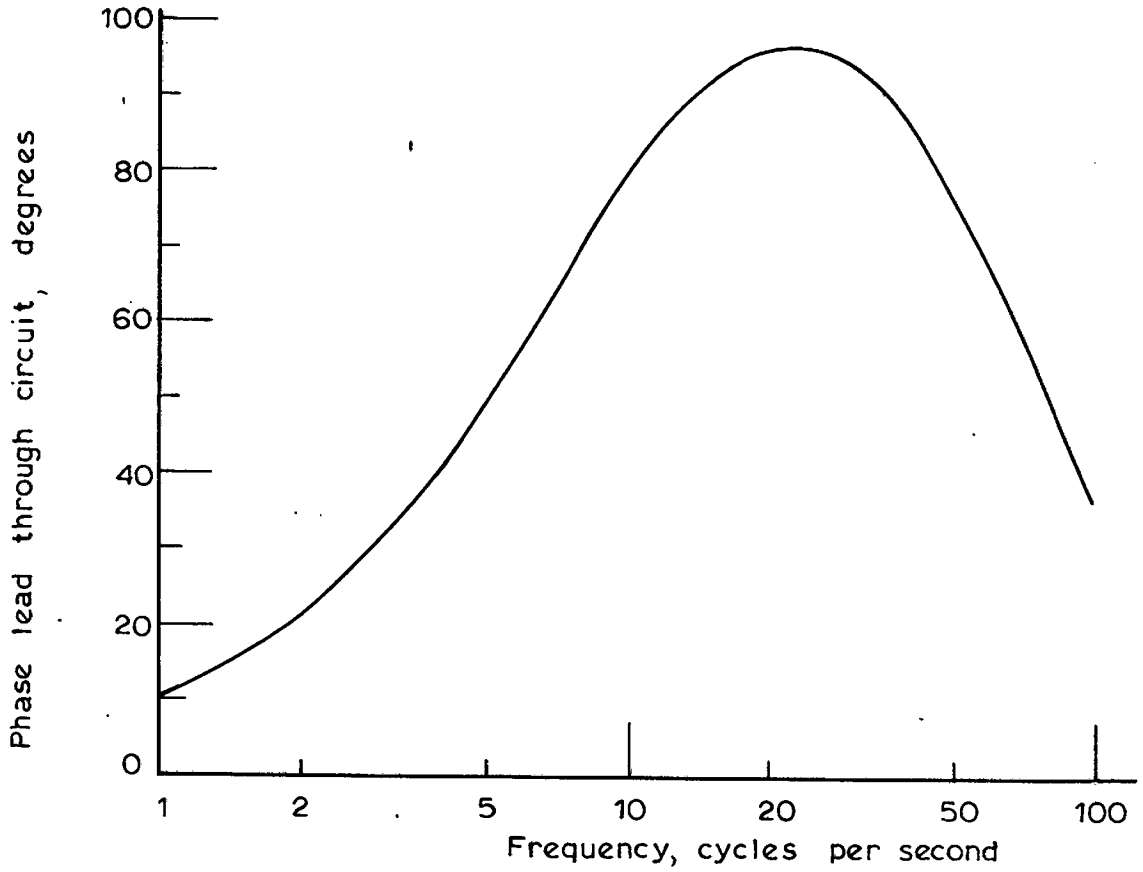

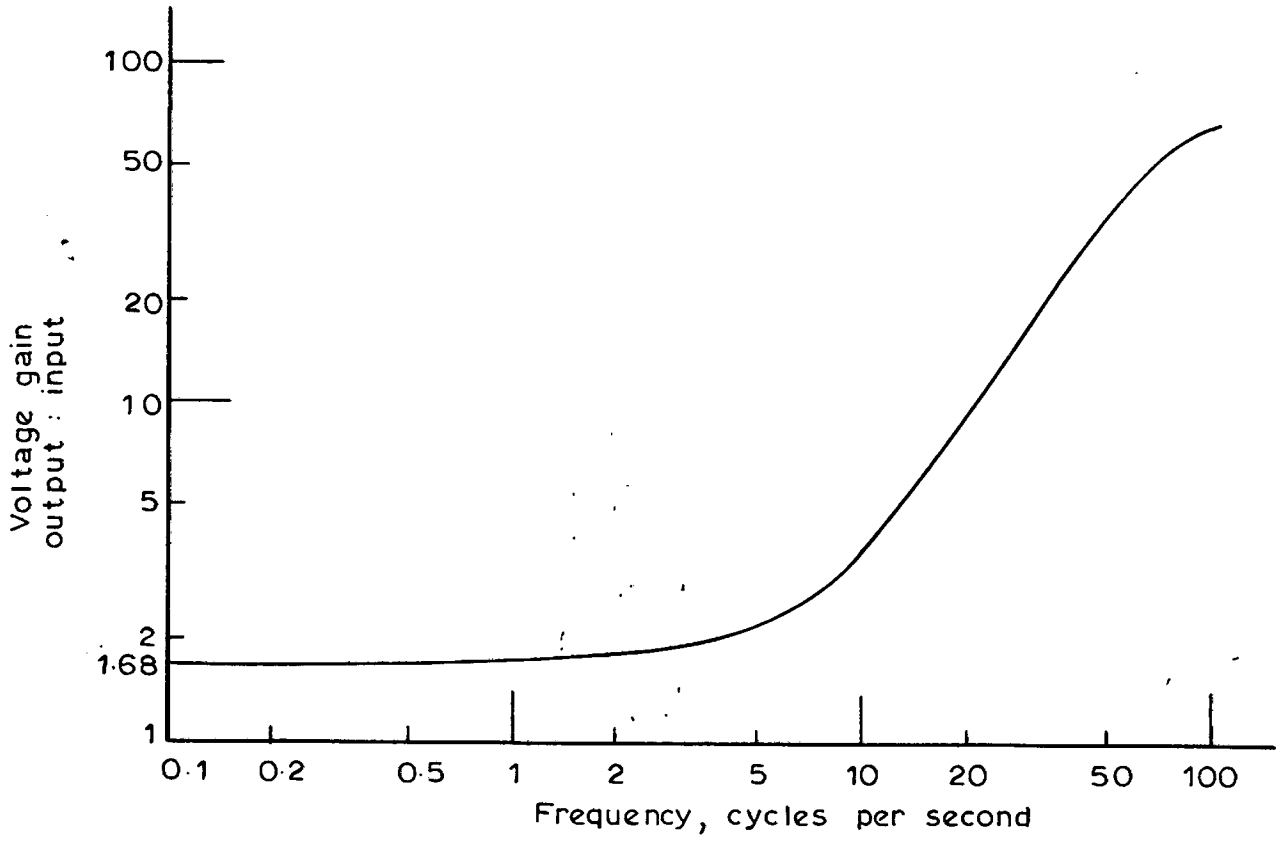

Fig. 7.19 The gain and phase characteristics of the lateral control system compensation circuits — solid model .

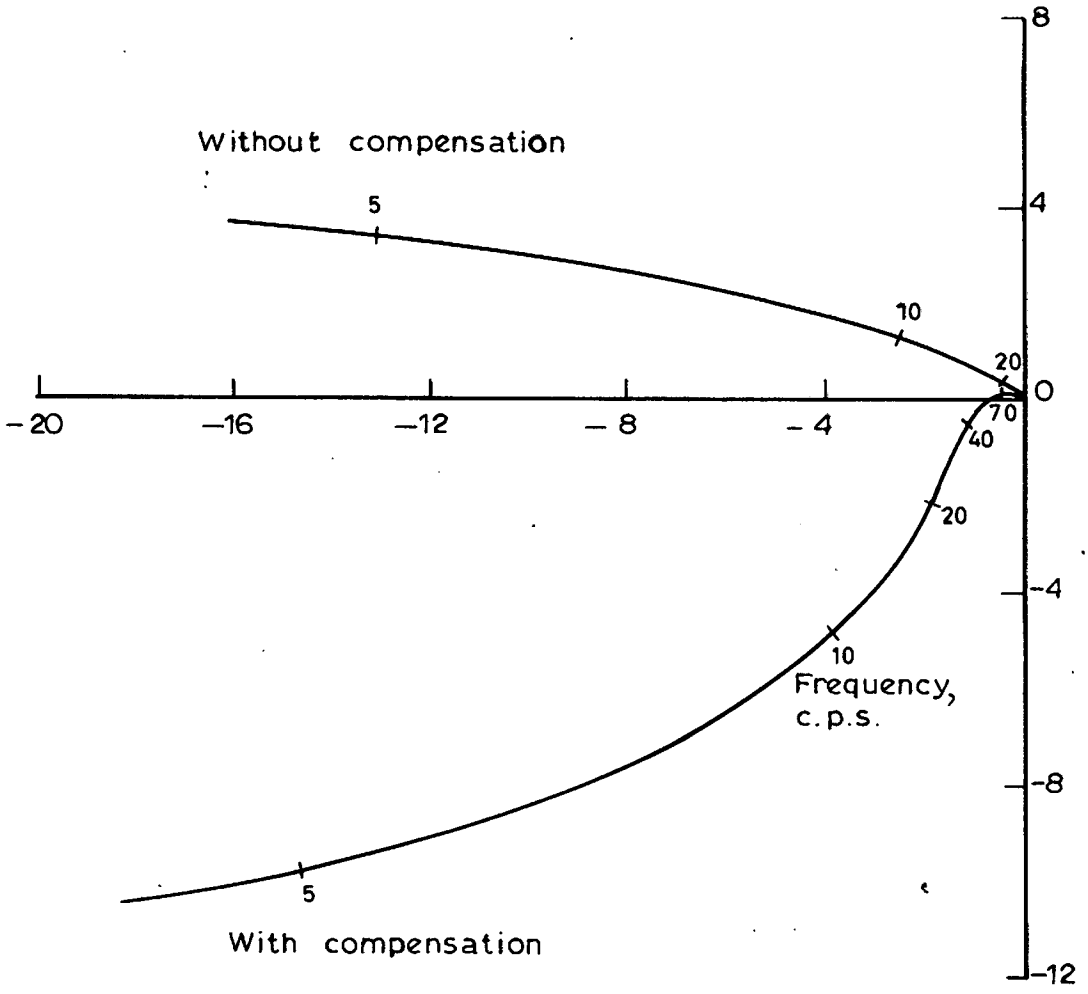

Fig. 7.20 Lateral position control loop Nyquist plot, with and without phase compensation.

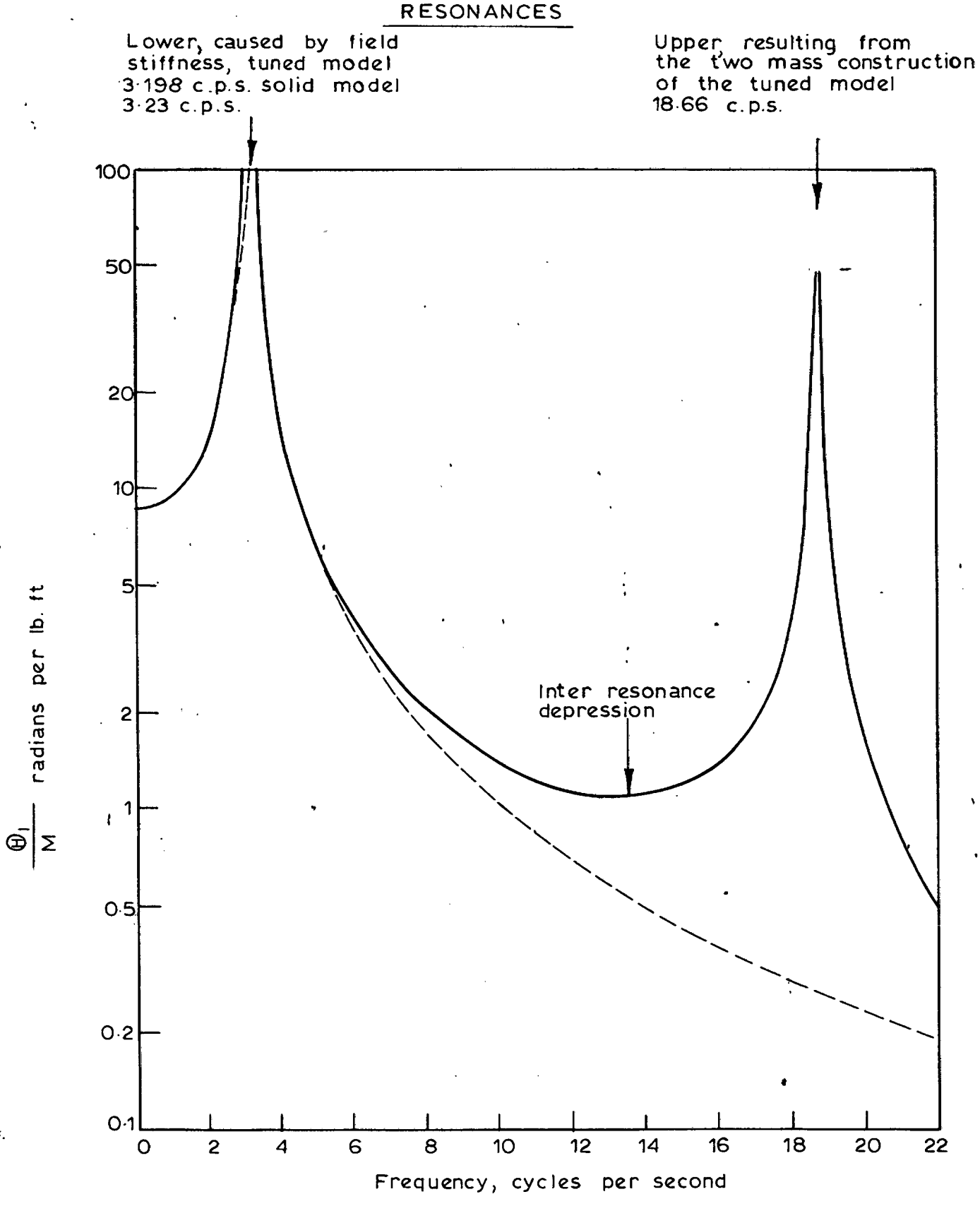

Fig. 7·21 The theoretical undamped frequency response of (i) a pitch tuned model, and (ii) the same model with the core locked, acting as a solid model.

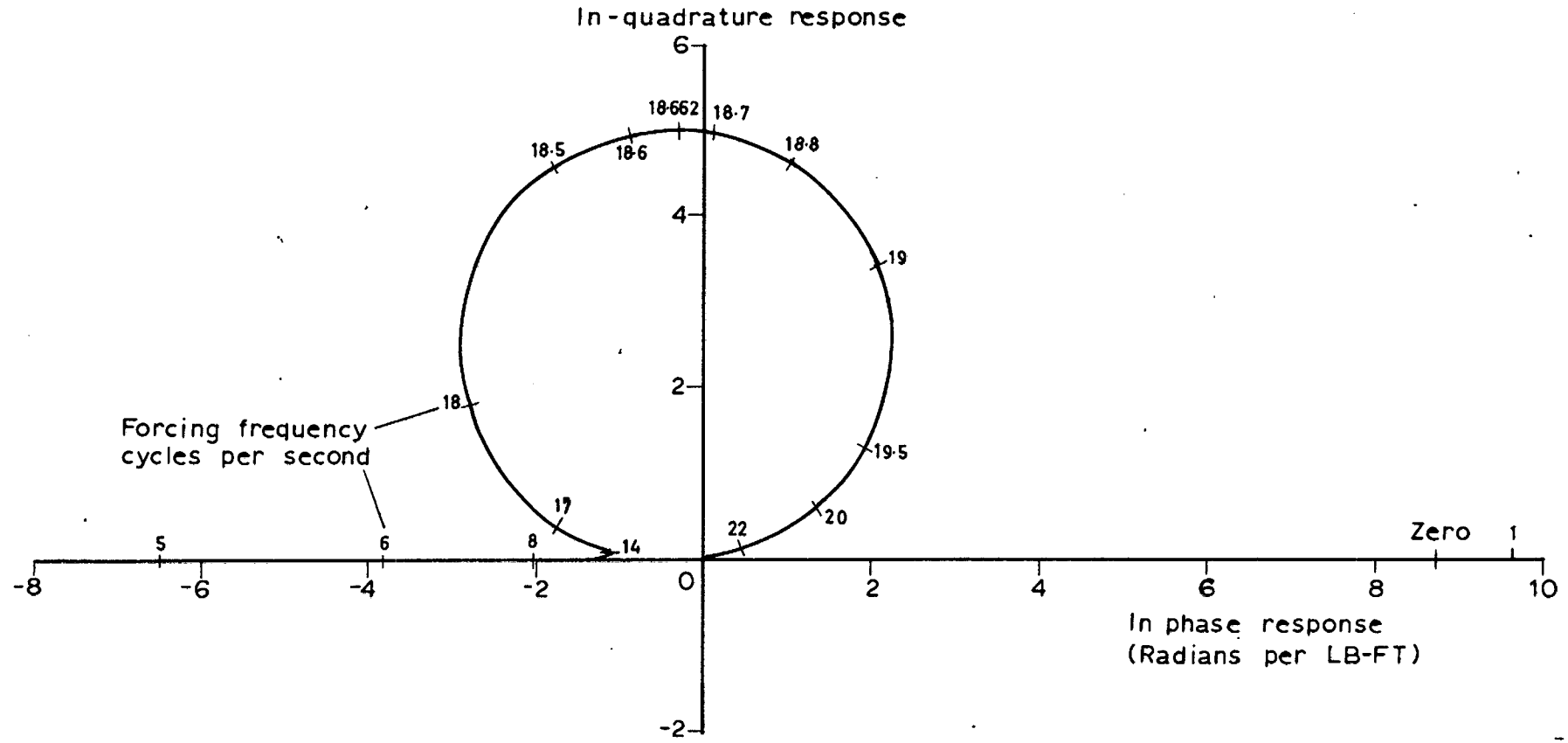

Fig. 7.22. The theoretical response $\frac{\Theta}{M}$ of a pitch tuned model showing the upper resonance in the region of the undamped natural frequency of 18·66 c.p.s.

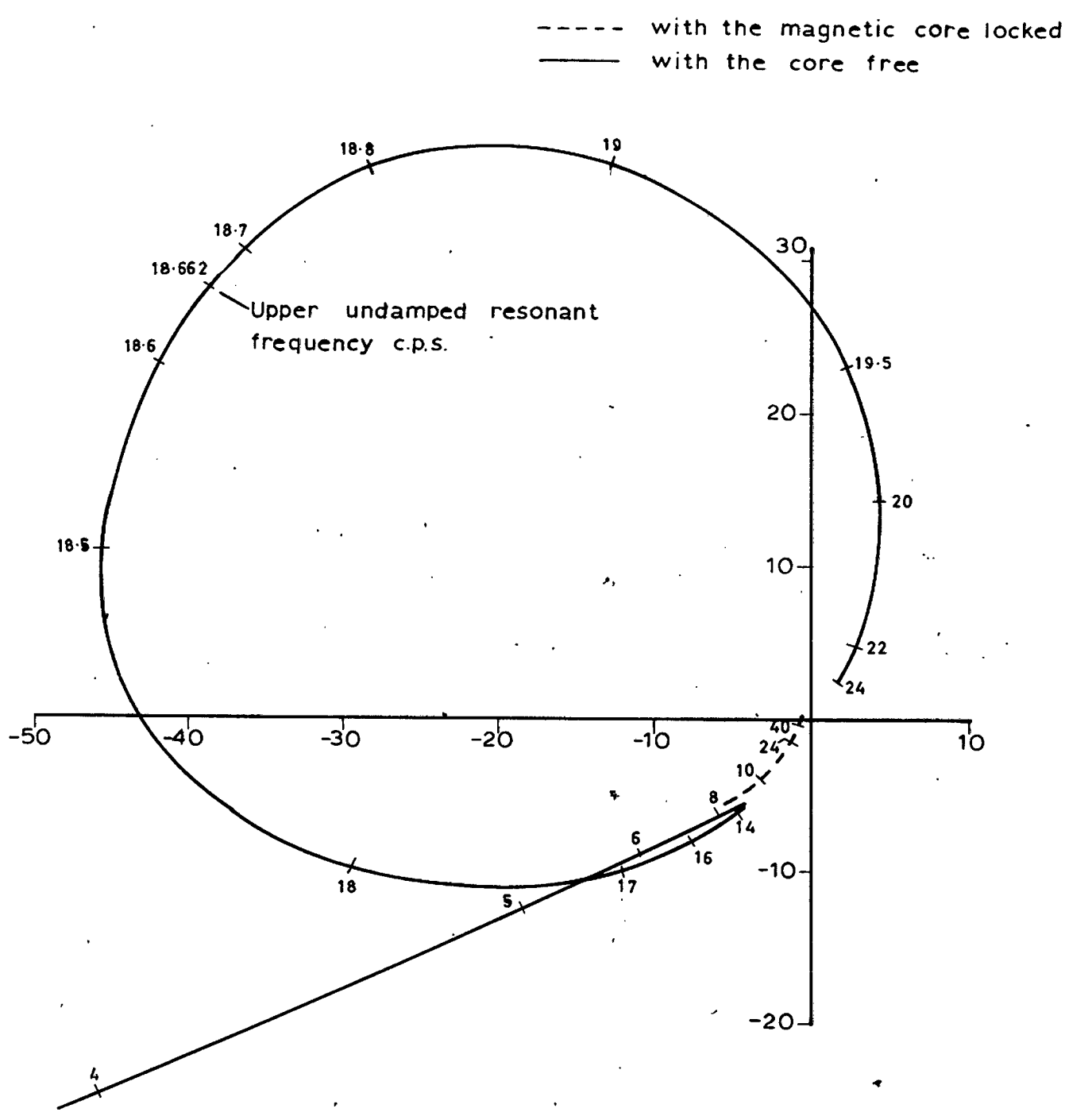

Fig. 7.23. Tuned model Nyquist plots, using the solid model compensation circuits (lateral pitching motion.)

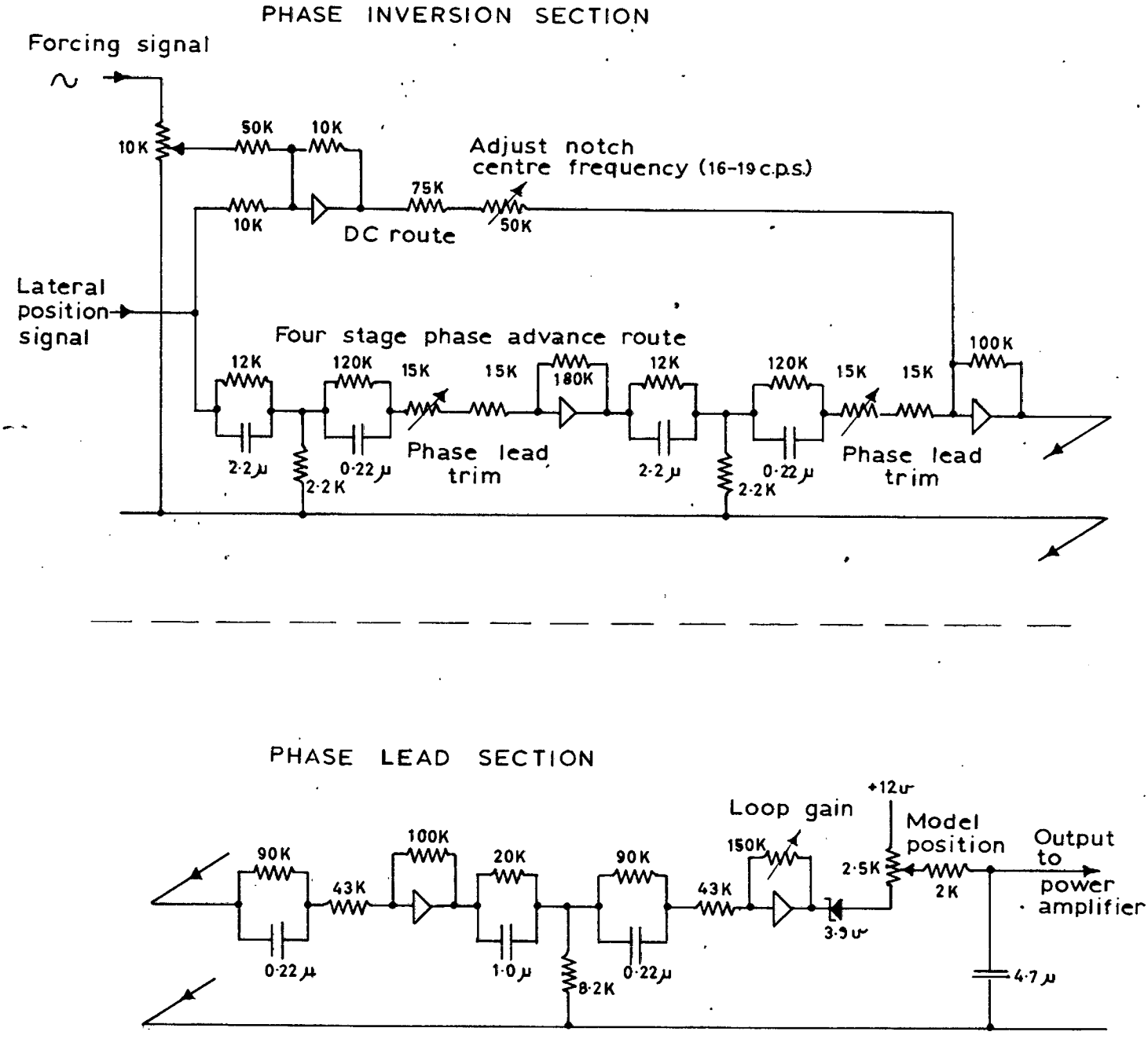

Fig. 7.24. The tuned model control loop compensation network, consisting of a phase inversion section in series with a phase lead section.

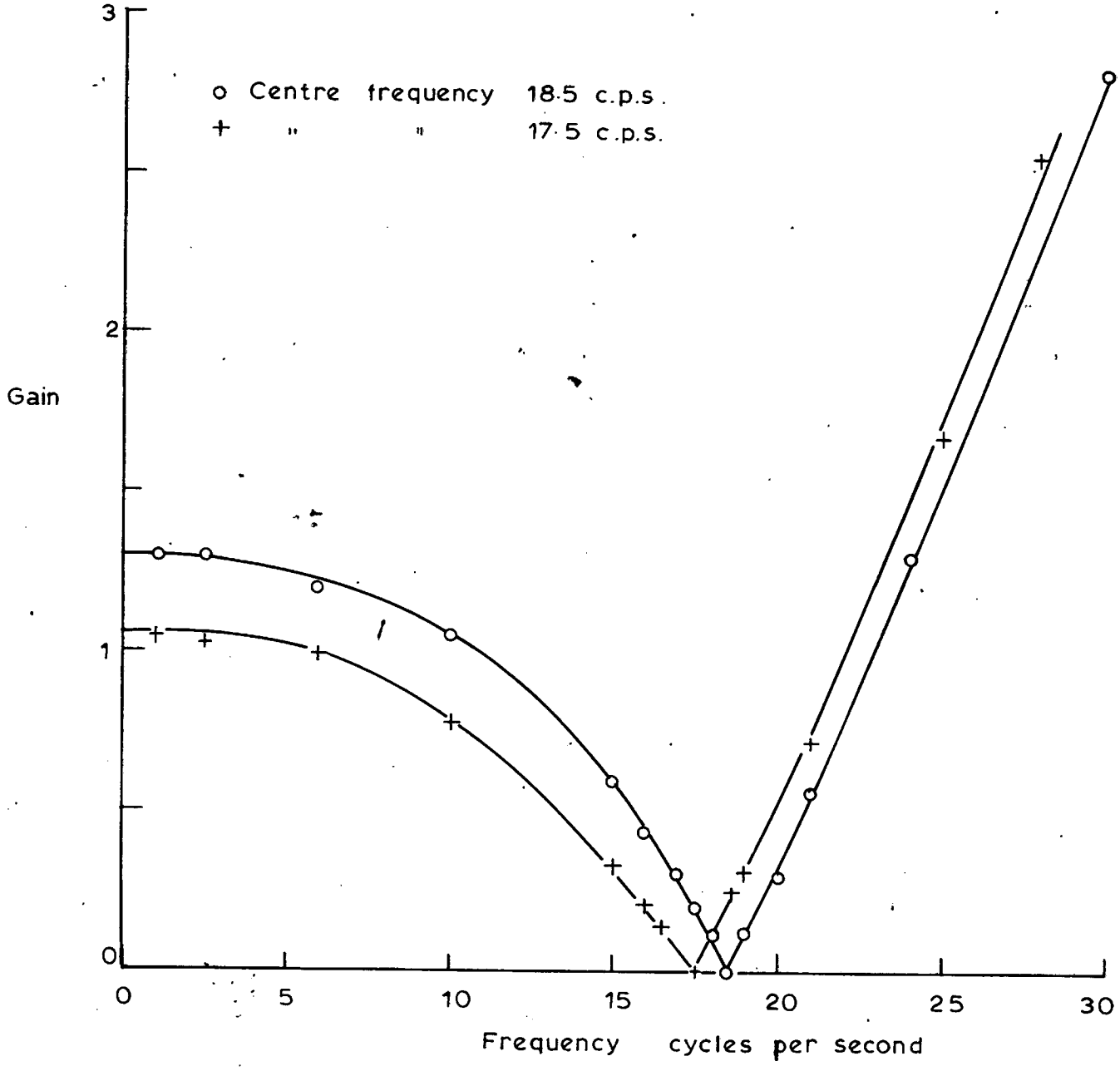

Fig. 7·25 The measured variation of gain with frequency for the phase inversion section of the tuned model lateral position control loop compensation network.

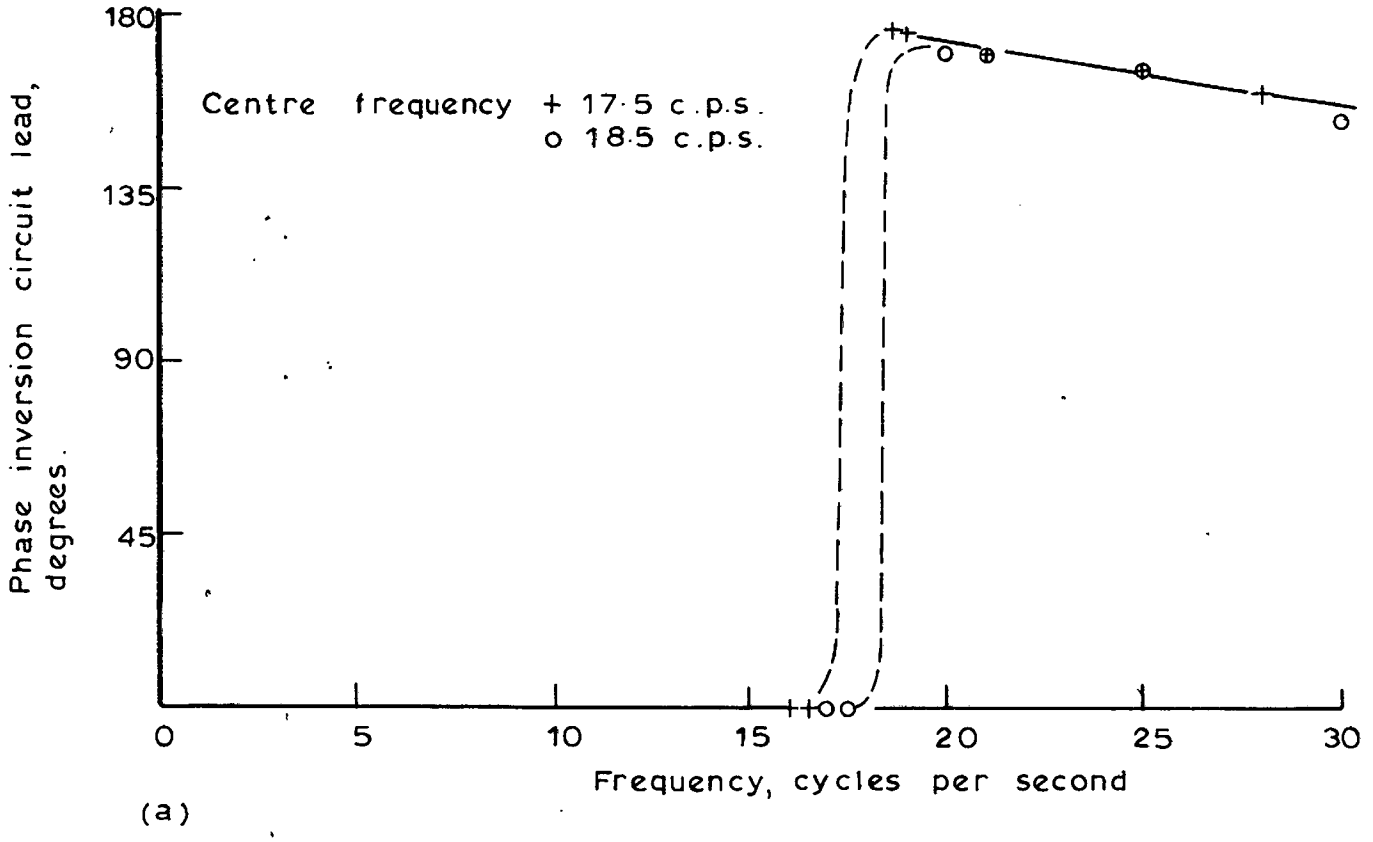

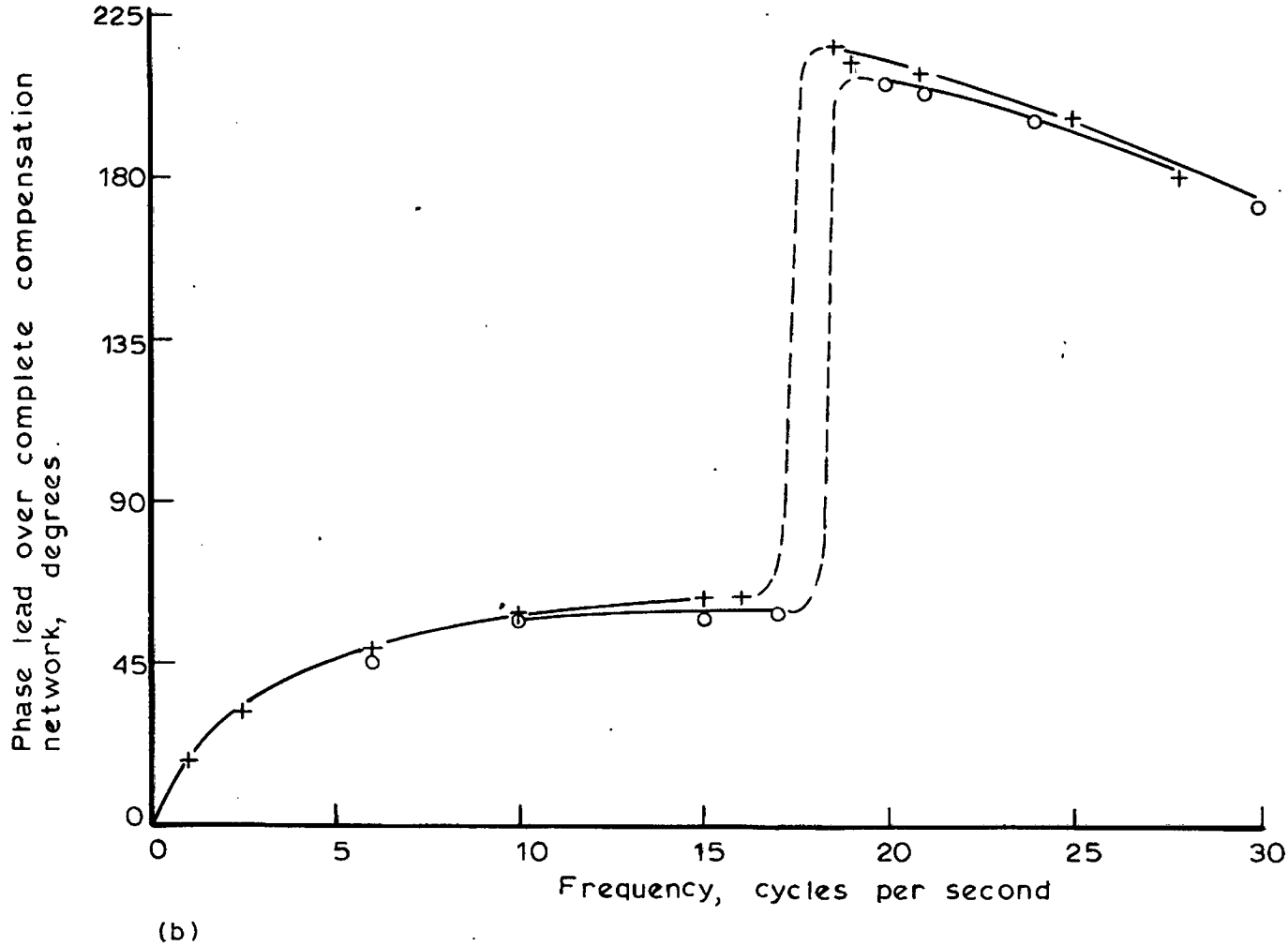

Fig. 7·26 The measured variation with frequency of the phase lead over (a) the phase inversion section and (b) the complete tuned model lateral position control loop compensation network.

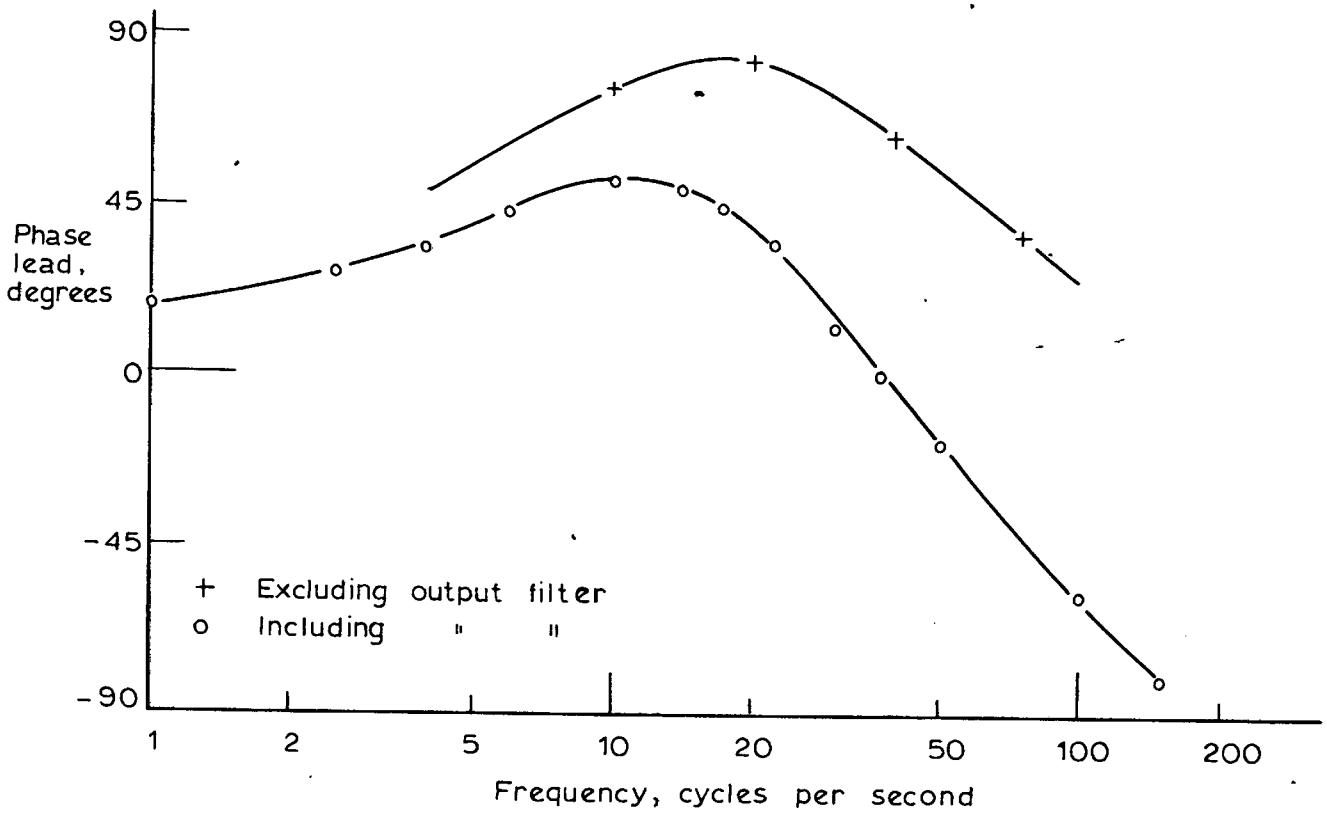

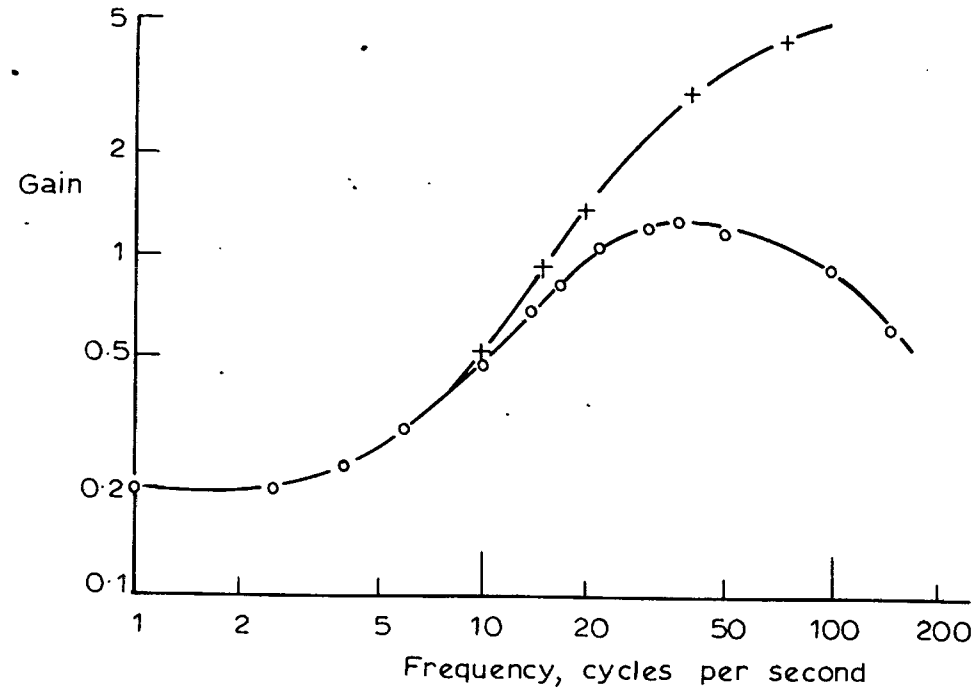

Fig. 7.27 The characteristics of the phase-lead section of the tuned-model lateral compensation network.

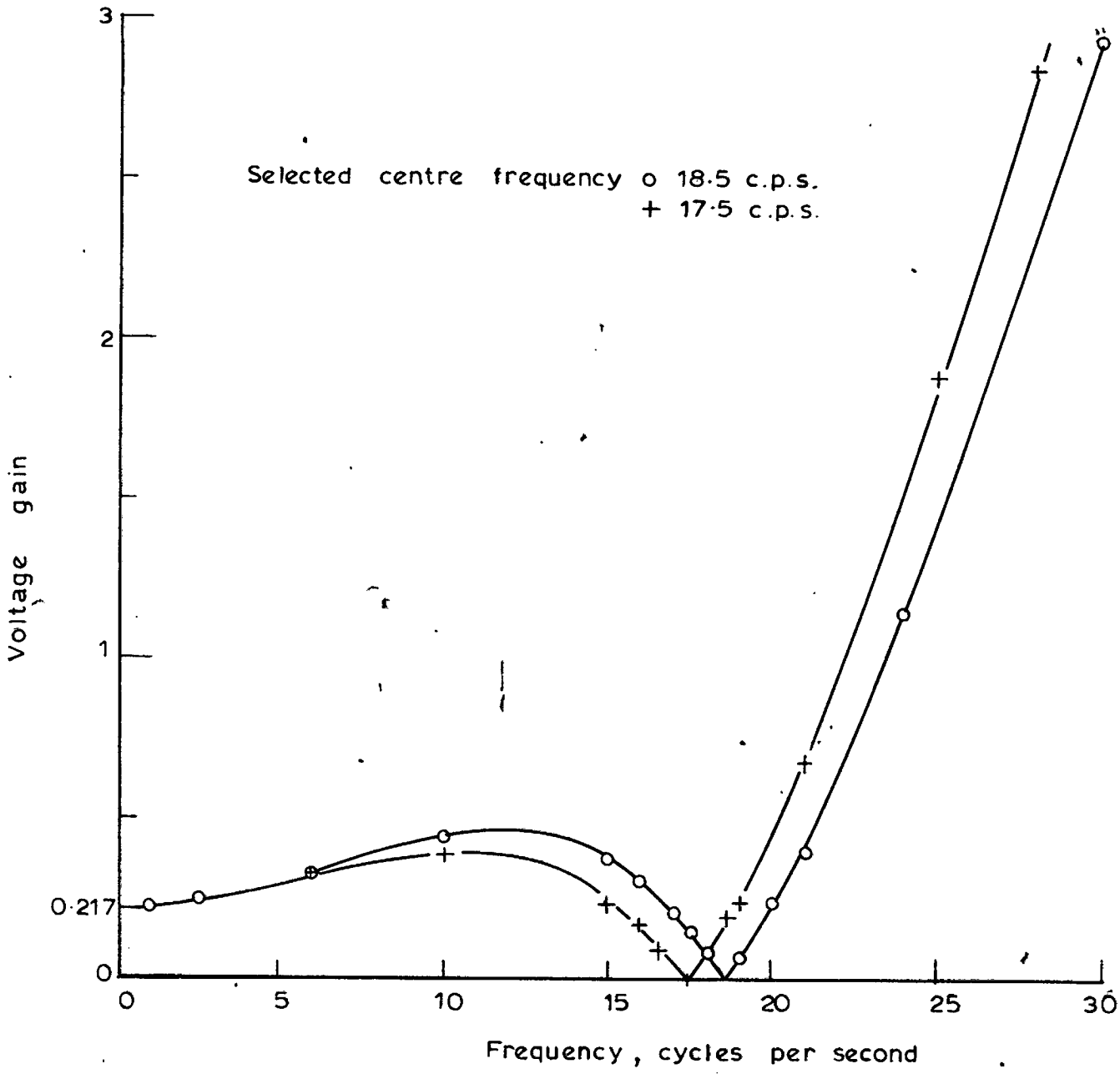

Fig. 7·28 The measured variation of gain with frequency for the complete tuned model lateral position control loop compensation network.

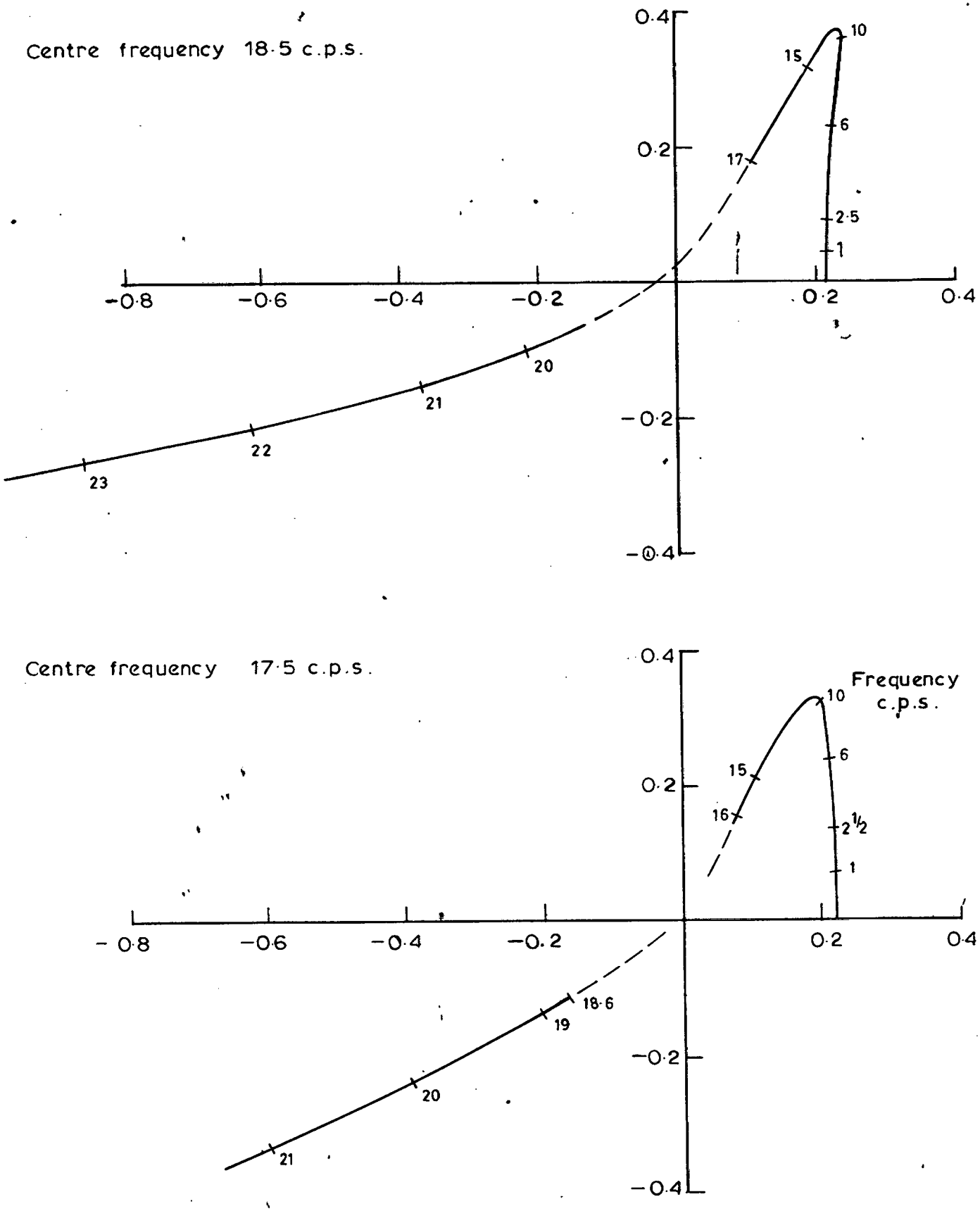

Fig. 7·29 The complete transfer function of the tuned model compensation network, at two values of the centre frequency.

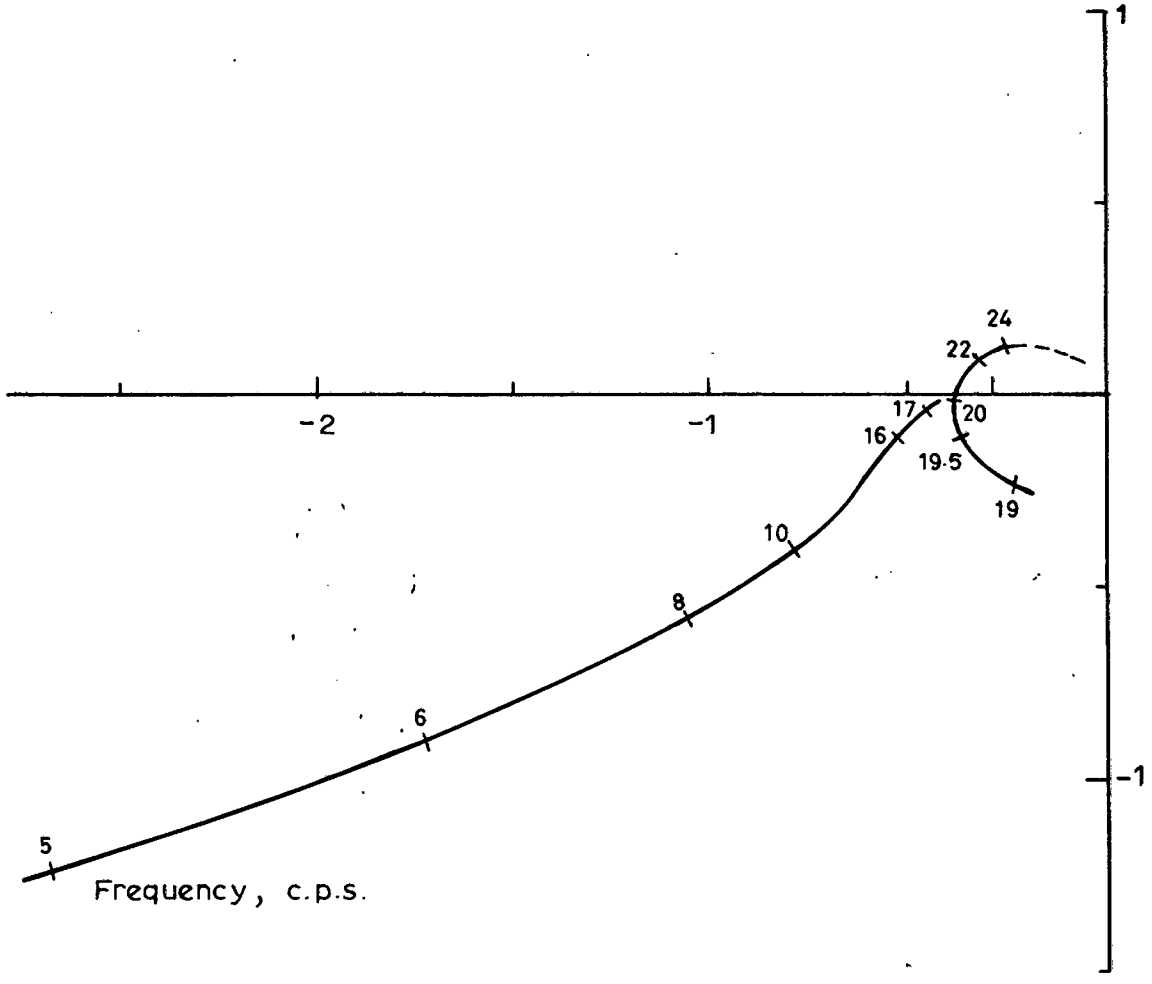

Fig. 7.30 A lateral position control Nyquist plot, using a phase inversion compensation network centred at 18·5 c.p.s. for stabilising the upper resonant frequency of a pitch tuned model.

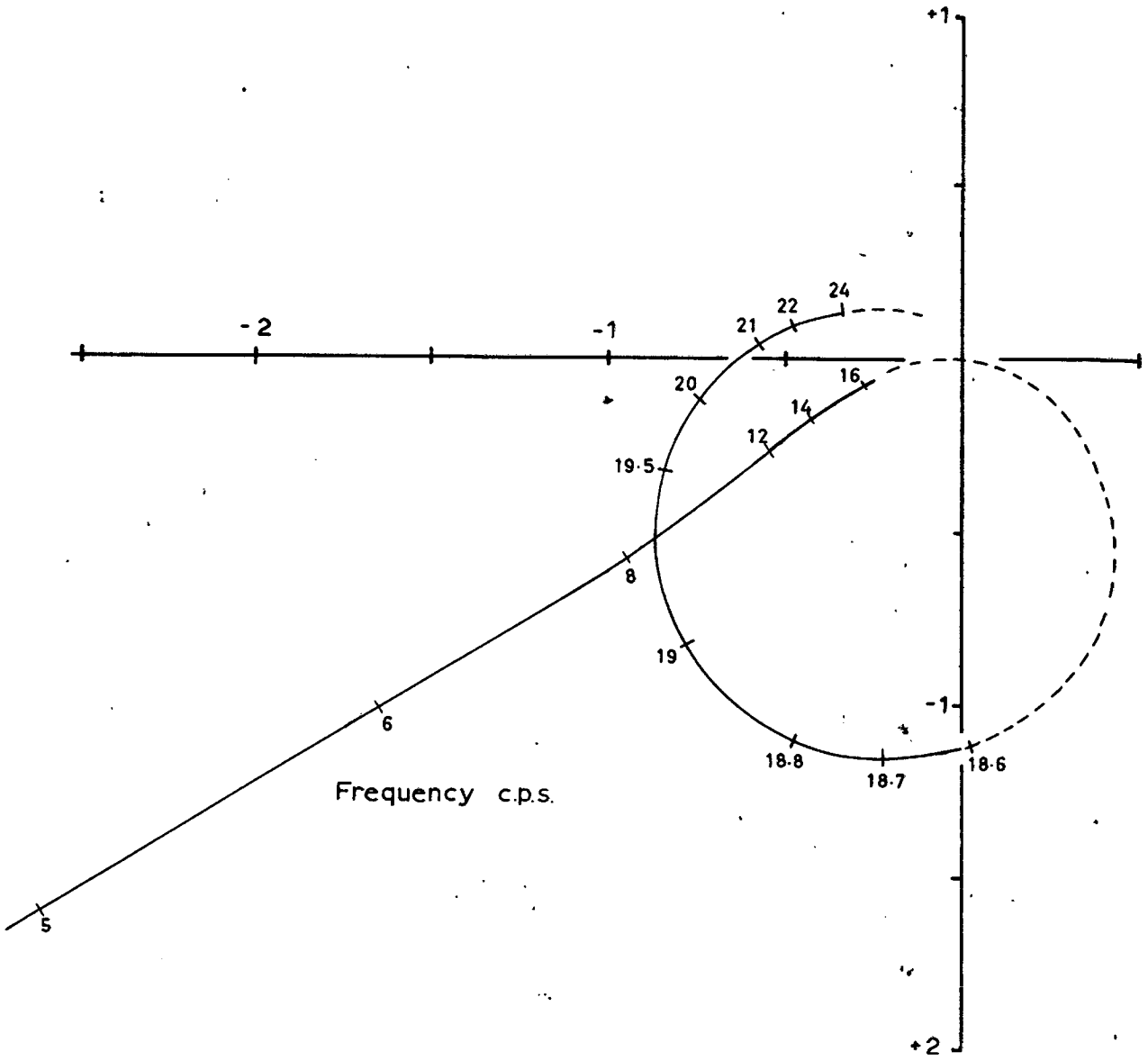

Fig. 7.31 A lateral position control Nyquist plot, using a phase inversion compensation network centered at 17.5 c.p.s. for stabilising the upper resonant frequency of a pitch-tuned model.

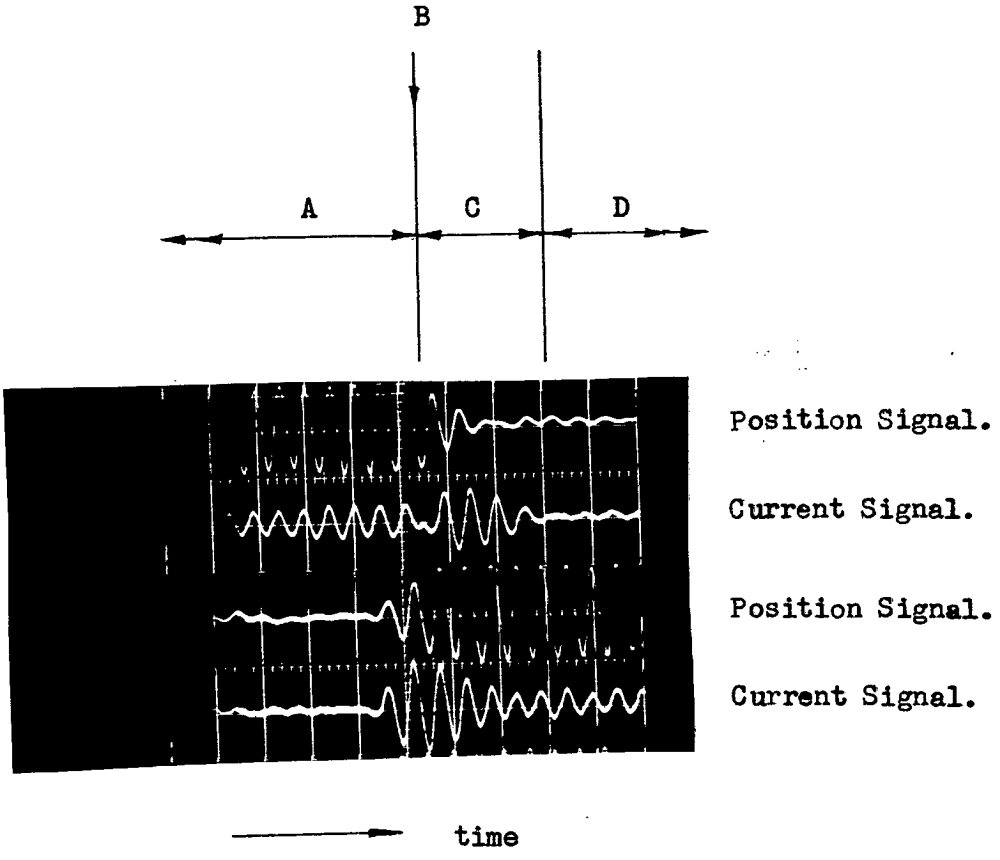

Time scale : 1 square = 0.1 second.

Upper traces: switching off the oscillation.

Lower traces: switching on the oscillation.

Fig.7.32 The Suppression and Initiation of Resonance of the Tuned Model.

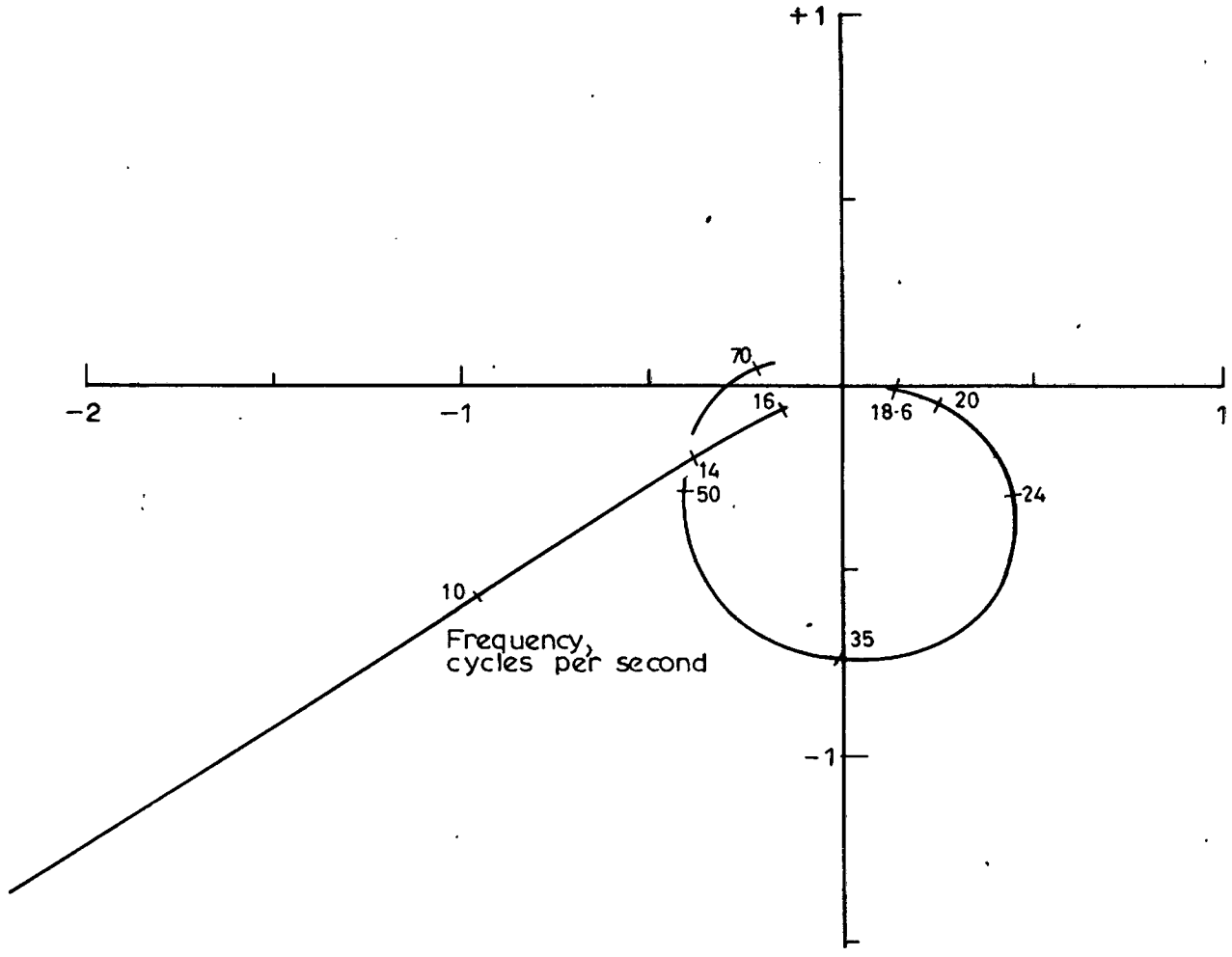

Fig. 7.33. A lateral position control loop Nyquist loop, for the heaving mode of a pitch tuned model, using a phase inversion compensation network centred at 17·5 c.p.s.

8. Model Position - Sensors.

A description of the optical systems which have been developed for monitoring model position, for the purposes of automatic position control and providing position information during aerodynamic measurements.

Contents:

8.1 Introduction.

Automatic control of the position of the model relative to the suspension magnet array requires the continuous monitoring of position. Optical position-sensors have been adopted because of the proven suitability and relative simplicity of such sensors[2]. The broad requirements of the position monitoring system were that the sensors should be capable of detecting an adequate range of model motion and model shapes. Also that the electrical signal derived from the optical system should be independant of motions in other degrees of freedom, and should respond sufficiently quickly to changes of model position in order to avoid complication in the form of additional lag compensation in the control feedback loops, or in the form of changing optical gain with frequency. The arrangement of the electromagnet system required that vertical and horizontal motions of the nose and tail of the model should be monitored, together with the

axial position and the roll attitude of the model.

Experience has shown that it is more convenient to alter the optical system from time to time to suit changes of model design, rather than to attempt to devise an all-purpose monitoring system. In fact it is probably impossible to do the latter with optical sensors because of the variety of model shapes that are likely to be suspended. The optical systems which were usually used on the apparatus are described in this Chapter (although some others were developed). The type of model that these sensors were suitable for monitoring had a fuselage of circular cross-section at the nose and tail, a blunt tail, and if roll attitude was to be controlled (this was not always the case) a fin was also required.

It was possible to define some of the requirements of the sensors reasonably clearly. For instance the range of model incidence that would be required for useful aerodynamic measurements was at least $\pm 10^{\circ}$, and on a typical 6 inch long model the optical system would be arranged to monitor the model about 2 inches ahead and behind the model centre. This suggested that the optical system should be capable of detecting the position of the fuselage of the model over a range of about $\frac{3}{8}$" either side of the tunnel centre-line. However, there were less clearly defined requirements as far as the range of motion that should be detectable by the roll and axial position sensors. There was no aerodynamic requirement to move the model axially, and the range of motion that required monitoring was dictated by the transient position changes that might occur during, for example, wind-on testing. In this case it was decided to use optical system components common with those in use elsewhere on the apparatus, which resulted

in the axial position sensor being capable of monitoring axial motions of about $\frac{3}{8}$" fore-and-aft of the normal position of the model. There was a possibility of making oscillatory measurements involving roll, and for this purpose a relatively small range of roll attitude would have been required, possibly 2° either side of normal, and initially a roll optical system was developed capable of controlling roll attitude over a range of $\pm 7^{\circ}$. However, this range was found to be too small for control purposes and the range was later doubled.

The remaining performance requirement that could be defined was optical system response. Phase errors could have effects in two ways, on the stability of the control system as a whole, and on aerodynamic measurements. At a representative frequency of oscillation of the model (for aerodynamic derivative measurements) of 20 c.p.s. a position signal lag of 5° would be acceptable as far as servo-loop stability was concerned because there were already much larger lags elsewhere in the loops. The electrical power supplies feeding the electro-magnets produced a certain amount of unwanted noise in the optical system pick-up circuits, principally in the form of spikes, and it was necessary to include a low-pass filter to reduce the amplitude of the spikes. As a result of the filter, the optical system output amplifier had a significant first-order lag, but the maximum acceptable lag dictated a time-constant of not greater than 0.5 milli-second. A lag of this order corresponds with a gain reduction of $\frac{1}{2}\%$ compared with the steady-state gain.

The signals from each pick-up were amplified using feedback stabilised single-ended input single-ended output operational amplifiers; a circuit showing typical component values is shown on Fig. 8.1 (a). The outputs from this type of circuit were used

directly as position signals for two degrees of freedom of model motion, namely axial position and roll attitude.

8.2. The Vertical and Lateral Position Sensors.

The restricted access to the wind tunnel resulting from the electro-magnet layout dictated that the nose and tail of the model should be monitored by four diagonal beams, and to obtain a signal dependent on the vertical position of one end of the model, the signals from the pair of beams monitoring the end were summed, and similarly to obtain a signal dependent on lateral position the signals were differenced. A pair of diagonal beams monitoring one end of the model is shown on Fig. 8.2. The operations of summing and differencing were carried out by three unity gain operational amplifiers, using the circuit shown on Fig. 8.1 (b).

The amount of light received by the pick-up solar cell varies linearly with movement of the edge of the shadow of the model over the pick-up lens, provided that the penumbra does not move off the lens. In order to make the best use of the size of the lenses chosen for the pick-ups, the shadow penumbra should have minimum width so that the traverse of the edge of the shadow over the lens will allow the maximum range of travel of the model.

The principle of this type of position sensor can be explained by reference to Fig. 8.3. The image of the filament of a 6 volt 6 watt bulb was directed past the model and focussed on the pick-up lens. In the region of the model, with the filament set at right angles to the edge of the model, the beam was in the form of a slit. The focal length of the lens was chosen so that the major axis of the beam cross section was about equal to the model diameter

at the model. A narrow penumbra was generated by masking the light source lens leaving a light transmission slit parallel to the model axis as shown on Fig. 8.3 (a). The narrower the penumbra can be made, the more nearly the maximum range of model movement that can be accepted with a linear calibration tends towards the maximum, equal to the model diameter.

In order to achieve the requirement for a narrow penumbra a pin-hole could be used, but the amount of light transmitted can be increased without widening the penumbra formed in the shadow of a straight edge, by extending the pin-hole in a direction parallel to the edge, to form a slit, so reducing either the light source power requirement or alternatively the gain of the pick-up amplifier.

On Fig. 8.3 (c) the straight edge representing the fuselage ofthe model is shown in the datum position, that is with the model axis lying along the wind tunnel axis. In this position the light beams were adjusted so that the model interrupted half of the beam, allowing the same movement in either direction. Also shown is a tapered screw, which was used as a means of source intensity adjustment so that the calibrations of the four source/pick-up sets forming the vertical and lateral position monitoring system could be matched.

The calibration technique was to traverse a cylinder, having the same diameter as the model, across the tunnel working section using a vernier traverser capable of setting the position of the cylinder to an accuracy of about $\pm$ 0.1 m.m. (0.0025 inches). By traversing in a lateral direction, in one pair of the diagonal beams, the intensity adjustment screws were trimmed in order to eliminate large differences in the performance of the two source/pick-up sets,

and the potentiometer marked R_1 on Fig. 8.1 (b) was trimmed to eliminate variations in the sum of A and B (the vertical position signal). Similarly, with a vertical traverse of the cylinder, potentiometer R_2 was trimmed to eliminate variations of A-B (the lateral position signal). Examples of the calibrations of the signals from the pick-up amplifiers of one diagonal pair of beams are shown on Fig. 8.4, taken with the cylinder in the region of the tunnel centre, the voltages being measured at the outputs of the section of circuit shown on Fig. 8.1 (a). Initially the calibration curves had shown some waviness which was produced by variations in the brightness of the filament image. The effect of these variations was virtually eliminated by slightly de-focussing the filament image on the pick-up lens. The pick-up lens was arranged to fucus the image entirely within the light sensitive surface of the $\frac{1}{4}$ inch square silicon solar cell.

The lenses used in all light sources were 1 inch overall diameter and had a focal length of 1 inch. In the four pick-ups of the vertical/lateral optical system the lenses were $1\frac{3}{8}$ inch diameter and 2 inch focal length.

Frequent re-calibrations of the optical system were necessary due to variations in the light transmission of the Perspex window in the tunnel underside.

8.3 The Drag Control Optical System.

A cross-section of the high speed wind tunnel viewed in the upstream direction is shown on Fig. 8.5, taken in the plane of the optical system monitoring the axial position of the model. The light beam was arranged to pass over the (blunt) tail of the model,

and in this case the major axis of the light slit formed by the source filament image was arranged parallel to the model axis. A stainless steel mirror was let into the top surface of the wind tunnel in order to simplify the positioning of the optical system components in the rather restricted space which was available. The pick-up lens was the same as used in the vertical/lateral pick-ups, and provided an adequate range of linear calibration without resorting to masking of the source lens at right angles to the filament. However, it was necessary either to limit the width of the beam, (the dimension of the minor axis) or to limit the amount of the width received by the pick-up, to allow adequate lateral movement of the model without change of pick-up output. The simpler approach was the latter, which was achieved by masking the source lens leaving a slit parallel to the model axis (producing a sharp penumbra of the shadow of the fuselage side, but a relatively wide shadow penumbra of the blunt tail) and by masking the pick-up lens leaving an open slit again parallel to the model axis. In this way the model could be traversed laterally a distance very nearly equal to its diameter without introducing variations in the pick-up signal.

A calibration of the optical system is given on Fig. 8.6. In the case of this optical system, calibration changes resulted from changes in the surface condition of the Perspex window, and as a result of surface erosion of the stainless steel mirror caused by dust etc. carried around the wind tunnel by the air stream.

8.4. <u>The Roll Attitude Monitoring System</u>.

The requirement for a roll control system resulted from the necessity to suspend and maintain the proper roll attitude of models having wings.

A desirable feature of any monitoring system is that it should only be sensitive to motion in the particular degree of freedom being monitored. The method which was adopted for monitoring roll attitude was an optical system, and the intensity of the beam received by the pick-up was modulated in the manner shown schematically on Fig. 8.7 by a comb-like grid mounted for convenience in the model fin. The location of the grid is shown on the drawing on Fig. 8.8, which is of a model in its normal attitude for this magnetic suspension system.

If the incident beam is assumed to be parallel, then although rotation of the grid in the rolling sense varies the amount of light transmitted, rotation about the remaining pair of axes initially produces only small variations of output, and translation in any direction (within the obvious limits set by the grid and beam geometry) has no effect on the amount of light transmitted. In practice the light source acts as a spherical radiator, and translation of the grid in a direction along the beam or across the beam in a direction normal to the slits in the grid did change the amount of transmitted light. However, the interactions can be reduced by placing the grid as far as practically possible from the source, and by masking the pick-up. These points will be discussed later.

An efficiency of a roll optical grid can be defined as the ratio of the maximum amount of light transmitted by a grid to the total incident light on the grid. The maximum amount of light will be transmitted when the grid is inclined at the angle β_o defined on Fig. 8.9, to align the openings with the vertical incident beam. The grid geometry is specified by the roll angle range $\pm \beta_o$ which it is intended to accomodate, and by the grid width b (which is

limited by the fin thickness) and the thickness t of the solid parts of the grid. The maximum opening of each gap in the grid is $2a\cos\beta_o$ which is taken as a measure of the transmitted light, and the equivalent measure of the incident light per grid element (considering an element as one gap and one solid part) with the grid inclined at β_o presenting the maximum opening to the incident light is given by $\cos\beta_o\,(2a+t)$. If we write $A = b/t$ then the transmission efficiency is given by

$$\eta = \frac{2\tan\beta_o}{2\tan\beta_o + 1/A}$$

The light source power requirement, or alternatively the pick-up amplifier gain, vary inversely as the transmission efficiency. The curves plotted on Fig. 8.9 show the variation of transmission efficiency with the design parameters A and β_o. The earlier grids were machined from the solid with $A = 1.5$ and $\beta_o = 7^\circ$ giving a transmission efficiency of about 25%. A later fabricated design for the tuned model has $A = 5$ and $\beta_o = 15^\circ$ giving a transmission efficiency of 72%. The significance of this is that although the roll angle range was doubled in the latter case, by improvement to the design the loss of gain of the optical system (defined as output signal change per unit angular change of roll attitude) was more than recovered by increased transmission efficiency.

The variation of transmitted light does not vary linearly with the roll angle. The general expression for the ratio of the transmitted light at the attitude β to the maximum light transmission for a particular grid is

$$\frac{g}{g_m} = \frac{1}{2}\left(\frac{\sin\beta}{\sin\beta_o} + \frac{\cos\beta}{\cos\beta_o}\right)$$

where β is taken as zero with the grid normal to the incident light (as shown on Fig. 8.9) and positive when the grid is rotated to transmit more light. The variation of g/g_m with β is shown on Fig. 8.10 for several values of β_o . Ambiguous signals are obtained with $\beta_o > 45^\circ$, and at $\beta_o = 45^\circ$ the sensitivity of the optical system tends to zero as $\beta \to +\beta_o$. Hence the practical upper limit of roll angle range that this particular system can be expected to monitor is less than $\pm 45^\circ$ about the mean position, but with β_o near to $\pm 45^\circ$ the calibration of the system would be very non linear. The calibration becomes progressively more linear as β_o tends to zero, and a compromise has to be accepted.

One measure of the non-linearity of the g/g_m — β/β_o curves is the ratio of g/g_m at $\beta = 0$ to g/g_m at $\beta = +\beta_o$ called the signal ratio $R_s = \frac{1}{2\cos\beta_o}$ and a second convenient measure of non-linearity is gain ratio R_g defined as the ratio of the gain at $\beta = +\beta_o$ to the gain at $\beta = -\beta_o$ This is the ratio of the slopes of the two ends of a g/g_m curve plotted on Fig. 8.10, and is given by

$$R_g = \frac{1}{1 - 2\sin^2\beta_o}$$

These two expressions are plotted on Fig. 8.11, from which it can be seen that the tuned model grid ($\beta_o = \pm 15^\circ$) could be expected to produce a 30% change of gain over the complete range of β , and the mid-range (β = o) output signal would be about 0.52 of the maximum signal.

The above analysis of the characteristics of the grid type of roll optical system has assumed a parallel light beam. However it was convenient to use a simple filament bulb and short focus lens

light source. The beam in the region of the model had a geometry close to that which would be produced by light radiating uniformly from a point source. The several interactions will be analysed separately and presented as the variation of the transmitted light with motion of the model in the other five degrees of freedom, with the model in the normal roll attitude, that is with $\beta = o$. The roll optical system is shown in Fig. 8.12. Light from the source is directed through the Perspex window in the underside of the working section, and reflected onto the fin containing the grid by the stainless steel mirror in the tunnel top. This particular beam path was chosen in order to place the model relatively far from the source to minimise one of the interactions. The grid and fin geometry allowed the same lateral and axial motion of the model as the other optical systems. The source and pick-up were moveable in order to accomodate different models, and to allow adjustments to the beam position and focus the lenses and bulb were adjustable.

The three translational modes of motion of the grid are defined as X , parallel to the model axis, Y in a direction vertically downwards and Z in a lateral direction, see Fig. 8.12; the three rotational modes are defined as β , ϕ, ψ taken as positive when clockwise viewed in a direction away from the origin along the X, Y, Z axes respectively. For convenience the origin has been taken as the grid centre. The basic roll attitude signal sensitivity is $\frac{\partial q}{\partial \beta}$ and the five possible interactions are $\frac{\partial q}{\partial \phi}$, $\frac{\partial q}{\partial \psi}$, $\frac{\partial q}{\partial X}$, $\frac{\partial q}{\partial Y}$ and $\frac{\partial q}{\partial Z}$

The roll signal sensitivity $\frac{\partial q}{\partial \beta}$ for any grid varies over the whole range, but for low values of β_o the variation is small as

shown above. For purposes of comparison the value of $\frac{\partial g}{\partial \beta}$ will be taken at the "normal" fin roll attitude, with $\beta = o$ corresponding with a horizontal fin and a vertical beam. For the case of a parallel beam only one interaction exists, the pitch interaction $\frac{\partial g}{\partial \phi} = \frac{\tan \phi}{\cos \phi}$. Pitch angles of $\pm$ 8° produce an error in the roll attitude signal of 1% and pitch angles of $\pm$ 18° produce an error of 5%. The change of roll attitude that, for example, 1% change of signal represents depends on the designed operating range β_o of the grid. For a grid designed for $\beta_o = \pm$ 15°, a 1% change of transmitted light due to the pitch interaction corresponds with a roll attitude angular error of approximately 0.3°. The approximation that has been assumed here is that the slope of the $g - \beta$ curve at $\beta = o$ is equal to the average slope, a good approximation at $\beta_o = \pm$ 15°.

In order to simplify the analysis of the likely interactions with the spherically radiating beam, it was assumed that the dimension of the grid measured across all of its elements was small compared with the beam path between the grid and the beam source, and that the part of the beam accepted by the pick-up measured at the grid in the X direction was very small compared with the beam length between source and grid. The conclusions were that in this case three interactions were significant, namely $\frac{\partial g}{\partial Y}$, $\frac{\partial g}{\partial \phi}$ and $\frac{\partial g}{\partial Z}$. The interaction $\frac{\partial g}{\partial \phi}$ was the same as for a parallel beam, and no action was taken to counter the effect, which has been shown to be small at small angles of pitch.

As a result of the offset of the grid from the axis of the model, a change of roll attitude of the model results in a translation of the fin in the Y and Z directions as well as a

change of β . For small angles of roll away from the normal attitude, the translation in the Z direction is small. The interaction $\frac{\partial q}{\partial Y}$ will enter directly into a roll optical system calibration obtained simply by varying the roll attitude of the model about its axis. The interaction $\frac{\partial q}{\partial Z}$ could appear in the roll attitude signal as a result of lateral pitching or heaving motions of the model, and exists because lateral movement of the grid across the beam varies the average alignment of the beam with the inclined openings in the grid. However, the interaction can be counteracted by fitting a tapered mask to the pick-up, allowing different amounts of light into the pick-up depending on the lateral position of the model in the beam. The pick-up lens for the roll optical system had a diameter of 1 inch, and over this distance a mask leaving an opening tapering from 0.2" at one side of the lens to 0.3" at the other was sufficient to suppress this particular interaction for the tuned-model grid shown on Fig. 8.13.

For small displacements in the Y direction $\frac{\partial q}{\partial Y} \propto \frac{-1}{l + 2Y}$ where l is the beam path length between the source and the grid, and the interaction can be minimised by arranging for the maximum convenient value of l . The total beam length for the roll optical system was about 20 inches, and the models were suspended relatively near to the pick-up giving a path length before the grid of about 14 inches. For the tuned model grid, for a one degree error in the indicated roll attitude at $\beta = o$ due to the interaction $\frac{\partial q}{\partial Y}$ the displacement Y would theoretically need to be about 1 inch.

The roll optical system was calibrated by attaching a protractor to the tail of the model, and magnetically suspending the model with control in five degrees of freedom (drag uncontrolled).

Re-calibration of the optical system was necessary from time to time because of changes in the condition of the mirror and the Perspex window. The range of roll angle which could be accomodated with this method of calibration was less than the maximum range provided by the grid, because it was necessary to maintain control in roll during calibration, and for this some margin was required at each end of the range. The roll attitude of the model, indicated by a pointer standing in the working section, was varied by the potentiometer R_9 shown on Fig. 7.14; the variation of the output of the pick-up amplifier with roll attitude is shown on Fig. 8.14. The calibration was slightly non-linear, as predicted. With the model removed from the wind tunnel there was increased illumination of the pick-up, and it was decided for convenience of launching and to avoid coil overheating to arrange for increased pick-up output to select reduced current from the power supply. This required that the inclination of the grid elements to the vertical should be opposite to the inclination of the shaped core, as shown in the sketches below:

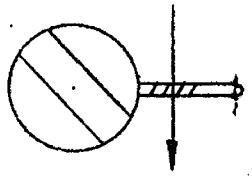

Normal roll attitude.

Rolling moment generated by increased current in electro-magnets.

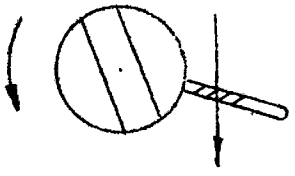

Reduced light transmission, selecting increased roll current.

Moment from reduced current.

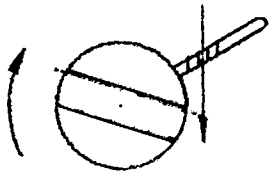

Increased light transmission, selecting reduced roll current.

8.5 Future Developments : A Brief Discussion.

8.5.1 One of the drawbacks with the optical system has been the gradual deterioration of the stainless steel mirror reflecting the drag and roll control beams. A surface reflecting mirror was chosen in order to avoid the small gain penalty arising from the interface losses of a back-silvered glass mirror. However, there is now no doubt that the latter type would be more suitable for this wind tunnel, the advantage of abrasion resistance outweighing any disadvantage.

The gradual deterioration of the Perspex window in the tunnel underside was expected: the working section was designed for a glass window, but the Perspex window was used for convenience during the development phase of the suspension system. It is intended to fit a glass window in the near future, and these two improvements are expected to cure the gradual changes of calibration that have been experienced.

8.5.2 The several adjustments that have been built into the optical system allow a fair range of models to be suspended. There is virtually no limit to the maximum diameter of the model, but todate the larger models have been about 1" diameter. The practical lower limit to the model diameter at present is about $\frac{1}{2}$", although a steel bar $\frac{1}{4}$" diameter has been suspended. However, there exists at least one optical method of monitoring small diameter models which allows movement of the model distances of more than one diameter across the beam, and so there is no fundamental limit to the minimum diameter.

Difficulties would arise with the optical monitoring of

a non-circular fuselage, in the form of lateral or vertical displacement of the model accompanying movement in roll; in this case some electrical coupling of the optical system signals might be necessary, and similarly in the case of axial movement with the vertical and lateral position sensors monitoring a tapered fuselage.

Changes of the design of the rear fuselage, for example to a shape tapering to a point, would require modification to the drag optical system. In anticipation of such a requirement, an optical system was developed for a plain conical afterbody using a modification of the normal drag control optical components, but this optical system has not yet been used.

8.5.3 There is at present a requirement for some means of detecting the position of the magnetic core inside a tuned model. This would allow the use of a more conventional stabilisation network than has been developed to cope with outer shell monitoring, with the possibility of suspension with increased lateral stiffness in pitch. However, although it may be possible to generate the signal optically, it may be simpler to use some entirely different principle, such as for example a magnetic induction technique under development at M.I.T.[1].

8.6 LIST OF SYMBOLS USED IN CHAPTER 8

Symbol	Meaning
a	The width of light slit admitted through an element of a roll control grid in the normal attitude.
A	The ratio of the width to thickness of the cross-section of the solid part of a grid.
b	The width of a grid measured in the direction of incident light.
g	A measure of the amount of light transmitted through a grid.
g_m	A measure of the maximum amount of light transmitted.
ℓ	The length of beam between the light source and grid.
R_s	Signal ratio. The ratio of the "normal" roll attitude signal to the maximum.
R_g	Gain ratio. The ratio of the maximum to minimum gain of an optical system.
t	The thickness of the solid parts of a grid.
X	The displacement of a grid from a datum position in a direction parallel to the tunnel axis, positive upstream.
Y	Grid displacement in the vertical direction, positive downwards.
Z	Grid displacement in the lateral direction, positive to the left viewed upstream.
β	Angular rotation of optical grid from horizontal , positive clockwise looking upstream.
$\lvert\beta_o\rvert$	The maximum roll angle capacity of a grid.
η	Light transmission efficiency.
θ	Displacement of model away from normal in roll, positive clockwise looking upstream.

List of Symbols, cont'd.

ϕ	Pitch angle of model and grid relative to tunnel centreline.
ψ	Yaw angle of model and grid relative to tunnel centreline.

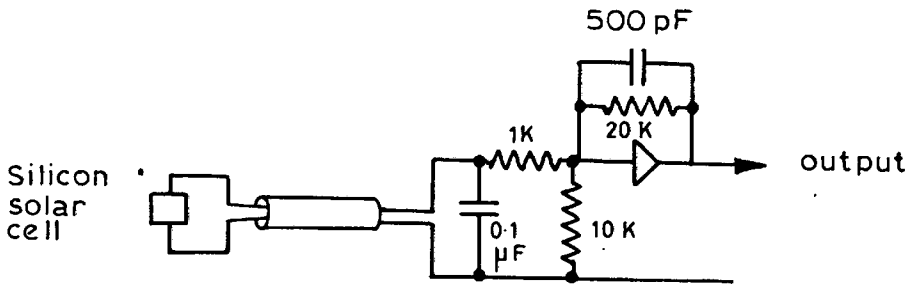

Fig. 8.1 (a) Position signal amplifier.

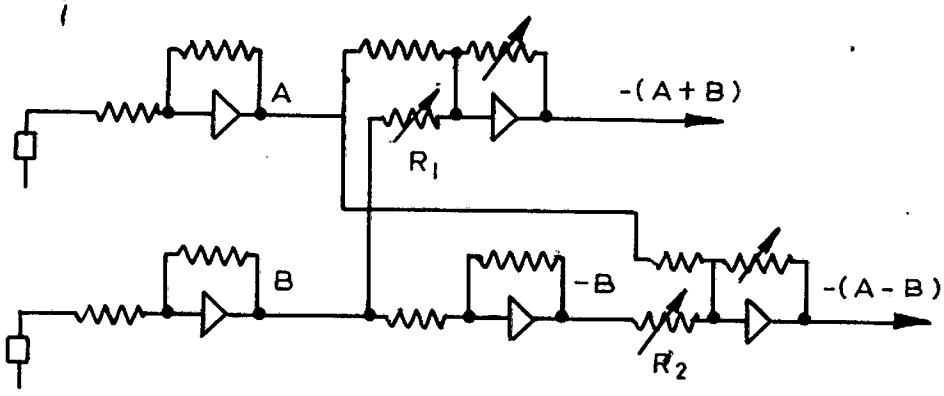

Fig. 8.1 (b) Summing and differencing of the signals from one pair of diagonal optic beams. The output signals A + B and A - B are proportional to the vertical and lateral motion respectively of one end of the model fuselage.

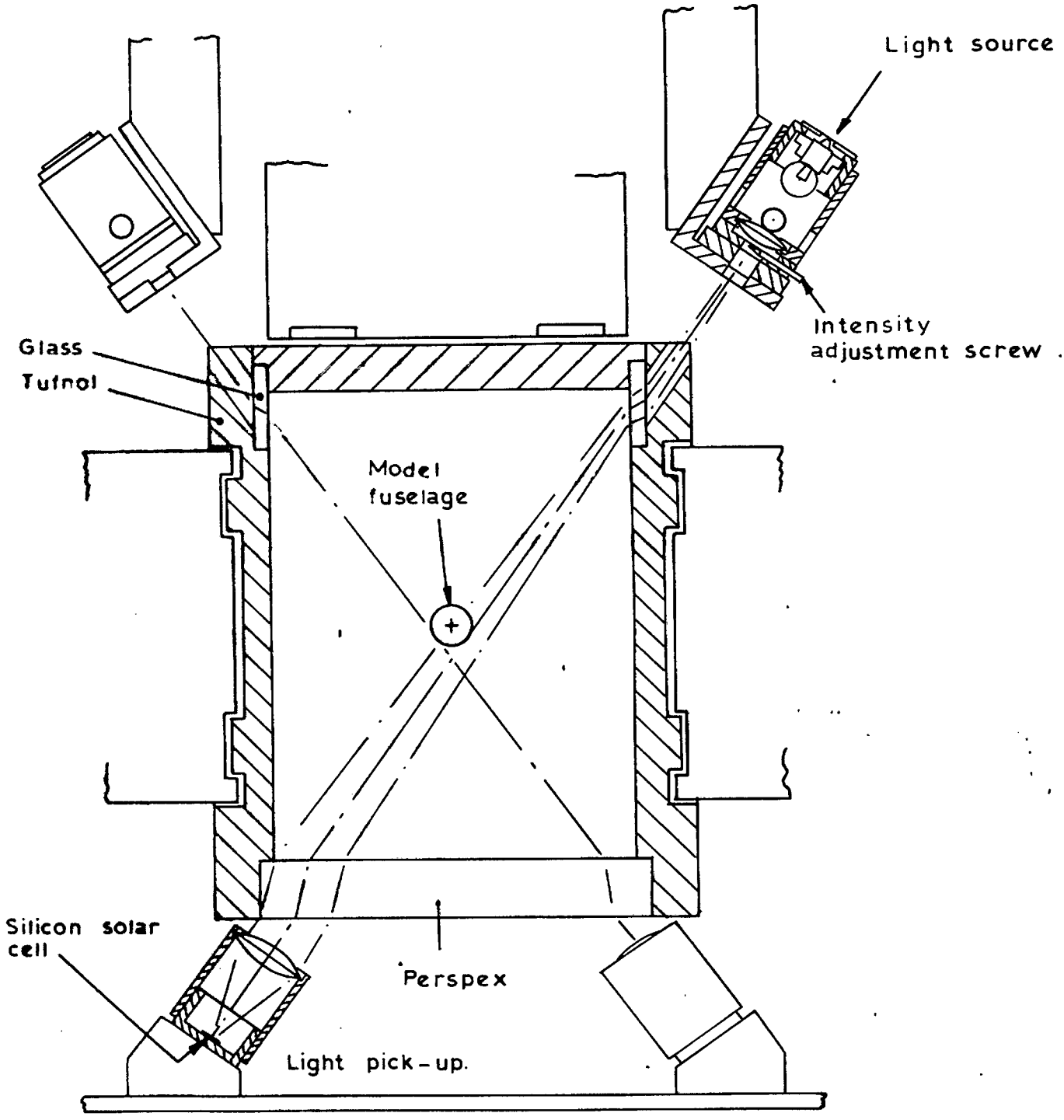

Fig.8.2 A cross-section through the high speed wind tunnel working section, showing the optical system monitoring vertical and horizontal motions of one end of the model.

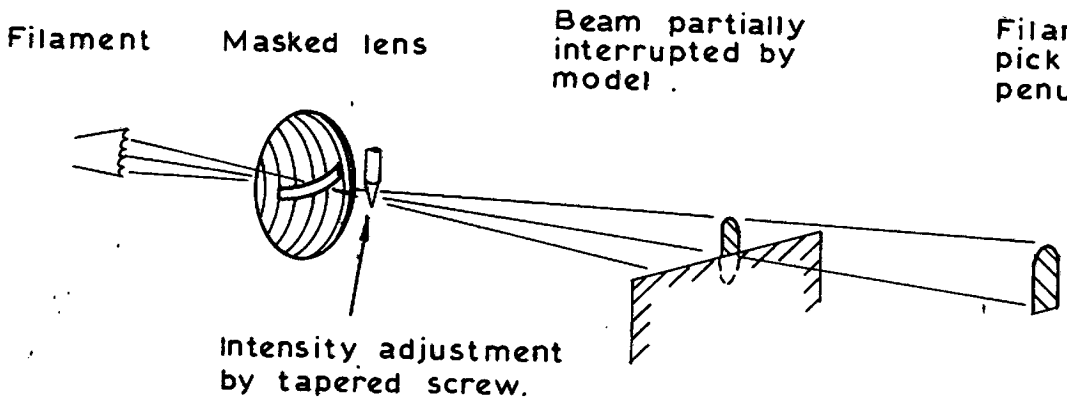

(a) Schematic arrangement of optical system.

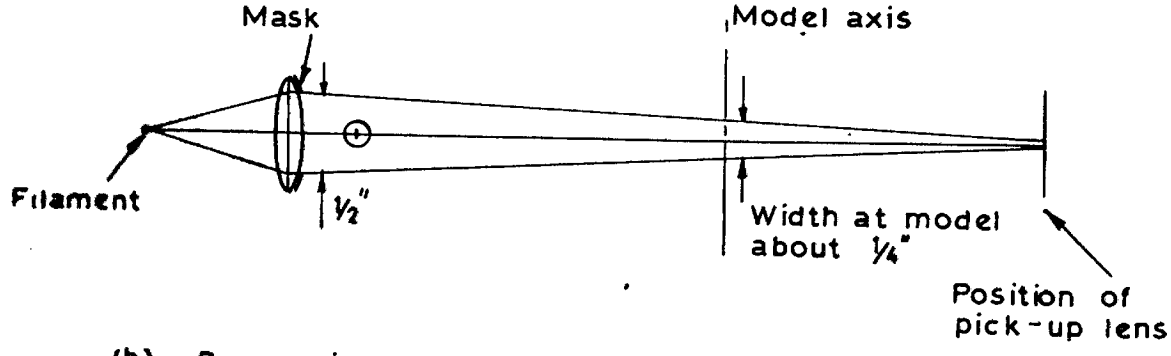

(b) Beam viewed at right-angles to model axis.

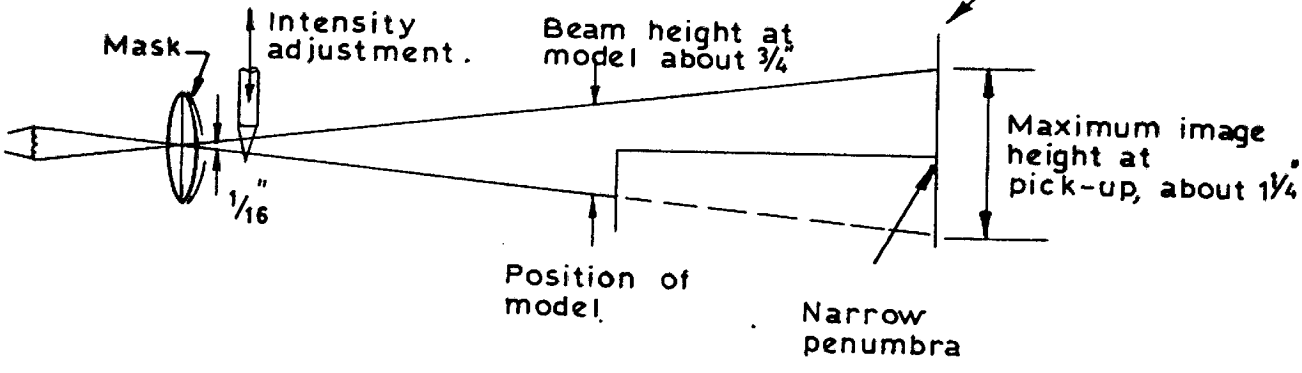

(c) Beam viewed parallel to model axis.

Fig. 8.3 Elements of the optical system type which is used for monitoring vertical and horizontal motions of the model fuselage.

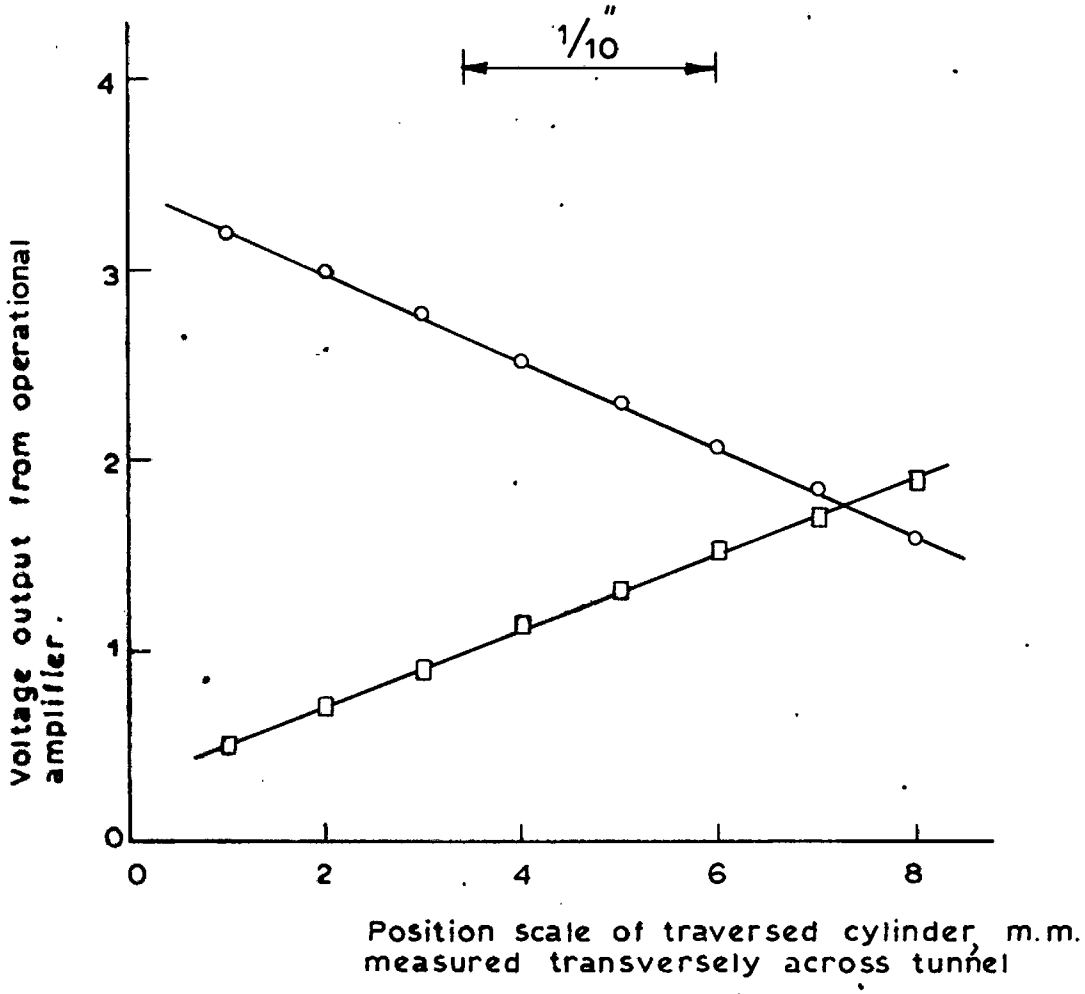

Fig.8.4 Representative position signals given by the solar cell amplifiers for the diagonal optical beams monitoring the position of one end of the model fuselage.

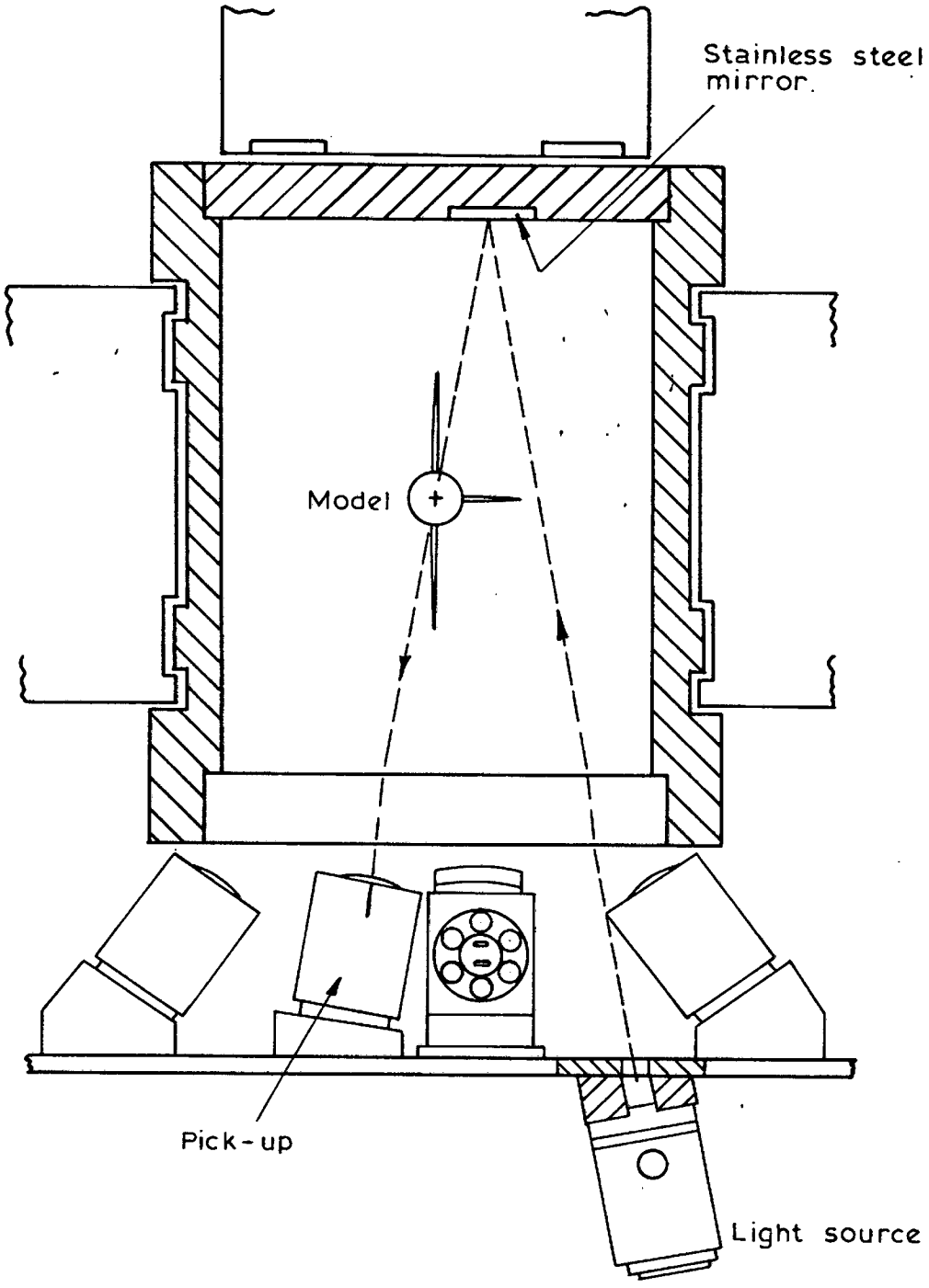

Fig. 8.5. The optical system for monitoring the axial position of the model and controlling the current supply to the drag coil.

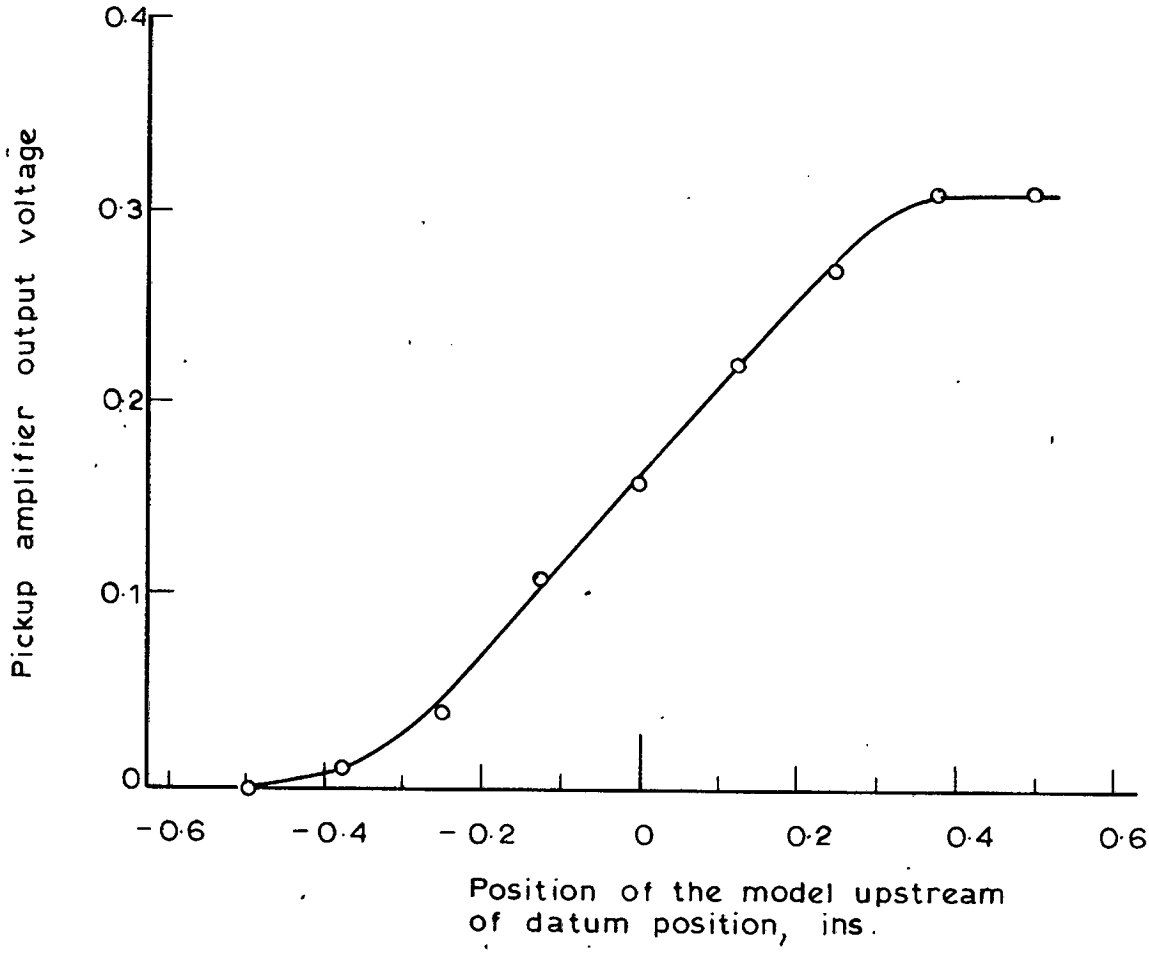

Fig. 8·6 A calibration of the optical system monitoring the axial position of the model

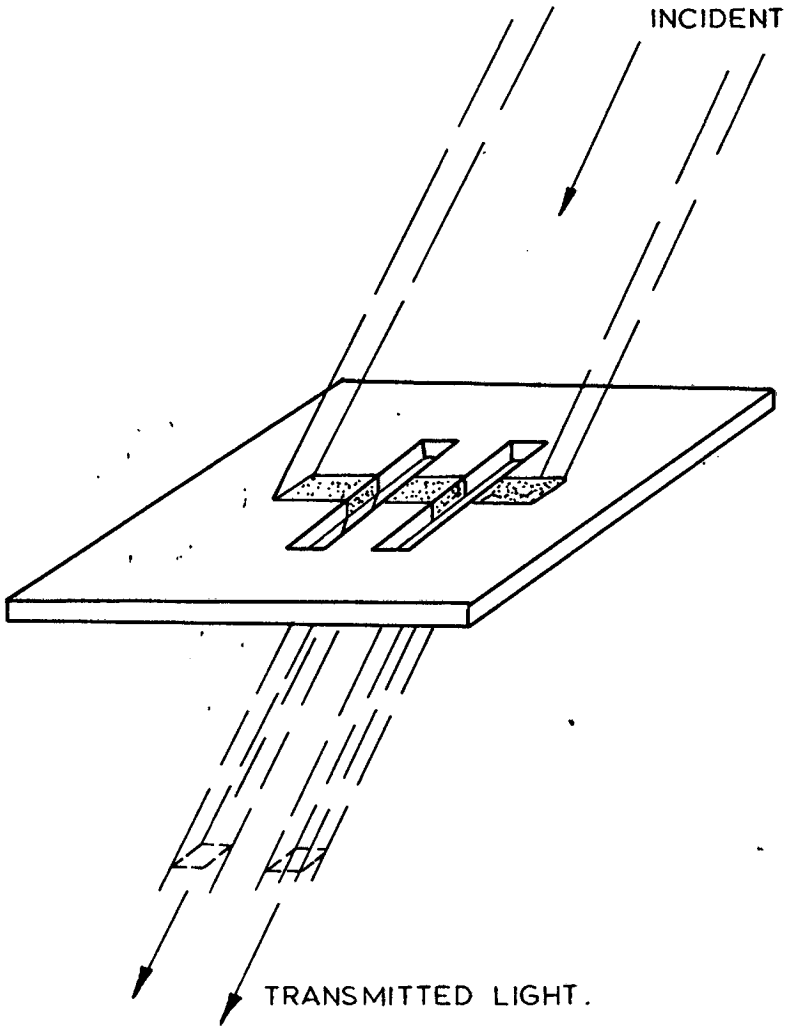

(a) Roll optical grid.

THE AMOUNT OF TRANSMITTED LIGHT IS ONLY STRONGLY AFFECTED BY ANGULAR MOTIONS OF THE GRID IN THE PLANE OF THE INCIDENT LIGHT SLIT.

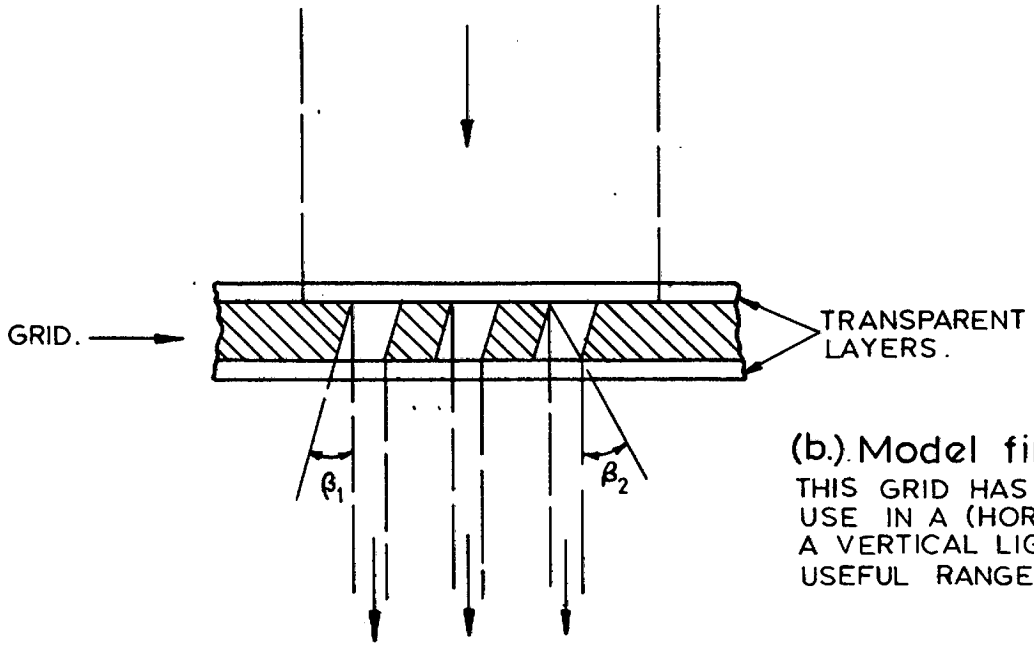

(b.) Model fin optical grid.

THIS GRID HAS BEEN DESIGNED FOR USE IN A (HORIZONTAL) FIN USING A VERTICAL LIGHT SLIT.
USEFUL RANGE $\beta_1 + \beta_2$

Fig. 8.7

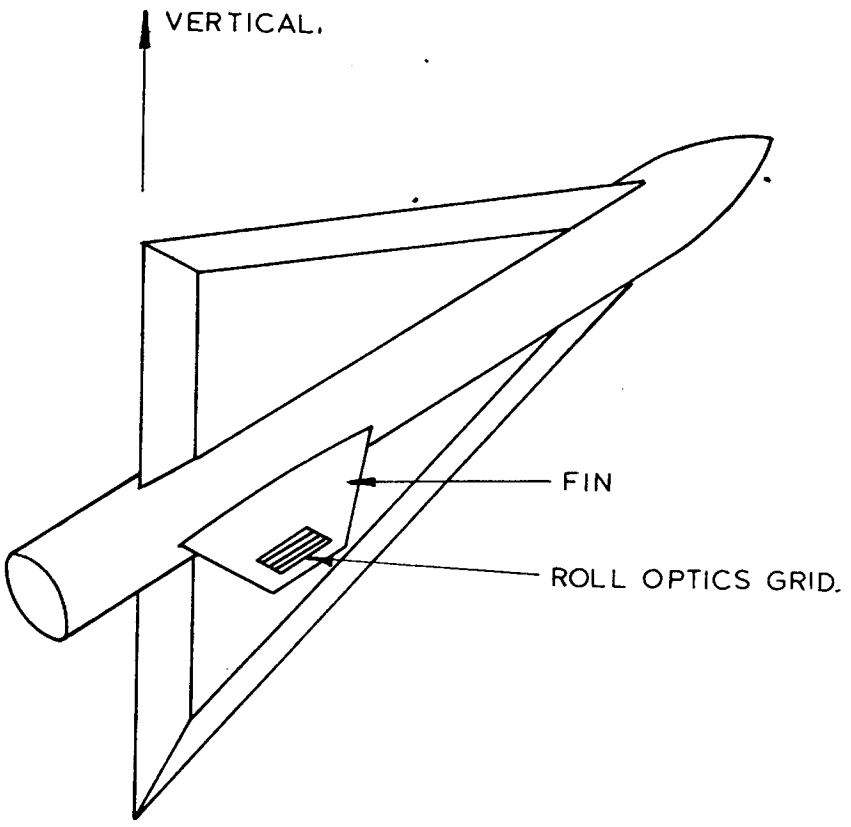

Figure 8.8. The location of the optical grid in the model, which is shown in the normal attitude for this suspension system.

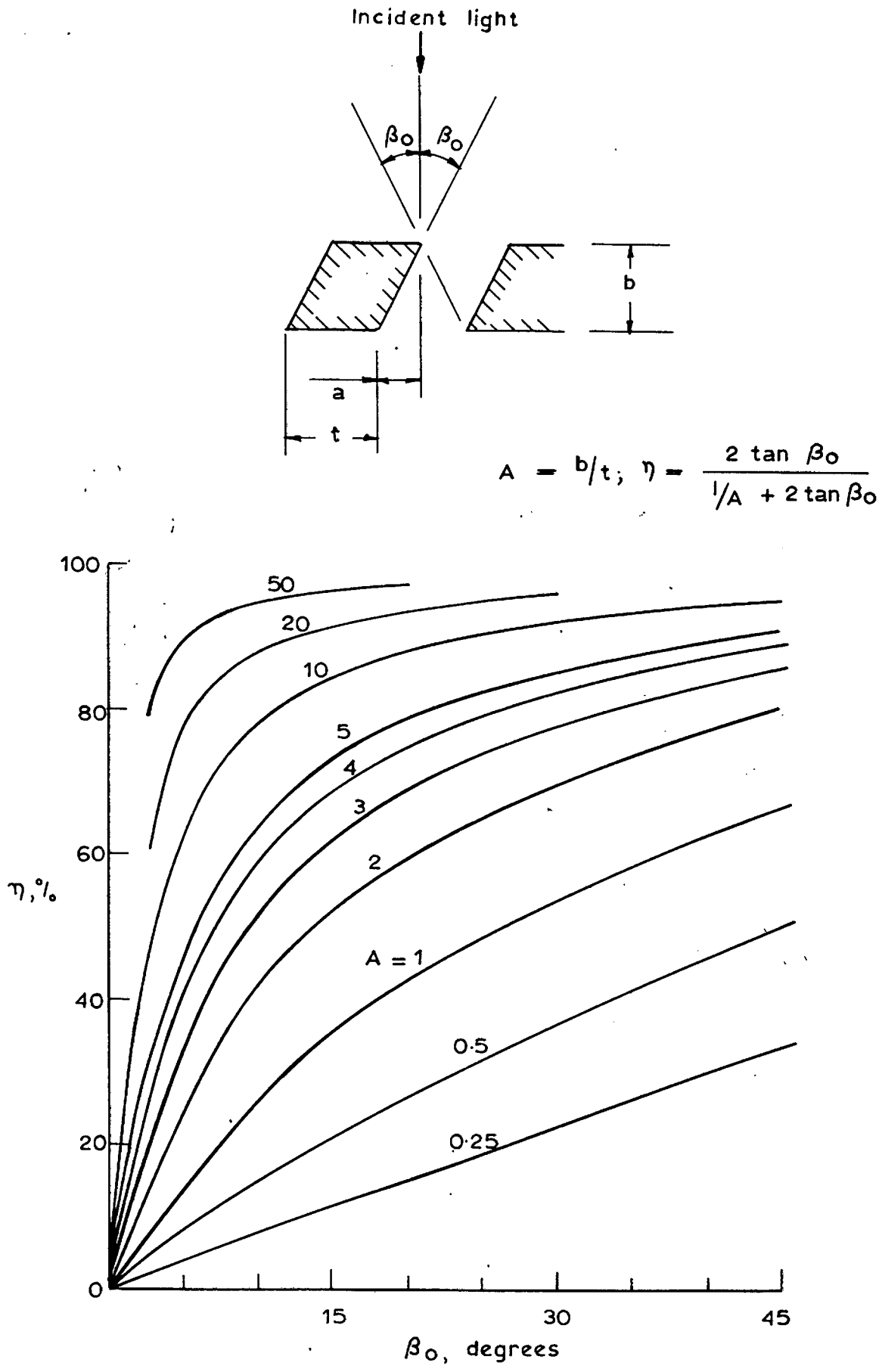

Fig.8.9 The light transmission efficiency of inclined solid grids.

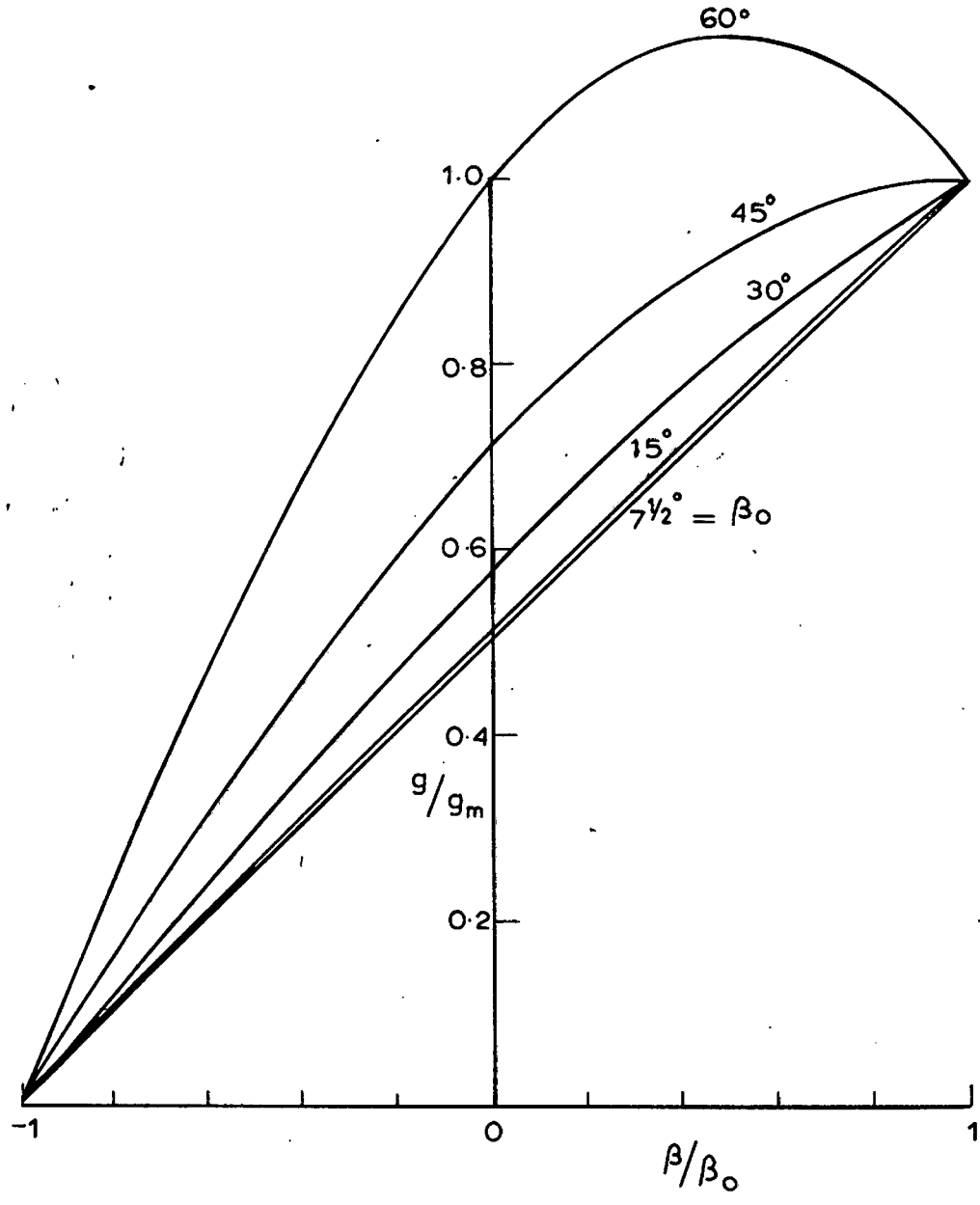

Fig. 8.10 The variation with operating range of the theoretical form of the grid optical system output.

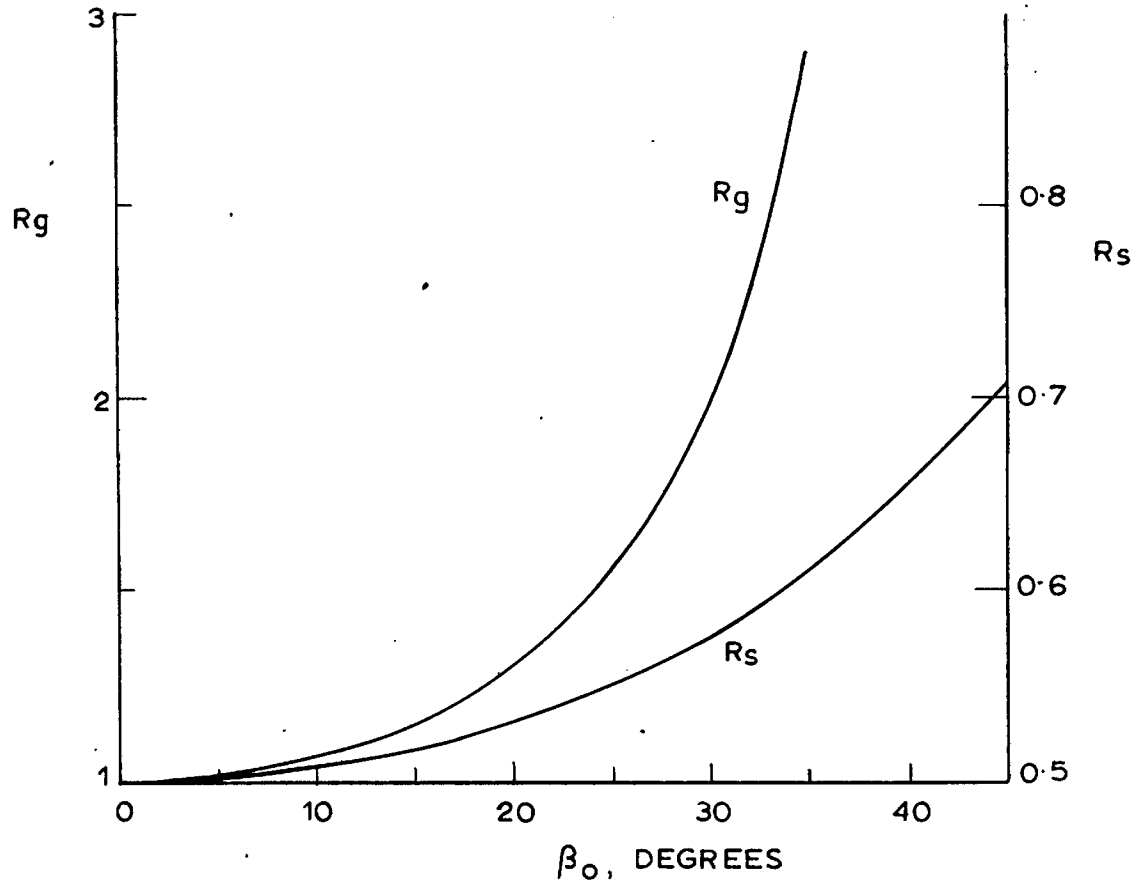

Fig. 8.11 The variation of gain ratio Rg and signal ratio Rs with β_o.

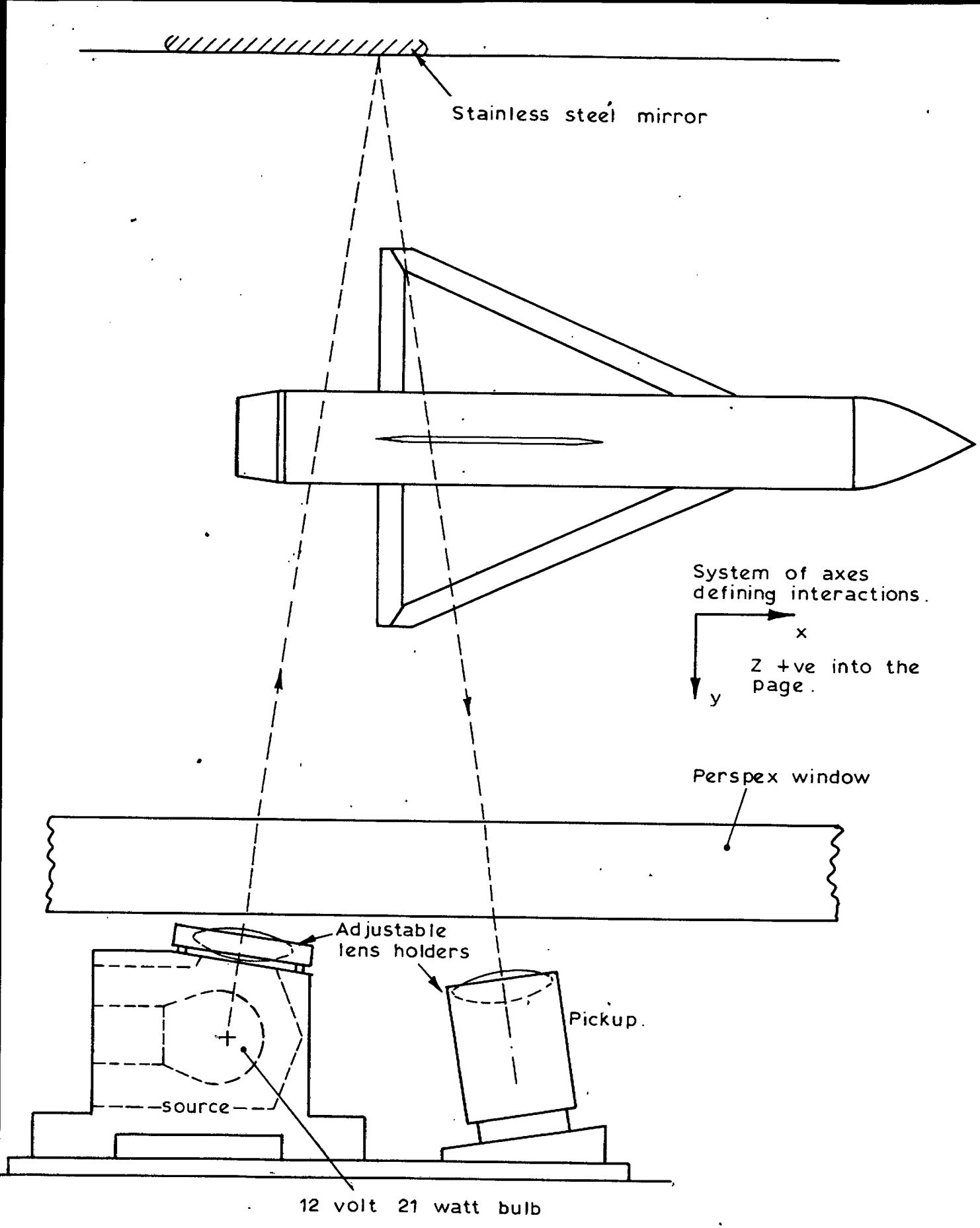

Fig. 8.12 A side view of a section through the wind tunnel showing the roll optical system and beam path.

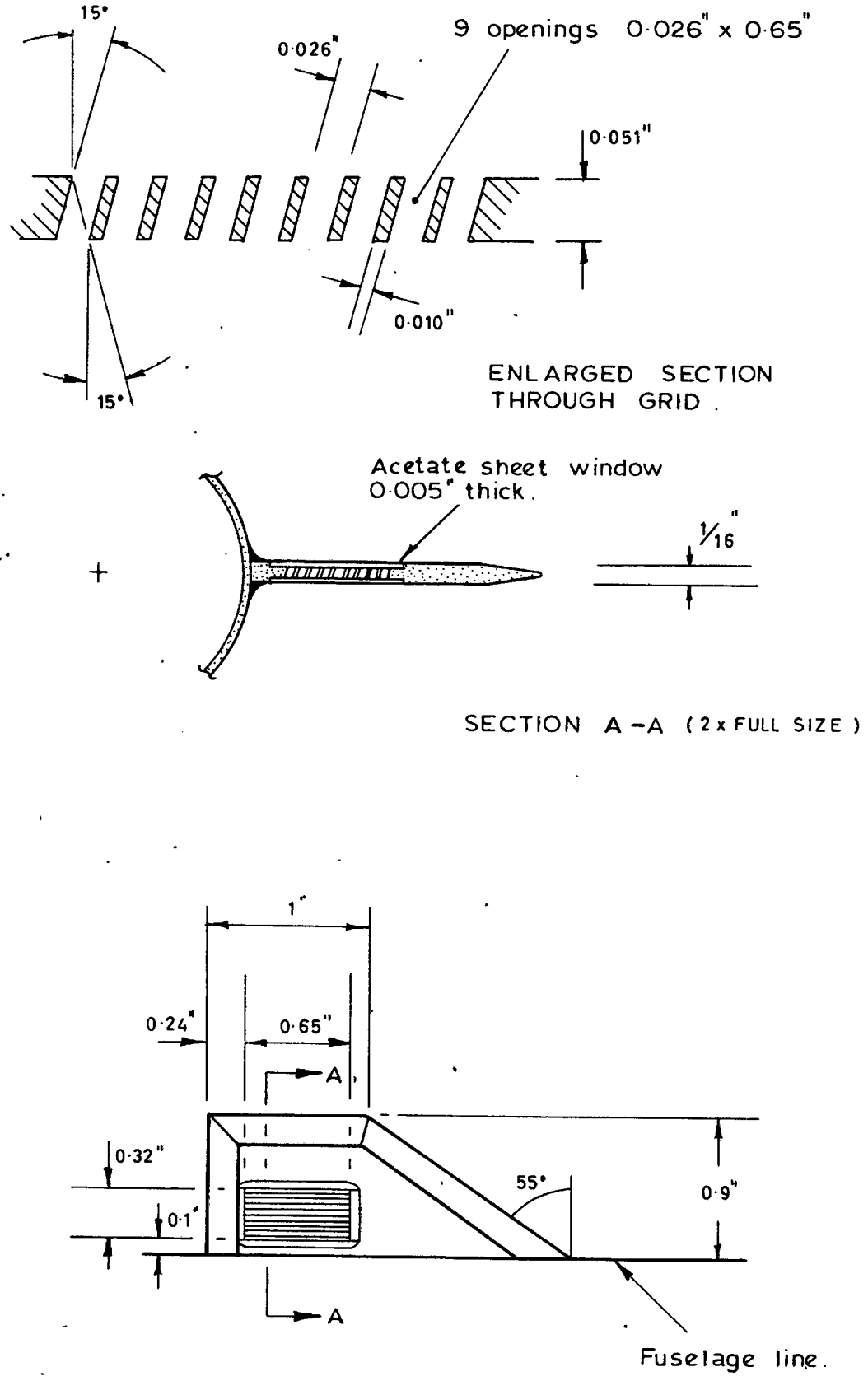

Fig. 8·13 The tuned model fin-mounted roll optical grid.

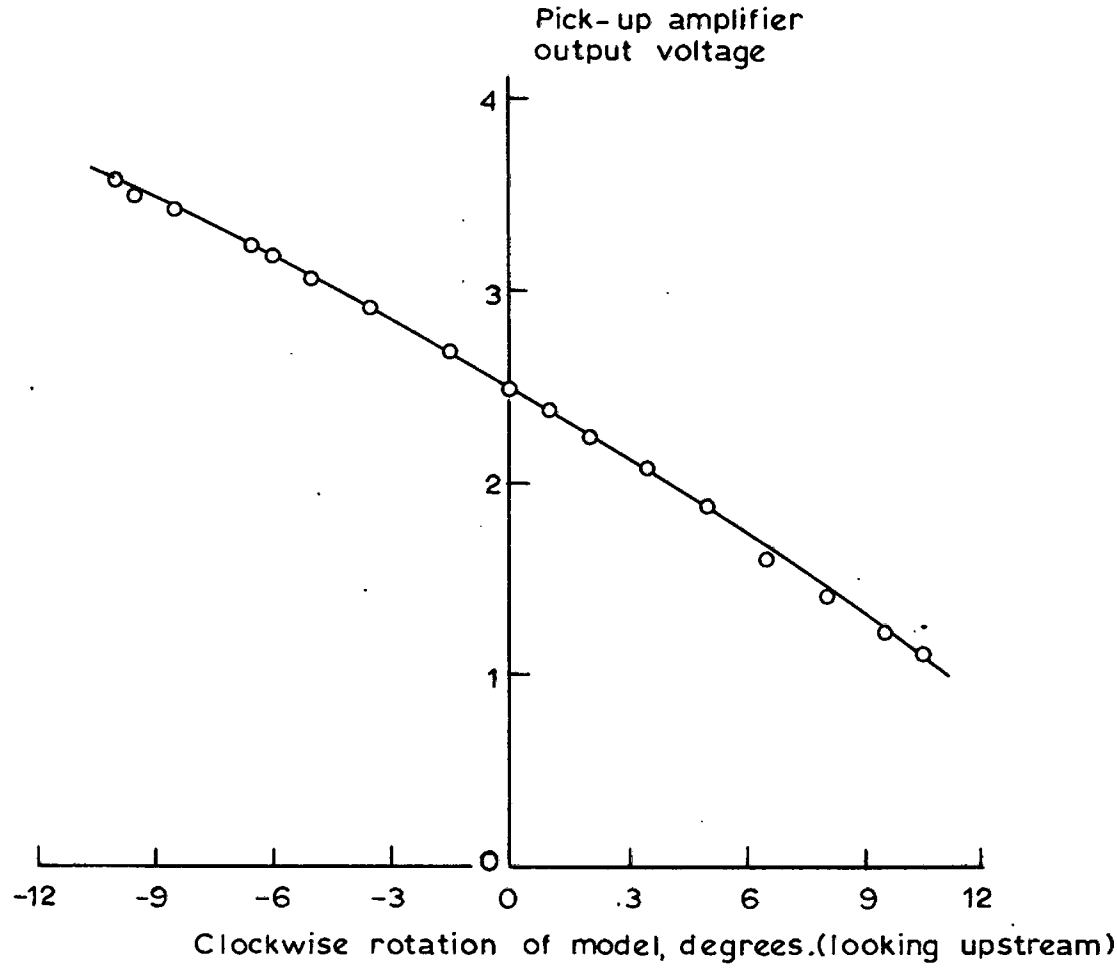

Fig. 8.14 Roll-attitude optical system calibration.

9. The Characteristics of the Power Supplies.

In this Chapter some details are given of the overall performance of the eight power supplies feeding current to the suspension magnets. Six of the supplies were of the type giving an output voltage varying in response to a low power input signal, i.e. they were power amplifiers, and were used as elements in servo-loops controlling six degrees of freedom of model motion. Some information on their internal design and transient performance was given by Weild[11], who concluded that for the purposes of control system stability analysis the power supplies can be assumed to have a negligible lag of output voltage following changes of input voltage.

Two D.C. power supplies were used in series to provide a bias current for the lateral electro-magnets.

Contents:

9.1 Introduction.

There are several different power supplies in use on the suspension system, feeding into a variety of loads. The supplies operated from 440 volt three phase mains, and produced uni-directional outputs. The main power supplies were required to respond rapidly to demands for changes of output voltage for model control purposes, and employed mains rectification by silicon controlled rectifiers. The mains frequency of 50 cycles per second resulted in 150 firing pulses per second. In order to maintain a rapid response rate there was no smoothing of the current flow apart

from that provided by the coils of the suspension system, and hence there was a considerable amount of ripple in the current supply. One problem which the ripple produced was that the frequency at which the output could be varied was limited by the acceptable distortion of the output wave-form.

The output voltage was varied by changes in the level of an input signal derived from the circuits of the model control system (see Chapter 7).

There were three basically different controllable power supplies, and a D.C. supply used in the lateral control of the model. The six controllable supplies were in the following groups:

Four independant supplies for the lift and lateral magnets,

One power supply for the drag coil,

One power supply for roll control.

Several of the power and coil circuits were provided with a series resistor as necessary to maintain the mean level of the supply voltage near to the mid-range for each supply at the mean current level, balancing the available voltage swings in each direction. This provided the same transient voltage capacity for satisfying demands for current changes above and below the mean. An additional advantage of the added resistance was a reduction of the time constants of the circuits. The resistors had a continuous rating of 30 amps., and had a negligible change of resistance with temperature in this current range.

9.2 The Controllable Power Supplies.

The lift and lateral power supplies each had load resistors amounting to 2 ohms in the coil circuit, giving a

total circuit resistance of about 2.6 ohms. . in the lift coil circuits, and 2.4 ohms. . in the lateral coil circuits. The mean current levels were typically 10 to 15 amps., and hence the mean supply voltage was in the range 24 to about 40 volts.

The variation with amplifier input voltage of the voltage across the terminals of one of the 0.6 ohm, . coils supplied by these types of amplifier (a lift magnet coil) is shown on Fig. 9.1. The curve is non-linear, a feature of the particular rectification method which was chosen, but in the mid region the variation of slope was not too pronounced. The slope at a representative current level was 12.6 volts/volt, giving an amplifier voltage gain of 54.6. The current drawn by the amplifier input from the model control loop compensation circuits was a maximum of 50 micro-amps and the maximum output current into the lift magnet coils was 35 amps at about 90 volts, hence the power gain of the amplifier was in the region of 10^7.

At maximum demand the power output from each amplifier was about 3.1 kW., but at the normal current required for model suspension the power dissipation was about 0.6 kW., giving a total power for the four supplies of this type at normal current levels of 2-2½ kW.

The drag coil had a relatively high resistance, the power requirements were high, and unlike the other supplies there was no normal output current level. For these reasons there was no load resistor in the circuit, but to reduce the time constant of the circuit the coil was wound in two halves, these being connected in series. The power amplifier was capable of producing a total

of 180 amperes, divided between the two windings. The maximum continuous rating of the coils with oil cooling was 40-50 amps. per section.

The measured variation of output voltage with input is shown on Fig. 9.2 taken with the amplifier supplying current to a coil, for part of the available range from the amplifier. The powerful heating effect at current levels above about 50 amperes per wire with the 12 S.W.G. wire of the coils precluded steady-state measurements at higher voltages. At mid-range the gain was 177 volts/volt.

The suspension system was designed for a maximum steady drag force of 1 lb. at a drag coil total current of 100 amps. At this condition the power output (dissipated in the coils) was 7.8 kW.; the maximum power output capability of the amplifier was about 25 kW.

A single power supply was used for generating rolling moment. In the coil circuit of this amplifier there was a 1 ohm load resistor, and the total circuit resistance was about 2 ohms, giving a power dissipation of 450 W. at the normal current level of 15 amperes. The maximum output of the amplifier into this load was 32 amperes, and the corresponding power output 2 kW. The variation of output voltage with input is shown on Fig. 9.3.

9.3 <u>The D.C. Power Supplies</u>.

Two D.C. power supplies were used in series, supplying a steady current to the lateral coils. The characteristics of one of the supplies are shown on Fig. 9.4; the continuous line shows the maximum output, and superimposed are broken lines showing power output and operating lines for different values of load resistor.

In order to suppress current fluctuations that might be induced in the bias circuit by inductive coupling in the lateral coils, a 0.75H choke was included in the circuit together with 2 ohm .w. load resistors giving a total circuit resistance of 6 ohms.s. The output of the supplies was variable, but the maximum bias current was 11½ amps with this circuit. With the load resistors removed the maximum could be increased to 16½ amps.

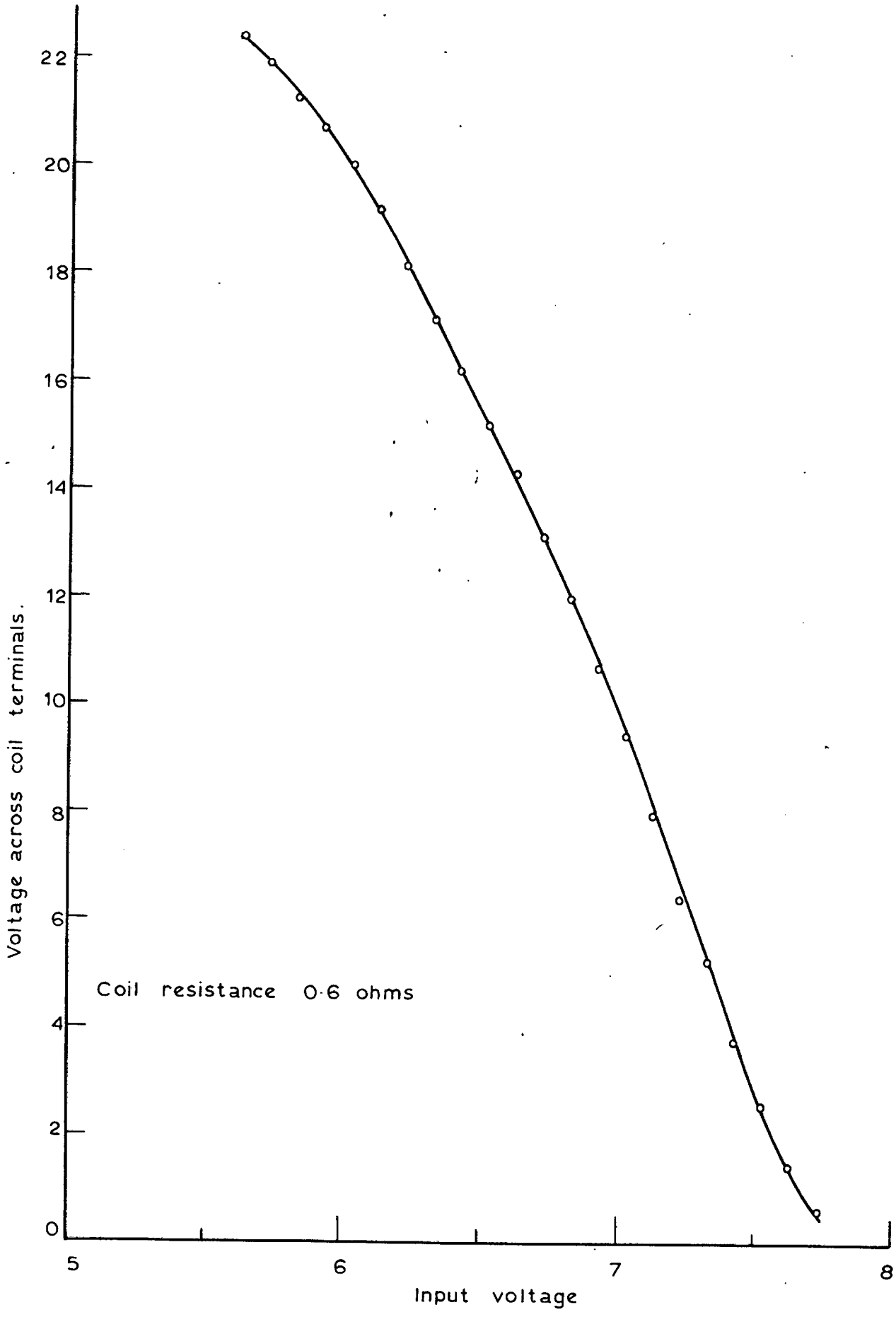

Fig. 9.1 The steady-state characteristics of a lift coil power amplifier coupled to a 2·6 ohm load.

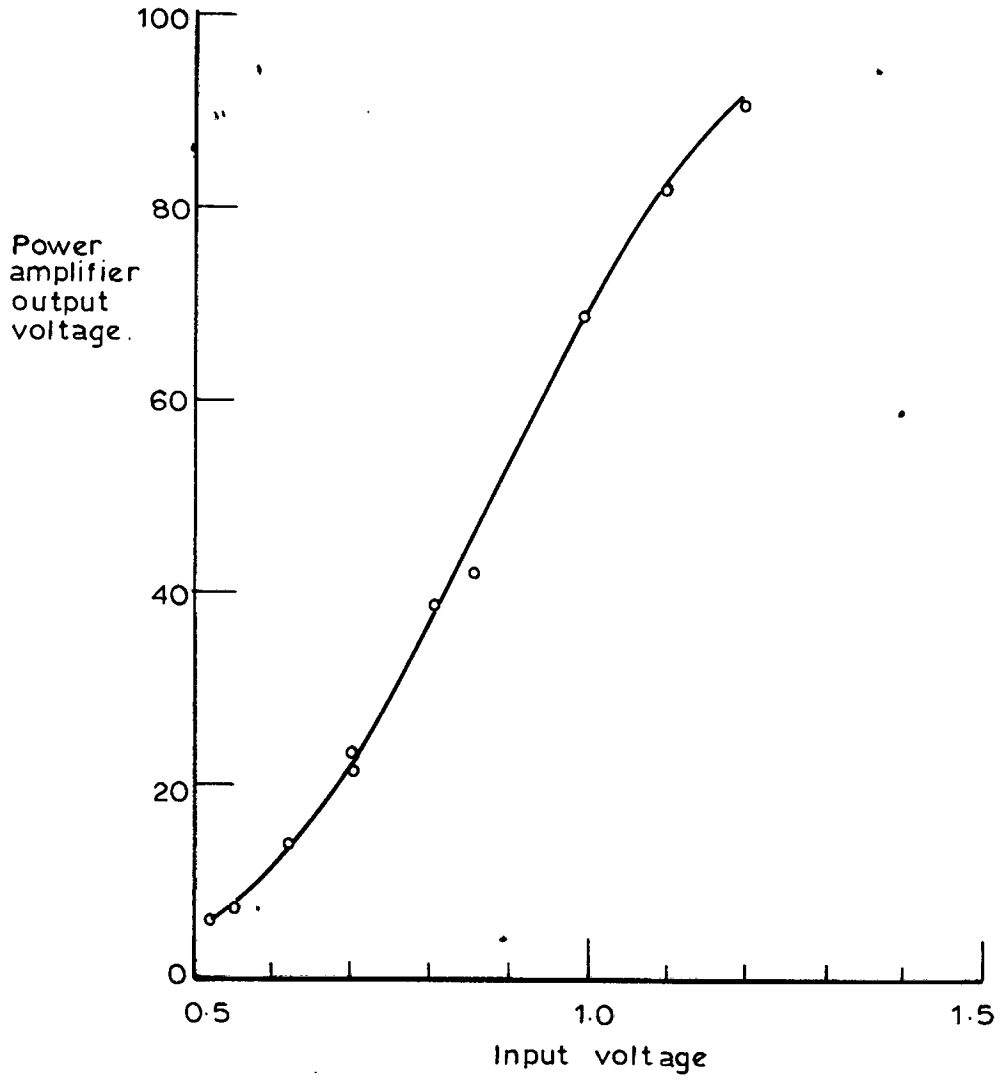

Fig. 9.2. The characteristics of the drag coil power amplifier.

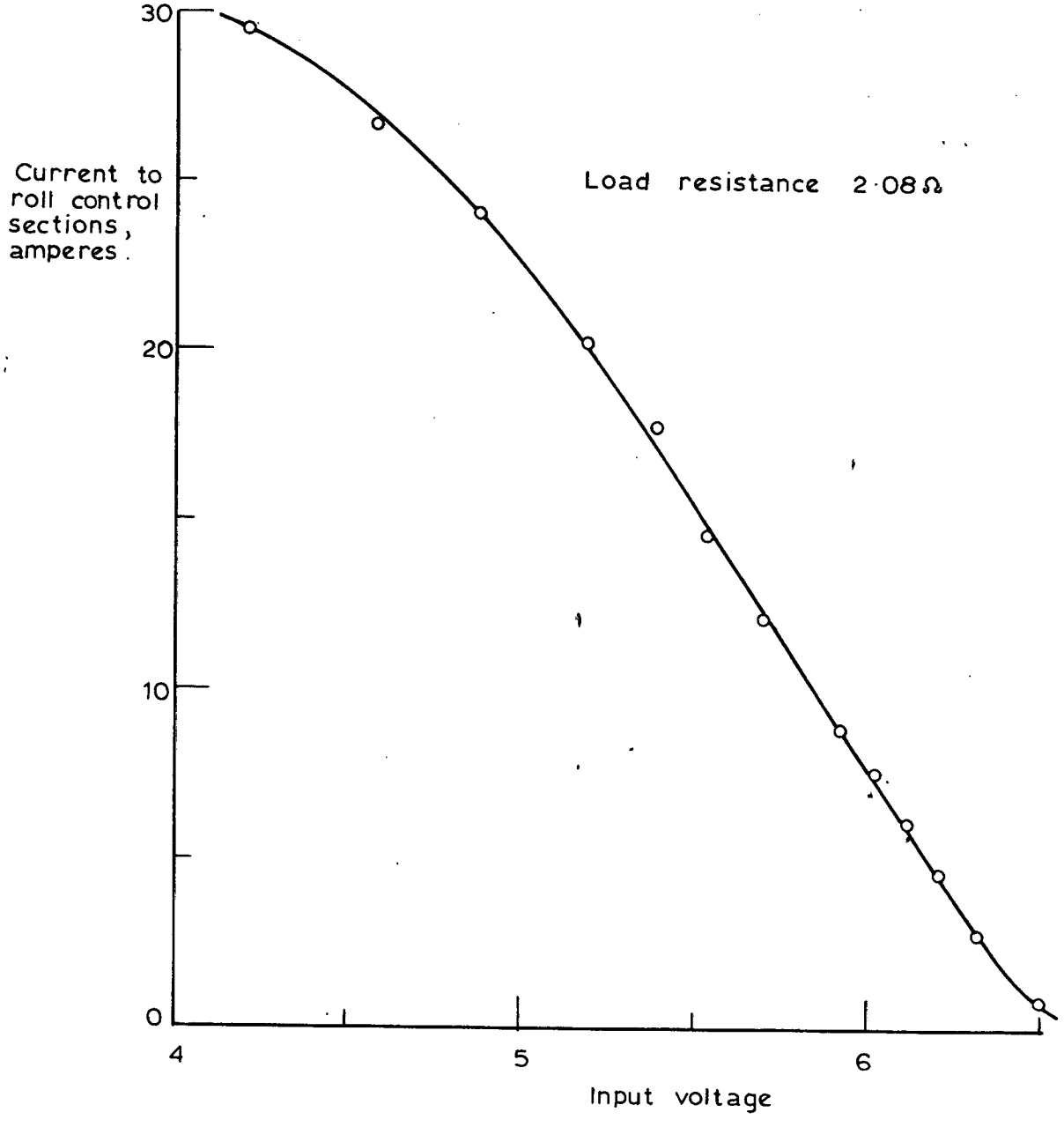

Fig. 9.3 The characteristics of the roll control power amplifier.

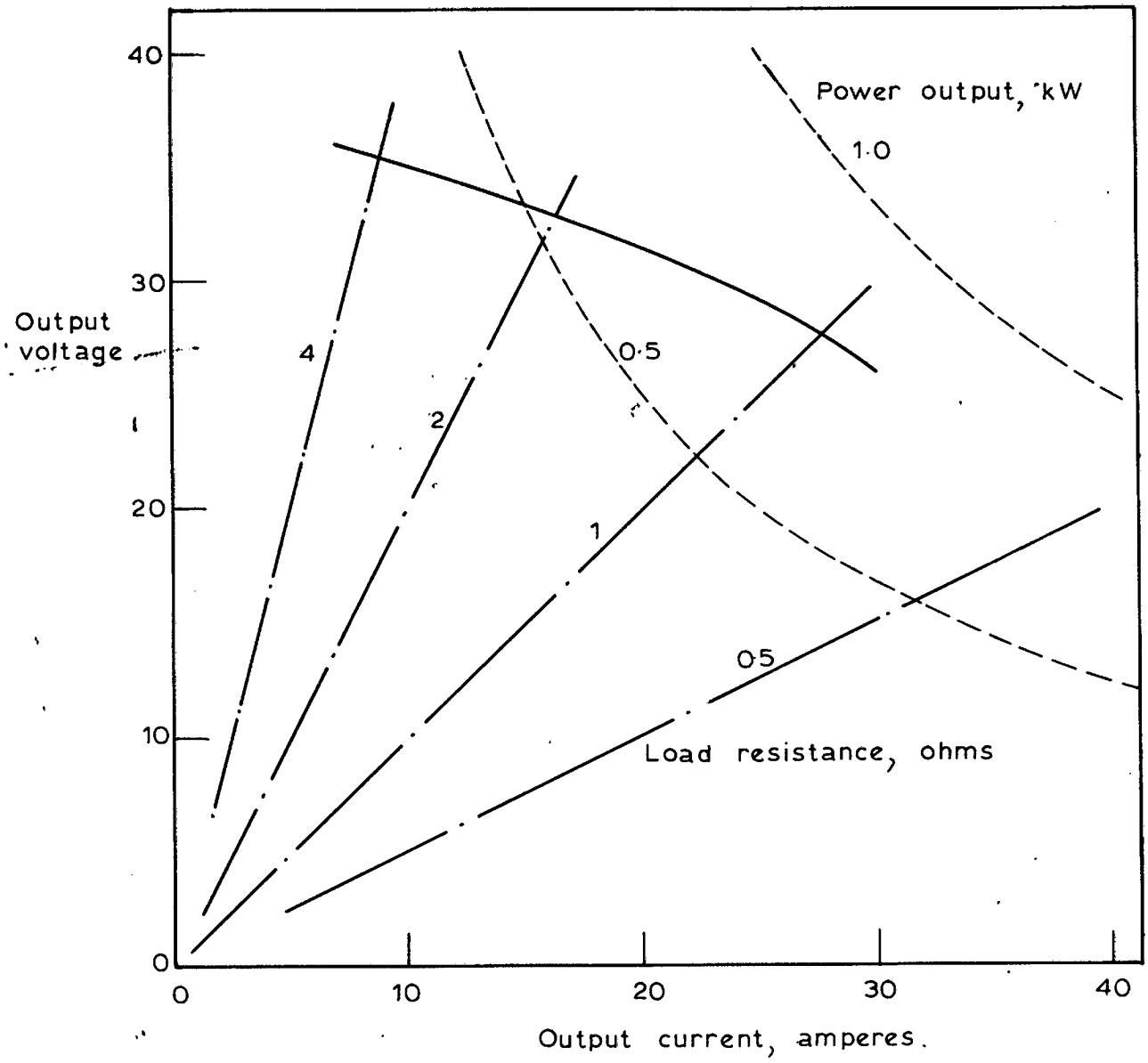

Fig. 9.4 The characteristics of a D.C. power supply.

10. The Magnetic Suspension System as a Low Speed Wind Tunnel Balance.

A magnetic suspension system can be a useful research tool when used as a balance, or just as a suspension system, for low Reynolds number and low speed experiments. In this Chapter some fields of application are discussed, together with brief details of some experiements carried out with models suspended in a low speed atmospheric stagnation pressure wind tunnel.

Contents:

10.1 Introduction.

There are two particular uses to which a magnetic suspension system can be applied to wind tunnel experiments at low air velocities, where the advantages of this form of suspension are particularly attractive. Accurate measurement of drag force is possible, and as the model would be suspended without wires or sting, the opportunity can be taken for measuring drag with a laminar boundary layer over the model and with no disturbance to the base flow.

With a laminar boundary layer over the model, at half of the maximum tunnel speed the total drag on an 11/16 inch diameter model was about 0.002 lb. (under 1 gram.). The normal drag resisting and measuring equipment on the suspension system was not

suitable for such small forces, being designed for a maximum drag force 500 times greater. Consequently a new measuring technique had to be developed, to make sufficiently accurate drag measurements in the range up to about 0.02 lb. (9 grams.).

Three possible alternative drag measuring techniques were considered, two making use of the stiffness imparted to the model in the axial sense by the suspension electro-magnets,

(i) The drag force could be resisted simply by making an alternative low-powered supply for the drag coil, with a suitable meter for indicating current and hence, from a calibration, drag force. The model position would be automatically controlled in the conventional manner using feedback from the optical system.

(ii) A more simple alternative would be to feed a direct-current supply to the drag coil, without stabilisation, but making use of the axial stiffness from the support magnets to obtain axial stability. This would be satisfactory provided that the field gradient from the drag coil did not cause axial motions to become unstable due to negative stiffness.

(iii) Another simple alternative was to make use of axial force components from suspension magnets, which come into play once the model is moved from its equilibrium position of suspension, giving stiffness comparable with that of a pendulum. For a given model, change of axial position could be calibrated against drag force.

Alternatives (ii) and (iii) would impart no significant

magnetic damping to axial motions of the model.

Alternative (iii) was chosen for experimental investigation partly because of the simplicity, but also because the drag calibration should be relatively insensitive to changes in the state of magnetisation of the permanent magnet core of the model.

The principles were described in Chapter 3 and the calibration technique is given in Chapter 5. A blunt based body of revolution has been the subject of a series of experiments[12] into the effects on drag of changes to the base design. The wind tunnel used for these experiments was an adaptation of an existing design, and is briefly described in section 10.2, and in section 10.3 examples are given of drag and base-pressure measurements made with this model.

The second application of the magnetic suspension system to low speed wind tunnel testing was the measurement of aerodynamic damping in roll of a winged model. If the rolling motion of a model is not controlled by the suspension system, then the damping in roll originating from the suspension system is low, allowing measurement of the relatively low aerodynamic damping forces. The technique, and an assessment of the accuracy of the measurements are given in section 10.4.

10.2 A Low Speed Wind Tunnel Adaptation to the Suspension System.

A wind tunnel was available which was well suited to the magnetic suspension system, requiring only a new working section for adaptation to the magnetic suspension system. The wind tunnel was fan driven, the fan drawing air through an intake to a 6 inch square working section. The maximum air speed in the working section was 110 ft./sec.

It was decided to construct an all-Perspex working section to allow passage of the optical system light beams. The wind tunnel and suspension system are shown on Fig. 10.1. The air intake is on the right of the picture, in the centre is the suspension system and at the left the fan exhausting into the room. Access to the inside of the working section was through a door in the working section side, just downstream of the suspension system. A view along the working section, looking upstream, is given on Fig. 10.2. A model is shown suspended, controlled in six degrees of freedom (the model is also shown on Fig. 6.17). The light sources for the diagonal beams can be seen either side of the central tank enclosing the lift magnet coils, over the wind tunnel, and the source for the optical system monitoring axial motion of the model is under the lower right side of the tunnel. Part of a honeycomb flow straightener in the air intake is visible through the tunnel.

10.3 Drag and Base-Pressure Measurements with a Body of Revolution.

The drag measurement technique was developed using the solid body of revolution weighing 10.2 oz., shown on Fig. 10.3, and measurements were confined to zero incidence, and for these experiments the model was controlled in four degrees of freedom. Force-displacement calibrations were taken before and after wind-on tests.

At the drag force realised with this model at the higher air speeds the drag measurement technique utilising the fore-and-aft stiffness from the lift magnets was satisfactory. However, it should be mentioned that the range of force measurements could be extended to a higher or lower range by introducing stiffness from the lateral

electro-magnets, by attracting or repelling the model respectively with equal forces from the magnets. By repelling the model the axial stiffness could be made negative resulting in an unstable model, but by adjusting the stiffness to a positive value near zero it might be possible to make drag measurements at very low air speeds.

An example of the results of a series of zero incidence drag measurements is shown on Fig. 10.4. The scatter in the calibration data given in Chapter 5 would indicate that in the upper third of the drag range the force could be measured accurate to about $\pm$ 1%. Some additional scatter occurred under wind-on conditions as a result of flow disturbances causing the model to wander slightly about the mean axial position appropriate to the mean drag force. The damping in the valve-voltmeter needle indicating model position assisted in reading the mean position of the model. However, the wind-on drag measurements that have been made indicate from the scatter obtained that wind-on force measurements can be obtained from a smoothed curve to an accuracy of about $\pm$ 2% with drag forces in the region of 0.01 lb. (4½ grams.)

As a check on whether the boundary layer over the model was turbulent, a 0.012" dia. transition wire was moved in steps along the length of the parallel part of the fuselage. The variation of drag coefficient with wire position is shown on Fig. 10.5. The drag coefficient was based on the model cross sectional area. The wire position x is measured downstream from the front of the parallel fuselage, as shown on Fig. 10.3. Movement of the wire towards the tail had the effect of reducing the drag coefficient except for wire positions very near the tail, within about 0.2" of the tail, where

an increased drag coefficient was measured. However, the trend of the curve as far as this region indicated that the no-wire drag coefficient would be reached by an extrapolation to $x = 6^{9}/_{16}$", which was some confirmation that the boundary layer was laminar when no trip-wire was in use. With the wire positioned just ahead of the tail, a wide scatter in drag coefficient was obtained, the lowest values being close to the laminar boundary layer drag coefficient of 0.21. The different values of drag coefficient were obtained on different occasions, with the wire in the same position on the model, and were not due to unsteadiness in the readings.

The special effect with the wire close to the tail was interesting, and it was decided to attempt to measure base pressure to see if base pressure changes could account for the drag rise. Base pressure was measured in a separate series of experiments using a slender non-magnetic probe mounted on the tunnel downstream of the model and extending towards the tail of the model, touching the model on the centre-line of the base. The probe consisted of an open ended tube, with the end chamfered 15° away from square to allow a small air flow into the tube when touching the model. The tube outside diameter was 0.046" for the 3" of tube adjacent to the tail, with a further 3" of $\frac{1}{8}$" diameter tube downstream of this, all lying on the tunnel axis. Thereafter the tube curved round through 90°, increased in diameter to $\frac{1}{4}$", and passed through the tunnel wall.

The main disadvantages with this method of measuring base pressure were that the probe could interfere with base flow, even though the probe was relatively slender, and that simultaneous drag measurements could not be made with the probe touching the base.

The base pressure data is also shown on Fig. 10.5 in coefficient form. Relatively large differences of base pressure coefficient were recorded on different occasions with the wire in a given position near the tail, and the range of values obtained suggested that the drag rise was due to changes of base pressure.

The ease with which these drag and pressure measurements had been made, and the accuracy obtained, were encouraging, and resulted in a series of experiments[12] on the effects of base design changes.

10.4 The Measurement of Damping in Roll.

10.4.1 A winged model was manufactured, for testing in the low speed wind tunnel described in section 10.2, with the object of developing a technique for measuring damping due to rate of roll.

A drawing of the model, carrying thin cropped delta wings, is shown on Fig. 10.6. The leading and trailing edges of the wings were tapered.

Several alternative methods were available for investigation:

(i) the model could be forced to oscillate in roll using the roll control system, and the aerodynamic damping of the motion detected by measuring phase-change between the applied rolling moment and the motion of the model,

(ii) the model could be motored about its roll axis by the roll control system using a method described in Chapter 6,

(iii) the model could be mechanically spun about its roll axis, released, and the rate of decay of the angular velocity used as a measure of aerodynamic damping.

Alternative (i) is not a particularly attractive technique,

because it would be necessary to apply a relatively large moment to the model to balance the inertial moment, which would tend to swamp any aerodynamic moment that might be present, and hence make the extraction of the required data rather difficult. In any case, at about the time that these experiments were being made, the more attractive tuned model oscillatory technique was being studied, and hence it was decided that little could be gained by pursuing this line of investigation.

Alternative (ii) would avoid the problem of large inertia moments by driving the model as a synchronous motor, nominally at constant speed. This does in fact appear to be a promising line of approach and may well be developed in the future. However, it is not as simple as the third method, because of the requirement of calibration and indication of power input to the rotor (i.e. the model).

Because of its relative simplicity, alternative (iii) was chosen for experimental evaluation. The only equipment that required special development was an optical system to monitor roll attitude through 360°, to give the rate of roll of the model.

10.4.2 The drag optical system was chosen for indicating roll rate and attitude. As a result of the low drag forces experienced with models in this low speed tunnel, no special provision was required for the control of axial motions. The field stiffness from the suspension magnet could be relied upon to cope with the drag force in the manner described in the previous section. Even when the model was spinning about its roll axis, there was no significant change of drag force and hence there was no tendency, from this source at least, for the model to wander axially during the time that it was spinning.

Sixteen radial slits were machined in an aluminium alloy tail-plug for the model. The light beam used for roll position indication was directed in the manner shown on Fig. 10.7, across the tail of the model. As two diametrically opposite slits moved into and out of alignment with the light beam axis, due to the model rotation, a triangular pulse was produced in the output from the pick-up. One diametrically opposite pair of slits were made wider than the rest, so that out of the sixteen pulses obtained in one revolution of the model, two could be identified on traces by broader bases and higher peaks. This allowed the fixing of the roll attitude to one of two alternatives. In fact ambiguity of attitude did not occur in practice, because asymmetry in the model magnetisation or manufacture, or both (which always seems to be present) gave some stiffness in roll which showed clearly in velocity-time plots in the form of tendencies to accelerate or decelerate more than normal when the roll attitude was about 90° away from the preferred attitude when suspended. Had there been some ambiguity in the roll attitude a simple modification was possible to result in a position-time trace giving just one large pulse per revolution.

A photograph of the model, which clearly shows the tail plug, is shown on Fig. 10.8, and a trace showing the output from the optical system pick-up, taken on a ultra-violet recorder, is shown on Fig. 10.9. A 500 cycle per second timing mark is also shown. Time increases from right to left. The pulses have well defined peaks, each corresponding precisely with the alignment of one pair of tail plug slits with the light beam, and the time interval between pulses corresponds with a rotation in roll of $22\frac{1}{2}$ degrees. During the analysis of the trace it was assumed that the average angular velocity

given by the time interval between pulses corresponded with the actual velocity at the time mid way between the pulses.

An angular velocity - time curve is shown on Fig. 10.10, taken from the trace on Fig. 10.9. Methods for the analysis of this curve will now be discussed.

10.4.3 It can be seen that about 2½ revolutions of the model have been recorded, the angular velocity changing from 7.62 to 1.91 revolutions per second during a period of about seven-tenths of a second, as a result of damping. There may have been some eddy-current damping; separate experiments would have been required to determine the magnitude of this contribution to the net damping measured and at the present time it is not known whether eddy currents within the model have any significant effect.

It has already been mentioned that the model had a preferred roll attitude as a result of some roll stiffness. The effects of this stiffness can be distinguished on the wind-on velocity-time curve. For example, in the second half of the first and second revolutions there was a clear tendency for the model to decelerate rapidly. This was attributed to the roll stiffness producing a decelerating torque. Similarly in the first half of the first, second and third revolutions a tendency can be seen for the model to reduce its rate of deceleration, and this can be attributed to the roll stiffness tending to accelerate the model. In this way, ambiguity was avoided with regard to model attitude. The preferred roll attitude happened to coincide with the large tail-plug slits nearly aligned with the light beam.

From a measurement of the moment of inertia of the model

about its roll axis, and the slope of the velocity-time curve at any particular angular velocity, one can determine the decelerating torque. Best accuracy was obtained by measuring a slope of the curve near an inflection. However, these points coincide with model roll attitudes about 90° away from equilibrium, where asymmetry was having the effect of increasing or reducing the deceleration of the model. Consequently some correction was necessary for the effects of roll stiffness.

The stiffness might have been from two sources : magnetic asymmetry and offset centre of gravity. The correction for an offset centre of gravity is relatively simple, because a measurement of the natural frequency of small amplitude roll oscillations (wind off) permits the calculation of the amount of offset. It was less easy to allow for the effects of magnetic asymmetry. However, it appears that the combined effects of offset centre of gravity and magnetic asymmetry may have the characteristics of an offset centre of gravity, and hence be corrected-for using the technique already mentioned.

Due to the uncertainty of the above procedure, a second method an analysis is proposed, based on energy balance considerations.

The instantaneous rate of extraction of energy from the model by the airstream, $\dot{E}$, is given by

$$\dot{E} = - L \dot{\theta} \qquad \text{10.1}$$

where L is the aerodynamic torque applied to the model by the airstream.

The work done on the airstream in time δt is $\dot{E} \delta t$.

Over any one revolution, the magnetic asymmetry and offset centre of gravity make no contribution to the energy balance.

Assume that at any given airstream velocity head

$$L = L_p . \dot{\theta} \qquad \text{10.2}$$

where L_p is the aerodynamic derivative required which may be written in non-dimensional form:

$$\ell_p = \frac{L_p}{\rho V_o S s^2}$$

From 10.1 and 10.2 $\quad \dot{E} = -L_p \dot{\theta}^2$

and over one revolution, the total work done is $-L_p \int \dot{\theta}^2 dt$ the integration being taken over the time required for the revolution.

This is equated to the change of kinetic energy of the model over the same period of time, given by $\frac{1}{2} A (\dot{\theta}_o^2 - \dot{\theta}_1^2)$

Hence $\quad L_p = \dfrac{-\frac{1}{2} A (\dot{\theta}_o^2 - \dot{\theta}_1^2)}{\int \dot{\theta}^2 dt}$ $\qquad$ 10.3

10.4.4 The experimental procedure was as follows:

The moment of inertia of the model about its roll axis, 7.2×10^{-4} lb.ft.^{2}, was determined by the bifilar suspension technique (the weight of the model being 11.31 oz., 321 gm.). The initial spin of the model was produced by unwinding a thread which had been wound into a groove located near the tail of the model, just ahead of the optical slits but clear of optical systems and passing through a hole in the wind tunnel alongside the model. The groove is shown on Figs. 10.6 and 10.8. As soon as the thread was clear of the model, the output from the roll monitoring optical system was recorded, together with timing marks giving the trace of Fig. 10.9. During this particular experiment the tunnel air speed was 86.2 ft./sec. (26.3 metres/sec.)

Some axial disturbance of the model position usually occurred as a result of the spin-up process, leaving an axial oscillation of approximately 1 c.p.s. which was poorly damped because

of the absence of proper control of that degree of freedom. This accounts for the rise and fall in the trace over its length. However, the change of relative velocity between the model and the airstream as a result of this motion was insignificant because of the small amplitude of the disturbance.

A large scale plot of $\dot{\theta}^2$ against time was then used for evaluating the denominator of equation 10.3. Four separate integrations were made, each over one revolution, covering the revolution ranges marked on Fig. 10.10 of 0 - 1, ½ - 1½, 1 - 2 and 1½ - 2½. The four ranges gave the results in Table 10.1.

TABLE 10.1

Revolution range	0 - 1	½ - 1½	1 - 2	1½ - 2½
Kinetic energy change - ft.lb.	0.01373	0.01097	0.00794	0.00548
$\int \dot{\theta}^2 dt$, radian^2/sec.	247	200.2	155	109
$-L_p \times 10^5$ lb.ft.sec./radian	5.56	5.47	5.12	5.03
$-l_p$	0.14	0.1378	0.129	0.1268
Mean wing-tip incidence, degrees	4.0	3.24	2.46	1.7

The rolling moment derivative is plotted against the mean tip incidence during the integration period on Fig. 10.11, curve A. There was a tendency for $-l_p$ to increase with increasing mean tip incidence. The significance of this tendency required some investigation. It might have been a correct representation of the aerodynamic characteristics of the model, but the unknown effects of eddy currents did leave some doubt about the trend. However, an extrapolation of curve A back to zero tip incidence should give a correct value for l_p, unaffected by eddy currents.

Some wind-off measurements of rate of deceleration were made, which place a maximum limit on the variation of torque due to eddy currents with speed. In fact these measurements would include a torque contribution from the air pumping effect of the wings; they do not show eddy current effect alone. However, curve C is drawn through points corrected by the full amount of wind-off torque at the appropriate mean rotational speeds. Two revolutions of free-rotation of the model under wind-off conditions are shown on Fig. 10.10. The effects of roll stiffness are clearly visible as a sinusoidal variation of rotational speed about a gradually reducing mean value. The wind-off mean rate of deceleration of the model is shown on Fig. 10.12, where a curve has been fitted according to the so-called propeller-law:

$\ddot{\theta}$ = constant x $\dot{\theta}^2$,(where $\ddot{\theta}$ is proportional to torque,)

which proved to be a good fit. There is reason for believing that torque due to eddy-currents would vary as the first power of $\dot{\theta}$, and hence the evidence of this curve would indicate that eddy-currents were not contributing a large part to the wind-off decelerating torque. However, in the absence of positive evidence on these effects, for the time being half of the wind-off torque has been deducted from the wind-on data of Fig. 10.11, giving curve B, with the errors due to the uncertainty over eddy-current effects shown on the same diagram.

The use of an identical model constructed from a non-conducting material would provide the essential data on the effects of eddy-currents.

10.4.5 At higher wind tunnel air speeds, where the drag forces would be higher, control of the axial position of the model might be required, together with a more refined method for producing the initial spin-up.

However, there does not appear to be any other problem facing its potential use at high speeds.

10.5 A Summarised Assessment of Low Speed Applications.

General comments:

A magnetic suspension system controlling the model position in four degrees of freedom (leaving drag and roll uncontrolled) can be a versatile piece of equipment. Experience has shown that with a modest amount of effort the system can be adapted to perform a variety of measurements. In this form the suspension system is relatively cheap.

On drag measurement:

(a) Drag measurements have been demonstrated to be practicable at drag forces up to 3% of the weight of a model, suspended in a horizontal working section.[12]

(b) A drag force of about 0.01 lb. can be measured within an accuracy of about $\pm$ 2%.

(c) A four component balance may be suitable for measuring higher drag forces, possibly up to 10% of the model weight. To date the maximum drag force that has been resisted, under calibration, is 10% of the model weight. However, this was not the force limit. Coil heating could be a limiting criterion.

(d) Drag forces equal to 0.3% of the weight of the model can be satisfactorily measured.

(e) Improved sensitivity might be obtained at lower drag forces by repelling the model with the lateral electro-magnets, thereby reducing the effective axial stiffness of the model.

(f) The force range might be increased by attracting the model equally by the lateral magnets, thereby increasing the axial stiffness of suspension.

On rolling moment due to rate of roll:

(a) The rate of deceleration of a model spinning freely about its roll axis can be used for the measurement of this roll derivative.

(b) Possible eddy-current effects at present throw some doubt on the accuracy of data obtained at high rotational speeds. More experimental or theoretical work is required to resolve this problem.

(c) The technique is potentially suitable for air speeds higher than used in these experiments.

10.6 LIST OF SYMBOLS USED IN CHAPTER 10

Symbol	Meaning
A	Moment of inertia of model about the roll axis
C_D	Drag coefficient, = drag/$\frac{1}{2}\rho V_o^2 S_f$
C_{P_B}	Base pressure coefficient, = $(p_B - p_o)/\frac{1}{2}\rho V_o^2$
E	Energy
L	Aerodynamic torque
L_P	$L/\dot{\theta}$
ℓ_P	$L_P/\rho V_o S s^2$
p_B	Base Pressure.
p_o	Airstream static pressure ahead of model.
S	Wing area.
S_f	Fuselage cross sectional area.
s	Wing semi-span.
t	Time.
V_o	Air velocity ahead of model.
θ	Roll angular attitude.
ρ	Air density.

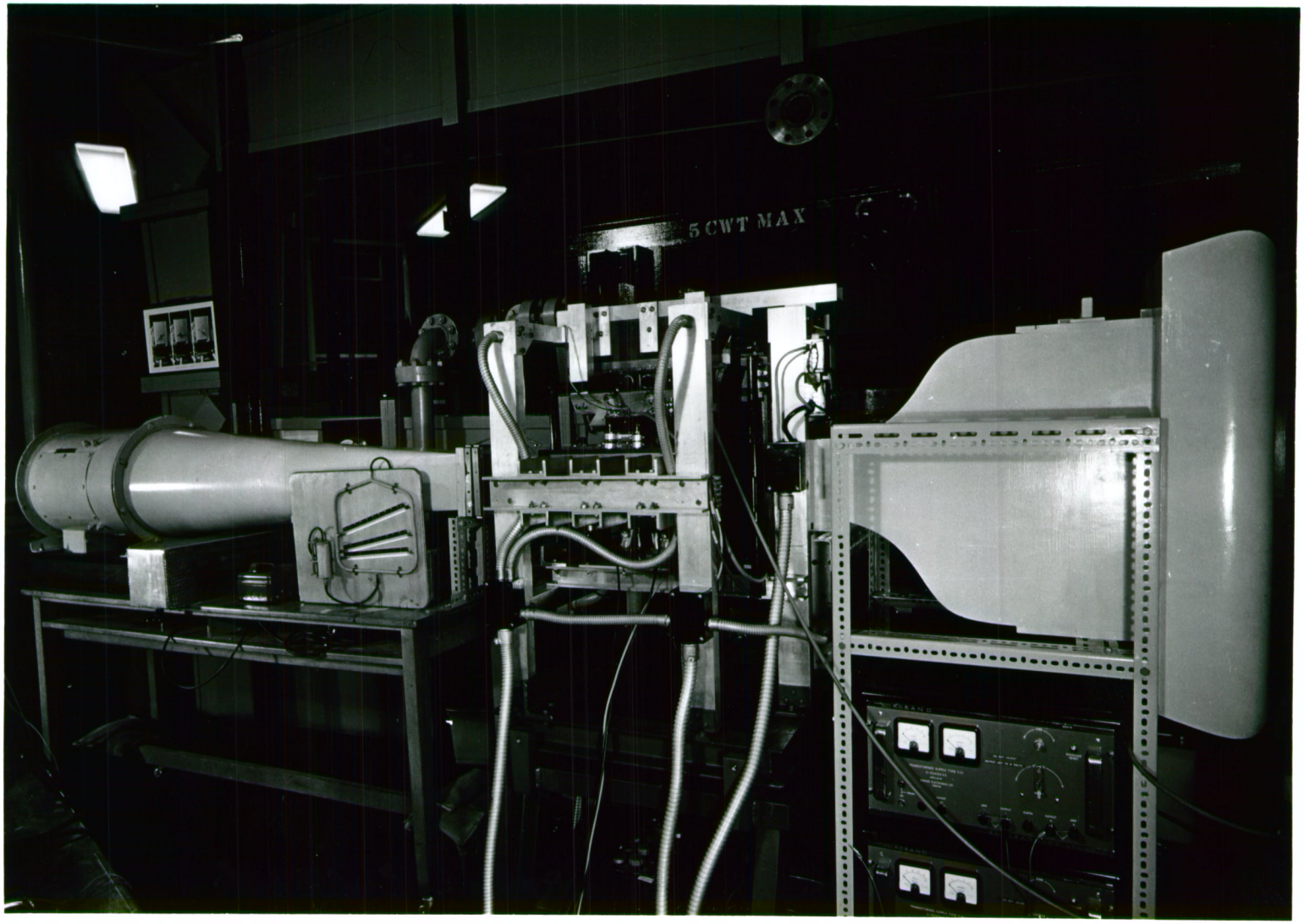

Fig. 10.1 The low speed wind tunnel and magnetic suspension system.

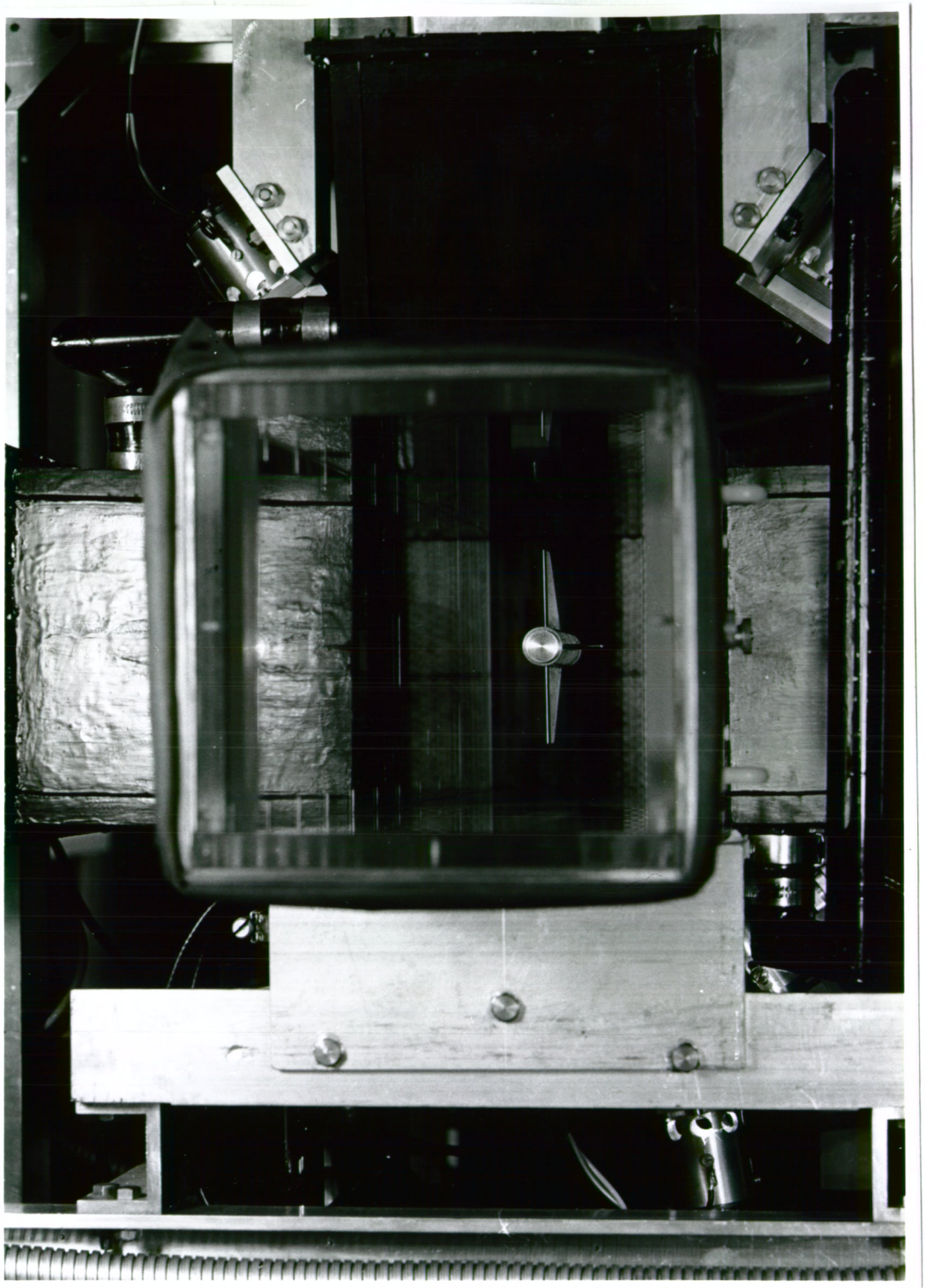

Fig.10.2 A view along the Perspex working section of the low speed wind tunnel, showing a winged model suspended in the six component magnetic balance.

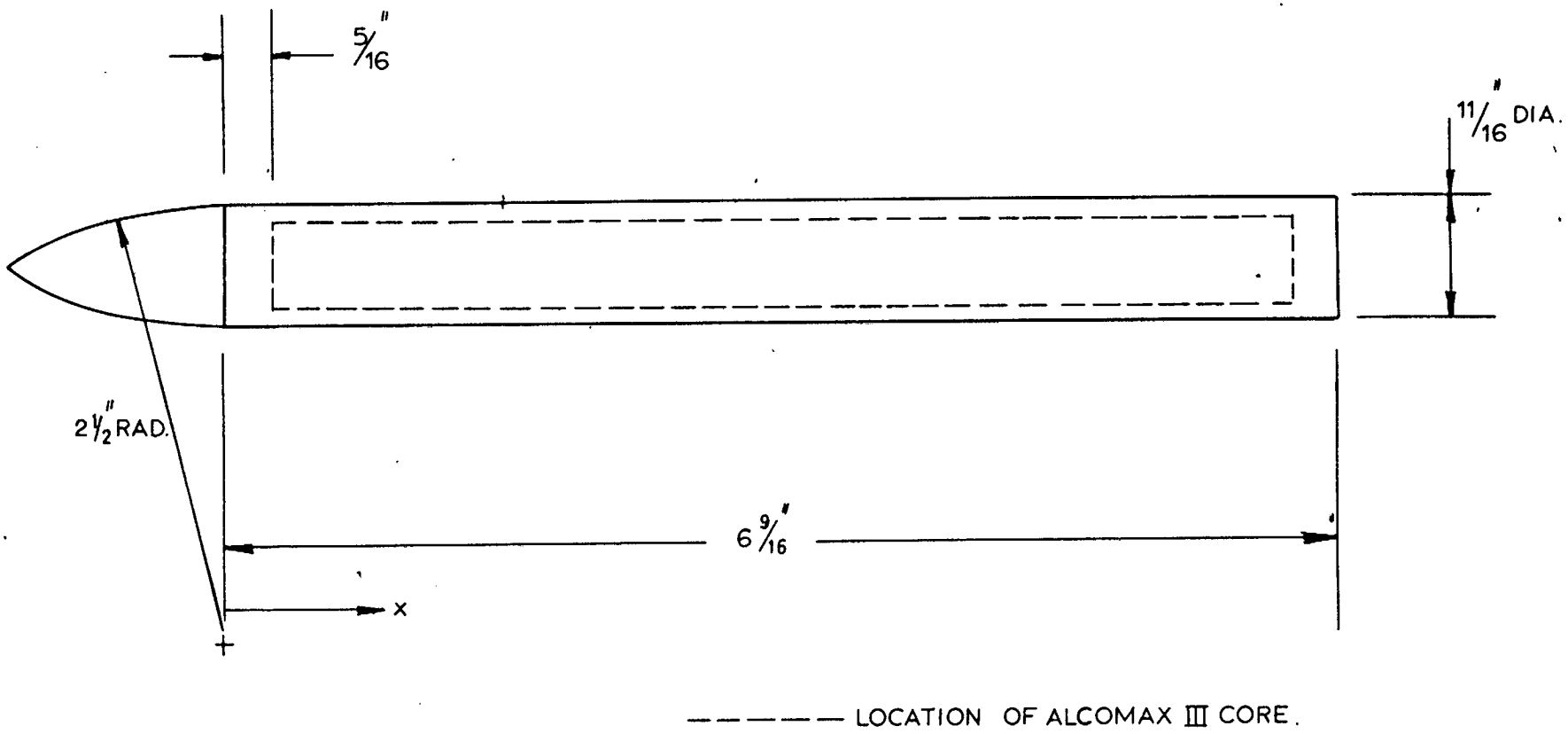

Figure 10.3. An outline drawing of the solid body of revolution.

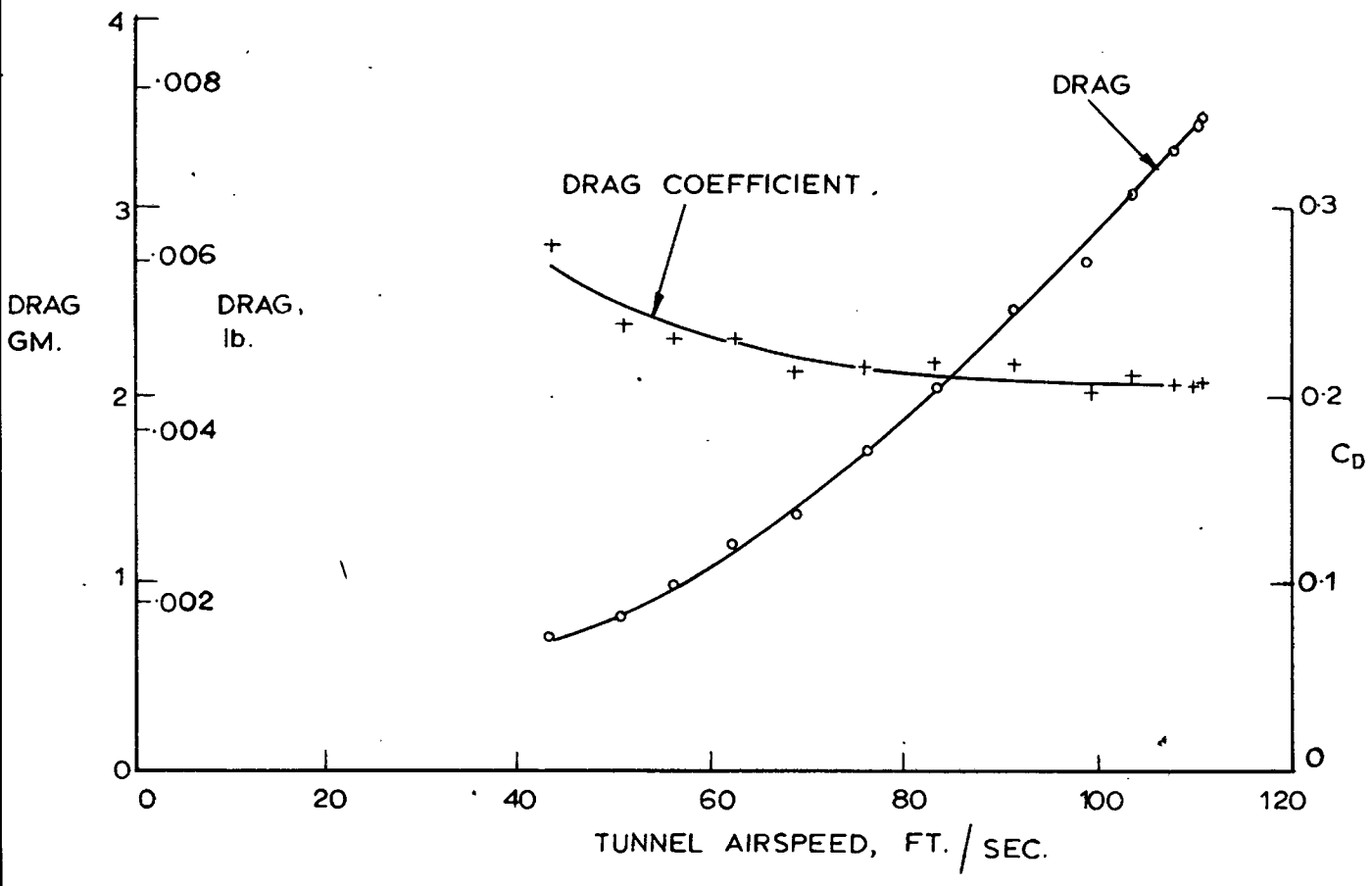

Figure 10.4. Drag measurements made on the body of revolution shown on figure 10.3.

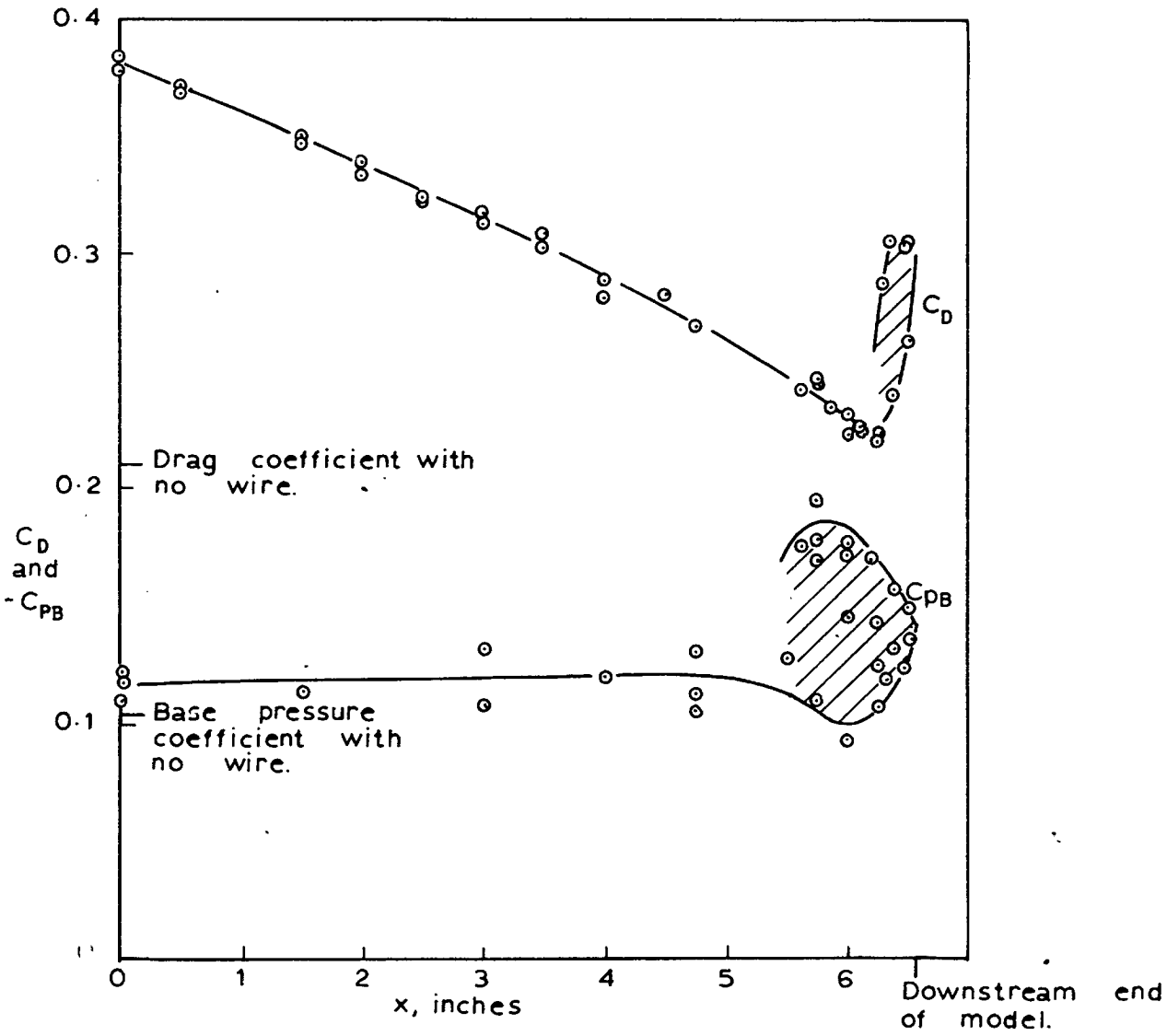

Figure 10.5. Variation with wire position of the bluff-tailed model drag and base pressure coefficients.

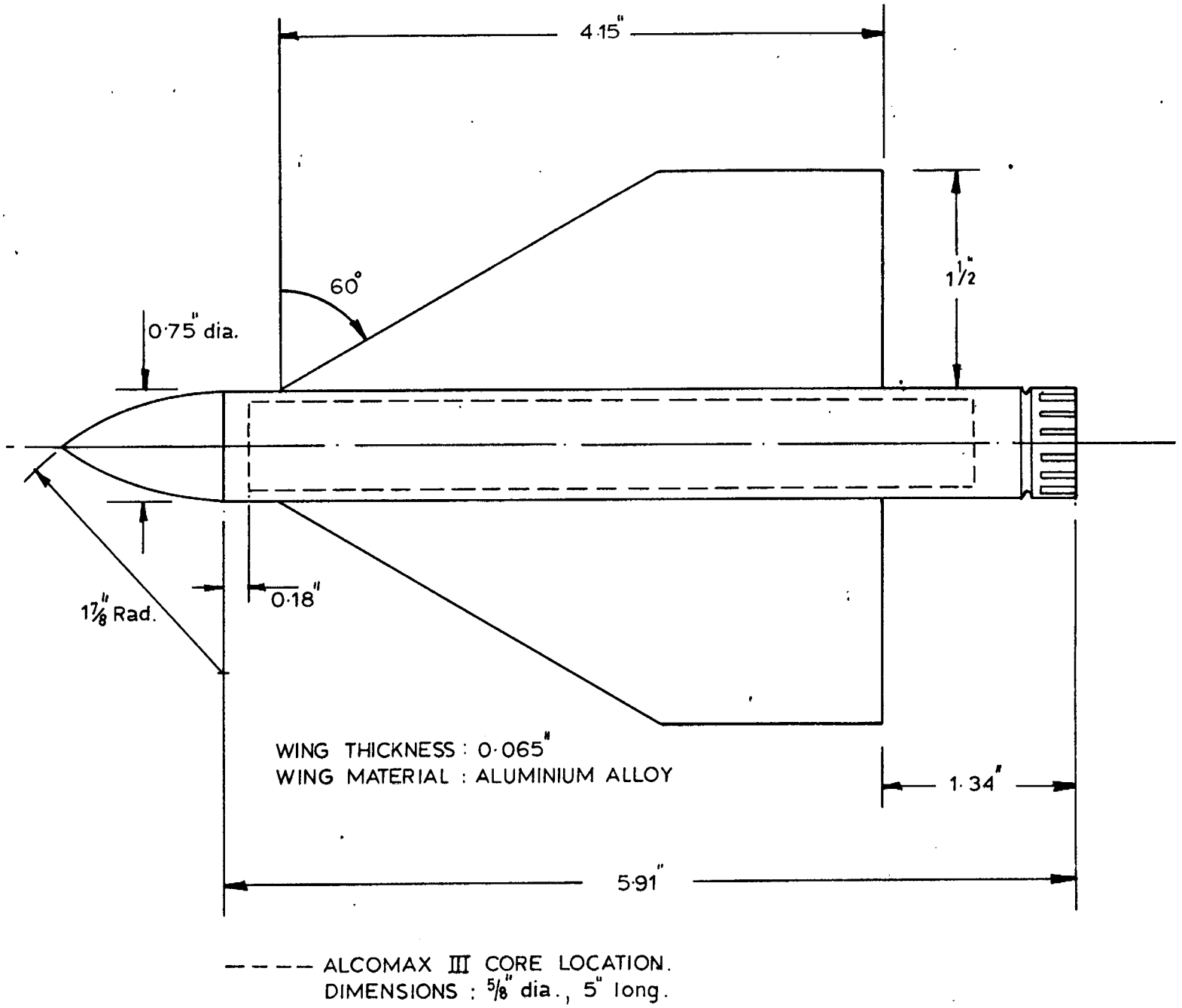

Figure 10.6. The planform of the model used for roll derivative measurements.

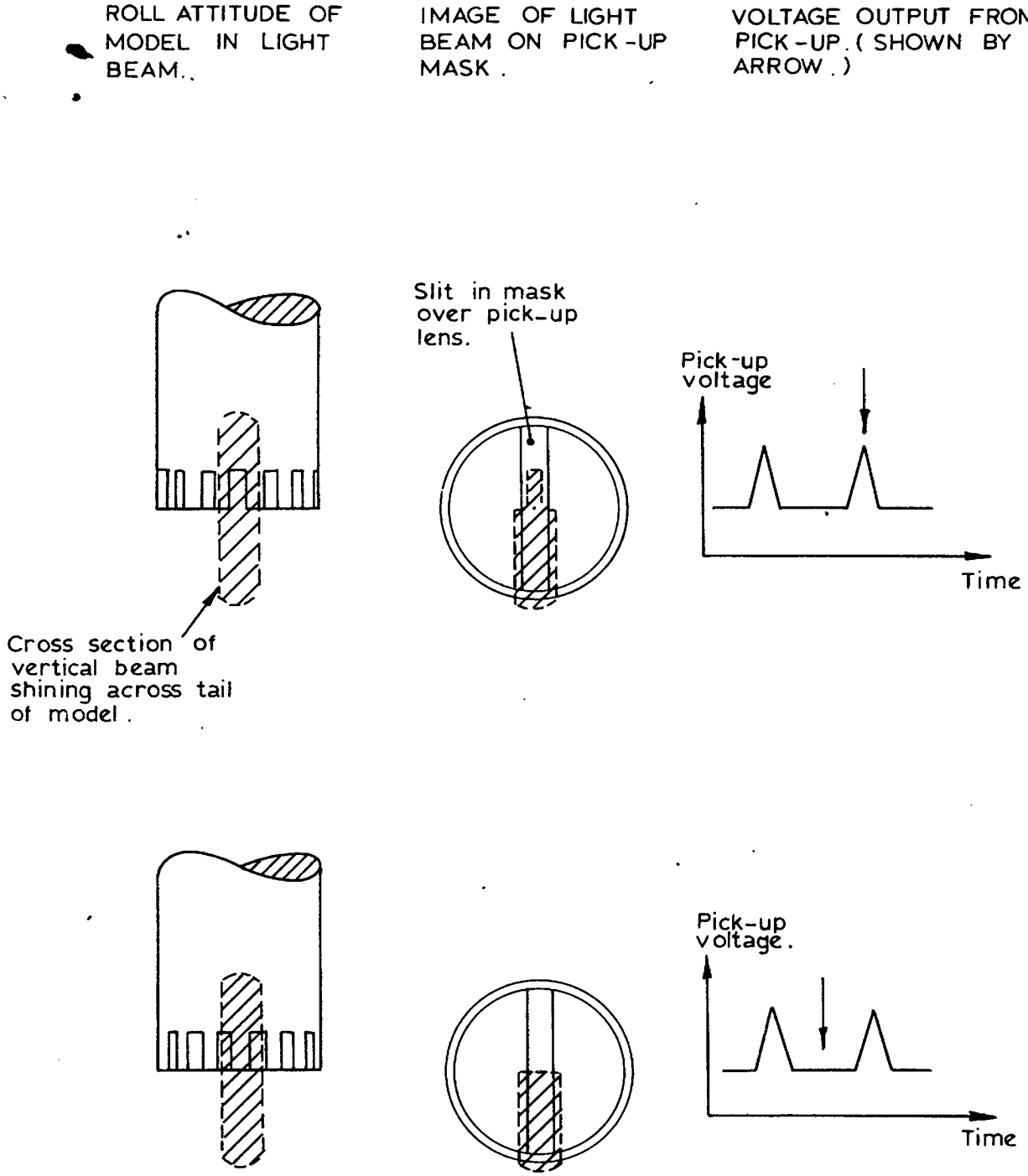

Figure 10.7 A roll attitude indication system.

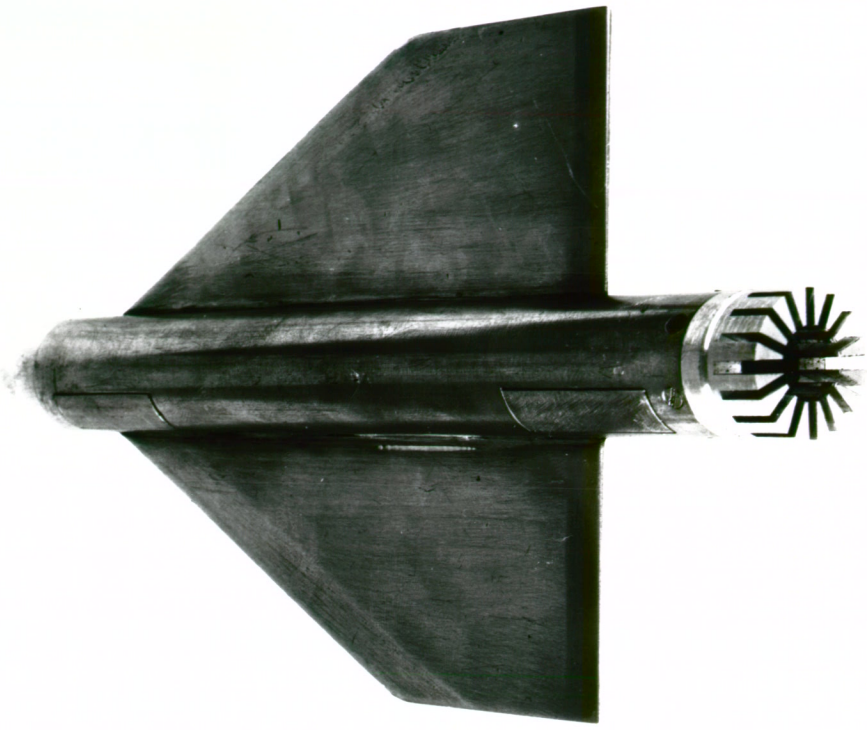

Fig. 10.8 The winged body used for roll damping measurements, showing the tail design which was used in conjunction with the optical system for monitoring rotational speed.

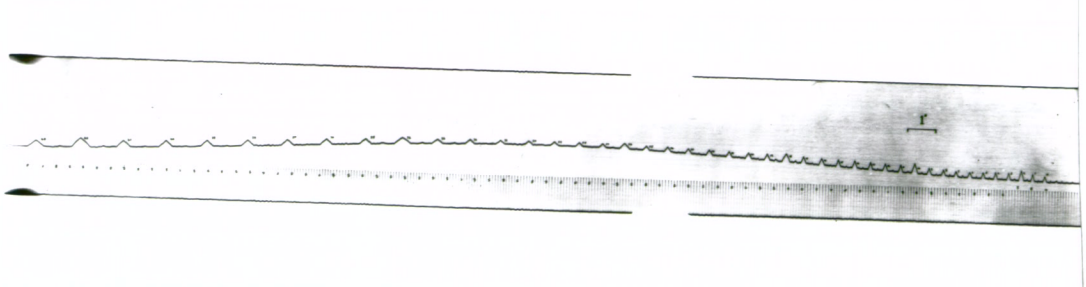

Fig. 10.9 The U.V. recording of the output from the roll monitoring system.

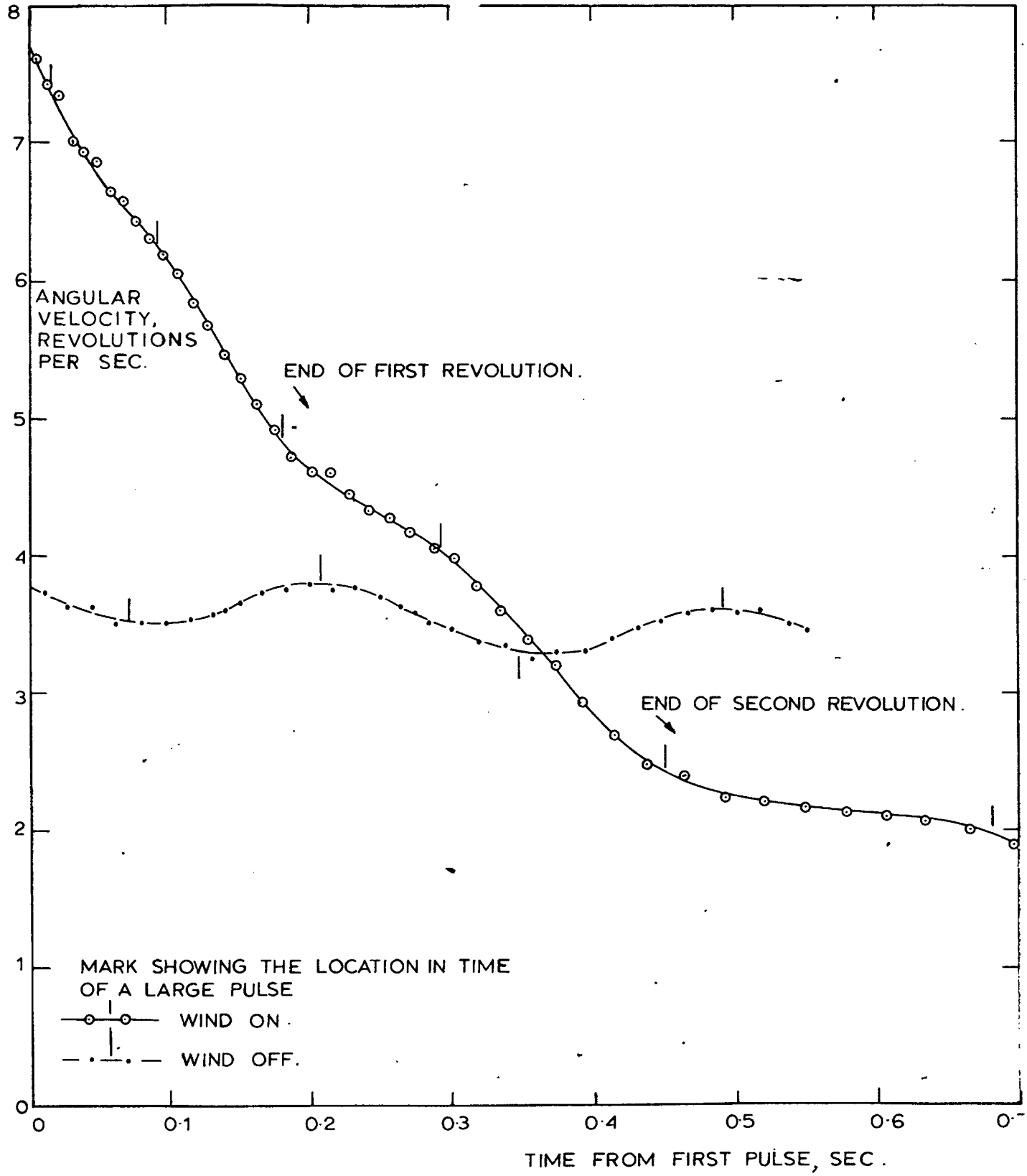

Figure 10.10
The velocity-time curve of the freely rotating model magnetically suspended in the low speed wind tunnel.

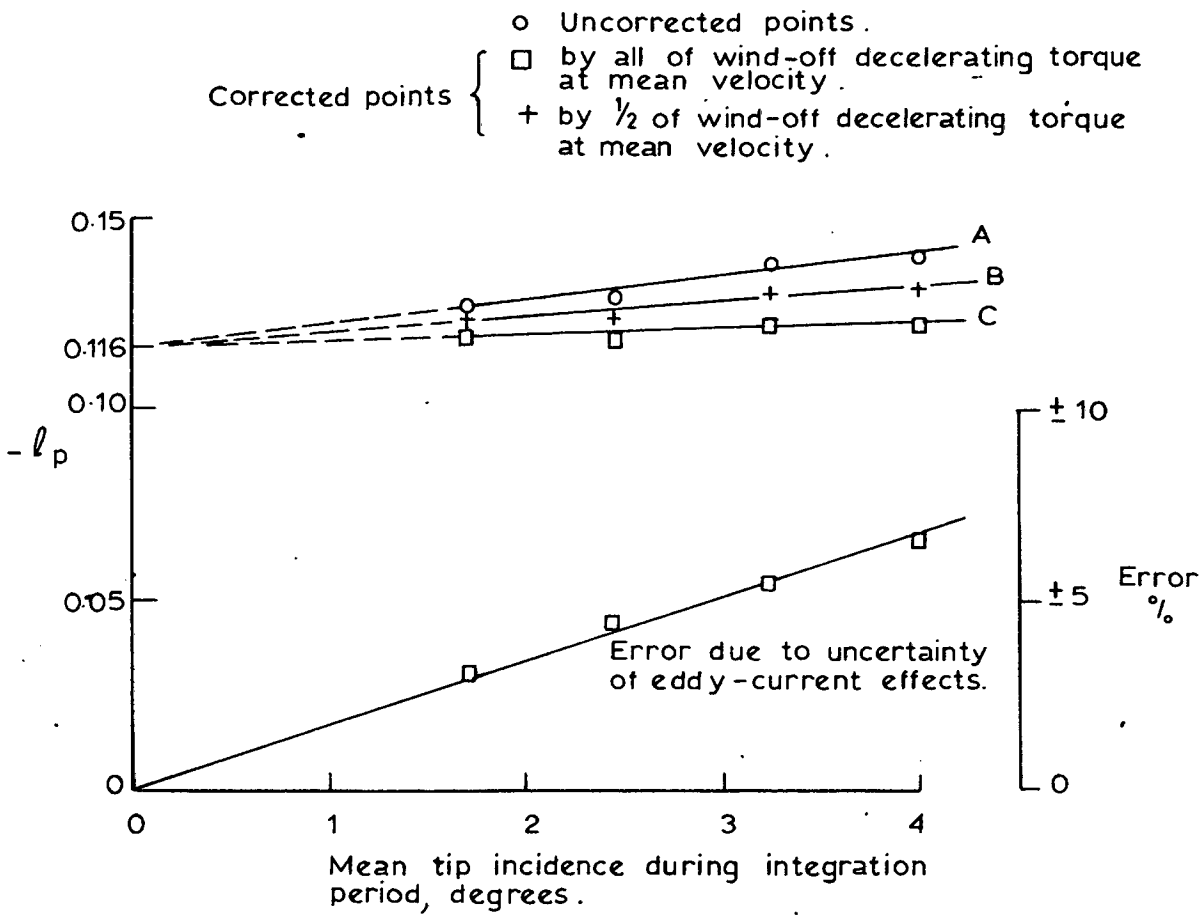

Figure 10.11. The variation of the rolling moment derivative with wing tip incidence.

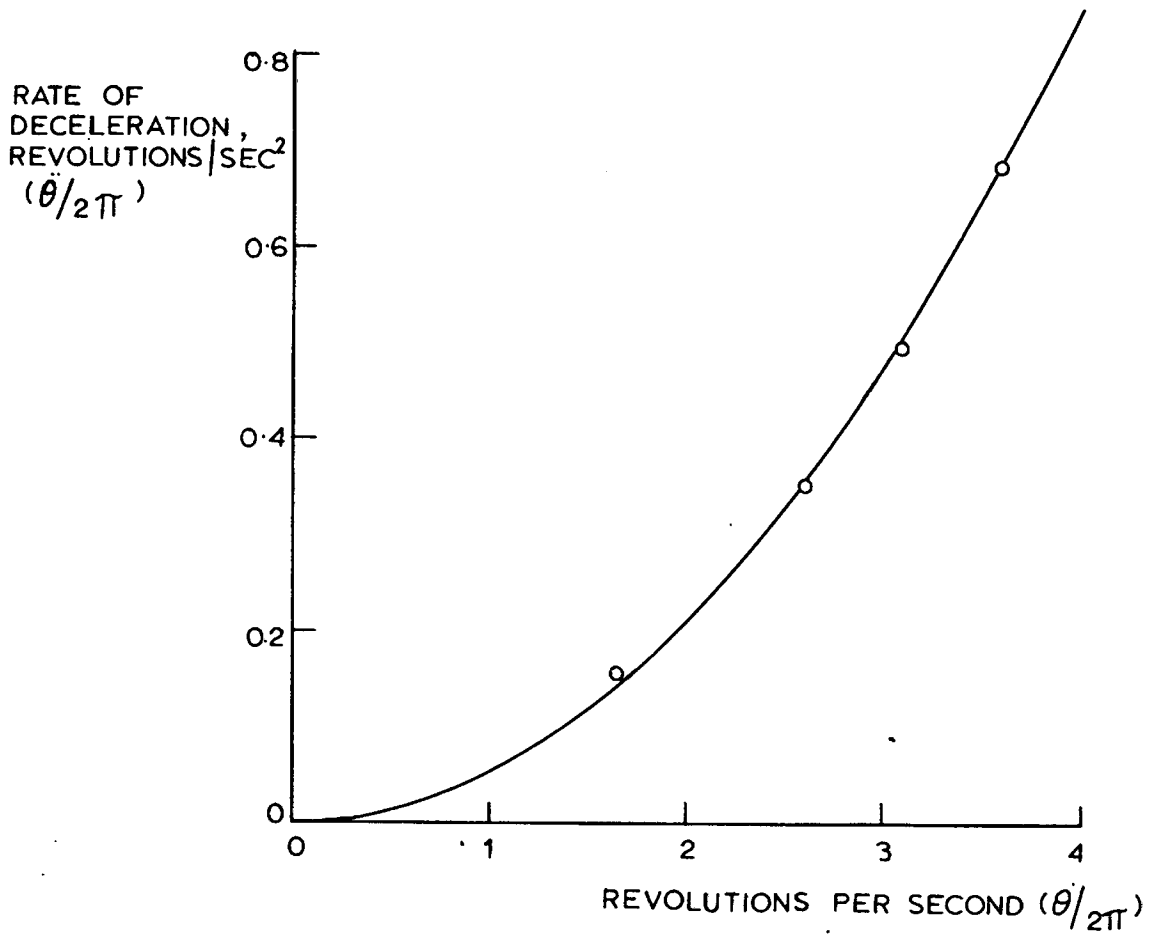

Figure 10.12. Rate of deceleration of the suspended model, wind off.

11. The Working Section for the High Speed Wind Tunnel.

The magnetic suspension system has been designed primarily for use with an existing induced flow return circuit supersonic wind tunnel. The existing working section was unsuitable for magnetic suspension, and a new working section was designed for the part of the circuit between the wooden contraction and the injector.

Contents:

11.1 The Requirements of a Working Section.

Where the wind tunnel working section of a magnetic suspension system is enclosed, as in this case, it is clear that the wall material which is used must not interfere to any large extent with the magnetic fields which are produced by the externally positioned electro-magnets. The working section must also allow the passage of the optical system light beams, and in the case of a high speed tunnel operating at atmospheric total pressure the walls must be strong enough to withstand a pressure differential. With rectangular working sections, deflections of the flat sides under load can dominate the design.

It is important to have a good surface finish on working sections, and highly polished materials are commonly used; however, in this case where the model position is monitored optically,

reflections from a bright polished surface could have proved troublesome. For this reason a relatively dark material, or dark coating, was desirable, but a mirror-like surface finish was avoided.

The working section can be regarded as consisting of three portions: a section upstream of the suspension system where the air is accelerated to the working speed, a section through the magnet region, and a section carrying the air to the injector. The original working section of this tunnel had cross sectional dimensions of 6" wide by 9" deep, but it was decided to reduce the vertical dimension to 8" for the new working section to reduce the current demands for the lift magnets. Otherwise the wind tunnel was as described by Judd[15].

One further design requirement of a working section was that provision must be made for the measurement of airspeed at the position of a suspended model. Blockage effects of the model dictate that speed should be measured by pressure sensors positioned well upstream of the model. The speed indicated by these sensors is related to the speed that would have existed at the position of the model, in the absence of the model, by separate calibration. In this particular wind tunnel the working section speed was indicated by the pressure difference given by two static pressure tappings, one located in an upstream settling chamber where the air pressure was near atmospheric and the air velocity relatively low, and another located further downstream in the tunnel wall where the air had been accelerated to close to the velocity at the model, but still positioned well ahead of the model.

11.2 Eddy-Current Generation in Conducting Walls.

A convenient non-magnetic material would have been Duralumin, but at the time that the working section was planned,

it was anticipated that large magnetic forces would be required from the lateral electro-magnets to induce oscillatory motions of the model, and it was necessary to determine the effects of eddy-current generation in conducting walls resulting from magnetic flux variation.

It was decided to induce eddy-currents by connecting the A.C. mains across windings on one of the lateral electro-magnets (these placed a load consisting of a resistance of 1 ohm and an inductance of about 0.08 Henries across 230 volts r.m.s.) The wave-form from this supply was much cleaner than could be provided by the normal lateral power supplies, and a search coil located on the wind-tunnel centre-line, connected to an oscilloscope, could be used to monitor the field produced by the magnets. Pieces of Dural sheet were positioned close to the pole faces, and the effects on centre-line field of a variety of sheet thickness and design were investigated by comparing the e.m.f. induced in the search coil with the value induced with no wall present.

Some comparative results are tabulated below, for the case where the coils were connected in a manner which would produce a pitching mode in the model. The $\frac{3}{8}$" dia. search coil was positioned with its axis pointing transversely across the tunnel.

Sheet thickness:	zero	0.036"	$\frac{1}{2}$"
Relative current:	1.0	0.99	0.61
Relative field on axis:	1.0	0.95	0.39
Axis field phase lag relative to current:	0	18.3°	52°

The Dural sheets had a depth of $8\frac{1}{2}$" and a length of $15\frac{1}{2}$", and were symmetrically placed relative to the electro-magnet. The

alternating fields induced fairly violent vibrations in the sheets, accompanied by heating. The heating was most pronounced on the thinner sheet; a temperature rise of 25°C was measured on this sheet. Clearly a thick sheet could not be used, because of the reduced field strength, but even the thin sheet, which would have required fairly extensive support in the form of ribs, exhibited a large phase lag. The phase lag was largely eliminated by slitting the sheet to break up the current paths, but a wind tunnel constructed in this way would have been too complicated. It was decided that conducting walls could not be used, and an alternative non-conducting non-magnetic material was sought.

11.3 The Choice of Wall Material, Design and Constructional Details.

A range of materials was considered, and some of the Tufnol brands of laminates appeared best suited, in particular the asbestos or paper base laminates which had a good surface finish. These materials have a relatively low ultimate tensile stress and Youngs Modulus, and consequently the wall would be relatively thick compared with a metal wall. In view of this, it was decided to wind the drag coil straight onto the wind tunnel to minimise the inner diameter of the coil; the wall material would be in direct contact with cooling oil and the windings which could at times be at a temperature above 100°C. All brands of Tufnol are unaffected by oil, but only one brand, Tufnol ASP, could satisfy the temperature requirement. This brand was chosen for the major part of the tunnel, and is an asbestos base laminate, synthetic resin-bonded, having the highest Youngs Modulus of the range. Some properties of the material are listed on the following page:

Maximum service temperature	165°C
Ultimate tensile stress	12,000 p.s.i.
Ultimate compressive stresses	
Edgewise	20,000 "
Flatwise	42,000 "
Shear strength, flatwise	12,000 "
Youngs Modulus in tension, E	2.4×10^6 p.s.i.
Specific gravity	1.7

One of the more important effects of wall deflection under the effect of the pressure differential would be a change in the effective ratio of the cross sectional areas of the throat to the working section. The effect would be for a deflection of the working section walls inwards to reduce the flow Mach number in that region. An estimate of the order of the Mach number changes was made by first estimating the reduction of area, using a simplified analysis, and then calculating the corresponding change of average Mach number.

It was assumed that the four walls of the tunnel were simply supported at their corners, a worst case. In fact bolts holding the sides together probably formed some sort of restraint. The deflection δ_x of a side at a position distance x from a corner is given by

$$\delta_x = \frac{px}{24EI}\left(L^3 - 2Lx^2 + x^3\right)$$

where p = pressure differential

I = second moment of area

L = corner to corner span of side

The reduction of working section cross-sectional area due to the deflection of a side is :

$$\int_0^L \delta_x . dx = \frac{P}{24EI} \int_0^L (L^3 - 2Lx^2 + x^3) dx = PL^5/120EI$$

For a pressure differential of 12 lb./in.^{2}, curves showing the variation with wall thickness of the maximum deflection of a side (at its mid point) and the reduction of working section area, are given on Fig. 11.1 for two values of wall span. The total reduction of working section area from the nominal value of 48 in.^{2} is given by the sum of the area changes due to the deflection of each wall.

The effect of the area change on mean Mach number has been calculated using the non-dimensional isentropic flow equation relating working section area A to sonic point area A_* and working section Mach number M:

$$\frac{A_*}{A} = M\left[\frac{\frac{\gamma+1}{2}}{1+\frac{\gamma-1}{2}M^2}\right]^{\frac{\gamma+1}{2(\gamma-1)}}$$ which for $\gamma = 1.4$ reduces to:

$$\frac{A_*}{A} = \frac{1.728\,M}{(1+0.2\,M^2)^3}$$

The variation of working section Mach number with area ratio is infinite at M = 1, reducing in value with increasing Mach number. At a representative value of M = 1.6, $\frac{A_*}{A} = 0.799$, and $\frac{dM}{dA_*/A} = -2.63$. If area A is assumed to be reduced by a value ΔA which is the total area reduction due to the deflection of four walls, then $d\frac{A_*}{A} \doteq \frac{A_* . \Delta A}{A^2}$ for small area changes, and it is assumed that the throat of the tunnel nozzle can be designed to deflect an insignificant amount because it is well clear of the region of the electro-magnets. For the particular Mach number of 1.6, and an area reduction $\Delta A = 0.01\,A$ (a 1% reduction of area) $dM = -0.021$.

This is a Mach number reduction of about 1⅓% of the nominal value of 1.6 which has been assumed.

The 6" wide top and bottom walls of the tunnel could have thicknesses of ¾"; from Fig. 11.1, the change of area would total about 0.02 in.^{2}, corresponding with a Mach number change of about 0.05%, an insignificant error. However, the 8" span of the tunnel sides produces a much larger change of area for a given wall thickness, by a factor of about 4.2.

It has already been mentioned that the tunnel was designed before the tuned model had been devised, and in order to produce the maximum possible lateral force or moment it was necessary to position the lateral electro-magnets close to the model. To achieve this, while at the same time minimising wall deflection, it was decided to make the side walls of 1" thick Tufnol ASP sheet, but to let the lateral magnets into machined recesses in the wall, leaving as much material on the walls as possible. The minimum wall thickness was ½", at the recesses and at the drag coil. The recesses were reinforced by leaving ribs where possible, and the drag coil region was reinforced by relatively heavy gauge formers. If we assume that the ribs have no effect, then the area reduction per side would be 0.13 in.^{2}, giving a total reduction of about 0.55% and a Mach number error of about ¾%. This is a worst possible case. Factors tending to reduce the error are

(i) at the recesses the thinnest region of the wall accounts for a maximum of 60% of the span,

(ii) the wall was machined from a slab of material 1" thick, giving an adequately stiff structure in regions which were not machined away,

(iii) some ribs varying in thickness from $\frac{3}{4}$" to 1" were left in the regions of the recesses, and metal ribs were bolted to the walls at the drag coil.

it was found that deflections, rather than stress limits, dictated the thickness of the wind tunnel walls.

A drawing of a side wall is given on Fig. 11.2. The top of the working section was $\frac{3}{4}$" thick Tufnol ASP downstream of the drag coil, $\frac{1}{2}$" thick Tufnol at the drag coil, and a profiled Dural liner upstream. The bottom of the tunnel was designed for $\frac{3}{4}$" thick glass downstream of the drag coil, although 1" thick Perspex has been used initially. At the drag coil, and upstream, the bottom of the tunnel was the same design as the top. The parts of the tunnel were bolted together using relatively coarse Whitworth thread brass bolts of $\frac{1}{4}$" diameter, screwing into the grain of the Tufnol. The only precaution that had to be taken was to clamp the material while tapping.

The side-walls of the tunnel were continuous from just downstream of the horse-shoe electro-magnets through the drag coil to about 23" upstream. The upstream section held Dural liners (of sub-sonic form initially) bolted in position with $\frac{3}{8}$" dia. brass bolts. Four small optical system light ports were bored through the top corners of the side-walls near the lateral coils, and $\frac{1}{4}$" thick glass windows were bonded to the walls on the inside edge to seal the ports.

The drag coil former was made from $\frac{1}{8}$" thick brass sheet on the downstream sides and $\frac{1}{4}$" thick Dural angle on the upstream sides, and these were bolted to the tunnel. The relatively heavy drag coil and the working section were supported through these Dural formers on Dural channel sections standing on a welded steel base. The only

other support for the working section was just downstream of the electro-magnets. The injector was designed for a 9" deep working section, and as this one was 8" deep, an 8" long detachable transition piece was made from Tufnol ASP tapering in depth from the working section to the injector, and containing a $4\frac{1}{2}$" square access door in one side. The complete suspension system with working section, including the transition piece, was isolated from vibrations of the remainder of the wind tunnel by $\frac{1}{8}$" gaps, sealed with tape. Adjusters were built into the system supports to allow alignment with the tunnel, and the system could be wheeled away from the tunnel circuit for the purposes of force and moment calibrations, etc.

Allowance for change of boundary layer displacement thickness was made by tapering the top and bottom walls of the tunnel by 0.008 inches per inch. The section was 8" deep at the drag coil, rising to 8.346" at the transition piece. The normal tolerance on machining, where it affected the working section size, was $\pm$ 0.002". The inside surface of the tunnel was the "as delivered" condition of the Tufnol. The material had a polish, but was dark olive green in colour and reflected very little light.

A photograph of the suspension system and high speed wind tunnel is given on Fig. 11.3. The airflow is from right to left. Just visible on the right is a 3 ft. square wooden contraction in which the air accelerates from a low velocity to the profiled liners which are clamped between the tunnel sidewalls. The main magnet and working-section support frames are light-coloured in the centre of the photograph; the bolts holding the liners can be seen on the dark section between these supports and the wooden contraction. Extending

off the left of the photograph is a wooden diffuser just downstream of the cast-iron injector and compressed air pipework. A mirror for viewing the model is between the working section and the steel base, and also shown are flexible steel tubes containing the power supply leads to the coils.

The nearest magnetic material to the model, apart from iron in the coils, is in the air injector, the base under the working section, a support for the wooden contraction, and an overhead crane (out of the picture). None of this iron is closer than 20" to the model.

11.4 Speed Calibration.

Speed measurement in this tunnel was by means of a calibration of the pressure difference between tappings upstream of the contraction and in the liner, against working section velocity head, the velocity head being measured with an otherwise empty working section by a pitot tube and a wall static pressure tapping in the Perspex window in the tunnel underside.

A calibration of the Mach number given by the pitot tube and its wall static tapping, (which was located 1¼" upstream of the pitot tube opening) against the Mach number indicated by the pressures at the static tappings in the throat of the liners and in the upstream settling chamber, is given on Fig. 11.4. For this calibration the pitot tube was positioned on the tunnel centre-line, mid-way between the legs of the horse-shoe electro-magnets. Check calibrations taken 1" above and below this position gave the same results. The Mach number at the centre of the working section was 0.99 of the Mach number indicated by the upstream tappings (referred to as the "liner" Mach number), this has been verified up to conditions where the tunnel was choked by the pitot tube, about Mach 0.87.

LIST OF SYMBOLS USED IN CHAPTER 11.

Symbol	Meaning
A	Working section cross sectional area.
A_*	Sonic point (or throat) area.
ΔA	Reduction of A due to wall deflection.
E	Youngs Modulus.
I	Second moment of area.
L	Corner to corner length of a side.
M	Working section Mach number.
p	Pressure differential.
x	Distance measured from a corner of the wind tunnel along a wall in a direction at right angles to the axis.
γ	Ratio of specific heats.
δ_x	Deflection of a wall at position x .

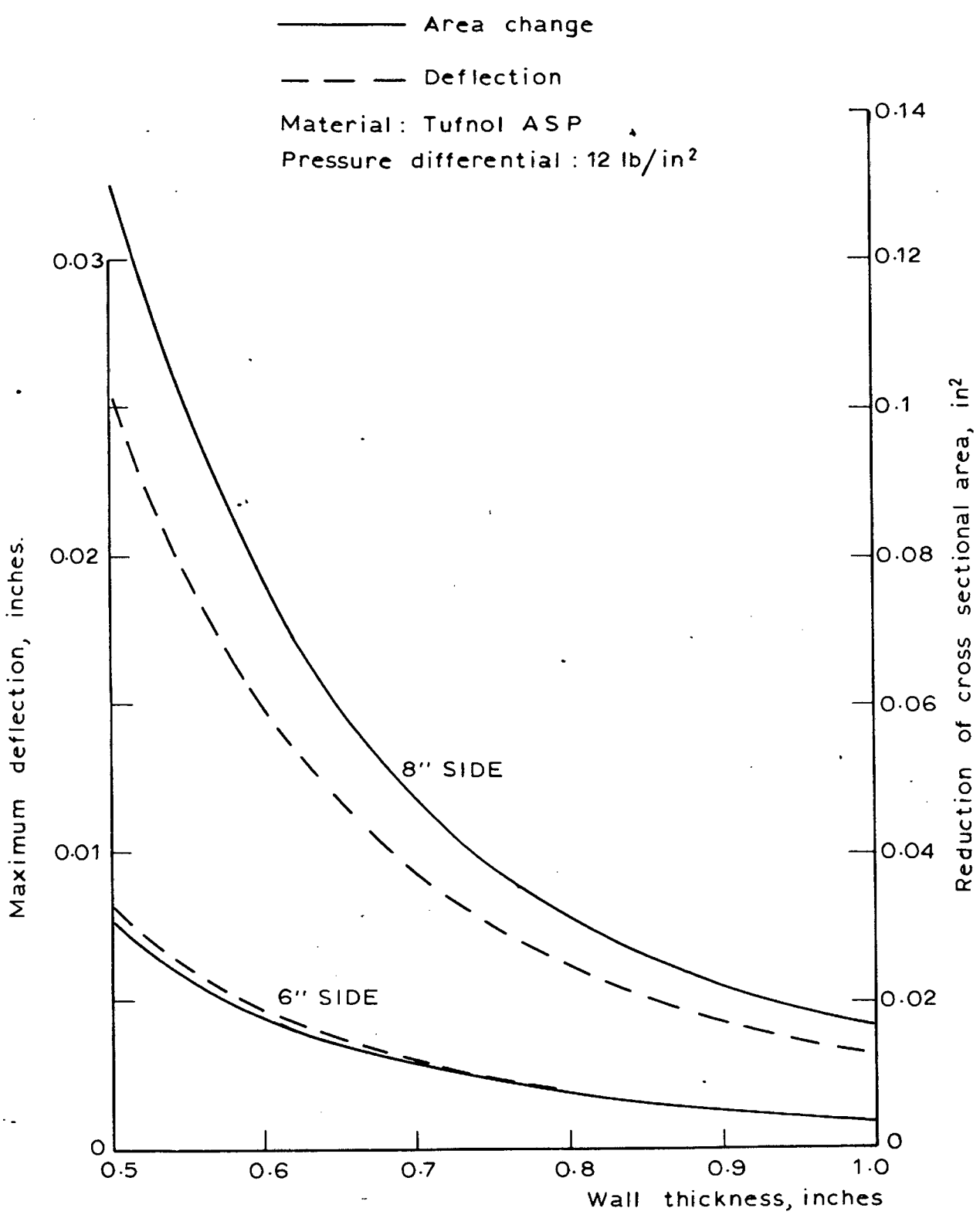

Fig. 11.1. The deflection, and resulting change for section area, for a simply supported wind tunnel wall.

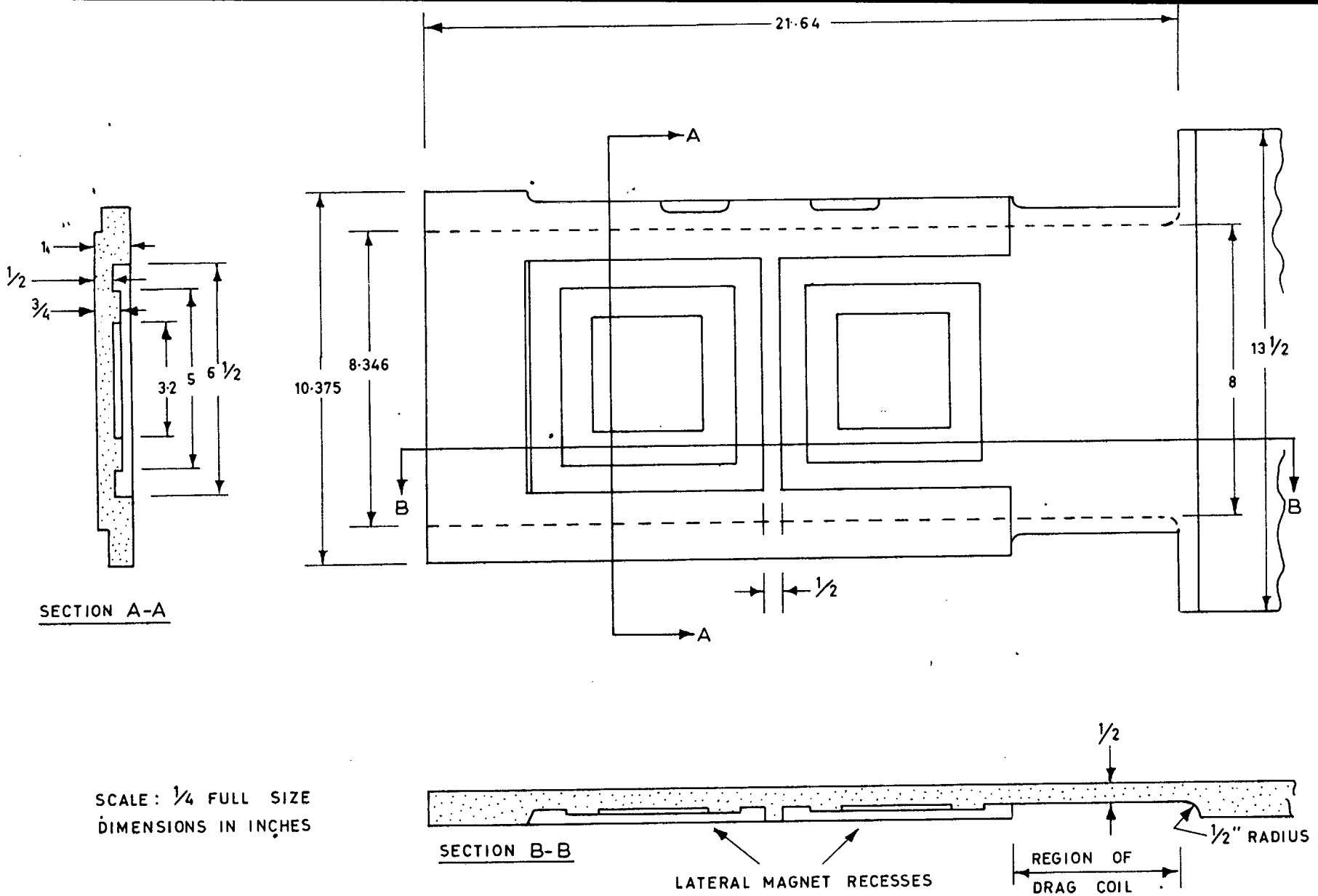

Fig. 11.2. A part side view and sections of the high speed wind tunnel showing regions where the wall has been recessed to accept the lateral magnets, and thinned for the drag coil.

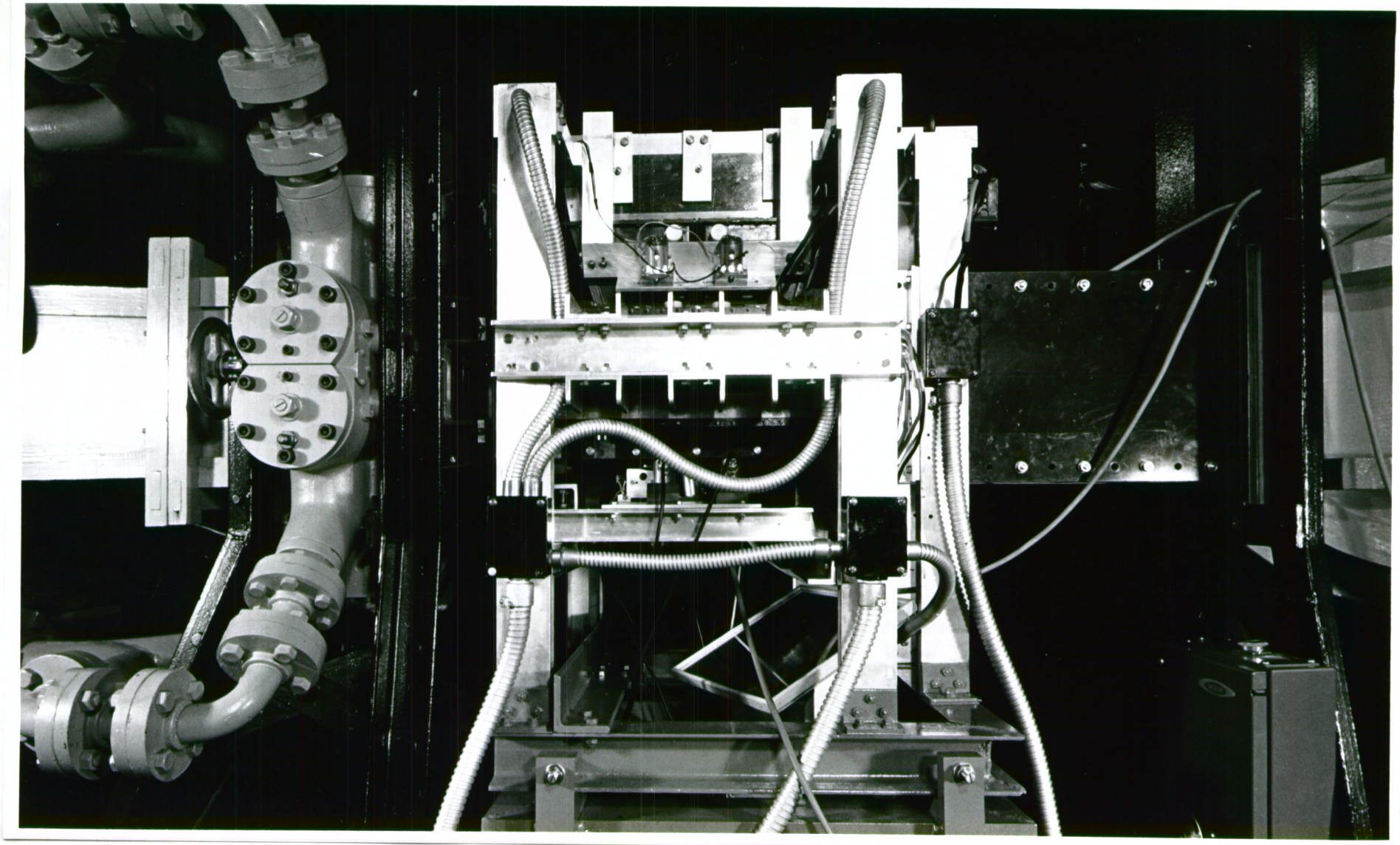

Fig. 11.3. A side view of the high speed wind tunnel and the Magnetic Suspension System.

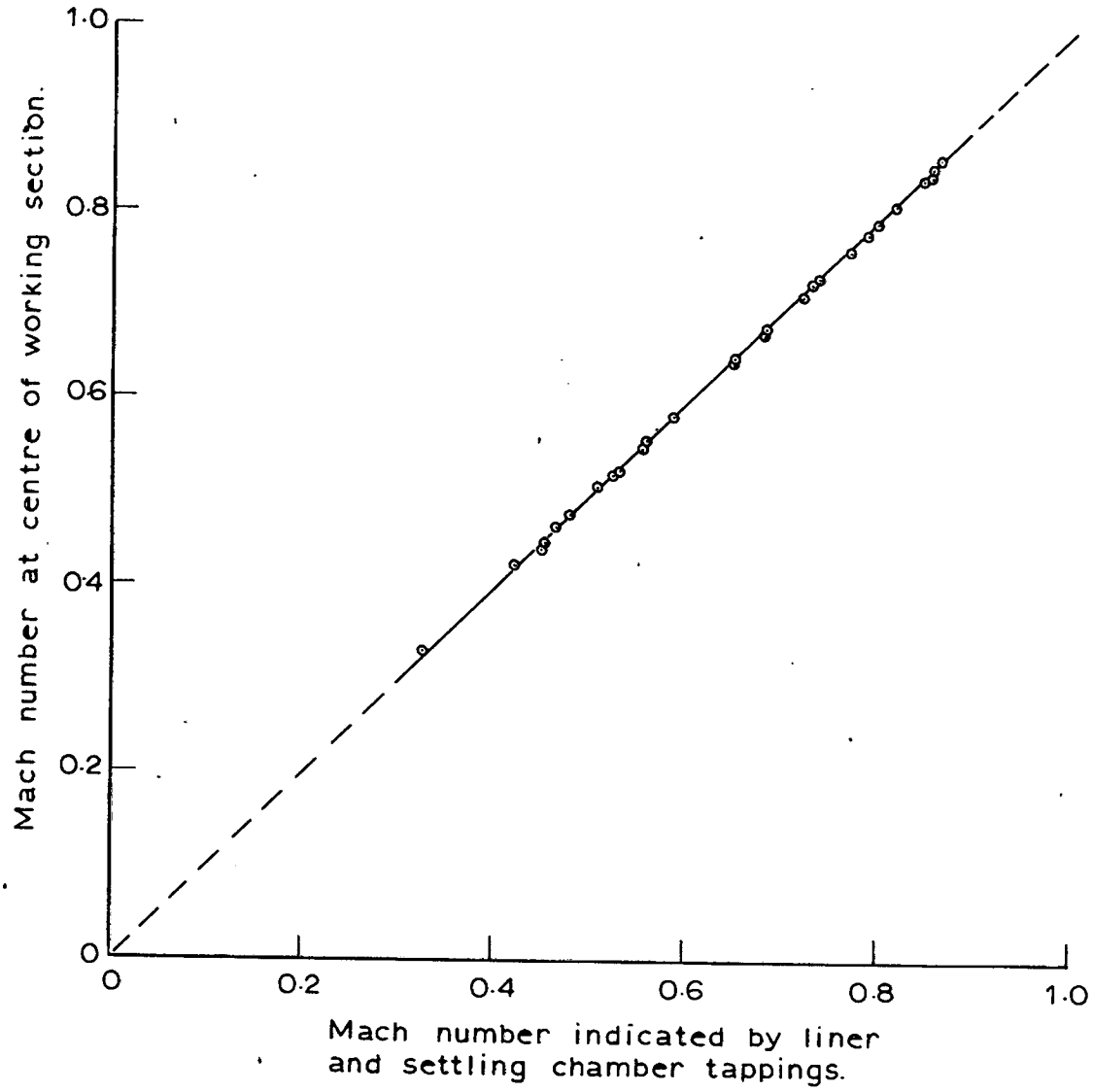

Fig. 11.4. A calibration of the tunnel wall tappings indicating working section Mach number.

12. Drag Measurements in the High Speed Tunnel.

As a step towards the development of a magnetic suspension system suitable for use with supersonic flow, a solid model was suspended at air speeds up to the limit set by the convergent liners and tunnel choking by the model, and the opportunity was taken to measure the drag of the model. In addition to this, the drag of a tuned model was measured, with and without wings, to provide some design data for future models of this type.

Contents:

12.1 Static Pressure Distributions Along the Working Section.

During the initial set of drag measurements with a solid body of revolution, a pressure tapping in the bottom of the tunnel alongside the model indicated that the flow in this region could be just supersonic while the Mach number indicated by the liner tapping (well ahead of the model) indicated a mean Mach number below 1. It was also noticed that the depression at the tapping alongside the model dropped suddenly from a value corresponding with subsonic flow to a value corresponding with supersonic flow as the injector pressure was taken above some critical value. It was decided to measure the static pressure distribution along the working section with the tunnel free from any blockage whatsoever, partly as a check on the allowance that had been made for boundary layer growth along

the tunnel, but also to find out if supersonic flow could be produced in the absence of what was effectively a "plug" in the centre of the tunnel formed by the model.

A line of static tappings was positioned along the tunnel centre-line in the Perspex window forming the underside of the working section alongside the model position. The tappings, totalling six in all, extended a distance of 6¼" upstream of the centre of the tunnel and 5¼" downstream. Pressure distributions, measured with mercury manometers, are plotted on Fig. 12.1, for several values of injector pressure. With subsonic flow in the tunnel the static pressure in this region was fairly constant, but increasing injector pressure first induced supersonic flow in the upstream region of the test section, and then supersonic flow right through. When only part of the working section contained super-sonic flow, the supersonic region was terminated by a fairly sharp rise of pressure (the wide spacing of the pressure tappings could not show how sharp the rise actually was) which was probably associated with a weak shock-wave. A pressure distribution in this transitional stage is shown on Fig. 12.1 at an injector gauge pressure of 39 lb./in.^{2}. At a higher injector pressure, the static pressure depression in this region become uniform within the limits 16.1 to 16.4" Hg., indicating a mean Mach number of about 1.105. According to one-dimensional isentropic flow theory this would require a flow area increase of about 1% from the sonic point: the allowance for boundary layer displacement thickness is at the rate of 0.1% change of section area per inch measured in the streamwise direction. This taper, with the subsonic liners, began at a point 16¾ inches upstream of the "tunnel centre"

marked on Fig. 12.1 (the tunnel centre corresponds with the centre of the horse-shoe magnets). An explanation of the production of supersonic flow with "subsonic" liners might be that the boundary layer displacement thickness remained constant for some distance downstream of the throat, in the presence of accelerating flow in the same region.

The static pressure distribution has been measured with a body of revolution suspended in the working section. The model was that shown on Fig. 10.3, and the pressure distributions were taken over a range of injector pressures. The model choked the tunnel at a Mach number M_L indicated by the liner tapping of 0.885, which required a minimum injector pressure of 39 lb./in.^{2}. As the injector pressure was further increased, the manometers indicated reducing pressure along the wall region alongside the forward part of the model, followed by a sharp rise of pressure over the aft part. The pressure step moved aft with increasing injector pressure until it passed the tail, when control over the model was lost and it was swept down the tunnel. Local wall values of Mach number can be calculated from the static pressures by assuming that the settling chamber pressure was the stream total pressure. Mach number distributions calculated in this way are shown on Fig. 12.2, together with the position of the model relative to the static pressure tappings. It can be seen that there could be a local region of supersonic flow; it is possible that when this region extended over the tail the reduced base pressure resulted in a sharp rise of drag which the drag coil was not able to withstand. The order of magnitude of the base pressure change might be inferred from the change of wall static

pressure across the shock. This was about 1½" Hg., and if applied over the base area would result in a drag rise of 0.27 lb. requiring a drag coil current increase of about 27 amps. This would be additional to the current of about 70 amps. which was required to hold the model while the distribution given by the upper curve on Fig. 12.2 was being measured. The large current demand, coupled with a step change, was probably beyond the capability of the drag stabilisation system.

The working section blockage of this model, amounting to 0.77% of the tunnel area, assuming one-dimensional flow and neglecting the model boundary layer displacement thickness, would theoretically allow a maximum Mach number ahead of the model of 0.906. The Mach number indicated by the liner tapping was about 0.88.

12.2 Drag Measurements with the Solid Model.

The relatively high drag forces to which this model was subjected would have resulted in a large shift of model axial position from still air to wind-on conditions, requiring manual correction for each change of airspeed and consequently slow operation of the system with an unacceptably large consumption of the stored compressed air supply for the tunnel. For this reason the drag position-error integrator was used to automatically return the model to its correct position following a change of airspeed. In order to retain some control over the axial position of the model under still air conditions, the model was drawn forward against the lift magnet stiffness using about 1½ amps in the drag coil. Drag force was calibrated against current with the model in this position, and the drag calibration is given on Fig. 5.4, the slope of the

curve giving a calibration constant of 93.7 amps./lb.

The variation of drag coil current with flow Mach number indicated by the liner pressure tapping is given on Fig. 12.3, and the variation of working section q ($q = \frac{1}{2}\rho v^2$) with Mach number is given on Fig. 12.4 for a constant total pressure of one atmosphere. The shape of the drag coil current - Mach number curve has the same form as the q-curve at Mach numbers up to about 0.8. The vertical part of the curve corresponds with tunnel choking.

In the Mach number range 0.3 to 0.8 the drag coefficient of this model in the clean condition was 0.26 $\pm$ 0.005 based on model cross sectional area, which compares with a value of about 0.21 measured in the low speed wind tunnel with the model in the same condition. The Reynolds number (based on model length) at Mach 0.8 was about 2.8×10^6, whereas the low speed measurements extended up to a Reynolds number of about 0.45×10^6. The increased Reynolds number at Mach 0.8 may have produced a region of turbulent boundary layer on the model, which would account for the difference between drag coefficients. Drag measurements in the high speed wind tunnel with a 0.013" diameter transition wire around the model near the nose gave a drag coefficient of 0.32 $\pm$ 0.01 in the Mach number range 0.45 to 0.75. This compares with a drag coefficient of about 0.38 measured with the model carrying a transition wire in the low speed wind tunnel. With a fixed area of turbulent boundary layer a reduction of drag coefficient would be expected to accompany an increase of Reynolds number.

12.3 Drag Measurements with the Tuned Model.

The tuned model consisted of a circular sectioned fuselage

carrying a pair of delta wings and a fin. A dimensioned outline drawing is given on Fig. 13.5. The drag of the model was measured with and without wings, but no attempt was made to fix the boundary layer transition point. No measurements were made with the model in the low speed wind tunnel.

The low stiffness of suspension of this model did not allow measurements at Mach numbers above about 0.35. The drag was measured at air speeds up to this limit to provide design data for future models of this type. The variation of drag coil current with Mach number is given on Fig. 12.3 for the two conditions of the model (in both cases the fin was carried). The drag coefficients at a Mach number of 0.35, based on fuselage cross sectional area were,

model with wings 0.27

model without wings 0.19

The drag force was obtained from the force-current calibration given on Fig. 5.3.

The drag coefficient of this model without wings is appreciably lower than that obtained with the body of revolution discussed in the previous section; this was probably because of a relatively lower base drag resulting from the boat-tail on the tuned model.

The experience on drag measurements that has been gained, particularly with the solid model, suggests that drag forces in the range $\frac{1}{2}$ - $\frac{3}{4}$ lb. can be measured to an accuracy of about $\pm$ 2%, but no particular effort was made to obtain the best possible accuracy with the equipment. With an improved technique, particularly in the calibration of force against drag coil current, the accuracy of drag measurements could probably be improved.

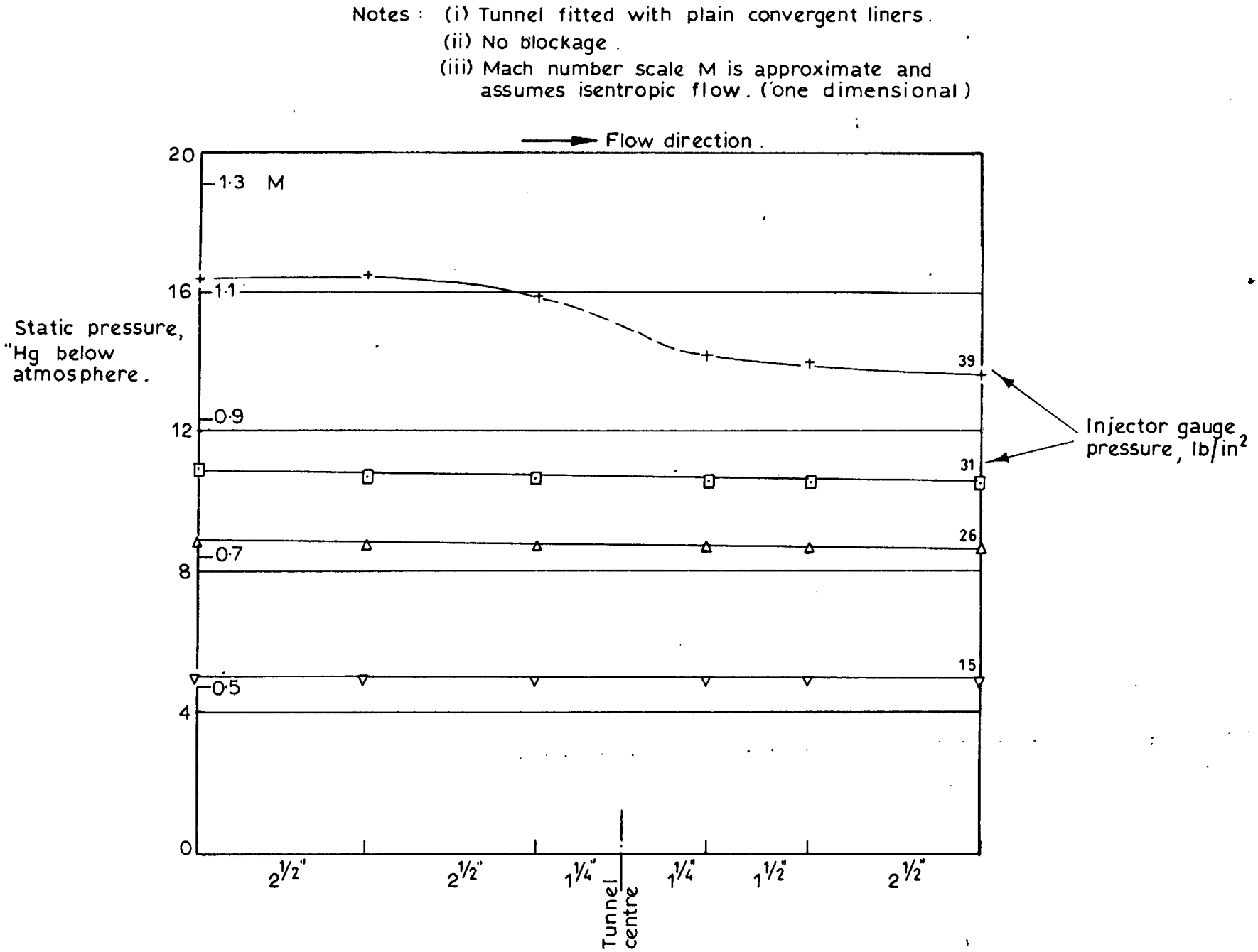

Fig.12.1. The static pressure distribution along the wind tunnel working section underside centre-line.

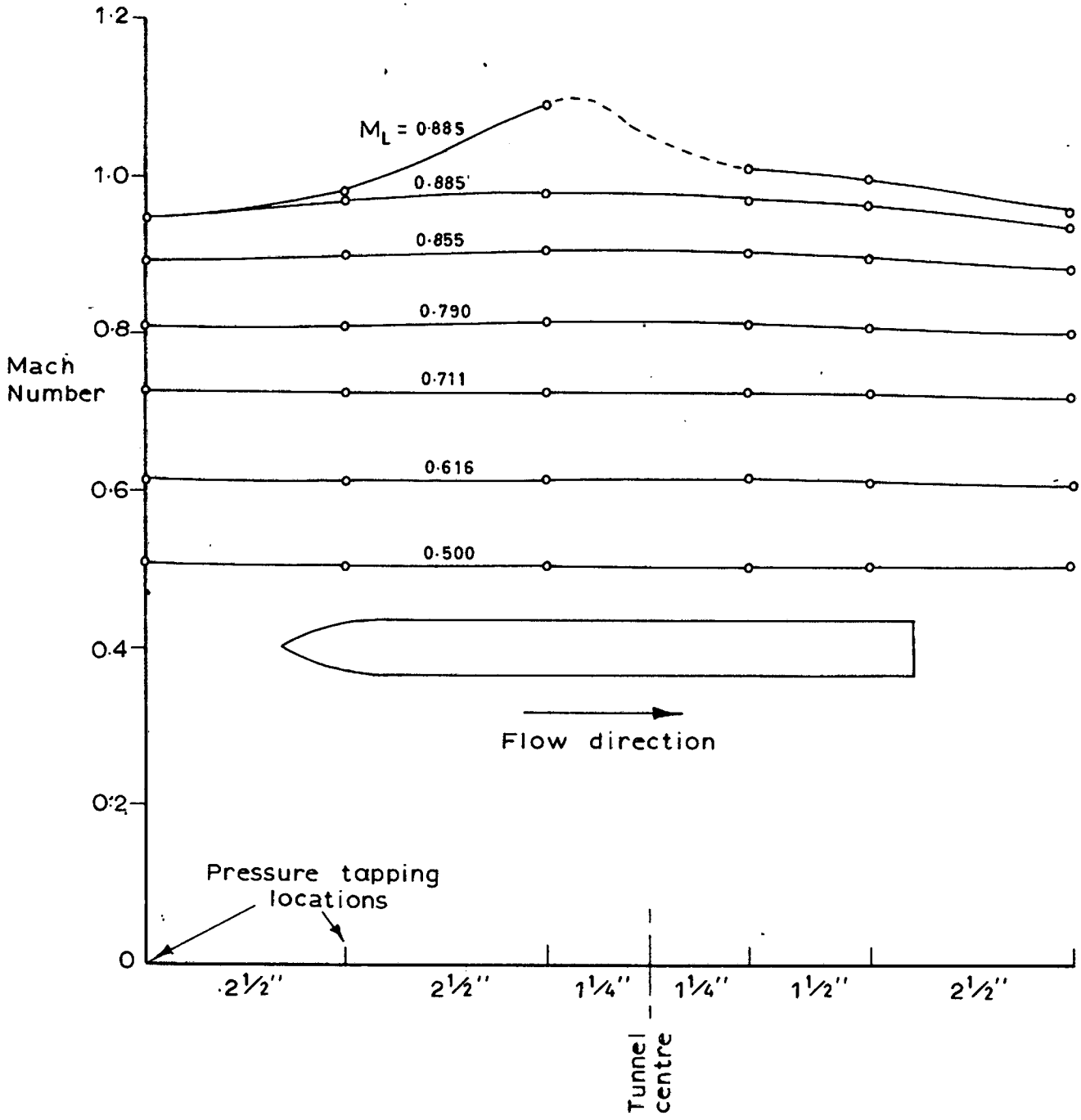

Fig. 12.2 Mach number distributions along the tunnel wall with a body of revolution suspended at zero incidence on the tunnel centre line.

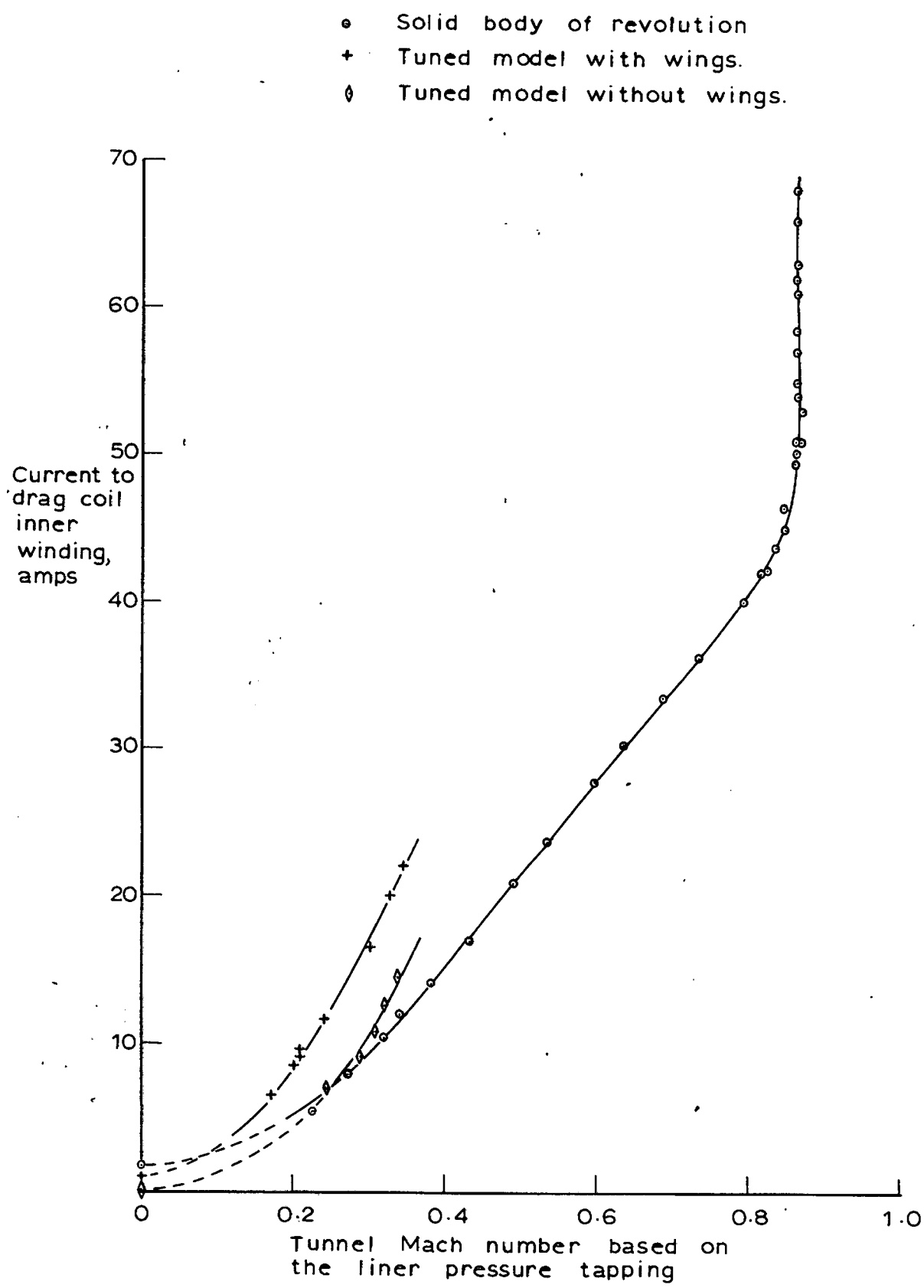

Fig. 12.3. The variation of drag coil current requirements with flow Mach number, for two models.

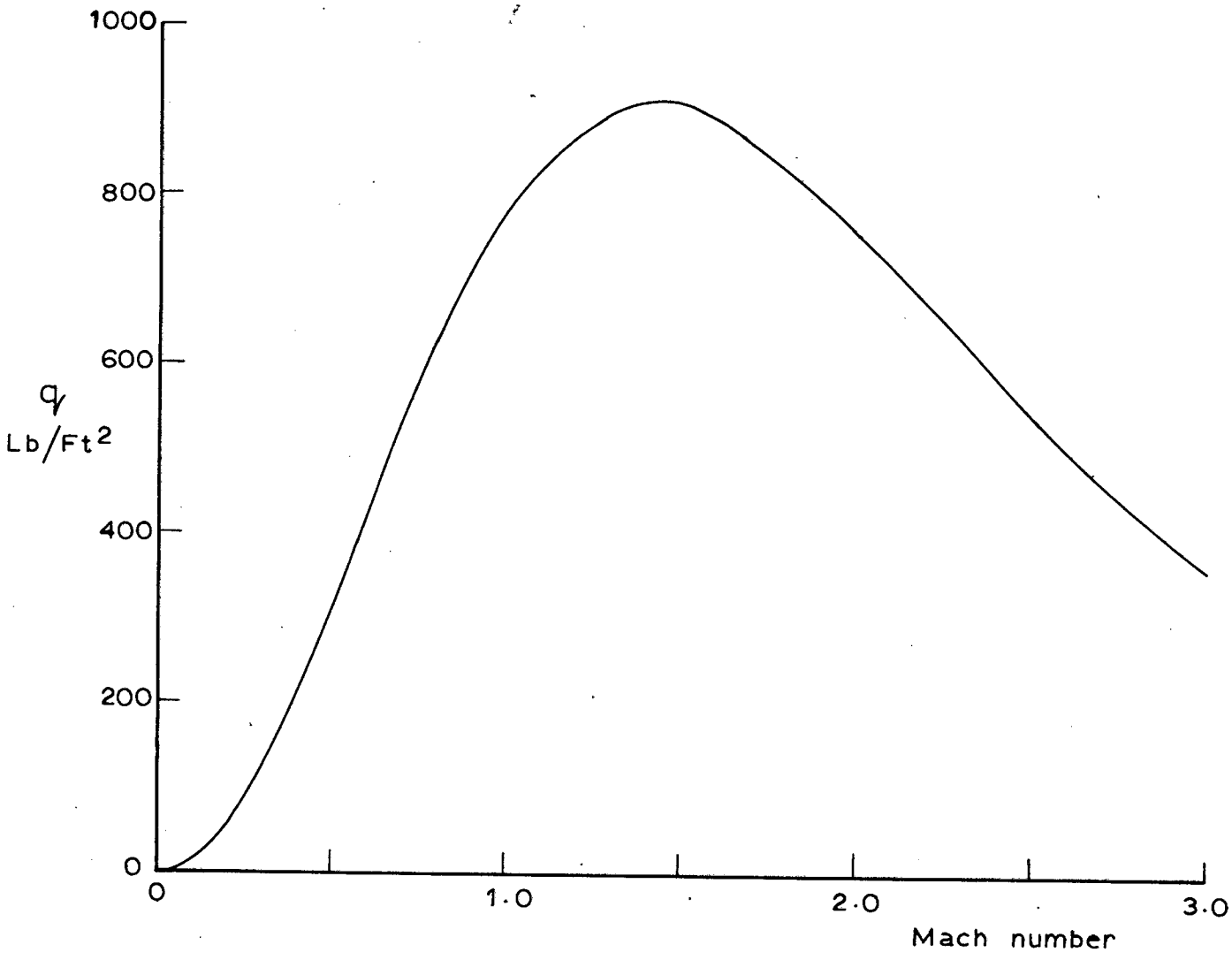

Fig. 12.4. The variation of q with Mach number, for an atmospheric stagnation pressure wind tunnel.

13. The Tuned Model.

In this chapter the advantages to be gained by using a tuned model for dynamic measurements are discussed, and the design and development of a particular model is described. The model design is intended to allow the measurement of pitching derivatives, as well as steady forces and moments. Methods for obtaining this aerodynamic data are given, together with an assessment of accuracy.

Contents:

13.1 Introduction.

The tuned-model concept arose as a possible solution to two problems associated with magnetic suspension systems when applied to dynamic measurements. Firstly, there was a clearly defined frequency/amplitude boundary associated with solid models which in general restricted the available amplitude of oscillation

of a model at any particular frequency. It has been described in Chapter 7 how a model suspended under the action of a field stiffness can produce a resonant system. The model can be excited in its resonant mode with amplitudes limited only by damping, or some other physical limitation which is not fundamental to magnetic suspension. The frequency/amplitude boundary is limiting except in the particular case of oscillations at this resonant frequency. However, this frequency is rather low. In the case of pitching motions of a model, the frequency would be in the range 2-7 cycles per second depending on the field stiffness generated by the drag coil. For the size of model involved, frequencies of this order are regarded as being too low for a supersonic wind tunnel. Higher frequencies of oscillation can be obtained by forcing the model above its resonant frequency, but there is a heavy penalty involved because of reduced response of the model to applied force or moment. The excitation force originates from the suspension magnet system, which is driven by power amplifiers which have a limitation to the possible output e.m.f. Increasing frequency of oscillation increases the reactive load of the electromagnets, so reducing the amplitude of current oscillations and hence excitation force and amplitude of motion of the model. This falling response of the model with increasing frequency was one fundamental limitation of the suspension system.

As an example of the severity of this limitation, the available amplitude of motion of a particular model oscillating in an undamped pitching mode over a range of frequencies has been calculated for this suspension system. The model was assumed to be excited by the lateral magnets to the limits of the power amplifiers.

Points on the frequency/amplitude boundary are tabulated below:

Frequency, cycles per second:	10	17	24
Pitch amplitude, degrees:	10.7	2.52	1.02

These amplitudes are the maximum that could be produced, and would involve the power amplifiers working to the limits of e.m.f. during a cycle, from zero to the maximum. There are two reasons for not operating at this condition. Firstly, some voltage would be kept in hand for control purposes, to cater for disturbances to the model, and secondly the amplifier output voltage wave-form would become distorted by operating to the extremes of amplitude due to non-linearities in the amplifiers.

There is one further problem involved with dynamic measurements using solid models oscillating above resonance, and that is the problem of detecting aerodynamic forces. A magnetic force applied to a model can be composed of three components: a force to balance the inertia force of the model, a force to balance aerodynamic stiffness, and a force to overcome aerodynamic damping. The first two components are in antiphase or inphase with the oscillatory motion of the model, and the third is in quadrature. For a given model, oscillation amplitude and flow conditions, the force component which must be exerted by the electro-magnets to balance the inertia force varies as frequency squared at frequencies well above resonance, whereas the force from aerodynamic stiffness is constant, and the damping force varies directly with frequency. Consequently the relative magnitude of the aerodynamic forces tends to reduce with increasing frequency, compared with the inertia force. The electro-magnets forcing the motion supplies the sum of these

three components. From a knowledge of the mass of the model (or the moment of inertia in the case of rotary motions) the inertia force component can be calculated and subtracted from the component of applied force in-phase with the motion. However, with increasing forcing frequency the difference becomes progressively smaller and more difficult to obtain accurately. The force component in quadrature with the motion of the model results in the applied force being out of phase with the model motion. The amplitude of this component may be calculated from measurements of the amplitude of the applied force and the phase difference between motion and applied force. However, the phase difference tends to become smaller with increasing frequency, and good quality wave forms are required for good accuracy. With this type of model the wave-form of the motion is likely to be distorted because of the non-linearity of the power amplifier, and the wave-form of the applied force (the current wave-form) from the power amplifiers would have superimposed firing frequency ripple which would make interpretation of the phase of the forcing signal difficult. (Provided that the forcing frequency is well below the firing frequency, the effect of the ripple on model motion is relatively small).

The problems associated with dynamic measurements using a solid model at relatively high forcing frequencies may be summarised as:

(i) The aerodynamic force component in-phase with model motion is proportional to the small difference between a measured applied force, and an inertia force calculated from a measured amplitude and frequency of model motion.

(ii) The calculation of the aerodynamic damping force component depends on the measurement of amplitude of applied force, and the small phase difference between force and motion. For accurate phase measurement, good wave-forms are required.

It was with these difficulties in mind that a search was made for an alternative solution to the problem of making aerodynamic derivative measurements with a magnetic suspension system.

Improved current wave-form, more nearly producing a pure sinusoidal model motion wave-form and allowing more accurate measurement of phase angles might be obtained by incorporating the forcing electro-magnets in a tuned circuit, (by connecting suitable capacitors in series with the coils, an R-L-C resonant circuit is formed, which can be relatively easily excited at the resonant frequency.) This might also extend the frequency/amplitude boundary by utilising a voltage higher than available from the normal position-control power amplifiers. This was one method which was available had not the more promising tuned model concept been devised.

In principle the tuned model is a two-part model, the parts being interconnected by a spring. The model has a resonant frequency which depends on the masses of the parts and on the stiffness of the spring. One of the parts is magnetic, and the model may be magnetically suspended and forced to oscillate over a range of frequencies. However, the resonant frequency is of most interest, because at this frequency the applied force has only to overcome any damping forces that might be present. At high frequencies of oscillation the damping forces are usually very much lower than the inertia forces. The inertia forces of the model are balanced internally at resonance because the motions of the two parts are in antiphase.

With this type of model, any change in the damping forces applied to the model requires a corresponding change of applied excitation force. Damping could arise in several ways. There could be eddy-current damping forces between the moving parts, and between these and any conducting material near the model; there is structural damping associated with the spring and spring end-fixings; in general there would be some aerodynamic damping. Aerodynamic damping forces are often small in still air, and can be neglected, but under wind-on conditions aerodynamic damping can be much greater than damping from other sources giving a large ratio of applied force wind-on to wind-off (for a given amplitude of motion and at the resonant frequency) and hence in principle the aerodynamic damping should be obtainable with good accuracy.

In cases where the airflow produces a force in phase with model motion (an aerodynamic stiffness), the resonant frequency of the model changes. The change of frequency is a measure of the stiffness.

For convenience the first wind-tunnel model was constructed with one mass forming the outer shell of the model, the aerodynamic shape including wings, and the second mass was a permanent magnet core. The model is described in the following sections, and some preliminary steady and unsteady aerodynamic measurements are given, with details of the equipment which had to be devised to measure small amplitude alternating currents.

13.2 The Design of a Pitch-Tuned Model.

It was decided at the outset to incorporate roll control in this model, and for the purposes of monitoring roll attitude a fin was required. Details of this optical system are given in Chapter 8, and

the design of the Dural fin and the brass grid insert is given on Fig. 8.13. Controlling rolling moments were generated using a shaped permanent magnet core, ground to shape from a $\frac{5}{8}$" diameter 5" long Alcomax III magnet.

At resonance, the two parts of a tuned model move in antiphase. This model was required to oscillate in pitch, and some internal clearance between the two parts was necessary.

If I_1 is the inertia of the outer shell and associated parts, and I_2 the inertia of the magnetic core, the ratio of the outer shell amplitude to the available relative amplitude of motion between shell and core, assuming negligible damping, is given by $\frac{I_2}{I_1 + I_2}$. A high inertia core and low inertia shell give the maximum shell amplitude for a given clearance. Rolling moment capacity increases with increased span of the major axis of the end of the core, but it is at this point where maximum clearance between core and fuselage is required in a pitching model. Compromise was accepted allowing a core fitted with pole-pieces having a maximum diameter of $\frac{3}{4}$" to be contained in a circular sectioned fuselage of outside diameter 0.794". The clearance allowed a relative amplitude between core and fuselage of 1.95°. The fuselage and its attached parts were made from Dural and kept as thin as possible for minimum inertia. With the available internal clearance the inertia ratio allowed a theoretical undamped maximum amplitude of motion of the fuselage of 1.19°.

A flexure design was required giving just one resonant mode of the model. In practice other modes do exist. With a suitable choice of flexure the frequencies of these modes can be kept well above the tuned frequency, high enough to have no effect on

the stability of the position-control loops. The flexure design which was chosen satisfied this requirement while developing sufficiently low stresses in the flexures under deflection in the tuned mode (at high frequencies of oscillation there is considerable kinetic energy to be stored in the springs). The flexure consisted of a pair of spring steel beams, mounted parallel to the model axis above and below the core, between the core and shell. The downstream ends of the beams were attached to a brass collar clamped to the core, and the upstream ends were attached to a brass strong point on the tube forming the fuselage.

A cross-section through the fuselage, showing the magnetic core and flexures, is given on Fig. 13.1. The fuselage had a wall thickness of 0.032" over most of its length, but near the ends the thickness was reduced to 0.015" to allow the maximum amplitude of motion. A hollow faired Dural nose plug and blunt tail plug completed the fuselage.

Flexures of this type provide adequate stiffness in the rotary mode of relative motion about a horizontal axis, and in the vertical and fore-and-aft heaving modes.

Drawings of the magnetic core and a flexure are given on Fig. 13.2. The core has flats ground on it to provide end-shaping for generation of rolling moments, and in the mid region to provide room for the two flexures and the brass end-fixings. The lateral heave and rolling modes of relative motion between core and shell had relatively low stiffnesses, giving a calculated natural frequency in the case of the heaving mode of about 20 cycles per second. In order to increase the natural frequencies of these modes, a short length of spring steel wire was built into the model, positioned at right

angles to the flexures in a horizontal direction mid-way along the model. The wire can be seen on the photograph of the core, flexures and end-fixings on Fig. 13.3. The wire also had the effect of locating the position of the flexural axis, one end of the wire being fixed relative to the core and the other end fixed relative to the outer shell. Also shown on Fig. 13.3 are mild steel pole-pieces stuck with epoxy resin to the ends of the core. It was the clearance between these pole-pieces and the shell which determined the relative motion between core and shell. In view of the unusual shape of the core, the rolling moment capacity was measured, using the techniques of Chapter 6. The capacity was 0.012 oz.inch per ampere in the roll control sections of the lateral magnets.

A cut-away sketch which has been used to illustrate the construction of a tuned model of this type is shown on Fig. 13.4, showing the locations of the principal parts. The main difference between the model in this drawing and that used for aerodynamic measurements was the shape of the wings and fin. A drawing of the model used for these experiments is given on Fig. 13.5. The flat-plate section wings had a thickness of 0.065", and the edges were straight tapered to a thickness of about 0.010". The gross and net wing areas of the model are 9.93 in.^{2}, and 6.05 in.^{2} respectively, and the aspect ratio 1.49 based on the net wing (this aspect ratio is used later to determine some theoretical aerodynamic derivatives). The centre of gravity of the complete model was within 1/10" of the flexural axis.

In the design of this model the main concern was to provide a model which could be used as a "hack" in the development of a

technique for derivative measurement, rather than to obtain date for a specific aerodynamic shape. Properties such as the surface finish of the model, tunnel blockage etc. were of secondary interest at this stage.

The main features of the model may be summarised as follows:

(i) Roll control was incorporated in order to maintain proper orientation of the model relative to the suspension magnets, and to prevent components of motion of the tuned mode affecting the lift magnet stabilisation circuits which were designed for solid body modes. The permissible angle of rotation in roll before the lift position stabilisation systems became unstable due to the influence of the tuned mode has not been measured precisely, but it is known to be small, of the order of $\pm 5^{\circ}$ to $\pm 15^{\circ}$ about normal. A tuned mode instability in conjunction with a solid body compensation circuit was discussed in Chapter 7, and an unstable Nyquist plot is given on Fig. 7.23. From this figure one would infer that only a small component of a tuned mode may be allowed to enter into feedback circuits designed for solid models.

(ii) A peak to peak amplitude of outer shell of about 2° was available as a result of a compromise between core size and end-clearance. Amplitudes somewhat less than this have to be used in practice: the core cannot be allowed to touch the outer shell without the model becoming unstable laterally.

(iii) The model was designed for oscillation in its tuned mode in pitch about an axis mid-way along the magnetic core, which was located centrally in the fuselage tube as shown on Fig. 13.1. The frequency of oscillation could most conveniently be adjusted by changing the

thickness of the flexures. This model has been tuned in the frequency range 18-27 cycles per second. All other modes of oscillation of the model occur at much higher frequencies. This range of frequencies was chosen in order to obtain an acceptable current wave-form from the power amplifiers. Frequencies up to 60 c.p.s. have been obtained on a demonstration model tuned in a rotational mode, with amplitudes up to 7°. The wind-tunnel model may be tuned for frequencies of this order in the future as more experience is gained with operation and stabilisation.

13.3 Steady Lift Force and Pitching Moment.

A limited range of lift forces and pitching moments have been measured for the tuned model in the high speed wind tunnel at a working section velocity head of 8"H_2O. The current levels recorded for the lateral bias and position control coils, from which lift force and pitching moment will be estimated, are tabulated below for two values of incidence:

Incidence degrees	q lb/ft^2	Current levels, amps. Lateral position control, Bias	Ford.	Aft.
	0	7.82	7.70	7.95
-0.95	41.6	7.85	9.35	9.40
	0	8.03	8.28	7.75
+0.95	41.6	8.10	6.85	6.40

Over this small incidence range the drag force, estimated from the drag coil current, was 0.058 lb. The "lift" magnets, which do not in fact resist the lift force with this model because of its orientation in the wind tunnel with wings vertical, carried a current of

12.4 amps. $\pm$2% in each leg throughout the measurements, wind on and off.

The procedure for calculating pitching moments will be explained first.

When analysing results from a magnetic suspension system, consideration must always be given to the effects of field gradients on calibrations, and to the effects of direct or indirect stiffnesses. In the case of lift force and pitching moment measurements with vertical wings, the lateral magnet currents are used as measures of force and moment, and in the case of this suspension system the symmetry of the lateral magnets gives zero field gradient effect. Stiffnesses come into play when the model is moved from its datum position. In the case of these measurements a change of model incidence is involved, and the stiffness which would produce a pitching moment would be a direct stiffness, now referred to as a field stiffness (see Appendix III for definitions and data on stiffnesses). A field stiffness is referred to the displacement of the core from the tunnel axis. When the core is locked to the shell, the analysis of results is simple. The measurements in the above table were taken with the core free, that is with the position of the core in the shell dependent on the stiffness of the model flexures and the aerodynamic pitching moment. Hence the moments due to field stiffnesses require a knowledge of the aerodynamic moment, and an iterative process of analysis must be used. Two field stiffnesses are involved with the moment calculation, $k_{\theta,vf}$ and $k_{\theta,d}$. Both have been measured, and are respectively 0.115 lb.ft. per radian and 0.42 lb.ft. per radian per pound drag force. These are stiffnesses tending to centre the core in an angular sense onto the tunnel axis.

The end step in the iterative solution will now be given, beginning with the information from the proceeding step that the angular rotation of the core corresponding with the total shell rotation of 1.9° was 1.658°, i.e. the relative rotation of the two parts was 0.242°. The stiffness of the model flexure is being taken as 0.893 lb.ft./radian (see section 5 of this Chapter), and the moment change due to deflection of the flexure through the angular displacement of $0.242/_{57.3}$ radians is 0.00377 lb.ft. The angular movement of the shell is greater than the core, hence the aerodynamic moment is tending to make the model diverge in pitch (in conventional aerodynamic notation, $\frac{dC_m}{d\alpha}$ is positive). The magnetic moments applied to the model by the lateral magnets, at each incidence, are obtained from equation 5.5 and current changes Δi from the above table, where Δi is a lateral control coil current minus the bias.

At -0.95° incidence, $\Delta i_f = 1.5$, $\Delta i_a = 1.55$ amps.

and $\Delta m = -0.00525\ (0.864\ \Delta i_a - \Delta i_f)$ lb.ft.,

(equation 5.5 with a sign change because moments applied to the model by the magnets are being calculated.)

$$\Delta m = +0.00084 \text{ lb.ft.}$$

(Δm is positive when the lateral magnets are tending to rotate the core clockwise viewed in plan. Positive incidence with this model is a clockwise rotation from the datum position, viewed in plan).

At $+0.95^{\circ}$ incidence, $\Delta i_f = -1.25$, $\Delta i_a = -1.7$ amps

and $\Delta m = +0.00115$ lb.ft.

Evidently most of the aerodynamic pitching moment was resisted by field stiffnesses. This now has to be checked. The centering moment from the lift magnets at a core rotational displace-

ment of 0.829° is 0.00166 lb.ft., and the centring moment from the drag field stiffness at the drag force of 0.058 lb. was 0.00035 lb.ft.

The moments (lb.ft.) applied to the model from the various sources are tabulated below for the two values of incidence.

Attitude	Aerodynamic Moment	Moment from Lateral Magnets	Moment from Stiffness
Negative incidence	-0.00188	+0.00084	+0.00201
Positive incidence	+0.00188	+0.00115	-0.00201
Change, nose up-nose down	+0.00377	+0.00031	-0.00402

The residual algebraic sum of these moment changes, which should be zero, is +0.00006 lb.ft., about 1½% of the calculated aerodynamic moment change. Although a more precise figure could be calculated from a further step in the iteration process, the accuracy of moment-current calibrations and current measurements does not justify the step.

An aerodynamic stiffness in pitch may now be calculated. At the particular dynamic head of this experiment, the stiffness, which would be given a positive sign if tending to centre the shell on the tunnel axis, is given by the change of aerodynamic moment of 0.00377 lb.ft. in 1.9° incidence change, a stiffness of -0.00199 lb.ft./degree. However, the stiffness may be presented in a more general way to allow for changes of dynamic head. At low incidence, drag varies in direct proportion to dynamic head and may be taken as a measure of dynamic head. Hence the stiffness may be quoted per unit drag force, for use at different air speeds, an assumption that remains valid while drag coefficient remains constant. The aerodynamic stiffness quoted in

these terms is

-1.97 lb.ft./radian/lb. drag force,

and this is the stiffness k_3 in the schematic arrangement of a tuned model shown on Fig. 7.3.

The procedure for calculating the lift force will now be explained. The type of stiffness entering into this calculation is an indirect stiffness, because a force is being calculated and the movement of the model during measurements was rotary. Account must be taken of any lateral forces which are generated as a result of rotation of the core away from its datum position in the magnetic fields. These stiffnesses are discussed in Appendix III, and one that enters this calculation is the indirect stiffness $Z_{\theta,d}$ from the drag coil field. The measured value of $Z_{\theta,d}$ was 1 lb./radian/lb.drag force, and as the core displacement was 0.829° and the drag force 0.058 lb. the force at $\pm$ 0.95° shell incidence was $\pm$ 0.00084 lb.

The force applied to the model by the lateral magnets is given by

$- 0.0315\ (0.972\ \Delta i_a + \Delta i_b)$ lb. (see equation 5.6)

and from the data tabulated at the beginning of this section the magnetic forces were

positive incidence +0.0914 lb.

negative incidence -0.0948 lb.

The aerodynamic force is equal and opposite to the sum of the forces exerted on the model by the lateral magnets and by the indirect stiffness from the drag coil. Hence the forces directed along the y-axis (see Fig. III.1) were

at positive incidence - 0.0922 lb.

at negative incidence + 0.0956 lb.

giving a total lift force change of 0.1878 lb. in 1.9° at a dynamic head of 41.6 lb./ft.^{2}. Expressed as an aerodynamic stiffness this becomes 0.099 lb./degree at 0.058 lb. drag, or 1.7 lb./degree/lb. drag force. The lift curve slope $\frac{dC_L}{d\alpha}$ for the tuned model, calculated from these results and based on the net wing area, is 3.24. Slender wing theory gives a slope $\frac{\pi A}{2}$ where A is the aspect ratio. For this model the theoretical slope would be 2.34 based on the net wing; however, the relatively large fuselage probably contributed significantly to lift force.

The aerodynamic stiffnesses derived in this section are compared in section 13.6 with values derived from dynamic measurements.

13.4 The Measurement of the Alternating Components of Current in the Lateral Magnets.

The adoption of the tuned model for dynamic measurements meant that it was necessary to measure relatively small sinusoidal variations of current in a large standing current which had a 150 c.p.s. ripple of relatively large amplitude. The technique which was adopted, described in its simplest terms, was to use the potential difference across a shunt in the current line as a current signal, and then to filter out the ripple from the signal.

Current measurement equipment was applied to the two lateral position control circuits; the equipment is shown schematically on Fig. 13.6. The shunt giving the current signal for each supply was the 2 Ω load resistor; each end of the resistor was subject to large potential variations during a firing cycle of the power supply. The required signal was the difference between the potentials of the two ends, and this was provided by a differential amplifier. The

amplifier, which was a transistor type having a permissible output voltage swing of $\pm$ 10 volts, had an excellent common mode rejection, (the common mode gain was of the order of $\frac{1}{3000}$) which eliminated in the out-put the common mode variations of potential across the shunt. However, to avoid subjecting the amplifier input to large potential variations, it was used with resistive feedback giving a gain of 0.1. The output of the differential amplifier was an unfiltered current signal, which was incidentally very useful for assisting with adjustment of the firing of the three phases of the power amplifiers to give symmetrical firing. The tuned model required symmetry in the firing of the lateral power supplies because it was readily excited by components of current ripple which appeared once symmetry was lost.

The current signal was fed through a Butterworth low pass filter (see Fig. 13.7) having a sharp reduction of gain with frequency above about 20 cycles per second. This filter removed most of the ripple, but attenuated the current signal by only a few percent at the tuned frequency of the model. There was a relatively large phase lag introduced by the filters at the tuned frequency. The lags were $80^{\circ} \pm 2^{\circ}$ at 20 c.p.s. Care was taken to match the filter gains and phase lags near the frequency of interest. Provided the filters are matched, there is no problem introduced by filter phase lag.

The pitching moment generated by the lateral magnets is proportional to $0.864\,\Delta i_a - \Delta i_f$, and for sinusoidal model motion Δi_a and Δi_f are sinusoidal variations of current. A signal proportional to $0.864\,\Delta i_a - \Delta i_f$ was obtained by differencing the current signals in appropriate proportions using another operational amplifier. The output from this amplifier was then measured on an A.C.

millivoltmeter (Solartron type VF 252). This particular meter is suitable for frequencies of 10 c.p.s. and upwards.

The initial experience with the current measurement equipment described above showed that the ripple passing the filters, which resulted in the A.C. meter showing a reading when the model was not being forced, should be further filtered. For this purpose another low pass filter, cutting off at a lower frequency than those on the differential amplifier outputs, was placed in the circuit between the current differencing amplifier and the A.C. meter. The variation with frequency of the gains of the three low pass filters is given on Fig.13.8.

The procedure for setting-up the current measuring circuits was as follows. The variation of the output e.m.f. e_3 from amplifier No. 3 on Fig. 13.6 with forward lateral D.C. current was first measured. This gave a calibration $\left(\frac{e_3}{i_f}\right)_{\omega=0}$ = +1.126 volts/amp. The required calibration $\left(\frac{e_3}{i_a}\right)_{\omega=0}$ (from equation 5.5) was $-0.864 \left(\frac{e_3}{i_f}\right)_{\omega=0}$ = -0.973 volts/amp. The 5k variable resistor on the input of amplifier 3 was adjusted to give this calibration. The calibration of the current measuring equipment was now $\Delta e_3 = -1.126 \left(0.864 \Delta i_a - \Delta i_f\right)$ volts/amp. under D.C. conditions, and the relationship between Δe_3 and Δm is $\frac{\Delta m}{\Delta e_3}$ = -0.00466 lb.ft./volt. _____13.1

Under A.C. conditions, the gain variations of the low pass filters have to be applied in the form of corrections from Fig. 13.8 to the voltage signals measured on the A.C. meter.

13.5 Measurements with the Tuned Model Oscillating in Still Air.

The preliminary frequency response measurements made with this model magnetically suspended and forced at frequencies near its upper resonance showed that the natural frequency was in the range

18.6 - 18.65 c.p.s. when fitted with the flexures shown on Fig. 13.2.

The moments of inertia of the parts of the model, measured using the bifilar method, were:

outer shell, including brass strong point and one flexure

$$I_1 = 0.00357 \text{ lb.ft}^2$$

$$= 1.11 \times 10^{-4} \text{ slug ft.}^2$$

magnetic core and one flexure $I_2 = 0.00557 \text{ lb.ft.}^2$

$$= 1.73 \times 10^{-4} \text{ slug ft.}^2$$

The measured value of the flexure stiffness k_1 was 0.867 lb.ft./radian, and the still air field stiffness k_2 was 0.1147 lb.ft./radian. Using these values in equation I.6 with aerodynamic stiffness $k_3 = 0$ one obtains a theoretical lower undamped resonant frequency of 3.17 c.p.s. and an upper resonant frequency of 18.21 c.p.s. During the measurement of frequency responses the frequencies were measured on a RACAL 1.2 Mc./sec. timer, and the oscillatory signals fed into the lateral position compensation circuits to produce current oscillations were derived from a DAWE low-frequency oscillator with an infinitely variable output. It is estimated that frequency could be set and measured accurate to at least 1 part in 2000. However, the frequency response also involved measurements of amplitudes of motion and current, and the combined effect of scatter resulted in the upper resonant frequency only being known to an accuracy of about 4 parts in 2000, i.e. about $\pm$ 0.2%. On this evidence the disparity between the measured and calculated values could not be attributed to an error in estimating the resonant frequency from the frequency response, but was probably due to an accumulationof errors involved in the measurements of I_1, I_2, k_1, k_2. The effect of

stiffness k_2 on the calculated natural frequency is rather small, and for this reason arbitrary adjustments were made to the values of I_1, I_2 and k_1 in order to obtain a theoretical upper resonance near the measured value. The chosen values are tabulated below:

I_1 reduced by 2% to 1.0878×10^{-4} slug ft.^{2}

I_2 reduced by 2% to 1.6954×10^{-4} slug ft.^{2}

k_1 increased by 3% to 0.89301 lb.ft./radian.

Table 13.1. Adjustments to Tuned Modal Component Constants.

These give a theoretical undamped upper resonance at . . 18.662 c.p.s. The changes in the values of these three constants are of the same order as the experimental error involved in their measurement, and are justified on this basis. Errors in the estimation of damping coefficients, resulting from the adoption of values for the constants which are in error, will be discussed later.

The measurement of the still air frequency response of the model involved the measurement of the following values:

(i) the amplitude of displacement of the nose and tail of the model shell, obtained from the optical system signal amplitudes measured on an A.C. milliameter (Solartron type VF 252), the meter indicating r.m.s. values,

(ii) the frequency of the oscillator feeding the disturbance signals into the two lateral position compensation circuits,

(iii) the r.m.s. amplitude of the voltage signal derived from the current measurement circuits shown on Fig. 13.6, measured on a Solartron milliameter.

The shell of the model was monitored in planes $2\frac{1}{4}$" ahead and $2\frac{1}{2}$" behind the flexural axis.

The check procedure which was necessary before or during these measurements, and wind-on measurements, was as follows:

(a) clean windows in working section, and check lateral optical system calibrations,

(b) check the firing symmetry of the two lateral power amplifiers,

(c) check the internal parts of the model for free movement, and inspect the lateral heave suppression wire for security (on this model one end periodically came adrift),

(d) with the model suspended, check the A.C. meter readings of position and current amplitude with no forcing,

(e) when the model is being forced, display the current signals from filters 1a and 1b (shown on Fig. 13.6) on a twin-beam oscilloscope and check for the correct current phase relationship (antiphase) and amplitudes. It was possible to hold the correct phase relationship, as near as could be estimated from the wave-forms, without resort to feeding the disturbance signals into the two compensation circuits at different phases relative to one another.

The ratio of alternating current amplitudes was adjustable over a wide range by means of variable amplitude disturbance signals. It was possible to maintain the ratio forward current amplitude to aft current amplitude at unity within the limits of about $\pm$ 5%. This was done to ensure that:

(i) inductive coupling in the lateral magnets did not occur. With symmetrical forcing as here proposed the coupling should be zero. However, to date no measurements have been made of possible induced current changes in the roll or bias sections. Variations of roll current would not affect the applied pitching moment or lateral force.

(ii) the lateral magnets did not apply a lateral force to the model. Strictly a lateral force would be produced if the current signals gave a non-zero value of $0.972\,\Delta i_a + \Delta i_f$ from equation 5.6. However, at this stage of development it was judged sufficient to hold the amplitudes nominally constant.

In different circumstances the conflict between the requirements of (i) and (ii) above could become a problem.

The checks (a) to (e) above were additional to checks on force and moment calibrations, and on the alternating current measuring circuits, which were necessarily carried out less frequently because of the time involved.

The still air variation of the forward end position signal r.m.s. amplitude with current circuit output filter r.m.s. amplitude at a constant forcing frequency of 18.6 c.p.s. is shown on Fig. 13.9. The response at this frequency was a maximum. When the model was not being forced the A.C. meters showed residual readings, probably due to the combined effects of the residue of the filtered ripple, model unsteadiness, and spike pick-up (the spikes were produced at the time of firing of the rectifiers). These readings are indicated on Fig. 13.9 near the origin. However, over most of the range the position signal amplitude varied in direct proportion to the current signal amplitude.

At this frequency the corrections to be applied to the current signal are for the reduction of the gain of filters 1a and 1b from the D.C. value (the reduction is 4%, from Fig. 13.8) and for the gain of filter 2 of 0.53 at 18.6 c.p.s. Hence the r.m.s. value of the current amplitude of 120 m V. r.m.s. read from the line on Fig.13.9 at position amplitude 167 m V. r.m.s., when corrected for filter gain

becomes 236 m V. r.m.s. From this corrected current amplitude, the r.m.s. moment amplitude from the calibration given by equation 13.1 is $|M| = 0.0011$ lb.ft.r.m.s.

The pitch amplitude represented by the position signal is obtained from the forward and optical system calibration of 13 volts/inch. The r.m.s. amplitude of nose displacement in the optical system was 0.0128 inches, from which the r.m.s. angular amplitude of motion $|\theta_1|$ was 0.00571 radians, giving a response $\left|\frac{\theta_1}{M}\right|$ of 5.19 radians per lb.ft.

Over a period of time many still air measurements of the response $\left|\frac{\theta_1}{M}\right|$ were taken with this model resonating at 18.6 c.p.s. with amplitudes of shell motion up to $\pm 0.7^{\circ}$, mainly as a check that the model was performing normally. The values of the response lay in the range 4.75 to 5.29 radians per lb.ft., and a value of 5 has been adopted in order to calculate a theoretical response over a range of frequencies for comparison with measurements.

Firstly a damping coefficient c_1 was required corresponding with this typical value of still air response. It can be shown theoretically that the maximum in the frequency - $\left|\frac{\theta_1}{M}\right|$ curve for the case when c_1 is small is very close to the value of $\left|\frac{\theta_1}{M}\right|$ at the upper undamped resonant frequency. Hence we can evaluate c_1 from equation I.5 (writing θ_1 in place of X_1 and moment M in place of F) at the resonant frequency with small loss of accuracy.

At the upper undamped resonant frequency ω_{ob}, Equation I.5 may be re-written for the case where $c_2 = c_3 = k_3 = 0$ as

$$c_1 = \frac{k_1/\omega_{ob}}{\left\{\left|\frac{\theta_1}{M}\right|^2_{\omega_{ob}}\left[k_2 - \omega_{ob}^2(I_1 + I_2)\right]^2 - 1\right\}^{1/2}}$$

and when $\left|\frac{\Theta_1}{M}\right|^2_{\omega_{ob}} \left[k_2 - \omega_{ob}(I_1 + I_2)\right]^2 \gg 1$

_____13.1

$$c_1 \doteq \frac{k_1/\omega_{ob}}{\left|\frac{\Theta_1}{M}\right|_{\omega_{ob}} \left[\omega_{ob}^2(I_1+I_2) - k_2\right]} \qquad \text{_____13.2}$$

where $\frac{1}{\omega_{ob}^2(I_1 + I_2) - k_2} = \left|\frac{\Theta_1}{M}\right|_{\substack{k_1=\infty \\ \omega_{ob}}}$,

the core-locked response of the model at ω_{ob}.

Then

$$c_1 \doteq \frac{\frac{k_1}{\omega_{ob}} \left|\frac{\Theta_1}{M}\right|_{\substack{k_1=\infty \\ \omega_{ob}}}}{\left|\frac{\Theta_1}{M}\right|_{\omega_{ob}}} \qquad \text{_____13.3}$$

The theoretical core-locked response at 18.662 c.p.s., using the adjusted constants of Table 13.1 is 0.2695 radians per lb.ft., and $\frac{k_1}{\omega_{ob}} = 0.007616$ (lb.ft., radian, second units) from which $c_1 = 0.000411$ lb.ft./radian per second. This value is valid provided that inequality 13.1 is satisfied. In this case the left-hand side of 13.1 has the value 344.47.

Internal damping in the tuned model was measured by a separate method as a check on the value of the coefficient c_1 determined from measurements with the model magnetically suspended. With the nose cone and tail plug removed, the magnetic core was clamped on its ends, and an optical system was arranged to monitor the position of the outer shell. The decaying oscillation technique was used to determine

the damping of pitching oscillations of the shell, and the derived value of damping coefficient was 0.00028 lb.ft./radian per second, at a resonant frequency of 24.4 c.p.s., and with a Dural collar fitted to the fuselage tube the damping coefficient was 0.00030 at the reduced frequency of 15.8 c.p.s. These measurements were a check on the order of magnitude of c_1; the differences between the various values may have been due to a reduction of eddy-current damping with the nose cone and tail removed.

An assessment of the likely accuracy of c_1 calculated from equation 13.3 must include the effects of the accuracy of measurement of the applied moment amplitude, the amplitude of motion of the shell, the moments of inertia I_1 and I_2 of the parts of the model, the flexure stiffness k_1, the field stiffness k_2 and frequency ω_{ob}.

Stiffness k_2 is probably known to an accuracy of $\pm$ 5%, but its effect on the calculation of c_1 is small. Ignoring k_2 altogether would only change the calculated c_1 by about 3% in this case, and a 5% change of k_2 would only change c_1 by about 0.15% which will be ignored in the light of other likely errors. The frequency ω_{ob} can be set to an accuracy of $\pm$ 1 part in 2000 if required, and in fact is the most accurately known factor entering into the calculation of c_1. Amplitude of shell motion $|\theta_1|$ can probably be measured to an accuracy of $\pm$ 2% at an amplitude of 0.7°. The moment amplitude measurement involves possible current D.C. calibration and filter errors of about $\pm$1% and a possible current-moment calibration error of about $\pm$5%.

It remains to consider the effects of errors in the model constants k_1, I_1 and I_2. It is quite possible that the assumed values were in error, but any changed value of one of these three constants must be accompanied by a suitable change in one or both of

the others, to maintain the theoretical undamped upper resonant frequency at a constant value, because this frequency is known fairly accurately.

If we write $k_1 = Ak_{1*}$ where a starred constant is the correct value of the constant, and similarly $I_1 = BI_{1*}$, $I_2 = CI_{2*}$, the correct value of the upper resonant frequency is given by

$$\omega_{ob} \doteq k_{1*} \frac{I_{1*} + I_{2*}}{I_{1*} \cdot I_{2*}} \qquad \text{13.4}$$

(this is equation 13 of Appendix I with some changed symbols to suit the pitch-tuned model. The approximation results from ignoring k_2, a small effect as noted above).

The factors A,B, C. have values which in combination give the correct measured value of resonant frequency ω_{ob}. The factors differ from unity because of experimental errors which are involved in the measurement of k_1, I_1 and I_2, and because of adjustments that are made to the measured values to give a theoretical resonant frequency close to the measured value.

As $\omega_{ob} = \omega_{ob*}$ we can use equation 13.4 to establish a relationship between the factors which must be satisfied:

$$\omega_{ob*} = k_{1*} \frac{I_{1*} + I_{2*}}{I_{1*} \cdot I_{2*}} \quad \text{and} \quad \omega_{ob} = Ak_{1*} \frac{BI_{1*} + CI_{2*}}{BC \cdot I_{1*} \cdot I_{2*}}$$

from which $I_{1*} + I_{2*} = \frac{A}{C} I_{1*} + \frac{A}{B} I_{2*}$ 13.5

The accuracy of constants k_1, I_1 and I_2 affects the calculation of c_1 through errors in the term $\frac{k_1}{\omega_{ob}^2(I_1 + I_2) - k_2}$ in equation 13.2. For the purpose of this analysis we are ignoring k_2 and assuming ω_{ob} is known accurately, and hence we are interested in the effects of errors on the ratio

$\frac{k_1}{I_1 + I_2}$. Using the relationship between A, B and C from 13.5 we may write

$$\frac{k_1}{I_1 + I_2} = \frac{k_{1*}}{I_{1*} + I_{2*}} \cdot \frac{A}{B} \cdot \frac{A}{C} \qquad \text{13.6}$$

Now in the case of this tuned model, $I_{2*} \doteq 1{\cdot}56\, I_{1*}$ and equation 13.5 may be re-written

$$\frac{A}{C} = 2{\cdot}56 - 1{\cdot}56\, \frac{A}{B} \qquad \text{13.7}$$

This is the relationship between A, B and C which has been satisfied to give $\omega_{ob} = \omega_{ob*}$. Suppose that, due to errors etc., $\frac{A}{C} = 1{\cdot}1$ The product $\frac{A}{B} \cdot \frac{A}{C}$ in equation 13.6 determines the effect on c_1 of errors. The corresponding value of $\frac{A}{B}$ which would be required to give the correct resonant frequency, obtained from equation 13.7 is 0.936, giving a product $\frac{A}{B} \cdot \frac{A}{C} = 1.03$. Hence the effect of small errors in the assumed values of the model constants k_1, I_1 and I_2 is relatively small on the derived value of internal damping c_1, provided that the theoretical resonant frequency equals the measured frequency. The conclusions are that errors in c_1 are dominated in this case by errors of measurement of the response $\left|\frac{\theta_1}{M}\right|$ at resonance. The sum of the estimated possible errors in this response amounts to $\pm 8\%$, and if an allowance for the effects of errors in k_1, I_1 and I_2 of $\pm 2\%$ is added, the likely maximum error in the calculation of the damping coefficient would be about $\pm 10\%$.

The still air frequency response of the model has been measured over the frequency range 10–23 c.p.s., and the measurements are compared with a theoretical response using the calculated value of c_1, on Fig. 13.10. The agreement between the responses is fair,

the maximum difference between the curves being about 10% near the inter resonance depression. Also shown on this figure is the theoretical solid model response ($k_1 = \infty$) which gives a response amplitude of about 5% of that of the tuned model at the upper resonance frequency. This is a measure of the amplitude advantage to be gained by employing a tuned model. Also shown is the theoretical undamped variation of the core to shell amplitude ratio. Below the anti-resonance frequency of 12.2 c.p.s. the parts move in phase, and above the motions are in anti-phase. At the upper resonant frequency the core amplitude is lower than the shell amplitude, one of the design features of the model: the shell inertia was minimised to reduce the relative motion at this frequency.

13.6 Aerodynamic Derivative Measurements Using the Tuned Model.

The main features of the preliminary measurements of model frequency response with wind-on may be summarised as follows:

(a) the peak in the response $\left|\frac{\theta}{M}\right|$ was changed compared with the still air value: a change was expected, due to aerodynamic damping.

(b) there was a shift in the frequency giving maximum response: this was due to the aerodynamic stiffness changing the natural frequency of the model system.

(c) there was a shift in the pitching axis: this was not anticipated. Evidently a heaving motion was accompanying the pitching motion. Within the limits of measurement the pitching axis was pure.

The axis shift was forwards with increasing head, and hence the heaving motion was in phase with the pitching motion. The heave amplitude was small, and can be derived from the shift of the pitching axis. At the typical conditions of air velocity of 258 ft./sec., and

a pitching amplitude of $\pm 0.51^{\circ}$ the axis shift measured at 18.6 c.p.s. was 0.49" forwards of the flexural axis of the model. This represents a heave amplitude of 0.00436 inches, and a corresponding maximum velocity in heave of 0.0426 ft./sec. The maximum flow incidence change resulting from the heaving motion was $\pm$ 0.0096 degrees in a pitching amplitude of $\pm 0.51^{\circ}$. The effect of the heaving mode of motion on the pitching mode will therefore be ignored.

The cause of the heaving motion was lift force due to incidence, in the main, but there were small additional force components in phase with the lift force, from the lift magnet field stiffness and from the indirect stiffness arising from the drag coil. The calculated sum of these forces agreed with the inertia force in one sample case within better than 10%. Some wind-on measurements with the wings removed showed that the axis shift was virtually eliminated. This evidence, coupled with the phasing of the heaving mode relative to the pitching mode, leaves no doubt over the origins of the motion.

Model frequency responses measured at tunnel dynamic heads (in undisturbed flow) of 26 and 78 lb./ft.^{2} (corresponding with air velocities of 148 and 255 ft./sec. respectively) are shown on Fig.13.11. The peaks in the responses are summarised below:

q, lb./ft.^{2}	0	26	78
$\left\|\frac{\theta}{M}\right\|$, radian/lb. ft.	4.85	3.85	3.27
Frequency, c.p.s.	18.63	18.57	18.42

A method for calculating the value of aerodynamic damping will now be given, which is suitable for cases when C_1 and C_3 are low. The method becomes increasingly less accurate with increasing

damping; the point where the accuracy becomes unacceptable is quite arbitrary. The accuracy of the calculation when c_3 has the higher value, at the higher air speed, will be indicated.

The method of analysis is as follows:

(i) Assume that the frequency corresponding with the peak of a response curve is the undamped natural frequency. Assume the damping coefficient c_2 between core and ground is negligible, and that the product $\omega^2 c_1 c_3$ is small compared with other terms in C of equation I.5 (Appendix I). Hence we assume $C = 0$, and the unknown term k_3 may be calculated to give this result.

(ii) The response $\left|\frac{\Theta}{M}\right| = \sqrt{\frac{A^2 + B^2}{C^2 + D^2}}$ from I.5. In the cases considered here where damping is low, $B^2 = c_1^2\omega^2 \ll A^2 = k_1^2$ and we have chosen k_3 to give $C = 0$, hence the response becomes $\left|\frac{\Theta_1}{M}\right| \doteq \frac{A}{D}$ (typically $B^2 = A^2/300$)

and as $D = \omega\left\{c_3(k_1 + k_2) + c_1(k_2 + k_3) - \omega^2\left[I_2(c_1 + c_3) + I_1 c_1\right]\right\}$

$$c_3 = \frac{k_1/\left|\frac{\Theta_1}{M}\right| - \omega c_1\left[\omega^2(I_1 + I_2) - (k_2 + k_3)\right]}{\omega\left[\omega^2 I_2 - (k_1 + k_2)\right]}$$

The values of aerodynamic stiffness k_3 and damping c_3 calculated in this way are as follows:

Head, lb./ft.^{2}	26	78
k_3, lb.ft./radian	-0.0325	-0.0909
c_3, lb.ft./radian per sec.	0.000332	0.000667

In determining c_3 a value for the internal damping coefficient c_1 of 0.000423 lb.ft./radian per sec. was used, calculated from the still air response measured on the same day as the wind-on measurements.

The steps listed under (i) and (ii) above have assumed that the peaks of the responses correspond with the undamped resonant frequency.

This is not the case. With positive damping the undamped resonant frequency lies to the right of the peak. At these levels of damping, the difference between $\left|\frac{\Theta_1}{M}\right|$ measured at the peak and measured at the undamped resonant frequency is very small. As the stiffness k_3 depends on the change of resonant frequency between wind-on and still air, which is small and in any case is not easily determined with accuracy, k_3 will be in error. Some check calculations using representative values of k_3 and c_3, corresponding with results obtained at the higher air speed, have shown that the method of analysis under (i) and (ii) above will in theory give the correct value of c_3 (to within 2%), but overestimates k_3 for positive values of c_3 and negative k_3. Typically the difference between the frequency corresponding with the peak of the response curve, and the undamped resonant frequency, is of the order of 1 part in 200. However, this small difference can have a large effect on k_3. It is estimated that k_3 could be 30% in error due to this feature of the analysis.

Techniques of analysis could be developed to give k_3 more accurately, but the main concern with the dynamic measurements was to determine aerodynamic damping. The stiffness can be measured separately.

The coefficient c_3 corresponds with the derivative $-M_{\dot{\alpha}}$, using conventional aerodynamic symbols, and the non-dimensional damping derivative $m_{\dot{\alpha}}$ is given by

$$m_{\dot{\alpha}} = M_{\dot{\alpha}} / \rho S V \bar{c}^2$$

For this model, $m_{\dot{\alpha}}$ will be based on the net wing area of 6.05 in.^{2} and the mean chord of 2.015". There was a shift in the pitching axis with airspeed, and also a change of frequency parameter V.

The measured values are listed below:

Airspeed V ft./sec.	148	255
h	0.444	0.356
v	0.132	0.076
$-m_{\dot{\alpha}}$	0.799	0.927

h is the distance of the pitching axis aft of the root leading edge, as a fraction of root chord.

These results will now be compared with some obtained by Miles and Bridgman, who have reported some measurements[16] of $m_{\dot{\alpha}}$ for an aspect ratio 1.5 cropped delta wing of similar planform to the wing on the tuned model. This wing will be called the reference wing. The Mach number range covered by their tests was 0.4 to 1.1, whereas the tuned model damping derivative measurements only extended up to Mach 0.23. However, some theoretical results reported in reference 16 indicate that $m_{\dot{\alpha}}$ is fairly constant at Mach numbers up to 0.4, and so the tuned model data will be compared with the Miles and Bridgman data at M = 0.4.

The wing geometries are compared below:

Wing:	Tuned Model	Aspect ratio 1.5 wing of reference 16
tip : root chord ratio	0.112	0.143
section :	Constant thickness, tapered leading and trailing edges.	R.A.E. 102
leading edge sweep:	65°	63.43°
mean chord $\bar{c}$:	2.015"	4"

The reference wing was tested as a half model, whereas the tuned model wing was complete, but subject to interference from the fuselage. In both cases, data for two pitching axis positions

is available. The pitching axis is defined by h, which is the ratio of the distance of the axis downstream of the root leading edge, to the root chord. The axis position has a strong effect on m_α, whereas frequency parameter V has a relatively small effect. The frequency parameter of the reference wing was in the region of 0.12 at Mach 0.4, and the non-dimensional derivatives measured at these conditions were:

h	0.3774	0.7346
$-m_\alpha$	0.736	0.093

The measurements with the tuned model were with h near to the lower value in this table, and generally $-m_\alpha$ for the tuned model is about 15% higher than those for the reference wing. The slopes dm_α/dh are similar.

The agreement between the derivative measurements is considered to be quite good, bearing in mind that these are preliminary measurements using a technique involving novel techniques and complex equipment : the differences could be due to interference from the tuned model fuselage, or to a contribution to m_α from the fuselage, or to differences in wing section.

13.7 A Discussion on Tuned Models and Derivative Measurements.

Now that the measurement technique has been developed, and proved in a gross sense, it would be useful to compare measurements of derivatives of a standard model using the magnetic suspension system, with measurements made on the same model with more conventional equipment.

With development, dynamic measurements with a tuned model of this type can be expected to provide reliable data on the variation of lift force with incidence, the variation of pitching moment with

incidence, and data on aerodynamic damping. The accuracy of measurements is dependent on the accuracies of several calibrations, and of these the force and moment calibrations require improvement.

At present the upper speed at which the tuned model can be suspended is limited by loop gain in roll, lateral heave and pitch. There are several possible methods of increasing the gains, discussed in Chapters 6 and 7 : these will be investigated during the future development of tuned-model techniques.

The axis shift wind-off to wind-on depends on the interplay of several factors, but general trends of the magnitude of the shift and the magnitude of the associated heaving motion can be stated for a given model:

at a given air speed, increased frequency of oscillation reduces the shift,

at a given frequency, increased velocity increases the amount of axis shift.

These trends point to a requirement for an increased value of tuned frequency at higher air speeds if the heaving motion is to be limited. Increased frequency would also be required to maintain the value of frequency parameter V' . With the power supplies which are in use at present there is little scope for increasing the tuned frequency because of wave-form distortion and the onset of beats in the forcing current amplitude at higher frequencies. These problems result from the relatively low firing frequency of the power supplies. A new pair of supplies are at present under development, the power to the supplies coming from a pair of 400 c.p.s. alternators driven from a 60 B.H.P. motor. The maximum output from each of the supplies will

be 20 k.V.A. The increased firing frequency should allow tuned frequencies to be used which are two or three times higher than in use at present.

Tuned modes of motion other than pitch can be provided, by changing the arrangement of the flexures in the model. Two modes which could be of interest are (i) bodily heaving motions, and (ii) roll. The arrangement of the flexures for the first would not be simple, because of the requirement that only one mode should have a relatively low natural frequency; there is scope for ingenuity in flexure design. However, a flexure design consisting of crossed springs at each end of the magnetic core should prove adequate for tuning in roll.

On the subject of designing for just one low frequency mode of oscillation it is appropriate to mention that the tests which were made with the tuned model reported in this Chapter, with the wings removed, were not easy to make. When the model was first suspended a vertical instability resulted. This was probably caused by a bending mode of oscillation of the fuselage, and was only cured by reducing the gain of the control circuits of the lift magnets. Evidently the wings themselves contributed significantly to the stiffness of the fuselage. Instabilities of this type can be expected to be more critical when the tuned frequency is increased. For example, with increased tuned frequency of a pitching model, the natural frequencies of the fuselage in lateral heave will presumably have to be increased in proportion.

In the foregoing analysis it has been assumed that the moment applied to the pitch-tuned model was proportioned to the signal from the lateral control current amplitude measuring equipment.

Magnetic hysteresis in the iron cores of the lateral magnets, or currents induced in magnetically coupled circuits, could introduce amplitude errors. The suspension system has been designed to minimise such effects. However, a check is desirable, and it has already been mentioned that an improved force and moment calibration technique is required. It is proposed to design and manufacture a strain gauge force and moment balance which will provide the necessary information on dynamic and static calibrations.

LIST OF SYMBOLS USED IN CHAPTER 13.

Symbol	Meaning.
A	Aspect ratio.
A, B, C, D	Terms in model equation of motion, or, ratios of assumed to actual model constants.
c_1	Shell to core damping coefficient.
c_3	Aerodynamic damping coefficient.
$\bar{c}$	Geometric mean chord.
e_3	e.m.f. output from current signal. differencing amplifier.
f	Lateral force produced by lateral magnets.
h	Distance of pitching axis downstream of root leading edge, as a fraction of root chord.
Δi	Change of current from normal wind-off value.
I_1	Moment of inertia of shell about flexure axis.
I_2	" " " " core " " "
k_1	Flexure stiffness.
k_2	Core-to-ground stiffness (a magnetic stiffness).
k_3	Aerodynamic stiffness.
m	Moment.
m_α	Non-dimensional form of M_α : $m_\alpha = \dfrac{M_\alpha}{\rho S V \bar{c}^2}$
M_α	Pitching derivative.
$\|M\|$	Moment amplitude
q	$\frac{1}{2}\rho V^2$
S	Net wing area.
V	Air speed.
α	Pitching displacement (positive nose up).

Symbol	Meaning
$\lvert\Theta_1\rvert$	Amplitude of shell pitching oscillations.
V'	Frequency parameter, = $\omega \bar{c}/V$
ρ	Air density.
ω	Angular frequency of pitching oscillations.
ω_{ob}	Upper undamped natural frequency of tuned model.

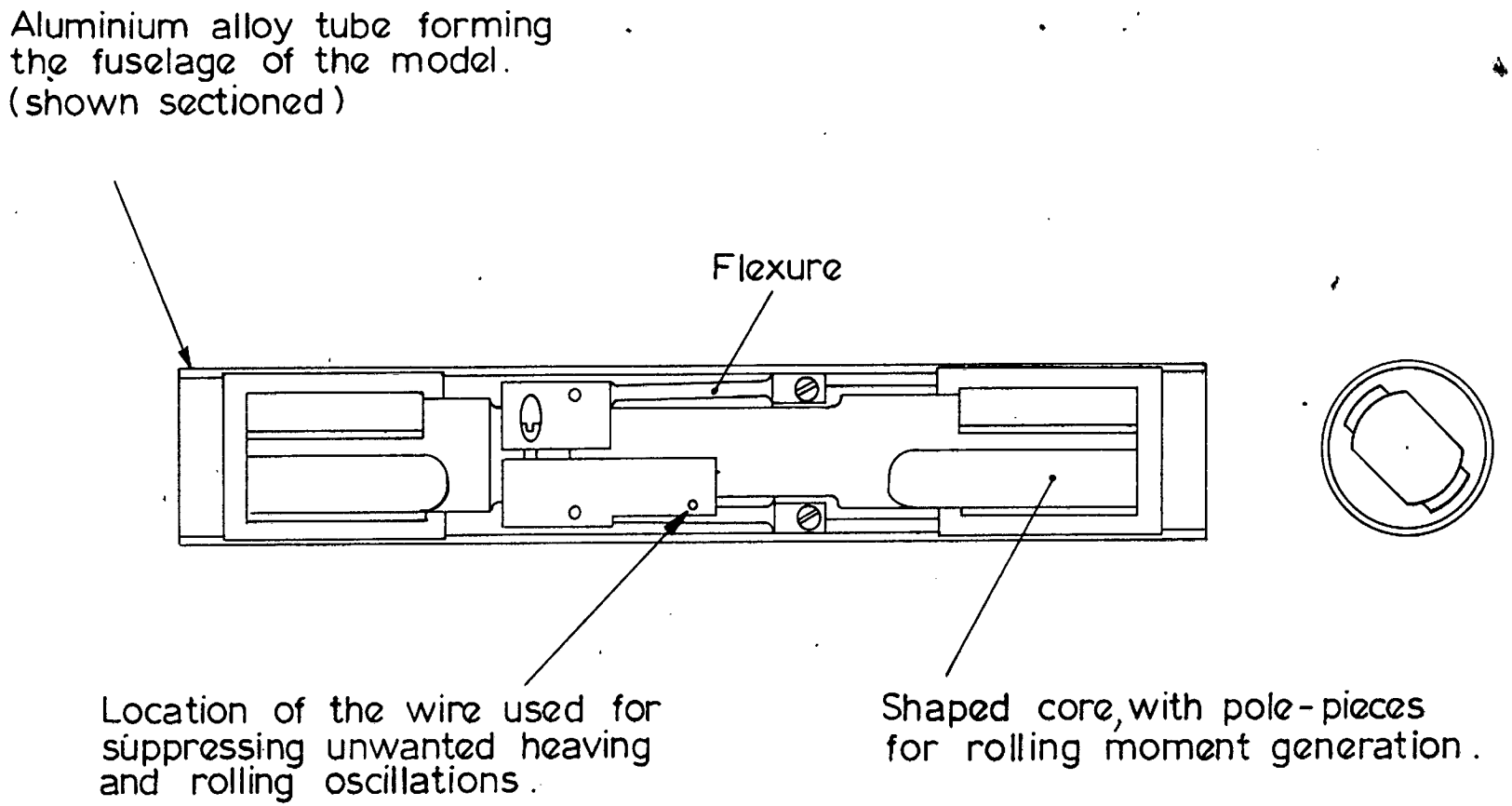

Figure 13.1 The internal arrangement of a tuned model, designed for pitching oscillations.

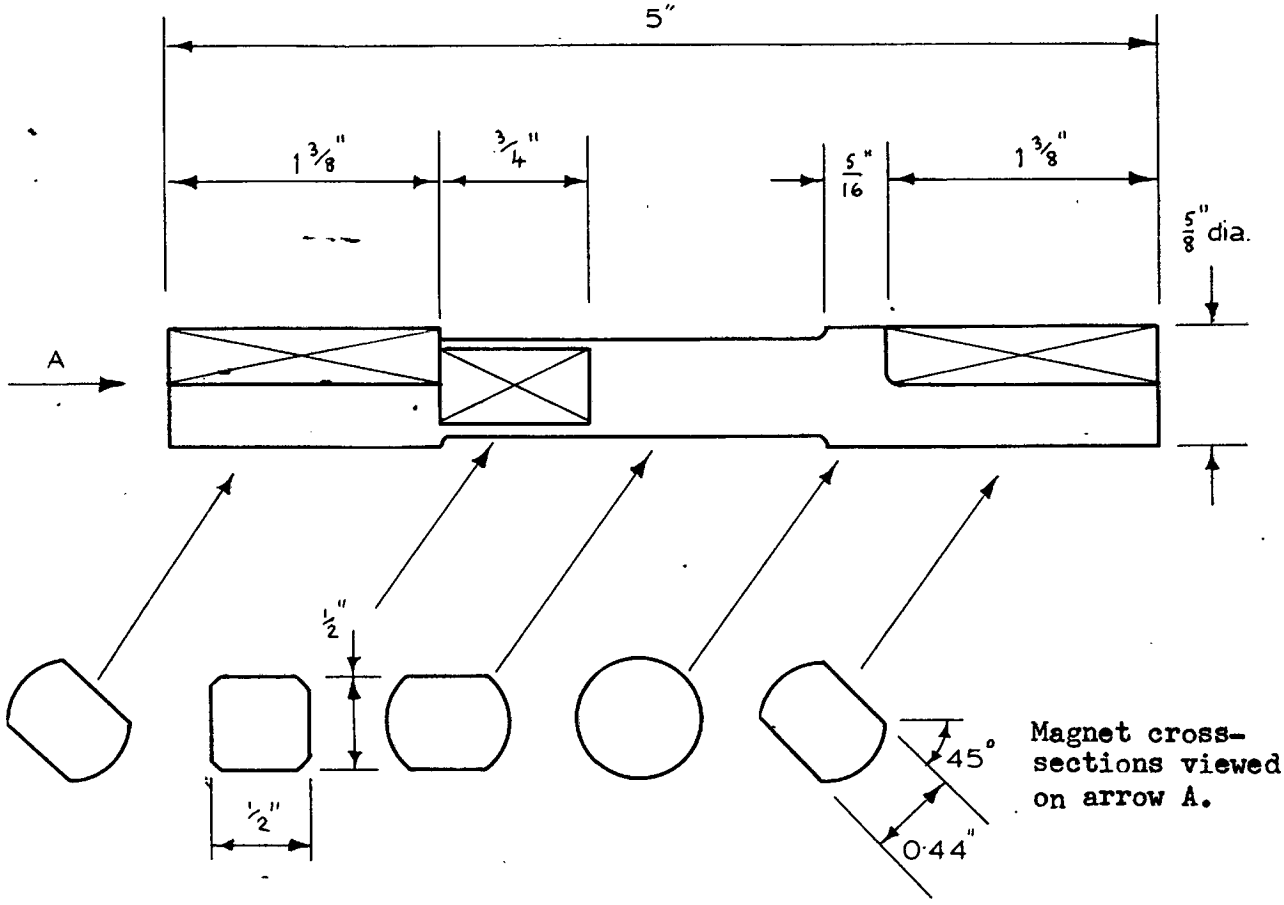

The magnetic core of the tuned model, showing the shaping necessary for roll control, and to provide space for flexures and flexure attachment. Material: Alcomax III.

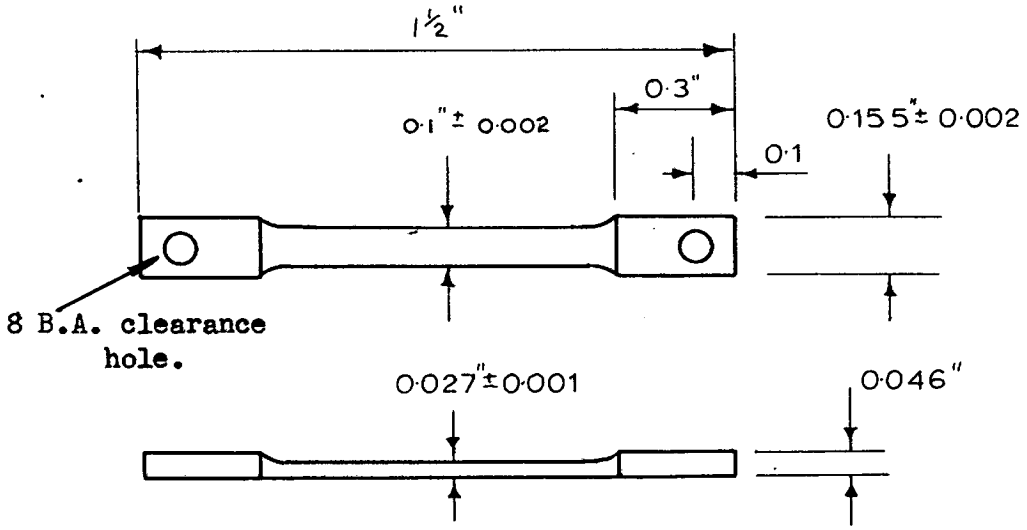

A tuned-model flexure. One of a pair contained within the model fuselage. Material: spring steel.

FIG.13.2. The principal internal parts of the tuned model.

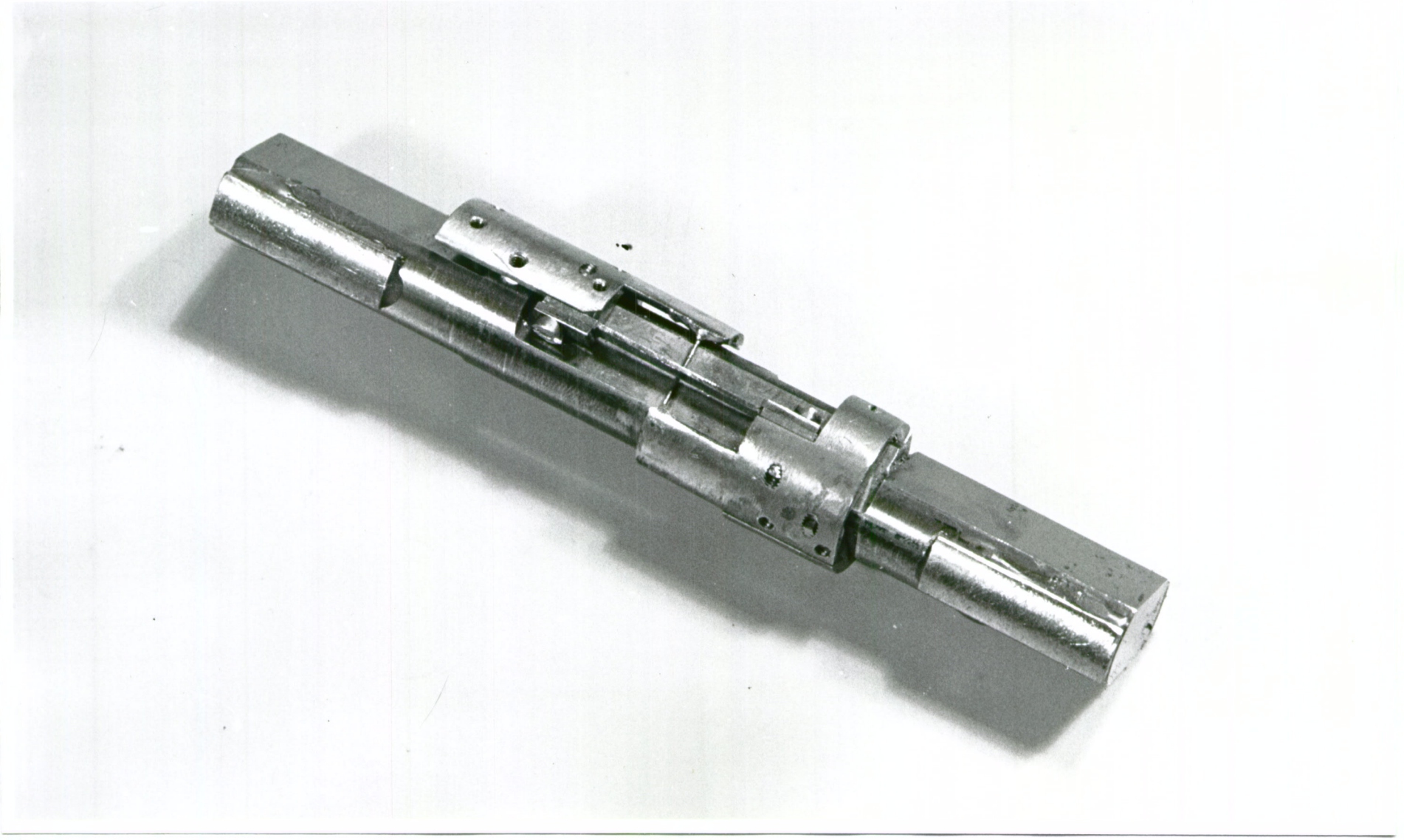

Fig. 13.3 The internal parts of the tuned model.

ey:

1. Wing, in vertical plane.
2. Flexure-magnetic core clamping point.
3. Pitching mode flexure.
4. Magnetic core.
5. End shaping of core, for roll control purposes.
6. Strong point on fuselage, acting as flexure clamping point.
7. Fin, with roll optical system grid.
8. Model tail, monitored optically together with nose for position control.

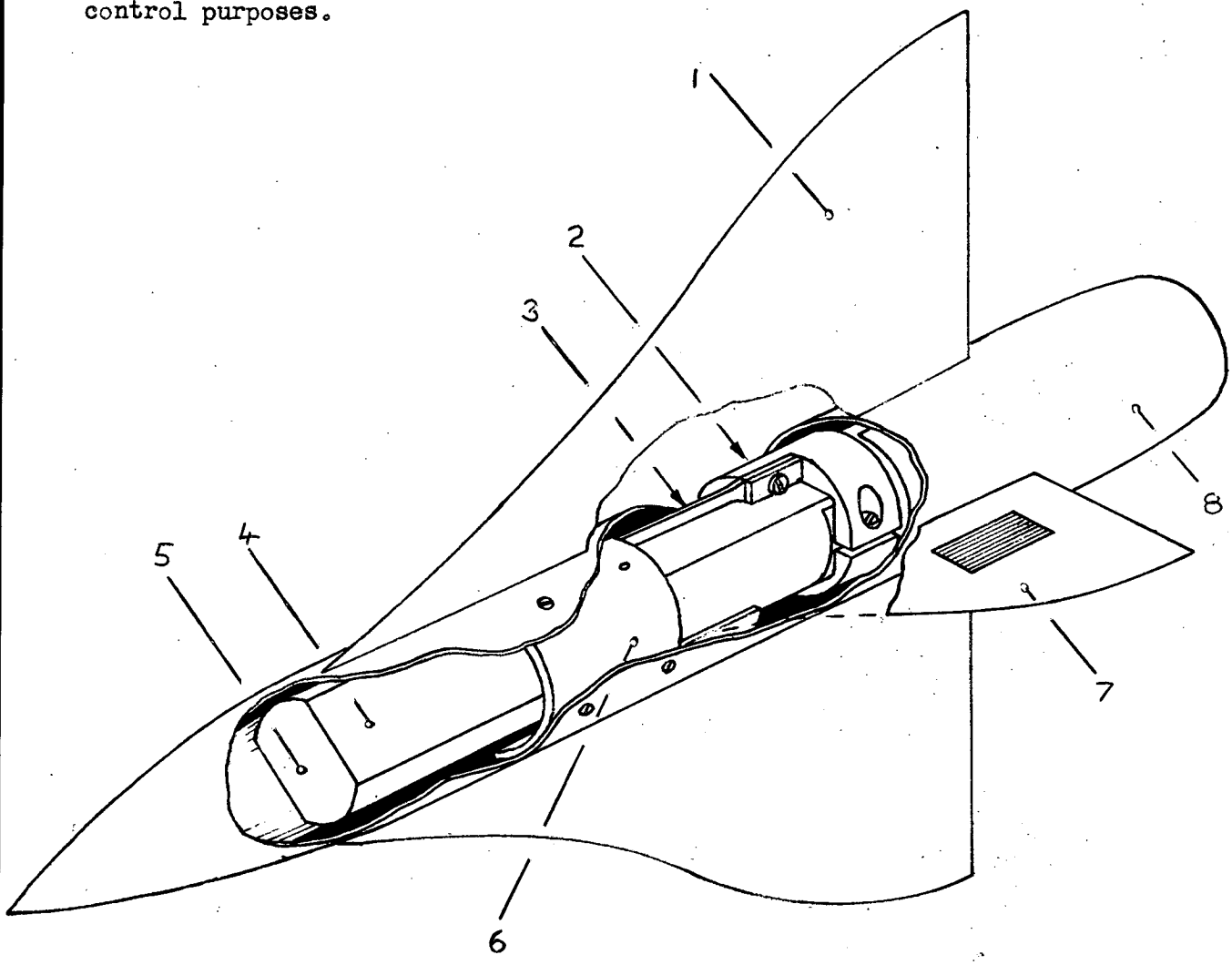

Fig.13.4 A tuned two-mass model.

This type of model, referred to as a "complex model", is being developed for the purpose of measuring aerodynamic pitching derivatives using the Southampton University Six Component Magnetic Suspension System. The fuselage, wings and fin can be induced to oscillate about a vertical axis by the electro-magnets comprising the suspension system, at frequencies close to the relatively high tuned frequency.

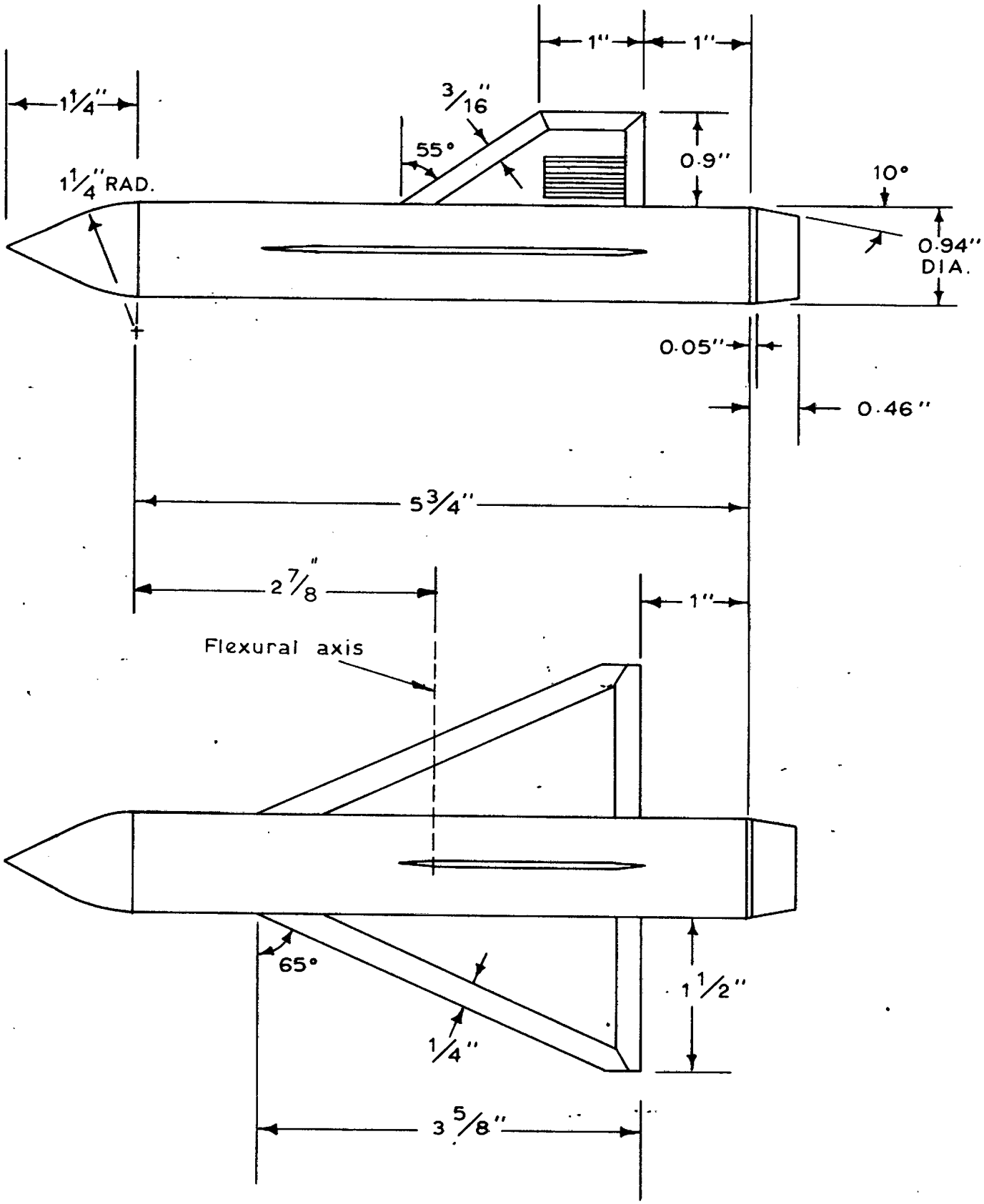

Fig.13·5 The external dimensions of the tuned model.

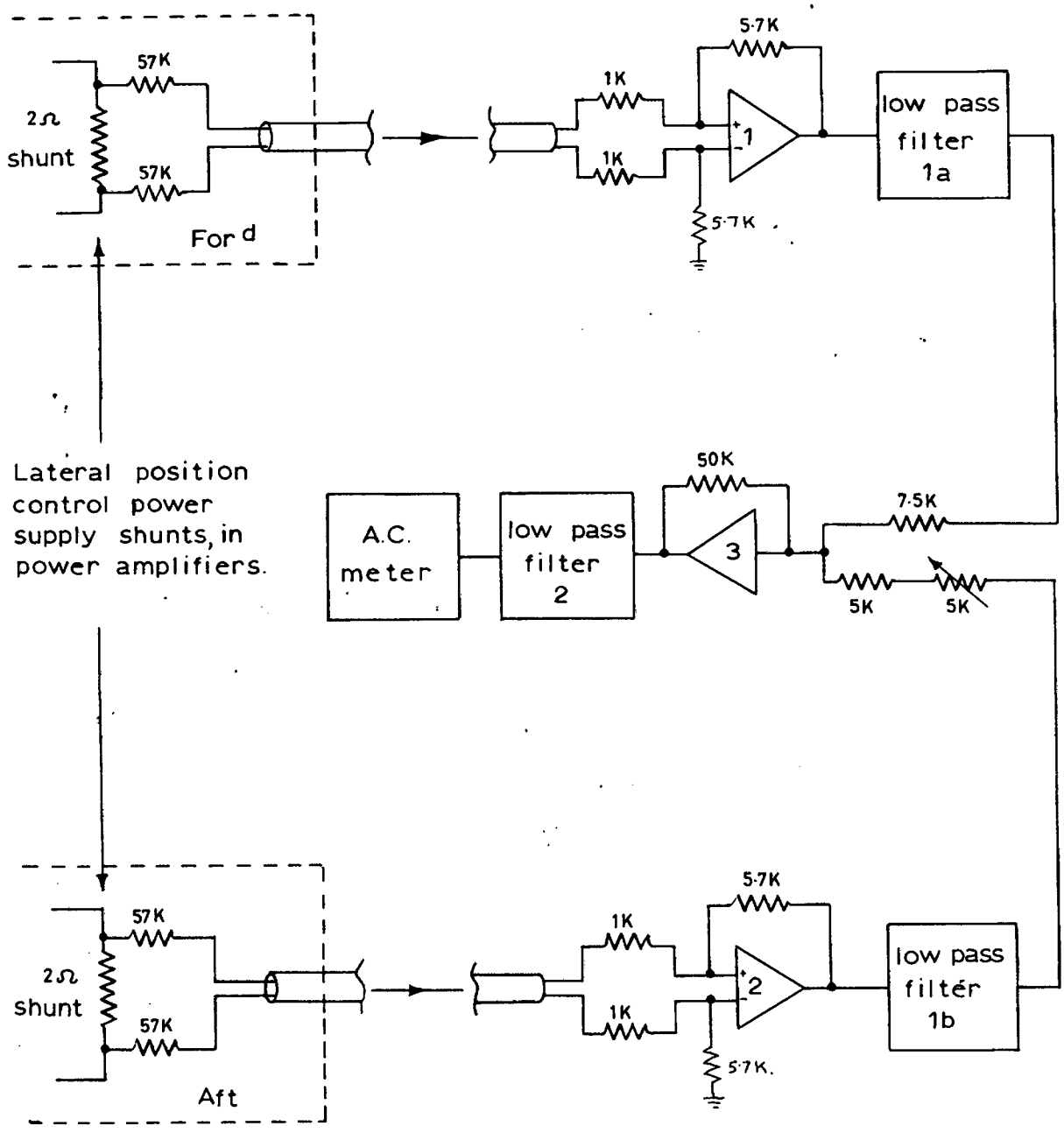

Fig. 13.6 The current measuring systems giving an output which is related to the alternating pitching moment applied to the model.

$$R_1 = R_3 = \frac{500\,k\Omega}{\alpha}\,; \quad R_2 = 1M\Omega$$

$$R_4 = \frac{2M\Omega}{\alpha}$$

$$R_5 = \frac{1M\Omega}{6\alpha}$$

$$C_1 = C_2 = C_3 = C_4 = \frac{2\mu F \times \alpha}{\omega_c}$$

$$C_5 = \frac{12\mu F \times \alpha}{\omega c}\,; \quad \omega_c = 2\pi f_c$$

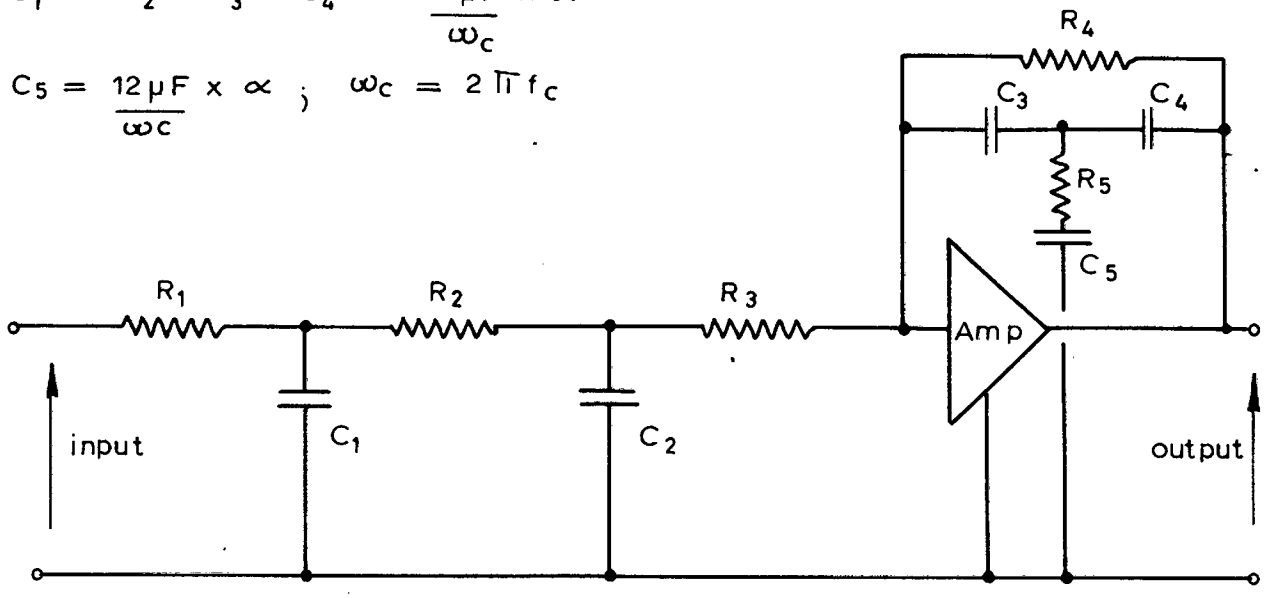

Cut off frequency = f_c; Attenuation rate = 18 dB/octave

α = Scaling factor selected to give reasonable impedance levels.

Fig. 13.7 Butterworth low pass active filter

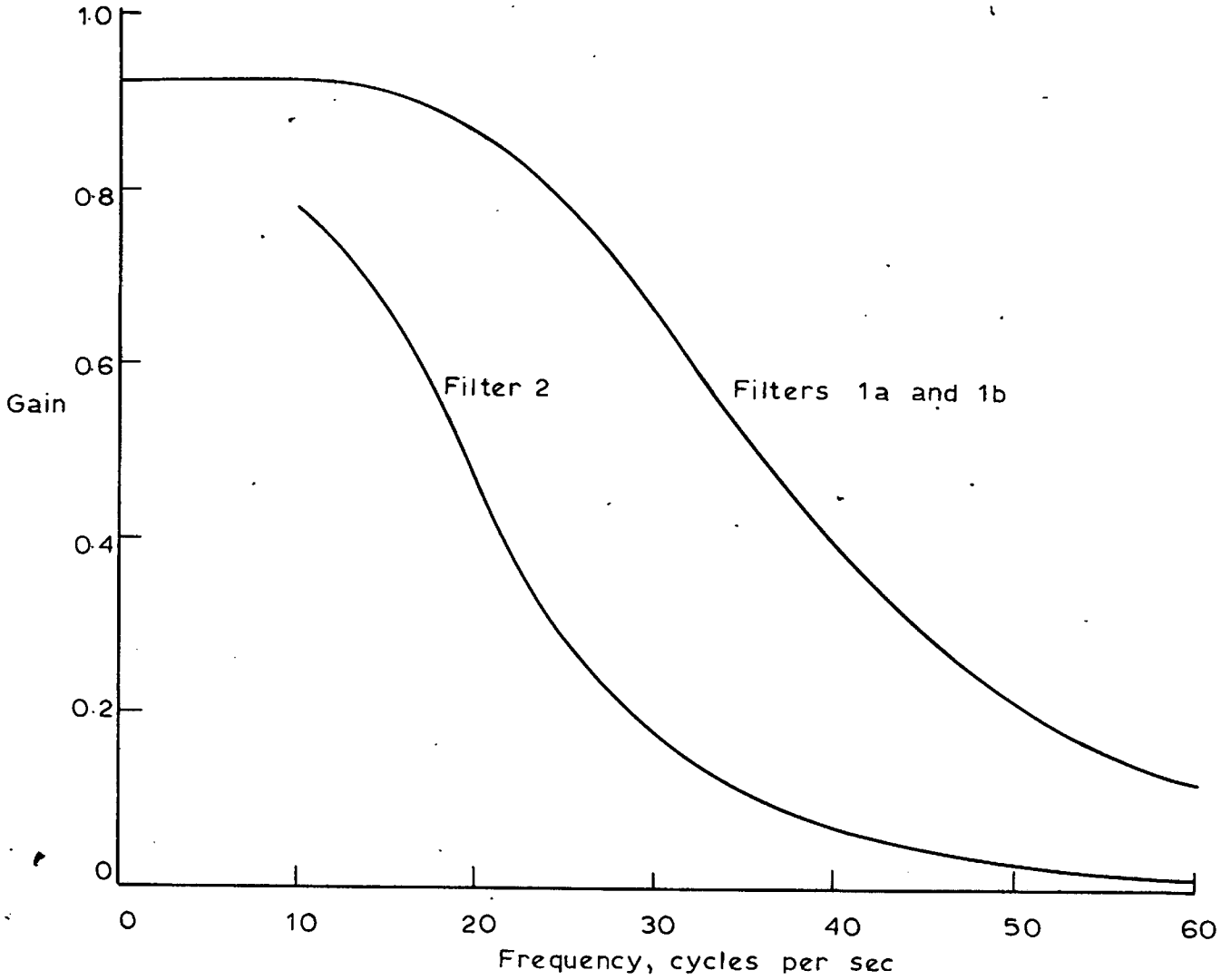

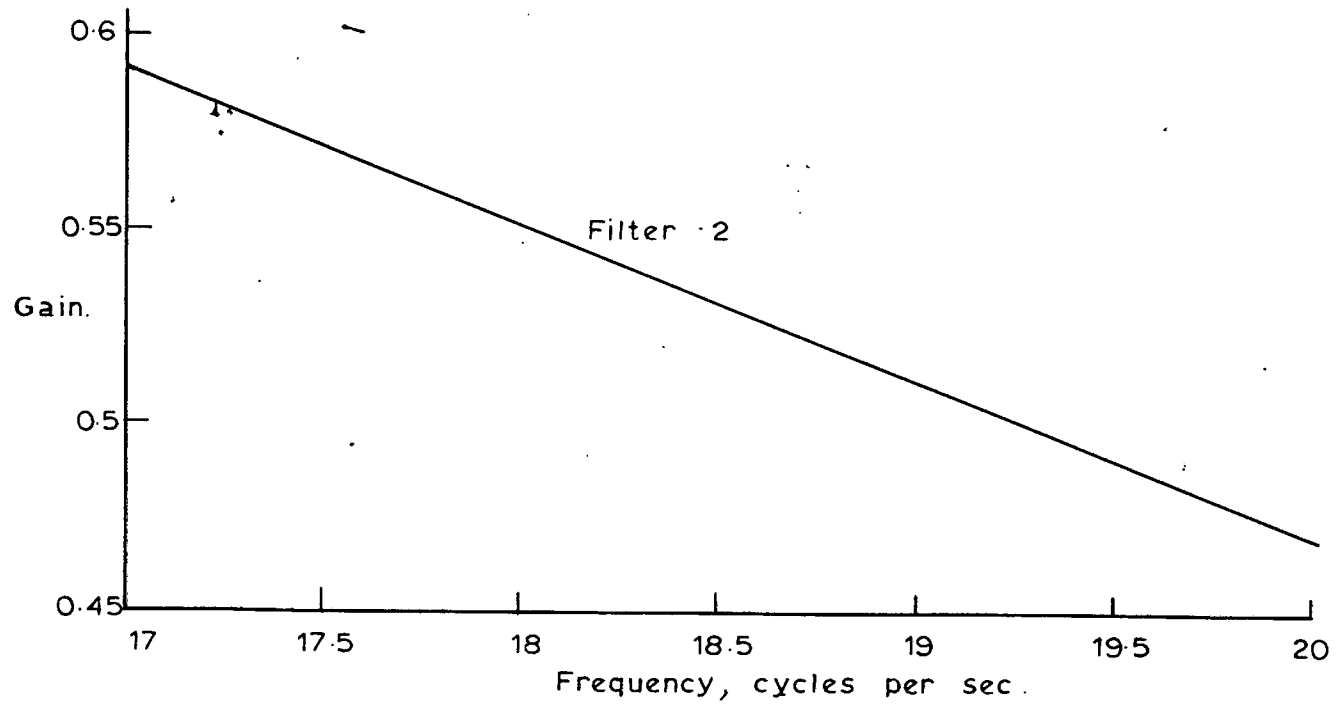

Fig. 13.8. The gain characteristics of the low pass filters in the lateral magnet current measuring circuits.

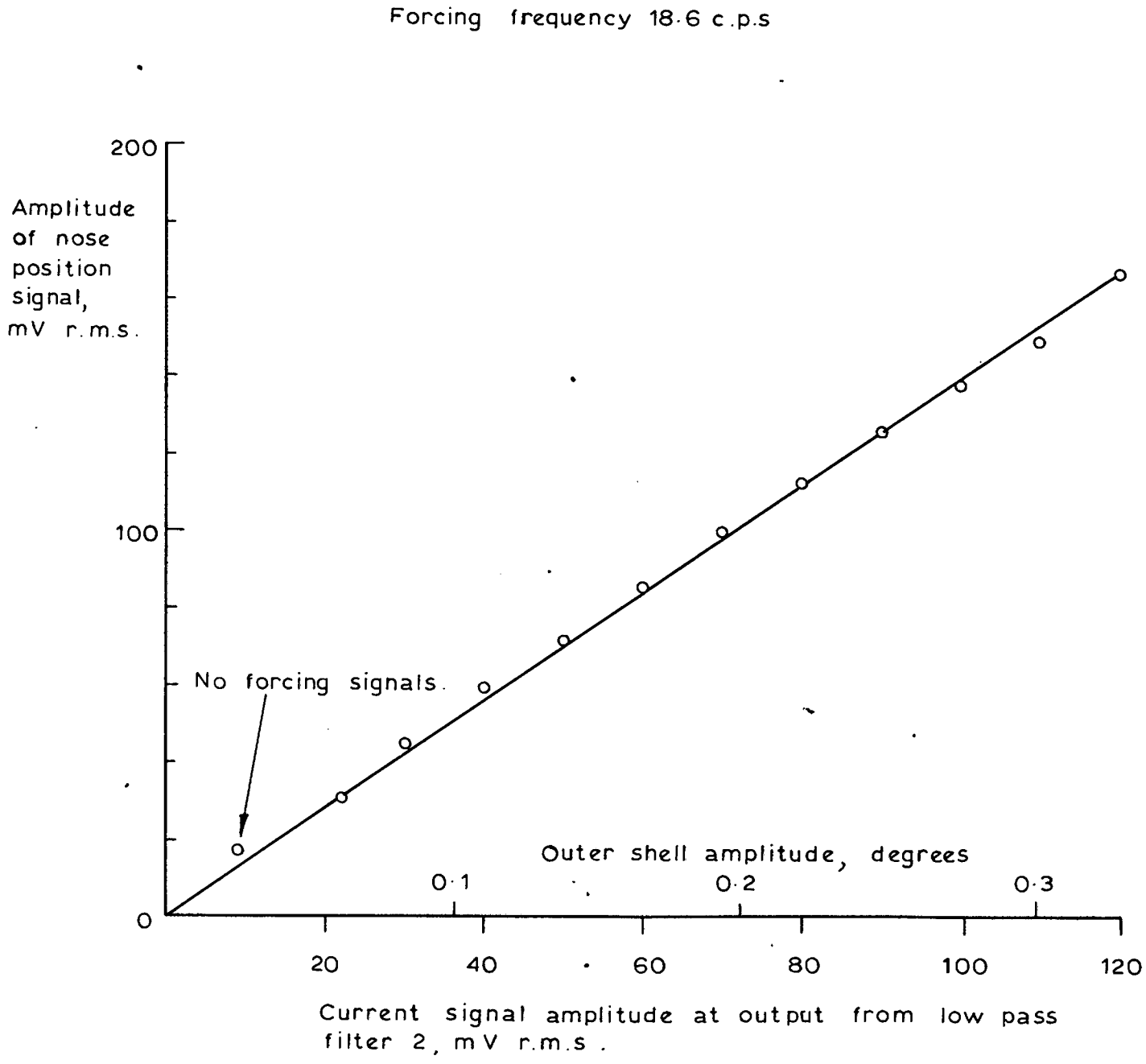

Fig. 13.9. The variation of the tuned model outer shell amplitude with a signal proportional to the amplitude of the applied moment, at a frequency close to the upper resonant frequency.

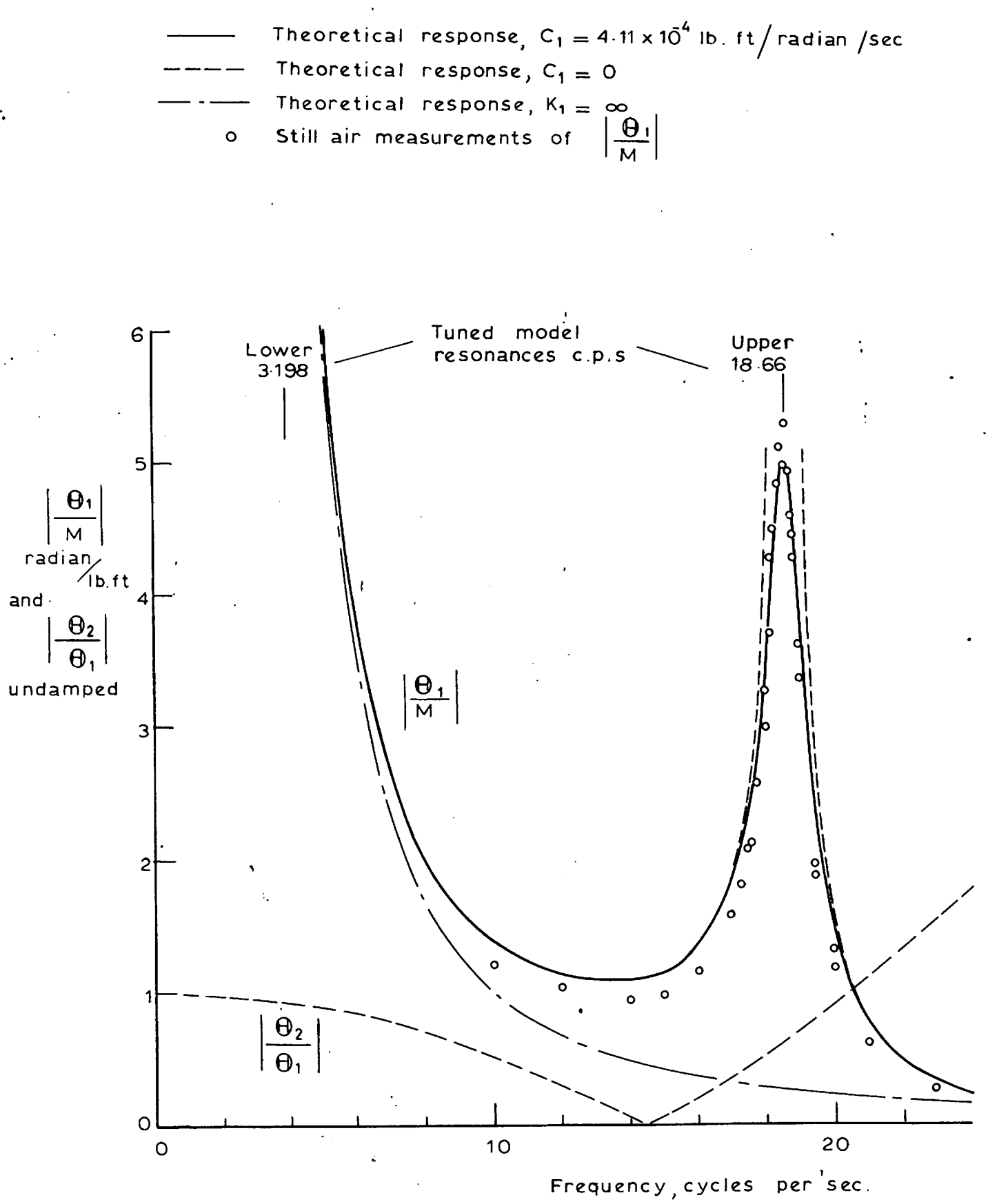

Fig. 13.10 Theoretical and measured frequency responses of the tuned model in still air.

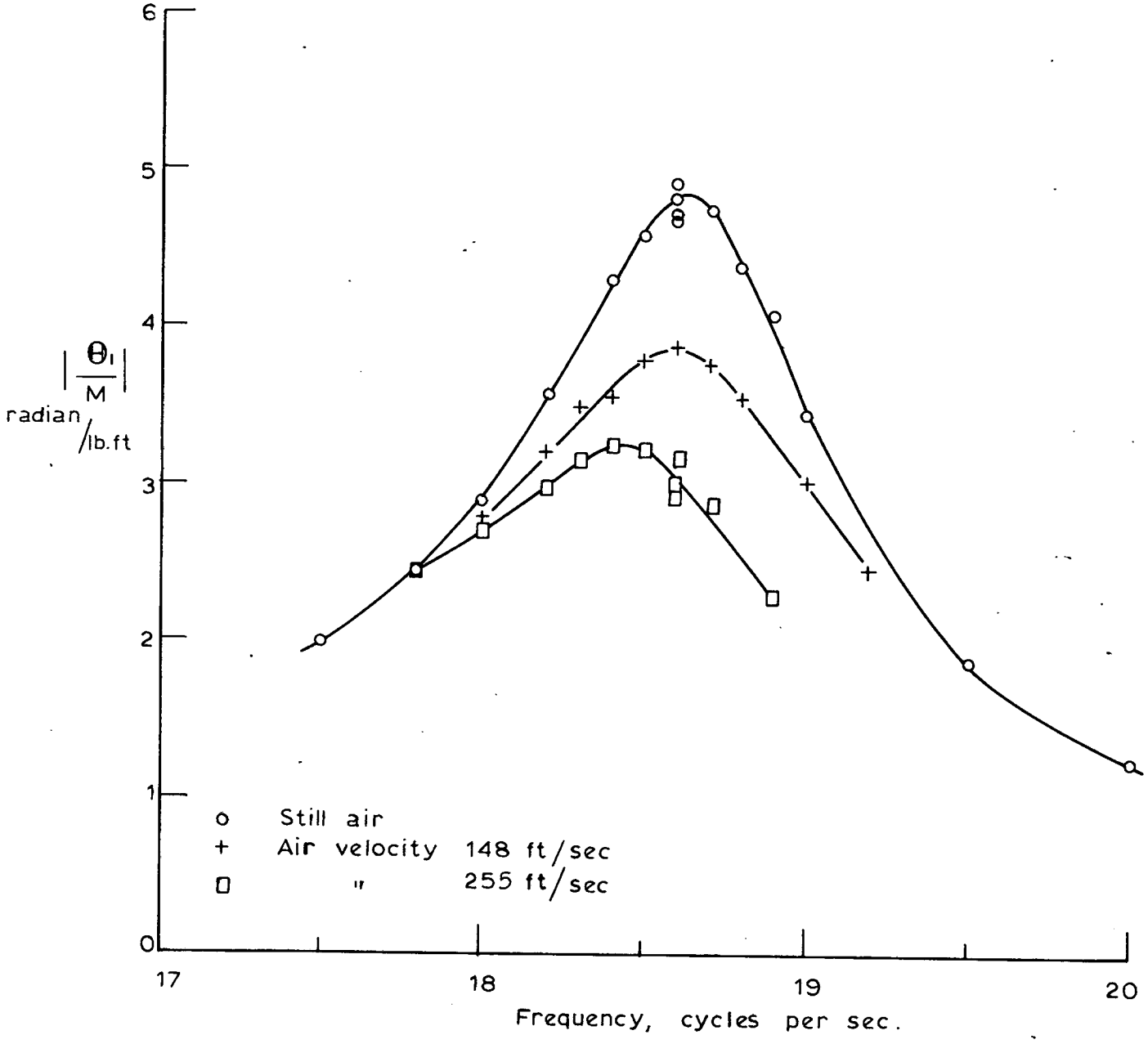

Fig. 13.11 The variation with air velocity of the frequency response of the tuned model in its pitch-tuned model.

14. Conclusions.

A. General conclusions.

(i) A simplified version of the suspension system, controlling in four degrees of freedom, is adequate for the measurement of model drag and for the measurement of aerodynamic damping due to roll, at low air speeds. Both of these measurements involve model motion in uncontrolled degrees of freedom. In the case of drag measurement, the drag force is calibrated against model displacement in the suspension magnetic fields. A simple theory predicted a linear calibration at low drag forces, which agreed with experiments at drag forces up to 3% of model weight. The technique may be suitable for use in horizontal wind tunnels where drag force is less than 10% of the model weight. Methods of measurement have been proposed which might extend the useful range of drag force.

The technique for measuring the roll derivative involved measuring the rate of rotation of a freely spinning model. In still air the measured damping was significant compared with wind-on, and may have been due to eddy current or aerodynamic damping. Further work is necessary to identify and separate these two possible sources, and until this is done, high accuracy for the wind-on measurements cannot be claimed. Such a four component balance is a useful facility for laminar boundary layer experiments, in particular for investigations into base flow.

(ii) The suspension system is suitable for suspending and for drag measurements on a body of revolution up to tunnel choking conditions. Drag measurement with an estimated accuracy of $\pm$ 2% have been made. There are prospects of improving this accuracy..

(iii) The still-air damping of pitching and heaving motions of a model fitted with (conducting) wings is small. The still-air pitch damping is small compared with the likely wind-on damping. Measurements have indicated that the still-air damping is predominently due to eddy-currents.

(iv) A symmetrical arrangement of lateral electro- magnets offers useful simplifications of lateral force and moment calibrations, because the calibrations are independent of model position near the centre of the working section. With conventional suspension systems the calibrations vary strongly with model position.

(v) Calibrations indicate that the suspension magnet system has adequate force and moment capacity in most degrees of freedom to suspend models in supersonic flow.

(vi) Integral control over model position is a useful facility, and has been demonstrated on drag control. The principle should be adapted to more degrees of freedom with models suspended in supersonic flow, to reduce the work-load of the operator.

(vii) A mechanical model launcher will be required to hold the model during the starting and shut-down phases of supersonic flow.

(viii) More accurate force and moment calibration techniques are required. A strain-gauged sting balance has been proposed.

(ix) Soft iron model cores give higher forces than permanent magnet cores of similar size. However, models are subjected to magnetising fields of varying intensity in magnetic suspension systems, and permanent magnet cores are less prone to changing their strength of magnetisation. They are therefore preferred for use when the suspension system is to be used as a balance, because calibrations are less likely

to change.

(x) With this suspension system, models are suspended with their wings in the vertical plane, and lift force is resisted by the lateral magnets. The electro-magnet symmetry in conjunction with the chosen wiring arrangement, results in the model not being subjected to magnetising or de-magnetising fields as a result of the production of lateral force or moment. Without this symmetry, models could be de-magnetised by a lateral force of repulsion.

(xi) It may not be possible to generate adequate moments on some models. A novel form of indirect control over model position has been proposed.

(xii) Steady lift force and pitching moment can be measured for a winged model in a six component magnetic balance.

B. Conclusions related to roll control.

(i) All of the known methods of controlling roll have been reviewed, and some methods are suitable for magnetic suspension systems.

(ii) Some promising control methods have been investigated, and in particular the "shaped core" roll control system has been the subject of a comprehensive theoretical and experimental investigation. The control system was suitable for this suspension system, and was incorporated to allow aerodynamic measurements to be made with winged models. A simple pole-theory was used to predict the general characteristics of this method of control.

(iii) The shaped-core roll control system provided adequate control for one particular model at low air speeds. However, the rolling moment capacity is fixed for a given core design, whereas moment requirements increase with air speed. With this model, a higher capacity would

probably be required at a higher Mach number, in particular for supersonic flow.

(iv) Methods of indirect control have been proposed which might be suitable for the control of roll, under wind-on conditions only, at high speeds.

(v) A roll attitude optical system has been developed and has proved satisfactory.

(vi) The ⊥ arrangement of suspension electro-magnets can be used for motoring a model about its roll axis. It may be possible to develop this into a roll derivative measuring technique. The available evidence suggests that some feedback between model motion and the excitation field would be necessary.

C. Conclusions relating to the tuned model.

(i) A tuned model greatly reduces the electrical power that is required to induce a particular frequency and amplitude of motion, compared with a similar solid model.

(ii) With given power supplies and suspension magnets, a tuned model can be excited at higher frequencies than an equivalent solid model.

(iii) Where the outer shell of a tuned model is monitored and the position signal used for control, control system stabilisation is difficult. In particular, it has not been possible to obtain lateral stiffness in a pitch-tuned model which is sufficient for suspension at high air speeds. A control system was developed which was adequate for still air suspension, and for use at low air speeds. Control was in six degrees of freedom.

(iv) A tuned model excited near resonance produces a more pure sinusoidal motion than a solid model. The distortions in the motion

of a solid model are due to non-linearities in the power supplies.

(v) The pitch-tuned model had adequate control system performance in drag, and vertical force and moment.

(vi) Techniques are available for improving the stiffness of the remaining degrees of freedom.

(vii) Pitch-tuned models have an absolute limit to the moment that may be applied. The limit increases with increased tuned frequency, with an otherwise fixed design of model.

(viii) A pitch damping derivative has been measured, with an estimated accuracy of $\pm$10%. There are good prospects of improving this accuracy, mainly as a result of improvements in calibration techniques.

(ix) A pitch tuned model can allow the simultaneous measurement of steady lift force and pitching moment during measurements of aerodynamic damping.

(x) The control system which has been developed for stabilising the tuned mode introduces positive damping of this mode. This should allow models which have negative aerodynamic damping to be suspended and controlled wind-on.

(xi) The aerodynamic damping force acting on an oscillating solid model is small compared with the inertia force of the model, and it is therefore difficult to separate and measure the damping force. The tuned model avoids this difficulty by balancing the inertia force internally. The excitation force from the suspension magnets is just required to overcome damping, and the problem of separation is therefore avoided.

The important features of this research work may be summarised as:

the exploitation of a unique electro-magnet layout for the development of a six component suspension system, involving research into roll attitude monitoring and control techniques. This has allowed aeroplane-like models to be suspended for the first time using a magnetic suspension system,

the concept of the tuned model, a study of the stabilisation problems introduced by the model followed by the development of a control system, the incorporation of roll control into the tuned model, and the use of a tuned model for the satisfactory measurement of the aerodynamic damping of pitching oscillations.

Improvements in magnetic suspension techniques applied to the tuned model are required in respect of the stiffness of suspension in some degrees of freedom, and of the force and moment calibration methods.

15. References.

1. Daum, F.L., (Editor) — "Summary of A.R.L. Symposium on Magnetic Wind Tunnel Model Suspension and Balance Systems", Aerospace Research Laboratories document A.R.L. 66-0135, Wright-Patterson Air Force Base, Ohio.

2. Tournier, M. and Laurenceau, P. — "Suspension Magnetique d'une maquette en soufflerie". La Recherche Aeronautique, p.21, July-August 1957.

3. Wilson, A. and Luff, B.F. — "Magnetic Suspension for Wind Tunnels", Electronic Engineering, Feb. 1966, p.72.

4. Chrisinger, J.E., Tilton, E.L., Parkin, W.J., Coffin, J.B., Covert, E.E. — "Magnetic Suspension and Balance System for Wind Tunnel Application", Journal of The Royal Aeronautical Society, Nov. 1963.

5. Jenkins & Parker. — Journal of Applied Physics, Vol. 30, P.2385 (1959).

6. Zapata, R.N., and Dukes, T.A. — "Electromagnetic Suspension System for Spherical Models in a Hypersonic Wind Tunnel". Report 682, Princeton University, Dept. of Aerospace & Mechanical Sciences, Princeton, New Jersey, (July 1964).

7. Copeland, B.A., Covert, E.E., Stephens, T. — "Recent Advances in the Development of a Magnetic Suspension System and Balance System for Wind Tunnels (Part III)", M.I.T. report A.R.L. 65-114, June 1965.

8. Stephens, T. — "Methods of Controlling the Roll Degree of Freedom in a Wind Tunnel Magnetic Balance", Aerospace Research Laboratories report A.R.L. 65-242, Dec. 1965.

9. Beecham, L.J. — A verbal proposal on 26th October 1967 by Mr. L.J. Beecham of R.A.E.

10. Goodyer, M.J., — "Roll Control Techniques on Magnetic Suspension Systems", The Aeronautical Quarterly, Vol. XVIII, Feb. 1967.

11. Wield, G. — "An investigation into the nature of the transfer function of the lift power amplifier in a magnetic suspension system". Honours project, year 1964-65, Dept. of Aeronautics & Astronautics, Southampton University.

12. Goodyer, M.J. — "Some Experimental Investigations into the Drag Effects of Modifications to the Blunt Base of a Body of Revolution". Institute of Sound & Vibration Research, Report I.S.A.V. No. 150, Southampton University, July 1966.

13. Earnshaw, S., "On the nature of the molecular forces which regulate the constitution of the luminiferous ether". Trans. Cambridge Philosophical Society, Vol. 7, 1842.

14. Judd, M. "Progress report on the feasibility study of magnetic suspension for derivative measurement", A.A.S.U. Report No. 191, Dept. of Aeronautics & Astronautics, Southampton University.

15. Judd, M. "Some aspects of Separated Flow", Ph.D. Thesis, 1960. Dept. of Aeronautics & Astronautics, Southampton University.

16. Miles, C.J.W., and Bridgman, K.B. "Measurements of the Direct Pitching Oscillation Derivatives for Three Cropped Delta and Three Arrowhead Planforms at Subsonic and Transonic Speeds". Aeronautical Research Council R. & M. 3397, 1965.

17. Tilton III, E.L. "Dynamic Stability Testing with a Wind Tunnel Magnetic Model Suspension System", M.Sc. Thesis, 1963, M.I.T., Dept. of Aeronautics and Astronautics.

Appendix I.

The Equations of Motion of Tuned Models.

A tuned model represented by the springs, masses and dashpots shown schematically on Fig. 7.3 is to be considered. The equilibrium of forces applied to masses 2 and 1 gives respectively

$$m_2 D^2 x_2 + c_2 D x_2 + k_2 x_2 + c_1 D(x_2 - x_1) + k_1(x_2 - x_1) - f = 0 \qquad \text{I.1.}$$

$$m_1 D^2 x_1 + c_1 D(x_1 - x_2) + k_3 x_1 + c_3 D x_1 + k_1(x_1 - x_2) = 0 \qquad \text{I.2.}$$

and from I.2. $$x_2 = x_1 \frac{m_1 D^2 + D(c_1 + c_3) + k_1 + k_3}{k_1 + c_1 D} \qquad \text{I.3.}$$

Substituting for x_2 in I.1. from I.3. we have

$$f = \frac{x_1 (m_2 D^2 + c_2 D + k_2 + c_1 D + k_1)(m_1 D^2 + [c_1 + c_3] D + k_1 + k_3) - (k_1 + c_1 D)^2}{k_1 + c_1 D} \qquad \text{I.4.}$$

If we assume the applied force to be periodic, and given by $f = F e^{j\omega t}$ resulting in responses of the two masses of $x_1 = X_1 e^{j\omega t}$ and $x_2 = X_2 e^{j\omega t}$, the response $\frac{X_1}{F}$ from equation I.4. by substitution for f and x_1 and simplification becomes

$$\frac{X_1}{F} = \frac{A + Bj}{C + Dj} \qquad \text{I.5.}$$

where $A = k_1$, $B = c_1 \omega$,

$$C = m_1 m_2 \omega^4 - \omega^2 [m_1(k_1 + k_2) + m_2(k_1 + k_3) + c_1 c_2 + c_2 c_3 + c_3 c_1] + k_1 k_2 + k_2 k_3 + k_3 k_1$$

$$D = \omega \{ c_3(k_1 + k_2) + c_2(k_1 + k_3) + c_1(k_2 + k_3) - \omega^2 [m_2(c_1 + c_3) + m_1(c_1 + c_2)] \}$$

The undamped resonant frequencies are given by $C = 0$,

i.e. $$m_1 m_2 \omega_o^4 - \omega_o^2 [m_1(k_1 + k_2) + m_2(k_1 + k_3)] + k_1 k_2 + k_2 k_3 + k_3 k_1 = 0 \qquad \text{I.6.}$$

a quadratic in ω_o^2 giving two positive real solutions. Continuing with the case of an undamped model, equation I.5. may be re-written

$$\frac{X_1}{F} = \frac{1}{m_1 m_2 \omega^4 - \omega^2\left[m_1 \frac{k_1+k_2}{k_1} + m_2 \frac{k_1+k_3}{k_1}\right] + k_2 + k_3 + \frac{k_2 k_3}{k_1}}$$

If mass m_1 is locked to mass m_2, which is equivalent to writing $k_1 = \infty$, the response becomes

$$\frac{X_1}{F} = \frac{1}{k_2 + k_3 - \omega^2 (m_1 + m_2)}$$

and the undamped natural frequency of this system is given by

$$\omega_l^2 = \frac{k_2 + k_3}{m_1 + m_2} \qquad \text{I.7.}$$

In the text, the stiffness k_2 has been identified with a magnetic stiffness, and k_3 with an aerodynamic stiffness which is taken to be zero in still air.

The steady-state response is

$$\frac{X_1}{F} = \frac{k_1}{k_1 k_2 + k_2 k_3 + k_3 k_1} \qquad \text{I.8.}$$

The response $\frac{X_2}{F}$ may be obtained by substituting for x_1 from I.3. in I.1, from which

$$\frac{X_2}{F} = \frac{A + k_3 - m_1 \omega^2 + (B + c_3 \omega) j}{C + Dj} \qquad \text{I.9.}$$

where A, B, C, D are as defined for equation I.5. An undamped antiresonance $\frac{X_2}{F} = 0$ occurs at the frequency ω_a which results in the real numerator of I.8. equalling zero, i.e. $A + k_3 = m_1 \omega_a^2$

from which $\omega_a^2 = \frac{k_1 + k_3}{m_1}$ I.10.

and the steady-state response is

$$\frac{X_2}{F} = \frac{k_1 + k_3}{k_1 k_2 + k_2 k_3 + k_3 k_1} \qquad \text{I.11.}$$

Under wind-off conditions it has been assumed that $k_3 = 0 = c_3 = c_2$, and the stiffness k_2 in some circumstances could be zero, giving the responses

$$\left.\begin{aligned} \frac{X_1}{F} &= \frac{k_1 + c_1\omega j}{m_1 m_2 \omega^4 - k_1\omega^2(m_1+m_2) - j\omega^3 c_1 (m_1+m_2)} \\ \frac{X_2}{F} &= \frac{k_1 - m_1\omega^2 + c_1\omega j}{m_1 m_2 \omega^4 - k_1\omega^2(m_1+m_2) - j\omega^3 c_1 (m_1+m_2)} \end{aligned}\right\} \quad \text{I.12}$$

An undamped resonance occurs when $m_1 m_2 \omega^4 = k_1\omega^2(m_1+m_2)$ from which

$$\omega_o^2 = \frac{k_1(m_1+m_2)}{m_1 m_2} \qquad \text{I.13.}$$

With the particular tuned model which has been used for the derivative measurements reported in Chapter 13, the mass m_1 was identified with the outer shell of the model, the mass m_2 with the magnetic core, k_1 with a spring in the model and k_2 with a magnetic stiffness. The response of the outer shell of this system is given by

$$\frac{X_1}{F} = \frac{k_1 + c_1\omega j}{m_1 m_2 \omega^4 - \omega^2\left[m_1(k_1+k_2) + m_2 k_1\right] + k_1 k_2 + j\omega c_1\left[k_2 - \omega^2(m_1+m_2)\right]} \qquad \text{I.14.}$$

under wind-off conditions.

List of symbols used in Appendix I.

Symbol	Meaning
c	Damping factor.
D	Operator d/dt.
f	Force.
$\|F\|$	Force amplitude.
k	Spring constant.
m	Mass.
x	Displacement from equilibrium.
$\|X\|$	Displacement amplitude.
ω_a	Antiresonance angular frequency.
ω_o	A resonant frequency of a tuned model.
ω_l	" " " " " " " with the masses locked together.

Appendix II

Multiple Staging of Lead-Lag Circuits.

If the maximum phase lead produced by a single lead-lag circuit is ϕ , then the ratio of the infinite frequency gain to the D.C. gain is given by

$$\frac{G_\infty}{G_o} = \frac{1+\sin\phi}{1-\sin\phi}$$

and if a total maximum phase-lead of α is produced by n identical lead-lag circuits staged in series, the gain ratio over the n stages is given by

$$\frac{G_\infty}{G_o} = \left[\frac{1+\sin \alpha/n}{1-\sin \alpha/n}\right]^n \qquad \text{II.1}$$

provided that there is no loading of one stage by another. For small values of α/n equation II.1 becomes

$$\frac{G_\infty}{G_o} \doteq \left[\frac{1+\alpha/n}{1-\alpha/n}\right]^n$$

and as $\left(1+\alpha/n\right)^n = e^{\alpha}$, $\left(1-\alpha/n\right)^n = e^{-\alpha}$

$$\frac{G_\infty}{G_o} \doteq e^{2\alpha} \qquad \text{II.2}$$

For $\alpha = \pi/2$, $n = \infty$, $\frac{G_\infty}{G_o} = e^{\pi} \doteq 23.1$

For $\alpha = \pi$, $n = \infty$, $\frac{G_\infty}{G_o} = e^{2\pi} \doteq 530$

The ratio of the gain at the frequency corresponding with the maximum phase lead ϕ in one stage (the "centre frequency" gain G_c) to the infinite frequency gain is given by

$$\frac{G_c}{G_\infty} = \frac{\cot\phi}{1+\operatorname{cosec}\phi}$$

and if a total phase lead of π is produced over n identical stages in series, the overall gain ratio is

$$\frac{G_c}{G_\infty} = \left[\frac{\cot \pi/n}{1 + \operatorname{cosec} \pi/n}\right]^n, \quad n = 3, 4, 5 \ldots\ldots \qquad \text{II.3}$$

For large values of n,

$$\frac{G_\infty}{G_c} \doteq \left(1 + \pi/n\right)^n \doteq e^\pi$$

and as $n \to \infty$,

$$\frac{G_\infty}{G_c} \to e^\pi \doteq 23{\cdot}1 \qquad \text{II.4}$$

Tabulated below are values of $\frac{G_\infty}{G_o}$ from equation II.1 for $\alpha = \pi/2$ and values of $\frac{G_\infty}{G_c}$ from equation II.3 for $\alpha = \pi$ for a range of values of n

n	2	3	4	7	10	∞
$\frac{G_\infty}{G_o}$, $\alpha = \pi/2$	34	27	25.2	23.6	23.2	23.1
$\frac{G_\infty}{G_c}$, $\alpha = \pi$	-	52.2	33.8	25.7	24.2	23.1

From the above argument it can be concluded that a given desired maximum phase lead should be divided between as many lead-lag stages as practically possible, in order to minimise the gain at high frequencies.

Appendix III.

System Data.

Contents:

III.1 Compensation Circuit Constants.

The tabulated data below refers to the circuits shown on Figs. 5, 11 and 14 of Chapter 7. Resistance values are given in k-ohms, and capacitance values are in micro-Farads.

Compensation Circuit.

Resistor		Lift.		Lateral		
	Roll	For^{d}.	Aft.	For^{d}.	Aft.	Drag.
R1	1	75	75	75	75	75
R2	100	9.1	9.1	9.2	9.2	9
R3	10	100	100	100	200	100
R4	20	1	1	1	75	1
R5	1000	75	75	75	10	75
R6	10	9.2	9.1	9.2	100	9
R7	250	100	100	100	1	100
R8	10	2.5	3	3	75	3
R9	10	10	15	10	0.5	15
R10	20	3.3	3	5	1	5
R11	100	10	10	2	0.5	25
R12	50					57
R13	2					5
R14						75
R15						10
R16						10
R17						5
R18						10
R19						0.22

Compensation Circuit.

Capacitor		Lift		Lateral		
	Roll	For^{d}.	Aft.	For^{d}.	Aft.	Drag
C1	0.1	0.32	0.32	0.25	0.22	0.25
C2	4.7	1	1	1	0.25	1
C3		0.22	0.22	0.22	1	1.25
C4						4.7
C5						4.7

III.2 Magnet Coil Resistances and Inductances.

The resistances have been measured by passing a steady current of 10 amperes through the coils, and measuring the potential difference across the coils, using AVO meters for the measurements. The current levels were low enough for short-period measurements to have only a small heating effect on the coils. The quoted values of resistance can be taken as applying to normal room temperature, 15-20°C.

Lift Magnets: with three winding sections in series, each leg of the horseshoe maget had a resistance of 0.61 ohm ± 0.01 ohm.

Lateral Magnets: the resistance of each winding section was separately measured, and variations exist between the limits of 0.17 and 0.23 ohm. The total resistance of the four sections of the lateral coils used for roll control, and including the circuit load resistance, was 2.09 ± 0.03 ohm.

Drag Coil: at the time of writing only half of the drag coil for the high speed wind tunnel had been wound. This section had a room temperature resistance of 1.46 ± 0.02 ohm.

The measurement of inductance was a little more involved, both in the measurement technique and in the attention that had to be given to possible coupling effects. The value of the inductance was calculated either from the time constant or the initial slope of the response of current to a step change of applied e.m.f., measured from an oscilloscope trace, and the current signal was obtained from the e.m.f. across a resistance in series with the coil. Significant inductive coupling can occur between the separate winding sections of one coil, and between the two coils

on one iron yoke. The latter form of coupling can occur between the two legs of the lift electro-magnet. The former, which would be a particularly strong source of inductive coupling, could occur between the various sections of the lateral electro-magnets: on each leg the three sections of the coil were connected to three separate power supplies, according to the wiring diagrams on Figs. 3.3 or 3.4. These particular wiring arrangements were chosen because it was anticipated that problems of model stability might occur in the presence of strong coupling effects: some forms of coupling are eliminated with these arrangements.

For example, we first consider inductive coupling of the R-C-B sections of the windings on say the two downstream legs of the lateral magnets. The three power supplies involved are roll, bias, and aft lateral position control. The bias power supply was arranged to generate a constant e.m.f. and hence a constant current provided that inductive coupling was suppressed, but the two remaining power supplies produced varying outputs for control purposes. An increasing lateral control current would tend to produce an induced e.m.f. reducing the roll current due to coupling in the left-hand coils because the two sections were connected in the same sense, each tending to increase the attraction of that leg, whereas on the right-hand leg the two sections were connected in opposite sense and an increasing lateral control current would tend to produce an e.m.f. in the roll section increasing roll current. Provided that the coil sections and iron cores are identical, the coupling effects cancel, and similarly the effects on lateral control current due to a changing roll sections current.

A similar argument applies to the coupling between roll control and bias: on the left-hand coils coupling tends to increase bias current as a result of an e.m.f. induced from increasing roll control current, but the e.m.f. is cancelled by an opposite e.m.f. from the right-hand coils.

In the case of lateral position/bias coupling, the coupling effects from the downstream legs are additive; increasing lateral position control current produces an e.m.f. tending to increase bias current on both legs. As a result of this coupling, a forced oscillation of one end of a model by means of variations of lateral control current could be expected to induce variations in the bias current, and variations in bias current would in turn affect the lateral force applied to the upstream end of the model. In general this particular form of coupling could not be suppressed. However, there were two special forcing cases in which the coupling effects could be arranged to cancel. These were the cases of forcing by lateral position control current variations of equal amplitude in the upstream and downstream legs. Uncoupled forcing either in heave or pitch could be arranged by a simple change of the arrangement of the supply connections to the upstream legs, as shown on the two wiring diagrams on Figs. 3.3 and 3.4. In these special cases, coupling effects from the downstream legs were counteracted by coupling of opposite sense in the upstream legs.

The sources of coupling so far considered can be summarised as follows:

between bias and roll: zero, resulting from cancellation,

between roll and lateral position: zero, resulting from cancellation,

between bias and lateral position: zero for the special cases of equal amplitude current variations upstream and downstream, as a result of cancellation.

It remains to consider the effects of coupling between upstream and downstream legs resulting from inductive coupling through the iron cores. In the case of roll, although there is no coupling between this supply and others, mutual coupling through the iron core could change the inductance of the roll circuit to a value greater than just the sum of the inductances of the individual winding sections obtained with the remaining five sections on one horseshoe yoke open circuit. Mutual inductance would probably have the effect of raising the inductance of the lateral position control circuits in a similar way in the case of symmetrical heave (i.e. with equal current amplitudes fore and aft) but of reducing the inductance with symmetrical pitch.

The measured inductances of the winding sections on one leg of a magnet have been measured, with the windings on the other leg open circuit. The results are tabulated below:

Arrangement:	Inductance, Henries
one section	0.008 ± 10%
two sections in series	0.034 "
three sections in series	0.076 "
two sections in parallel	0.008 "
three sections in parallel	0.008 "

The inductances were calculated from the time constants of the circuits, and any sections not in use were open circuit.

A measurement has been made of the effects of mutual inductance. The time constant for the four series connected sections

used for roll control has been measured, and the derived total inductance was 0.042 H ± 10%. Had the mutual inductance been zero, from the above table an inductance of about 0.032 H would be expected. The difference, amounting to about 30%, can probably be attributed to mutual inductance. However, the significance of a difference of this order must be regarded with some reserve because of the estimated accuracy of the inductance measurements. Consequently, for the purpose of calculating the time constants of the lateral position control circuits, which differ according to the chosen mode of excitation of the model, an approximate fixed value of inductance of 0.02 H has been assumed which could be in error by as much as 30 or 40%.

For the same reasons, a fixed value of 0.076H for the inductance of the lift magnet coils has been assumed for the purpose of calculating the control circuit Nyquist plots given in Chapter 7, irrespective of the mode of model motion being considered.

A similar measurement technique applied to the part of the drag coil which has been wound (the inner of the two sections) gave an inductance of 0.073 Henries. In this case there should be no coupling effects, and the probable accuracy of this measurement was ± 10%.

III.3 Field Stiffnesses for Some Combinations of Model and Field.

The forces and moments arising from model motion within the magnetic fields are of interest because of their effect on model control system stability and because of their influences on the dynamic behaviour of a model when subjected to a forced oscillation by means of oscillations of the magnetic fields.

A system of axes has been defined on Fig. III.1. The suspension magnet array in general can be regarded as a device subjecting the model to three forces and three moments when the model is in the datum position. These are given in Table III.1 below:

a vertical force from the lift magnets,	given suffix	vf
a moment about z axis from lift magnets,	" "	vm
a horizontal force from the lateral magnets,	" "	hf
a moment about y axis from lateral magnets,	" "	hm
a rolling moment about x axis,	" "	r
an axial force from the drag coil,	" "	d

TABLE III.1.

Forces and moments resulting from model movement in fields resulting from constant coil excitation are of interest, and it is assumed that for small displacements of the model the resultant forces and moments vary in direct proportion to the displacement.

For each model, movement in each of six degrees of freedom could in the general case produce three forces and three moments as a result of the fields arising from the generation of the three forces and three moments listed above, giving a permutation of 216possible terms, which can be assumed independant provided that the magnetisation of the model does not change with changing field strengths.

A force directed along a particular axis resulting from motion along that axis is referred to as a "field stiffness", as is a moment about an axis resulting from rotation about that axis. Six degrees of freedom are involved, and field stiffnesses can be generated

by the six forces or moments listed in Table III.1, giving 36 possible field stiffnesses. The remaining 180 possible terms are referred to as "indirect stiffnesses".

The field stiffnesses are identified by the symbol k, with suffixes specifying the displacement and origin of the stiffness in that order. Rotations of the model are given the symbols ϕ, θ, ψ positive in the clockwise sense about the x, y, z axes respectively defined in Fig. III.1. As an example, the stiffness $k_{x,\ vf}$ refers to a stiffness due to translation in the x direction in the field from the lift magnets subjecting the model to a vertical force; the force resulting from the displacement is the component directed along the x axis and when the stiffness $k_{x,\ vf}$ is positive the force is tending to restore the model to its datum position.

Table III.2 summarises the present state of knowledge of the 36 field stiffnesses, for the tuned model discussed in Chapter 13.

TABLE III.2.

	vf	vm	hf	hm	r	d
k_x	measured	zero?	$zero_1$?	$zero_1$?	measured	negative from field gradient$_4$
k_y	negative, from field gradient$_4$	zero?	$zero_1$?	$zero_1$?	not known	measured zero$_2$
k_z	measured	zero?	$zero_1$?	$zero_1$?	$zero_1$?	$zero_3$?
k_ϕ	measured $zero_7$	zero?	$zero_1$?	$zero_1$?	measured $zero_1$?	not known$_5$
k_θ	measured	zero?	$zero_1$?	$zero_1$?	$zero_1$?	measured
k_ψ	zero?	zero?	$zero_1$	$zero_1$?	not known	measured$_6$?

Notes: ? An assumption based on the layout of the electro-magnet array.

1 Resulting from the symmetry of the lateral magnets.

2 A stiffness was expected, but the measured value was small.

3 Assumed equal to $k_{z,d}$.

4 Discussed under III.4.

5 A uniformly magnetised axi-symmetric model core would give $k_{\phi,d} = 0$, but the shaped cores in association with the field from the non-circular drag coil could produce a finite value.

6 Assumed equal to $k_{\theta,d}$: this is an approximation because of a non-circular drag coil.

7 Measured during the development of roll control for the tuned model.

The values of the measured stiffnesses are given in Table III.3, and the units are as follows:

linear motion	lb/ft.
angular motion	lb.ft./radian.

Clearly the stiffnesses depend on the magnitude of the six forces or moments listed in Table III.1 applied to the model. In most cases, at the time of measurement these were the "normal" values, but in the case of the force from the drag coil there was no convenient normal value. Consequently stiffnesses involving the drag coil force are quoted per pound of drag force. The normal vertical force was taken as the weight of the model (under wind-on conditions, aerodynamic force could change the stiffnesses due to v_f). The stiffnesses arising from current supplied to the roll control sections of the lateral magnets are quoted for the normal roll current level of 15 amperes.

The most convenient method for measuring the field stiffnesses in most cases was to derive each stiffness from the natural frequency of the model when oscillating in a mode influenced by the stiffness. The vf stiffnesses were measured by oscillating the model separately in translational and rotational modes with the model suspended under control only from the lift magnet. To determine the stiffnesses due to the roll current field a steady roll current was applied and the appropriate stiffness calculated from the changed natural frequency of oscillation. In the case of stiffnesses due to the drag coil field, it was necessary to apply a steady drag force to the model by means of threads attached to pegs mounted at the centre of the model on the y-axis. The stiffnesses $k_{x,d}$ and $k_{z,vf}$ are derived in section 4 of this Appendix. The measured stiffnesses are tabulated below:

TABLE III.3.

Tuned-model field stiffnesses.

$k_{x,vf}$	1.49	$k_{x,r}$	3.19	$k_{x,d}$	-7.88/lb.
$k_{y,vf}$	-1.86				
$k_{z,vf}$	2.4				
$k_{\theta,vf}$	0.115	$k_{\theta,d}$	0.42/lb.		

Very few indirect stiffnesses have been measured. It is quite likely that a large proportion of the 180 possible are zero or negligible. However, two values were measured because they could influence derivative measurements made with the tuned model; both originate from the drag coil field.

One indirect stiffness was the force due to the drag coil field in the z direction resulting from angular displacement θ, and

as this varies with the drag-coil field it is quoted per unit drag force. The stiffness is given the symbol $Z_{\theta,d}$. The second stiffness was the moment about the y-axis resulting from displacement in the z direction, given the symbol $M_{z,d}$. These stiffnesses were determined from measurements made with the model suspended with a drag force applied mechanically, by measuring the forces and moments required from the lateral coils to translate or rotate the model, and noting the changes associated with changes of drag force. The values are given below:

$Z_{\theta,d}$ = 1 lb./radian/lb.drag force; $M_{z,d}$ = 1.35 lb.ft./ft./lb.drag force.

The force is taken as positive directed away from the axis origin, and the moment as positive in the clockwise sense. In applying these stiffnesses, it has to be remembered that they refer to movement of the magnetic core in the fields, not to the outer shell.

A few field stiffnesses have been measured for the solid body of revolution, where required for the calculation of Nyquist plots. The values are given in Table III.4 below:

TABLE III.4.

Field stiffnesses for solid body of revolution.

$k_{y,vf}$ = -2.05 $k_{z,vf}$ = 2.20 $k_{\theta,vf}$ = 0.19

III.4 Field Gradient Constants in the Lift and Drag Coil Force Calibrations.

III.4.1 The tuned model.

At the datum position of the model, the sum of the currents in two legs of the lift magnet required to support the model weight of 0.571 lb. was 24.8 amps., hence for the lift magnet:-

$b_1 = \left(\frac{\partial f}{\partial i}\right)_{\bar{y}} = \frac{0.571}{24.8} = 0.023$ lb./amp., using the notation of Chapter 7.

By moving the model vertically from its datum position, the current required to support the weight varies because of the field gradient. Movement of the model downwards away from the lift magnet (negative values of δy) increases the current requirement. From equation 7.8 for a constant force we can write

$$b_1 \delta i + b_2 \bar{i}\, \delta y = 0$$

and from a measurement of δi corresponding with a small movement away from datum, the value of $b_2 = \left(\frac{\partial f}{\partial y}\right)_{\bar{i}}$ may be determined. For the tuned model this was 0.15 lb./ft. per ampere for each leg of the electro-magnet, giving $\bar{i}\, b_2 = 1.86$ lb./ft.

For the drag coil, the constant b_1 applicable to the datum position of the model was determined by applying an axial force to the model and calibrating force against current (a linear calibration for a permanent magnet model), an example of which is included in Chapter 5 giving b_1 for the drag coil of 1/97 lb./ampere (for the tuned model, over a period of several months the calibration of this constant lay within the range 1/99 lb./ampere $\pm$ 3%). The constant is applicable only to the inner half of the drag coil, and by definition to constant model position.

The constant b_2 could be determined by re-calibrating drag force against current at a different model position, or in practice more conveniently by drawing the model in the upstream direction by the drag coil against known field stiffnesses, and determining from the difference between the current required to hold the model

in a given displaced position and the current which would have been required had k_2 been zero. The latter technique gave $k_2 = 0.0773$ lb./ft. per ampere in the drag coil inner winding, or around 7.7 lb./ft. per lb. drag force.

III.4.2 The solid body of revolution.

Identical measurement techniques applied to this model gave, for the lift magnet: $k_1 = 0.0208$ lb./ampere, $k_2 = 0.134$ lb./ft. per ampere) for each leg

and $k_1 \bar{i} = 2.05$ lb./ft., the current in each leg required to suspend the model being 15.3 amps.

The constant k_1 for the drag coil was 1/93.7 lb./amp. (see Chapter 5), but k_2 has not been measured.

III.5 Model Data.

Model weights:

Tuned model: 9.14 oz. (0.571 lb.)

Solid body of revolution: 10.2 oz. (0.637 lb.)

Roll derivative model: 11.31 oz. (0.708 lb.)

(see Chapter 10).

Moments of inertia:

	Axis (see Fig. III.1)		
Model	x	y	z
Tuned (core	(combined	54.6_2	(combined
Tuned (shell	(6.28	35.0_2	(89.6_1
Body of revolution	-	154.5	154.5_1
Roll derivative	7.04	-	-

Units are lb.ft.^{2} x 10^4.

Notes: 1: The values for the z-axis are assumed equal to those for the y-axis.

2: See Chapter 13 for the derivation of these figures.

The damping forces applied to models in still air.

Data under this heading is included more appropriately in Chapter 10 for the Roll Derivative model. For the tuned model and the body of revolution (which are the subjects of Chapters 12 and 13) the damping of oscillations induced by field stiffnesses in several degrees of freedom have been measured, by photographing the oscillations displayed on an oscilloscope and determining the decay rates of the natural oscillations. In each degree of freedom the model was assumed to behave as a single degree of freedom system under the action of a force proportional to displacement, and a damping force proportional to the velocity of the model (the system shown on Fig. 7.1 (b)) The damping coefficient is given by

$$c = \frac{2m}{t} \log_e \frac{x_o}{x}$$

where m = mass of model (or moment of inertia for rotational modes) and x_o, x are the amplitudes of motion at two points during the decay separated by time t .

Table III.5 below summarises the available data:

Mode of motion:	Translation in z direction	rotation about y axis, at roll current zero	15 amps.
Tuned model:	-	0.10	0.2 *
Body of revolution:	0.75	0.11	-

Units: in translation, lb. per ft./sec. x 10^4

in rotation, lb.ft./ radian per sec. x 10^4.

* This value was estimated from a large extrapolation from a measurement taken at 3.7 amps. roll current, and hence must be regarded as very approximate.

The damping forces measured in this way could originate from eddy currents or from aerodynamic forces. However, measurements

made with the working section filled with helium instead of air gave no significant change of damping. The ratio of the densities of these two atmospheres was 1/7 . This suggested that most of the damping was due to eddy currents.

Compared with other damping forces present in the system, those discussed above are unimportant. In the tuned model, damping between the shell and inner core was an order of magnitude greater, and was measured in two ways. In Chapter 13 the damping was measured by forced oscillations of the model. However, as a check on the value obtained a separate measurement was made using a decaying oscillation technique.

The core of the model was clamped, and the shell (with the nose and tail removed to allow the core to be clamped) was monitored optically during decaying natural oscillations, from which the damping between shell and core was determined at 2.8 $/10^4$ lb.ft. radian per sec. At the same time the opportunity was taken to measure the stiffness of the spring system in the model. This measurement gave 0.867 lb.ft./radian, but a slightly different value was later adopted as explained in Chapter 13.

It is likely that the energy loses represented by this damping occur in the end-fixings of the springs.

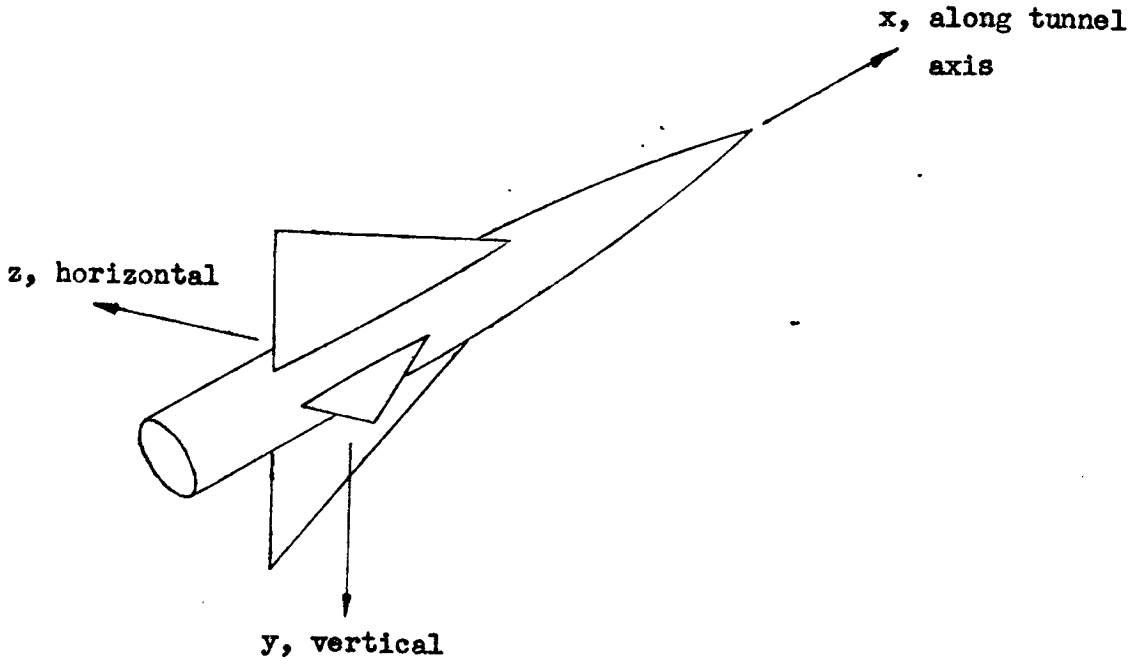

Fig. III.1 The axis system used in defining the magnetic stiffnesses. The stiffnesses are given a positive sign when they act as a spring tending to restore the model to its datum position, which is with its axis lying along the tunnel axis, at the correct roll attitude (usually with the wings upright on this system as shown above), and at a prescribed fore-and-aft position.

Appendix IV. The Theoretical Rolling Moment Capacity of Magnetically Suspended Shaped Cores.

Contents:

LIST OF SYMBOLS

a	defined on Fig.IV.4.
b	thickness of shaped core.
b_m	core thickness giving the maximum moment
D	the ratio r_o/g
f	force
F	non-dimensional force
g	defined on Fig.
I	intensity of magnetisation of the core material
j	the ratio of the thickness of a core to the semi-width
m	distance between an elemental pole in the shaped core and the near pole of the horse-shoe magnet
p	equivalent pole strength of a leg of the horse-shoe magnet
Q, R	non-dimensional forms of b, x respectively, used in section IV.3
r	radius of an element in an optimum core
r_o	maximum radius of optimum core
s	the distance between the poles in a horse-shoe magnet
t	moment about model axis
T, T'	non-dimensional forms of rolling moment
x	position along the major axis of the core, measured from the centre outwards
x_o	the semi-width of the core cross section
A, B, G, X, X_o	non-dimensional forms of a, b, g, x, x_o respectively used in section IV.2
ϵ	a thickness of pole elements, used in section IV.3
θ	the rotation of the major axis in a rolling sense out of the plane including the core axis and the horse-shoe poles.

IV.1. The principles of moment production.

The magnetic suspension system which has been constructed at Southampton University makes use of three horse-shoe shaped electro-magnets together with one hollow solenoid-like coil for the control of the position of the wind tunnel model in six degrees of freedom, the model itself containing a permanent magnet. A schematic arrangement of these magnets is shown in Fig.IV.1,suitably disposed to suspend a model in the horizontal working section of a wind tunnel. The drag force is resisted by the action of coil A wound around the wind tunnel, and the weight of the model is taken by the horse-shoe electro-magnet B. The control of the lateral position and the roll attitude of the model is by means of the two horse-shoe electro-magnets C and D, and it is the mechanism of the control of roll which is to be explained in this section.

As mentioned above, the model contains a magnetic core, and the core is arranged to lie along the axis of the model. The usual practice has been to use cores having circular cross sections, but such cores do not impart any resistance to disturbances in roll. However, if a core having a non-circular cross section is carried in the model, the core will adopt preferred roll attitudes when suspended in the field of the model supporting magnet, B in Fig.IV.1. The number of equilibrium roll attitudes that the core can adopt depends upon the shape of the cross section of the core. For example, a core having a square cross section will adopt any of the four attitudes with a corner uppermost. A rectangular core can have two equilibrium attitudes, the two attitudes where the narrow edge is uppermost.

Rotating such a core away from the equilibrium attitude requires the application of a moment varying very nearly as $\sin 2\theta$, where θ is the displacement in roll away from equilibrium. Hence the maximum moment that the support magnet B can generate on the core occurs when the major

axis of the cross section of the core is displaced about 45° away from the vertical. The same property applies to the influence on the core of the fields generated by the two remaining horse-shoe magnets, C and D in Fig. IV.1, lying in the horizontal plane through the model axis, namely that the maximum moment that these magnets can generate occurs when the model roll attitude is 45° out of the plane of the magnets.

In Fig.IV.2 an end view of a rectangular cross-sectioned core is shown, together with one pole corresponding with the poles in each adjacent end of the three horse-shoe electro-magnets. As will be shown later, in addition to force components acting through the core axis, the model weight supporting pole B generates an anti-clockwise moment about the model axis, which is very nearly a maximum for a given pole strength with the core in the position shown. Similarly each lateral pole generates its own force components and moment, but in the case of these poles the force components cancel one another for equal lateral (horse-shoe) pole strengths whereas the moments generated are additive and in opposite sense to that generated by B. Consequently such a core suspended magnetically would experience a fixed anti-clockwise moment from the support magnet, which can be opposed by an equal and opposite moment as a result of the two lateral magnets attracting the core equally with an appropriate field strength. Because of the cancellation of force components from the lateral magnets, they have no influence upon the position of the model. By varying the strength of the lateral poles away from that value which just has the effect of opposing the fixed anti-clockwise moment resulting from the support magnet field, the magnetic core of the model can be made to oppose any disturbing rolling moment that might be applied to the model. This roll control principle can allow the exertion of lateral forces and yawing moments upon the model by the lateral magnets without at the same time disturbing the magnitude

of the rolling moment. The mechanism for the simultaneous control of lateral bodily motions and rolling motions of the model with the lateral electro-magnets will now be discussed.

It would be possible to exert a lateral force on the magnetic core of the model by increasing the strength of the pole of one of the lateral magnets, say pole C in Fig.IV.2, but if this was done without changing the strength of pole D there would be a change of rolling moment generated by the shaped core because the net moment generated by the two lateral magnets is additive. To avoid this rolling moment change the technique can be adopted of reducing the strength of one of the lateral electro-magnet poles by the same amount that the other has its strength increased. In this way the net rolling moment would remain constant, while the required lateral force would be generated. If corresponding changes equal in magnitude but of opposite sign (because of the opposite polarity) were made at the other ends of the two lateral horse-shoe magnets, a lateral force would be generated on the core, the line of action of the force passing through the centre of the model. Similarly, if changes of the same sign were made at the other ends of the lateral magnets, a pure yawing moment would be generated on the model, again acting about its centre, assuming that the magnetic core of the model was symmetrically disposed relative to the electro-magnet array. Combinations of unequal changes of pole strengths of the lateral magnets, as between the upstream and downstream ends, would have the effect of producing a yawing moment and side force simultaneously without disturbing the rolling moment, provided that at all times the pole strength change of one lateral magnet pole adjacent to a given end of the model is matched by an equal and opposite change to the strength of the lateral magnet pole on the other side of the wind tunnel adjacent to the same end of the model.

Theories covering some aspects of moment and force production by shaped cores are now considered, using simplified mathematical models invoking classical magnetic pole theory, with modifications.

IV.2 The theory of slender cores.

IV.2.1 One possible shape for a rolling moment generating core is a strip of magnetic material having a slender cross-section, rectangular in form. The magnetic poles in such a core are here assumed to consist of uniform line distributions near the ends of the core, rather than to be the point sources of magnetism assumed in classical theory. The assumed disposition of the poles is shown in Fig.IV.3. Each of these distributions, which in this slender-core theory are assumed to be line distributions, is acted on by both poles of an adjacent horse-shoe electro-magnet. The theory below gives the rolling moment and three force components generated by one such line distribution of poles when acted upon by the magnetic field produced by both equally energised poles of one horse-shoe electro-magnet. To calculate the net forces and rolling moment for a symmetrically disposed model the results merely require doubling, except in the case of the axial force component f_a, where the net force is zero.

The geometrical arrangement of the core and the two horse-shoe magnet poles is given on Fig.IV.4. Three elemental force components are defined, as generated by an element of the line of poles within the core, under the action of the nearest horse-shoe pole. Two of these components, namely δf_v and δf_h, contribute to the rolling moment.

The resultant of the three force components, δf, is given by

$$\delta f = pIb\,\delta x / m^2 \qquad \text{—— (IV.1)}$$

where b and δx are defined on Fig.IV.4, and

I is the intensity of magnetisation of the core (unit poles per unit area)

$|p|$ is the pole strength of the poles in the horse-shoe magnet.

m is the distance between the elemental pole in the shaped core and the near pole of the horse-shoe magnet.

For this core it is assumed that $b \ll 2c$.

The force components of δf are

$$\left.\begin{aligned} \delta f_v &= \delta f\,(g - x\cos\theta)/m \\ \delta f_a &= \delta f\, a/m \\ \delta f_h &= \delta f\, x\sin\theta/m \end{aligned}\right\} \quad \text{—— (IV.2)}$$

where $m^2 = g^2 + a^2 + x^2 - 2xg\cos\theta$

As mentioned above, the components δf_v and δf_h contribute to the rolling moment δt

where $\delta t = \delta f_h \cdot x\cos\theta + \delta f_v\, x\sin\theta = \delta f\, \frac{xg}{m}\sin\theta$ —— (IV.3)

positive when the moment is anti-clockwise viewed from the left of Fig. IV.2.

At this stage it is convenient to write several of the terms in the above equations in non-dimensional form. For this write

$$g/s = G\,, \quad a/s = A\,, \quad x/s = X\,, \quad b/s = B$$

then $m^2 = s^2(G^2 + A^2 + X^2 - 2XG\cos\theta)$

and the three force components can be written in the non-dimensional form

$$\left.\begin{aligned} \frac{\delta f_v}{pIB} &= \frac{(G - X\cos\theta)\,\delta X}{(G^2 + A^2 + X^2 - 2XG\cos\theta)^{3/2}} = \delta F_v \\ \frac{\delta f_a}{pIB} &= \frac{A\,\delta X}{(G^2 + A^2 + X^2 - 2XG\cos\theta)^{3/2}} = \delta F_a \\ \frac{\delta f_h}{pIB} &= \frac{X\sin\theta\,\delta X}{(G^2 + A^2 + X^2 - 2XG\cos\theta)^{3/2}} = \delta F_h \end{aligned}\right\} \quad \text{—— (IV.4)}$$

and a non-dimensional form of δm is

$$\frac{\delta t}{pIb} = \frac{GX\sin\theta\,\delta X}{(G^2 + A^2 + X^2 - 2XG\cos\theta)^{3/2}} = \delta T \quad \text{—— (IV.5)}$$

hence $\delta T = G\,\delta F_h$ —— (IV.6)

Equations IV.4 - 6 give three force components and the rolling moment about the model axis, due to the near horse-shoe magnet pole. The effect of the far horse-shoe pole is accounted for by repeating the equations with $a+s$ in place of a ($[A+1]s$ in place of As), and deducting the resulting forces and moment. The alteration involves changing the denominators to

$$\left[G_1^2 + (A+1)^2 + X^2 - 2XG\cos\theta\right]^{3/2}$$

Integrating the expression for δF_v between the limits $X = \pm X_o$ gives, for both poles of the horse-shoe electro-magnet acting on one end of the slender shaped core

$$F_v = \frac{X_o}{G + \frac{A^2}{G\sin^2\theta}}\left(\frac{1}{u_1}+\frac{1}{v_1}\right) + \frac{\cos\theta}{1+\left(\frac{G\sin\theta}{A}\right)^2}\left(\frac{1}{u_1}-\frac{1}{v_1}\right) - \frac{X_o}{G+\frac{(A+1)^2}{G\sin^2\theta}}\left(\frac{1}{u_2}+\frac{1}{v_2}\right) - \frac{\cos\theta}{1+\left(\frac{G\sin\theta}{1+A}\right)^2}\left(\frac{1}{u_2}-\frac{1}{v_2}\right) \quad \text{—— (IV.7)}$$

where $u_1 = \left[X_o^2 + G^2 + A^2 - 2GX_o\cos\theta\right]^{1/2}$

$v_1 = \left[X_o^2 + G^2 + A^2 + 2GX_o\cos\theta\right]^{1/2}$

$u_2 = \left[X_o^2 + G^2 + (A+1)^2 - 2GX_o\cos\theta\right]^{1/2}$

$v_2 = \left[X_o^2 + G^2 + (A+1)^2 + 2GX_o\cos\theta\right]^{1/2}$

$$F_h = \frac{\sin\theta}{\frac{A^2}{G^2}+\sin^2\theta}\left[\frac{X_o}{G}\cos\theta\left(\frac{1}{u_1}+\frac{1}{v_1}\right) - \left(1+\frac{A^2}{G^2}\right)\left(\frac{1}{u_1}-\frac{1}{v_1}\right)\right] - \frac{\sin\theta}{\left(\frac{A+1}{G}\right)^2+\sin^2\theta}\left[\frac{X_o}{G}\cos\theta\left(\frac{1}{u_2}+\frac{1}{v_2}\right) - \left(1+\frac{(A+1)^2}{G^2}\right)\left(\frac{1}{u_2}-\frac{1}{v_2}\right)\right] \quad \text{—— (IV.8)}$$

$$F_a = \frac{A/G}{\frac{A^2}{G^2}+\sin^2\theta}\left[\frac{X_o}{G}\left(\frac{1}{u_1}+\frac{1}{v_1}\right) - \cos\theta\left(\frac{1}{u_1}-\frac{1}{v_1}\right)\right] - \frac{(A+1)/G}{\left(\frac{A+1}{G}\right)^2+\sin^2\theta}\left[\frac{X_o}{G}\left(\frac{1}{u_2}+\frac{1}{v_2}\right) - \cos\theta\left(\frac{1}{u_2}-\frac{1}{v_2}\right)\right] \quad \text{—— (IV.9)}$$

and $T = G.F_h$ —— (IV.10)

Values of the force components F_v and F_h and the rolling moment T have been computed over the range of interest of the variables G, A, θ, X_o

in a comprehensive manner in the following ranges:

G from + 0.4 to + 1.2

A from − 0.2 to + 0.4

θ from 20° to 60°

X_o from + 0.04 to + 0.08

with a small amount of additional data at $\theta = 45^\circ$ extending the range of A down to − 0.4.

Fortunately, it is unnecessary to present all of the data in the form of curves, because the effects of some of the variables, in the range investigated, can be summarised without introducing errors of practical significance.

Each of the force components and the rolling moment, which will be considered individually, are functions of the above four variables.

The non dimensional force component F_v can be summarised with the aid of Fig.IV.5, on which F_v is shown plotted against A, for two values of X_o over the complete range of G. No values of θ are quoted on the diagram, and this is because, within the quoted range of variables, θ has little effect on F_v. The curves are most accurate at the higher values of G and to illustrate the error involved by ignoring the effect of θ, two examples are given below for $X_o = 0.08$, $A = 0$

(a) for $G = 0.4$, at $\theta = 20^\circ$, $F_v = 0.98282$

at $\theta = 60^\circ$, $F_v = 0.94352$

where the percentage change of F_v is 4.3

(b) for $G = 1.2$, at $\theta = 20^\circ$, $F_v = 0.06115$

at $\theta = 60^\circ$, $F_v = 0.06072$

where the percentage change of F_v is 0.7

The two sets of curves given on Fig.IV.5, exhibit very nearly a linear variation of F_v with X_o, other variables remaining constant. In order

to illustrate the maximum errors that are involved in making this assumption of linearity, consider what is probably the worst case, $A = 0$, $G = 0.4$, with $\theta = 20^\circ$. At $X_o = 0.04$, $F_v = 0.47857$, whereas at $X_o = 0.08$, $F_v = 0.98282$. The ratio of these two force components is 2.05366, only 2.7% different from the figure that would have been obtained had the relationship between F_v and X_o been linear.

The force component F_h is rather small, within the range of variables considered, and the data is here presented for convenience in the form of the ratio F_h/F_v. There are two reasons for choosing to present the F_h data in this way. The first is that the strong variation of F_h with G does not show, but can be accounted for by referring to Fig. IV.5. The second is that in practice the ratio is important when considering force-coupling, a topic dealt with in section IV.2.2. The ratio is a very weak function of A and G, but varies more strongly with X_o, as shown on Fig. V.6. In fact, to a close approximation, F_h/F_v can be assumed to vary as X_o^2 for particular values of A, G and θ. The likely errors, at constant $\theta = 45^\circ$, resulting from this assumption are illustrated by the following example:

with $G = 0.6$, $A = -0.1$

at $X_o = 0.04$, $F_h/F_v = 0.0024809$

whereas with the same values of G and A

at $X_o = 0.08$, $F_h/F_v = 0.0099149$

The second ratio is 3.9965 times the first.

The variation of F_h with θ closely follows a $\sin 2\theta$ law, consequently as F_v is relatively insensitive to θ, the above example at $\theta = 45^\circ$ probably represents a worst case. Certainly this attitude is the one of most practical interest.

The rolling moment data is presented in the form of the ratio T/F_v for convenience. The variation of T/F_v with θ is shown on Fig. IV.7 for $X_o = 0.08$, $A = 0$, where, for a particular value of G, T/F_v varies

as $\sin 2\theta$, to a close approximation. The maximum distortion occurs at $G = 0.4$, where the peak occurs at about $\theta = 44^{\circ}$. The variation of this ratio with A is shown on Fig.IV.8 for two values of X_o over the full range of G , at constant $\theta = 45^{\circ}$. In order to show the values of A giving the peak non-dimensional moment T , Fig.IV.9 is included. Here it can be seen that, within the range $0.6 \leq G \leq 0.9$ a maximum moment would be obtained with $0 < A < 0.05$

T/F_v varies nearly as X_o^2 (because F_h varies in the same way) and the errors involved in adopting this assumption are identical with those applying to F_h , from equation IV.10.

It is interesting to note that for constant $b/X_o = j$, $G, A,$ and θ , the rolling moment generated by a shaped core is

$$\frac{t}{pIBs} = T = \phi(X_o, G, A, \theta)$$

and at constant $G, A, \theta,$

$$T = kX_o^3 \qquad \text{where } k \text{ is a constant}$$

Now, $\quad Bs = b = jX_o$

hence $\quad t = kpIjX_o^4$

Therefore with given values of p, I etc., the rolling moment capacity of a shaped core varies as the fourth power of the scale of the cross-section, provided that the proportions of the cross-section are held constant (i.e. constant j).

IV.2.2. The practical effects of the force component F_h require some comment. Referring to Fig.IV.2, the component F_h from magnet B is a horizontal force to the left, which must be resisted by magnet D being more strongly energised than C. The lateral force involved mainly depends upon

the size of the model core, but in practice the force would probably be less than 1% of the model weight. The lateral magnets C and D themselves generate F_h components, acting vertically upwards and downwards respectively. With the lateral magnets energised equally, because of the symmetry of the system the two components would cancel. However, circumstances can occur where the two horse-shoe magnets have significant differences in strength, for example, when a large lateral aero-dynamic force must be resisted, or alternatively when it is desired to oscillate the model laterally. The lateral force would be generated by increasing the energisation of one lateral magnet and reducing the energisation of the other, to maintain a constant rolling moment. In these circumstances the two F_h components from the lateral magnets would no longer cancel (except for the roll attitude of 0°, 90° etc., which are of no interest). The net vertical force resulting from the unbalance constitutes a force coupling, and in the case of lateral oscillation of the model there would be a periodic component of force, and hence motion, in the vertical plane. The magnitude of the coupling can be estimated from Fig.IV.6 if required, but because the ratio F_h/F_v is small (at least for the values of X_o and G of interest) the force coupling would be correspondingly small.

IV.3. The optimum thickness of rectangular or circular-based cores.*

The analysis in the preceeding section, while usefully indicating trends and also the effects of some variables on the moment and force capacity of slender rectangular cores, becomes inaccurate when applied to cores of useful thickness with regard to

(i) the force component f_h

(ii) the rolling moment t

For example, if the core thickness b was increased until it equalled $2x_o$, (the case of a square cross-section), the above force and moment would be zero at $\theta = 0^\circ$, 45°, 90° etc., but not at attitudes

* The word "optimum here refers to the rectangular sectioned core which will generate the maximum rolling moment, for given values of x_o etc.

between these. Hence at $\theta = 45^{\circ}$ and with a given x_o, the moment generated by a rectangular core is zero at $t = 0$, rises to a maximum in the range $0 < t < 2x_o$ and falls again to zero at $t = 2x_o$, in the manner shown below

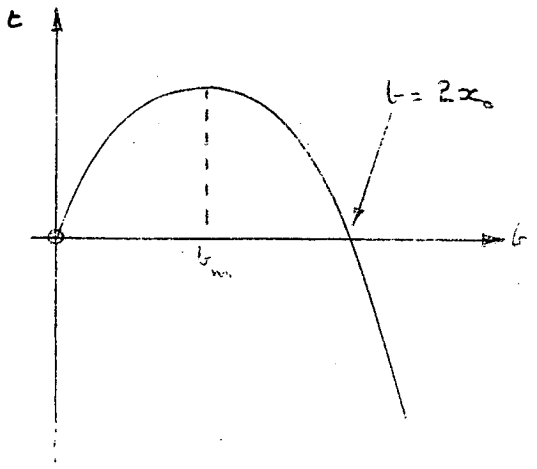

In this section a method is given for calculating the value of t corresponding with the peak of the $t - t$ curve.

IV.3.1. The special case is considered of $a = 0$ and $s \gg g$. A diagram showing the core cross-section and the near horse-shoe magnet pole is given on Fig.IV.10. The core is assumed to be uniformly magnetised, the area distribution of poles being affected by the near horse-shoe pole but not by the far pole. The convenience a set of cartesian axes is established with the origin on the core centre-line.

The calculation of the optimum core thickness for maximum moment is based on the following reasoning. Suppose a value of t is chosen between the values 0 and t_m. If now two thin layers of core material are added, each of thickness ϵ, so that the total thickness becomes $t + 2\epsilon$ the total moment generated by the core will increase, (provided that $\theta \neq 0^{\circ}, 90^{\circ}$ etc.) even though the layer nearer to the horse-shoe pole p of Fig.IV.10 might be generating a negative moment about the model axis. As the value of t is increased towards t_m the addition of thin layers (which might be considered as line distributions of poles) will have

less effect upon t until at $b = b_m$ adding the two lines of poles will have no net effect; the positive moment from the lower right line of poles will just balance the negative moment from the upper left line. This balance will be used as a test for the correct value of b_m .

The moment generated by an element δx of a line distribution of poles at position b , is given by

$$\delta t = p I \epsilon c \, \delta x / m^2$$

where $m^2 = b^2 + x^2 + g^2 + 2g(b \sin\theta - x\cos\theta)$

and $$c = \frac{g}{m}(b\cos\theta + x\sin\theta)$$

hence $$\frac{\delta t}{p I \epsilon g} = \frac{(b\cos\theta + x\sin\theta)\,\delta x}{[x^2 + b^2 + g^2 + 2g(b\sin\theta - x\cos\theta)]^{3/2}}$$

Put $b/g = Q$, $x/g = R$

then $$\frac{\delta t}{p I \epsilon} = \delta T' = \frac{(Q\cos\theta + R\sin\theta)\,\delta R}{[R^2 + Q^2 + 1 + 2(Q\sin\theta - R\cos\theta)]^{3/2}}$$

This elemental moment is how integrated along the line, between the limits R_o and $-R_o$ corresponding with $x = +x_o$ and $x = -x_o$:

$$T' = \left[\frac{Q\cos\theta(R - \cos\theta) - \sin\theta(Q^2 + 1 + 2Q\sin\theta - R\cos\theta)}{(Q^2 + 1 + 2Q\sin\theta - \cos^2\theta)[R^2 + Q^2 + 1 + 2(Q\sin\theta - R\cos\theta)]^{1/2}} \right]_{-R_o}^{R_o}$$

This expression, evaluated at $Q = b_1/2g$ gives the non-dimensional moment generated by the line distribution of poles on the lower right face of the core, Fig. IV.10, and the moment is designated T_{Q+} . The corresponding non-dimensional moment from the upper left face of the core is obtained by

substituting $Q = -b_1/2g$ and integrating between the same limits, giving T_{Q-}. The test for $b_1 = b_m$ is $T_{Q+} + T_{Q-} = 0$

IV.3.2. Values of b_m have been computed for several values of R_o ranging from 0.04 to 0.3, at $\theta = 45^\circ$. The residual moment $T_Q = T_{Q+} + T_{Q-}$ is shown plotted on Figs.IV.11 (a) and (b) against the core thickness to width ratio (i.e. $b_1/2x_o = Q/R_o$) as abscissa. For each value of R_o several values of T_Q have been calculated for b_1 close to b_m.

The conclusion is that over a wide range of core sizes relative to the separation of the core from the horse-shoe magnet, the maximum rolling moment would be obtained with a thickness to width ratio of 0.575 - 0.584, the trend being from the lower value to the higher as R increases through the range.

IV.3.3. Wind tunnel models frequently employ fuselages of circular cross section, and within the confines of this shape one can accomodate a core having basically a circular section, machined with two similar diametrically opposite flats so that its cross-section is comparable with a rectangle, as shown below in the 45° attitude.

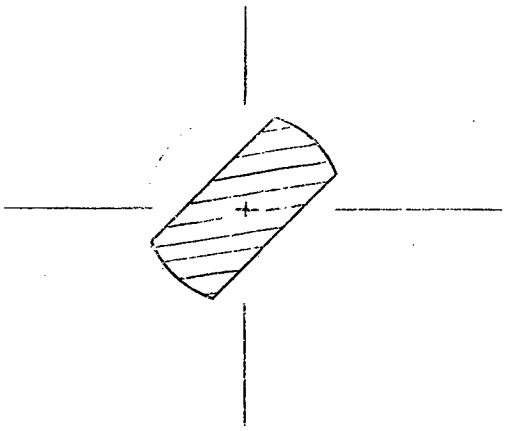

The analysis of section IV.3.1 can also be applied to this circular based core, to give an optimum value of the ratio core thickness to width of flats. This results in the optimum thickness to diameter ratio for this type of core of almost exactly 0.5, within the investigated range

$$0.04 \leq \frac{\text{width of flats}}{g} \leq 0.3$$

IV.4 The moment capacity of the optimum "shaped core".

The principle of moment generation by shaped cores relies upon some parts of the core being attracted more strongly than others by the horse-shoe electro magnet. The maximum moment is achieved when the major axis of the cross-section is more or less in the 45° attitude. Referring again to the core and pole B shown in Fig.IV.2, it can be seen that core material in the top right quadrant is attracted more strongly to B than material in the lower left quadrant. However, core material in the top left and lower right quadrants contributes a moment opposite to that required, reducing the net moment generated by the core. Evidently a thick rectangular core is not the best that could be devised, because if there was no material in the latter quadrants, the net moment would be greater. To give some idea of the penalty arising from using such a core the case of the optimum rectangular core can be considered being made up of two parts as shown below:

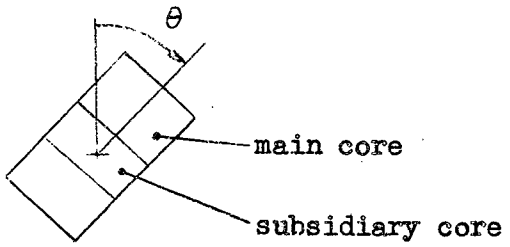

The thickness : width ratio of the main core is assumed to be 0.58, with its major axis inclined at $\theta = 45^{\circ}$. Part of this core could be looked upon as a subsidiary core with its major axis at $\theta = -45^{\circ}$, again with a thickness : width ratio of 0.58.

As shown in Section IV.2, the moment generating capacity of slender cores varies as the fourth power of the scale - assuming geometric similarity. If this law applies to thick cores as here considered, then an estimate can be made of the negative moment generated by the subsidiary core, assuming that the whole core generates a positive moment.

The subsidiary core is a scaled version of the main core, the scaling factor being 0.58. The moment generated by this part of the main

core would be $-0.58^4 = -0.1135$ of that from the main core. Hence, if this section were removed, the net moment would be increased by about 13%. However, this argument can be taken further : account could be taken of the fact that the subsidiary core itself contained some material which contributed a small positive moment because this material resided in the top right and lower left quadrants.

With this roll control system a core must be used which is symmetrical either side of the minor axis of the cross section. Any material which lies in the top right quadrant, in conjunction with the corresponding material in the lower left quadrant, would generate a positive (anti-clockwise) moment under the action of magnet B, Fig.IV.2. The moment would increase with an increase in the amount of magnetic material in these quadrants. Any material in the remaining two quadrants would reduce the rolling moment. Hence, one can arrive at an "optimum" shape of core contained within a circular cross-section of model fuselage, as shown in Fig.IV.12.

A theoretical expression can be derived for the moment that such a core would generate, in the 45° attitude shown on Fig.IV.12, assuming that the shaded areas are planar distributions of poles. Similar assumptions are made to those in the preceeding section, namely that only the near pole of the horse-shoe magnet need be considered, and that this pole lies in the same plane as the core poles. A diagram of the horse-shoe pole and one quadrant of the core is shown on Fig.IV.13.

The pole strength of an element of the core is $I r \delta r \delta\alpha$

and the elemental force $\delta f = p I r \delta r \delta\alpha / m^2$

where r is the radius of the element measured from the model axis.

The moment generated by this force element about the model axis is

$$\delta\epsilon = \frac{p I g r^2 \sin\alpha}{m^3} \delta r \delta\alpha$$

where $m^2 = r^2 + g^2 - 2rg\cos\alpha$

The total moment from both quadrants, covering the α range of 0° to 90° and 180° to 270° is given by

$$t = pI_g \int_0^{r=r_o} \int_0^{\alpha=\pi/2} \frac{r^2 \sin\alpha \, dr \, d\alpha}{(r^2+g^2-2rg\cos\alpha)^{3/2}} + pI_g \int_0^{r=r_o} \int_{\alpha=\pi}^{3\pi/2} \frac{r^2 \sin\alpha \, dr \, d\alpha}{(r^2+g^2-2rg\cos\alpha)^{3/2}}$$

$$= pI \int_0^{r=r_o} \left\{ \frac{r}{(r^2+g^2-2rg)^{1/2}} + \frac{r}{(r^2+g^2+2rg)^{1/2}} - \frac{2r}{(r^2+g^2)^{1/2}} \right\} dr$$

hence $$\frac{t}{pI_g} = 2 - \log_e (1-D^2) - 2(1+D^2)^{1/2} \qquad \text{(IV.11)}$$

where $D = r_o/g$

Using the series expansions for the second and third terms on the right hand side of equation IV.11, and ignoring the sixth and higher powers of D one obtains

$$t = \frac{3pI_g}{4} D^4 \qquad \text{(IV.12)}$$

Equation IV.12, which is only valid for low values of r_o/g, shows that the moment generated by this type of core varies as the fourth power of the radius, for a given value of g; a similar conclusion was reached for the slender rectangular cores considered in section IV.2.

IV.5. General observations.

(a) on the slender core data:

(i) At a constant thickness to width ratio, the rolling moment generated varies as the fourth power of the width.

(ii) The maximum rolling moment occurs with the major axis of the cross-section rotated in a rolling sense about 45° out of the horse-shoe magnet - core axis plane.

(iii) The force component at right angles to this plane is small, for core sizes of interest.

(iv) Maximum force components and rolling moment occur with cores having

pole lengths slightly greater than the distance between the two poles in the horse-shoe magnet, other factors remaining constant.

(b) on the optimum proportions of thick rectangular or circular based cores:

(i) For cases where the magnetic affects of the horse-shoe pole furthest from a core pole can be ignored, and where the core pole length equals the distance between the horse-shoe magnet poles, the optimum thickness to width ratio for maximum rolling moment from a rectangular sectioned core is about 0.58.

(ii) In cases where the core is manufactured from a circular sectioned bar by machining diametrically opposite flats, (the circular based core) the optimum thickness to diameter ratio is about 0.5.

(c) on the rolling moment generated by the optimum shaped core:

the moment varies as the fourth power of the core radius, other factors remaining constant. This strictly applies only in situations where the core pole-length is equal to the distance between the horse-shoe magnet poles etc., as under (b) (i) above. However, as a similar conclusion was reached for slender rectangular cores, valid over a wide range of core length, it might be assumed that the law would also apply to thick rectangular cores, circular based cores and "optimum" cores over a similar range of core lengths.

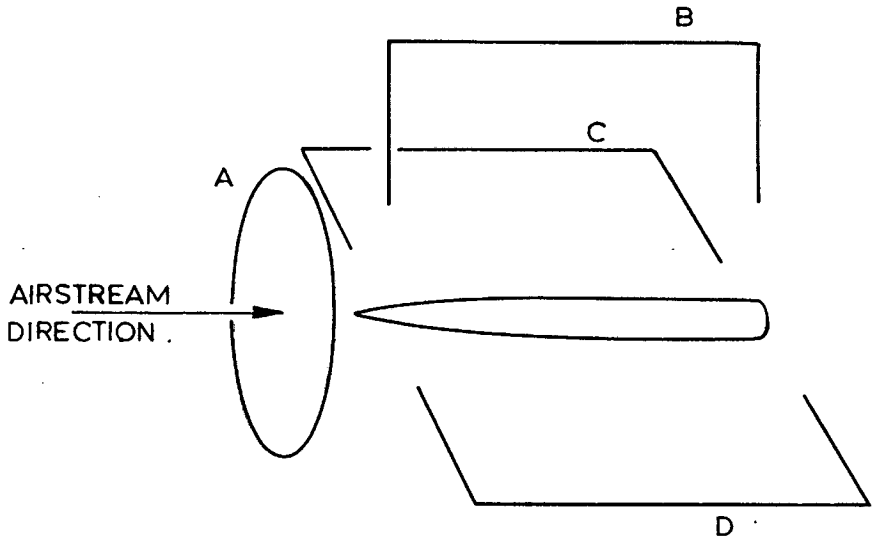

Fig. IV 1. A schematic diagram of the suspension magnet array of a six component magnetic wind tunnel balance and suspension system.

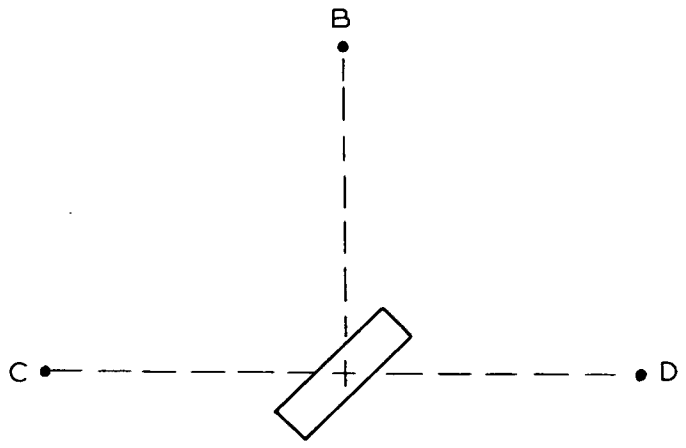

Fig. IV 2.. A view along the axis of the model, taken in a plane through the upstream poles of the support and lateral horse-shoe electro-magnets.

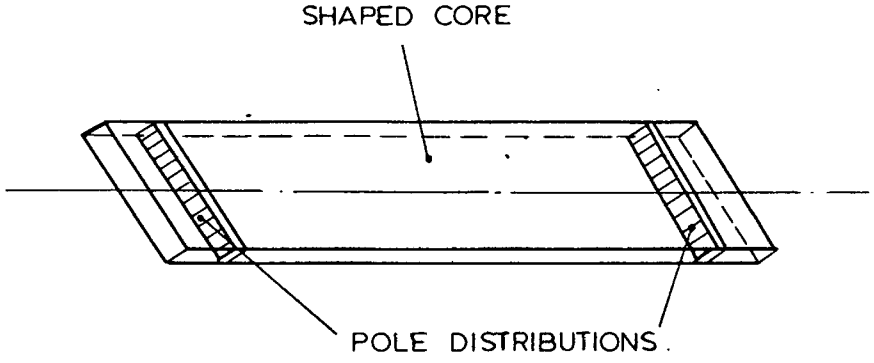

Fig. IV 3 The pole distributions assumed for the force and moment theory.

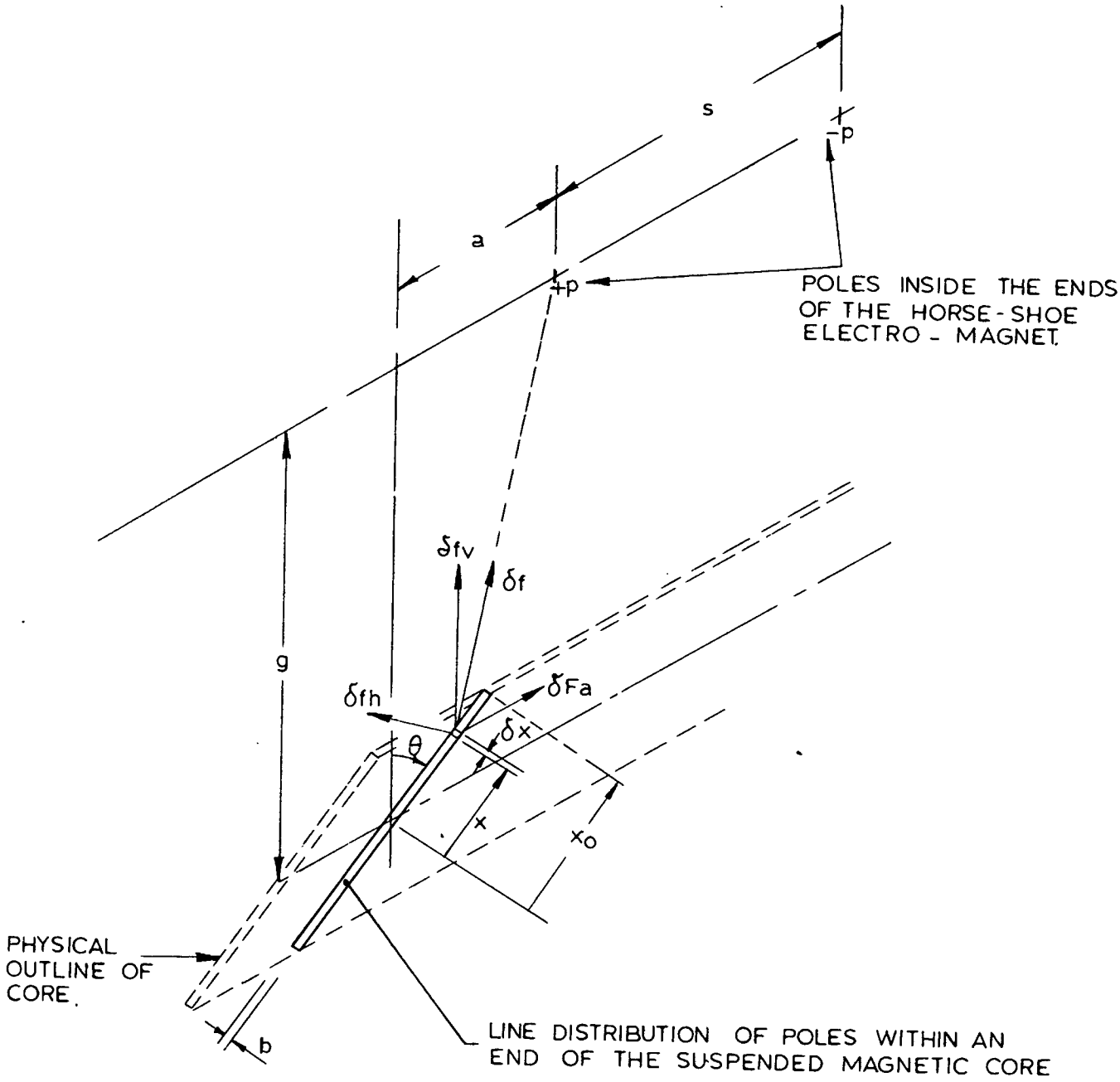

Fig IV 4 The "slender core" mathematical model.

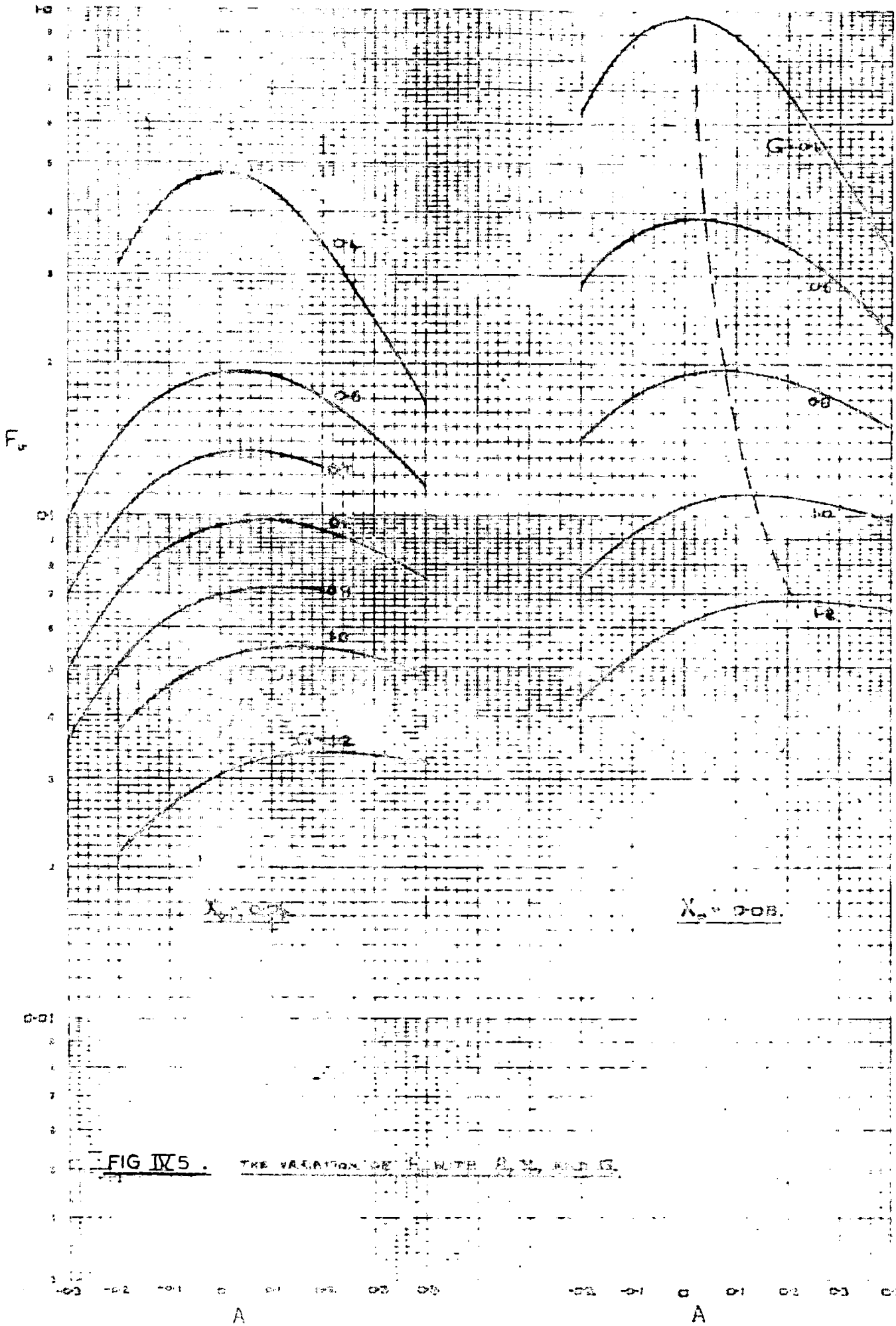

FIG IV 5. THE VARIATION OF F_s WITH A, X_0 AND G.

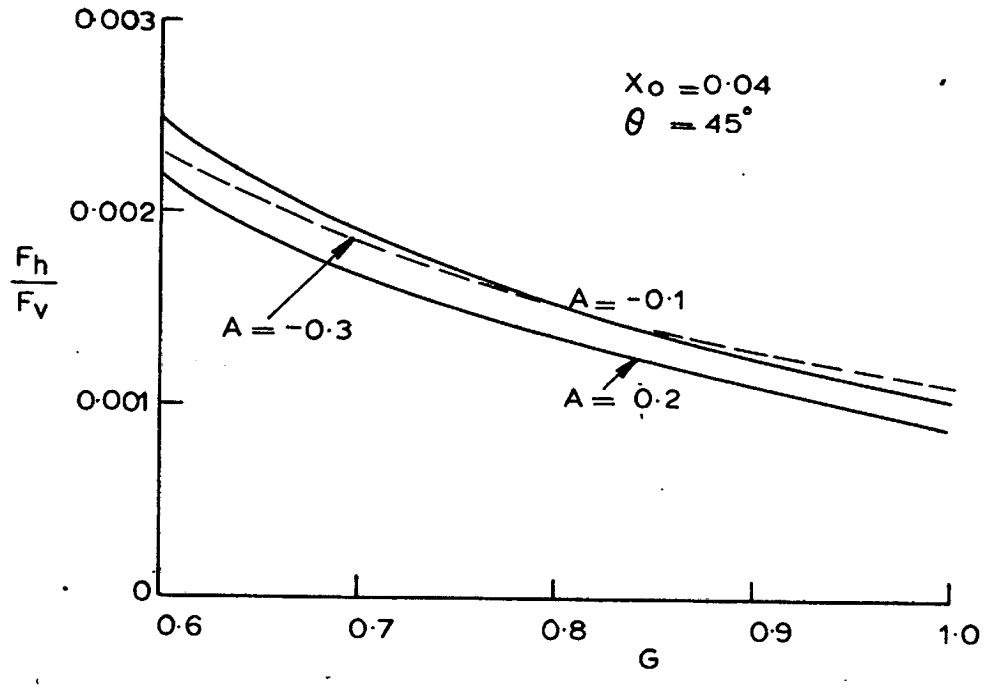

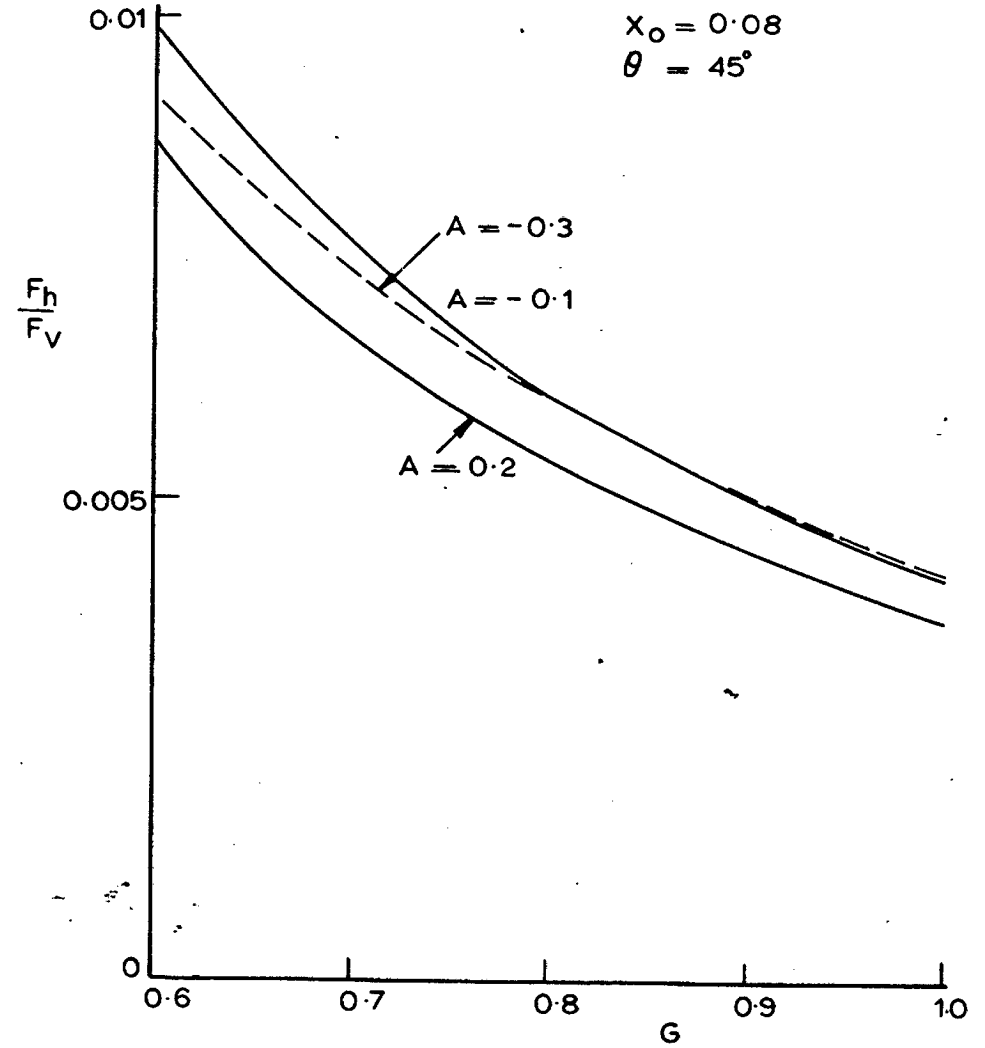

Fig IV 6. The ratio F_h/F_v with the core in the normal roll attitude.

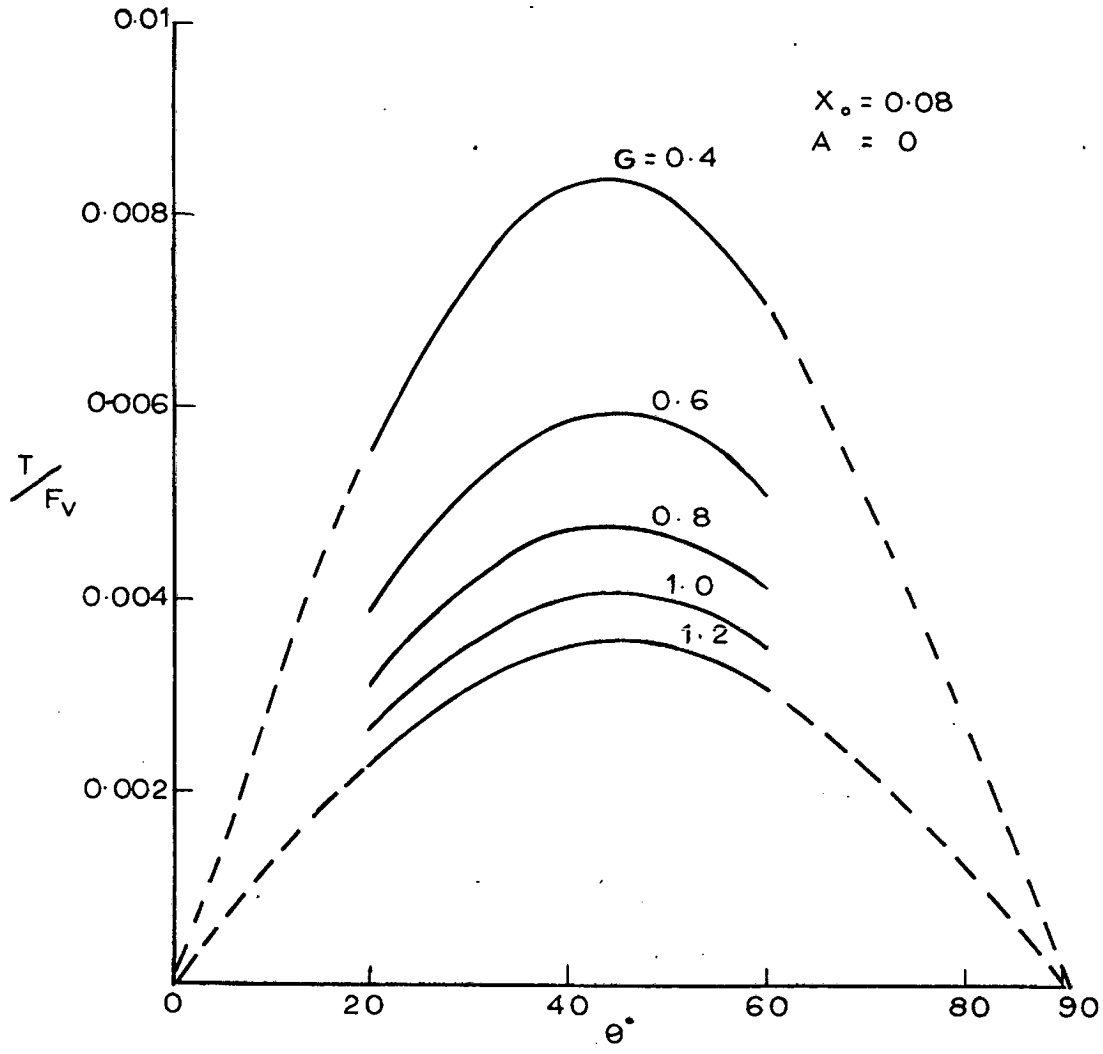

Fig. IV 7. The variation of T/F_v with θ and G.

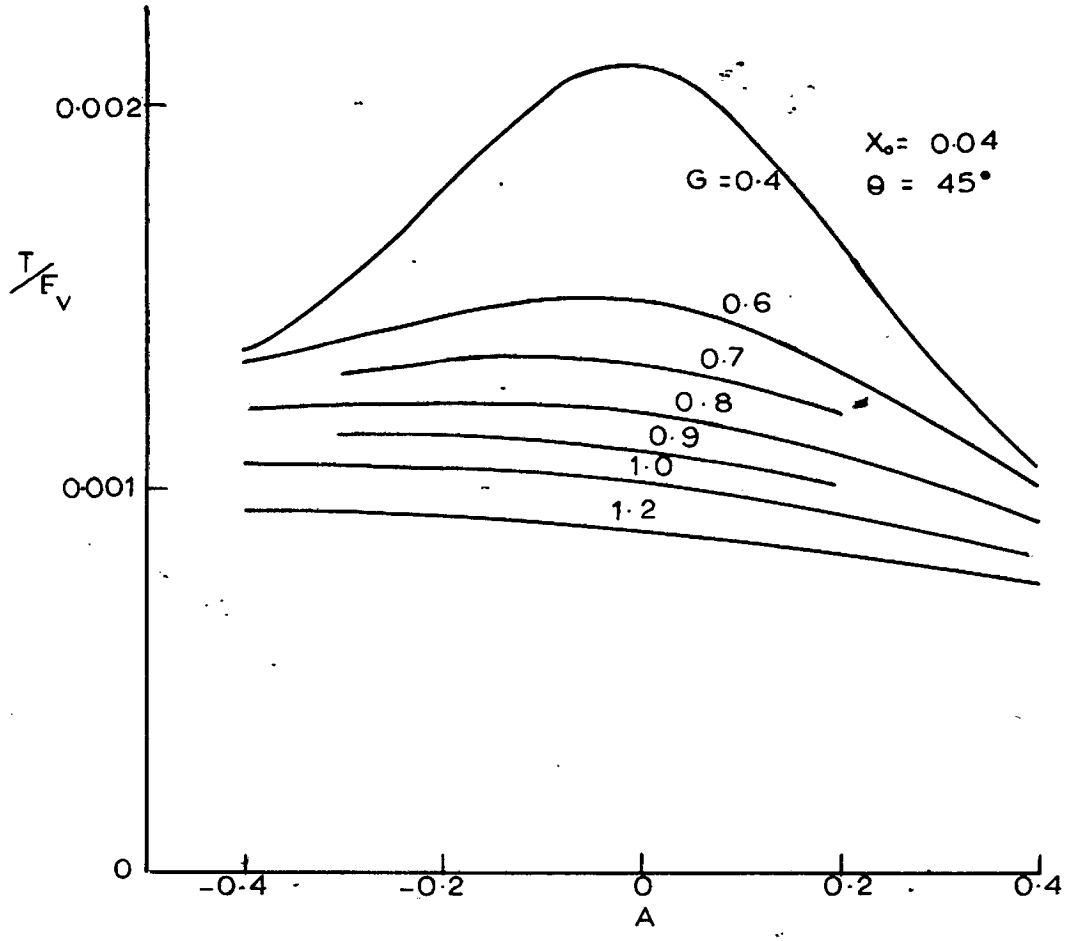

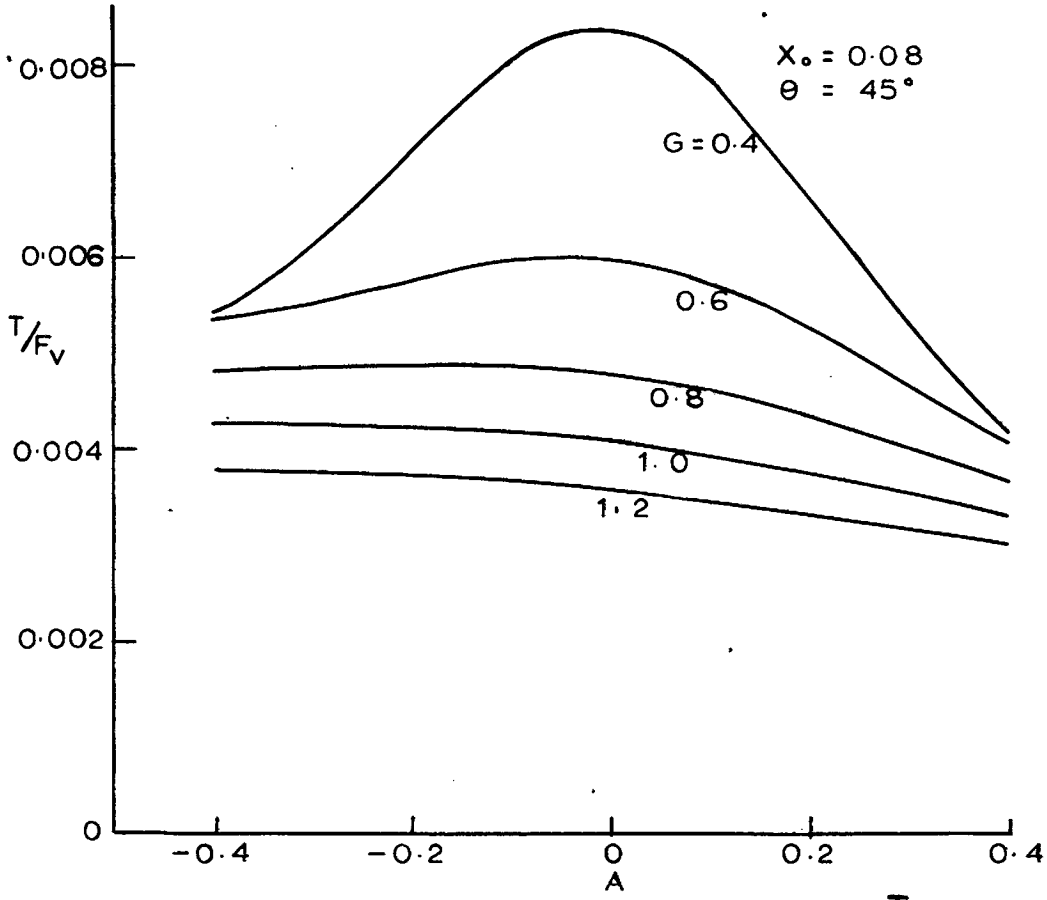

Fig IV 8. The variation of T/F_V with A and G. Normal roll attitude.

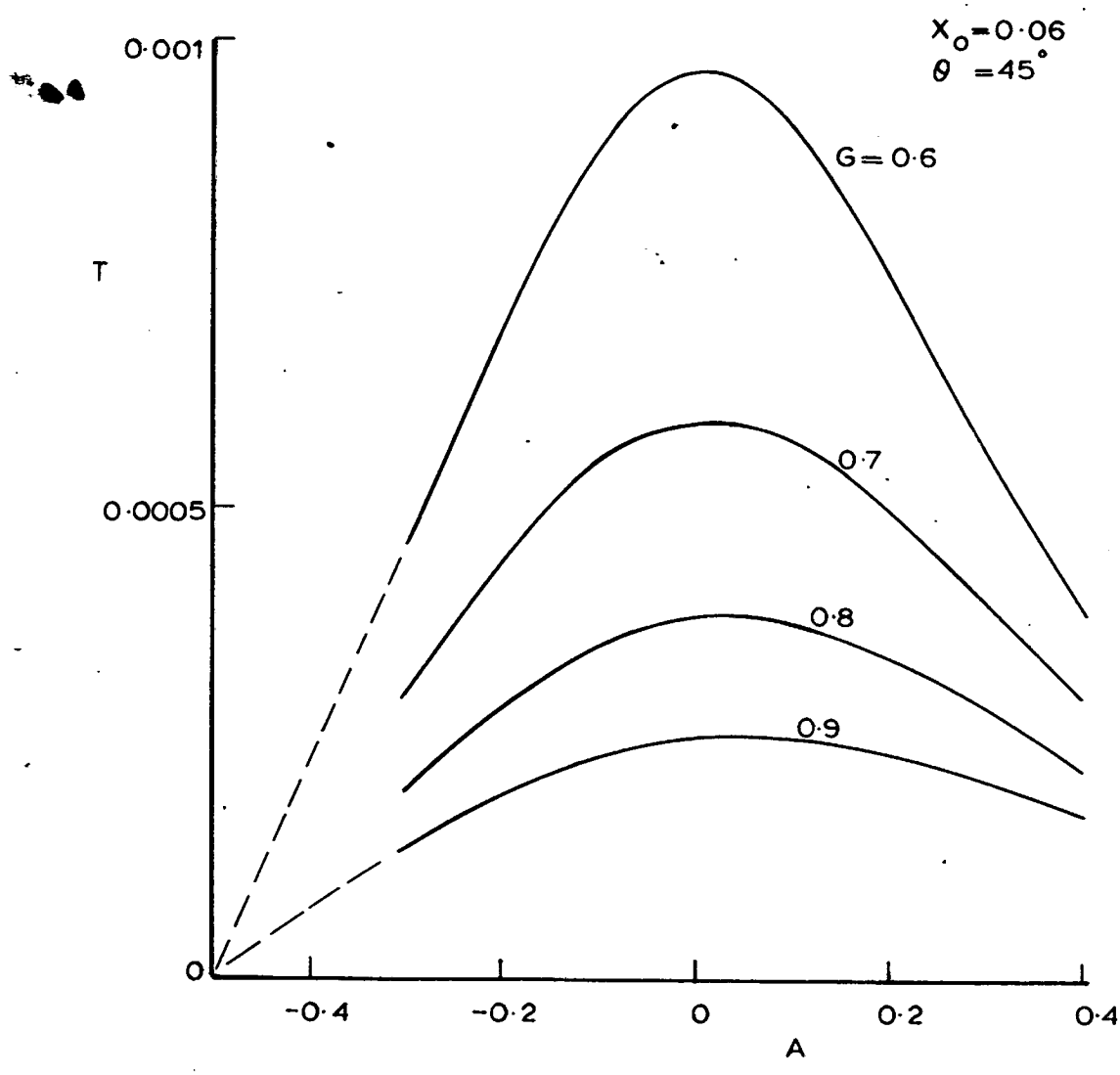

Fig IV 9 The variation of non-dimensional moment with A and G. Normal roll attitude.

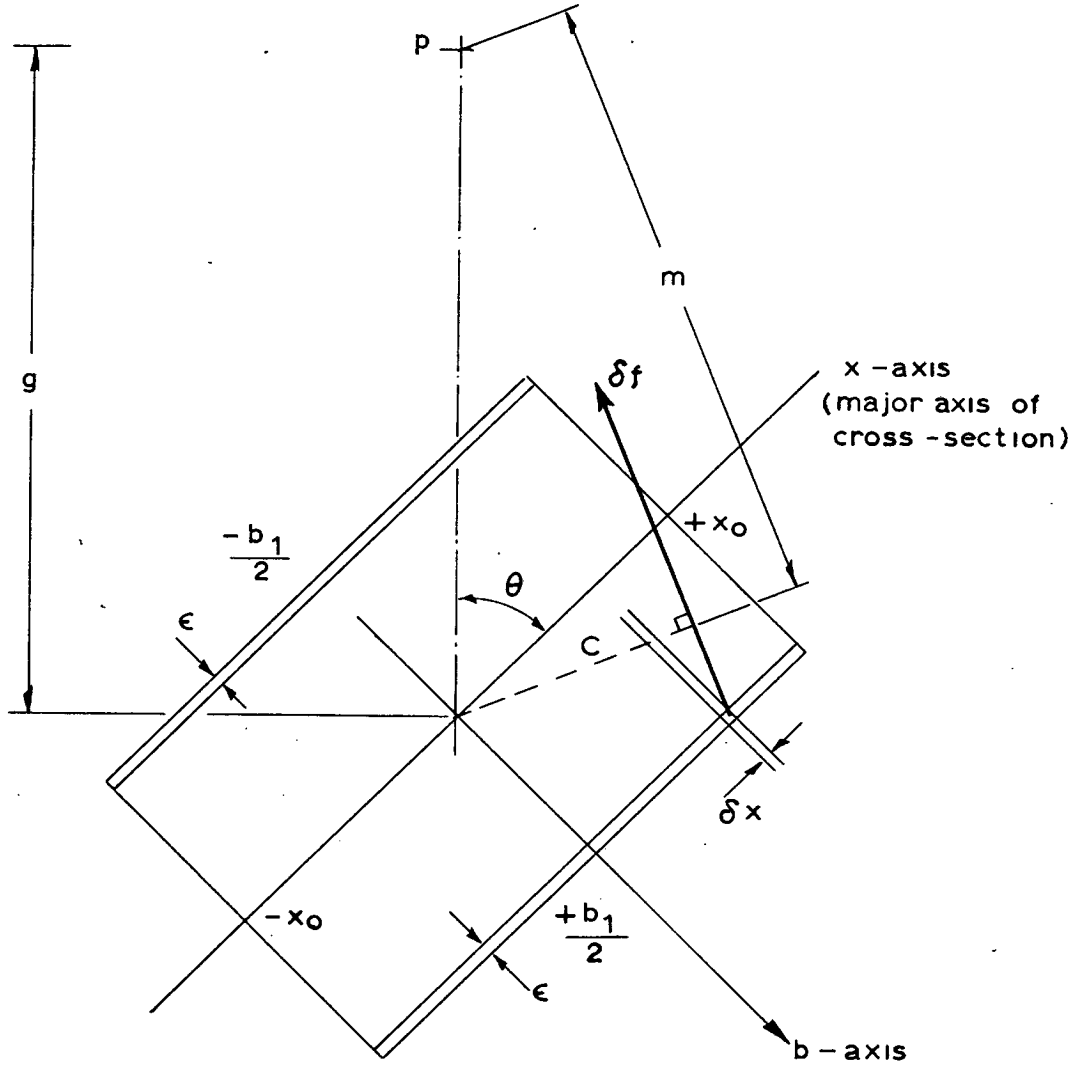

Fig IV 10 The rectangular cross-section of a thick Shaped Core.

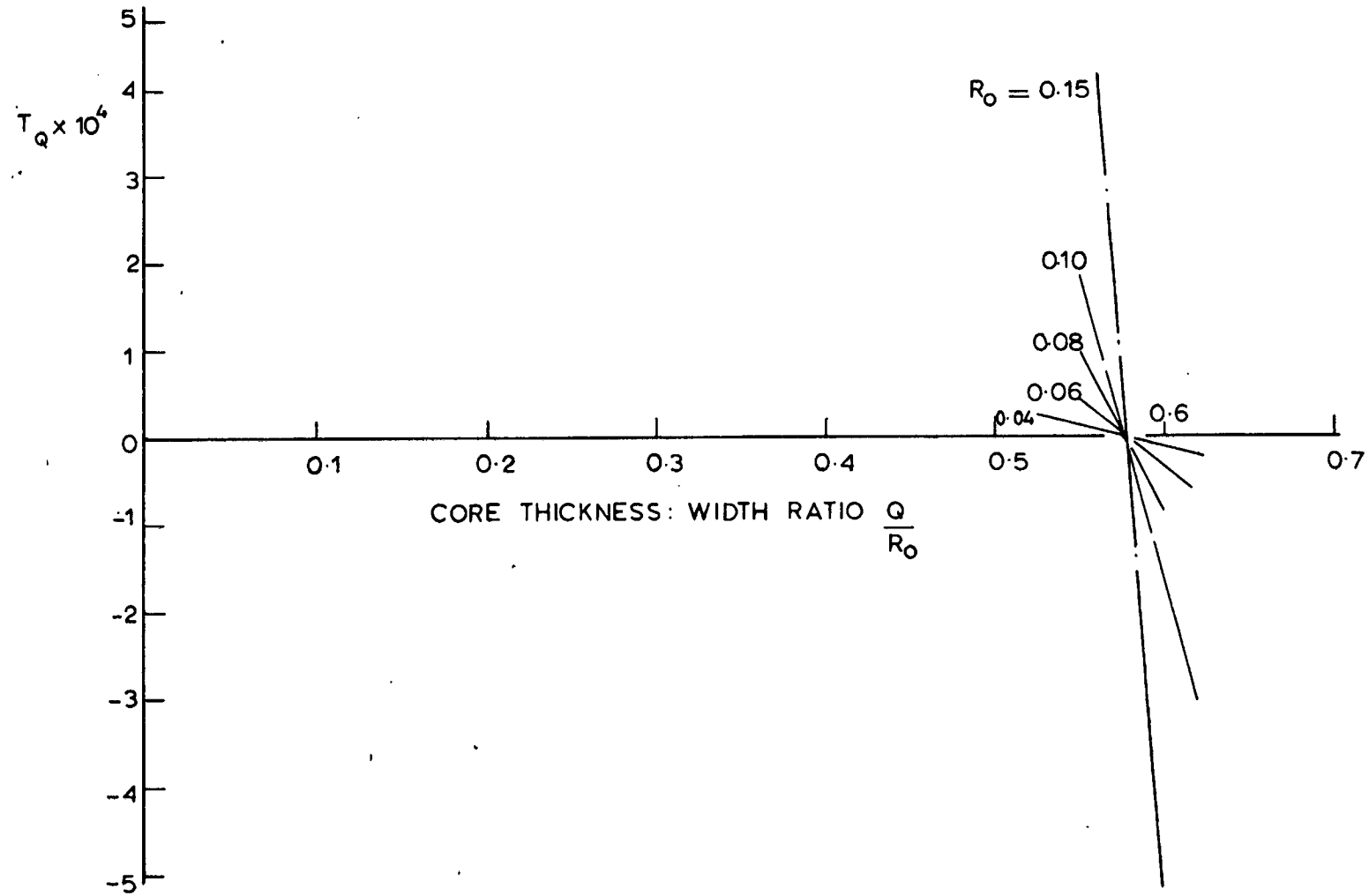

Fig. IV 11(a) The variation of the residual moment with the core thickness: width ratio for different core sizes.

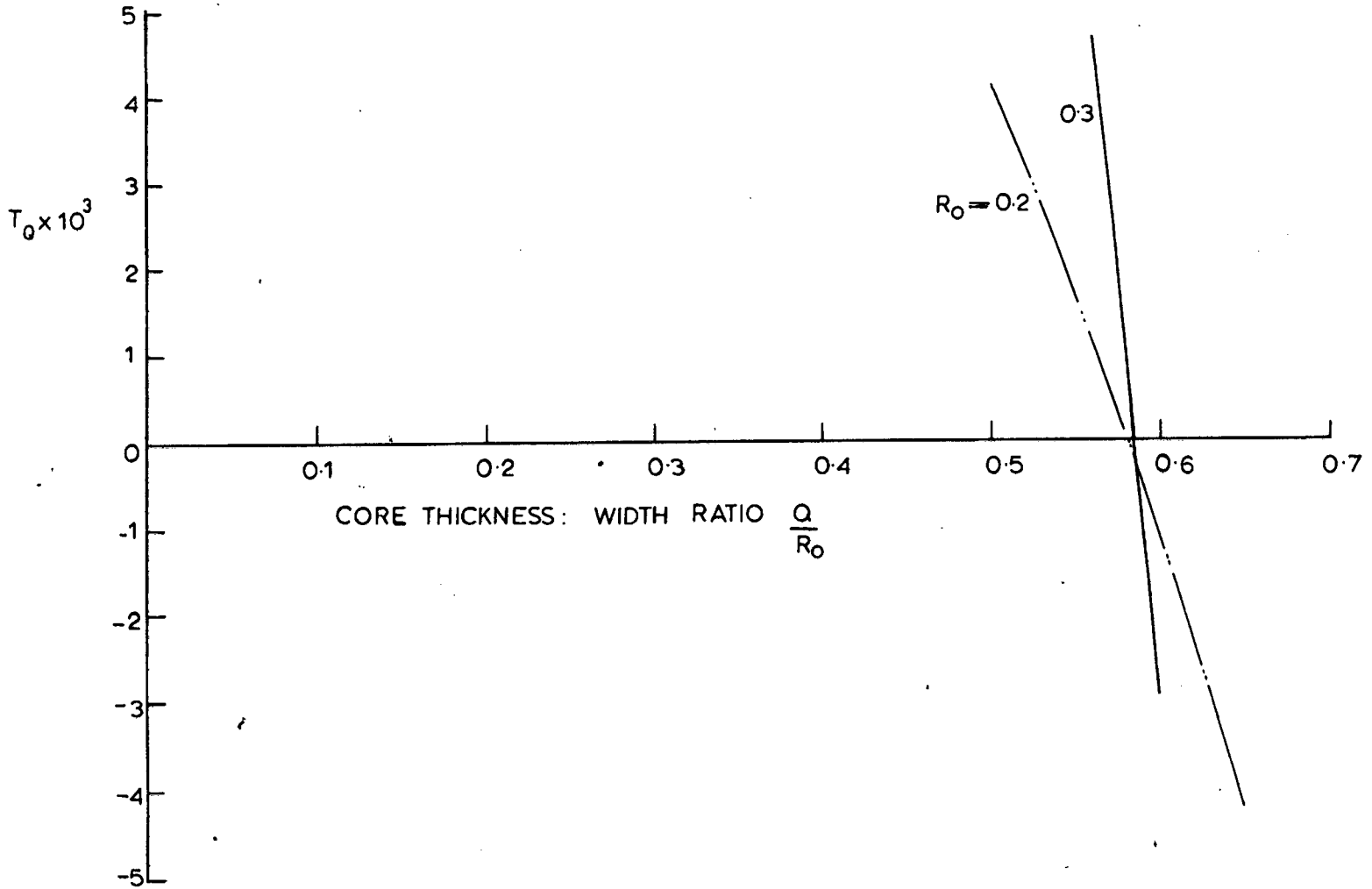

Fig. IV 11 (b) The variation of the residual moment with the core width: thickness ratio for different core sizes.

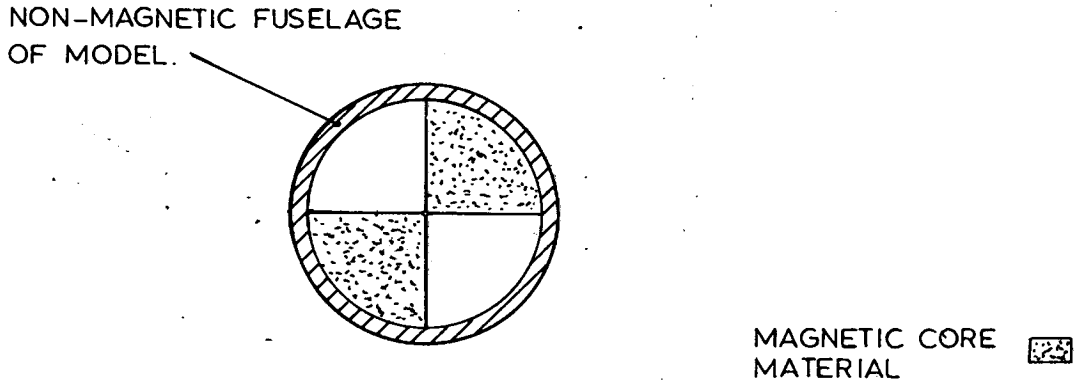

Fig. IV 12 The optimum "shaped core".
A cross section through the fuselage of a model, showing the core shape having the maximum rolling moment capability for a given diameter.

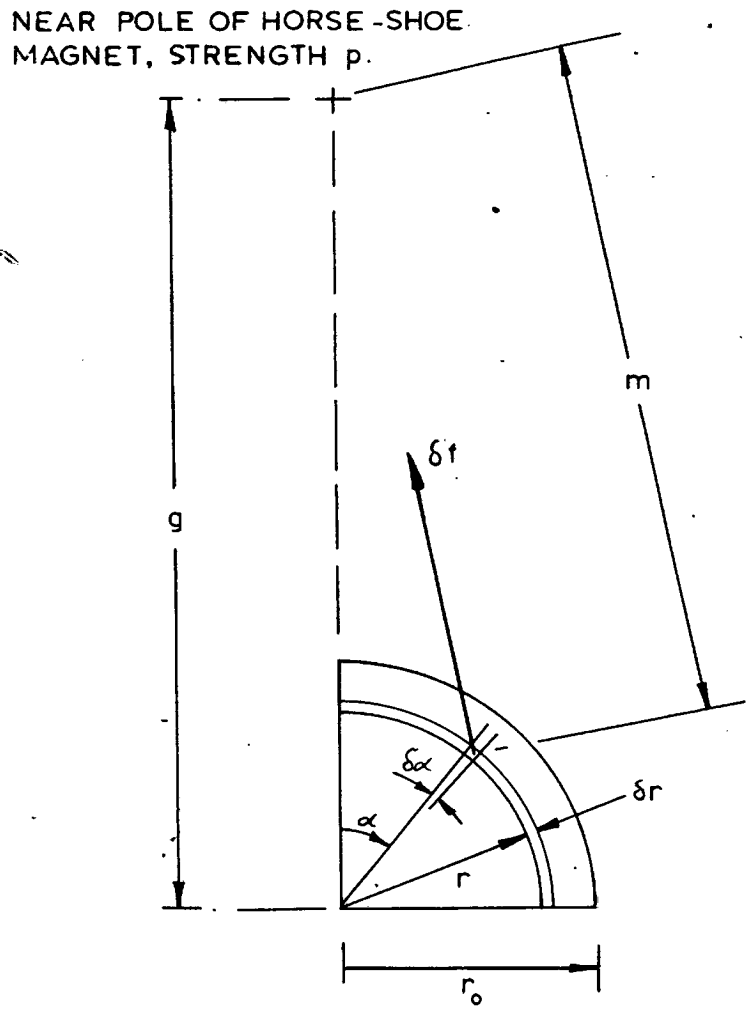

Fig. IV 13. An area distribution of poles lying in one quadrant of the "optimum" shaped core.